

Understanding Complex Systems

Springer :
COMPLEXITY

Petter Holme
Jari Saramäki *Editors*

Temporal Networks

 Springer

Springer Complexity

Springer Complexity is an interdisciplinary program publishing the best research and academic-level teaching on both fundamental and applied aspects of complex systems – cutting across all traditional disciplines of the natural and life sciences, engineering, economics, medicine, neuroscience, social and computer science.

Complex Systems are systems that comprise many interacting parts with the ability to generate a new quality of macroscopic collective behavior the manifestations of which are the spontaneous formation of distinctive temporal, spatial or functional structures. Models of such systems can be successfully mapped onto quite diverse “real-life” situations like the climate, the coherent emission of light from lasers, chemical reaction-diffusion systems, biological cellular networks, the dynamics of stock markets and of the internet, earthquake statistics and prediction, freeway traffic, the human brain, or the formation of opinions in social systems, to name just some of the popular applications.

Although their scope and methodologies overlap somewhat, one can distinguish the following main concepts and tools: self-organization, nonlinear dynamics, synergetics, turbulence, dynamical systems, catastrophes, instabilities, stochastic processes, chaos, graphs and networks, cellular automata, adaptive systems, genetic algorithms and computational intelligence.

The three major book publication platforms of the Springer Complexity program are the monograph series “Understanding Complex Systems” focusing on the various applications of complexity, the “Springer Series in Synergetics”, which is devoted to the quantitative theoretical and methodological foundations, and the “SpringerBriefs in Complexity” which are concise and topical working reports, case-studies, surveys, essays and lecture notes of relevance to the field. In addition to the books in these two core series, the program also incorporates individual titles ranging from textbooks to major reference works.

Editorial and Programme Advisory Board

Henry Abarbanel, Institute for Nonlinear Science, University of California, San Diego, USA

Dan Braha, New England Complex Systems Institute and University of Massachusetts Dartmouth, USA

Péter Érdi, Center for Complex Systems Studies, Kalamazoo College, USA and Hungarian Academy of Sciences, Budapest, Hungary

Karl Friston, Institute of Cognitive Neuroscience, University College London, London, UK

Hermann Haken, Center of Synergetics, University of Stuttgart, Stuttgart, Germany

Viktor Jirsa, Centre National de la Recherche Scientifique (CNRS), Université de la Méditerranée, Marseille, France

Janusz Kacprzyk, System Research, Polish Academy of Sciences, Warsaw, Poland

Kunihiko Kaneko, Research Center for Complex Systems Biology, The University of Tokyo, Tokyo, Japan

Scott Kelso, Center for Complex Systems and Brain Sciences, Florida Atlantic University, Boca Raton, USA

Markus Kirilionis, Mathematics Institute and Centre for Complex Systems, University of Warwick, Coventry, UK

Jürgen Kurths, Nonlinear Dynamics Group, University of Potsdam, Potsdam, Germany

Andrzej Nowak, Department of Psychology, Warsaw University, Poland

Linda Reichl, Center for Complex Quantum Systems, University of Texas, Austin, USA

Peter Schuster, Theoretical Chemistry and Structural Biology, University of Vienna, Vienna, Austria

Frank Schweitzer, System Design, ETH Zurich, Zurich, Switzerland

Didier Sornette, Entrepreneurial Risk, ETH Zurich, Zurich, Switzerland

Stefan Thurner, Section for Science of Complex Systems, Medical University of Vienna, Vienna, Austria

Understanding Complex Systems

Founding Editor: J.A. Scott Kelso

Future scientific and technological developments in many fields will necessarily depend upon coming to grips with complex systems. Such systems are complex in both their composition – typically many different kinds of components interacting simultaneously and nonlinearly with each other and their environments on multiple levels – and in the rich diversity of behavior of which they are capable.

The Springer Series in Understanding Complex Systems series (UCS) promotes new strategies and paradigms for understanding and realizing applications of complex systems research in a wide variety of fields and endeavors. UCS is explicitly transdisciplinary. It has three main goals: First, to elaborate the concepts, methods and tools of complex systems at all levels of description and in all scientific fields, especially newly emerging areas within the life, social, behavioral, economic, neuro- and cognitive sciences (and derivatives thereof); second, to encourage novel applications of these ideas in various fields of engineering and computation such as robotics, nano-technology and informatics; third, to provide a single forum within which commonalities and differences in the workings of complex systems may be discerned, hence leading to deeper insight and understanding.

UCS will publish monographs, lecture notes and selected edited contributions aimed at communicating new findings to a large multidisciplinary audience.

For further volumes:

<http://www.springer.com/series/5394>

Petter Holme • Jari Saramäki
Editors

Temporal Networks

 Springer

Editors

Petter Holme
Ice Lab, Department of Physics
Umeå University
Umeå
Sweden

Department of Energy Science
Sungkyunkwan University
Suwon
Korea

Jari Saramäki
Department of Biomedical Engineering
and Computational Science
Aalto University
Espoo
Finland

ISSN 1860-0832

ISBN 978-3-642-36460-0

DOI 10.1007/978-3-642-36461-7

Springer Heidelberg New York Dordrecht London

ISSN 1860-0840 (electronic)

ISBN 978-3-642-36461-7 (eBook)

Library of Congress Control Number: 2013938946

© Springer-Verlag Berlin Heidelberg 2013

This work is subject to copyright. All rights are reserved by the Publisher, whether the whole or part of the material is concerned, specifically the rights of translation, reprinting, reuse of illustrations, recitation, broadcasting, reproduction on microfilms or in any other physical way, and transmission or information storage and retrieval, electronic adaptation, computer software, or by similar or dissimilar methodology now known or hereafter developed. Exempted from this legal reservation are brief excerpts in connection with reviews or scholarly analysis or material supplied specifically for the purpose of being entered and executed on a computer system, for exclusive use by the purchaser of the work. Duplication of this publication or parts thereof is permitted only under the provisions of the Copyright Law of the Publisher's location, in its current version, and permission for use must always be obtained from Springer. Permissions for use may be obtained through RightsLink at the Copyright Clearance Center. Violations are liable to prosecution under the respective Copyright Law.

The use of general descriptive names, registered names, trademarks, service marks, etc. in this publication does not imply, even in the absence of a specific statement, that such names are exempt from the relevant protective laws and regulations and therefore free for general use.

While the advice and information in this book are believed to be true and accurate at the date of publication, neither the authors nor the editors nor the publisher can accept any legal responsibility for any errors or omissions that may be made. The publisher makes no warranty, express or implied, with respect to the material contained herein.

Printed on acid-free paper

Springer is part of Springer Science+Business Media (www.springer.com)

Preface

Neither Finland nor Sweden qualified for the 2010 Football World Cup in South Africa. Wouldn't that have been the case, you might not hold this book in your hands. With Finland vs. Sweden in the finals, our excitement would have been elsewhere than in science. At this time, at a workshop organized by Pieter Trapman, Tom Britton and Fredrik Liljeros of Stockholm University in the quaint Swedish seaside town Öregrund, we started discussing temporal networks. A month earlier, we had both within days put e-prints on the arXiv with intriguing results—"Small but slow world" by Saramäki et al. and "Simulated epidemics in an empirical spatiotemporal network of 50,185 sexual contacts" by Holme et al. In those papers, we used the same randomization technique, independently of each other, to discover that the temporal structures of two different datasets responded differently to spreading processes. In Saramäki's mobile phone communication data, randomization sped up spreading; in Holme's data from sexual encounters in prostitution, randomization slowed down spreading. While our beer-fueled discussion did not solve that question, we agreed that it was a good time to write a review paper on temporal networks. After about a year of off-and-on writing, we had a manuscript to submit to *Physics Reports*. About the same time, we both met at the European Conference on Complex Systems in Vienna and came up with the idea of this book volume as a follow-up to the review paper. Luckily Christian Caron, the editor-in-chief of Springer's Complexity series, was also at the conference and with his encouragement we moved on, gathering material to the book.

Temporal networks is a growing subfield of network science, probably with most of its discoveries still ahead in the future. As an example, we still don't have the answer to the question that sparked our collaboration—what are the conditions for temporal network structure to speed up spreading? However, we do know much more. This volume gathers 17 chapters and much new knowledge, many new methods and observations. We are very grateful to the authors and their contributions, all meeting our high expectations and most submitted by the deadlines. Last but not least, we want to thank our families. Fate or coincidence, during the making of this book we both got married and provided the future generation of network scientists (or football players, who knows) with two baby

boys: Jari's & Kaarina's son Paavo was born in August 2012 and Petter's & Hyunok's son Minu was born in February 2013.

Suwon
Espoo
April 2013

Petter Holme
Jari Saramäki

Contents

Temporal Networks as a Modeling Framework	1
Petter Holme and Jari Saramäki	
Graph Metrics for Temporal Networks	15
Vincenzo Nicosia, John Tang, Cecilia Mascolo, Mirco Musolesi, Giovanni Russo, and Vito Latora	
Burstiness: Measures, Models, and Dynamic Consequences	41
Byungjoon Min and K.-I. Goh	
Temporal Scale of Dynamic Networks	65
Rajmonda Sulo Caceres and Tanya Berger-Wolf	
Models, Entropy and Information of Temporal Social Networks	95
Kun Zhao, Márton Karsai, and Ginestra Bianconi	
Temporal Motifs	119
Lauri Kovanen, Márton Karsai, Kimmo Kaski, János Kertész, and Jari Saramäki	
Applications of Temporal Graph Metrics to Real-World Networks	135
John Tang, Ilias Leontiadis, Salvatore Scellato, Vincenzo Nicosia, Cecilia Mascolo, Mirco Musolesi, and Vito Latora	
Spreading Dynamics Following Bursty Activity Patterns	161
Alexei Vazquez	
Time Allocation in Social Networks: Correlation Between Social Structure and Human Communication Dynamics	175
Giovanna Miritallo, Rubén Lara, and Esteban Moro	
Temporal Networks of Face-to-Face Human Interactions	191
Alain Barrat and Ciro Cattuto	

Social Insects: A Model System for Network Dynamics	217
Daniel Charbonneau, Benjamin Blonder, and Anna Dornhaus	
Self-Exciting Point Process Modeling of Conversation Event Sequences	245
Naoki Masuda, Taro Takaguchi, Nobuo Sato, and Kazuo Yano	
Infering and Calibrating Triadic Closure in a Dynamic Network	265
Alexander V. Mantzaris and Desmond J. Higham	
Dynamic Communicability Predicts Infectiousness	283
Alexander V. Mantzaris and Desmond J. Higham	
Random Walks on Stochastic Temporal Networks	295
Till Hoffmann, Mason A. Porter, and Renaud Lambiotte	
A Temporal Network Version of Watts’s Cascade Model	315
Fariba Karimi and Petter Holme	
Timing Interactions in Social Simulations: The Voter Model	331
Juan Fernández-Gracia, Víctor M. Eguíluz, and Maxi San Miguel	

Temporal Networks as a Modeling Framework

Petter Holme and Jari Saramäki

Abstract To understand large, connected systems we cannot only zoom into the details. We also need to see the large-scale features from afar. One way to take a step back and get the whole picture is to model the systems as a network. However, many systems are not static, but consisting of contacts that are off and on as time progresses. This chapter is an introduction to the mathematical and computational modeling of such systems, and thus an introduction to the rest of the book. We will cover some of the earlier developments that form the foundation for the more specialized topics of the other chapters.

1 Introduction

Life, at many levels, is about large connected systems. In the biological sense, life is a consequence of macromolecules building cells and carrying information. More mundanely, our everyday life happens in amid a network of friends, acquaintances and colleagues. To understand life, at every level, we need to zoom out from macromolecules or friendships and look at their global organization from a distance. Here, zooming out means discarding the less relevant information in a systematic way. One approach to this, successful the last decade, is network modeling. This means that one focusses on the units of the system, be it proteins or persons, and how they are connected, and nothing else. Of course, this is a very strong

P. Holme (✉)

IceLab, Department of Physics, Umeå University, 90187 Umeå, Sweden

e-mail: petter.holme@physics.umu.se

Department of Energy Science, Sungkyunkwan University, Suwon 440-746, Korea

J. Saramäki

Department of Biomedical Engineering and Computational Science, School of Science,

Aalto University, FI-00076 AALTO, Espoo, Finland

e-mail: jari.saramaki@aalto.fi

simplification. One often has more information about a system that would enrich rather than obscure the picture. One such additional type of information regards when the interactions happen between the units. The essence of temporal-network modeling is to zoom out by excluding all information except which pairs of units that are in contact and when these contacts happen.

There is a large number of systems that could, potentially, be modeled as temporal networks. In addition to the cellular processes and social communication mentioned above large technological infrastructures—technologies based on the Internet or mobile-phone networks for example—have both network and time aspects that make them interesting for temporal network modeling. Neural networks—perhaps primarily at a functional level of brain regions that are considered connected if there is a measurable information transfer between them—are another example. A third example is ecological networks and species and their interaction. Such networks—like food webs, depicting which species feed on which other species, or mutualistic networks of species providing mutual benefits, such as plants and pollinators—experience time varying changes with the seasons and other environmental changes.

In this chapter, we will review the essential mathematical and computational techniques for extracting information from a temporal network representation of a system. We will discuss quantitative measures of network structure, computational techniques of successive randomization to study these measures, and models to generate and explain temporal networks and studies seeking to explain the effects of the temporal-topological structures on dynamics taking place on the networks. For a more comprehensive review of the field, see Holme and Saramäki [1].

2 Measuring Temporal Network Structure

In this section, we will review some of the proposed structural measures that strive to capture both temporal and topological features and correlations. For the rest of the chapter, we will consider systems that can be represented as lists of contacts—triplets of pairs of vertices together with the time of their contact, or alternatively as quadruples containing the beginning and end times of contacts, if these are not instantaneous. We call the first type of temporal network a *contact sequence*, the other one an *interval graph*.

Before we start discussing effects of structural measures, we note that temporal networks are notoriously difficult to visualize in a way that would both show all possible temporal information and highlight the important structural features (similarly to what e.g. spring-embedding can successfully do for static networks). Two representations, labeled graphs and time-line plots, are illustrated in Fig. 1. Of these, the time-line plots can help to visualize the temporal structure (including temporal heterogeneities such as bursts) while the labeled graphs highlight the network topology. However, neither of them can be scaled up to more than a dozen or so vertices. There are other attempts of combining time and simplified

topology—most notably the *alluvial diagrams* of Rosvall and Bergstrom [2]—that however typically miss the non-transitivity of temporal networks, or some other important aspects.

2.1 *Reachability and Latency*

One of the most fundamental differences between temporal and static networks is that the former are not transitive. Even if vertex A is related to B and B is related to C, it might be that A is not related to C (see Fig. 2). The relation in question is in essence the possibility of something spreading from one vertex to another through a series of contacts where the times of the contacts are increasing (anything else would not be feasible in reality). For this reason, the statistics of such *time-respecting paths* are very informative. Authors have e.g. investigated the average durations of time-respecting paths [3–6]. Given a pair of vertices (i, j) and a time t , the *latency* is the shortest time to go from i to j at time t following only time-respecting paths.

The latency is not the entire story, since just like regular graphs, temporal networks can be disconnected. This is, in practice, more common in temporal than static networks, as the paths joining vertices need to be traversed in the order of contacts. A practical measure for capturing this would be the expected value of the number of vertex pairs that have infinite latency values [3]. For empirical data, the finite period of observation may also play a role, because paths whose realization takes a very long time may not ever be completed within the observed period. It should be emphasized that connectivity is only defined within some time window: the fact that A is connected to B via a time-respecting path that begins at t does not guarantee that such a connection exists at any later point in time. Furthermore, connectivity is always directed as dictated by the arrow of time (see the transitivity example above).

One can elaborate on latency-like measures in many ways in order to capture different aspects of reachability and dynamical influence between nodes. It could for example be interesting to monitor the number of time-respecting paths between pairs of vertices in order to capture frequently appearing pathways, or to resolve the average latency in time—it might be that the average latency follows e.g. a daily pattern where time-respecting paths are faster to traverse during the time of day when the contacts are more frequent. Additional constraints may also be set on time-respecting paths; e.g. one may require that the contacts forming a path follow each other rapidly enough, so that long waiting times between contacts destroy the path [6].

2.2 *Clustering and Correlations*

In static networks, the local structure—focusing on the immediate surroundings of an average vertex—is an important predictor of the behavior of dynamic systems on

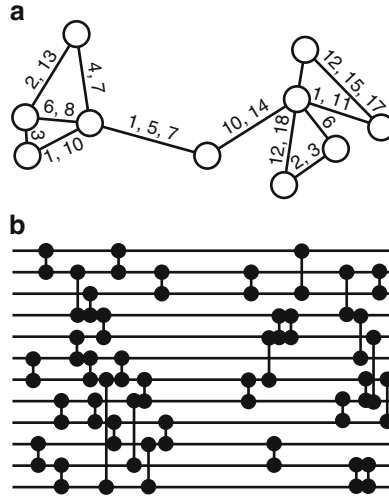


Fig. 1 Visualization of temporal networks. (a) Shows a labeled aggregate network where the labels denote times of contact, and (b) shows a time-line plot, where each of the lines corresponds to one vertex and time runs from *left to right*

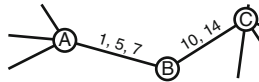


Fig. 2 Illustrating the non-transitive nature of temporal networks. Information can spread from A to B, from B to C, from C to B, from B to A, it can also spread from A to C via B, but not from C to A since by the time the information can have reached B all contacts between A and B have already happened. Note that static networks are transitive, even directed networks, so one cannot simply reduce a temporal network to a static one

the network. Adding the temporal dimension is not straightforward, which perhaps explains the rather few attempts to do so. Below, we sketch one possible approach and illustrate some of the inherent difficulties.

In static networks, the level of connectivity in the neighborhood of a vertex can be measured with the (local) topological clustering coefficient. Its values are normalized, such that a value of 0 indicates no connectivity and a value of 1 the existence of all possible connections. Adding a temporal dimension, we would like to measure the connectedness of a neighborhood around a given moment of time t . In other words, we would like to put a larger weight on contacts that are closer to t in time. This can be done by an summation kernel $F(t)$ with the properties that it is bounded, non-negative, monotonically increasing for $t < 0$, monotonically decreasing for $t > 0$, and $F(0) = 1$. A temporal clustering coefficient for a contact sequence would then be the following sum divided by some normalizing factor

$$\sum_{c,c',c''} F(t(c) - t) F(t(c') - t) F(t(c'') - t) \quad (1)$$

where $c = (i, j, t)$, $c' = (j, k, t')$ and $c'' = (k, i, t'')$ are contacts with $i \neq j \neq k$. However, there is no obvious choice of denominator to balance this with. If one calculates the denominator by assuming that there can be one contact per time step between all vertices that are in contact with i at some point, then this would for the very most datasets be a number many orders of magnitude larger than the denominator. One can perhaps set the maximal number of contacts as the total number of contacts in the dataset and assume that they all happened at time t , but also this would in practice be a very much larger number than that given by (1). A third option would be to replace the F -factors by 1 (their maximal value), but this would be equal to assuming that the number of contacts per vertex pair that has been in contact at some time is fixed, which would be strange for most types of temporal networks. This example is not meant to discourage from constructing measures capturing both temporal and topological structures, but rather the other way around. It shows how moving away from the assumption that all edges are equivalent (an assumption underlying most static network representations) requires new ways to think about network concepts. In this case, the best solution, we believe, would be to compare the raw sum to that obtained from a carefully chosen reference model.

In static networks, one important class of measures quantifies the relationship between the degrees of connected nodes. Is there an overrepresentation of edges between, say mid-degree vertices and other mid-degree vertices? Such an analysis can be made at different levels, from plotting the entire correlation profile [7] to measuring a scalar-valued correlation coefficient [8]. These degree-correlation measures can be generalized to temporal networks more straightforwardly than the clustering coefficient. One can use similar summation kernels as discussed above to replace node degrees by a time-dependent activity level, and then perform the same analysis. Then again, while this would capture something similar in spirit to the degree-correlation measures designed for static networks, in temporal networks there is a multitude of other conceivable concepts of correlations across links that could well prove more important.

As a temporal networks evolve, some subsets of their nodes and links may be more continuously active than others. Such persistent patterns are subnetworks that are prime candidates for functional subunits of some sort; they could also be an interesting alternative to aggregating all contacts if one wants to reduce the system to a static network. As an example of how to investigate persistent contact patterns, one can let a time window slide through an interval graph and calculate the adjacency *correlation function*, or *vertex persistency*

$$\gamma_i(y) = \frac{\sum_{j \in \phi(i,t)} a(i, j, t) a(i, j, t + 1)}{\sqrt{\sum_{j \in \phi(i,t)} 1} \sqrt{\sum_{j \in \phi(i,t+1)} 1}} \quad (2)$$

where t is the beginning of the time window, and $\phi(i, t)$ are the non-zero indices of the (time-dependent) adjacency matrix.

2.3 Centrality

Network centrality measures form one of the most important classes of measures of static network structure. These quantities try to capture various facets of the question how central a vertex is. Pan and Saramäki discuss a centrality measure akin to *closeness* in static graphs [8]. Essentially, the authors define centrality as the average reciprocal value of the time from the focal vertex to all others. Tang et al. also defines a (somewhat different) closeness centrality for temporal networks together with a temporal version of the *betweenness centrality* [9].

Takaguchi et al. take a slightly different approach in [10] when they measure a kind of influence (called *advance*) related to concepts of centrality by focusing on the importance of the events the vertex participates in. This work draws on previous results from [4]. Mantzaris et al. [11] use a spectral centrality measure for temporal graphs to study learning in the human brain.

2.4 Motifs

Network motifs were first proposed for static directed networks [12] and are, briefly described, overrepresented subgraphs formed by a few vertices and their directed links. Motifs are often interpreted as functional units, or candidates for such, and motif analysis is commonly applied e.g. in systems biology. In static directed networks, motifs can be mapped to component-like structures such as feedforward loops, but in temporal networks, this is harder. Rather, motifs in temporal networks correspond to typical sequences of events. There are many ways of defining such motifs. To take one example, Kovanen et al. [13] look at sequences of contacts between vertices that are maximally separated by a time δt . More precisely, two contacts e_i and e_j are δt -adjacent if they share a vertex and are separated in time by no more than δt . Pairs of events are then defined as δt -connected if there is a sequence of δt -adjacent events joining them and temporal subgraphs are defined as sets of events that are δt -connected. By counting such subgraphs and mapping them into isomorphic classes on the basis of their order of events, Kovanen et al. find an overrepresentation of temporal motifs that are causal, i.e. where the contacts may have triggered one another (such as A contacts B who contacts C and D, as opposed to the non-causal sequence where B contacts C and D, and A only then contacts B). As an application of a temporal-network motif method (slightly different from that of [13]) Jurgens and Lu [14] use motifs to study behavior in the evolution of Wikipedia.

2.5 *Mesoscopic Structures*

In static networks, there has recently been a flood of methods proposed to discover mesoscopic structures (a.k.a. clusters, communities or modules [15]). These are loosely defined as groups of vertices more densely connect within than between each other. Much of the community structure literature regarding static networks only focuses on deriving a method for decomposing the network on the basis of some conceptually simple principle. The few methods that incorporate the time dimension into community detection typically operate on aggregated time-slices of the contact sequence [16, 17] or networks of links that have happened and will happen again [18]. One can imagine clustering algorithms based on more elaborate temporal structures, like time-respecting paths (an exception is Lin et al. [19]). As mentioned earlier, visualizing temporal networks as two-dimensional, printable diagrams is difficult and this is a major obstacle to intuitive reasoning about mesoscopic temporal-topological structure. Reducing the network to a network of clusters that split and merge with time is perhaps the most promising path in this direction. Unfortunately, such a reduction would also destroy any non-transitive features of the original structure, especially when time slices or aggregation are involved, and smear out the effects of all temporal structures associated with shorter time scales than the time window that is used (such as bursts) [20].

3 Models of Temporal Networks

As in all other areas of theoretical science, our understanding of temporal networks hinges on mathematical and computational models. These models have different purposes. The simplest class of models, already mentioned above, involves *null* or *reference models* that are used together with various measures in order to infer their statistical significance, or in order to assess the contribution of chosen types of correlations to the values of the measures. Related to this are generative models that can serve both as reference models and as a method to synthesize temporal structures to run simulations of dynamic systems on. The third class comprises mechanistic models for explaining the emergent network structures that one measures; and finally we also have predictive models that are tailored to forecast future aspects of a temporal network.

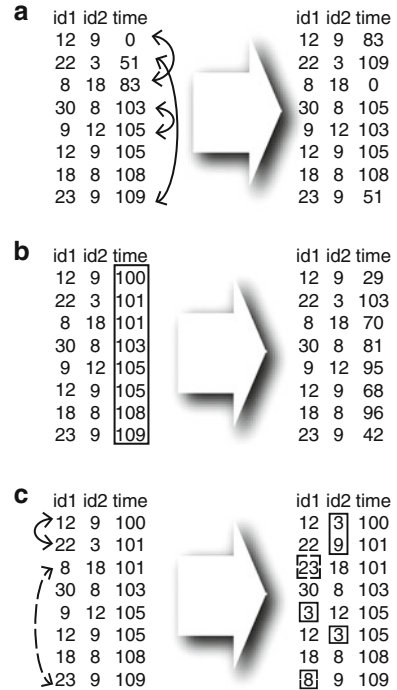
Much remains to be done in the development of temporal-network models in all above-mentioned areas. This is somewhat in contrast to the theory of static networks where a very large number of models were developed at an early stage [8].

3.1 *Randomized Null or Reference Models*

In order to interpret the significance of temporal-network measures, or to understand what effects different temporal and structural features have on them, one needs

Fig. 3 Illustration of some randomization methods.

(a) Shows the randomly permuted times (*PT*) scheme that removes structures in the order of events. (b) Shows the random times scheme (*RT*) and (c) displays a static network rewiring as it appears in a contact sequence. The contacts of an edge is conserved in the process. Note that one need to allow edges (A,B) and (C,D) to be rewired to both (A,D), (C,B) and (A,C), (D,B) to make the sampling ergodic



something for comparing against. One approach is to compare observations against the same measures computed for an ensemble of randomized networks that are “neutral” in some chosen sense, i.e. where certain correlations and features are removed by randomization procedures such that only the chosen fundamental constraints of empirical networks are retained. The way the empirical network differs from the null model gives meaning to the structure observed in the empirical data, and points out effects that are due to the removed correlations. One can also give a scale to the “raw” measures of temporal network structure, e.g. by normalizing by the corresponding values for the reference models or subtracting such values. More elaborately, one can assess the statistical significance of observed measures by calculating the *Z*-score, or similar, of their values in the empirical network against their distribution in the randomized ensemble. Strictly speaking, the term “null model” should be used only in this context: *Z*-scores are then used to reject or verify the null hypothesis that the observed features can be explained by the randomized ensemble, and the removed correlations do not play a role.

For static networks, perhaps the most popular reference model is to rewire the edges randomly while keeping the degree and number of vertices constant [7]. See Fig. 3. This model is very closely related to the *the configuration model* which is rigorously defined as an ensemble of vertices of given degrees that are connected in a maximally random way [8]. For practical purposes, randomization by edge swapping and the configuration model are equivalent. This is helpful since the configuration model is theoretically well understood.

For temporal networks, randomization plays a slightly different role than for static networks. On one hand, there is no mathematically well-understood null model like the configuration model. On the other hand, there is a much larger number degrees of freedom, and subsequently there is also a much larger number of possible randomization models. In fact, such models allow for going through a sequence of randomization procedures, where one progressively removes chosen types of correlations from the empirical temporal network. This provides a detailed, continuous picture of temporal-network structure and the correlations that underlie observations.

Below, we will discuss some of the most important temporal network models. For a longer list, see Holme and Saramäki [1].

3.1.1 Randomly Permuted Times (RP)

As a temporal counterpart to the randomization of edges discussed above, one can randomly permute the times of contacts, while keeping the network's static topology and the numbers of contacts between all pairs of vertices fixed. As this randomization scheme retains all static network structure and the number of contacts for each edge, its application can be used to study the effects of the exact order and timings of contacts. The reference model destroys burstiness and inter-contact times of nodes and edges, and subsequently also all correlations between timings of contacts on adjacent edges. The model also keeps the overall rate of events in the network over time, such as daily or weekly patterns. See Fig. 3.

3.1.2 Random Times (RT)

The set of time stamps is conserved in the RP ensemble. Hence, the intensities of contacts at an aggregate level follow the same patterns as the real data—if there are circadian rhythms (like in many human, and other biological and social systems) they will still be there in randomized networks. If one wants to explore the impact of these rhythms, one may draw the interaction times from a random distribution and compare the outcome to the RP ensemble. See Fig. 3.

3.2 *Generative, Mechanistic and Predictive Models*

A large amount of numerical temporal network studies have been performed on empirical networks. Since there is not yet any commonly-agreed-upon set of temporal network characteristics, and since it is not yet clear what the most important features of temporal networks are and whether there is any universality in such features, the focus has been on what the data can tell us, which can be seen as an advantage. The disadvantage is that we do not get a systematic understanding of the

effects of temporal network structure. In order to arrive at such an understanding, we need generative models that can output temporal networks with tunable structure.

In cases where topological and temporal structures are decoupled, creating a generative model is straightforward. One could perhaps first generate the topology according to some model from the static network literature, and then generate time series of contacts over the edges for tuning some quantity of interest (like the vertex persistency, (2)). Studies that successfully utilize generative models to study the effects of temporal network structure include [21, 22].

Another type of models that are very common in the static network literature but not for temporal networks are mechanistic models trying to explain the emergence of large-scale structure from simple underlying driving mechanisms. Indeed, the whole field of complex network theory took off in the 1990s with the Watts–Strogatz model of small-world networks and the Barabási–Albert model of scale-free networks, which makes this lack of mechanistic temporal network models even more conspicuous.

A third type of models for temporal networks (largely still waiting to be realized) is predictive models, solely targeted at forecasting the future development of the contact structure. Such models, drawing from machine-learning and statistical techniques, would not necessarily attempt to explain why a temporal network is like it is, or to generate contact sequences from scratch. Rather, given a contact sequence or interval graph, such models could predict its continuation in the near future.

4 Processes on Temporal Networks

Networks are never just a collection of vertices and edges (or contacts in the case of temporal networks), except in very trivial cases. Rather, they are the underlying structure that determines how dynamical processes over the graph unfold, from contagion of infections to Internet traffic. Thus, they in reality define the system’s function. Obviously, temporal effects can strongly affect any dynamics that follow the shortest paths between vertices (see the above discussion on latency). Especially, temporal features of networks affect the dynamics of diffusion and spreading. This has been investigated by comparing spreading dynamics—often, with the help of compartmental models of infectious disease spreading—on empirical contact sequences and their randomized reference counterparts. At the moment, we do not have a comprehensive theory of how temporal-network structure affects disease spreading. For some systems the temporal structure speeds up spreading [23], in other systems the temporal structure seems to slow it down [24]. The structure in focus of these studies is *burstiness*—the property that contact activity (often human) is very inhomogeneously distributed in time—that can be readily removed from temporal networks by applying randomized reference models.

Another type of models of social spreading phenomena is threshold models, in particular targeted for studies of social influence and opinion spreading. In threshold models, an agent (or vertex) changes its state whenever the impact from

the surrounding vertices exceeds some threshold value. The dynamics of such models seem to have a tendency to speed up if there is burstiness, but also in this case there is no general theory. Coming up with a general theory might even be impossible, since there are different aspects of how to measure and quantify the impact that triggers state changes in such models. Furthermore, it is hard to observe or experimentally study human threshold behavior, which additionally may largely depend on circumstances (for one such experiment, see [25]). Regarding threshold models on temporal networks, Karimi and Holme [26] studied a modification of Watts's threshold models of cascades [27] for contact sequences and Takaguchi, Masuda and Holme [28] studied a threshold model of exponentially decaying influence. Both these studies were performed on empirical networks.

5 Summary and Discussion

We have given an overview of the different aspects that the field of temporal network so far has covered. Furthermore, we have explained the challenges in extending static network measures to temporal networks. We argue these challenges should be encouraging rather than the opposite, both since they are intellectually fascinating and since there are useful applications waiting once they are resolved.

The study of temporal networks is a fast advancing field with a great potential for the future. However, many challenges remain. The extra level of information added by the temporal dimension does not only make it difficult to develop theory and computational methods, it also changes the questions one can ask about the structure of the system. Probably many advances can be made by connecting and integrating temporal networks with other extensions of network models such as *spatial networks* [29] where the coordinated of spatially embedded nodes and links are incorporated in the modeling framework, or *adaptive networks* [17, 30] where there is a focus on the feedback from the dynamics on the networks to the evolution of the network evolution.

Open questions for future studies ranges from how to make static visualizations of temporal networks, via how to predict missing links in incomplete temporal network data [31] or how to make sport-ranking systems [32], to classic questions like if there is any universal law that involves both temporal structure and network topology.

6 In This Book

This book aims at presenting an overview of the state-of-the-art in temporal networks. Its chapters are contributed by leading researchers and research teams from a variety of backgrounds and disciplines. Our target has been to cover the emerging field of temporal networks both in breadth and in depth, and because of

this, some chapters are essentially reviews on key topics—such as temporal network metrics and burstiness—whereas others provide detailed accounts of investigations building on the temporal networks framework, from networks of face-to-face human proximity to the collective behaviour of social insects.

The following five chapters focus on metrics, measures and methods for characterizing temporal network structure. In chapter “Graph Metrics for Temporal Networks”, Nicosia, Tang, Mascolo, Musolesi, Russo, and Latora present an overview of key temporal network metrics and measures, from walks and paths to connectedness and centrality measures. This is followed by a chapter that focuses on one of the key characteristics of temporal networks, especially those related to human interactions: in chapter “Burstiness: Measures, Models, and Dynamic Consequences”, Min, Goh, and Kim discuss burstiness, from measuring and characterizing bursty activity to modeling its origins and assessing its effects on dynamical processes. Then, in chapter “Temporal Scale of Dynamic Networks”, Caceres and Berger-Wolf address the important problem of the underlying temporal scales in interaction streams that define temporal networks, focusing on identifying inherent temporal scales and finding network representations that match those scales. These overviews are followed by two chapters that focus on specific temporal network features and measures: Zhao, Karsai and Bianconi discuss the entropy of temporal networks in chapter “Models, Entropy and Information of Temporal Social Networks”, combining modeling efforts with studies of large, time-stamped empirical data sets. In chapter “Temporal Motifs”, Kovanen, Karsai, Kaski, Kertész and Saramäki present the temporal motifs approach that is designed to detect, categorize and quantify recurrent temporal mesoscopic patterns of link activations.

In the second part of the book, temporal network metrics and measures are put to use in empirical studies. In chapter “Applications of Temporal Graph Metrics to Real-World Networks”, Tang, Leontiadis, Scellato, Nicosia, Mascolo, Musolesi, and Latora apply the metrics discussed in chapter “Graph Metrics for Temporal Networks” to the analysis of a number of empirical and simulated data sets. Then, in chapter “Spreading Dynamics Following Bursty Activity Patterns”, Vazquez returns to the topic of burstiness, and analyzes how bursty dynamics impacts spreading processes in computer and social systems. The effects of burstiness on spreading processes are further studied in chapter “Time Allocation in Social Networks: Correlation Between Social Structure and Human Communication Dynamics” by Miritello, Lara, and Moro in the context of networks of human interactions, and connected to the social, topological structure around individuals. This is followed by an account of temporal networks of face-to-face human interactions by Cattuto and Barrat in chapter “Temporal Networks of Face-to-Face Human Interactions”; spreading dynamics are also used here to probe the temporal structure of proximity patterns. Finally, in chapter “Social Insects: A Model System for Network Dynamics”, Charbonneau, Blonder, and Dornhaus present an inspiring overview of social insects as model systems for network dynamics, and discuss how temporal network analysis methods can provide novel ways to view the complexity of collective behavior of social insects.

The third and last part of the book discusses models of temporal networks and processes taking place on such networks. In chapter “Self-exciting Point Process Modeling of Conversation Event Sequences”, Masuda, Takaguchi, Sato, and Yano consider the origins of the long-tailed inter-event interval distributions in human dynamics, and model them with the Hawkes process, a self-exciting point process that is fitted to data on face-to-face interactions in company offices. Mantzaris and Higham then address the micro-scale dynamics of triadic closure in social networks with the help of a model and time-stamped electronic records in chapter “Inferring and Calibrating Triadic Closure in a Dynamic Network”. The same authors then move on to dynamic communicability measures, and show that they can be used to predict macro scale features of simulated epidemics on temporal networks in chapter “Dynamic Communicability Predicts Infectiousness”. The last three chapters focus on the behavior of other archetypal dynamic processes than spreading, when the dynamics unfolds through the interactions sequences of temporal networks. In chapter “Random Walks on Stochastic Temporal Networks”, Hoffmann, Porter and Lambiotte develop a mathematical framework for random walks on temporal networks using an approach that provides a compromise between abstract but unrealistic models and data-driven but non-mathematical approaches. Karimi and Holme then develop and study a version of Watts’s cascade model for the spreading of opinions and innovations in the temporal network setting in chapter “A Temporal Network Version of Watts’s Cascade Model”, and finally, Fernández-Gracia, Eguíluz, and San Miguel present version of the Voter model of opinion dynamics that is able to account for heterogeneous temporal activity patterns in chapter “Timing Interactions in Social Simulations: The Voter Model”.

Acknowledgements The authors acknowledge financial support by the Swedish Research Council (PH), the WCU program through NRF Korea funded by MEST R31-2008-10029 (PH), and EU’s 7th Framework Program’s FET-Open to ICTeCollective project no. 238597 (JS) and the Academy of Finland project “Temporal networks of human interactions”, no. 260427 (JS).

References

1. Holme, P., Saramäki, J.: Temporal networks. *Phys. Rep.* **519**, 97–125 (2012)
2. Rosvall, M., Bergstrom, C.T.: Mapping change in large networks. *PLoS ONE* **5**, e8694 (2010)
3. Holme, P.: Network reachability of real-world contact sequences. *Phys. Rev. E* **71**, 046119 (2005)
4. Kossinets, G., Kleinberg, J., Watts, D.J.: The structure of information pathways in a social communication network. In: *Proceedings of 14th ACM SIGKDD International Conference on Knowledge Discovery and Data Mining*, pp. 435–443. Association for Computing Machinery, New York (2008)
5. Tang, J., Scellato, S., Musolesi, M., Mascolo, C., Latora, V.: Small-world behavior in time-varying graphs. *Phys. Rev. E* **81**, 055101 (2010)
6. Pan, R.K., Saramäki, J.: Path lengths, correlations, and centrality in temporal networks. *Phys. Rev. E* **84**, 016105 (2011)
7. Maslov, S., Sneppen, K.: Specificity and stability in topology of protein networks. *Science* **296**, 910–913 (2002)

8. Newman, M.E.J.: *Networks: An Introduction*. Oxford University Press, Oxford (2010)
9. Tang, J., Musolesi, M., Mascolo, C., Latora, V., Nicosia, V.: Analysing information flows and key mediators through temporal centrality metrics. In: *Proceedings of the 3rd ACM EuroSys Workshop on Social Networks Systems (SNS'10)*, p. 3. Association for Computing Machinery, New York (2010)
10. Takaguchi, T., Sato, N., Yano, K., Masuda, N.: Importance of individual events in temporal networks. *New J. Phys.* **14**, 093003 (2012)
11. Mantzaris, A.V., Bassett, D.S., Wymbs, N.F., Estrada, E., Porter, M.A., Mucha, P.J., Grafton, S.T., Higham, D.J.: Dynamic network centrality summarizes learning in the human brain (2012). E-print [arXiv:1207.5047]
12. Alon, U.: Network motifs: theory and experimental approaches. *Nat. Rev. Genet.* **8**, 450–461 (2007)
13. Kovanen, L., Karsai, M., Kaski, K., Kertész, J., Saramäki, J.: Temporal motifs in time-dependent networks. *J. Stat. Mech.* P11005 (2011)
14. Jurgens, D., Lu, T.C.: Temporal motifs reveal the dynamics of editor interactions in Wikipedia. In: *Proceedings of the Sixth International AAAI Conference on Weblogs and Social Media*, pp. 162–169 (2012)
15. Fortunato, S.: Community detection in graphs. *Phys. Rep.* **486**, 75–174 (2010)
16. Braha, D., Bar-Yam, Y.: From centrality to temporary fame: dynamic centrality in complex networks. *Complexity* **12**, 1–15 (2006)
17. Braha, D., Bar-Yam, Y.: Time-dependent complex networks: dynamic centrality, dynamic motifs, and cycles of social interaction. In: Gross, T., Sayama, H. (eds.) *Adaptive Networks: Theory, Models and Applications*, pp. 39–50. Springer, Berlin (2008)
18. Holme, P.: Network dynamics of ongoing social relationships. *Europhys. Lett.* **64**, 427–433 (2003)
19. Lin, Y.R., Chi, Y., Zhu, S., Sundaram, H., Tseng, B.L.: Facetnet: a framework for analyzing communities and their evolutions in dynamic networks. In: *Proceedings of the 17th International Conference on World Wide Web*, pp. 685–694. Association for Computing Machinery, New York (2008)
20. Krings, G., Karsai, M., Bernharsson, S., Blondel, V.D., Saramäki, J.: Effects of time window size and placement on the structure of aggregated networks. *EJP Data Sci.* **1**, 4 (2012)
21. Perra, N., Gonçalves, B., Pastor-Satorras, R., Vespignani, A.: Activity driven modeling of time varying networks. *Sci. Rep.* **2**, 469 (2012)
22. Rocha, L.E.C., Decuyper, A., Blondel, V.D.: Epidemics on a stochastic model of temporal network (2012). E-print [arXiv:1204.5421]
23. Karsai, M., Kivelä, M., Pan, R.K., Kaski, K., Kertész, J., Barabási, A.L., Saramäki, J.: Small but slow world: how network topology and burstiness slow down spreading. *Phys. Rev. E* **83**, 025102 (2011)
24. Rocha, L.E.C., Liljeros, F., Holme, P.: Simulated epidemics in an empirical spatiotemporal network of 50,185 sexual contacts. *PLoS Comp. Biol.* **7**, e1001109 (2011)
25. Centola, D.: The spread of behavior in an online social network experiment. *Science* **329**(5996), 1194–1197 (2010)
26. Karimi, F., Holme, P.: Threshold model of cascades in temporal networks (2012). E-print [arXiv:1207.1206]
27. Watts, D.J.: A simple model of global cascades on random networks. *Proc. Natl. Acad. Sci. U.S.A.* **99**, 5766–5771 (2002)
28. Takaguchi, T., Nakamura, M., Sato, N., Yano, K., Masuda, N.: Predictability of conversation patterns. *Phys. Rev. X* **1**, 011008 (2011)
29. Barthélemy, M.: Spatial networks. *Phys. Rep.* **499**, 1–101 (2011)
30. Gross, T., Sayama, H. (eds.): *Adaptive Networks: Theory, Models and Applications*, pp. 39–50. Springer, Berlin (2008)
31. Sarkar, P., Chakrabarti, D., Jordan, M.I.: Nonparametric link prediction in dynamic networks. In: *Proceedings of the 29th International Conference on Machine Learning* (2012)
32. Motegi, S., Masuda, N.: A network-based dynamical ranking system. *Sci. Rep.* **2**, 904 (2012)

Graph Metrics for Temporal Networks

Vincenzo Nicosia, John Tang, Cecilia Mascolo, Mirco Musolesi,
Giovanni Russo, and Vito Latora

Abstract Temporal networks, i.e., networks in which the interactions among a set of elementary units change over time, can be modelled in terms of time-varying graphs, which are time-ordered sequences of graphs over a set of nodes. In such graphs, the concepts of node adjacency and reachability crucially depend on the exact temporal ordering of the links. Consequently, all the concepts and metrics proposed and used for the characterisation of static complex networks have to be redefined or appropriately extended to time-varying graphs, in order to take into account the effects of time ordering on causality. In this chapter we

V. Nicosia (✉)

Computer Laboratory, University of Cambridge, 15 JJ Thomson Avenue,
Cambridge CB3 0FD, UK

e-mail: V.Nicosia@qmul.ac.uk

Laboratorio sui Sistemi Complessi, Scuola Superiore di Catania, Via Valdisavoia 9,
95123 Catania, Italy

J. Tang · C. Mascolo

Computer Laboratory, University of Cambridge, 15 JJ Thomson Avenue,
Cambridge CB3 0FD, UK

M. Musolesi (✉)

School of Computer Science, University of Birmingham, Edgbaston, Birmingham B15 2TT, UK

e-mail: m.musolesi@cs.bham.ac.uk

G. Russo

Dipartimento di Matematica e Informatica, Università di Catania, Via S. Sofia 64,
95123 Catania, Italy

V. Latora

Laboratorio sui Sistemi Complessi, Scuola Superiore di Catania, Via Valdisavoia 9,
95123 Catania, Italy

School of Mathematical Sciences, Queen Mary, University of London, E1 4NS London, UK

Dipartimento di Fisica e Astronomia and INFN, Università di Catania, Via S. Sofia 64,
95123 Catania, Italy

discuss how to represent temporal networks and we review the definitions of walks, paths, connectedness and connected components valid for graphs in which the links fluctuate over time. We then focus on temporal node–node distance, and we discuss how to characterise link persistence and the temporal small-world behaviour in this class of networks. Finally, we discuss the extension of classic centrality measures, including closeness, betweenness and spectral centrality, to the case of time-varying graphs, and we review the work on temporal motifs analysis and the definition of modularity for temporal graphs.

1 Introduction

Whenever a system consists of many single units interacting through a certain kind of relationship, it becomes natural to represent it as a *graph*, where each *node* of the graph stands for one of the elementary units of the system and interactions between different units are symbolised by *edges*. If two nodes are connected by an edge they are said to be *adjacent*. According to the nature of the units and to the characteristics of adjacency relationship connecting them, it is possible to construct different kind of graphs, such as friendship graphs—where nodes are people and edges connect two people who are friends, functional brain networks—where nodes are regions of the brain and edges represent the correlation or causality of their activity, communication graphs—where nodes are terminals of a communication systems, such as mobile phones or email boxes, and edges indicate the exchange of a message from a terminal to another, just to make some examples. Thanks to the availability of large data sets collected through modern digital technologies, in the last decade or so there has been an increasing interest towards the study of the structural properties of graph representations of real systems, mainly spurred by the observation that graphs constructed from different social, biological and technological systems show surprising structural similarities and are characterised by non-trivial properties. In a word, they are *complex* networks. Independently of the peculiar nature and function of the original systems, the corresponding graphs are usually *small-worlds*, i.e., they show high local cohesion and, at the same time, extremely small node–node distance [47]; the distribution of the number of neighbours of a node (its *degree*) is often heterogeneous, and decays as a power-law (i.e., they are *scale-free* [2]); they are locally organised as tightly-knit groups of nodes (called *communities*), which are in turn loosely interconnected to each other [33]. The concepts, metrics, methods, algorithms and models proposed so far to study the structure of real networks has led to the formation of theoretical framework known as *complex network theory* [1, 5, 31].

However, the relationships among the units of a real networked system (e.g., node adjacency) are rarely persistent over time. In many cases, the static interpretation of node adjacency is just an oversimplifying approximation: contacts among individuals in a social network last only for a finite interval and are often intermittent and recurrent [8, 13, 18]; different intellectual tasks are usually associated to different brain activity patterns [9, 45]; communication between agents in a

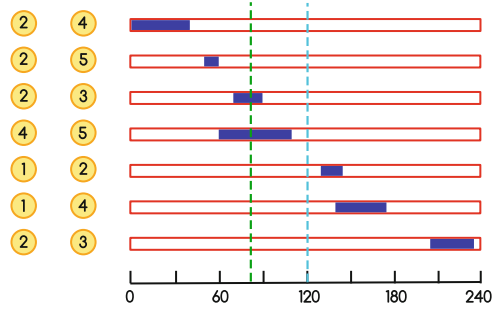
telecommunication system are typically bursty and fluctuate over time [4, 26, 40]; transportation networks show fluctuations in their microscopic organisation, despite the stability of their global structural properties [11]. Consequently, whenever we deal with a networked system that evolves over time, the concept of adjacency needs to be appropriately redefined. The extension of node adjacency to the case of time-evolving systems has lately led to the definition of *temporal graphs* (sometimes also called *time-varying graphs* or *dynamic graphs*), in which *time* is considered as another dimension of the system and is included in the same definition of the graph. Since most of the metrics to characterise the structure of a graph, including graph connectedness and components, distance between nodes, the different definitions of centrality etc., are ultimately based on node adjacency, they need to be appropriately redefined or extended in order to take into account of the presence, frequency and duration of edges at different times. In general, the temporal dimension adds richness and complexity to the graph representation of a system, and demands for more powerful and advanced tools which allow to exploit the information on temporal correlations and causality. Recently, Holme and Saramäki have published a comprehensive review which presents the available metrics for the characterisation of temporal networks [14]. A description of some potential applications of these metrics can be found in [44].

This chapter presents the basic concepts for the analysis of time-evolving networked systems, and introduces all the fundamental metrics for the characterisation of time-varying graphs. In Sect. 2 we briefly discuss different approaches to encode some temporal information into static graphs and we introduce a formal definition of time-varying graph. In Sect. 3 we examine how reachability and connectedness are affected by time-evolving adjacency relationships and we introduce the definitions of node and graph temporal components, showing the intimate connections between the problem of finding temporal connected components and the maximal-clique problem in static graphs. In Sect. 4 we focus on the concepts of temporal distance, efficiency and temporal clustering, and we discuss the temporal small-world phenomenon. In Sect. 5 we present the extensions of betweenness, closeness and spectral centrality to time-varying graphs. Finally, in Sect. 6 we report on the definition of temporal motifs and on the extension of the modularity function to time-varying graphs.

2 Representing Temporal Networks

From a mathematical point of view a networked time-evolving system consists of a set \mathcal{C} of *contacts* registered among a set of nodes $\mathcal{N} = \{1, 2, \dots, N\}$ during an *observation interval* $[0, T]$ [37, 43]. A *contact* between two nodes $i, j \in \mathcal{N}$ is represented by a quadruplet $c = (i, j, t, \delta t)$, where $0 \leq t \leq T$ is the time at which the contact started and δt is its duration, expressed in appropriate temporal units. As we stated above the relationship between i and j is usually not persistent (it could represent the co-location at a place, the transmission of a message, the temporal correlation between two areas of the brain etc.), so that in general we will observe

Fig. 1 The set of contacts registered among five nodes within an observation period of 4 h. *Blue bars* indicate the duration of each contact. The two *dashed lines* correspond to two instantaneous cuts of the contact set, respectively for $t = 80$ min (*green*) and $t = 120$ min (*cyan*)



more than one contact between i and j in the interval $[0, T]$. In Fig. 1 we report an example of a set of seven contacts observed between a set of $N = 5$ nodes within an interval of $T = 240$ min. The contacts in the figure are considered *symmetric*, i.e., $(i, j, t, \delta t) = (j, i, t, \delta t)$, even if in general this is not the case. Each contact is represented by a pair of nodes and a blue bar indicating the start and duration of the contact. Notice that in this example, which is indeed representative of many social and communication systems, the typical overlap between contacts is relatively small with respect to the length of the observation interval.

Before explaining how the temporal information about such a set of contacts can be represented by means of a time-varying graph, we first review some simple approaches to deal with time-evolving systems based on static graphs, and we discuss why they are inadequate for analyzing time-evolving systems.

2.1 Aggregated Static Graphs

The classic approach to represent networked systems evolving over time consists in constructing a single *aggregated static graph*, in which all the contacts between each pair of nodes are flattened in a single edge. An aggregated graph can be represented by an *adjacency matrix* $A = \{a_{ij}\} \in \mathbb{R}^{N \times N}$, in which the entry $a_{ij} = 1$ if at least one contact (i, j, \cdot, \cdot) has been registered in $[0, T]$ between i and j , and $a_{ij} = 0$ otherwise. If the relationship between any pair of nodes i and j is symmetric, such as in the case of co-location or collaboration graphs, also the corresponding adjacency matrix is symmetric, i.e., $a_{ij} = a_{ji} \quad \forall i, j \in \mathcal{N}$. Conversely, whenever a directionality is implied, for instance when the contact is a phone call from i to j or represents goods transferred from i to j , the adjacency matrix is in general non-symmetric.

Representing a time-evolving system by means of an adjacency matrix, i.e., an unweighted graph, is usually a severe oversimplification: the information about the number, frequency and duration of contacts between two nodes i and j is flattened down into a binary digit (i.e., $a_{ij} = 1$ if there is at least one contact, of any duration, between i and j , while $a_{ij} = 0$ otherwise). In general, a binary adjacency information does not take into account the heterogeneity observed in real

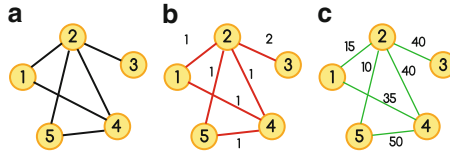


Fig. 2 Three different aggregated static graphs obtained from the set of contacts in Fig. 1. **(a)** The unweighted aggregated graph; **(b)** the weighted aggregated graph where each weight w_{ij} between node i and node j corresponds to the number of contacts observed; **(c)** the weighted aggregated graph where each weight w_{ij} is the total duration of all the contacts between i and j

systems. Just to make an example, both the number of phone calls made by a single node during a certain time interval and the duration of a call between two nodes exhibit large fluctuations, and their distribution is well approximated by a power-law [4, 16, 26]. This means that assigning the same weight to all the relationships can lead to misleading conclusions. This problem can be partially solved by constructing a *weighted aggregated graph*, in which the edge connecting i to j is assigned a weight w_{ij} proportional to the number of contacts observed, their duration, their frequency or a combination of these three dimensions.

In Fig. 2 we show three different aggregated static graphs corresponding to the same set of contacts reported in Fig. 1. The leftmost graph (Panel a) is the unweighted aggregated graph; in the middle graph (Panel b) the weights correspond to the number of contacts observed between the nodes; in the rightmost one (Panel c) the weight of each edge w_{ij} is equal to the sum of the duration of all the contacts between i and j . However, both unweighted and weighted aggregated graphs fail to capture the temporal characteristics of the original system. In fact, by considering all the links as always available and persistent over time, the number of walks and paths between two nodes is overestimated, while the effective distance between two nodes is instead systematically underestimated. For instance, in all the three aggregated representations, node 2 and node 4 are connected by an edge, but their interaction is limited just to the beginning of the observation period, so that these nodes cannot directly communicate for most of the time.

Despite not being powerful enough to represent networks in which the temporal aspects are crucial, static aggregated graphs and the metrics proposed for their analysis still constitute an invaluable framework to investigate the structure and function of systems in which the topological characteristics are more relevant than the temporal ones. After all, most of the classic examples of complex networks, including the graph of the Internet at Autonomous Systems level [46], co-authorship networks [29, 30], the graph of the World Wide Web [2, 6] and functional brain networks [7] have been obtained so far by aggregating all the contacts observed among a certain number of nodes within a given temporal interval, and the analysis of their structure has provided new insights about the organisation of different complex systems.

2.2 Time-Varying Graphs

The natural way to work out a graph representation that can properly take into account all the temporal correlations of a set of contacts consists into including time as an additional dimension of the graph [17]. We notice that a set of contacts implicitly defines a graph for each instant t , made by the set of edges corresponding to all the contacts $(\cdot, \cdot, t_i, \delta t_i)$ such that $t_i \leq t \leq t_i + \delta t_i$. In the example shown in Fig. 1, if we consider $t = 80$ min, corresponding to the dashed green line in the figure, the graph constructed from contacts active at that time contains only two edges, namely (2, 3) and (4, 5). However, we notice that the graph corresponding to $t = 120$ min (the dashed cyan line in the figure) is an empty graph, since no contact is active at that time. For practical reasons, and especially when contacts are instantaneous, i.e., $\delta t \rightarrow 0$, it is convenient to consider a finite *time-window* $[t, t + \Delta t]$ and to construct a graph by creating an edge between all pairs of nodes for which there is at least a contact which overlaps with the interval $[t, t + \Delta t]$. A generic contact $(\cdot, \cdot, \tau_i, \delta \tau_i)$ overlaps with $[t, t + \Delta t]$ if it satisfies at least one of the three following conditions:

$$t \leq \tau_i < t + \Delta t \quad (1)$$

$$t \leq \tau_i + \delta \tau_i < t + \Delta t \quad (2)$$

$$\tau_i < t \quad \wedge \quad \tau_i + \delta \tau_i > t + \Delta t \quad (3)$$

A graph G_t obtained by aggregating all the contacts appearing in a given interval $[t, t + \Delta t]$ represents the state of the system in that interval, i.e., it is a *snapshot* which captures the configuration of the links at that particular time interval. If we consider a sequence of successive non-overlapping time-windows $\{[t_1, t_1 + \Delta t_1], [t_2, t_2 + \Delta t_2], [t_3, t_3 + \Delta t_3], \dots, [t_M, t_M + \Delta t_M]\}$ then we obtain a *time-varying graph*, which is the simplest graph representation of a set of contacts that takes into account their duration and their temporal ordering [19,43]. A time-varying graph is an ordered sequence of M graphs $\{G_1, G_2, \dots, G_M\}$ defined over N nodes, where each graph G_m in the sequence represents the state of the network, i.e., the configuration of links, in the time-window $[t_m, t_m + \Delta t_m]$, $m = 1, \dots, M$. In this notation, the quantity $t_M + \Delta t_M - t_1$ is the temporal length of the observation period. In general the graphs in the sequence can correspond to any ordered sequence of times such that $t_1 < t_1 + \Delta t_1 = t_2 < t_2 + \Delta t_2 = t_3 < \dots < t_M + \Delta t_M$ [12]. In the following we assume, without loss of generality, that $t_1 = 0$ and $t_M = T$ and, at the same time, that the sequence of snapshots is uniformly distributed over time, i.e., $t_{m+1} = t_m + \Delta t$, $\forall m = 1, \dots, M - 1$ [43]. In compact notation, we denote the graph sequence forming a time-varying graph as $\mathcal{G} \equiv \mathcal{G}_{[0, T]}$. Each graph in the sequence can be either undirected or directed, according to the kind of relationship represented by contacts. Consequently, the time-varying graph \mathcal{G} is fully described by means of a time-dependent adjacency matrix $A(t_m)$, $m = 1, \dots, M$, where

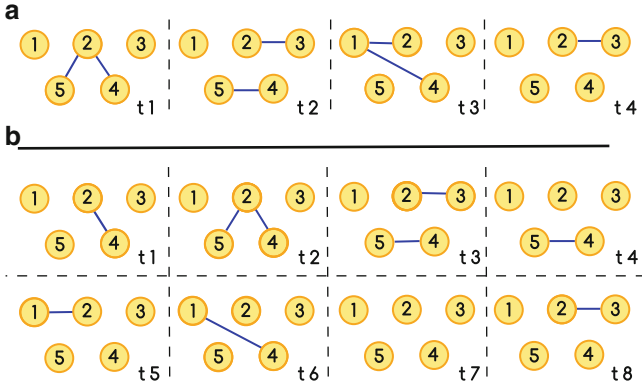


Fig. 3 Two time-varying graphs corresponding to the set of contacts in Fig. 1. Panel (a) the four snapshots obtained setting $\Delta t = 60$ min; Panel (b) the eight snapshots of the time-varying graph constructed using $\Delta t = 30$ min. The smaller the size of the time-window, the higher the probability that a snapshot contains no edges (this happens for the snapshot $t7$ in panel (b))

$a_{ij}(t_m)$ are the entries of the adjacency matrix of the graph at time t_m , which is in general a non-symmetric matrix.

Notice that, by tuning the size of the time-window used to construct each snapshot, it is possible to obtain different representations of the system at different temporal scales. In Fig. 3 we present two time-varying graphs obtained from the same set of contacts in Fig. 1 but using two different lengths for the time-window. The graph on the top panel is constructed by setting $\Delta t = 60$ min, and consists of four snapshots, while the graph on the bottom panel corresponds to a time-window of $\Delta t = 30$ min and has eight snapshots. It is usually preferable to set the size of the time-window to the maximum temporal resolution available. For instance, if the duration of contacts is measured with an accuracy of 1 s (such as in the case of email communications or phone calls), it makes sense to construct time-varying graphs using a time-window $\Delta t = 1$ s.

In the limit case when $\Delta t \rightarrow 0$, we obtain an infinite sequence of graphs, where each graph corresponds to the configuration of contacts at a given instant t . This sequence of graphs might include a certain number of empty graphs, corresponding to periods in which no contacts are registered. On the contrary, if we set $\Delta t = T$, the time-varying graph degenerates into the corresponding unweighted aggregated graph, where all the temporal information is lost.

3 Reachability, Connectedness and Components

In a static graph the *first neighbours* of a node i are the nodes to which i is connected by an edge, i.e., nodes j such that $a_{ij} = 1$. We say that the neighbours of i are *directly reachable* from i . If k is a neighbour of j and j is in turn a neighbour

of i , then the node k is indirectly reachable from i , i.e., by following first the edge connecting i to j and then the one which connects j to k . In general, the direct and indirect reachability of nodes is important to characterise the global structure of a network and to investigate the dynamics of processes occurring over it. For instance, if node i has got a contagious disease, then there is a high probability that the disease will sooner or later be transmitted to the nodes that are directly reachable from i (its first neighbours). However, if a disease starts from a node i , also the nodes which are not directly connected to i but are still indirectly reachable from i have a finite probability to get the disease through a chain of transmissions.

The reachability between nodes is related to the concept of *walk*. In a static graph a walk is defined as an ordered sequence of ℓ edges $\{a_{i_0,i_1}, a_{i_1,i_2}, \dots, a_{i_{\ell-1},i_\ell}\}$ such that $a_{i_k,i_{k+1}} = 1, k = 0, 1, \dots, \ell - 1$. The *length* of a walk is equal to the number of edges traversed by the walk. We say that the node j is *reachable* from i if there exists a walk which starts at i and ends up at j . If each vertex in a walk is traversed exactly once, then the walk is called a *simple walk* or a *path*. For instance, in the graph shown in Fig. 2 the sequence of nodes [2, 4, 5, 2, 1, 4] is a walk of length 5 which starts at node 2 and ends at node 4, while the sequence [3, 2, 5] is a path of length 2 going from node 3 to node 5 passing by node 2. In a static graph the length of the shortest path connecting two nodes is called *geodesic distance*.

Since the definitions of walk and path depend on the adjacency of nodes, and given that node adjacency is a function of time in time-varying graphs, an appropriate extension of these concepts is necessary in order to define node reachability and components in time-varying graphs.

3.1 Time-Respecting Walks and Paths

In a time-varying graph, a *temporal walk* from node i to node j is defined as a sequence of L edges $[(n_{r_0}, n_{r_1}), (n_{r_1}, n_{r_2}), \dots, (n_{r_{L-1}}, n_{r_L})]$, with $n_{r_0} \equiv i, n_{r_L} \equiv j$, and an increasing sequence of times $t_{r_1} < t_{r_2} < \dots < t_{r_L}$ such that $a_{n_{r_{l-1}}, n_{r_l}}(t_{r_l}) \neq 0, l = 1, \dots, L$ [12, 43]. A *path* (also called *temporal path*) of a time-varying graph is a walk for which each node is visited at most once. For instance, in the time-varying graph of Fig. 3a, the sequence of edges [(5, 2), (2, 1)] together with the sequence of times t_1, t_3 is a temporal path of the graph. This path starts at node 5 at time t_1 and arrives at node 1 at time t_3 . Notice that the aggregated static graph flattens down most of the information about temporal reachability. In fact, if we look at the static aggregated graph corresponding to this time-varying graph (shown in Fig. 2a), there are different paths going from node 1 to node 5 and vice versa; however, if we look at the time-varying graphs of Fig. 3 we notice that in both of them there is no temporal path connecting node 1 to node 5. The reason is that node 5 could be reached from node 1 only by passing through either node 2 or node 4, but node 1 actually is connected to both these nodes *after* they have been in contact to node 5.

3.2 Temporal Connectedness and Node Components

The concept of connectedness is fundamental in complex network theory. A message, a piece of information or a disease can be transferred from one node to all the other nodes to which it is connected, but will never be conveyed to nodes that are disconnected from it. For this reason, the study of node connectedness and node components is the very basic tool to investigate the structure of a graph.

In a static undirected graph two nodes are said to be connected if there exists a path between them. In this particular case connectedness is an equivalence relation: it is *reflexive* (i.e., i is connected to itself), *symmetric* (i.e., if i is connected to j then j is connected to i) and *transitive* (i.e., if i is connected to j and j is connected to k , then i is also connected to k). Instead, in a directed graph, due to the directionality of the edges, symmetry is broken and the existence of a path from i to j does not guarantee that a path from j to i does indeed exist. For this reason, the notions of strong and weak connectedness are introduced. In a word, two nodes i and j of a static directed graph are said to be *strongly connected* if there exist a path from i to j and a path from j to i , while they are *weakly connected* if there exists a path connecting them in the underlying undirected graph, i.e., in the static graph obtained from the original by discarding edge directions.

Starting from the definitions of temporal walk and path, it is possible to define temporal connectedness (in a weak and in a strong sense) for pairs of nodes in a time-varying graph. A node i of a time-varying graph $\mathcal{G}_{[0,T]}$ is *temporally connected* to a node j if there exists a temporal path going from i to j in $[0, T]$. Due to the temporal ordering of edges, this relation is trivially not symmetric, so that if i is temporally connected to j , in general j can be either temporally connected or disconnected to i . Two nodes i and j of a time-varying graph are *strongly connected* if i is temporally connected to j and also j is temporally connected to i .

Temporal strong connectedness is a reflexive and symmetric relation, so that if i is strongly connected to j , then j is strongly connected to i . However, strong connectedness still lacks transitivity, and, therefore, it is not an equivalence relation. In fact, if i and j are strongly connected and j and l are strongly connected, nothing can be said, in general, about the connectedness of i and l . For instance, in the time-varying graph shown in Fig. 3a, nodes 5 and 2 are strongly connected and also 2 and 1 are strongly connected, but nodes 5 and 1 are not strongly connected because, as we have already explained above, there exists no temporal path that connects node 1 to node 5.

Similarly to the case of static directed graphs, it is possible to define weak connectedness among nodes. Given a time-varying graph \mathcal{G} , we consider the underlying undirected time-varying graph \mathcal{G}^u , which is obtained from \mathcal{G} by discarding the directionality of the links of all the graphs $\{G_m\}$, while retaining their time ordering. Two nodes i and j of a time-varying graph are *weakly connected* if i is temporally connected to j and also j is temporally connected to i in the underlying undirected time-varying graph \mathcal{G}^u . Also weak connectedness is a reflexive and symmetric relation, but not transitive.

It is worth noting that strong and weak connectedness propagate over different time scales. In fact, if we consider two time-varying graphs obtained from the same set of contacts by using two different time-windows, such as for instance Δt_1 for the graph \mathcal{G}_1 and $\Delta t_2 > \Delta t_1$ for \mathcal{G}_2 (as in the two time-varying graphs of Fig. 3), then it is easy to prove that if i and j are strongly connected in \mathcal{G}_1 then they are also strongly connected in \mathcal{G}_2 . The contrary is trivially not true. Thanks to this property, strong and weak connectedness in time-varying graphs are consistent with the corresponding definitions given for static graphs. In fact, as a limiting case, if two nodes are strongly (weakly) connected in a time-varying graph, then they are also strongly (weakly) connected in the corresponding aggregated static graph, which is the degenerate time-varying graph obtained by setting $\Delta t = T$.

By using reachability, strong and weak connectedness, different definitions of node components can be derived. For instance, the *temporal out-component of node i* (resp. *in-component*), denoted as $\text{OUT}_T(i)$ (resp. $\text{IN}_T(i)$), is the set of vertices which can be reached from i (resp. from which i can be reached) in the time-varying graph \mathcal{G} . Similarly the *temporal strongly connected component of a node i* (resp. *weakly connected component*), denoted as $\text{SCC}_T(i)$ (resp. $\text{WCC}_T(i)$), is the set of vertices from which vertex i can be reached, and which can be reached from i , in the time-varying graph \mathcal{G} (resp. in the underlying undirected time-varying graph \mathcal{G}^u).

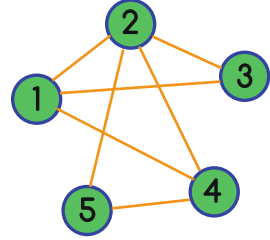
In general, temporal node components have quite heterogeneous composition and sizes, and reveal interesting details about the structure of the graph. For instance, the out-component of node 3 in the two graphs of Fig. 3 contains only nodes 1, 2, 4 and node 3 itself, since there is no way for node 3 to reach node 5. Conversely, in the corresponding aggregated graphs (as shown in Fig. 2) the out-components of all the nodes are identical and contain all the nodes of the graph.

The importance of temporal node components has been pointed out in [36], which reports the results of temporal component analysis on time-varying graphs obtained from three different data sets. The authors compared the size of node temporal in- and out-components in these time-varying graphs with the size of the giant component of the corresponding aggregated graphs, and they found that in general temporal node components are much smaller than the giant component of the aggregated graph, and exhibit a high variability in time. This is another example of the fact that time-varying graphs are able to provide additional information that is not captured by aggregated graphs.

3.3 Graph Components and Affine Graphs

Differently from the case of directed static graphs, it is not possible to define the strongly (weakly) connected components of a time-varying graph starting from the definition of connectedness for pairs of nodes. Formally, this is due to the fact that strong and weak connectedness are not equivalence relations. For this reason, the following definition of strongly connected component of a time-varying graph has

Fig. 4 Affine graph associated to the time-varying graph of Fig. 3a. Pairs of strongly connected nodes are linked by an edge, and the cliques of the affine graph correspond to the strongly connected components of the associated time-varying graph



been proposed [36]: a set of nodes of a time-varying graph \mathcal{G} is a temporal strongly connected component of \mathcal{G} if each node of the set is strongly connected to all the other nodes in the set. A similar definition exists for weakly connected components. These definitions enforce transitivity but have the drawback that in order to find the strongly connected components of a time-varying graph, it is necessary to check the connectedness between all pairs of nodes in the graph. In [36] it has been shown that the problem of finding the strongly connected components of a time-varying graph is equivalent to the well-known problem of finding the maximal-cliques of an opportunistically constructed static graph. We define such graph as the *affine graph* corresponding to the time-varying graph. The affine graph $G_{\mathcal{G}}$ is defined as the graph having the same nodes as the time-varying graph \mathcal{G} , and such that two nodes i and j are linked in $G_{\mathcal{G}}$ if i and j are strongly connected in \mathcal{G} . In Fig. 4 we report the affine graph corresponding to the time varying graph shown in Fig. 3a. In this graph, node 1 is directly connected to nodes $\{2, 3, 4\}$, since it is temporally strongly connected to them in the time-varying graph. Similarly, node 2 is connected to nodes $\{1, 3, 4, 5\}$, node 3 is connected to $\{1, 2\}$, node 4 is connected to $\{1, 2, 5\}$ and node 5 is connected to $\{2, 4\}$. Hence, the affine graph $G_{\mathcal{G}}$ has only 7 of the 10 possible links, each link representing strong connectedness between two nodes. By construction, a clique of the affine graph $G_{\mathcal{G}}$ contains only nodes which are strongly connected to each other, so that the *maximal-cliques* of the affine graph, i.e., all the cliques which are not contained in any other clique, are temporal strongly connected components (SCC_T) of \mathcal{G} . Similarly, all the *maximum-cliques* of the affine graph $G_{\mathcal{G}}$, i.e., its largest maximal-cliques, are the largest temporal strongly connected components (LSCC_T) of \mathcal{G} .

We notice that the problem of finding a partition of \mathcal{G} that contains the minimum number of disjoint strongly connected components is equivalent to the well-known problem of finding a partition of the corresponding affine graph $G_{\mathcal{G}}$ in the smallest number of disjoint maximal-cliques [15]. Unfortunately, this problem is known to be NP-complete, and in practice can be exactly solved only for small graphs. In the case of the affine graph reported in Fig. 4, it is possible to check by hand that there are only three possible partitions of $G_{\mathcal{G}}$ into maximal-cliques, namely

1. $\{1, 2, 3\} \cup \{4, 5\}$
2. $\{1, 2, 4\} \cup \{3\} \cup \{5\}$
3. $\{2, 4, 5\} \cup \{1, 3\}$

The second partition contains two isolated nodes, which are indeed degenerated maximal-cliques. Therefore, the original time-varying graph admits only two different partitions into a minimal number of non-degenerated strongly connected components, namely into two components containing at least two nodes each. This is a quite different picture from that we obtain using static aggregated graphs. In fact, all the static aggregated representations of the same time-varying graph (see Fig. 2) are composed by just one strongly connected component which includes all the nodes.

We notice that in general the largest temporal strongly connected components of a time-varying graph can be much smaller than the giant connected component of the corresponding aggregated graph. For instance, in [36] the authors performed temporal component analysis on time-varying graphs constructed from three different time-stamped data sets (i.e. the MIT Reality Mining project, co-location at INFOCOM 2006 and Facebook communication), and they found that despite the giant connected component of the corresponding aggregated graphs usually included almost all the nodes in the network, the maximal cliques of the affine graphs were indeed much smaller. Particularly interesting was the case of the Facebook communication data set: the giant connected components of the aggregated graphs contained from 10^4 to 10^5 nodes, while the largest temporal strongly connected components counted around 100 nodes at most. Disregarding such discrepancies could result in misleading conclusions. For example, the potential number of individuals infected by a disease which spreads through the system is in the order of tens if we correctly take into account temporal correlations, but could be erroneously estimated to be thousand times larger if one considers the aggregated graph.

4 Distance, Efficiency and Temporal Clustering

One of the most relevant properties of static complex networks is that they exhibit, on average, a surprising small geodesic distance between any pairs of nodes, where the geodesic distance between i and j is defined as the length of the shortest path connecting them. The average geodesic distance is important to characterise how fast (for example, in terms of number of hops), a message can be transmitted from a node to another in the network; therefore, it is related to the overall efficiency of communication among nodes. Having a small average geodesic distance (where the average is computed over all the pairs of connected nodes) is a desirable property when one wants to spread a message throughout the network; conversely, small geodesic distance becomes a problem if we want to control the propagation of a disease.

4.1 Temporal Distance and Efficiency

When we consider time-varying graphs, the temporal dimension is an essential element of the system, so that the concept of geodesic distance cannot be limited to the number of *hops* separating two nodes but should also take into account the temporal ordering of links. As a matter of fact, any path in a time-varying graph is characterised by two different lengths: (a) a *topological length*, measured as the number of edges traversed by the path, and a (b) *temporal length* or duration, measured as the time interval between the first and the last contact in the path.

Both the topological and the temporal lengths of a path usually depend on the time at which the path starts. Consider for instance two of the paths connecting node 5 to node 3 in Fig. 3a. The first path starts from 5 at snapshot t_1 which traverses the edge (5, 2) at (t_1) and arrives at node 3 following the edge (2, 3) at time (t_2). The second one starts from 5 at time t_2 and arrives at node 3 at time t_4 , after traversing the edges (5, 4) at t_2 , (4, 1) and (1, 2) at t_3 and finally (2, 3) at t_4 . The first path has a topological length equal to 2 and a temporal length of two snapshots (e.g., 2 h), while the second path has a topological length equal to 4 and a temporal length equal to three snapshots (e.g., 3 h).

The *temporal shortest path* from node i to node j is defined as the temporal path connecting i to j which has minimum temporal length. Similarly, the *temporal distance* $d_{i,j}$ between i and j is the temporal length of the temporal shortest path from i to j . In the example discussed above, the temporal shortest path connecting node 5 to node 3 is the one starting at t_1 and having temporal length equal to two snapshots.

The natural extension of the average geodesic distance to the case of time-varying graphs is the *characteristic temporal path length* [42, 43], which is defined as the average temporal distance over all pairs of nodes in the graph:

$$L = \frac{1}{N(N-1)} \sum_{ij} d_{ij} \quad (4)$$

It is also possible to define the *temporal diameter* of a graph as the largest temporal distance between any pair of nodes:

$$D = \max_{ij} d_{ij} \quad (5)$$

However, in real time-varying graphs it is quite common to have many pairs of temporally disconnected nodes. The problem is that if a node j is not temporally reachable from i , then $d_{ij} = \infty$, and the characteristic temporal path length diverges. In order to avoid such divergence, the *temporal global efficiency* [42, 43] of a time-varying graph has been defined as follows:

$$\mathcal{E} = \frac{1}{N(N-1)} \sum_{ij} \frac{1}{d_{ij}} \quad (6)$$

The temporal global efficiency is the straightforward generalisation of the global efficiency already defined for static graphs [22], and has been successfully employed to study and quantify the robustness of temporal graphs (see for instance [38] and [44] in this book).

4.2 Edge Persistence and Clustering

The characteristic temporal path length and the temporal efficiency provide a quantitative representation of the global structure of a graph in terms of the average temporal distance among any pair of nodes. However, in time-varying systems contacts are usually *bursty*, meaning that the distribution of the time between two contacts has a heavy tail, and *persistent*, i.e., if two nodes are connected at a time t , there is a non-negligible probability that they will still be connected at time $t + \Delta t$. This characteristic can be quantified in the following way. If we consider a node i and two adjacent snapshots of a time-varying graph, respectively starting at time t_m and $t_{m+1} = t_m + \Delta t$, we can define the *topological overlap* of the neighbourhood of i in $[t_m, t_{m+1}]$ as:

$$C_i(t_m, t_{m+1}) = \frac{\sum_j a_{ij}(t_m) a_{ij}(t_{m+1})}{\sqrt{\left[\sum_j a_{ij}(t_m)\right] \left[\sum_j a_{ij}(t_{m+1})\right]}} \quad (7)$$

and the *average topological overlap* of the neighbourhood of node i as the average of $C_i(t_m, t_{m+1})$ over all possible subsequent temporal snapshot, i.e.:

$$C_i = \frac{1}{M-1} \sum_{m=1}^{M-1} C_i(t_m, t_{m+1}) \quad (8)$$

The average topological overlap of a node i is a natural extension of the concept of local clustering coefficient which includes temporal information. In fact, while in a static graph the local clustering coefficient of a node measures the probability that its neighbours are in turn connected by an edge, the average topological overlap estimates the probability that an edge from i to one of its neighbours j persists across two consecutive time-windows. In a word, it is a measure of the *temporal clustering* of edges, i.e., of their tendency to persist across multiple windows. The average of C_i computed over all the nodes in the network, namely the quantity:

$$C = \frac{1}{N} \sum_i C_i \quad (9)$$

is called *temporal-correlation coefficient* [43], and is a measure of the overall average probability for an edge to persist across two consecutive snapshots. Notice

Table 1 Temporal-correlation, characteristic temporal path length and efficiency for brain functional networks (in four different frequency bands) [9], for the social interaction networks of INFOCOM'06 (time periods between 1 p.m. and 2:30 p.m., four different days) [39], and for messages over Facebook online social network (4 different months of year 2007) [48]

	C	C^{rand}	L	L^{rand}	E	E^{rand}
α	0.44	0.18 (0.03)	3.9	4.2	0.50	0.48
β	0.40	0.17 (0.002)	6.0	3.6	0.41	0.45
γ	0.48	0.13 (0.003)	12.2	8.7	0.39	0.37
δ	0.44	0.17 (0.003)	2.2	2.4	0.57	0.56
d1	0.80	0.44 (0.01)	8.84	6.00	0.192	0.209
d2	0.78	0.35 (0.01)	5.04	4.01	0.293	0.298
d3	0.81	0.38 (0.01)	9.06	6.76	0.134	0.141
d4	0.83	0.39 (0.01)	21.42	15.55	0.019	0.028
Mar	0.044	0.007 (0.0002)	456	451	0.000183	0.000210
Jun	0.046	0.006 (0.0002)	380	361	0.000047	0.000057
Sep	0.046	0.006 (0.0002)	414	415	0.000058	0.000074
Dec	0.049	0.006 (0.0002)	403	395	0.000047	0.000059

Results are compared with the averages measured over 1,000 time-varying graphs obtained by reshuffling the sequences of snapshots. The values in parenthesis next to C^{rand} are the respective standard deviations. The values of L and L^{rand} are computed considering only the connected pairs of nodes. Table adapted from [43]

that $C = 1$ if and only if all the snapshots of the time-varying graphs have exactly the same configuration of edges, while it is equal to zero if none of the edges is ever observed in two subsequent snapshots.

In [43] the authors considered time-varying graphs constructed from three data sets, namely functional brain networks [9], the co-location at INFOCOM 2006 [39] and personal messages exchanged among Facebook users [48]. They compared the characteristic temporal path length and the temporal correlation coefficient of these temporal graphs with those obtained from the same data sets by reshuffling the sequence of snapshots. Notice that by reshuffling the snapshots one destroys all the existing temporal correlations while retaining the average connectivity of each node and the configuration of edges in the corresponding aggregated graph. They showed that the original time-varying graphs usually exhibit both a relatively smaller characteristic temporal path length and a relatively higher temporal correlation coefficient, when compared with those measured on reshuffled sequences of snapshots. This finding is the temporal analogous to the small-world effect observed in static complex networks, and has consequently been named *small-world behaviour in time-varying graphs*. Table 1 reports the results obtained for the three different data sets.

5 Betweenness, Closeness and Spectral Centrality

The structural properties of a complex network usually reveal important information about its dynamics and function. This is particularly true if we take into account the relationship between the position occupied by a node in a static graph and the *role* played by the node for the evolution of a dynamic process. For instance, not all nodes have the same impact on the transmission of a disease (or the spreading of a rumour) over a network: intuitively, the nodes having a higher number of neighbours should contribute much more to the spreading than nodes having few connections. However, if we perform a deeper analysis, we observe that not just the number of edges is important to identify good spreaders, since also the actual organisation of these edges has an impact on the speed of the spreading process. In fact, nodes mediating a large number of shortest paths are indeed those that contribute the most to the transmission of diseases and information over a network. The identification of nodes that play a central role, i.e., nodes having high *centrality*, has been a quite active research field in complex network theory. Here we review some standard centrality measures and their extension to the case of time-varying graphs.

5.1 Betweenness and Closeness Centrality

Two basic centrality measures based on shortest paths are *betweenness* centrality and *closeness* centrality. The betweenness centrality of a node i in a static graph is defined as follows:

$$C_i^B = \sum_{j \in V} \sum_{\substack{k \in V \\ k \neq j}} \frac{\sigma_{jk}(i)}{\sigma_{jk}} \quad (10)$$

where σ_{jk} is the number of shortest paths from node j to node k , while $\sigma_{jk}(i)$ is the number of such shortest paths that pass through the node i . The higher the number of shortest paths passing through i , the higher the value of C_i^B . Betweenness centrality can be also defined for single edges, by counting the fraction of shortest paths between any pair of nodes to which a given edge participate.

A simple way to extend betweenness centrality to time-varying graphs consists in counting the fraction of temporal shortest paths that traverse a given node. The formula would be exactly the same as (10), with the only difference that σ_{jk} and $\sigma_{jk}(i)$ will be, respectively, the total number of temporal shortest paths between j and k and the number of those paths which make use of node i .

Sometimes it can be important to take into account not only the number of temporal shortest paths which pass through a node, but also the length of time for which a node along the shortest path retains a message before forwarding it to the next node [41]. For example, let us consider the simple case of nodes i and j being connected by just one shortest path which consists of the two edges $(i, k)_{t_\ell}$ and $(k, j)_{t_m}$. This means that the edge connecting i to k appears at time t_ℓ , while

the edge connecting k to j appears at time t_m . Since the path through k is the only way for i to temporally reach j , then we would say that k plays an important mediatory role and is “central” for communication between i and j . Nevertheless, the vulnerability of node k heavily depends on the interval $[t_\ell, t_m]$: the longer this temporal interval, the higher the probability that a message forwarded to k is lost if k is removed from the network. In order to take into account the effect of waiting times, the *temporal betweenness centrality* [41] of the node i at time t_m is defined as:

$$C_i^B(t_m) = \frac{1}{(N-1)(N-2)} \sum_{\substack{j \neq i \\ k \neq j \\ k \neq i}} \sum_{\substack{k \neq j \\ k \neq i}} \frac{U(i, t_m, j, k)}{\sigma_{jk}} \quad (11)$$

where σ_{jk} is the number of temporal shortest path from j to k , and $U(i, t_m, j, k)$ is the number of temporal shortest paths from i to j in which node k is traversed from the path in the snapshot t_m or in a previous snapshot $t' < t_m$, so that the next edge of the same path will be available at a later snapshot $t'' > t_m$. The *average temporal betweenness* of node i is defined as the average of $C_i^B(t_m)$ over all the snapshots:

$$C_i^B = \frac{1}{M} \sum_m C_i^B(t_m) \quad (12)$$

The closeness centrality of a node i is a measure of how close i is to any other node in the network. It can be measured as the inverse of the average distance from i to any other node in the network:

$$C_i^C = \frac{N-1}{\sum_j d_{ij}} \quad (13)$$

where d_{ij} is the distance between i and j in a static graph. The *temporal closeness centrality* is defined in an analogous way, the only difference being that for time-varying graphs d_{ij} denotes the length of the temporal shortest path from i to j .

As shown in [41] and elsewhere in this book [44], temporal closeness and betweenness centrality have proven useful to identify key spreaders and temporal mediators in corporate communication networks. In particular, it was found that traders indeed played an important mediatory role in time-varying graphs constructed from the ENRON email communication data set, being consistently ranked among the first ones both for temporal betweenness and for temporal closeness centrality. This result is qualitatively and substantially different from the one obtained by computing betweenness and closeness centrality in the corresponding aggregated graph, where the most central nodes are the people who interacted with the most number of other people, i.e., a secretary and a managing director. This apparently unimportant discrepancy between the centrality rankings actually turns out to be fundamental for the spreading of information (or diseases) throughout the system. In fact, simulation reported in [41] confirmed that when a spreading process

is initiated at the nodes having the highest temporal closeness centrality the number of other nodes reached by the spreading was higher and the time needed to reach them was smaller than in the case in which the spreading starts at nodes having higher static closeness centrality.

5.2 Spectral Centrality and Communicability

The total number of shortest paths passing through a node is not always the best way of measuring its centrality, especially because the shortest paths are not always the most relevant for a process. For instance, a disease could propagate through any path (not just through the shortest ones), and the rumours usually follow walks which are much longer (and somehow less efficient) than shortest paths. Consequently, other definitions of centrality exist which take into account walks instead of shortest paths. The classic example for static graphs is represented by the so called *Katz centrality* [28]. The basic idea is that the propensity for node i to communicate with node j can be quantified by counting how many walks of length $\ell = 1, 2, 3, \dots$ lead from i to j . The importance of a walk of length $\ell = 1$ (i.e., the direct edge (i, j)) is higher than that of a walk of length $\ell = 2$, which in turn is higher than that of a walk of length $\ell = 3$ and so forth. For this reason, it makes sense to appropriately rescale the contribution of longer walks. The original proposal consisted into scaling walks of length ℓ by a factor α^ℓ , where α is an appropriately chosen real value. We notice that the element a_{ij}^{ℓ} of the ℓ^{th} power of the adjacency matrix corresponds to the number of existing walks of length ℓ between i and j . Consequently, the entry s_{ij} of the matrix sum $S = I + \alpha A + \alpha^2 A^2 + \dots$ measures the propensity of i to interact with j (notice that I is the $N \times N$ identity matrix). It is possible to prove that the sum S converges to $(I - \alpha A)^{-1}$ if $\alpha < \rho(A)$, where $\rho(A)$ is the spectral radius of the adjacency matrix. In this case, the Katz centrality of node i is measured as the sum of the i^{th} row of S :

$$C_i^K = \sum_j [(I - \alpha A)^{-1}]_{ij} \quad (14)$$

Katz centrality can be extended to the case of time-varying graphs by using a similar reasoning [12]. We notice that each entry of the product of the adjacency matrices corresponding to an increasing sequence of ℓ snapshots $[t_{r_1}, t_{r_2}, \dots, t_{r_\ell}]$ represents the number of temporal walks in which the first edge belongs to the snapshot t_{r_1} , the second edge to t_{r_2} and so on. So, in order to count all the possible temporal walks of any length we should sum over all possible products of the form:

$$\alpha^k A(t_{r_1})A(t_{r_2}) \cdots A(t_{r_k}), \quad t_{r_1} \leq t_{r_2} \leq \cdots \leq t_{r_k} \quad (15)$$

for any value of the length k . It is possible to prove that if $\alpha < \min_m \rho(A(t_m))$ then the sum of all these products can be expressed as:

$$Q \equiv [I - \alpha A(t_0)]^{-1} [I - \alpha A(t_1)]^{-1} \cdots [I - \alpha A(t_m)]^{-1} \quad (16)$$

The matrix Q is called *communicability matrix*. Starting from this matrix one can define the *broadcast centrality*:

$$C_i^{Broad} = \sum_j Q_{ij} \quad (17)$$

which quantifies how well node i can reach all the other nodes in the time-varying graph, and the *receive communicability*:

$$C_i^{Recv} = \sum_j Q_{ji} \quad (18)$$

which is an estimation of how well node i can be reached from any other node in the network. In [12] it has been found that broadcast and receive communicability can be useful to spot the most influential spreaders in different time-evolving communication networks.

6 Meso-scale Structures

Real static networks differ from random graphs in many ways. In fact, together with heterogeneous distributions of node properties (e.g. degree and centrality) and with specific global characteristics (e.g. high average clustering and small average path length), complex networks show a non-trivial organisation of subsets of their nodes and exhibit a variety of meso-scale structures, including *motifs* and *communities*. The characterisation of the abundance of specific motifs has helped to explain why biological and technological networks are relatively resilient to failures [24, 25], while the analysis of communities has revealed that there exists a tight relationship between structure of a network and its functioning [10]. In the following we discuss how motifs analysis can be performed also in time-varying graphs and we present the extension of the modularity (a function for measuring the quality of a partition in communities, defined for static graphs by Newman in [34]) to temporal communities.

6.1 Temporal Motifs

In static graphs a *motif* is defined as a class of isomorphic subgraphs. We recall that two graphs G' and G'' , having adjacency matrices A' and A'' , are *isomorphic*

if there exists a permutation of the labels of the nodes of A' such that, after the permutation, $A' \equiv A''$. A permutation is represented by a matrix P that has the effect of swapping the rows and columns of the matrix to which it is applied. If A' and A'' are isomorphic, then there exists a permutation matrix P such that:

$$P^{-1}A'P = A'' \quad (19)$$

If two graphs are isomorphic then they are topologically equivalent, i.e., the arrangement of the edges in the two graphs is exactly the same, up to an appropriate relabelling of the nodes. Consequently, a motif can be thought as the typical representative of a class of subgraphs sharing the same arrangement of edges. It has been shown that in real networks, especially in biological ones, motifs are not uniformly distributed and some motifs are over-represented while others are rare [24, 25].

As for all the metrics described so far, the extension of *motifs* to time-varying graphs has to take into account time in a meaningful way. In a recent paper Kovanen et al. [20] propose an extension of motifs to time-varying graphs, based on the definition of $\Delta\tau$ -adjacency and $\Delta\tau$ -connectedness of contacts.¹ For practical reasons, the authors made the simplifying assumption that each node can be involved in no more than one contact at a time. This assumption is in general too restrictive, but it could be valid in some cases, e.g. when the contacts represent phone calls or when the duration δt of a contact is so small that the probability for a node to have two simultaneous contacts is negligible.

We say that two contacts $c_a = (i, j, t_a, \delta t_a)$ and $c_b = (k, \ell, t_b, \delta t_b)$ are $\Delta\tau$ -adjacent if they have at least one node in common and the time difference between the end of the first contact and the beginning of the second one is no longer than $\Delta\tau$. We assume, without loss of generality, that $t_a < t_b$, so that c_a and c_b are $\Delta\tau$ -adjacent if $0 \leq t_b - t_a - \delta t_a \leq \Delta\tau$. We say that an ordered pair of contacts (c_a, c_b) is *feasible* if $t_a < t_b$. Notice that $\Delta\tau$ -adjacency is defined only for the subset of feasible pairs of contacts. Two contacts c_a and c_b are $\Delta\tau$ -connected if there exists a sequence of m contacts $S = \{c_a = c_{n_0}, c_{n_1}, c_{n_2}, \dots, c_{n_m} = c_b\}$ such that each pair of consecutive contacts in S is feasible and $\Delta\tau$ -adjacent. From $\Delta\tau$ -connectedness, we derive the definition of *connected temporal subgraph*, which is a set of contacts such that all feasible pairs of contacts in the set are $\Delta\tau$ -connected.

For the definition of temporal motifs, we restrict ourselves to the subset of *valid temporal subgraphs*. A temporal subgraph is considered valid if all the $\Delta\tau$ -adjacent contacts of the nodes in the subgraph are consecutive. This means that if a node j appears in the pair of $\Delta\tau$ -adjacent contacts $c_a = (i, j, t_a, \delta t_a)$ and $c_b = (j, k, t_b, \delta t_b)$ of the subgraph, then does not exist any contact $c_x = (j, k, t_x, \delta t_x)$

¹In order to avoid confusion with the size Δt of the time-window used to define the temporal snapshot of a time-varying graph, here we preferred to use $\Delta\tau$ instead of the original Δt proposed by the authors of [20]. Also, notice that the authors use to call *events* what we have called here *contacts*.

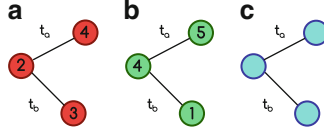


Fig. 5 Connected temporal subgraphs and motifs. The subgraph in panel (a) is not a valid temporal subgraph, because node 2 is involved in another contact after the contact with node 4 at time t_a and before the contact with node 3 at time t_b . Conversely, the subgraph in panel (b) is valid. Panel (c) shows the motif associated to the valid subgraph in panel (b)

such that $t_a < t_x < t_b$. In Fig. 5 we report two temporal subgraphs of three nodes obtained from the set of contacts in Fig. 1 considering $\Delta\tau = 30$ min. The subgraph of Panel (a) corresponds to the sequence of contacts $S_1 = \{c_1 = (2, 4, 0, 40), c_3 = (2, 3, 70, 20)\}$, and is not valid because node 2 is involved in another contact, namely $c_2 = (2, 5, 50, 10)$ after c_1 and before c_3 . Conversely, the connected temporal subgraph reported in Panel (b) and corresponding to the pair of contacts $S_2 = \{c_4 = (4, 5, 60, 50), c_6 = (1, 4, 140, 35)\}$, is valid, since node 4 is not involved in any contact between c_4 and c_6 .

A *temporal motif* is a class of isomorphic valid temporal subgraphs, where two temporal subgraphs are considered isomorphic if they are topologically similar (i.e., the organisation of the links in the subgraph is equivalent up to an appropriate relabelling of the nodes) and represent the same temporal pattern, i.e., the order of the sequence of contacts is the same. The typical element of the temporal motif corresponding to the graph reported in Fig. 5b is shown in Fig. 5c, where the labels on the edges of the graph correspond to the ordering of contacts. In [20] the authors report also an algorithm to discover temporal motifs, and discuss the problems connected with the estimation of the significance of motifs.

6.2 Temporal Communities and Modularity

The identification of communities, i.e., groups of tightly connected nodes, has allowed to reveal the richness of static graphs and has helped to understand their organisation and function. The simplest way to partition a graph is by dividing it into a set of \mathcal{M} non-overlapping groups, so that each node of the graph is assigned to one of the \mathcal{M} communities. The quality of a non-overlapping partition in communities can be measured by the *modularity function*. This function, originally proposed by Newman in [34], estimates the difference between the fraction of edges among nodes belonging to the same community and the expected fraction of such edges in a null-model graph with no communities. More formally, it is defined as follows:

$$Q = \frac{1}{2K} \sum_{ij} (a_{ij} - P_{ij}) \delta(c_i, c_j) \quad (20)$$

where a_{ij} are the elements of the adjacency matrix, P_{ij} is the expected number of edges between i and j in the null-model graph, c_i is the community to which node i belongs, $\delta(c_i, c_j) = 1$ if and only if node i and node j belong to the same community and K is the total number of edges in the graph. The simplest null-model is represented by a configuration model graph, where all the nodes of the graph have the same degree as in the real graph but edges are placed at random. In this case the modularity function reads:

$$Q = \frac{1}{2K} \sum_{ij} \left(a_{ij} - \frac{k_i k_j}{2K} \right) \delta(c_i, c_j) \quad (21)$$

where k_i is the degree of node i . Different extensions of the modularity function have been proposed for directed graphs, weighted graphs and graphs with overlapping communities [3, 23, 32, 35].

The extension of modularity for time-varying graphs is based on an interesting result valid for the modularity of static graphs and presented in [21], which connects the modularity function with the dynamics of a random walk over the graph. The authors of [21] show that the modularity function can be considered a particular case of a class of functions that measure the dynamical stability of a partition \mathcal{P} , where the stability of \mathcal{P} at time t is defined as:

$$R(t) = \sum_{\mathcal{C} \in \mathcal{P}} P(\mathcal{C}, t) - P(\mathcal{C}, \infty) \quad (22)$$

Supposing that the random walk has reached the stationary state,² then $P(\mathcal{C}, t)$ is the probability that a random walker which starts from a node in the community \mathcal{C} is found in a node of \mathcal{C} after time t . Similarly, $P(\mathcal{C}, \infty)$ is the probability that a random walker that started from a node in \mathcal{C} is found in \mathcal{C} after an infinite number of steps; when the walk has reached the stationary state, this corresponds to the probability that two independent random walks are found in \mathcal{C} at the same time. It is possible to show that if we consider a discrete-time random walk, in which a walker jumps from a node to another at equally-spaced time-steps of length $\Delta\tau$, then the stability of a partition at one step $R(t = \Delta\tau)$ is identical to the modularity function.

In [27] Mucha et al. propose an extension of modularity to multi-slice graphs which exploits the connection between the modularity function and the stability of a random walk on the multi-slice graph. Indeed, a time-varying graph can be considered a multi-slice graph if we connect each node of a snapshot with the other instances of itself in neighbouring snapshots by means of *multi-slice edges*. For brevity, we give here the definition of the modularity function for multi-slice graphs,

²It is possible to prove that a random walk on a graph always converges towards a stationary state, independently of the initial condition, if the adjacency matrix of the graph is primitive, which is the case for the vast majority of real graphs.

which corresponds to the stability at one step of a random walk on the multi-slice graph, but we omit the derivation of the formula.³ The modularity for multi-slice graphs reads:

$$Q_{multi} = \frac{1}{2\mu} \sum_{ijsr} \left[\left(a_{ij}(s) - \gamma_s \frac{k_i(s)k_j(s)}{2m_s} \right) \delta_{sr} + C_{jsr} \delta_{ij} \right] \delta(g_{is}, g_{jr}) \quad (23)$$

The indices i and j are used for nodes while the indices r and s indicate different slices. Here $a_{ij}(s)$ are the elements of the adjacency matrix of slice s , $k_i(s)$ represents the degree of node i in slice s (i.e., the number of neighbours to which i is connected in that slice) and $m_s = \frac{1}{2} \sum_i k_i(s)$ is the total number of edges in the slice s . The term C_{jsr} is the weight of the link that connects node j in slice s to itself in slice r , and γ_s is a resolution parameter. The terms δ_{ij} and δ_{rs} indicate the Kronecker function and $\delta(g_{is}, g_{jr})$ is equal to 1 only if node i in slice s and node j in slice r belong to the same community. The definition looks a bit complicated but it is essentially composed of two parts. The term in parentheses represents the standard modularity for the graph at slice s (the only difference being the resolution parameter γ_s), while the term C_{jsr} accounts for inter-slice connections. Once we have defined modularity for multi-slice networks, the search for the best partition can be performed by using one of the standard methods for modularity optimisation [10].

This definition of modularity is quite general, works well for any kind of multi-slice network, and is also applicable to assess the quality of a partition of a time-varying graph, which can be considered a multi-slice network. However, when using (23) one should take into account that in order to derive it as the stability of a random walk on the graph, the edges connecting different slices have to be undirected.⁴ Consequently, this definition of modularity is invariant under inversion of the sequence of slices which, in the particular case of time-varying graphs, implies invariance under time inversion. This means that (23) gives the same result on the time-varying graph $\mathcal{G}_{[0,T]}$ and on the graph $\mathcal{G}_{[T,0]}$ in which the sequence of time-windows is given in the opposite order.

In general, invariance under time inversion is not a desirable property for a metric used to characterise the structure of time-varying graphs, because most of the interesting characteristics of time-evolving systems, including temporal correlation of links and reachability, are due to the asymmetry introduced by the *arrow of time*. Time-invariance disregards this asymmetry completely, washing out most of the richness of time-varying systems. Consequently, we believe that the definition of appropriate metrics for the evaluation of community structures in time-varying graphs is still an open field of investigation.

³The interested reader can find the derivation of (23) in [27] and in the Supplemental Information of the same paper.

⁴This is required to ensure the existence of a stationary state for the Laplacian dynamics on the graph.

7 Final Remarks

The description of temporal networks in terms of time-varying graphs and the analysis of their structural properties is still in its infancy but has already produced many encouraging results, showing that complex networks theory is a quite flexible and promising framework for the characterisation of different real systems. There are still some open problems to be tackled, such as the definition of appropriate methods to detect temporal communities and the construction of analytical methods to assess how the structure of a time-varying graph can affect the dynamics of processes occurring over it, including spreading, synchronisation and evolutionary games. However, even if the community has not yet converged towards a unified notation and a fully consistent set of definitions and approaches is still lacking, the metrics and concepts devised so far for time-varying graphs constitute a valid and consistent alternative to the standard methods for the study of time-evolving systems, and will certainly represent a fundamental contribution to our understanding of complex systems in general.

Acknowledgements This work was funded in part through EPSRC Project MOLTEN (EP/I017321/1).

References

1. Albert, R., Barabasi, A.-L.: Statistical mechanics of complex networks. *Rev. Mod. Phys.* **74**, 47 (2002)
2. Albert, R., Jeong, H., Barabasi, A.-L.: Internet: diameter of the world-wide web. *Nature* **401**(6749), 130–131 (1999)
3. Arenas, A., Duch, J., Fernández, A., Gómez, S.: Size reduction of complex networks preserving modularity. *New J. Phys.* **9**(6), 176 (2007)
4. Barabasi, A.-L.: The origin of bursts and heavy tails in human dynamics. *Nature* **435**(7039), 207–211 (2005)
5. Boccaletti, S., Latora, V., Moreno, Y., Chavez, M., Hwang, D.-U.: Complex networks: structure and dynamics. *Phys. Rep.* **424**, 175–308 (2006)
6. Broder, A., Kumar, R., Maghoul, F., Raghavan, P., Rajagopalan, S., Stata, R., Tomkins, A., Wiener, J.: Graph structure in the web. *Comput. Network* **33**(1–6), 309–320 (2000)
7. Bullmore, E., Sporns, O.: Complex brain networks: graph theoretical analysis of structural and functional systems. *Nat. Rev. Neurosci.* **10**(3), 186–198 (2009)
8. Clauset, A., Eagle, N.: Persistence and periodicity in a dynamic proximity network. In: *Proceedings of DIMACS Workshop on Computational Methods for Dynamic Interaction Network*, Piscataway, 2007
9. De Vico Fallani, F., Latora, V., Astolfi, L., Cincotti, F., Mattia, D., Marciani, M.G., Salinari, S., Colosimo, A., Babiloni, F.: Persistent patterns of interconnection in time-varying cortical networks estimated from high-resolution EEG recordings in humans during a simple motor act. *J. Phys. A: Math. Theor.* **41**(22), 224014 (2008)
10. Fortunato, S.: Community detection in graphs. *Phys. Rep.* **486**, 75–174 (2009)
11. Gautreau, A., Barrat, A., Barthélemy, M.: Microdynamics in stationary complex networks. *Proc. Natl. Acad. Sci. U.S.A.* **106**(22), 8847–8852 (2009)

12. Grindrod, P., Parsons, M.C., Higham, D.J., Estrada, E.: Communicability across evolving networks. *Phys. Rev. E* **83**, 046120 (2011)
13. Holme, P.: Network reachability of real-world contact sequences. *Phys. Rev. E* **71**, 046119 (2005)
14. Holme, P., Saramäki, J.: Temporal networks. *Phys. Rep.* **519**(3), 97–125 (2012). doi:10.1016/j.physrep.2012.03.001.<http://www.sciencedirect.com/science/article/pii/S0370157312000841>
15. Karp, R.M.: Reducibility among combinatorial problems. In: Miller, R.E., Thatcher, J.W. (eds.) *Complexity of Computer Computations: Proceedings of a Symposium on the Complexity of Computer Computations*. The IBM Research Symposia Series. Plenum, New York (1972)
16. Karsai, M., Kivela, M., Pan, R.K., Kaski, K., Kertész, J., Barabási, A.-L., Saramäki, J.: Small but slow world: how network topology and burstiness slow down spreading. *Phys. Rev. E* **83**, 025102 (2011)
17. Kempe, D., Kleinberg, J., Kumar, A.: Connectivity and inference problems for temporal networks. *J. Comput. Syst. Sci.* **64**(4), 820–842 (2002)
18. Kossinets, G., Kleinberg, J., Watts, D.: The structure of information pathways in a social communication network. In: *Proceedings of the 14th ACM SIGKDD International Conference on Knowledge Discovery and Data Mining (KDD'08)*, pp. 435–443. ACM, New York (2008)
19. Kostakos, V.: Temporal graphs. *Phys. A: Stat. Mech. Appl.* **388**, 1007–1023 (2008)
20. Kovanen, L., Karsai, M., Kaski, K., Kertész, J., Saramäki, J.: Temporal motifs in time-dependent networks. *J. Stat. Mech.: Theor. Exp.* **2011**(11), P11005 (2011)
21. Lambiotte, R., Delvenne, J.-C., Barahona, M.: Laplacian dynamics and multiscale modular structure in networks. December (2008). arXiv:0812.1770
22. Latora, V., Marchiori, M.: Efficient behavior of small-world networks. *Phys. Rev. Lett.* **87**, 198701 (2001)
23. Leicht, E.A., Newman, M.E.J.: Community structure in directed networks. *Phys. Rev. Lett.* **100**, 118703 (2008)
24. Milo, R., Itzkovitz, S., Kashtan, N., Levitt, R., Shen-Orr, S., Ayzenshtat, I., Sheffer, M., Alon, U.: Superfamilies of evolved and designed networks. *Science* **303**(5663), 1538–1542 (2004)
25. Milo, R., Shen-Orr, S., Itzkovitz, S., Kashtan, N., Chklovskii, D., Alon, U.: Network motifs: simple building blocks of complex networks. *Science* **298**(5594), 824–827 (2002)
26. Miritello, G., Moro, E., Lara, R.: Dynamical strength of social ties in information spreading. *Phys. Rev. E* **83**, 045102 (2011)
27. Mucha, P.J., Richardson, T., Macon, K., Porter, M.A., Onnela, J.-P.: Community structure in time-dependent, multiscale, and multiplex networks. *Science* **328**(5980), 876–878 (2010)
28. Newman, M.: *Networks: An Introduction*. Oxford University Press, New York (2010)
29. Newman, M.E.J.: Scientific collaboration networks. I. Network construction and fundamental results. *Phys. Rev. E* **64**, 016131 (2001)
30. Newman, M.E.J.: Scientific collaboration networks. II. Shortest paths, weighted networks, and centrality. *Phys. Rev. E* **64**, 016132 (2001)
31. Newman, M.E.J.: The structure and function of complex networks. *SIAM Rev.* **45**, 167–256 (2003)
32. Newman, M.E.J.: Analysis of weighted networks. *Phys. Rev. E* **70**, 056131 (2004)
33. Newman, M.E.J.: Modularity and community structure in networks. *Proc. Natl. Acad. Sci. U.S.A.* **103**(23), 8577–8582 (2006)
34. Newman, M.E.J., Girvan, M.: Finding and evaluating community structure in networks. *Phys. Rev. E* **69**, 026113 (2004)
35. Nicosia, V., Mangioni, G., Carchiolo, V., Malgeri, M.: Extending the definition of modularity to directed graphs with overlapping communities. *J. Stat. Mech.: Theor. Exp.* **2009**(03), P03024 (2009)
36. Nicosia, V., Tang, J., Musolesi, M., Russo, G., Mascolo, C., Latora, V.: Components in time-varying graphs. *Chaos* **22**, 023101 (2012)
37. Pan, R.K., Saramäki, J.: Path lengths, correlations, and centrality in temporal networks. *Phys. Rev. E* **84**, 016105 (2011)

38. Scellato, S., Leontiadis, I., Mascolo, C., Basu, P., Zafer, M.: Evaluating temporal robustness of mobile networks. *IEEE Trans. Mob. Comput.* **12**(1), 105–117 (2013)
39. Scott, J., Gass, R., Crowcroft, J., Hui, P., Diot, C., Chaintreau, A.: CRAWDDAD trace [cambridge/haggle/imote/infocom2006](http://crawdad.cs.dartmouth.edu/cambridge/haggle/imote/infocom2006) (v. 2009-05-29). Downloaded from <http://crawdad.cs.dartmouth.edu/cambridge/haggle/imote/infocom2006>. Accessed May 2009
40. Stehlé, J., Barrat, A., Bianconi, G.: Dynamical and bursty interactions in social networks. *Phys. Rev. E* **81**, 035101 (2010)
41. Tang, J., Musolesi, M., Mascolo, C., Latora, V., Nicosia, V.: Analysing information flows and key mediators through temporal centrality metrics. In: *Proceedings of the 3rd Workshop on Social Network Systems (SNS'10)*, pp. 3:1–3:6. ACM, New York (2010)
42. Tang, J., Musolesi, M., Mascolo, C., Latora, V.: Characterising temporal distance and reachability in mobile and online social networks. *SIGCOMM Comput. Comm. Rev.* **40**(1), 118–124 (2010)
43. Tang, J., Scellato, S., Musolesi, M., Mascolo, C., Latora, V.: Small-world behavior in time-varying graphs. *Phys. Rev. E* **81**, 055101 (2010)
44. Tang, J., Leontiadis, I., Scellato, S., Nicosia, V., Mascolo, C., Musolesi, M., Latora, V.: Applications of temporal graph metrics to real-world networks. In: Saramäki, J., Holme, P. (eds.) *Temporal Networks*. Springer, Heidelberg (2013)
45. Valencia, M., Martinerie, J., Dupont, S., Chavez, M.: Dynamic small-world behavior in functional brain networks unveiled by an event-related networks approach. *Phys. Rev. E* **77**, 050905 (2008)
46. Vazquez, A., Pastor-Satorras, R., Vespignani, A.: Large-scale topological and dynamical properties of internet. *Phys. Rev. E* **65**, 066130 (2002)
47. Watts, D.J., Strogatz, S.H.: Collective dynamics of ‘small-world’ networks. *Nature* **393**(6684), 440–442 (1998)
48. Wilson, C., Boe, B., Sala, R., Puttaswamy, K.P.N., Zhao, B.Y.: User interactions in social networks and their implications. In: *Proceedings of ACM EuroSys'09, Nuremberg* (2009)

Burstiness: Measures, Models, and Dynamic Consequences

Byungjoon Min and K.-I. Goh

Abstract Various human activities were shown to exhibit heavy-tailed dynamics, dubbed “burstiness,” which manifests itself as a fat tail in the waiting time distribution. Such a heavy-tailed activity crucially deviates from the traditional assumption of Poisson random activity which had been used for over a century in many theoretical and practical modelings of human activity-based problems. In this survey article, we will overview some recent studies on burstiness, focusing on (a) how to characterize the burstiness, (b) how to model the bursty human activity at the individual and population levels, and (c) how the bursty activity could modify the collective dynamics of spreading processes in social networks.

1 Introduction

The quantitative understanding of temporal complexity of human dynamics underlies better comprehension and proper control of social systems which are among the most challenging goals of contemporary science [26]. Given the lack of appropriate data on how humans behave in reality, it has been assumed for a long time that human activities were uniform in time, thus modeled by the Poisson process [23]. Recent technological advances, however, changed the situation fundamentally. During the last few years, researchers have had access to large-scale datasets of human behaviors such as online and offline digital communications, from which the researchers could extract information on how people behave in reality [13, 14, 24, 56]. Studies on these data almost unanimously demonstrated a strong departure from the Poisson model. Human activities are highly heterogeneous in time, typically showing significantly enhanced activity levels over short periods,

B. Min · K.-I. Goh (✉)

Department of Physics, Korea University, Seoul 136–713, Korea

e-mail: kgoh@korea.ac.kr

followed by long periods of inactivity; human activities are dubbed to exhibit “burstiness” [4, 5].

“Burstiness” has become one of the keywords in the study of complex systems, since theories of microscopic individual behaviors as well as macroscopic social and economic dynamic phenomena should be rewritten in terms of bursty activity patterns instead of Poisson model. In so doing, a number of general questions can be raised. First, how should one quantify the burstiness of activity patterns? Second, how could one model the bursty activity patterns? Third, which consequences would the burstiness of individual’s activity have in the collective dynamics of the whole system? These are the questions some partial answers to which we will try to review in this survey article, centered on recent works contributed by the authors [10, 18, 39, 40].

This survey article is organized as follows: In Sect. 2, we overview the methods of characterizing burstiness of time series in a quantitative manner. A newly-proposed measure of burstiness in terms of waiting time distributions and short-term memory is discussed and applied to classify complex systems. Section 3 covers models of bursty activities based on the concept of priority-queues, both at the individual, group, and network levels. In Sect. 4, we discuss how burstiness could affect spreading processes over the network, as an example of impact of burstiness on collective dynamics. Section 5 will conclude the survey article with summaries.

2 Measures to Characterize the Burstiness

Although it gained a resumed interest in the context of human activities just recently, the dynamics showing temporal inhomogeneity had been documented and studied in a wide range of natural, physical, cellular, physiological, and technological complex systems, under various concepts such as punctuated, intermittent, chaotic, and fractal dynamics [3, 12, 20, 35, 37, 52]. Measures directly or indirectly addressing the inhomogeneity of signals had been proposed and applied under corresponding contexts [1]. These measures can be divided into two categories, the one based on the distribution of waiting times, the time intervals between two consecutive activities in the activity sequence, such as the coefficient of variation and Fano factor [37], and the other based on the correlations of the time series, such as autocorrelation function and Hurst exponent [1]. In human dynamics studies, burstiness had often been characterized by the fat-tailed nature of the response or waiting time distributions [4, 56]. Studies of natural systems such as earthquake and meteorological signals have also focused on the effect of correlations [7, 36]. To quantify the magnitude and potential origin of bursty dynamics seen in different systems, a two-way characterization scheme has recently been proposed [18]. This approach uses both distribution-based and correlation-based measures, respectively called burstiness parameter and memory parameter, putting them into a combined framework to compare signals from systems coming from diverse and apparently unrelated domains.

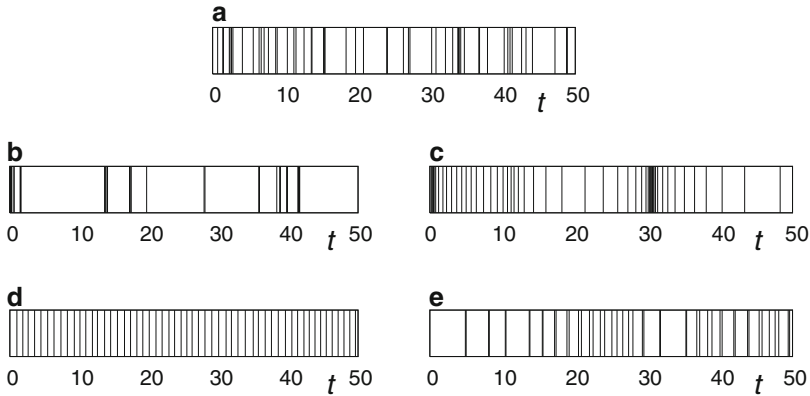


Fig. 1 (a) A synthetic signal generated by a Poisson process with a unit rate. (b, c) Bursty signals generated with a power-law waiting time distribution (b) and shuffled Poisson signal for positive short-term memory (c). (d, e) Anti-bursty signals generated with Gaussian waiting time distribution (d) and shuffled Poisson signal for negative short-term correlation (e). Note that signals in (a), (c) and (e) have identical waiting time distributions. Adopted from [18]

2.1 Measures: Burstiness and Memory Parameters

Distribution of and correlation between waiting times are two means that can generate bursty (or anti-bursty) signals in orthogonal way (Fig. 1). A uniformly random activity pattern can be obtained by a Poisson process in which the probability of an event is time-independent (Fig. 1a). In this case the waiting time, τ , between two consecutive events follows an exponential distribution, $P_{\text{Poisson}}(\tau) = (1/\tau_0) \exp(-\tau/\tau_0)$. An apparently bursty (or anti-bursty) signal emerges if $P(\tau)$ is different from the exponential. For example, one can generate a bursty pattern from a power-law $P(\tau)$ (Fig. 1b), or a more regular pattern with a Gaussian $P(\tau)$ (Fig. 1d). Alternatively, one can also modulate the burstiness of a signal by correlation without altering $P(\tau)$. For example, the signals shown in Fig. 1c, e have exactly the same $P(\tau)$ as the signal in Fig. 1a, yet they have a more bursty or a more regular character, respectively. In Fig. 1c the waiting times are correlated in such a way that short waiting times tend to follow short ones, resulting in a bursty look. On the contrary, in Fig. 1e the relative regularity is due to the anti-correlation between waiting times, such that short (long) waiting times tend to be followed by long (short) ones. Therefore, the apparent burstiness of a signal can be attributed to two mechanistically different origins of deviations from Poisson process: differences in the distribution of or the correlation between waiting times.

To distinguish these orthogonal effects, it was proposed to use simultaneously the two metrics, one addressing the properties of $P(\tau)$ and the other the correlations. These two measures are called the burstiness parameter B for the former, and the memory parameter M for the latter. The corresponding definitions will be introduced shortly. The proposed framework is readily applicable to systems with a

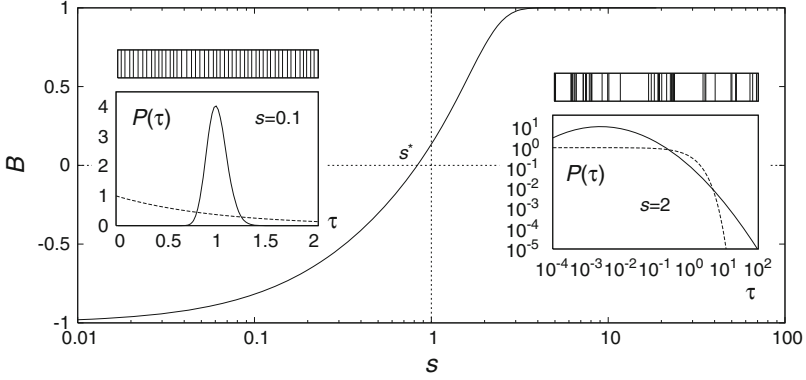


Fig. 2 The burstiness parameter B for log-normal waiting time distributions, interpolating between a highly bursty ($B = 1$), neutral ($B = 0$), and a regular ($B = -1$) signal. Insets show the form of $P(\tau)$ in bursty- and anti-bursty regime of each distribution along with a typical time signal generated with the corresponding $P(\tau)$. Dashed line in the insets corresponds to the exponential distribution for the Poisson process. Adopted from [18]

discrete activity pattern, as in human email communication signal. For systems with continuous signals as in earthquakes, one can apply the framework after transforming the signal into a discrete one by thresholding. In many systems the statistical properties of the obtained signal are known to be threshold-independent [7, 12].

To characterize the deviation of $P(\tau)$ from the Poisson signal, perhaps the simplest way is to use the so-called coefficient of variation, defined as the ratio of the standard deviation to the mean, σ_τ/m_τ , where m_τ and σ_τ are the mean and the standard deviation of $P(\tau)$, respectively. It has a value 1 for a Poisson signal with an exponential $P(\tau)$, 0 for completely regular δ -function-like $P(\tau)$, and ∞ for signals with a heavy-tailed $P(\tau)$ with infinite variance. Higher order characteristics such as skewness or kurtosis, or yet more complicated quantities based on the form of $P(\tau)$ can also be used for this purpose. For the sake of simplicity, we use the coefficient of variation to define the burstiness parameter B as

$$B \equiv \frac{(\sigma_\tau/m_\tau - 1)}{(\sigma_\tau/m_\tau + 1)} = \frac{(\sigma_\tau - m_\tau)}{(\sigma_\tau + m_\tau)}. \quad (1)$$

This definition is readily applicable when the mean of $P(\tau)$ exist, which is the case for real-world finite signals. The case with infinite mean m_τ , such as the power-law $P(\tau)$ with the power-law exponent smaller than 2, should be treated with care.

The particular definition of B was chosen to keep its value in the bounded range $(-1, 1)$. Also, the magnitude of B correlates with the signal's burstiness: $B = 1$ is the most bursty signal, $B = 0$ is neutral, and $B = -1$ corresponds to a completely regular (periodic) signal. For instance, for the synthetic signals shown in Fig. 1a, b, d the burstiness coefficient are $B = -0.05$ (neutral; a), $B = 0.44$ (bursty; b), and $B = -0.81$ (anti-bursty; c), respectively. In Fig. 2 we show the behavior of B for the log-normal distribution,

$$P_{\log\text{-normal}}(\tau) = \frac{1}{\tau s \sqrt{2\pi}} \exp\left(-\frac{[\ln(\tau) - \mu]^2}{2s^2}\right). \quad (2)$$

Here the larger the parameter s is, the larger is the variance of $P(\tau)$ hence the signal gets burstier ($B \rightarrow 1$). On the other hand, the smaller s is, the more regular is the signal, and B approaches to -1 as $s \rightarrow 0$. Note however that even though B becomes zero for a specific value s^* , $P(\tau)$ does not become an exponential there.

Deviation from the Poisson signal in the correlations can be quantified in many ways. Basically, the joint probability distribution of waiting times, parameterized by a time lag k , $P(\tau, \tau'; k)$, defined as the probability density that we have two waiting times τ and τ' separated by k events, contains the most information about the two-point correlation properties. The autocorrelation function $C(k) = \langle (\tau_i - m_\tau)(\tau_{i+k} - m_\tau) \rangle / \sigma_\tau^2$, where $\langle \cdot \rangle$ denotes the average over the index i , is also widely used in many applications. Again for the sake of simplicity, we use the correlation coefficient of consecutive waiting times (τ_i, τ_{i+1}) , defining the memory coefficient M as

$$M \equiv \frac{1}{n_\tau - 1} \sum_{i=1}^{n_\tau-1} \frac{(\tau_i - m_1)(\tau_{i+1} - m_2)}{\sigma_1 \sigma_2}, \quad (3)$$

where n_τ is the number of waiting times measured from the signal and $m_1(m_2)$ and $\sigma_1(\sigma_2)$ are sample mean and sample standard deviation of τ_i 's (τ_{i+1} 's), respectively ($i = 1, \dots, n_\tau - 1$). It might be noted that M is a biased estimator for $C(k = 1)$.

With this definition, the memory coefficient also has a value in the bounded range $(-1, 1)$ and is positive when a short (long) waiting time tends to be followed by a short (long) one, and it is negative when a short (long) waiting time is likely to be followed by a long (short) one. For example, the synthetic signals shown in Fig. 1a, c, e with identical $P(\tau)$ have the memory coefficient $M = 0.02$ (neutral; a), $M = 0.90$ (positive memory; c) and $M = -0.74$ (negative memory; e), respectively.

2.2 Characterizing Complex Systems with (M, B) Parameters

Most complex systems display a remarkable heterogeneity: some components may be very active, and others much less so. For example, some users may send dozens of emails during a day, while others only one or two; seismic activities can vary across regions, resulting in different frequencies of earthquake time series. As shown in the insets of Fig. 3, $P(\tau)$ of components with different activity levels can apparently differ significantly, questioning the validity of a unique system-specific value of B parameter in systems with heterogeneous activity levels. It turns out, however, that the apparently different-looking $P(\tau)$ curves behave in the same ways, when we properly rescale time: If we plot $\tau_0 P(\tau)$ as a function of τ/τ_0 , with τ_0 being the mean waiting time, the data collapse into a single curve $\mathcal{F}(x)$ (Fig. 3), indicating that the waiting time distribution takes a scaling form

$$P(\tau) = (1/\tau_0) \mathcal{F}(\tau/\tau_0), \quad (4)$$

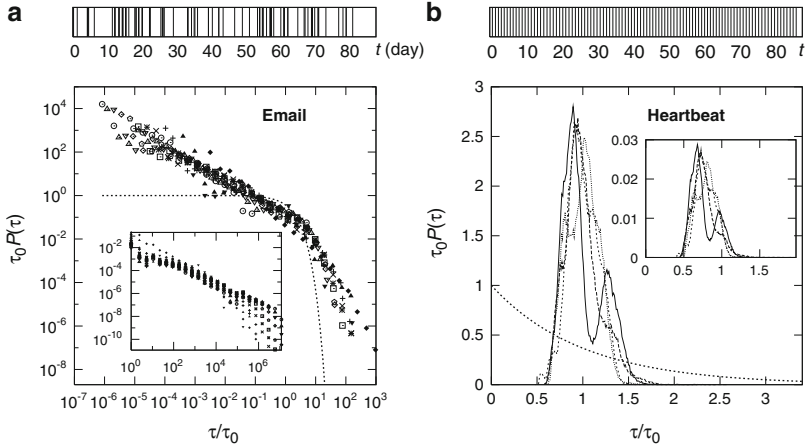


Fig. 3 Scaled plots of waiting time distribution $P(\tau)$ for some real signals. (a) $P(\tau)$ for the e-mail activity of individuals from a University [14]. τ corresponds to the time interval between two emails sent by the same user. (b) $P(\tau)$ of the cardiac rhythm of individuals [44]. Each event corresponds to the beat in the heartbeat signal and τ is the time interval between two consecutive heartbeats for an individual. In each panel, we also show for reference the exponential waiting time distribution (dotted). Unscaled waiting time distributions are shown in the inset for each dataset. Adopted from [18]

where $\mathcal{F}(x)$ is an activity-level-independent scaling function characteristic of the particular system [8, 12, 50]. Furthermore, the burstiness parameter B is invariant under such time rescaling, enabling us to assign to each system a characteristic B parameter in terms of the scaling function \mathcal{F} .

Having defined the two orthogonal measures B and M addressing two qualitatively different origins of bursty activities, it becomes feasible to characterize real-world complex systems by placing them in the (M, B) space (Fig. 4). Non-random distribution of complex systems in such “burstiness map” would imply possible classification scheme of complex systems from a dynamics perspective.

The first example examined is written texts, in which a waiting time represents the spacing between the consecutive occurrences of the same letter. *David Copperfield* by Dickens and *Isten Rabjai* by Géza were chosen as example texts of different kind, era, and language [45]. For these signals, it was shown that $P(\tau)$ follows closely an exponential so that $B \approx 0$, and that they have almost no short-term memory, as $M \approx 0.01$. Therefore these signals are found near the origin of the (M, B) space.

As the second class signals from natural phenomena such as the earthquake sequences near Japan [28] and the daily precipitation records in New Mexico, USA [41] were examined. They are found in the vicinity of the diagonal, indicating that both $P(\tau)$ and memory contribute to their bursty character.

Thirdly, signals for human activities, ranging from email and phone communication to web browsing and library visitation patterns [13, 14, 24, 25, 56] are

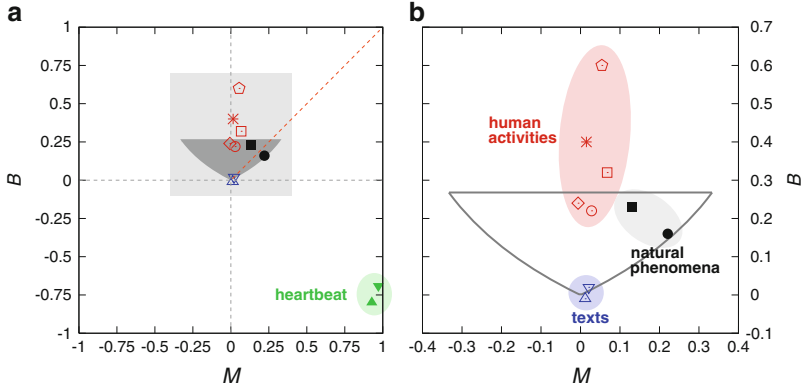


Fig. 4 (a) The burstiness map in (M, B) space. Human activities (red) are captured by activity patterns pertaining to email (star symbol) [14], library loans (open circle) [56], and printing (pentagon symbol) [25] of individuals in Universities, call center record (open square) [24], and phone initiation record (open diamond). Data for natural phenomena (black) are earthquake records in Japan (filled circle) [28] and daily precipitation records in New Mexico, USA (filled square) [41]. Data for written texts (blue) [45] are the English text *David Copperfield* (open triangle) and the Hungarian text *Isten Rabjai* (open inverted triangle). Data for physiological behaviors (green) are the normal sinus rhythm (filled inverted triangle) and the cardiac rhythm with CHF (filled triangle) [44]. (b) Close-up of the most populated region [light grey region in (a)]. Data in each class are indicated by grouping for the eye. Adopted from [18]

considered. For these a high B and small or negligible M were obtained, indicating that while these systems display significant burstiness rooted in $P(\tau)$, short-term memory plays a small role in their temporal inhomogeneity. This lack of memory is quite unexpected, if not counter-intuitive, and it may suggest the lack of short-term predictability [51]. This suggests that consideration of higher-order correlation may need to be included for better characterization [33].

Finally as an example of physiological signal, the cardiac rhythms describing the time interval between two consecutive heartbeats [44] were examined. It was obtained that $B_{\text{healthy}} = -0.69(6)$ for healthy individuals and $B_{\text{CHF}} = -0.8(1)$ for patients with congestive heart failure, both signals being highly regular. It is noteworthy that the B parameter captures the fact that cardiac rhythm is more regular in heart failure condition than in healthy condition [52].

The usefulness of burstiness map is illustrated by the clustering of the different systems by their class in the (M, B) plane: human activity patterns locate themselves in the high B , low M region, natural phenomena near the diagonal, heartbeats in the high M , negative B region and written texts near the origin, suggesting the possibility of existence of distinct classes or compositions of underlying mechanisms driving the temporal complexity of these systems. Further empirical testing of the clustering and its theoretical understanding should follow for conclusive understanding and setting the boundaries between these classes and categorization of complex system dynamics.

3 Priority-Queue Network Models of Bursty Human Dynamics

3.1 Priority Queue Models

A primary quantity in studying temporal heterogeneity of human dynamics is the waiting time distribution $P(\tau)$. $P(\tau)$ for many different types of human activities are found to deviate strongly from the exponential distribution for Poisson process. In particular, they exhibit so-called fat or heavy tail, possessing much larger statistical weight for long waiting times compared to Poisson process with the same mean waiting time. A number of models of such heavy-tailed $P(\tau)$ have been proposed. An asymptotic power-law distribution,

$$P(\tau) \sim \tau^{-\alpha}, \quad (5)$$

was proposed by Barabási and colleagues [4, 42, 56] and adopted widely [21, 46, 59, 60]; alternatively, the log-normal distribution of the form (2) was proposed by Amaral and colleagues [38].

Aside from technical issues from the point of view of statistical analysis, attempts to understand the origins and consequences of the heavy-tailed waiting time distributions in human dynamics with dynamical models may help provide conceptual insight. A family of dynamical models based on priority queues has been proposed to this end [4]. In such models, priority queues are used to mimic human decision making processes, under the assumption that humans decide what to do next among the list of tasks according to priorities assigned to the tasks. Here we briefly overview the main ideas.

The original priority queue model by Barabási [4] is a model of autonomous individual's activity, consisting of a single, fixed-length queue. The queue is filled with tasks, each of which is assigned a priority value drawn randomly when it enters into the queue. At each step the task with the highest priority is executed and is replaced by a new task with a random priority value. Upon execution, the waiting time τ , defined as the time interval for which the task has sat (waited) on the queue, is measured. The distribution of waiting times $P(\tau)$ of the Barabási model has been shown both numerically and analytically to exhibit a power-law tail for large τ with the exponent $\alpha = 1$ [2, 4, 16, 56]. Exact analytic results for the Barabási model was first obtained for queue length $L = 2$ case [56], and then extended to more general case with arbitrary queue length L [2]. The scaling behaviors were also obtained by mapping the problem into invasion percolation [16].

If the restriction of fixed queue length in the Barabási model is relaxed and the number of tasks can vary from time to time, the model becomes the classical priority queue model by Cobham [11]. For Cobham model, $P(\tau)$ has a power-law tail, but with a different exponent $\alpha = 3/2$ [11, 22]. The power-law waiting time distribution with the exponent $\alpha = 3/2$ was derived by mapping the variable-length priority queue model into the biased diffusion [22].

3.2 *Interacting Queues and Priority-Queue Networks*

Both Barabási model and Cobham model are simplified models to be used as a starting framework, and they neglect many aspects of potential importance in realistic human dynamics. Various detailed factors of human dynamics have recently been embedded in the priority-queue model framework [6, 21]. Such variants of priority-queue models have exhibited diverse dynamic behaviors dependent on the model-specific details. For instance, when a group of tasks is selected to execution at each time step, waiting time distribution decays as the power-law with the exponent $\alpha = 1.25$ [21]. Blanchard and Hongler studied the effect of time-dependent priorities on the basis of population dynamics [6]. They showed that when the priority of each task increases due to aging or deadlines in tasks, it could be possible that prioritization alone cannot produce heavy-tailed waiting time distributions.

Another important factor that has not been taken into account until recently is the interaction among queues, which can be employed to provide a simple model of human interactions. Due to a large array of interactions among people in various modes, typical activity of an individual is not an outcome of completely autonomous decisions, but of delicate compromises and balanced conflicts between often competing priorities. The impact of such human interactions on the patterns of human dynamics has first been addressed by Oliveira and Vazquez (OV) [43]. They introduced a minimal model consisting of two interacting priority queues with interacting (I) and non-interacting (O) tasks. The human interaction is taken into account in a way that the I -task is executed only when both individuals choose to execute them, that is, an AND-type protocol. Through this model they showed that the power-law waiting time distribution still persists against the introduction of human interaction, but the exponent α of $P(\tau)$ can take many different values other than 1, depending on the length of the queues.

The effect of human interactions for a system of more than two queues, or the queue *network* in general, can also be studied by generalizing the OV model [10,39]. A priority-queue network (PQN) of N queues is constructed as follows:

- A queue has one I -task for each neighbor in the network, in addition to an O -task. Thus a queue node i with degree k_i in the network (degree is the number of links connected to the node) has a queue with fixed length $L_i = k_i + 1$.
- The I -task of the node i paired with the node j is denoted as I_{ij} , and the O -task of the node i as O_i .
- In addition to the network configuration, the queue discipline has to be specified for a complete specification of a PQN. The protocol consists of a specification of the type of interaction for I -tasks (e.g., AND- or OR-type interaction) and an update rule (e.g., parallel or sequential update).

Having specified the PQN, the dynamics runs as follows:

1. Initially each task in the PQN is given a priority value drawn from a uniform distribution in $[0, 1)$.
2. At each step, one or more tasks are executed, following the queue discipline.

3. The waiting times of the executed tasks are recorded, and the executed tasks are replaced with new tasks each with a random priority value uniformly sampled $[0, 1)$.
4. N such elementary steps constitute a Monte Carlo step (MCS), which is the time unit of waiting time measurement.

In the following subsections, we will review existing variants of PQN models [10, 39]. As illustrated therein, variations of interaction rules in PQNs can lead to diverse power-law behaviors dependent on model details. Persisting power-law tails in various PQNs suggests that the power-law waiting time distribution is a robust feature of priority-based queuing models. At the same time, the power-law exponents are non-universal but dependent on model factors such as network topology, local position of a queue on the networks, interaction discipline, and reciprocity of influence. These results may provide theoretical background to identify essential factors in temporal human activity patterns. Sensitivity of the exponent dependent on model details supports diverse values of the exponent observed in empirical data [4, 21, 42, 46, 56, 59]. Finally, analytic treatment of interacting priority-queue models has largely remained to be fulfilled.

3.3 *OV Model on Networks*

An example of queue discipline is the AND-type protocol, random sequential update case, which is a direct extension of the OV model. In this queue discipline, a random node is chosen at each step, say node i . If the highest priority task of i is O_i , then it is executed. If it is an I -task, say I_{ij} , it is executed only if I_{ji} is also the highest priority task of the conjugate node j (AND-type interaction). In this case, the conjugate task I_{ji} is also executed. Otherwise, node i executes O_i .

Two representative network configurations, the star graph and fully-connected network, are studied (Fig. 5). The OV model on networks exhibits an interesting phenomenon of dynamic freezing due to priority conflict. The priority conflict occurs when a node i has I_{ij} as highest priority task, but the node j has another, say I_{jk} , as its highest priority, in conflict with each other. The star topology is less vulnerable to such a dynamic freezing since leaf-nodes can resolve it, primarily by updating the priority of the O -task repeatedly. As a result, we have a power-law decaying $P(\tau)$ (Fig. 5a, b). The power-law exponent α is found to be independent of the network size N ; for the I -tasks $\alpha_I \approx 2$, and for the O -tasks $\alpha_O \approx 3$ for both hubs and leaf nodes. These exponent values share common values with those of original OV model with $L = 2$; so for star graphs the model essentially behaves in the same way as the binary OV model.

On the other hand, the dynamics is quite different in networks with cycles, such as fully-connected graphs, which are highly susceptible to conflicts that cannot be resolved readily. As a consequence, the number of executed I -tasks, $\eta(t)$, decays rapidly in time, either algebraically for small N , or exponentially

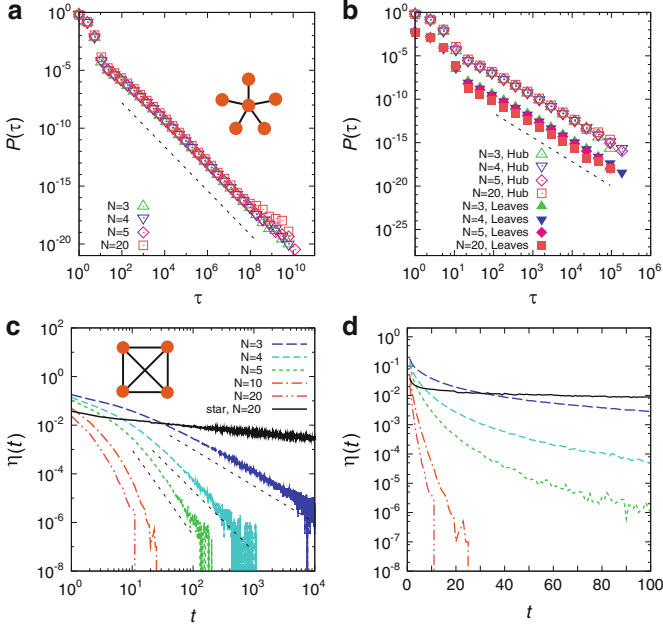


Fig. 5 (a–b) The waiting time distribution $P(\tau)$ of the OV model on star networks for I -tasks (a) and for O -tasks (b), with various $N = 3, 4, 5, 20$. Both $P(\tau)$ show power-law asymptotic with $\alpha_I \approx 1.9$ (a) and $\alpha_O \approx 2.8$ (b), indicated respectively with *dotted lines*. (c–d) The double logarithmic (c) and semi-logarithmic (d) plots of the number of executed I -tasks, $\eta(t)$, for the OV model on fully-connected networks versus time. Different *dotted line patterns* are used for different network size N (see legend). $\eta(t)$ decays algebraically for small N (c) and exponentially for large $N \gtrsim 10$ (d). Indicated slopes of *dotted line* are 1.5, 2.5, and 3.5, from *right to left*, drawn for the eye. Also shown is $\eta(t)$ for $N = 20$ with the star graph topology (*black solid*) for comparison. Adopted from [39]

for large $N \gtrsim 10$ (Fig. 5c, d), and eventually the dynamics gets frozen, with the timescale decreasing with N . In real social networks, we have strong empirical evidences of high clustering and clique structure [58], suggesting that the AND-type interaction protocol would strongly suffer the dynamic freezing, rendering itself alone inadequate for the realistic modeling of the network effects in human dynamics.

3.4 PQN with OR-Type Interactions: The OR Model

Not all human I -tasks should follow the AND-type protocol. Rather, an OR-type protocol would be more reasonable for the tasks which require simultaneous actions of two or more individuals but for which the action can be initiated primarily by either of them, such as a phone call conversation. For this class of I -tasks, potential priority conflicts can be instantly resolved; for instance, we normally answer the

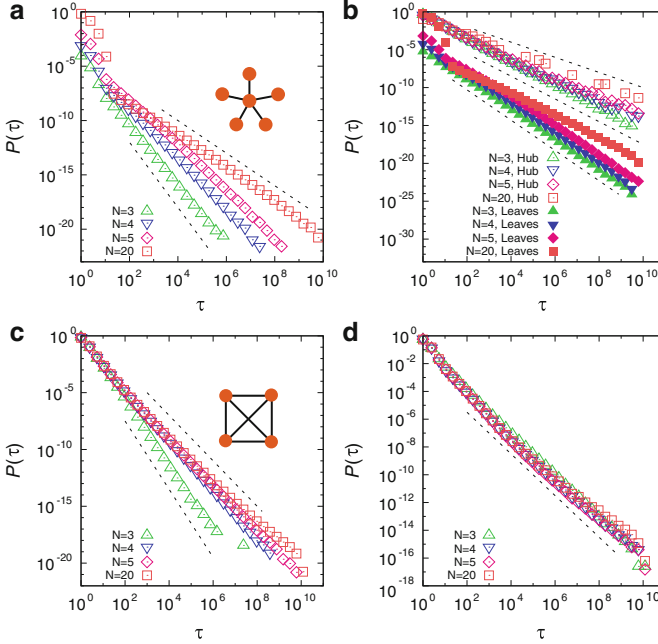


Fig. 6 (a–b) $P(\tau)$ of the OR model on star topology. **(a)** $P(\tau)$ for I -tasks decay as power laws with the exponent decreasing as N from $\alpha_I \approx 3$ for $N = 3$ to $\alpha_I \approx 1.5$ for $N = 20$. **(b)** $P(\tau)$ for O -tasks show distinct behaviors between the hub node (*open symbols*) and leaf nodes (*full symbols*). For the hubs, the power-law exponent varies from $\alpha_{O,hub} \approx 1.5$ for $N = 3$ to $\alpha \approx 1$ for $N = 20$. For the leaf nodes, $P(\tau)$ the exponents range from $\alpha_{O,leaf} \approx 2$ for $N = 3$ to $\alpha_{O,leaf} \approx 1.5$ for $N = 20$. $P(\tau)$ curves were shifted vertically for visibility. **(c–d)** $P(\tau)$ of the OR model on fully-connected topology. **(c)** $P(\tau)$ for I -tasks decay with asymptotic powers, with exponents decreasing with N from $\alpha_I \approx 3$ for $N = 3$ to $\alpha_I \approx 2$ for $N = 20$. **(d)** $P(\tau)$ for O -tasks follow the power-law decay with the exponent $\alpha_O \approx 1.5$. All quoted slopes are indicated with *dotted lines* for the eye. Adopted from [39]

incoming phone call while we are performing other tasks. By incorporating such an OR-type interaction protocol, the dynamic rule of what we call the OR model is given as follows:

- At each step we choose a random node, say node i .
- If its highest priority task is an I -task, say I_{ij} , the two tasks I_{ij} and I_{ji} are executed regardless of the priority value of I_{ji} ; If O_i is the highest priority task, only that is executed.
- Priorities of all the executed tasks are randomly reassigned.

For the OR model, $P(\tau)$ still exhibit power-law tails for both star and fully-connected network topology, yet the power-law exponent α depends on the network size N as well as the network topology in a diverse way. First, in the star topology, α decreases as N increases: For I -tasks, it exhibits values from $\alpha_I \approx 3$ for $N = 3$ to $\alpha_I \approx 1.5$ for $N = 20$ (Fig. 6a); For O -tasks, the exponent exhibits distinct

values for the hub and leaf nodes, changing from $\alpha_{O,hub} \approx 1.5$ for $N = 3$ to $\alpha_{O,hub} \approx 1.0$ for $N = 20$ for the hub node, whereas for the leaf nodes it changes from $\alpha_{O,leaf} \approx 2.0$ for $N = 3$ to $\alpha_{O,leaf} \approx 1.5$ for $N = 20$ (Fig. 6b). Moreover, for the hub-node, the mean waiting time $\langle \tau \rangle_{O,hub}$ of O -tasks diverges, as the power-law exponent $\alpha < 2$. For other tasks, however, power-law $P(\tau)$ with $\alpha < 2$ for large N is accompanied by the peak at $\tau = 1$, making the average waiting time finite.

In the fully-connected topology, the power-law exponent α weakly depends on N . For the I -tasks, it decreases with N from $\alpha_I \approx 3$ for $N = 3$ to $\alpha_I \approx 2$ for $N = 20$ (Fig. 6c). For the O -tasks, on the other hand, α_O is rather stable against N as $\alpha_O \approx 1.5$ (Fig. 6d). This result implies that on the fully-connected networks, I -tasks are executed with finite mean waiting times while O -tasks on average have to wait on the queue infinitely long to be executed. Taken together, the OR model on networks implicates the importance of not only the overall network structure but also individual node's topological position on determining the dynamics of networking priority-queue nodes.

3.5 The OR Model with Team-Based Execution

Further variations of the OR model were considered, by including more complicated forms of human interactions [10]. First is the team-based task execution, referring to the situation when a task demands simultaneous actions of more than two individuals. The second is the hierarchy in decision making, occurring when a node in higher hierarchy can order the nodes in lower hierarchy to execute a task together. Both forms of human interaction are encountered in many real-life situations, thus the understanding of their impact is of use for a more complete human dynamics modeling.

In the team-based task execution OR model, each I -task is associated with a group G of queue nodes of size r , meaning that r individuals form a group or a team in executing the task. Here the size of a team r is an important parameter characterizing the model. In this model, each queue has $n_I = \binom{N-1}{r-1}$ I -tasks and $n_O = 1$ O -task. Note that the case with $r = 2$ is the same as the original OR model on fully-connected network. As $r > 2$, the number of I -tasks n_I varies drastically and it is therefore interesting to study its impact on the queue dynamics. Then the dynamics of the model proceeds as follows:

- At each step, a queue node is chosen randomly (say it to be μ) and its highest priority task is identified. If it is an I -task, all the r nodes in the associated team execute the task simultaneously; if it is an O -task, only node μ executes the task.
- The waiting times τ of executed tasks are recorded, and the priority of executed tasks are refreshed with independent random values in $[0, 1)$.
- Repeat the previous steps, N repeats of which constitute one Monte Carlo step.

This model is called the (N, r) -model.

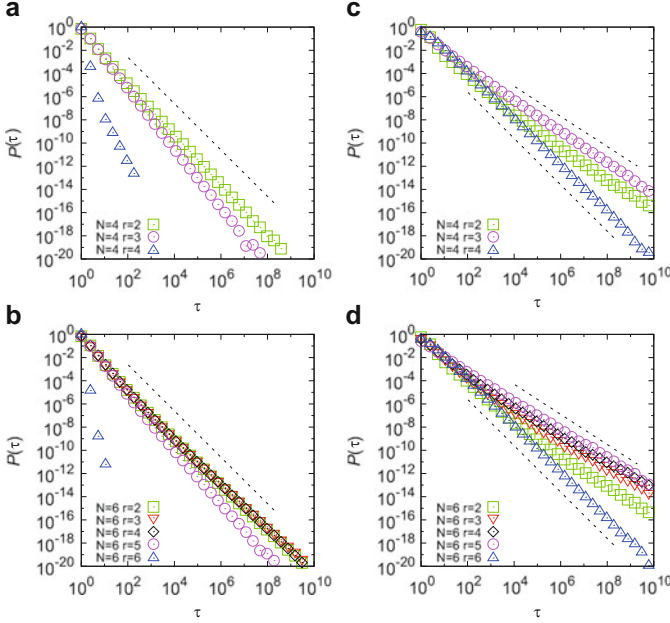


Fig. 7 Waiting time distribution $P(\tau)$ of (N, r) -model. $P(\tau)$ of (a, b) I -tasks and (c, d) O -tasks for various team sizes r with $N = 4$ (a, c), and 6 (b, d). Slope of the straight lines in (a, b) is -2 ; those in (c, d) are -1.3 (upper) and -2 (lower), respectively, drawn for the eye. Adopted from [10]

Waiting time distributions of (N, r) -model with $N = 4$ and 6 and $r = 2 \dots N$ are shown in Fig. 7. In all cases shown, we observe a power-law decaying $P(\tau)$ whose exponent depends on the model parameters. For I -tasks, $\alpha \approx 2$ in the range $2 \leq r \leq N - 2$ (Fig. 7a, b). Team execution does not have an apparent effect in these cases. However, the case $r = N - 1$ exhibits a distinct power law, with slightly larger exponent $\alpha \approx 2.3 \sim 2.5$. Interestingly, a distinct power-law behavior for $r = N - 1$ is similarly observed in OR model ($r = 2$) on fully-connected networks. The case $N = 3$ exhibits a distinct power-law exponent than other cases $N \geq 4$ [39]. For $r = N$, $P(\tau)$ decays rapidly with an apparent power-law tail whose exponent increases with N . This apparent power-law behavior is, however, a finite-size effect, and the distribution is dominated by the $\tau = 1$ peak approaching to unity in the long-time limit. This means that when $r = N$ the I -task tends to be executed in an overwhelmingly long succession, so that $P(\tau)$ has a finite second moment, contrast with the case $r < N$ where it is divergent.

Results for $P(\tau)$ of O -tasks are shown in Fig. 7c, d. For the O -task dynamics, the power-law exponent α remains unchanged as $\alpha \approx 1.3$ for $2 \leq r \leq N - 1$, even though the probability density for large τ becomes systematically elevated with r . We note the absence of distinct power law in $r = N - 1$ case for O -tasks, which is also consistent with the result of $N = 3$ pairwise-interaction OR model. The case

with $r = N$ exhibits a distinct power-law behavior with the exponent $\alpha \approx 2$. This can be understood as follows. From the perspective of the O -task, the case $r = N$ is similar to the $N = 2$ OR model, in which each queue has one I -task and one O -task. Therefore we have the same exponent $\alpha \approx 2$ for O -tasks in both cases.

Taken together, these results indicate that in the (N, r) -model, mean I -task waiting time is marginally divergent (as $\alpha \approx 2$) for $r < N - 1$, but is finite for $r \geq N - 1$. The variance diverges for $r < N$ (as $\alpha < 3$), while it is finite only for $r = N$. For O -tasks, not only the variance but also mean waiting time would diverge ($\alpha \lesssim 2$) in the long-time limit, implying the lack of characteristic scale in the waiting times dynamics. Further properties of the team-based task execution OR model have also been studied such as the effect of number of O -tasks [10].

3.6 The OR Model with Hierarchy-Based Execution

When making a decision of what to do next, often the decision is followed in a hierarchical manner: a node in higher hierarchy can order the nodes in lower hierarchy to execute a task together. Incorporating such a hierarchy-based task execution, what is called the H -model is defined as follows.

- Each of the N individuals is assigned a hierarchy value h in the interval $1, 2 \dots N$. The node with $h = 1$ sits on the top of the hierarchy, while the one having $h = N$ is at the bottom.
- Each node has two tasks, $n_I = 1$ I -task and $n_O = 1$ O -task.
- If a node μ (μ -th in the hierarchy) is chosen for task-execution, and it has the I -task as highest priority, all the lower hierarchy nodes (from $h = \mu + 1$ to $h = N$) follow to execute the I -task simultaneously with node μ . If the O -task is chosen, only node μ executes it.
- Waiting times are recorded and priorities are refreshed for all the executed tasks.
- Repeat the previous two procedures.

Depending on the node's position in the hierarchy, the degree of intervention (number of I -task execution orders from upper-hierarchy nodes) varies.

The waiting time distributions of H -model are shown in Fig. 8. In the H -model, the node at the top of hierarchy ($h = 1$) is not affected by any other nodes in its decision making. Thus the $h = 1$ node's dynamics, having two independent tasks, is the same as that of the simple Barabási queue with length $L = 2$; therefore, we have the same $P(\tau)$ for both the I -task and O -task as that of the Barabási model [4], the nonstationary $P(\tau)$ with a strong peak at $\tau = 1$ accompanied by a power-law tail with exponent $\alpha = 1$ (Fig. 8, \square) [54].

The I -task dynamics of nodes with $h > 1$ is found to follow a power-law $P(\tau)$ with the same exponent $\alpha \approx 1$, but with an h -dependent cutoff τ_c (Fig. 8a, b);

$$P(\tau) \sim \tau^{-1} \exp(-\tau/\tau_c). \quad (6)$$

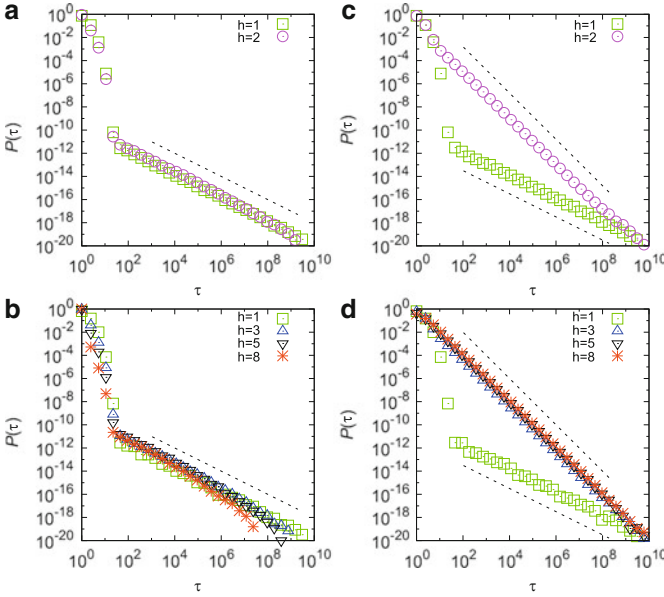


Fig. 8 $P(\tau)$ of the hierarchy-based H -model. **(a, b)** $P(\tau)$ of I -tasks for various hierarchy index h with $N = 2$ **(a)** and 8 **(b)**. Slope of the *straight lines* is -1 , drawn for the eye. **(c, d)** $P(\tau)$ of O -tasks for various hierarchy index h with $N = 2$ **(c)** and 8 **(d)**. Slopes of the *straight lines* in each panel are -2 (*upper*) and -1 (*lower*), respectively, drawn for the eye. Adopted from [10]

This cutoff waiting time is introduced by the intervention from higher-hierarchy nodes, due to which the node executes an I -task that is not the highest priority task at the moment. Without the intervention, the I -task would have had to wait longer. The characteristic time scale of such intervention introduces the cutoff in $P(\tau)$ for $h > 1$ nodes. The cutoff timescale τ_c decreases approximately exponentially with h [10]. Yet, these interventions do not change the exponent of the tail. Note that despite the fat-tailed $P(\tau)$ with $\alpha \approx 1$ the mean I -task waiting time is finite, as the tail part contributes only marginally to the mean value in the long-time limit [54]. The O -task dynamics of nodes with $h > 1$ exhibits a different behavior. We have $P(\tau)$ decaying as a power law with the exponent $\alpha \approx 2$ in all cases. The peak at $\tau = 1$ disappears and the distributions become stationary. As in $r = N$ case of (N, r) -model, the power-law exponent $\alpha \approx 2$ for O -tasks has the same dynamic origin as the O -tasks of $N = 2$ OR model. Each $h > 1$ node has one I -task and one O -task; its I -task can be executed not only by its own priority, but also by the requests from other nodes. Such setting is identical to $N = 2$ OR model's O -tasks. Therefore they share the same exponent. For $h > 1$ nodes, mean O -task waiting time is marginally divergent as $\alpha \approx 2$, suggesting a lack of the characteristic O -task waiting time in the model.

An interesting point can be made from comparison of $N = 2$ cases of H -model and OR model. They differ only by directional property of interaction for I -task, for which we have directional or unilateral influence in the former and unidirectional or reciprocal influence in the latter. We have seen that this simple difference has dynamic consequences, as the two model exhibit different $P(\tau)$. Furthermore, I -tasks and O -tasks are found to respond differently to breaking of interaction symmetry, revealing intricate interplay between the interaction structure and resulting dynamics of priority-queue networks.

3.7 Other Works

Further variants of priority-queue models have steadily been studied. A variant priority-queue model incorporating the interaction between individuals was proposed by Wu et al. [59] to describe a bimodal combination of the Poisson and power-law waiting time distributions in short message communication. The interaction in this model is similar to OR model, but a new I -task is added with a small probability after the interaction, while in the OR model a new I -task is added immediately after the execution of a previous I -task. This model fits well the bimodal distribution of short message communication using the parameters extracted from the empirical data [59]. Recently, Jo et al. [30] introduced a priority-queue model with time-varying priorities. They solved the priority-queue model with the priority of task either increasing or decreasing analytically and obtained the bimodal and unimodal waiting time distributions with power-law tails. They also compared their results with updating time distribution of arXiv.org and the processing time distribution of papers in Physical Review journals.

4 Spreading Dynamics with Bursty Activity Patterns

As surveyed in the previous section, priority-queue models mimicking human decision process were shown to reproduce fat-tailed waiting time distributions on the individual level. While these modelings were successful, how the activity modeling at the individual level translates into the collective phenomena at the population or network level was not addressed in those works.

In this perspective, spreading process has been a paradigmatic subject for studying the impact of individual dynamics on collective dynamics. The impact of the non-Poisson statistics on spreading processes was first addressed by Vazquez et al. [57] using email communication patterns. They show that the decay of the number of new infections based on empirical waiting time distributions is significantly slower than that expected with the Poissonian assumption [57]. Iribarren and Moro provided another empirical evidence of slower spreading dynamics using a viral email experiment [27]. More recently, Karsai et al. [32] examined dynamics of information spreading on communication networks using the empirical event sequences of phone calls data, showing dynamics with temporal heterogeneity.

4.1 Long-Time Behavior of SI Dynamics

Here we outline the main results for the long-time behaviors of susceptible-infected (SI) model dynamics with bursty activity models [40]. To start understanding the impact of power-law waiting time distribution on long-time behavior of SI dynamics, we first outline a general theory of irreversible spreading processes in a social network. The network structure is assumed to be tree-like, and the activity pattern is characterized by the waiting time distribution $P(\tau)$. The generation time Δ [55] is defined as the time interval between the infection of an agent in the social network (primary case) and the transmission of the infection to a neighbor agent (secondary case). The generation time distribution $g(\Delta)$ then characterizes the timings of infection transmissions.

In this setting, an outbreak starting from a single infected individual at $t = 0$ results in the average number of new infections at time t , $n(t)$, given by [55]

$$n(t) = \sum_{d=1}^D z_d g^{*d}(t). \quad (7)$$

Here z_d is the average number of individuals d contacts away from the first infected node and D is the maximum of d . $g^{*d}(t)$ is the d -th order convolution of $g(\Delta)$, that is, $g^{*1}(t) = g(t)$ and $g^{*d}(t) = \int_0^t dt' g(t') g^{*(d-1)}(t - t')$, representing the probability density function of the sum of d generation times.

Long-time behaviors of $n(t)$ can be extracted from (7). For example, when $g(\Delta) \sim \Delta^{-\beta}$ with $1 < \beta < 2$, that is in the Lévy-stable regime, one obtains in the limit $d \gg 1$, independently of the network structure, $g^{*d}(t) \sim t^{-\beta}$ as $t \rightarrow \infty$ and thus the asymptotic behavior of the prevalence decay as

$$n(t) \sim t^{-\beta}. \quad (8)$$

Therefore, quite generically, with heavy-tailed activity patterns the long-time spreading dynamics would decay with the same tail behavior as the generation time distribution by the above theory.

4.2 SI Dynamics with Power-Law Waiting Time Distribution

The generation time distribution can be determined from the waiting time distribution and the type of interactions between the social agents in the network. As the simplest scenario, we consider the case when the activities of individuals in the network are completely uncorrelated and so are the timings of consecutive interactions. In such a case, the time series of interactions can be modeled by a simple renewal process [15] with waiting time distribution $P(\tau)$. Specifically, let us consider the case where agent A is infected at time t_A ; agent B, who is connected to

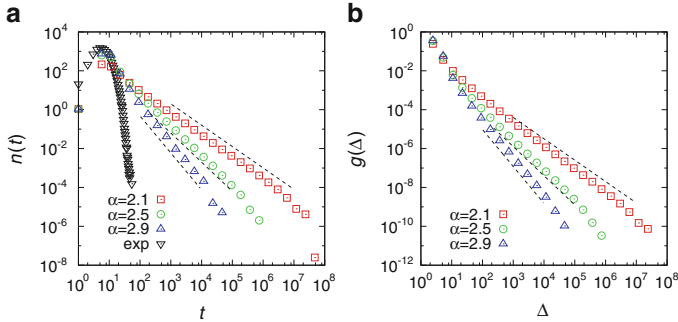


Fig. 9 (a) The average number of new infections $n(t)$ of the SI model with uncorrelated identical power-law $P(\tau)$ with exponent $\alpha = 2.1$ (open square), 2.5 (open circle), 2.9 (open triangle), and with an exponential $P(\tau)$ (open inverted triangle), respectively. All $P(\tau)$ have the same mean waiting time $\langle \tau \rangle = 2$. It decays with the exponent $\approx \alpha - 1$ for power-law $P(\tau)$, whereas it decays exponentially for exponential $P(\tau)$. (b) The generation time distribution $g(\Delta)$ for power-law $P(\tau)$. It decays as a power law with the same exponent as $n(t)$. Simulations were performed on a scale-free network with $\gamma = 3$ and size $N = 10^4$, and averaged over 10^8 independent runs. Initial infected node is selected to be the hub. In both panels, dotted lines have slopes -1.1 , -1.5 , and -1.9 , drawn as a guide. Data are binned logarithmically. Adopted from [40]

A, is still susceptible at time t_A and becomes infected, after interacting with agent, at time $t_B > t_A$. From the perspective of B, the time A was infected is random and therefore, the generation time $t_B - t_A$ is the residual waiting time, the time interval between a randomly selected time and the time A and B will perform their next interaction.

For the waiting time distribution with finite mean $\langle \tau \rangle$, the residual waiting time probability density function is related to the waiting time probability density function, leading to [15]

$$g_{\text{uncorr}}(\Delta) = \frac{1}{\langle \tau \rangle} \int_{\Delta}^{\infty} P(\tau) d\tau. \quad (9)$$

Therefore, for the uncorrelated activity patterns with $P(\tau) \sim \tau^{-\alpha}$, $2 < \alpha < 3$, we have

$$g_{\text{uncorr}}(\Delta) \sim \Delta^{-(\alpha-1)} \quad \text{and} \quad n_{\text{uncorr}}(t) \sim t^{-(\alpha-1)}. \quad (10)$$

When $1 < \alpha < 2$, $P(\tau)$ does not have a finite mean, but thanks to more complicated theory [15] we still obtain the long-time behavior of power-law form, $n_{\text{uncorr}}(t) \approx t^{-1}$, in this regime.

Numerical simulations of the SI process on the static model [19] of scale-free networks confirmed the predicted power-law decay of $n(t)$ (Fig. 9). For $2 < \alpha < 3$, $n(t)$ is found to decay as a power law with the exponent $\alpha - 1$ for large t as predicted by the theory. For comparison, the same SI dynamics with exponential (Poisson-type) $P(\tau)$ with the same mean waiting time $\langle \tau \rangle = 2$ (Fig. 9a, ∇) is shown, where $n(t)$ decays exponentially fast. The effective duration \mathcal{T} of the epidemic

process, given by the expected infection time of an individual after the outbreak, $\mathcal{T} = \sum_{t=0}^{\infty} tn(t)/N$, is measured to be $\mathcal{T}_{exp} \approx 5$ for the exponential $P(\tau)$, whereas $\mathcal{T} \approx 4 \times 10^5$ for the power-law $P(\tau)$ with $\alpha = 2.1$. Therefore, the power-law waiting time distribution indeed impacts the long-time dynamics of the spreading process significantly.

4.3 SI Dynamics over Priority-Queue Networks

As a second example, the SI dynamics following the OR model of PQN has also been studied. This may model the spreading of infectious entity through mutual communications or contacts between individuals that can be initiated primarily by any one of the individuals, as in the case of phone calls and face-to-face interactions. The dynamics basically follows that of the OR model in Sect. 3.4. The infection is transmitted whenever an infected and a susceptible node perform an I -task together. This dynamics proceeds until all nodes are infected.

We consider first the SI dynamics on a PQN having a power-law degree distribution with exponent $\gamma = 3$. In the long time limit, $n(t)$ is found to decay as a power law with exponent approximately 2 (Fig. 10a, \circ). The power-law decay of $n(t)$ is much slower than the exponential decay on the random execution queue network (Fig. 10a, ∇). Such a longer prevalence time than predicted by the Poisson process had been observed for spreading dynamics controlled by empirical human activity patterns, such as an E-mail virus outbreak [57].

To understand the $n(t) \sim t^{-2}$ behavior, we turn to the waiting time distribution of the OV model PQN, through which the generation time distribution can be obtained. There is a local variation of the $P(\tau)$ exponent α in the OV model PQN as shown in Sect. 3, which makes the identification of network-level exponent α_{PQN} nontrivial. However, the following statistical reasoning, supported by numerical simulations, offers key insights about long-time dynamic characteristics. We first observe that different I tasks (links) manifest different exponents $P_{kk'}(\tau) \sim \tau^{-\alpha_{kk'}}$, parameterized by the degrees k and k' of the associated nodes. Putting the contribution of all tasks together, the smallest exponent $\alpha_{kk'}$ makes biggest contribution to the tail of $P_{PQN}(\tau)$. Note that links with $\alpha_{kk'} < 2$ cannot contribute statistically because of the strong peak of $P_{kk'}(\tau)$ at $\tau \approx 1$. So the net result is that links with $\alpha_{kk'} \approx 2$ contribute the most, resulting in (Fig. 10b, \circ),

$$P_{PQN}(\tau) \sim \tau^{-\alpha_{PQN}}, \quad \alpha_{PQN} = 2. \quad (11)$$

In relating the waiting time distribution to the generation time distribution, we further note that the interaction timings between connected pairs are not completely independent in the PQN. To see this explicitly, let us consider three linearly connected nodes (B – A – C) in the PQN. When node A interacts with node B (I_{AB} task is being executed), node A cannot interact at the same time with node C (I_{AC} task has to wait). So the waiting time of I_{AC} begins at the execution of I_{AB}

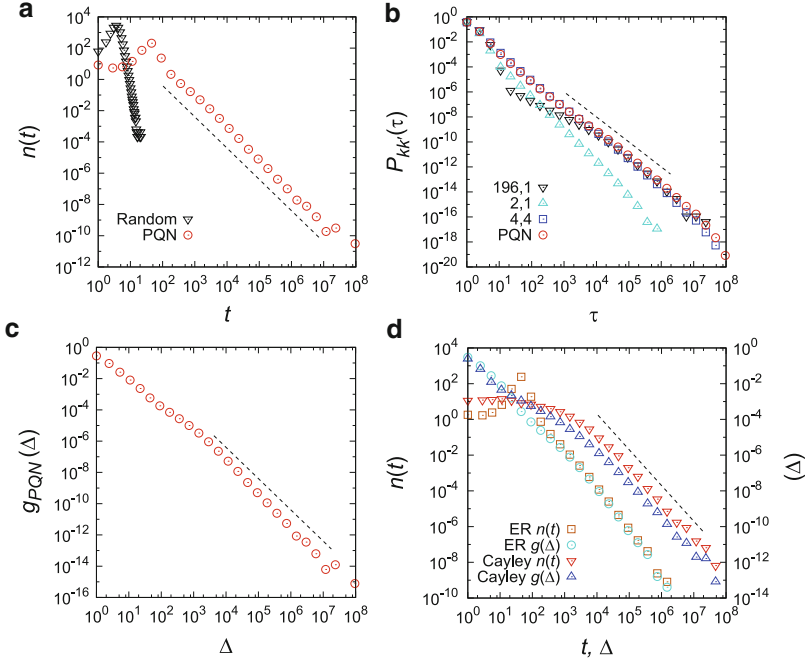


Fig. 10 (a) The average number of new infection $n(t)$ of the SI model on the PQN (*open circle*) and on the random execution queue network (*open inverted triangle*). After the initial increase, $n(t)$ after the peak decays with a power-law tail with exponent $\beta \approx 2$ for the PQN (*open circle*) and exponentially for the random execution case (*open inverted triangle*). (b) The waiting time distribution of the whole network, $P_{PQN}(\tau)$, and those of links connecting nodes with degree k and k' , $P_{kk'}(\tau)$, of the same process for the PQN. Both $P_{PQN}(\tau)$ and $P_{kk'}(\tau)$ decay as a power law, yet with different exponents dependent on the local topological position, $\alpha_{PQN} \approx 2$, $\alpha_{196,1} \approx 1$, $\alpha_{2,1} \approx 3$, and $\alpha_{4,4} \approx 2$. (c) The generation time distribution $g_{PQN}(\Delta)$ of the same process for the PQN. In (a–c), simulations were performed on a scale-free network with $\gamma = 3$ and size $N = 10^4$, and averaged over 10^3 different initial conditions. (d) $n(t)$ (*left scale*) and $g(\Delta)$ (*right scale*) of the SI model on the Erdős-Rényi network with mean degree $\langle k \rangle = 4$ and size $N = 10^4$ and Cayley tree with branching number 4 and six generations ($N = 1456$). In each case, $n(t)$ and $g(\Delta)$ show power-law tails with the same exponent. In all panels, *dotted lines* have slope -2 , drawn as a guide. Data are binned logarithmically. Adopted from [40]

task. If node B has been infected, the generation time of infection of C from A is the same as the waiting time. Therefore, in the PQN the generation time distribution $g_{PQN}(\Delta)$ has the same power-law exponent as the waiting time distribution $P_{PQN}(\tau)$ (Fig. 10c), which in turn, according to our general theory, leads to $n_{PQN}(t)$ decaying with the same power law as $P_{PQN}(\tau)$, that is $\beta_{PQN} = \alpha_{PQN} = 2$ consistent with our numerical findings.

The power-law decay with $\alpha = 2$ has been checked to hold quite independently with the network structure (Fig. 10d). We have examined the influence of the network structure on the spreading dynamics over the PQN by considering Erdős-Rényi networks and Cayley trees. On both network structures, $n(t)$ is found to decay

as a power law also with $\beta = \alpha$, $n(t) \sim t^{-\alpha}$ (Fig. 10d). Since every node except the root in Cayley tree is topologically indistinguishable, all I tasks show the same $P(\tau)$, which decays as a power law with $\alpha \approx 2$ for degree $k \geq 3$. In this respect, this is an example where the temporal heterogeneity dominates over the structural heterogeneity.

5 Summary and Outlook

In this survey article, we have briefly overviewed recent works on the measurements, modeling, and dynamics consequences of burstiness in human dynamics. A two-way method for assessing the burstiness of a system using both the distribution-based and the correlation-based measures was proposed. The modeling framework of human dynamics based on priority queues has been generalized to a network level, called the priority-queue network, to take interactions between individuals into account. Finally, we have shown how individual bursty activity can slow down spreading dynamics on a social network in the context of the simple SI model.

The stream of studies of temporal heterogeneity in human dynamics still continues to flow, fuelled mainly by a variety of new datasets. In addition to digital communication data from email [14], mobile phone [8], and short message [59], other data from as diverse domains as face-to-face contact [9], online chat [17], Wikipedia edit [31], internet prostitution [47], and online game behavior [53] have been studied. Those studies on one hand reinforce the universal characteristics of bursty, non-Poissonian activity in human dynamics; on the other, they have also uncovered further features of human dynamics, such as the activity-topology relation [32], the persistence pattern of emotional expressions [17], the effect of circadian and seasonal patterns [29], and the temporal correlations in bursty pattern [33], in particular the presence of long-term correlations [48, 49]. All these intellectual effort, and surely more to come, will collectively contribute to the ultimate goal of fulfilling the promise of better understanding of social dynamics [34] and the physics of complex systems with temporal heterogeneity in general [26].

Acknowledgements The authors would like to thank A.-L. Barabási, W.-k. Cho, I.-M. Kim, and A. Vazquez for the fruitful collaborations on the works reviewed in this article. This work was supported by Basic Science Research Program (No. 2011-0014191) through NRF grant funded by MEST.

References

1. Abarbanel, H.D.I., Brown, R., Sidorowich, J.J., Tsimring, L.Sh.: Rev. Mod. Phys. **65**, 1331 (1993)
2. Anteneodo, C.: Phys. Rev. E **80**, 041131 (2009)
3. Bak, P., Christensen, K., Danon, L., Scanlon, T.: Phys. Rev. Lett. **88**, 178501 (2002)

4. Barabási, A.-L.: *Nature* **207**, 435 (2005)
5. Barabási, A.-L.: *Bursts*. Dutton, New York (2010)
6. Blanchard, P., Hongler, M.O.: *Phys. Rev. E* **75**, 026102 (2007)
7. Bunde, A., Eichner, J.F., Kantelhardt, J.W., Havlin, S.: *Phys. Rev. Lett.* **94**, 048701 (2005)
8. Candia, J., González, M.C., Wang, P., Scheonharl, T., Madey, G., Barabási, A.-L.: *J. Phys. A* **41**, 224015 (2008)
9. Cattuto, C., Van den Broeck, W., Barrat, A., Colizza, V., Pinton, J.-F., Vespignani, A.: *PLoS ONE* **5**, e11596 (2010)
10. Cho, W.-k., Min, B., Goh, K.-I., Kim, I.-M.: *Phys. Rev. E* **81**, 066109 (2010)
11. Cobham, A.: *J. Oper. Res. Soc.* **2**, 70 (1954)
12. Corral, A.: *Phys. Rev. E* **68**, 035102(R) (2003)
13. Dezső, Z., Almaas, E., Lukács, A., Rácz, B., Szakadát, I., Barabási, A.-L.: *Phys. Rev. E* **73**, 066132 (2006)
14. Eckmann, J.P., Moses, E., Sergi, D.: *Proc. Natl. Acad. Sci. USA* **101**, 14333 (2004)
15. Feller, W.: *An Introduction to Probability Theory and Its Applications*, vol. 2. Wiley, New York (1966)
16. Gabrielli, A., Caldarelli, G.: *Phys. Rev. Lett.* **98**, 208701 (2007)
17. Garas, A., Garcia, D., Skowron, M., Schweitzer, F.: *Sci. Rep.* **2**, 402 (2012)
18. Goh, K.-I., Barabási, A.-L.: *Europhys. Lett.* **81**, 48002 (2008)
19. Goh, K.-I., Kahng, B., Kim, D.: *Phys. Rev. Lett.* **87**, 278701 (2001)
20. Golding, I., Paulsson, J., Zawilski, S.M., Cox, E.C.: *Cell* **123**, 1025 (2005)
21. Gonçalves, B., Ramasco, J.J.: *Phys. Rev. E* **78**, 026123 (2008)
22. Grinstein, G., Linsker, R.: *Phys. Rev. Lett.* **97**, 130201 (2006)
23. Gross, D., Harris, C.M.: *Fundamentals of Queueing Theory*. Wiley, New York (1998)
24. Guedj, I., Mandelbaum, A.: <http://iew3.technion.ac.il/serve/callcenterdata/>
25. Harder, U., Paczuski, M.: *Phys. A* **361**, 329 (2006)
26. Holme, P., Saramäki, J.: *Phys. Rep.* **519**, 97 (2012)
27. Iribarren, J.L., Moro, E.: *Phys. Rev. Lett.* **103**, 038702 (2009)
28. Japan University Network Earthquake Catalog. <http://www.eri.u-tokyo.ac.jp/CATALOG/junec/>
29. Jo, H.-H., Karsai, M., Kertész, J., Kaski, K.: *New J. Phys.* **14**, 013055 (2012)
30. Jo, H.-H., Pan, R.K., Kaski, K.: *Phys. Rev. E* **85**, 066101 (2012)
31. Kämpf, M., Tismer, S., Kantelhardt, J.W., Muchnik, L.: *Phys. A* **391**, 6101 (2012)
32. Karsai, M., Kiveli, M., Pan, R.K., Kaski, K., Kertész, J., Barabási, A.-L., Saramäki, J.: *Phys. Rev. E* **83**, 025102 (2011)
33. Karsai, M., Kaski, K., Barabási, A.-L., Kertész, J.: *Sci. Rep.* **2**, 397 (2012)
34. Lazer, D., Pentland, A., Adamic, L., Aral, S., Barabási, A.-L., Brewer, D., Christakis, N., Contractor, N., Fowler, J., Gutmann, M., Jebara, T., King, G., Macy, M., Roy, D., Van Alstyne, M.: *Science* **323**, 721 (2009)
35. Leland, W.E., Taqqu, M.S., Willinger, W., Wilson, D.V.: *IEEE/ACM Trans. Netw.* **2**, 1 (1994)
36. Livina, V.N., Havlin, S., Bunde, A.: *Phys. Rev. Lett.* **95**, 208501 (2005)
37. Lowen, S.B., Teich, M.C.: *Fractal-Based Point Processes*. Wiley, Hoboken (2005)
38. Malmgren, R.D., Stouffer, D.B., Motter, A.E., Amaral, L.A.: *Proc. Natl. Acad. Sci. USA* **105**, 18153 (2008)
39. Min, B., Goh, K.-I., Kim, I.-M.: *Phys. Rev. E* **79**, 056110 (2009)
40. Min, B., Goh, K.-I., Vazquez, A.: *Phys. Rev. E* **83**, 036102 (2011)
41. National Resources Conservation Service. <http://www.nm.nrcs.usda.gov/snow/data/historic.html>
42. Oliveira, J.G., Barabási, A.-L.: *Nature* **437**, 1251 (2005)
43. Oliveira, J.G., Vazquez, A.: *Phys. A* **388**, 187 (2009)
44. PhysioBank. <http://www.physionet.org/physiobank/>
45. Project Gutenberg. <http://gutenberg.org>
46. Radicchi, F.: *Phys. Rev. E* **80**, 026118 (2009)
47. Rocha, L.E.C., Liljeros, F., Holme, P.: *Proc. Natl. Acad. Sci. USA* **107**, 5706 (2010)

48. Rybski, D., Buldyrev, S., Havlin, S., Liljeros, F., Makse, H.A.: Proc. Natl. Acad. Sci. USA **106**, 12640 (2009)
49. Rybski, D., Buldyrev, S.V., Havlin, S., Liljeros, F., Makse, H.A.: Sci. Rep. **2**, 560 (2012)
50. Saichev, A., Sornette, D.: Phys. Rev. Lett. **97**, 078501 (2006)
51. Song, C., Blumm, N., Wang, P., Barabási, A.-L.: Science **327**, 1018 (2010)
52. Thurner, S., Feurstein, M.C., Teich, M.C.: Phys. Rev. Lett. **80**, 1544 (1998)
53. Thurner, S., Szell, M., Sinatra, R.: PLoS ONE **7**, e29796 (2012)
54. Vázquez, A.: Phys. Rev. Lett. **95**, 248701 (2005)
55. Vázquez, A.: Phys. Rev. Lett. **96**, 038702 (2006)
56. Vázquez, A., Oliveira, J.G., Dezső, Z., Goh, K.-I., Kondor, I., Barabási, A.-L.: Phys. Rev. E **73**, 036127 (2006)
57. Vázquez, A., Rácz, B., Lukács, A., Barabási, A.-L.: Phys. Rev. Lett. **98**, 158702 (2007)
58. Wasserman, S., Faust, K.: Social Network Analysis. Cambridge University Press, Cambridge (1994)
59. Wu, Y., Zhou, C., Xiao, J., Kurths, J., Schellnhuber, H.J.: Proc. Natl. Acad. Sci. USA **107**, 18803 (2010)
60. Zhou, T., Kiet, H.A.T., Kim, B.J., Wang, B.-H., Holme, P.: Europhys. Lett. **82**, 28002 (2008)

Temporal Scale of Dynamic Networks

Rajmonda Sulo Caceres and Tanya Berger-Wolf

Abstract Interactions, either of molecules or people, are inherently dynamic, changing with time and context. Interactions have an inherent rhythm, often happening over a range of time scales. Temporal streams of interactions are commonly aggregated into dynamic networks for temporal analysis. Results of this analysis are greatly affected by the resolution at which the original data are aggregated. The mismatch between the inherent temporal scale of the underlying process and that at which the analysis is performed can obscure important insights and lead to wrong conclusions. In this chapter we describe the challenge of identifying the range of inherent temporal scales of a stream of interactions and of finding the dynamic network representation that matches those scales. We describe possible formalizations of the problem of identifying the inherent time scales of interactions and present some initial approaches at solving it, noting the advantages and limitations of these approaches. This is a nascent area of research and our goal is to highlight its importance and to establish a computational foundation for further investigations.

1 Introduction

Whether it is on-line communications [11, 33, 34], animal social interactions [15, 19, 48, 55], or gene regulatory processes [25], the dynamic systems they represent have inherent rhythms at which they function. Some of these inherent rhythms come from the system itself, others are imposed by outside circumstances. Circadian patterns of cell regulatory systems, seasonality in mobility patterns of animals, daily and weekly communication patterns of humans are just a few examples of these characteristic temporal scales. Not only do these complex systems have inherent rhythms, different patterns within them form and live at different scales

R.S. Caceres (✉) · T. Berger-Wolf
University of Illinois at Chicago, Chicago, IL 60607, USA
e-mail: rsulo1@uic.edu; tanyabw@uic.edu

[32]. For example, when analyzing animal population behavior, three temporal scales are considered to be important for capturing the hierarchical nature of its social structure [21]: the scale of the interactions themselves, the scale of patterns of interactions (relationships), and, finally, the scale of patterns of relationships (network structures). In this context, grooming interactions of baboons usually have a temporal scale ranging from seconds to minutes, mother to infant or peer to peer relationships have a scale extending over years, while an individual troop membership, splitting or formation of new troops extends from years to decades [52]. Similarly, in human social behavior, the patterns of interaction of conversations, friendships, and kinship occupy different temporal scales. Every dynamic complex system exhibits this kind of multi-scalar behavior.

We view the system through the filter of data we collect. These data are typically collected opportunistically, with the temporal rate of data not always matching that of the system. In order to ask questions about these systems, the tools we use to answer the questions, and the temporal scale of analysis have to match the temporal scale of the process underlying the question. Whether the question of interest is the detection of anomalies, the understanding of cohesiveness and persistence of interactions, or the prediction of the system behavior, the temporal scale at which the analysis is applied needs to reflect the temporal scale that captures what is essential for the question. When we analyze millions of IP network traces in order to detect outlying behavior, should we analyze their communication patterns every 5 min, every hour, every day? How long should social interactions persist to be considered meaningful relationships in a social network [21, 41]? Just like the cell has the “capacity” to compute the temporal scope of mRNA expression [58], we would like to develop an understanding of how to estimate the tempo of a given dynamic system by analyzing its expression as a series of interactions occurring in time (i.e. temporal stream).

1.1 The Dynamic Network Abstraction

The abstract representation of choice for modeling a dynamic system has been that of the *dynamic network*, also referred to as *temporal network* [23, 27, 29, 35, 36]. A dynamic network is a time series of network snapshots. Each snapshot represents a state of the system over the interval of time such as a minute, a day, or a year in the life of the system. The duration of the snapshot represents the temporal scale of the dynamic network since all the interactions are lumped together discarding their order in time. Little thought, to date, has been given to matching this temporal scale to that of the system under study. A snapshot of a year is not appropriate for analyzing human conversation, but maybe right for understanding kinship relations, minute-long snapshots could be suitable for analysis of gene regulatory systems, but too fine for the baboon troop membership. **How, then, should we go about finding the “right” temporal scale for the dynamic network?** This is the central question of this book chapter.

In the abstraction of the dynamic network, the temporal ordering of interactions within a snapshot is lost. All these interactions are represented as living in the same temporal scale, whether we have the finer temporal information or not. In some instances, the data already comes as a series of aggregated snapshots; in other instances, we are given a stream of interactions in time which we have to aggregate. We have to make sure that as we transition from the temporal interaction stream or a collection of finer snapshots to a dynamic network representation, the information that we discard is not critical. It is not clear how to decide what the right temporal scale of dynamic networks should be. While in many cases the system under observation naturally suggests the size of such a temporal scale [35], it is more often the case that the choice of temporal scale is arbitrary and is done for the convenience of the data representation and analysis. For example, it is convenient and sometimes meaningful to analyze human interaction patterns in calendaric scales, but it does not always make sense to analyze animal social interactions in similar scales. Studies of periodic behavior of animals have shown that animals do not care much about week days and weekends [35].

Within the complex system there are subsets of interactions that form functional units that naturally co-occur together and their analysis as a cohesive unit allows us to see critical system behavior such as collective emergent behavior [41, 42, 46, 58]. For example, when studying molecular mechanisms of diseases, it is important to study the interactions of relevant genes concurrently in order to observe their temporal coordination [58]. Similarly, epidemiological studies show that analysis of concurrent relations allows for a more accurate estimation of the magnitude of spread of an infectious agent [42, 46]. In all these scenarios, analysis of interactions as series of network snapshots allows us to uncover inherent concurrent sets of interactions while maintaining only the critical temporal orderings. In this transition from data streams to dynamic networks we have to know to discard the little noisy perturbations of functional units, while retaining the meaningful temporal ordering at the scale of natural functionality as a whole.

1.2 Empirical Motivation

The level of aggregation of the temporal stream has great implications on the patterns observed in the corresponding dynamic network and the inference made about the network and the processes on it [10, 13, 23, 29, 32, 41, 53]. As Moody et al. [41] point out, if analysis is applied at too fine temporal resolution, we end up observing a network that has lots of temporal detail, yet the interesting and meaningful co-occurring patterns, such as communities, may not be fully formed. On the other end of the spectrum, when we aggregate the network at a too coarse of a temporal scale, we lose critical temporal information and cannot observe meaningful temporal changes to the system or processes over it. For example, ecologists Baldock et al. [2] have shown that analyzing plant pollinator interactions at a daily temporal scale misses temporal variations during the span of the day that

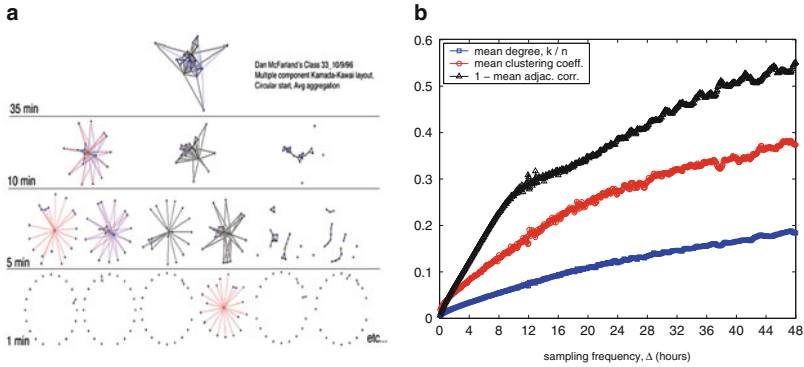


Fig. 1 Representation of a social network aggregated at different windows of aggregation [(a), [7]] and network measures of Reality Mining dataset as functions of the window of aggregation [(b), [13]]

are critical for correctly interpreting interactions as either competitive or facilitative. Figure 1a gives an illustration of the effect of the level of aggregation on the kind of network structures that we observe (image reprinted from [7], with authors' permission). Figure 1b also illustrates how measures computed over the dynamic network critically depend on the level of aggregation that generated this network (image reprinted from [13], with authors' permission).

1.3 Data Collection

Data about dynamic interaction systems is often collected as a sequence of interactions together with temporal information about their occurrences. Depending on the nature of the dynamic system, it might be more meaningful to represent the temporal dynamics as a stream of instantaneous interactions (i.e. *point-based* interaction streams). At other times, a stream of interactions with temporal durations (i.e. *interval-based* interaction streams) is more suitable. For systems such as email communications, point-based streams offer a better representation. On the other hand, friendships in a social network or grooming in baboon troops are better characterized as interval-based streams. Interval-based interaction streams can be viewed as a generalization of point-based interaction streams, where we can think of the duration time as zero. Figure 2 gives an illustration of both types of interaction streams.

Whether the collected data comes from GPS sensors, digital recording of emails, or human observation of animals grooming, most often, what we record is the instantaneous times at which the interactions were observed to be present. This process often introduces different kinds of artificial noise that can be described both in terms of topological structure and in terms of temporal structure. Topological noise arises when we attempt to represent continuous behavior discretely (GPS).

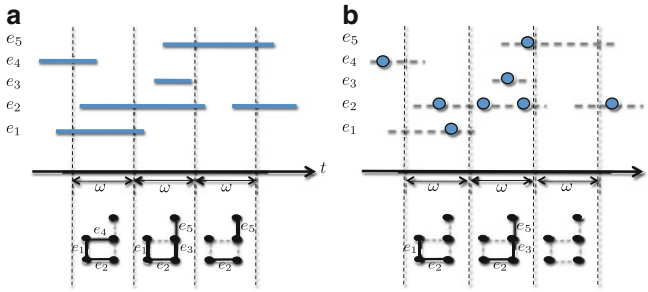


Fig. 2 Illustration of two different types of temporal interactions: interval-base interactions (a), point-based interactions (b)

We might miss interactions that should be present in the network. At the same time, we might record interactions that occur spuriously, but are not meaningful. For example, when collecting proximity-based networks of students at MIT using bluetooth devices or zebras in Kenya using GPS collars, an interaction, then, is being at the same place at the same time for a sufficiently long interval. If two zebras happen to cross paths without actually interacting, devices that sample positions sufficiently frequently will record this occurrence even though this “interaction” should not be included in the network. On the other hand, observing baboon interactions once a day, will miss many important dynamics.

1.4 Oversampling of Temporal Streams

Oversampling is an aspect of the data collection process that can help with the issue of representing continuous time discretely. Oversampling helps reduce the number of missing or spurious interactions. It allows us to better understand what interactions are persistent in the network. On the other hand, oversampling affects our ability to distinguish between local noisy temporal orderings and critical temporal ordering. For example, when we observe human interactions at much higher rate than necessary, it is maybe hard to distinguish between interactions that develop independently of each other and those that are transient. When emails arrive within seconds of each other, is their ordering meaningful? Is it important in what order people walk in to a meeting room or is it more important to know that they were present at the meeting? With the advent of electronic data collection of interactions using communication devices, GPS, and proximity sensors, it is often the case that data are oversampled at orders of magnitude higher temporal resolution than the temporal scale of the underlying process. Therefore, it is important that the aggregation process correctly accounts for the oversampling effects.

So far we have discussed scenarios when the aggregation of interactions streams into a series of network snapshots is useful in capturing both the topological and

temporal structure of the underlying system. The characteristic of the system that makes the dynamic network the right abstraction is the notion of local concurrency, or temporal independence. *In dynamic systems where the temporal ordering of the interactions is absolutely critical, and there are no hidden concurrencies buried due to the data collection process, aggregation is not a useful tool.*

In addition, we have discussed how temporal networks have an inherent rhythm that governs their dynamics. This is one natural way to define what is the “right” temporal scale. An alternative way would be to define the “right” temporal scale in terms of what is useful about networks. This leads to an orthogonal approach which is application driven. For example, the identification of the most frequent sub-graphs, or the identification of dynamic communities are useful applications that give us meaningful insight about the network. The natural question that arises here is to identify the optimal temporal scale at which application-specific patterns become detectable.

In summary, the dynamics of complex systems evolve at characteristic temporal scales. Understanding the mapping between structure and the temporal scale at which it lives is critical, and when done appropriately can lead to meaningful and insightful analysis. The subtle interplay between the temporal concurrency and temporal ordering is at the core of what is essential about the right temporal resolution for analysis of dynamic networks. The notions of temporal concurrency and temporal ordering depend on the context of analysis and they often lead to discovery of complex multi-scalar nature of the structure. When temporal concurrency is something inherent to the system or analysis, aggregation of interactions streams helps in capturing this aspect of system functionality.

Although we have illustrated the challenges related to temporal scale identification in the context of dynamic complex systems, the problem of identifying the right resolution for analysis of temporal data in general is very broad and covers many research areas. The relevant literature spans fields from signal processing [18,44] and information theory [50] to time series analysis, time series segmentation [28,43,45], and model granularity [5,20,47]. While the literature mentioned above offers a solid foundation for the problem of temporal scale identification in general, it does not explicitly address data that are represented as networks. It is not clear, for example, how techniques like aggregation or smoothing of numerical values relate to the same techniques applied to network structures [10,38,53]. There is, however, the opportunity for great research in trying to translate and adapt these methods for the analysis of temporal scale of networks. Caceres, Berger-Wolf and Grossman [10] show that for special classes of network generative processes, the class of linear network measures (such as density and average degree) capture essential characteristics of the network at different scales, while Miller, Bliss and Wolfe [38] aim to develop a general signal processing theory for networks (graphs).

The understanding and identification of the right temporal scale of dynamic networks is a nascent area of research. In this chapter, we formalize this problem and present some of its associated challenges. We also present an overview of existing methods for this problem, noting their advantages and limitations. Finally, we propose a conceptual framework designed to offer a common ground for translating empirical evidence, intuition and insight into a cohesive theory.

2 Related Work

Following is a brief review of related work in the areas of signal processing, information theory and time series analysis.

2.1 *Signal Processing and Information Theory*

Temporal aggregation is a natural pre-processing step when the frequency at which the data are generated is lower than the frequency at which the data are sampled. Usually the approach involves formulating a trade-off between loss of information and reduction of noise present in the signal. The goal in this context is to identify the window at which the original continuous signal can be fully recovered from the discretized signal. The Nyquist-Shannon sampling theorem [50] gives a necessary condition for the length of the sampling window in this context.

Minimum description length (MDL) is another information theoretic technique that is used to find the best granularity for data analysis [5, 20, 47]. In this context, information is defined in terms of its algorithmic complexity. It assumes that the best hypothesis for a given set of data is the one that leads to the largest compression. Several works have used MDL principle to learn the best model granularity. Identifying the intrinsic temporal scale of time series can be viewed as a special case of model granularity and there are a few approaches that apply the MDL concept directly to such data [24, 56]. In the next section we review the approach by Sun et al. [54] that applies the MDL concept to dynamic networks.

2.2 *Time Series Smoothing*

Smoothing techniques are prevailing in the domain of time series analysis. In this context, some of the variation in the data is assumed to be due to random noise. The goal of the smoothing techniques is, therefore, to cancel some of the variations and to reveal inherent properties of the time series, such as trends or seasonal and cyclic behavior. The two main groups of smoothing methods are the averaging methods and the exponential smoothing methods.

While the literature mentioned in this section offers a solid foundation on how to properly aggregate data for analysis, it does not explicitly address datasets that are represented as networks and, furthermore, it does not address the dynamic nature of these networks. In this chapter, we focus explicitly on understanding how the process of aggregation or smoothing of interaction streams affects the quality of dynamic network that we get.

2.3 *Temporal Scale for Dynamic Networks*

The problem of identifying the right temporal scale for dynamic networks has only recently started getting the deserved attention. James Moody explicitly points out the problem in [41]. Existing literature on the topic is preliminary and mainly of empirical nature. Clauset and Eagle [13] illustrate the effect of the aggregation window in understanding the periodic dynamics of the Reality Mining dataset [16]. They recommend the use of Fourier Transform analysis and auto-correlation analysis of time series of network measures. While these techniques have been successfully applied to understand stationary time series, their application to time series of measures originating from highly dynamic and complex networks might not be appropriate. It is not clear how the aggregation of time series of measures in networks relates to the underlying aggregation of interactions. Caceres et al. [10] theoretically show that for the special class of oversampled stationary processes and the special class of linear network measures (such as density and average degree), there is a direct relation between the two. We do not know, however, whether the same is true for more general dynamic network processes and network measures. Sulo, Berger-Wolf and Grossman [53] propose a heuristic that applies aggregation at the level of the dynamic network rather than at the level of time series of network measures in order to preserve as much of the network structure. They also give an explicit formulation of the optimal window of aggregation using the information theoretic framework.

The approach by Sun et al. [54] developed initially for the purpose of efficiently clustering dynamic networks consists of grouping similar network snapshots into one time-interval using the Minimum Description Length principle. The idea of compressing the graph to maintain only the more relevant aspects is very promising and relevant for the problem of aggregating at the right time scale and is similar to the approach in [53]. The contribution of the method by Sun et al. [54] is to use drastic changes in the time series of compression levels to segment the timeline of the temporal network. Rather than focusing explicitly on change detection, the goal of the research in [53] is more general, that is, identifying the inherent temporal scale that governs the overall dynamics of the network, as well as the changes in that scale.

However there is no definitive principled and rigorous framework for the problem of temporal scale for dynamic networks. Partially this due to the fact that problem itself has not been explicitly stated.

3 Problem Definition

We now formally define the main concepts that will be used throughout the chapter. We formalize the notion of a stream of interactions as a probabilistic process. We define the process of aggregation of interactions leading to a probabilistic dynamic

network. We further define special random interaction streams and corresponding networks. The definition of the optimal temporal scale for these streams is straightforward, yet stating these special cases explicitly allows us to gain further insight into more complex interaction streams. Finally, we formally state the **Temporal Scale Inference** (TSI) problem for dynamic networks.

3.1 Preliminary Definitions

In this section we present some basic definitions and descriptions of concepts and used throughout this thesis.

4 Definitions and Notation

Let V be a set of vertices and E the set of edges defined over $V \times V$. For $\forall e_{ij} \in E, i, j \in V$ and $t \in [1, \dots, T]$, the pair (e_{ij}, t) is the time labeled instance of e_{ij} .

Definition 1. A *temporal stream of edges* E_t is a sequence of edges ordered by their time labels:

$$E_t = \{(e_{ij}, t) | e_{ij} \in E, t \in [1, \dots, T]\}$$

Let \mathcal{P} be a partition of the timeline $[1, \dots, T]$:

$$\mathcal{P} = [t_0, t_1), [t_1, t_2), \dots, [t_k, T]$$

As a special case, we consider the *uniform partition* \mathcal{P}_ω , where each interval p_i has length ω :

$$\mathcal{P}_\omega = \{p_k\} \text{ s.t. } \forall p_k, |p_k| = \omega$$

Definition 2. A *dynamic graph* DG is a sequence of graphs defined over stream E_t and a fixed partition \mathcal{P} of E_t :

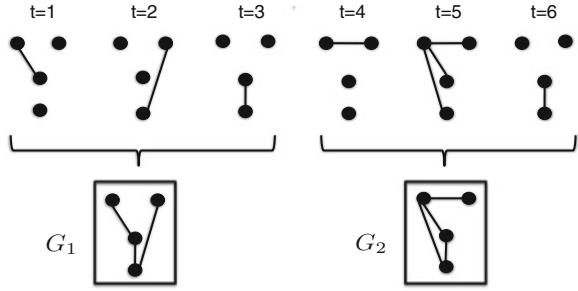
$$DG : \langle (V, E_t^k) \rangle$$

$$DG = \langle G_1, G_2, \dots, G_k, \dots, G_{|P|} \rangle$$

with $E_t^k = \{(e_{ij}, t) | e_{ij} \in E_t, t \in p_k\}$ and each G_k is associated with the k th interval p_k in \mathcal{P} .

We now define the operation of aggregation of a temporal stream of edges into the time series of graphs comprising a dynamic network. Given the temporal stream of edges E_t , and a fixed partition of the stream \mathcal{P} , we define the aggregation function that takes as an input the temporal stream of edges and the partition and outputs a time series of graphs.

Fig. 3 Aggregation of temporal edges with window of aggregation $\omega = 3$



Definition 3. An aggregation function A on a temporal stream E_t , and a fixed partition \mathcal{P} is defined as:

$$A : E_t \times \mathcal{P} \rightarrow \langle (V, E^k) \rangle$$

$$A(E_t, \mathcal{P}) = DG$$

The aggregation function A takes all the edges occurring in a stream within a time interval $p_k \in \mathcal{P}$ and constructs a graph. Consider the scenario when A is applied to the uniform partition \mathcal{P}_ω . Figure 3 shows an illustration of the aggregation function when the window of aggregation ω is three. Note, that edges can occur within each temporal window more than once, but they get represented in the corresponding aggregated graph at most once. Throughout this chapter, we use this definition for the aggregation function. Another possible extension to this definition of A could take the multiplicity of edge occurrence into account.

In a more general sense, an aggregation function could also use as a parameter a “goodness of fit” measure μ , that allows to map an interval $p_k \in \mathcal{P}$ to the best fit graph G_k^* with respect to μ :

$$A(E_t, \mathcal{P}, \mu) = \langle G_k^* \rangle$$

Note that in the general definition, G_k^* does not necessarily have to include all the edges that occur during p_k .

Let Q be a function that measures the quality of this dynamic graph:

$$Q : \mathcal{P} \times DG \rightarrow \mathbb{R}^+$$

Quality function Q maps the pair (\mathcal{P}, DG) to the set of non-negative real numbers so that these values capture how “good” the dynamic network is. Q can also be used to compare different dynamic network representations of the same temporal stream. The notion of the quality function is different from that of the objective function for a particular algorithm that generates a dynamic network. Thus, the use of quality function as a model selection tool allows us to use it for comparing different algorithms on the same data.

5 Problem Formulation

The abstraction and identification of the right temporal scale for transitioning from a dynamic stream of interactions into a meaningful and representative dynamic network is not a straight forward task. One natural way to define the “right” temporal scale of dynamic systems is as the scale of the inherent rhythm that governs their dynamics. Alternatively, one can argue that the definition of the temporal scale depends on the analysis objective for a given dynamic network. In either case, there is an implicit notion of a quality function that characterizes the optimal aggregation of the interaction stream. Ultimately the goal is to identify the temporal resolution that corresponds to either global or local optima of this quality function. With this in mind, we now formally define the Temporal Scale Inference problem:

Definition 4. TEMPORAL SCALE INFERENCE (TSI) PROBLEM: Given a temporal stream E_t and a quality function Q , find the partition \mathcal{P}^* of the timeline $[1, \dots, T]$, and the corresponding dynamic graph DG^* , that optimizes the quality function Q :

$$\langle \mathcal{P}^*, DG^* \rangle = \arg \max_{\mathcal{P}, DG} Q(\langle \mathcal{P}, DG \rangle).$$

Now that we have given the definitions, and stated the problem we are ready to discuss in more detail some results for the TSI problem.

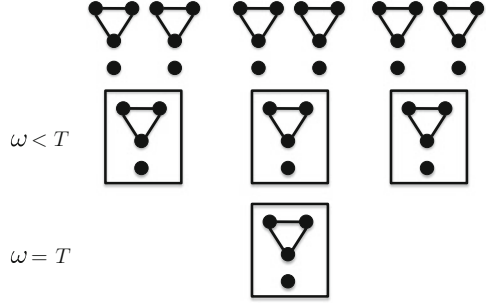
6 Special Cases of Temporal Interaction Streams

In this section, we study a collection of interaction streams for which we have some intuitive understanding on what is the “right” temporal scale. As we carefully define their generative processes and the properties they inherit, the goal is to understand more rigorously, and gain insight into what happens as we aggregate the streams at different temporal scales. We discuss examples ranging from the very simple constant stream with no temporal scale, to realistic interaction streams coming from real-world data. Each one of the examples touches on different aspects of temporal scale and helps us formalize the notion the “right” temporal scale.

6.1 Constant Streams

Constant streams are the simplest possible temporal streams and one might even argue whether they are indeed temporal at all. They are streams where the same set of interactions occurs at each time step. The corresponding static graph SG is defined as follows:

Fig. 4 Aggregation of a static stream at different levels of aggregation



Definition 5. *Static Graph (SG)* is the graph $G(V, E', p)$ defined over the set of nodes V and the set of edges $E' \subseteq V \times V$. Each edge in this graph occurs with probability $p = 1$ at any time t :

$$\forall (e_{ij}, t) \in E' \subseteq V \times V, \quad Pr[(e_{ij}, t) \in G] = 1$$

Clearly there is no dependence on time and no algorithm should choose a particular temporal scale other than the entire time line. More explicitly, as illustrated in Fig. 4, any aggregation of the constant stream over any aggregation window will produce a network identical to the original stream.

A more interesting case of a “stream with no temporal scale” is the stream where the set of interactions that appear at each step is not constant, yet, the occurrence of each interaction does not depend on time.

6.2 *DynUR Stream*

We define the *Dynamic Uniform Random Graph (DynUR)* as the graph where each edge occurs at any time uniformly at random with probability p . This is the temporal equivalent of the Erdős-Rényi graph.

Definition 6. *Dynamic Uniform Random Graph (DynUR)* is the graph $G(V, E_t, p)$ with a constant probability $0 \leq p \leq 1$ for all edges:

$$\forall (e_{ij}, t) \in \langle E, T \rangle \quad Pr[(e_{ij}, t) \in G] = p.$$

Consider what happens when the aggregation function A (Definition 3) is applied to the *DynUR* stream with aggregation window ω . The result is a time series of graphs, which we call $DynUR_\omega = A(DynUR, \mathcal{P}_\omega)$. Intuitively it is clear that the $DynUR_\omega$ graph is generated by a process with no temporal dependencies or correlations. This is true for any window of aggregation ω , therefore, such a graph

becomes a perfect candidate for a network that has no temporal scale. Sulo et al. [10] give several characterizations of this model. At any temporal scale, the resulting dynamic network is a time series of *ER* graphs and, therefore, topologically the dynamic network is a time series of probabilistically identical in time. Also, any permutations of the times of edges occurrences does not have any effect on the probabilistic topology of the dynamic network. These characterizations all point to the important property: no temporal scale is qualitatively better than any other for analyzing the *DynUR* temporal stream. The picture changes when processes that have an embedded temporal structure (e.g. periodicity) are analyzed at different temporal scales. In such cases, inherent structural properties of the dynamic network only emerge at specific scales and not all scales carry this property [10].

In general, a null model provides a baseline and a sanity check for evaluating any algorithm claiming to solve a problem or assessing the significance of any discovered pattern. For static networks, the Erdős-Rényi graph has been used as the simplest null model [17]. It is a simple graph where each edge occurs independently at random with the same probability p . This model generates a network where each vertex has the same expected degree. More sophisticated null models that can approximate the skewed degree distribution of empirical networks [4] have been proposed by Molloy and Reed [39,40], and later on by Chung-Lu [12].

The definition of the null model becomes more complicated when we add time. In addition to correctly representing the relevant topological structure of the network, these models need to incorporate aspects of the temporal structure such as order, concurrency, and delay of interactions, among others. Null models for temporal networks have been proposed by Holme [22] and Karsai [14,26]. They use temporal reshuffling as a tool to generate streams where different aspects of temporal structure get randomized. Holme and Karsai discuss these null models in the context of analyzing processes, such as spread of a virus or information, over the temporal stream (to which they refer to as the contact sequence). Holme in [23] points to the issue that scale plays a role in capturing the critical temporal correlations:

... there are several kinds of possible temporal correlations and several time scales where the correlations are important, and thus no single, general-purpose null model can be designed (the temporal configuration model). Rather, by designing appropriate null models, one may switch off selected types of correlations in order to understand their contributions to the observed time-domain characteristics of the empirical temporal network.

In the absence of knowing the right temporal scale for the given temporal stream or the spread process over it, permutations at all the scales need to be tried and tested in order to generate the relevant null model. A null model is a way to test the importance of structure found at any given scale. It does not allow us, however, to find the temporal scale (or scales) in and of itself. We can use a null model in conjunction with a quality function to do so. In Sect. 7 we formalize and generalize this observation for any quality function.

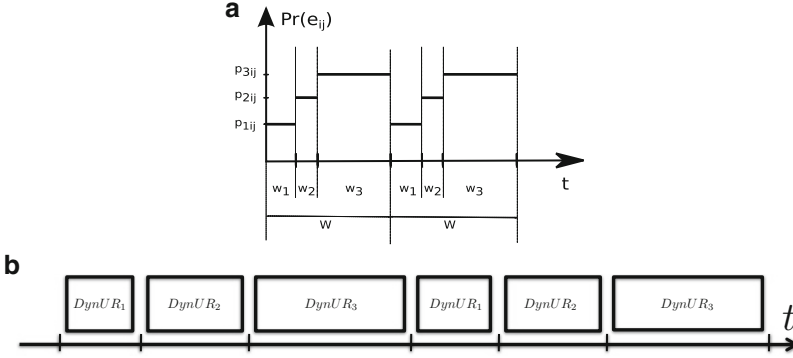


Fig. 5 Illustration of two cases of *DynMix* graph with three alternating probability distributions ($M=3$). (a) Illustrates Case 1 of *DynMix*, with a cycle of constant probabilities, and (b) illustrates Case 2 of *DynMix*, with a cycle of random graphs

6.3 Structured Temporal Streams

6.3.1 Periodic Stream

We will now consider periodic streams for which we expect the period to be related to the concept of the “right” temporal scale. We give a general definition of the corresponding probabilistic graph, the *Dynamic Mixture* (*DynMix*) graph.

Definition 7. *Dynamic Mixture Graph* ($DynMix_{M,\{w_l\}}$) on M fixed probability distributions $\{P_l\}_{l=1}^M$ and a set of temporal windows $\{w_l\}_{l=1}^M$ with $W = \sum_{l=1}^M w_l$, is the graph $G(V, E_t, P_l)$ where:

$$\forall (e_{ij}, t) \in E_t, \quad \Pr[(e_{ij}, t) \in G] = p_{lijt}, \quad l = \text{mod}_M \left\lfloor \frac{t}{W} \right\rfloor.$$

The Dynamic Mixture Graph is a repeating sequence of dynamic graphs.

Consider two special cases for the probability distribution functions generating the $DynMix_{M,\{w_l\}}$ graph:

Case 1. A sequence of constant probability distribution P_l , so the probability of an edge e_{ij} does not depend on the time index t :

$$\Pr[(e_{ij}, t) \in DynMix_{M,\{w_l\}} | (e_{ij})] = p_{lij}.$$

Figure 5a gives an illustration of such a Dynamic Mixture Graph when the number of repeating probability distributions M is 3.

Case 2. A sequence of *DynUR* graphs, where for any given probability distribution P_t , and a given time index t , the probability of all edges e_{ij} at t is the same:

$$Pr((e_{ij}, t) \in \text{DynMix}_{M, \{w_l\}} | t) = p_t \quad \forall i, j \in V.$$

Figure 5b gives an illustration of such a Dynamic Mixture Graph with $M = 3$.

Note that *DynUR* can be viewed as a special instance of both Case 1 and Case 2 of the $\text{DynMix}_{M, \{w_l\}}$ graph with $p_{lij} = p_t = p$ for all tuples $\{l, i, j, t\}$. Sulo et al. [10] showed that for a periodic stream, a linear function on the corresponding dynamic graph becomes stationary at specific windows of aggregation. These windows of aggregation correspond to the period (or any multiple of the period) of the underlying edge probability process.

6.3.2 Stationary Stream

One of the most intuitive properties that we want the dynamic network to have is stability or stationarity [8, 32]. In physics this property is typically referred to as steady state, while in statistics it is called stationarity. Whether we are trying to identify long term trends or typical behavior, or whether we want to predict new behavior, a stable system is a necessary condition for a meaningful analysis if we wish to infer something about the system from a history of observations. Furthermore, as perturbation analysis has increasingly become a powerful tool for untangling the complex structure of networks [22, 26], it is important to apply such analysis over a stable system. Otherwise, it is difficult to distinguish between changes due to the instability of the systems and changes due to the perturbation [8]. Stability is a property analyzed extensively in the context of numerical time series. The interest here is to understand this property in the context of temporal interaction streams. Ultimately, the goal is to be able to identify aggregation levels (temporal scales) of the interaction stream so that the corresponding dynamic system represents a system in a steady state and, therefore, appropriate for analysis.

In this chapter, we will use the statistical definition of stability. More precisely, we define a stationary probabilistic function that generates the temporal stream.

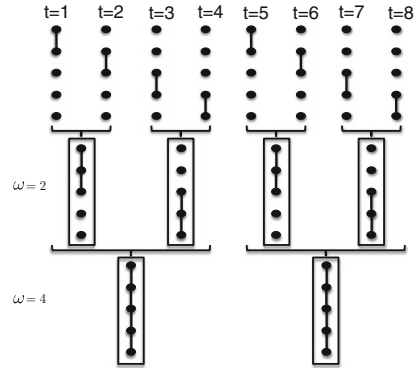
Let $P_t = Pr[(e_{ij}, t) \in E_t]$ be the general case of a (weak) stationary probability distribution function generating the stream of edges $E_t = \{(e_{ij}, t), e_i j \in E, t \in [1, \dots, T]\}$. That is,

1. $\mathbb{E}[p_{ijt}] = \mu_{ij}$, s.t. μ_{ij} does not depend on t .
2. $Cov(p_{ijt}, p_{ij(t+\tau)}) = \gamma_{ij}$, s.t. γ_{ij} does not depend on t .

6.3.3 Theseus Ship Stream

So far we have discussed streams whose structure is stable over time. We now turn our attention to a stream that appears to be stable, yet it changes slowly over time.

Fig. 6 Aggregation of Theseus Ship stream at different scales. The original Theseus Ship stream has no interactions as the base set and one interaction changes every time step



What kind of issues does a stream like this introduce to our problem of scale? The notion of an object changing slowly over time is an old one, and is illustrated by the Theseus Ship paradox [49].

The ship wherein Theseus and the youth of Athens returned [from Crete] had thirty oars, and was preserved by the Athenians down even to the time of Demetrius Phalereus, for they took away the old planks as they decayed, putting in new and stronger timber in their place, insomuch that this ship became a standing example among philosophers, for the logical question of things that grow; one side holding that the ship remained the same, and the other contending that it is not the same. [Plutarch, Life of Theseus]

The Theseus Ship paradox raises the question of whether the identity of an object fundamentally changes when all of the object's components have changed. Many great minds from ancient Greece to the present have struggled to find the right answer to the dilemma posed by this paradox. A translation of the Theseus Ship paradox in the framework of dynamic networks has been discussed in [57] to describe the notion of communities whose members change over time.

There is an analog of this paradox in the context of temporal interaction streams. Consider a process, where every k time steps, the same set of interactions occurs, except for a small change; one of the occurring interactions is replaced with a new interaction (illustrated in Fig. 6). After enough time steps, the initial set of interactions is replaced completely with a new set of interactions. The question that arises here is "What is the right temporal scale for aggregating such a stream?" At a fine temporal scale we observe change that is too gradual. At the same time, we are able to capture the persistence structure of the network. At a coarser temporal scale, we will lose this persistence structure, but we will be able to identify periodicity. This is a good example of the complexity of the definition of the "right" temporal scale. The dichotomy of persistence versus periodicity motivates the position that the definition of the "right" temporal scale is context- and question-specific. Furthermore, the aggregation the Theseus Ship stream illustrates the multi-scalar nature property of temporal streams. Depending on the magnitude of change we want to observe in such a stream, different levels of aggregation are suitable for the analysis.

6.3.4 Oversampled Stream

Another property of the streams that is critical for the TSI problem is the oversampling property. The assumption that the process is oversampled is a natural one for any good data set. An under-sampled process cannot be guaranteed to contain sufficient information for analysis, by definition. Furthermore, given the pervasiveness of fast and automated data collection systems, oversampling is more of a realistic property rather than a wishful one. It does, however, introduce some unwanted side effects, such as artificial time orderings and spurious patterns. Naturally, we are interested in identifying aggregation levels of the stream that take the oversampling factor into consideration. At such temporal scale, the oversampling noise has been smoothed out, and the corresponding dynamic network is a true representative of the underlying dynamics. Specifically, if we have an existing stream where we know the optimal window of aggregation is ω , then, intuitively, if we over-sample by a factor of α , the new optimal window of aggregation should be $\alpha\omega$. Although the size of the window of aggregation changes proportionally to the oversampling factor, the process of finding the optimal window should not be sensitive to the oversampling factor. In this sense, uniformly modifying the frequency of interactions should not affect the relative temporal distances between interactions.

We now formally define the process of oversampling of interaction streams. Let $P_t = Pr[(e_{ij}, t) \in E_t]$ be the probability distribution function generating the stream of edges $E_t = \{(e_{ij}, t), e_{i,j} \in E, t \in [1, \dots, T]\}$.

Definition 8. An α -stretching mapping ϕ_α of the time line $[1, \dots, t, \dots, T]$, where $\alpha > 0$, is defined as follows:

$$\phi_\alpha : [1, \dots, t, \dots, T] \rightarrow [1, \dots, t', \dots, \alpha T]$$

$$t' = [t\alpha - (\alpha - 1), t\alpha - (\alpha - 2), \dots, t\alpha]$$

Definition 9. An oversampled probabilistic interaction process $P_{t'} = Pr[(e_{ij}, t') \in E_{t'}]$, over the time sequence $t' \in [1, \dots, \alpha T]$, and probability function $P_{t'}$, is defined as follows:

$$P_{t'} = P_{\phi_\alpha(t)} = \frac{1}{\alpha} P_t$$

An illustration of a simple oversampled periodic stream is given in Fig. 7. Note an oversampled periodic stream is still periodic (in this case the period is $W = 2$, and the oversampling factor is $\alpha = 3$). The right scale for such a process takes into account the oversampling rate and recaptures what is essential about this process, whether that is the alternating change ($\omega^* = \alpha \frac{W}{2} = 3$) or the stationarity ($\omega^* = \alpha W = 6$).

Throughout this chapter, we are assuming oversampling at a uniform rate. In reality, data and the processes they represent are messy and oversampling could happen at nonuniform rates.

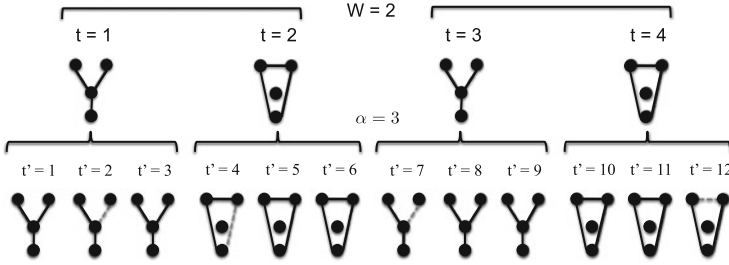


Fig. 7 Oversampled periodic stream

6.3.5 Noisy Stream

Similar to the definition of structure in dynamic networks, noise comes in two flavors: topological and temporal. Topological noise has to do with the presence or absence of an observed interaction (or a set of interactions) that does not reflect the behavior of the underlying system. The addition of time adds to the complexity of noise in dynamic networks. Specifically, the occurrence time of an interaction could be noisy as well as the ordering of this occurrence time with respect to that of other interactions. Alternatively, we can view noise as the antithesis of structure. In this context, we discussed in Sect. 6.2 the characteristics for the *DynUR* stream, the completely structureless stream.

In general, the topological and temporal aspects of noise are coupled in ways that make it difficult to analyze them individually. Yet, throughout Sect. 6, we attempt to state the characteristics of temporal noise more explicitly. In Sect. 6.3.6, we analyze a simple case of temporal noise, by introducing gaussian noise to the temporal probabilities of each interaction. In addition, we use perturbation analysis as a way to detect noisy temporal orderings of interactions. Clearly, in real-world datasets, noise is generated by much more complex models and can have other manifestations that we do not consider in this chapter. In addition, we would expect the magnitude of noise to have an effect on the “right” level of aggregation. We would expect that, at some threshold, the large magnitude of noise overwhelms structure and the stream essentially becomes the *DynUR* stream. Despite the fact that we do not address these aspects of noise explicitly, they provide interesting and important directions for future work.

6.3.6 Oversampled, Noisy Stationary Stream

A periodic process is just one example of a stationary process. Now that we have also discussed oversampled and noisy streams individually, we can discuss a much more general class of interaction streams: the oversampled noisy stationary streams.

Let $P_t = Pr[(e_{ij}, t) \in E_t]$ be the general case of a (weak) stationary probability distribution function generating the stream of edges $E_t = \{(e_{ij}, t), e_i, j \in E, t \in$

$[1, \dots, T]$. An *oversampled noisy probabilistic process* $P_{t'} = Pr[(e_{ij}, t') \in E_{t'}]$ over time sequence $[1, \dots, t', \dots, \alpha T]$, and probability function P_t , is defined as follows:

$$P_{t'} = \frac{1}{\alpha} P_t + \epsilon,$$

with $\epsilon \in N(0, \sigma)$ representing Gaussian noise.

Caceres et al. [10] showed that for the class of oversampled, stationary, noisy interaction streams, a linear function on the corresponding dynamic graph becomes stationary at specific windows of aggregation. These windows of aggregation correspond to the multiple of the oversampling rate.

7 Axiomatic Framework: Desired Properties of the Quality Function Q

In Sect. 6, we demonstrated some intuitive properties one would expect to observe for temporal streams. We showed that for a stream with no temporal scale, the re-ordering of interactions along the time line had no effect on the resulting dynamic network. We described some simple cases of interaction streams (e.g. *DynUR* and constant stream) for which we have a clear understanding of the right temporal scale. Finally, we illustrated the effect of oversampling on the aggregation of different temporal streams and how it intuitively relates to the notion of the “right” temporal scale.

We now propose an axiomatic approach to capture this collection of insights in a formal way and to allow future rigorous analysis of the TSI problem. The axiomatic approach has recently gained a lot of interest in the field of spatial clustering. Similar to the TSI problem, the goal of spatial clustering is to postulate important sets of properties both in terms of the optimal partitioning [30], and in terms of the qualitative functions over such partitions [1, 6]. The axiomatic view has also been applied to the analysis of graphs in the context of graph clustering [37] and graph complexity [9].

The TSI problem shares many of the characteristics and challenges of the clustering problem, both in metric and non-metric space, yet an axiomatic framework that synthesizes the characteristics of the TSI problem is lacking.

8 Axiomatic Framework: Desired Properties of the Quality Function Q

In the formulation of the TSI problem in Sect. 5, we defined the optimal temporal scale through the proxy of the quality function. This shifts the burden from finding the “real” temporal scale to optimizing the quality function. Ideally the two are the

same. *What properties, then, should the quality function possess in order to correctly reflect the behavior of the underlying temporal scale?*

Here we present a set of axioms that delineate desired properties of the quality function Q . Let Ω be the set of all temporal streams E_t defined over the fixed set of vertices V and the finite time line $[0, \dots, T]$. Since V is a fixed set and $[0, \dots, T]$ is finite, there is a finite number of temporal streams in Ω , and therefore, Ω is a discrete probability space. Let \mathcal{A} be a *TSI* algorithm, that takes as input a temporal stream E_t and outputs a set of pairs $\langle \mathcal{P}, DG \rangle$ as solutions:

$$\mathcal{A} : \{V \times V, [1, \dots, T]\} \rightarrow \{\langle \mathcal{P}, DG \rangle\}$$

We can then think of Q as a random variable defined over the set $\{\langle \mathcal{P}, DG \rangle\}$. The range of Q is $[0, Q^*]$, where Q^* is the maximal value of quality associated with a specific partition \mathcal{P} of E_t , and the corresponding dynamic network DG .

$$Q : \Omega \rightarrow \mathbb{R}^+$$

Let Φ be a transformation function on the temporal stream E_t :

$$\Phi : E_t \rightarrow E_t.$$

An example of a transformation function is the permutation function π defined as follows:

Definition 10. Given a temporal stream E_t , a fixed partition \mathcal{P} of the stream, a *probabilistic permutation function* π picks a pair of edges $\langle (e_{i_1 j_1}, t_l), (e_{i_2 j_2}, t_k) \rangle$, at random from E_t and swaps their timestamps:

$$\begin{aligned} \pi : E_t &\rightarrow E_t \\ \langle (e_{i_1 j_1}, t_l), (e_{i_2 j_2}, t_k) \rangle &\rightarrow \langle (e_{i_1 j_1}, t_k), (e_{i_2 j_2}, t_l) \rangle \end{aligned}$$

We consider two special cases of function π :

- The *within-interval* permutation function π_w chooses the pair of edges from the same interval $p_i \in \mathcal{P}$ such that $t_l, t_k \in p_i$.
- The *across-interval* permutation function π_a chooses the pair of edges from two different intervals $p_i, p_j \in \mathcal{P}$ such that $t_l \in p_i$ and $t_k \in p_j$.

The goal of the following axioms will be to characterize the change in the quality of dynamic network DG defined over a given temporal stream E_t due to transformation function Φ . Let $\epsilon \geq 0$ represent a fixed threshold parameter characterizing the amount of change in quality. If the change is less or equal ϵ , we consider the change ‘‘small’’. Let $\delta \geq 0$ be a confidence parameter about the probability of the change in Q being small. We are now ready to formally define the axioms.

[Q1] Within Interval Order Invariance: *For an optimal partition, permutations of interactions within the same interval do not drastically change the quality of the dynamic graph.*

Formally, let \mathcal{P}^*, DG^* be the optimal (with respect to a particular quality function Q) partition and the optimal dynamic graph for the temporal stream E_t . Let $\mathcal{P}^{*'}, DG^{*'}$ be the optimal partition and optimal dynamic graph corresponding to the perturbed stream $E'_t = \pi_w(E_t, \mathcal{P}^*)$. Then, with high probability, the change in the quality function after the perturbation is small:

$$\forall \pi_w, \forall p_i \in \mathcal{P}^*, P(|Q(DG^*) - Q(DG^{*'})| \leq \epsilon) \geq 1 - \delta.$$

Intuitively, the process of aggregating temporal interactions into a dynamic graph has the effect of assigning the same time to interactions within each partition, while preserving the temporal ordering across partitions. At the optimal temporal scale, the temporal ordering of interactions that fall within the same partition is not essential. The fact that, locally, some interactions are observed as happening in a particular order is an artifact of looking at them at too fine of a temporal resolution. They could have happened in any order as long as they happened within a certain time frame.

[Q2] Across Interval Order Criticality: *For an optimal partition, permutations of edges across different intervals change the quality of the partition.*

Formally, we define the neighborhood of a given interval $p_i \in \mathcal{P}$ the following way:

$$N(p_i) = \{p_j \mid |i - j| \leq r, r > 0\}.$$

Let $DG^{*'}$ be the optimal dynamic graph corresponding to $E'_t = \pi_a(E_t, \mathcal{P}^*)$: Then, with high probability, the change of the quality function after the permutation is substantial:

$$\exists \pi_a, \forall p_i \in \mathcal{P}^*, p_j \in N(p_i), P(|Q(DG^*) - Q(DG^{*'})| > \epsilon) \geq 1 - \delta.$$

Intuitively, at the optimal temporal scale, the temporal ordering of sets of interactions across the partitions is crucial and reflects the time dependence of the network structures. While this might not be true for all edges, there must exist a subset of interactions for which the ordering is critical. Otherwise, time does not play a role in the structure of the interactions.

[Q3] Measure Unit Invariance: *Uniform scaling of the oversampling factor does not change the quality of the dynamic network.*

Formally, let E_t and E'_t be two temporal streams generated by oversampling the same underlying process at rates α and α' , such that $\alpha \neq \alpha'$. Let DG^* and $DG^{*'}$ be the optimal dynamic graphs for E_t and E'_t respectively. Then, with high probability, the change in the quality function is small:

$$P(|Q(DG^*) - Q(DG^{*'})| \leq \epsilon) \geq \delta.$$

This axiom bears resemblance to the scale invariance axiom in spatial clustering. In this context, the partitioning of the data into clusters does not depend on the units of the distance function. The oversampling invariance axiom represents an analogous intuition: oversampling rate is a measure of the time unit used to measure how far apart interactions occur along the timeline. In this sense, uniformly modifying the frequency of interactions should not affect relative temporal distances between interactions.

[Q4] Constant Stream: *The constant stream has no time scale, the optimal partition is the whole timeline.*

A constant stream is the stream for which the same set of edges occurs at every time step. Let DG be a dynamic graph over the constant stream. Let DG' be a coarsening of DG . Then, the quality function of the coarsening is better:

$$\forall DG, DG', Q(DG) < Q(DG').$$

Consequently, the optimal DG^* with respect to the quality function Q on the constant stream is the aggregation of the whole timeline.

[Q5] Stream with no Temporal Scale: *The quality function is the same for any partition of the stream with no temporal scale.*

Formally, let DG and DG' be any two dynamic networks corresponding to any two partitions \mathcal{P} and \mathcal{P}' of the stream with no temporal scale. Then, the quality function of the two dynamic networks should not be different:

$$\forall DG, DG', |Q(DG) - Q(DG')| \geq \epsilon.$$

[Q6] Temporal Shift Invariance: *A shift of the time line of a temporal stream, does not drastically change the quality of the dynamic network. The optimal partition of the stream is independent of the time line's starting point.*

Formally, let $[0, \dots, T]$ be the time line of the temporal stream E_t . Let $[\Delta, \dots, T + \Delta]$ be the new timeline shifted by parameter $\Delta > 0$. Let DG^* represent the optimal dynamic network for E_t and $DG^{*'}$ be the optimal dynamic network for the shifted temporal stream. Then, the change of the quality function due to the shift is small:

$$|Q(DG^{*'}) - Q(DG^*)| < \epsilon.$$

An interval in a partition of the stream identifies a temporal cohesive unit in the dynamic network, similar to the notion of a building block. It is more important that interactions happen a specific time apart rather than where in the stream they happen. Temporal shift invariance is a strong assumption, considering the absolute time dependency of complex systems. For example, empirical analysis of mobile phone calls [32] shows that, especially for a finer time scale, the start time of the partition matters a lot. In general, it is of great interest to characterize interaction streams (and their generative mechanisms) that are independent of the start time, and those streams that are highly sensitive.

Axioms [Q1] and [Q2] view the underlying dynamic process and the temporal structure it contains as a sequential process. These axioms specify when the ordering of the interactions matters and when it is just temporal noise. Axioms [Q3] through [Q5] are formalizations of some intuitive observations about the TSI problem. As a collection, axioms presented here are not exhaustive of all the properties characterizing the temporal scale of interaction streams. Yet, these axioms provide a starting point for formally addressing the TSI problem in a rigorous and consistent manner. The axioms serve as external evaluators of the quality of a dynamic network, in the sense that they do not depend on the type of the partitioning algorithm used, objective function, or the generative process of the temporal stream. Therefore, the usefulness of the axiomatic framework is two-fold. The framework can be used to:

1. Evaluate the performance of a partitioning algorithm in a unbiased way.
2. Provide a taxonomy of different partitioning algorithms.

9 Heuristics for the TSI Problem

We conclude this chapter with two heuristics for the TSI problem. We have already discussed the very few approaches for inferring the temporal scale of an interaction stream. We now present in greater detail two heuristics that follow more closely the formalism of the TSI problem. These are by no means the best solutions for the problem, but they are the best to date and take a very different route to solving the problem. We hope they would serve as a starting point and a foundation for a variety of practical techniques for solving the TSI problem. Both heuristics are based on ideas from information theory. The concept of “information” embedded in interaction streams is general and includes the notion of persistence of structure as a special case. Patterns that persist for awhile truly represent what is more “essential” for the underlying system. In social network analysis, one point of view considers persistent interactions over time as defining more complex sociological structures such as relationships or kinship [41]. In another context, the notion of persistence is critical in extending the static definition of communities to that of dynamic communities [57]. Finally, persistence is a property that allows us to construct a network with the “core” interactions, discarding the noisy transient interactions. Therefore, the notion of persistence lends itself to yet another formulation of the “right” temporal scale: the temporal scale that best captures the persistent nature of the underlying complex system.

Following, we give a summary of the TWIN (Temporal Window In Networks) [53] and GraphScope heuristic [54]. TWIN takes the approach of looking at the temporal scale as a global inherent characteristic of the interaction stream. Graphscope on the other hand, takes an objective-specific approach by identifying levels of aggregation where drastic changes in the structure of the stream are easier to identify.

Fig. 8 Illustration of computation of variance and compression ratio for a given level of aggregation (ω), and a given graph-theoretic measure d (diameter)

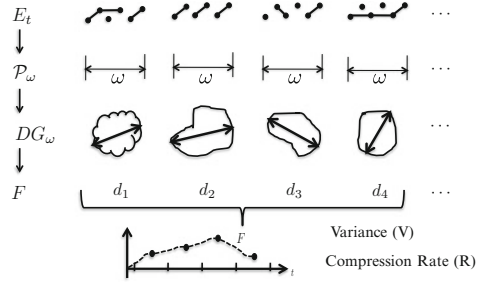
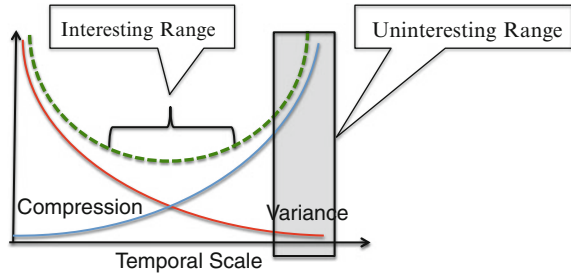


Fig. 9 Trade-off plot of variance and compression measures



9.1 TWIN

The TWIN (Temporal Window In Networks) heuristic uses graph-theoretic measures as proxies of different aspects of network structure. Given a temporal stream of edges and a graph-theoretic measure (Fig. 8), the heuristic generates time series of graphs (dynamic graphs) at different levels of aggregation. It then computes the variance and compression ratio for each time series. Finally, the algorithm analyzes the window size for which the variance is relatively small and compression ratio is relatively high.

Variance and compression ratio are not mathematical compliments of each other, but they do have opposite behavior as functions of window size. As illustrated in Fig. 9, when we increase the value of ω , we expect the variance to decrease and compression rate to increase. There is a region in Fig. 9 where variance is very small and compression is very high. However, low variance and high compression in this region are achieved artificially by aggregating the underlying stream at too coarse a scale, so that all the critical temporal information is removed. We call the range of window sizes that fall in this region *uninteresting*. Instead, there is a range of window sizes for which we can expect both relatively low variance and relatively high compression levels of time series F_ω . This insight allows TWIN to formulate the process of finding the range of appropriate discretization window sizes

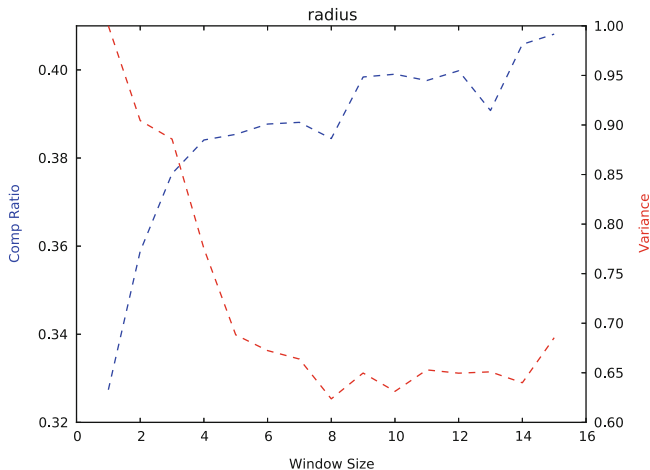


Fig. 10 TWIN’s trade-off plot of variance (V) and compression rate (R) of network radius with respect to window size ω (in days)

as a search problem guided by the values of variance and compression (Fig. 10). Figure 11 gives an illustration of TWIN’s results for the Enron dataset [51].

9.2 Graphscope

Graphscope uses the notion of compression cost to capture the persistence of network structures (in this case of communities) in time [54]. Similar graph snapshots will incur low compression cost, therefore they can be grouped together in one temporal segment. Whenever the compression cost increases substantially with the addition of a new graph snapshot, Graphscope starts a new temporal segment. Figure 12 shows the relative difference in compression cost between grouping consecutive temporal segments versus starting a new temporal segment for the Enron dataset. High peaks in this plot correspond to key events of the Enron corporation during the period of January 2002 [54].

9.3 Comparison of TWIN and Graphscope

Since GraphScope focuses on variations of graph compression levels, it is the magnitude of change in the graph structure that drives the timeline segmentation. TWIN analyzes the regularity of compression levels of different metrics on the graph, and therefore, it is the *rate of change*, not the *magnitude*, that will have the most affect in the aggregation.

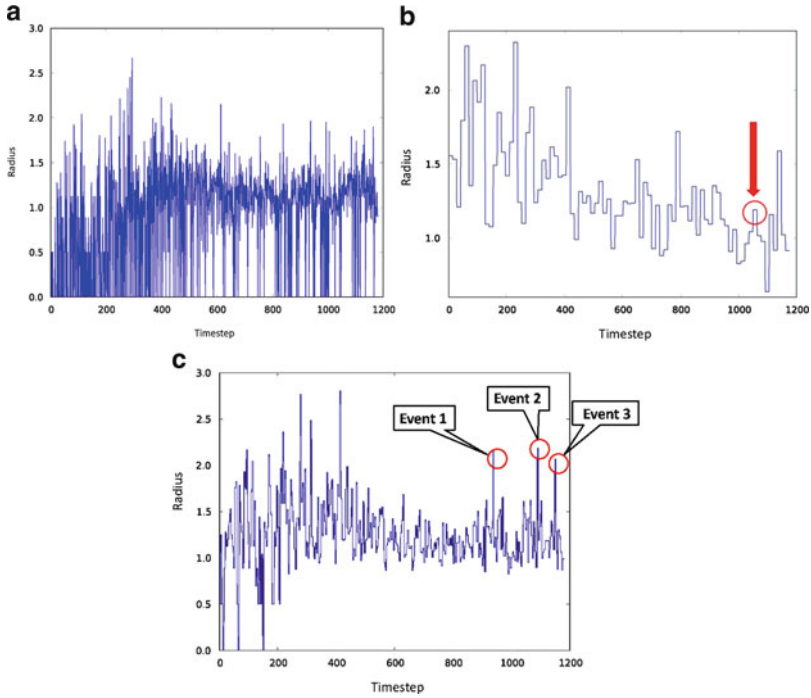


Fig. 11 Network radius time series for the Enron dataset at three levels of aggregation: **(a)** fine level of aggregation, $\omega = 1$ day, **(b)** coarse level of aggregation, $\omega = 12$ days, **(c)** the right level of aggregation, $\omega = 4$ days. The three important events (Karl Rove selling off his energy stocks (Event 1), the unsuccessful attempt of Dynegy to acquire the bankrupt Enron (Event 2), beginning of the FBI investigation (Event 3)) can be discerned only at the right level of aggregation. They are obscured by noise at too fine level of aggregation and smoothed out at the coarse level of aggregation

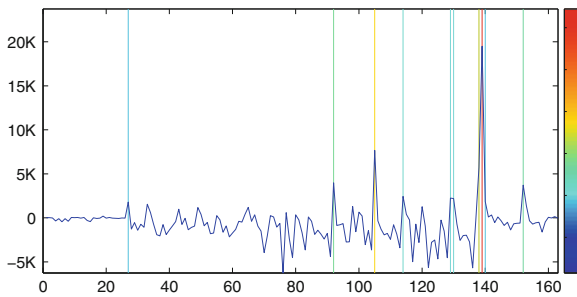


Fig. 12 Relative compression cost versus time for the Enron dataset. Large cost indicates change points which coincide with key events (with red representing maximal values of change). Vertical lines on the plot correspond to top ten change points. Reprinted with authors' permission

A nice feature of the Graphscope heuristic is the fact that it generates a non-uniform partitioning of the timeline. The non-uniform partitioning is a more realistic representation of real-world interaction streams which are commonly characterized by bursty behavior [3, 31]. On the other hand, Graphscope determines this partitioning for a fixed aggregation step and it does not take into account the affect the aggregation step has on the computation of the compression cost. The estimation of persistent structures leading to the low compression costs is highly sensitive on the size of aggregation level. TWIN overcomes this dependency by analyzing the persistent nature of the stream across different scale, and picking those scales where persistence is more pronounced.

10 Conclusions and Future Outlook

There is both the intuitive understanding and the mounting amount of evidence that temporal scale of an interaction stream plays an important role in the analysis of that stream. Moreover, it is clear that many streams have a set of relevant scales and that those may change over time. Some of the scales are inherent to the dynamics of the interactions, while others are only relevant depending on the context of the analysis performed on the stream. All of this makes the problem of identifying and inferring the temporal scale of interaction streams important. All of this also make the problem elusive and maddeningly difficult to state.

In this chapter we brought together the various interpretations of the concept of temporal scale and pointed out the evidence that supports those interpretations. We formalized the problem of the temporal scale inference and its properties, and discussed several existing approaches for solving the problem.

The problem of temporal scale inference is very new. The few existing approaches to stating or solving it are just the beginning. Every research direction in this area is open. We hope this chapter brings the problem to the forefront of research consciousness, makes the problem explicit, and provides the tools for making progress in this area. Understanding the rhythm of interacting systems is not only necessary for the proper analysis of these systems, but will provide us with the fundamental insight into what makes these systems tick. It is an important, challenging, and worthy endeavor.

References

1. Ackerman, M., Ben-David, S., Loker, D.: Towards property-based classification of clustering paradigms. In: Lafferty, J., Williams, C.K.I., Shawe-Taylor, J., Zemel, R.S., Culotta, A. (eds.) *Neural Information Processing Systems*, pp. 10–18 (2010). <http://nips.cc/>
2. Baldock, K., Memmott, J., Ruiz-Guajardo, J., Roze, D., Stone, G.S.: Daily temporal structure in african savanna flower visitation networks and consequences for network sampling. *Ecology* **92**, 687–698 (2011)

3. Barabasi, A.L.: *Bursts: The Hidden Pattern Behind Everything We Do*. Dutton, New York (2010)
4. Barabási, A.L., Albert, R.: Emergence of scaling in random networks. *Science* **286**(5439), 509–512 (1999)
5. Barron, A.R., Rissanen, J., Yu, B.: The minimum description length principle in coding and modeling. *IEEE Trans. Inf. Theor.* **44**(6), 2743–2760 (1998)
6. Ben-David, S., Ackerman, M.: Measures of clustering quality: a working set of axioms for clustering. *Neural Information Processing Systems*, pp. 121–128 (2008)
7. Bender-deMoll, S., McFarland, D.A.: The art and science of dynamic network visualization. *J. Soc. Struct.* **7**(2), 1206–1241 (2006)
8. Blonder, B., Wey, T.W., Dornhaus, A., James, R., Sih, A.: Temporal dynamics and network analysis. In: *Methods in Ecology and Evolution*, pp. 958–972. Blackwell Publishing Ltd., Oxford (2012)
9. Butts, C.T.: An axiomatic approach to network complexity. *J. Math. Sociol.* **24**, 273–301 (2000)
10. Caceres, R.S., Berger-Wolf, T., Grossman, R.: Temporal scale of processes in dynamic networks. In: *IEEE 11th ICDM Workshops*, pp. 925–932 (2011)
11. Chapanond, A., Krishnamoorthy, M., Yener, B.: Graph theoretic and spectral analysis of enron email data. *Comput. Math. Organ. Theor.* **11**, 265–281 (2005)
12. Chung, F., Lu, L., Vu, V.: Spectra of random graphs with given expected degrees. *Proc. Natl. Acad. Sci.* **100**(11), 6313–6318 (2003)
13. Clauset, A., Eagle, N.: Persistence and periodicity in a dynamic proximity network. In: *DIMACS Workshop on Computational Methods for Dynamic Interaction Networks*. DIMACS, Piscataway (2007)
14. Clauset, A., Shalizi, C.R., Newman, M.E.J.: Power-law distributions in empirical data. *SIAM Rev.* **51**(4), 661–703 (2009)
15. Cross, P.C., Lloyd-Smith, J.O., Getz, W.M.: Disentangling association patterns in fission-fusion societies using african buffalo as an example. *Anim. Behav.* **69**, 499–506 (2005)
16. Eagle, N., Pentland, A.: Reality mining: sensing complex social systems. *Pers. Ubiquitous Comput.* **V10**(4), 255–268 (2006)
17. Erdos, P., Renyi, A.: On the evolution of random graphs. *Publ. Math. Inst. Hung. Acad. Sci.* **5**, 17–61 (1960)
18. Feldmann, A., Gilbert, A.C., Willinger, W., Kurtz, T.: The changing nature of network traffic: scaling phenomena. *Comput. Comm. Rev.* **28**, 5–29 (1998)
19. Fischhoff, I.R., Sundaresan, S.R., Cordingley, J., Larkin, H.M., Sellier, M.J., Rubenstein, D.I.: Social relationships and reproductive state influence leadership roles in movements of plains zebra, *equus burchellii*. *Anim. Behav.* **73**(5), 825–831 (2007). doi:10.1016/j.anbehav.2006.10.012
20. Gao, Q., Li, M., Vitányi, P.M.B.: Applying MDL to learn best model granularity. *Artif. Intell.* **121**(1–2), 1–29 (2000)
21. Hinde, R.A.: Interactions, relationships, and social structure. *Man* **11**, 1–17 (1976)
22. Holme, P.: Network reachability of real-world contact sequences. *Phys. Rev. E* **71**, 046119 (2004)
23. Holme, P., Saramäki, J.: Temporal networks. *Phys. Rep.* **519**(3), 97–125 (2012) ArXiv e-prints (2011)
24. Hu, B., Rakthanmanon, T., Hao, Y., Evans, S., Lonardi, S., Keogh, E.J.: Discovering the intrinsic cardinality and dimensionality of time series using mdl. In: *ICDM*, pp. 1086–1091. IEEE Computer Society, Washington (2011)
25. Jeong, H., Tombor, B., Albert, R., Oltvai, Z.N., Barabasi, A.L.: The large-scale organization of metabolic networks. *Nature* **407**(6804), 651–654 (2000)
26. Karsai, M., Kivela, M., Pan, R.K., Kaski, K., Kertész, J., Barabási, A.L., Saramäki, J.: Small but slow world: how network topology and burstiness slow down spreading. *Phys. Rev. E* **83**, 025102 (2011)
27. Kempe, D., Kleinberg, J., Kumar, A.: Connectivity and inference problems for temporal networks. *J. Comput. Syst. Sci.* **64**(4), 820–842 (2002)

28. Keogh, E.J., Chu, S., Hart, D., Pazzani, M.J.: An online algorithm for segmenting time series. In: ICDM, pp. 289–296. IEEE Computer Society, Washington (2001)
29. Kivelä, M., Pan, R.K., Kaski, K., Kertész, J., Saramäki, J., Karsai, M.: Multiscale analysis of spreading in a large communication network. *J. Stat. Mech. Theor. Exp.* **3**, 5 (2012)
30. Kleinberg, J.: An impossibility theorem for clustering. In: *Advances in Neural Information Processing Systems*, pp. 446–453 (2002)
31. Kleinberg, J.: Bursty and hierarchical structure in streams. *Data Min. Knowl. Discov.* **7**(4), 373–397 (2003)
32. Krings, G., Karsai, M., Bernharsson, S., Blondel, V.D., Saramäki, J.: Effects of time window size and placement on the structure of aggregated networks. *CoRR* **abs/1202.1145** (2012). <http://arxiv.org/abs/1202.1145> ArXiv e-prints (2012)
33. Kumar, R., Raghavan, P., Rajagopalan, S., Tomkins, A.: Trawling the web for emerging cyber-communities. *Comput. Netw.* **31**(11–16), 1481–1493 (1999)
34. Kumar, R., Novak, J., Tomkins, A.: Structure and evolution of online social networks. In: *Proceedings of the 12th ACM SIGKDD International Conference on Knowledge Discovery and Data Mining*, pp. 611–617. ACM, New York (2006)
35. Lahiri, M., Berger-Wolf, T.Y.: Structure prediction in temporal networks using frequent subgraphs. In: *Proceedings of the IEEE Symposium on Computational Intelligence and Data Mining*, pp. 35–42. IEEE, New York (2007)
36. Lahiri, M., Maiya, A.S., Caceres, R.S., Habiba, Berger-Wolf, T.Y.: The impact of structural changes on predictions of diffusion in networks. In: *Workshops Proceedings of the 8th IEEE International Conference on Data Mining*, pp. 939–948. IEEE, New York (2008)
37. Meila, M.: Comparing clusterings: an axiomatic view. In: *In ICML '05: Proceedings of the 22nd international conference on Machine learning*, pp. 577–584. ACM, New York (2005)
38. Miller, B.A., Bliss, N.T., Wolfe, P.J.: Toward signal processing theory for graphs and non-euclidean data. In: *ICASSP*, pp. 5414–5417. IEEE, New York (2010)
39. Molloy, M., Reed, B.: A critical point for random graphs with a given degree sequence. *Random Struct. Algorithms* **6**(2–3), 161–180 (1995)
40. Molloy, M., Reed, B.: The size of the giant component of a random graph with a given degree sequence. *Comb. Probab. Comput.* **7**(3), 295–305 (1998)
41. Moody, J., McFarland, D., Bender-deMoll, S.: Dynamic network visualization. *Am. J. Sociol.* **110**(4), 1206–1241 (2005)
42. Morris, M., Kretzschmar, M.: Concurrent partnerships and transmission dynamics in networks. *Soc. Netw.* **17**, 299–318 (1995)
43. Papadimitriou, S., Li, F., Kollios, G., Yu, P.S.: Time series compressibility and privacy. In: *VLDB*, pp. 459–470. VLDB Endowment, Vienna (2007)
44. Partridge, C., Cousins, D., Jackson, A.W., Krishnan, R., Saxena, T., Strayer, W.T.: Using signal processing to analyze wireless data traffic. In: *Proceedings of the ACM Workshop on Wireless Security*, pp. 67–76. ACM, New York (2002)
45. Pesaran, M.H., Timmermann, A.: Model instability and choice of observation window. *Economics Working Paper Series 99–19*, Department of Economics, UC San Diego, 1999
46. Riolo, C., Koopman, J., Chick, S.: Methods and measures for the description of epidemiologic contact networks. *J. Urban Health* **78**, 446–457 (2001)
47. Rissanen, J.: Modeling by shortest data description. *Automatica* **14**, 465–471 (1978)
48. Rubenstein, D., Sundaresan, S., Fischhoff, I., Saltz, D.: Social networks in wild asses: comparing patterns and processes among populations, pp. 159–176. Martin-Luther-University Halle-Wittenberg, Halle (2007)
49. Sedley, D.: The stoic criterion of identity. *Phronesis* **27**, 255–75 (1982)
50. Shannon, C.E.: A mathematical theory of communication. *Bell Syst. Tech. J.* **27**, 379–423, 623–656 (1948)
51. Shetty, J., Adibi, J.: Enron email dataset. Institute, USC Information Sciences (2004). <http://www.isi.edu/adibi/Enron/Enron.htm>
52. Silk, J., Alberts, S., Altmann, J.: Social relationships among adult female baboons (*papio cynocephalus*) ii. variation in the quality and stability of social bonds. *Behav. Ecol. Sociobiol.* **61**(2), 197–204 (2006)

53. Sulo, R., Berger-Wolf, T., Grossman, R.: Meaningful selection of temporal resolution for dynamic networks. In: Proceedings of the 8th Workshop on Mining and Learning with Graphs, MLG '10, pp. 127–136. ACM, New York (2010)
54. Sun, J., Faloutsos, C., Papadimitriou, S., Yu, P.S.: Graphscope: parameter-free mining of large time-evolving graphs. In: KDD '07: Proceedings of the 13th ACM SIGKDD on Knowledge Discovery and Data Mining, pp. 687–696. ACM, New York (2007)
55. Sundaresan, S.R., Fischhoff, I.R., Dushoff, J., Rubenstein, D.I.: Network metrics reveal differences in social organization between two fission-fusion species, grevy's zebra and onager. *Oecologia*, 140–149 (2006)
56. Tanaka, Y., Iwamoto, K., Uehara, K.: Discovery of time-series motif from multi-dimensional data based on mdl principle. *Mach. Learn.* **58**(2–3), 269–300 (2005)
57. Tantipathananandh, C., Berger-Wolf, T., Kempe, D.: A framework for community identification in dynamic social networks. In: KDD '07: Proceedings of the 13th ACM SIGKDD on Knowledge Discovery and Data Mining, pp. 717–726. ACM, New York (2007)
58. Yosef, N., Regev, A.: Impulse control: temporal dynamics in gene transcription. *Cell* **144**, 886–896 (2011)

Models, Entropy and Information of Temporal Social Networks

Kun Zhao, Márton Karsai, and Ginestra Bianconi

Abstract Temporal social networks are characterized by heterogeneous duration of contacts, which can either follow a power-law distribution, such as in face-to-face interactions, or a Weibull distribution, such as in mobile-phone communication. Here we model the dynamics of face-to-face interaction and mobile phone communication by a reinforcement dynamics, which explains the data observed in these different types of social interactions. We quantify the information encoded in the dynamics of these networks by the entropy of temporal networks. Finally, we show evidence that human dynamics is able to modulate the information present in social network dynamics when it follows circadian rhythms and when it is interfacing with a new technology such as the mobile-phone communication technology.

1 Introduction

The theory of complex networks [1–6] has flourished thanks to the availability of new datasets on large complex systems, such as the Internet or the interaction networks inside the cell. In the last 10 years attention has been focusing mainly on static or growing complex networks, with little emphasis on the rewiring of the links. The topology of these networks and their modular structure [7–10] are able to affect the dynamics taking place on them [5, 6, 11, 12]. Only recently temporal

K. Zhao

Physics Department, Northeastern University, Boston, 02115 MA, USA
e-mail: zhao.k@husky.neu.edu;

M. Karsai

BECS, School of Science, Aalto University, Aalto, Finland
e-mail: karsai.marton@gmail.com

G. Bianconi (✉)

School of Mathematical Sciences, Queen Mary University of London, London, E1 4NS, UK
e-mail: ginestra.bianconi@gmail.com

networks [13–18], dominated by the dynamics of rewirings, are starting to attract the attention of quantitative scientists working on complexity. One of the most beautiful examples of temporal networks are social interaction networks. Indeed, social networks [19, 20] are intrinsically dynamical and social interactions are continuously formed and dissolved. Recently we are gaining new insights into the structure and dynamics of these temporal social networks, thanks to the availability of a new generation of datasets recording the social interactions of the fast time scale. In fact, on one side we have data on face-to-face interactions coming from mobile user devices technology [21, 22], or Radio-Frequency-Identification-Devices [16, 17], on the other side, we have extensive datasets on mobile-phone calls [23] and agent mobility [24, 25].

This new generation of data has changed drastically the way we look at social networks. In fact, the adaptability of social networks is well known and several models have been suggested for the dynamical formation of social ties and the emergence of connected societies [26–29]. Nevertheless, the strength and nature of a social tie remained difficult to quantify for several years despite the careful sociological description by Granovetter [19]. Only recently, with the availability of data on social interactions and their dynamics on the fast time scale, it has become possible to assign to each acquaintance the strength or weight of the social interaction quantified as the total amount of time spent together by two agents in a given time window [16].

The recent data revolution in social sciences is not restricted to data on social interaction but concerns all human activities [30–33], from financial transaction to mobility. From these new data on human dynamics evidence is emerging that human activity is bursty and is not described by Poisson processes [30, 31]. Indeed, a universal pattern of bursty activities was observed in human dynamics such as broker activity, library loans or email correspondence. Social interactions are not an exception, and there is evidence that face-to-face interactions have a distribution of duration well approximated by a power-law [16, 34–37] while they remain modulated by circadian rhythms [38]. The bursty activity of social networks has a significant impact on dynamical processes defined on networks [39, 40]. Here we compare these observations with data coming from a large dataset of mobile-phone communication [41, 42] and show that human social interactions, when mediated by a technology, such as the mobile-phone communication, demonstrate the adaptability of human behavior. Indeed, the distribution of duration of calls does not follow any more a power-law distribution but has a characteristic scale determined by the weights of the links, and is described by a Weibull distribution. At the same time, however, this distribution remains bursty and strongly deviates from a Poisson distribution. We will show that both the power-law distribution of durations of social interactions and the Weibull distribution of durations and social interactions observed respectively in face-to-face interaction datasets and in mobile-phone communication activity can be explained phenomenologically by a model with a reinforcement dynamics [35, 36, 41, 42] responsible for the deviation from a pure Poisson process. In this model, the longer two agents interact, the smaller is the probability that they split apart, and the longer an agent is non interacting, the

less likely it is that he/she will start a new social interaction. We observe here that this framework is also necessary to explain the group formation in simple animals [43]. This suggests that the reinforcement dynamics of social interactions, much like the Hebbian dynamics, might have a neurobiological foundation. Furthermore, this is supported by the results on the bursty mobility of rodents [44] and on the recurrence patterns of words encountered in online conversations [45]. We have therefore found ways to quantify the adaptability of human behavior to different technologies. We observe here that this change of behavior corresponds to the very fast time dynamics of social interactions and it is not related to macroscopic change of personality consistently with the results of [46] on online social networks.

Moreover, temporal social networks encode information [47] in their structure and dynamics. This information is necessary for efficiently navigating [48, 49] the network, and to build collaboration networks [50] that are able to enhance the performance of a society. Recently, several authors have focused on measures of entropy and information for networks. The entropy of network ensembles is able to quantify the information encoded in a structural feature of networks such as the degree sequence, the community structure, and the physical embedding of the network in a geometric space [10,51,52]. The entropy rate of a dynamical process on the networks, such a biased random walk, are also able to characterize the interplay between structure of the networks and the dynamics occurring on them [53]. Finally, the mutual information for the data of email correspondence was shown to be fruitful in characterizing the community structure of the networks [54] and the entropy of human mobility was able to set the limit of predictability of human movements [55].

Here we will characterize the entropy of temporal social networks as a proxy to characterize the predictability of the dynamical nature of social interaction networks. This entropy will quantify how many typical configuration of social interactions we expect at any given time, given the history of the network dynamical process. We will evaluate this entropy on a typical day of mobile-phone communication directly from data showing modulation of the dynamical entropy during the circadian rhythm. Moreover we will show that when the distribution of duration of contacts changes from a power-law distribution to a Weibull distribution the level of information and the value of the dynamical entropy significantly change indicating that human adaptability to new technology is a further way to modulate the information content of dynamical social networks.

2 Temporal Social Networks and the Distribution of Duration of Contacts

Human social dynamics is bursty, and the distribution of inter-event times follows a universal trend showing power-law tails. This is true for e-mail correspondence events, library loans, and broker activity. Social interactions are not an exception

to this rule, and the distribution of inter-event time between face-to-face social interactions has power-law tails [30, 31]. Interestingly enough, social interactions have an additional ingredient with respect to other human activities. While sending an email can be considered an instantaneous event characterized by the instant in which the email is sent, social interactions have an intrinsic duration which is a proxy of the strength of a social tie. In fact, social interactions are the microscopic structure of social ties and a tie can be quantified as the total time two agents interact in a given time-window. New data on the fast time scale of social interactions have been now gathered with different methods which range from Bluetooth sensors [21], to the new generation of Radio-Frequency-Identification-Devices [16, 17]. In all these data there is evidence that face-to-face interactions have a duration that follows a distribution with a power-law tail. Moreover, there is also evidence that the inter-contact times have a distribution with fat tails. In this chapter we report a figure of [16] (Fig. 1 of this chapter) in which the duration of contact in Radio-Frequency-Device experiments conducted by Sociopatterns experiments is clearly fat tailed and well approximated by a power-law (straight line on the log–log plot). In this figure the authors of [16] report the distribution of the duration of binary interactions and the distribution of duration of a the triangle of interacting agents. Moreover they report data for the distribution of inter-event time.

How do these distributions change when human agents are interfaced with a new technology? This is a major question that arises if we want to characterize the universality of these distributions. In this book chapter we report an analysis of mobile-phone data and we show evidence of human adaptability to a new technology.

We have analysed the call sequence of subscribers of a major European mobile service provider. In the dataset the users were anonymized and impossible to track. We considered calls between users who called each other mutually at least once during the examined period of 6 months in order to examine calls only reflecting trusted social interactions. The resulted event list consists of 633,986,311 calls between 6,243,322 users. We have performed measurements for the distribution of call durations and non-interaction times of all the users for the entire 6 months time period. The distribution of phone call durations strongly deviates from a fat-tail distribution. In Fig. 2 we report these distributions and show that they depend on the strength w of the interactions (total duration of contacts in the observed period) but do not depend on the age, gender or type of contract in a significant way. The distribution $P^w(\Delta t_{in})$ of duration of contacts within agents with strength w is well fitted by a Weibull distribution

$$\tau^*(w)P^w(\Delta t_{in}) = W_\beta \left(x = \frac{\Delta t}{\tau^*(w)} \right) = \frac{1}{x^\beta} e^{-\frac{1}{1-\beta} x^{1-\beta}}. \quad (1)$$

with $\beta = 0.47\dots$ The typical times of interactions between users $\tau^*(w)$ depend on the weight w of the social tie. In particular the values used for the data collapse of Fig. 3 are listed in Table 1. These values are broadly distributed, and there is evidence that such heterogeneity might depend the geographical distance between the users [56]. The Weibull distribution strongly deviates from a power-law

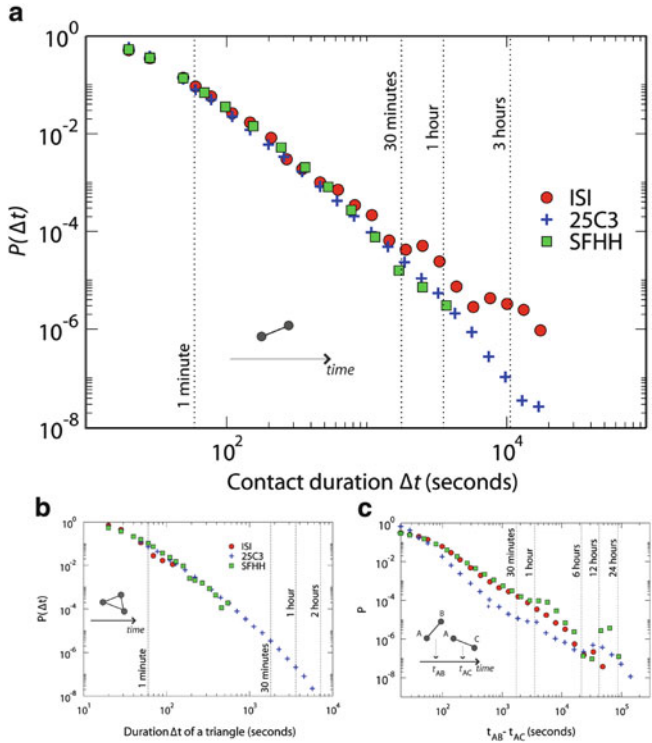


Fig. 1 Probability distribution of human social interaction. Figure from [16]. (a) Probability distribution of duration of contacts between any two given persons. Strikingly, the distributions show a similar long-tail behavior independently of the setting or context where the experiment took place or the detection range considered. The data correspond to respectively 8,700, 17,000 and 600,000 contact events registered at the ISI, SFHH and 25C3 deployments. (b) Probability distribution of the duration of a triangle. The number of triangles registered are 89, 1,700 and 600,000 for the ISI, SFHH and 25C3 deployments. (c) Probability distribution of the time intervals between the beginning of consecutive contacts AB and AC. Some distributions show spikes (i.e., characteristic timescales) in addition to the broad tail; for instance, the 1 h spike in the 25C3 data may be related to a time structure to fix appointments for discussions

distribution to the extent that it is characterized by a typical time scale $\tau(w)$, while power-law distribution does not have an associated characteristic scale. The origin of this significant change in the behavior of humans interactions could be due to the consideration of the cost of the interactions (although we are not in the position to draw these conclusions (see Fig. 3 in which we compare distribution of duration of calls for people with different type of contract) or might depend on the different nature of the communication. The duration of a phone call is quite short and is not affected significantly by the circadian rhythms of the population. On the contrary, the duration of no-interaction periods is strongly affected by the periodic daily or weekly rhythms. In Fig. 4 we report the distribution of duration of no-interaction periods in the day periods between 7 a.m. and 2 a.m. next day. The typical times

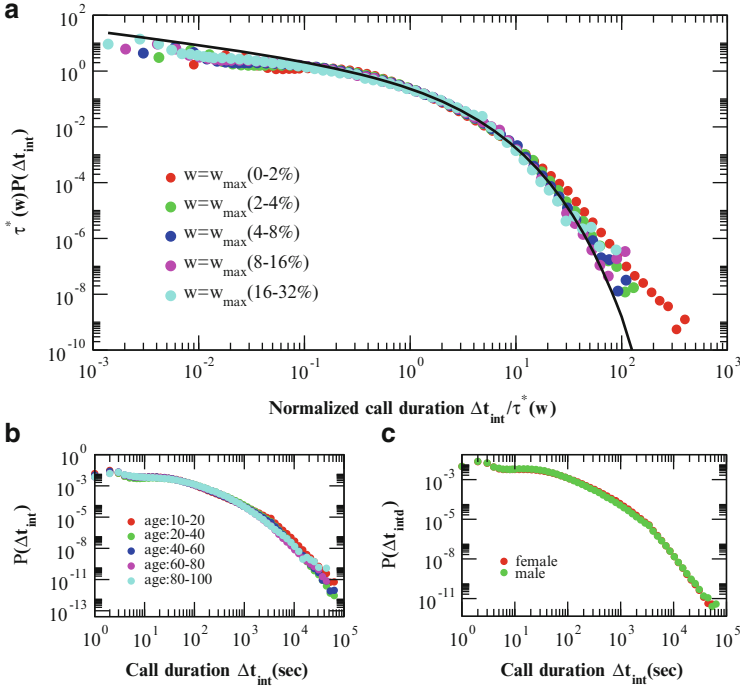
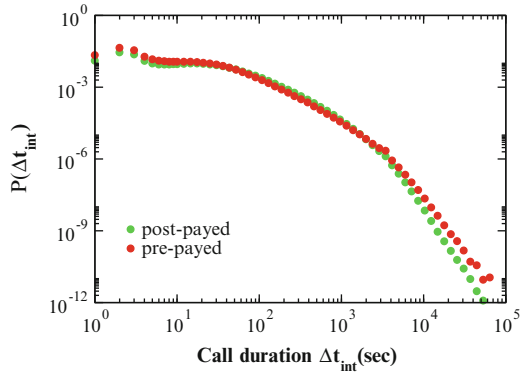


Fig. 2 (a) Distribution of duration of phone-calls between two users with weight w . The data depend on the typical scale $\tau^*(w)$ of duration of the phone-call. (b) Distribution of duration of phone-calls for people of different age. (c) Distribution of duration of phone-calls for users of different gender. The distributions shown in the panel (b) and (c) do not significantly depend on the attributes of the nodes. Figure from [41]

Fig. 3 Distribution of duration of phone-calls for people with different types of contract. No significant change is observed that modifies the functional form of the distribution. Figure from [41]



$\tau^*(k)$ used in Fig. 6 are listed in Table 2. The distribution of non-interacting times is difficult to fit due to the noise derived by the dependence on circadian rhythms. In any case the non-interacting time distribution if it is clearly fat tail.

Table 1 Typical times $\tau^*(w)$ used in the data collapse of Fig. 2

Weight of the link	Typical time $\tau^*(w)$ in seconds (s)
(0–2 %) w_{max}	111.6
(2–4 %) w_{max}	237.8
(4–8 %) w_{max}	334.4
(8–16 %) w_{max}	492.0
(16–32 %) w_{max}	718.8

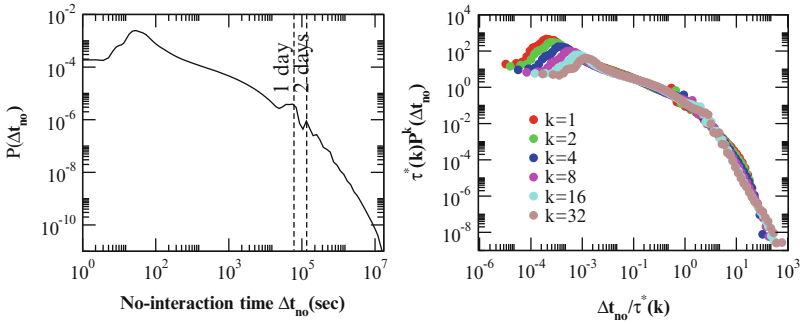


Fig. 4 Distribution of non-interaction times in the phone-call data. The distribution strongly depends on circadian rhythms. The distribution of rescaled time depends strongly on the connectivity of each node. Nodes with higher connectivity k are typically non-interacting for a shorter typical time scale $\tau^*(k)$. Figure from [41]

Table 2 Typical times $\tau^*(k)$ used in the data collapse of Fig. 4

Connectivity	Typical time $\tau^*(k)$ in seconds (s)
$k=1$	158,594
$k=2$	118,047
$k=4$	69,741
$k=8$	39,082
$k=16$	22,824
$k=32$	13,451

3 Model of Social Interaction

It has been recognized that human dynamics is not Poissonian. Several models have been proposed for explaining a fundamental case study of this dynamics, the data on email correspondence. The two possible explanations of bursty email correspondence are described in the following.

- A queueing model of tasks with different priorities has been suggested to explain bursty interevent time. This model implies rational decision making and correlated activity patterns [30, 31]. This model gives rise to power-law distribution of inter event times.
- A convolution of Poisson processes due to different activities during the circadian rhythms and weekly cycles have been suggested to explain bursty inter event time. These different and multiple Poisson processes are introducing a set of distinct characteristic time scales on human dynamics giving rise to fat tails of interevent times [57].

In the previous section we have showed evidence that the duration of social interactions is generally non Poissonian. Indeed, both the power-law distribution observed for duration of face-to-face interactions and the Weibull distribution observed for duration of mobile-phone communication strongly deviate from an exponential. The same can be stated for the distribution of duration of non-interaction times, which strongly deviates from an exponential distribution both for face-to-face interactions and for mobile-phone communication. In order to explain the data on duration of contacts we cannot use any of the models proposed for bursty interevent time in email correspondence. In fact, on one side it is unlikely that the decision to continue a conversation depends on rational decision making. Moreover the queueing model [30, 31] cannot explain the observed stretched exponential distribution of duration of calls. On the other side, the duration of contacts it is not effected by circadian rhythms and weekly cycles which are responsible for bursty behavior in the model [57]. This implies that a new theoretical framework is needed to explain social interaction data. Therefore, in order to model the temporal social networks we have to abandon the generally considered assumption that social interactions are generated by a Poisson process. In this assumption the probability for two agents to start an interaction or to end an interaction is constant in time and not affected by the duration of the social interaction.

Instead, to build a model for human social interactions we have to consider a reinforcement dynamics, in which the probability to start an interaction depends on how long an individual has been non-interacting, and the probability to end an interaction depends on the duration of the interaction itself. Generally, to model the human social interactions, we can consider an agent-based system consisting of N agents that can dynamically interact with each other and give rise to interacting agent groups. In the following subsections we give more details on the dynamics of the models. We denote by the state n of the agent, the number of agents in his/her group (including itself). In particular we notice here that a state $n = 1$ for an agent, denotes the fact that the agent is non-interacting. A reinforcement dynamics for such system is defined in the following frame.

Reinforcement dynamics in temporal social networks

The longer an agent is interacting in a group the smaller is the probability that he/she will leave the group.

The longer an agent is non-interacting the smaller is the probability that he/she will form or join a new group.

The probability that an agent i change his/her state (value of n) is given by

$$f_n(t, t_i) = \frac{h(t)}{(\tau + 1)^\beta} \quad (2)$$

where $\tau := (t - t_i)/N$, N is the total number of agents in the model and t_i is the last time the agent i has changed his/her state, and β is a parameter of the model. The reinforcement mechanism is satisfied by any function $f_n(t, t_i)$ that is decreasing with τ but social-interaction data currently available are reproduced only for this particular choice $f_n(t, t_i)$.

The function $h(t)$ only depends on the actual time in which the decision is made. This function is able to modulate the activity during the day and throughout the weekly rhythms. For the modelling of the interaction data we will first assume that the function $h(t)$ is a constant in time. Moreover in the following subsections we will show that in order to obtain power-law distribution of duration of contacts and non-interaction times (as it is observed in face-to-face interaction data) we have to take $\beta = 1$ while in order to obtain Weibull distribution of duration of contacts we have to take $\beta < 1$. Therefore, summarizing here the results of the following two sections, we can conclude with the following statement for the adaptability of human social interactions.

The adaptability of human social interactions

The adaptability of human social interactions to technology can be seen as an effective way to modulate the parameter β in (2) parametrizing the probability to start or to end the social interactions.

3.1 Model of Face-to-Face Interactions

Here we recall the model of face-to-face interactions presented in [35, 36] and we delineate the main characteristics and outcomes. A simple stochastic dynamics is imposed to the agent-based system in order to model face-to-face interactions. Starting from given initial conditions, the dynamics of face-to-face interactions at each time step t is implemented as the following algorithm.

1. An agent i is chosen randomly.
2. The agent i updates his/her state $n_i = n$ with probability $f_n(t, t_i)$.
If the state n_i is updated, the subsequent action of the agent proceeds with the following rules.
 - (i) If the agent i is non-interacting ($n_i = 1$), he/she starts an interaction with another non-interacting agent j chosen with probability proportional to $f_1(t, t_j)$. Therefore the coordination number of the agent i and of the agent j are updated ($n_i \rightarrow 2$ and $n_j \rightarrow 2$).
 - (ii) If the agent i is interacting in a group ($n_i = n > 1$), with probability λ the agent leaves the group and with probability $1 - \lambda$ he/she introduces a non-interacting agent to the group. If the agent i leaves the group, his/her coordination number is updated ($n_i \rightarrow 1$) and also the coordination numbers of all the agents in the original group are updated ($n_r \rightarrow n - 1$, where r represent a generic agent in the original group). On the contrary, if the agent i introduces another isolated agent j to the group, the agent j is chosen with probability proportional to $f_1(t, t_j)$ and the coordination numbers of all the interacting agents are updated ($n_i \rightarrow n + 1$, $n_j \rightarrow n + 1$ and $n_r \rightarrow n + 1$ where r represents a generic agent in the group).
3. Time t is updated as $t \rightarrow t + 1/N$ (initially $t = 0$). The algorithm is repeated from (1) until $t = T_{max}$.

We have taken in the reinforcement dynamics with parameter $\beta = 1$ such that

$$f_n(t, t') = \frac{b_n}{1 + (t - t')/N}. \quad (3)$$

In (3), for simplicity, we take $b_n = b_2$ for every $n \geq 2$, indicating the fact the interacting agents change their state independently on the coordination number n .

We note that in this model we assume that everybody can interact with everybody so that the underline network model is fully connected. This seems to be a very reasonable assumption if we want to model face-to-face interactions in small conferences, which are venues designed to stimulate interactions between the participants. Nevertheless the model can be easily modified by embedding the agents in a social network so that interactions occur only between social acquaintances.

In the following we review the mean-field solution to this model. For the detailed description of the solution of the outline non-equilibrium dynamics the interest reader can see [35, 36]. We denote by $N_n(t, t')$ the number of agents interacting with $n = 0, 1, \dots, N - 1$ agents at time t , who have not changed state since time t' . In the mean field approximation, the evolution equations for $N_n(t, t')$ are given by

$$\frac{\partial N_1(t, t')}{\partial t} = -2 \frac{N_1(t, t')}{N} f_1(t - t') - (1 - \lambda)\epsilon(t) \frac{N_1(t, t')}{N} f_1(t - t') + \sum_{i>1} \pi_{i,2}(t) \delta_{t'}$$

$$\begin{aligned}\frac{\partial N_2(t, t')}{\partial t} &= -2 \frac{N_2(t, t')}{N} f_2(t - t') + [\pi_{1,2}(t) + \pi_{3,2}(t)] \delta_{tt'} \\ \frac{\partial N_n(t, t')}{\partial t} &= -n \frac{N_n(t, t')}{N} f_n(t - t') + [\pi_{n-1,n}(t) + \pi_{n+1,n}(t) + \pi_{1,n}(t)] \delta_{tt'}, \quad n > 2.\end{aligned}\quad (4)$$

In these equations, the parameter $\epsilon(t)$ indicates the rate at which isolated nodes are introduced by another agent in already existing groups of interacting agents. Moreover, $\pi_{mn}(t)$ indicates the transition rate at which agents change its state from m to n (i.e. $m \rightarrow n$) at time t . In the mean-field approximation the value of $\epsilon(t)$ can be expressed in terms of $N_n(t, t')$ as

$$\epsilon(t) = \frac{\sum_{n>1} \sum_{t'=1}^t N_n(t, t') f_n(t - t')}{\sum_{t'=1}^t N_1(t, t') f_1(t - t')}.\quad (5)$$

Assuming that asymptotically in time $\epsilon(t)$ converges to a time independent variable, i.e. $\lim_{t \rightarrow \infty} \epsilon(t) = \hat{\epsilon}$, the solution to the rate equations (4) in the large time limit is given by

$$\begin{aligned}N_1(t, t') &= N_1(t', t') \left(1 + \frac{t - t'}{N}\right)^{-b_1[2+(1-\lambda)\hat{\epsilon}]} \\ N_2(t, t') &= N_2(t', t') \left(1 + \frac{t - t'}{N}\right)^{-2b_2} \\ N_n(t, t') &= N_n(t', t') \left(1 + \frac{t - t'}{N}\right)^{-nb_2} \quad \text{for } n > 2,\end{aligned}\quad (6)$$

with

$$\begin{aligned}N_1(t', t') &= \sum_{n>1} \pi_{n,1}(t') \\ N_2(t', t') &= \pi_{1,2}(t') + \pi_{3,2}(t') \\ N_n(t', t') &= \pi_{n-1,n}(t') + \pi_{n+1,n}(t') + \pi_{0,n}(t') \quad \text{for } n > 2.\end{aligned}\quad (7)$$

We denote by $P_n(\tau)$ the distribution of duration of different coordination number n which satisfies the relation

$$P_n(\tau) = \int_{t'=0}^{t'-\tau} f_n(t - t') N(t, t') dt'.\quad (8)$$

and using (3) and (6) we find that $P_n(\tau)$ simply satisfy

$$\begin{aligned}P_1(\tau) &\propto (1 + \tau)^{-b_1[2+(1-\lambda)\hat{\epsilon}]-1} \\ P_n(\tau) &\propto (1 + \tau)^{-nb_2-1}.\end{aligned}\quad (9)$$

Fig. 5 Distribution $P_n(\tau)$ of durations of groups of size n in the stationary region. The simulation is performed with $N = 1,000$ agents for a number of time steps $T_{max} = N \times 10^5$. The parameter used are $b_0 = b_1 = 0.7, \lambda = 0.8$. The data is averaged over ten realizations

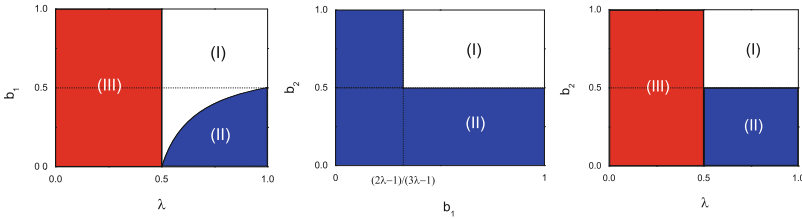
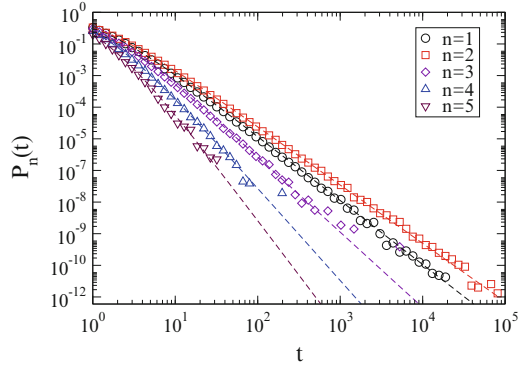


Fig. 6 Phase diagram of arbitrary state number n : the red area indicates the regime where a large group is formed and the solution is divergent. The blue area indicates the non-stationary regime. The white area indicates the stationary regime

As shown in Fig. 5, the analytic prediction (9) is in good agreement with the computer simulation.

Despite the simplicity of this model, the non-equilibrium dynamics of this system is characterized by a non trivial phase diagram. The phase-diagram of the model is summarized in Fig. 6. We can distinguish between three phases:

- *Region I—the stationary region:* $b_2 > 0.5, b_1 > (2\lambda - 1)/(3\lambda - 3)$ and $\lambda > 0.5$ — This region corresponds to the white area in Fig. 6. The region is stationary and the transition rates between different states are constant.
- *Region II—the non-stationary region:* $b_2 < 0.5$ or $b_1 > (2\lambda - 1)/(3\lambda - 3)$, and $\lambda > 0.5$ —This region corresponds to the blue area in Fig. 6. The region is non-stationary and the transition rates between different states are decaying with time as power-law.
- *Region III—formation of a big group:* $\lambda < 0.5$ —In this region there is an instability for the formation of a large group of size $\mathcal{O}(N)$.

In both regions I and region II the distribution of the duration of groups of size n follows a power-law distribution with an exponent which grows with the group size n . This fact is well reproduced in the face-to-face data [36] and implies the following principle on the stability of groups in face-to-face interactions.

Stability of groups in face-to-face interactions

In face-to-face interactions, groups of larger size are less stable than groups of smaller size. In fact the stability of a group depends on the independent decisions of the n agents in the group to remain in contact.

3.2 Model of Phone-Call Communication

To model cell-phone communication, we consider once again a system of N agents representing the mobile phone users. Moreover, we introduce a static weighted network G , of which the nodes are the agents in the system, the edges represent the social ties between the agents, such as friendships, collaborations or acquaintances, and the weights of the edges indicate the strengths of the social ties. Therefore the interactions between agents can only take place along the network G (an agent can only interact with his/her neighbors on the network G). Here we propose a model for mobile-phone communication constructed with the use of the reinforcement dynamic mechanism. This model shares significant similarities with the previously discussed model for face-to-face interactions, but has two major differences. Firstly, only pairwise interactions are allowed in the case of cell-phone communication. Therefore, the state n of an agent only takes the values of either 1 (non-interacting) or 2 (interacting). Secondly, the probability that an agent ends his/her interaction depends on the weight of network G . The dynamics of cell-phone communication at each time step t is then implemented as the following algorithm.

1. An agent i is chosen randomly at time t .
2. The subsequent action of agent i depends on his/her current state (i.e. n_i):
 - (i) If $n_i = 1$, he/she starts an interaction with one of his/her non-interacting neighbors j of G with probability $f_1(t_i, t)$ where t_i denotes the last time at which agent i has changed his/her state. If the interaction is started, agent j is chosen randomly with probability proportional to $f_1(t_j, t)$ and the coordination numbers of agent i and j are then updated ($n_i \rightarrow 2$ and $n_j \rightarrow 2$).
 - (ii) If $n_i = 2$, he/she ends his/her current interaction with probability $f_2(t_i, t|w_{ij})$ where w_{ij} is the weight of the edge between i and the neighbor j that is interacting with i . If the interaction is ended, the coordination numbers of agent i and j are then updated ($n_i \rightarrow 1$ and $n_j \rightarrow 1$).
3. Time t is updated as $t \rightarrow t + 1/N$ (initially $t = 0$). The algorithm is repeated from (1) until $t = T_{max}$.

Here we take the probabilities $f_1(t, t')$, $f_2(t, t'|w)$ according to the following functional dependence

$$\begin{aligned}
f_1(t, t') &= f_1(\tau) = \frac{b_1}{(1 + \tau)^\beta} \\
f_2(t, t'|w) &= f_2(\tau|w) = \frac{b_2 g(w)}{(1 + \tau)^\beta}
\end{aligned} \tag{10}$$

where the parameters are chosen in the range $b_1 > 0$, $b_2 > 0$, $0 \leq \beta \leq 1$, $g(w)$ is a positive decreasing function of its argument, and τ is given by $\tau = (t - t')/N$.

In order to solve the model analytically, we assume the quenched network G to be annealed and uncorrelated. Here we outline the main result of this approach and we suggest for the interested reader to look at papers [41, 42] for the details of the calculations. Therefore we assume that the network is rewired while the degree distribution $p(k)$ and the weight distribution $p(w)$ remain constant. We denote by $N_1^k(t, t')$ the number of non-interacting agents with degree k at time t who have not changed their state since time t' . Similarly we denote by $N_2^{k,k',w}(t, t')$ the number of interacting agent pairs (with degree respectively k and k' and weight of the edge w) at time t who have not changed their states since time t' . In the annealed approximation the probability that an agent with degree k is called by another agent is proportional to its degree. Therefore the evolution equations of the model are given by

$$\begin{aligned}
\frac{\partial N_1^k(t, t')}{\partial t} &= -\frac{N_1^k(t, t')}{N} f_1(t - t') - ck \frac{N_1^k(t, t')}{N} f_1(t - t') + \pi_{21}^k(t) \delta_{tt'} \\
\frac{\partial N_2^{k,k',w}(t, t')}{\partial t} &= -2 \frac{N_2^{k,k',w}(t, t')}{N} f_2(t - t'|w) + \pi_{12}^{k,k',w}(t) \delta_{tt'}
\end{aligned} \tag{11}$$

where the constant c is given by

$$c = \frac{\sum_{k'} \int_0^t dt' N_1^{k'}(t, t') f_1(t - t')}{\sum_{k'} k' \int_0^t dt' N_1^{k'}(t, t') f_1(t - t')}. \tag{12}$$

In (11) the rates $\pi_{pq}(t)$ indicate the average number of agents changing from state $p = 1, 2$ to state $q = 1, 2$ at time t . The solution of the dynamics must of course satisfy the conservation equation

$$\int dt' [N_1^k(t, t') + \sum_{k', w} N_2^{k,k',w}(t, t')] = Np(k). \tag{13}$$

In the following we will denote by $P_1^k(t, t')$ the probability distribution that an agent with degree k is non-interacting in the period between time t' and time t and we will denote by $P_2^w(t, t')$ the probability that an interaction of weight w is lasting from time t' to time t which satisfy

$$\begin{aligned}
P_1^k(t, t') &= (1 + ck) f_1(t, t') N_1^k(t, t') \\
P_2^w(t, t') &= 2f_2(t, t'|w) \sum_{k, k'} N_2^{k, k', w}(t, t').
\end{aligned} \tag{14}$$

As a function of the value of the parameter of the model we found different distribution of duration of contacts and non-interaction times.

- *Case* $0 < \beta < 1$. The system allows always for a stationary solution with $N_1^k(t, t') = N_1^k(\tau)$ and $N_2^{k, k', w}(t, t') = N_2^{k, k', w}(\tau)$. The distribution of duration of non-interaction times $P_1^k(\tau)$ for agents of degree k in the network and the distribution of interaction times $P_2^w(\tau)$ for links of weight w is given by

$$\begin{aligned}
P_1^k(\tau) &\propto \frac{b_1(1 + ck)}{(1 + \tau)^\beta} e^{-\frac{b_1(1+ck)}{1-\beta}(1+\tau)^{1-\beta}} \\
P_2^w(\tau) &\propto \frac{2b_2g(w)}{(1 + \tau)^\beta} e^{-\frac{2b_2g(w)}{1-\beta}(1+\tau)^{1-\beta}}.
\end{aligned} \tag{15}$$

Rescaling (15), we obtain the Weibull distribution which is in good agreement with the results observed in mobile-phone datasets.

- *Case* $\beta = 1$. Another interesting limiting case of the mobile-phone communication model is the case $\beta = 1$ such that $f_1^k(\tau) \propto (1 + \tau)^{-1}$ and $f_2^w(\tau|w) \propto (1 + \tau)^{-1}$. In this case the model is much similar to the model used to mimic face-to-face interactions described in the previous subsection [35, 36], but the interactions are binary and they occur on a weighted network. In this case we get the solution

$$\begin{aligned}
N_1^k(\tau) &= N\pi_{21}^k(1 + \tau)^{-b_1(1+ck)} \\
N_2^{k, k', w}(\tau) &= N\pi_{12}^{k, k', w}(1 + \tau)^{-2b_2g(w)}.
\end{aligned} \tag{16}$$

and consequently the distributions of duration of given states (14) are given by

$$\begin{aligned}
P_1^k(\tau) &\propto \pi_{21}^k(1 + \tau)^{-b_1(1+ck)-1} \\
P_2^w(\tau) &\propto \pi_{12}^{k, k', w}(1 + \tau)^{-2b_2g(w)-1}.
\end{aligned} \tag{17}$$

The probability distributions are power-laws. This result remains valid for every value of the parameters $b_1, b_2, g(w)$ nevertheless the stationary condition is only valid for

$$\begin{aligned}
b_1(1 + ck) &> 1 \\
2b_2g(w) &> 1.
\end{aligned} \tag{18}$$

Indeed this condition ensures that the self-consistent constraints (12), and the conservation law equation (13) have a stationary solution.

- *Case $\beta = 0$.* This is the case in which the process described by the model is a Poisson process and there is no reinforcement dynamics in the system. Therefore we find that the distribution of durations are exponentially distributed. In fact for $\beta = 0$ the functions $f_1(\tau)$ and $f_2(\tau|w)$ given by (10) reduce to constants, therefore the process of creation of an interaction is a Poisson process. In this case the social interactions do not follow the reinforcement dynamics. The solution that we get for the number of non interacting agents of degree k , $N_1^k(\tau)$ and the number of interacting pairs $N_2^{k,k',w}(\tau)$ is given by

$$\begin{aligned} N_1^k(\tau) &= N\pi_{21}^k e^{-b_1(1+ck)\tau} \\ N_2^{k,k',w}(\tau) &= N\pi_{12}^{k,k',w} e^{-2b_2g(w)\tau}. \end{aligned} \quad (19)$$

Consequently the distributions of duration of given states (14) are given by

$$\begin{aligned} P_1^k(\tau) &\propto e^{-b_1(1+ck)\tau} \\ P_2^w(\tau) &\propto e^{-2b_2g(w)\tau}. \end{aligned} \quad (20)$$

Therefore the probability distributions $P_1^k(\tau)$ and $P_2^w(\tau)$ are exponentials as expected in a Poisson process.

4 Entropy of Temporal Social Networks

In this section we introduce the entropy of temporal social networks as a measure of information encoded in their dynamics. We can assume that the following stochastic dynamics takes place in the network: according to this dynamics at each time step t , different interacting groups can be formed and can be dissolved giving rise to the temporal social networks. The agents are embedded in a social network G such that interaction can occur only by acquaintances between first neighbors of the network G . This is a good approximation if we want to model social interactions on the fast time scale. In the case of a small conference, where each participant is likely to discuss with any other participant we can consider a fully connected network as the underlying network G of social interactions. In the network G each set of interacting agents can be seen as a connected subgraph of \mathcal{G} , as shown in Fig. 7. We use an indicator function $g_{i_1,i_2,\dots,i_n}(t)$ to denote, at time t , the maximal set i_1, i_2, \dots, i_n of interacting agents in a group. If (i_1, i_2, \dots, i_n) is the maximal set of interacting agents in a group, we let $g_{i_1,i_2,\dots,i_n}(t) = 1$ otherwise we put $g_{i_1,i_2,\dots,i_n}(t) = 0$. Therefore at any given time the following relation is satisfied,

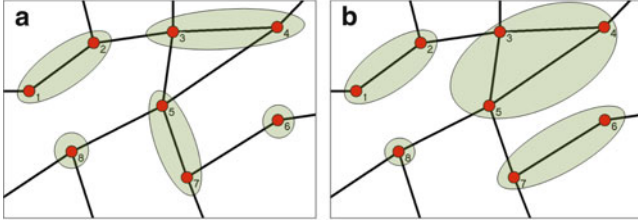


Fig. 7 The dynamical social networks are composed by different dynamically changing groups of interacting agents. **(a)** Only groups of size one or two are allowed as in the phone-call communication. **(b)** Groups of any size are allowed as in the face-to-face interactions

$$\sum_{\mathcal{G}=(i_1, i_2, \dots, i_n) | i \in \mathcal{G}} g_{i_1, i_2, \dots, i_n}(t) = 1. \quad (21)$$

where \mathcal{G} is an arbitrary connected subgraph of G . Then we denote by $\mathcal{S}_t = \{g_{i_1, i_2, \dots, i_n}(t') \forall t' < t\}$ the history of the dynamical social networks, and $p(g_{i_1, i_2, \dots, i_n}(t) = 1 | \mathcal{S}_t)$ the probability that $g_{i_1, i_2, \dots, i_n}(t) = 1$ given the history \mathcal{S}_t . Therefore the likelihood that at time t the dynamical social networks has a group configuration $g_{i_1, i_2, \dots, i_n}(t)$ is given by

$$\mathcal{L} = \prod_{\mathcal{G}} p(g_{i_1, i_2, \dots, i_n}(t) = 1 | \mathcal{S}_t)^{g_{i_1, i_2, \dots, i_n}(t)}. \quad (22)$$

We denote the entropy of the dynamical networks as $S = -\langle \log \mathcal{L} \rangle_{|\mathcal{S}_t}$ indicating the logarithm of the typical number of all possible group configurations at time t which can be explicitly written as

$$S = -\sum_{\mathcal{G}} p(g_{i_1, i_2, \dots, i_n}(t) = 1 | \mathcal{S}_t) \log p(g_{i_1, i_2, \dots, i_n}(t) = 1 | \mathcal{S}_t). \quad (23)$$

The value of the entropy can be interpreted as following: if the entropy is larger, the dynamical network is less predictable, and several possible dynamic configurations of groups are expected in the system at time t . On the other hand, a smaller entropy indicates a smaller number of possible future configuration and a temporal network state which is more predictable.

4.1 Entropy of Phone-Call Communication

In this subsection we discuss the evaluation of the entropy of phone-call communication. For phone-call communication, we only allow pairwise interaction in the system such that the product in (22) is only taken over all single nodes and edges of

the quenched network G which yields

$$\mathcal{L} = \prod_i p(g_i(t) = 1 | \mathcal{S}_t)^{g_i(t)} \prod_{ij | a_{ij}=1} p(g_{ij}(t) = 1 | \mathcal{S}_t)^{g_{ij}(t)} \quad (24)$$

with

$$g_i(t) + \sum_j a_{ij} g_{ij}(t) = 1. \quad (25)$$

where a_{ij} is the adjacency matrix of G . The entropy then takes a simple form

$$S = - \sum_i p(g_i(t) = 1 | \mathcal{S}_t) \log p(g_i(t) = 1 | \mathcal{S}_t) - \sum_{ij} a_{ij} p(g_{ij}(t) = 1 | \mathcal{S}_t) \log p(g_{ij}(t) = 1 | \mathcal{S}_t). \quad (26)$$

4.2 Analysis of the Entropy of a Large Dataset of Mobile Phone Communication

In this subsection we use the entropy of temporal social networks to analyze the information encoded in a major European mobile service provider, making use of the same dataset that we have used to measure the distribution of call duration in Sect. 2. Here we evaluate the entropy of the temporal networks formed by the phone-call communication in a typical week-day in order to study how the entropy of temporal social networks is affected by circadian rhythms of human behavior.

For the evaluation of the entropy of temporal social networks we consider a subset of the large dataset of mobile-phone communication. We selected 562,337 users who executed at least one call a day during a weeklong period. We denote by $f_n(t, t')$ the transition probability that an agent in state n ($n = 1, 2$) changes its state at time t given that he/she has been in his/her current state for a duration $\tau = t - t'$. The probability $f_n(t, t')$ can be estimated directly from the data. Therefore, we evaluate the entropy in a typical weekday of the dataset by using the transition probabilities $f_n(t, t')$ and the definition of entropy of temporal social networks (readers should refer to the supplementary material of [41] for the details). In Fig. 8 we show the resulting evaluation of entropy in a typical day of our phone-call communication dataset. The entropy of the temporal social network is plotted as a function of time during one typical day. The mentioned figure shows evidence that the entropy of temporal social networks changes significantly during the day reflecting the circadian rhythms of human behavior.

Fig. 8 Evaluation of the entropy of the dynamical social networks of phone calls communication in a typical week-day. In the nights the social dynamical network is more predictable. Figure from [41]

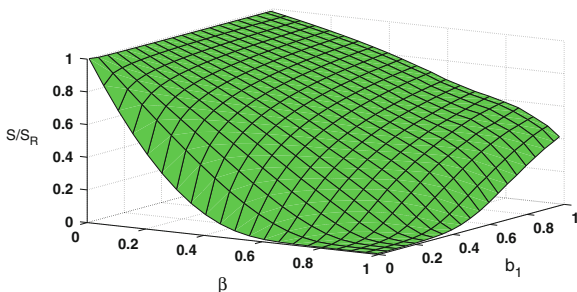
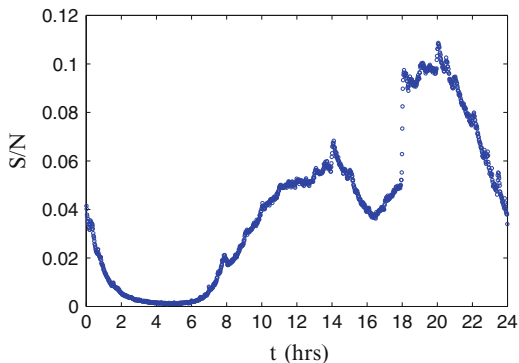


Fig. 9 Entropy S of social dynamical network model of pairwise communication normalized with the entropy S_R of a null model in which the expected average duration of phone-calls is the same but the distribution of duration of phone-calls and non-interaction time are Poisson distributed. The network size is $N = 2,000$ the degree distribution of the network is exponential with average $\langle k \rangle = 6$, the weight distribution is $p(w) = Cw^{-2}$ and $g(w)$ is taken to be $g(w) = b_2/w$ with $b_2 = 0.05$. The value of S/S_R is depending on the two parameters β, b_1 . For every value of b_1 the normalized entropy is smaller for $\beta \rightarrow 1$. Figure from [41]

4.3 Entropy Modulated by the Adaptability of Human Behavior

The adaptability of human behavior is evident when comparing the distribution of the duration of phone-calls with the duration of face-to-face interactions. In the framework of the model for mobile-phone interactions described in Sect. 3.2, this adaptability, can be understood, as a possibility to change the exponent β in Eq. (2) and Eq. (10) regulating the duration of social interactions.

Changes in the parameter β correspond to different values entropy of the dynamical social networks. Therefore, by modulating the exponent β , the human behavior is able to modulate the information encoded in temporal social networks. In order to show the effect on entropy of a variation of the exponent β in the dynamics of social interaction networks, we considered the entropy corresponding to the model described in Sect. 3.2 as a function of the parameters β and b_1

modulating the probabilities $f_1(t, t')$, $f_2(t, t'|w)$ (10). In Fig. 9 we report the entropy S of the proposed model a function of β and b_1 . The entropy S , given by (26), is calculated using the annealed approximation for the solution of the model and assuming the large network limit. In the calculation of the entropy S we have taken a network of size $N = 2,000$ with exponential degree distribution of average degree $\langle k \rangle = 6$, weight distribution $P(w) = Cw^{-2}$ and function $g(w) = 1/w$ and $b_2 = 0.05$. Our aim in Fig. 9 is to show only the effects on the entropy due to the different distributions of duration of contacts and non-interaction periods. Therefore we have normalized the entropy S with the entropy S_R of a null model of social interactions in which the duration of groups are Poisson distributed but the average time of interaction and non-interaction time are the same as in the model of cell-phone communication (readers should refer to the supplementary material of [41] for more details). From Fig. 9 we observe that if we keep b_1 constant, the ratio S/S_R is a decreasing function of the parameter β . This indicates that the broader is the distribution of probability of duration of contacts, the higher is the information encoded in the dynamics of the network. Therefore the heterogeneity in the distribution of duration of contacts and no-interaction periods implies higher level of information in the social network. The human adaptive behavior by changing the exponent β in face-to-face interactions and mobile phone communication effectively changes the entropy of the dynamical network.

5 Conclusions

The goal of network science is to model, characterize, and predict the behavior of complex networks. Here, in this chapter, we have delineated a first step in the characterization of the information encoded in temporal social networks. In particular we have focused on modelling phenomenologically social interactions on the fast time scale, such a face-to-face interactions and mobile phone communication activity. Moreover, we have defined the entropy of dynamical social networks, which is able to quantify the information present in social network dynamics. We have found that human social interactions are bursty and adaptive. Indeed, the duration of social contacts can be modulated by the adaptive behavior of humans: while in face-to-face interactions dataset a power-law distribution of duration of contacts has been observed, we have found, from the analysis of a large dataset of mobile-phone communication, that mobile-phone calls are distributed according to a Weibull distribution. We have modeled this adaptive behavior by assuming that the dynamics underlying the formation of social contacts implements a reinforcement dynamics according to which the longer an agent has been in a state (interacting or non-interacting) the less likely it is that he will change his/her state. We have used the entropy of dynamical social networks to evaluate the information present in the temporal network of mobile-phone communication, during a typical weekday of activity, showing that the information content encoded in the dynamics of the

network changes during a typical day. Moreover, we have compared the entropy in a social network with the duration of contacts following a Weibull distribution, and with the duration of contacts following a power-law in the framework of the stochastic model proposed for mobile-phone communication. We have found that a modulation of the statistics of duration of contacts strongly modifies the information contents present in the dynamics of temporal networks. Finally, we conclude that the duration of social contacts in humans has a distribution that strongly deviates from an exponential. Moreover, the data show that human behavior is able to modify the information encoded in social networks dynamics during the day and when facing a new technology such as the mobile-phone communication technology.

Acknowledgements We thank A. Barrat and J. Stehlé for a collaboration that started our research on face-to-face interactions. Moreover we especially thank A.-L. Barabási for his useful comments and for the mobile call data used in this research. MK acknowledges the financial support from EUs 7th Framework Programs FET-Open to ICTeCollective project no. 238597.

References

1. Dorogovtsev, S.N., Mendes, J.F.F.: *Evolution of Networks: From Biological Nets to the Internet and WWW*. Oxford University Press, Oxford (2003)
2. Newman, M.E.J.: The structure and function of complex networks. *SIAM Rev.* **45**, 167–256 (2003)
3. Boccaletti, S., Latora, V., Moreno, Y., Chavez, M., Hwang, D.U.: Complex networks: structure and dynamics. *Phys. Rep.* **424**, 175–308 (2006)
4. Caldarelli, G.: *Scale-Free Networks*. Oxford University Press, Oxford (2007)
5. Dorogovtsev, S.N., Goltsev, A.V., Mendes, J.F.F.: *Rev. Mod. Phys.* **80**, 1275 (2008)
6. Barrat, A., Barthélemy, M., Vespignani, A.: *Dynamical Processes on Complex Networks*. Cambridge University Press, Cambridge (2008)
7. Castellano, C., Fortunato, S., Loreto, V.: Statistical physics of social dynamics. *Rev. Mod. Phys.* **81**, 591–646 (2009)
8. Palla, G., Barabási, A.L., Vicsek, T.: Quantifying social group evolution. *Nature* **446**, 664–667 (2007)
9. Ahn, Y.Y., Bagrow, J.P., Lehmann, S.: Link communities reveal multiscale complexity in networks. *Nature* **466**, 761–764 (2010)
10. Bianconi, G., Pin, P., Marsili, M.: Assessing the relevance of node features for network structure. *Proc. Natl. Acad. Sci. U.S.A.* **106**, 11433–11438 (2009)
11. Bianconi, G.: *Phys. Lett. A* **303**, 166 (2002)
12. Bradde, S., Caccioli, F., Dall’Asta, L., Bianconi, G.: *Phys. Rev. Lett.* **104**, 218701 (2010)
13. Holme, P.: Network reachability of real-world contact sequences. *Phys. Rev. E* **71**, 046119 (2005)
14. Tang, J., Scellato, S., Musolesi, M., Mascolo, C., Latora, V.: Small-world behavior in time-varying graphs. *Phys. Rev. E* **81**, 055101 (2010)
15. Parshani, R., Dickison, M., Cohen, R., Stanley, H.E., Havlin, S.: Dynamic networks and directed percolation. *Europhys. Lett.* **90**, 38004 (2010)
16. Cattuto, C., Van den Broeck, W., Barrat, A., Colizza, V., Pinton, J.F., Vespignani, A.: Dynamics of person-to-person interactions from distributed RFID sensor networks. *PLoS One* **5**, e11596 (2010)

17. Isella, L., Stehlé, J., Barrat, A., Cattuto, C., Pinton, J.F., Van den Broeck, W.: What's in a crowd? Analysis of face-to-face behavioral networks. *J. Theor. Biol.* **271**, 166–180 (2011)
18. Holme, P., Saramäki, J.: *Phys. Rep.* **519**, 97–125 (2012)
19. Granovetter, M.: The strength in weak ties. *Am. J. Sociol.* **78**, 1360–1380 (1973)
20. Wasserman, S., Faust, K.: *Social Network Analysis: Methods and Applications*. Cambridge University Press, Cambridge (1994)
21. Eagle, N., Pentland, A.S.: Reality mining: sensing complex social systems. *Pers. Ubiquit. Comput.* **10**, 255–268 (2006)
22. Hui, P., Chaintreau, A., Scott, J., Gass, R., Crowcroft, J., Diot, C.: Pocket switched networks and human mobility in conference environments. In: *Proceedings of the 2005 ACM SIGCOMM Workshop on Delay-Tolerant Networking*, Philadelphia, PA, pp. 244–251 (2005)
23. Onnela, J.P., Saramäki, J., Hyvönen, J., Szabó, G., Lazer, D., Kaski, K., Kertész, J., Barabási, A.L.: Structure and tie strengths in mobile communication networks. *Proc. Natl. Acad. Sci. U.S.A.* **104**, 7332–7336 (2007)
24. Brockmann, D., Hufnagel, L., Geisel, T.: The scaling laws of human travel. *Nature* **439**, 462–465 (2006)
25. González, M.C., Hidalgo, A.C., Barabási, A.L.: Understanding individual human mobility patterns. *Nature* **453**, 779–782 (2008)
26. Davidsen, J., Ebel, H., Bornholdt, S.: Emergence of a small world from local interactions: modeling acquaintance networks. *Phys. Rev. Lett.* **88**, 128701 (2002)
27. Marsili, M., Vega-Redondo, F., Slanina, F.: The rise and fall of a networked society: a formal model. *Proc. Natl. Acad. Sci. U.S.A.* **101**, 1439–1442 (2004)
28. Holme, P., Newman, M.E.J.: Nonequilibrium phase transition in the coevolution of networks and opinions. *Phys. Rev. E* **74**, 056108 (2006)
29. Vazquez, F., Eguíluz, V.M., San Miguel, M.: Generic absorbing transition in coevolution dynamics. *Phys. Rev. Lett.* **100**, 108702 (2008)
30. Barabási, A.L.: The origin of bursts and heavy tails in humans dynamics. *Nature* **435**, 207–211 (2005)
31. Vázquez, A., et al.: *Phys. Rev. E* **73**, 036127 (2006)
32. Rybski, D., Buldyrev, S.V., Havlin, S., Liljeros, F., Makse, H.A.: Scaling laws of human interaction activity. *Proc. Natl. Acad. Sci. U.S.A.* **106**, 12640–12645 (2009)
33. Malmgren, R.D., Stouffer, D.B., Campanharo, A.S.L.O., Nunes Amaral, L.A.: On universality in human correspondence activity. *Science* **325**, 1696–1700 (2009)
34. Scherrer, A., Borgnat, P., Fleury, E., Guillaume, J.L., Robardet, C.: Description and simulation of dynamic mobility networks. *Comput. Netw.* **52**, 2842–2858 (2008)
35. Stehlé, J., Barrat, A., Bianconi, G.: Dynamical and bursty interactions in social networks. *Phys. Rev. E* **81**, 035101 (2010)
36. Zhao, K., Stehlé, J., Bianconi, G., Barrat, A.: Social network dynamics of face-to-face interactions. *Phys. Rev. E* **83**, 056109 (2011)
37. Karsai, M., Kaski, K., Barabási, A.L., Kertész, J.: Universal features of correlated bursty behaviour. *Sci. Rep.* **2**, 397 (2012)
38. Jo, H.H., Karsai, M., Kertész, J., Kaski, K.: Circadian pattern and burstiness in mobile phone communication. *New J. Phys.* **14**, 013055 (2012)
39. Vázquez, A., Rácz, B., Lukacs, A., Barabási, A.L.: Impact of Non-Poissonian activity patterns on spreading processes. *Phys. Rev. Lett.* **98**, 158702 (2007)
40. Karsai, M., Kivela, M., Pan, R.K., Kaski, K., Kertész, J., Barabási, A.-L., Saramäki, J.: Small but slow world: how network topology and burstiness slow down spreading. *Phys. Rev. E* **83**, 025102 (2011)
41. Zhao, K., Karsai, M., Bianconi, G.: Entropy of dynamical social networks. *PLoS One* **6**, e28116 (2011)
42. Zhao, K., Bianconi, G.: Social interaction model and adaptability of human behavior. *Front. Physiol.* **2**, 101 (2011)
43. Bisson, G., Bianconi, G., Torre, V.: The dynamics of group formation among leeches. *Front. Physiol.* **3**, 133 (2012)

44. Anteneodo, C., Chialvo, D.R.: Unraveling the fluctuations of animal motor activity. *Chaos* **19**, 033123 (2009)
45. Altmann, E.G., Pierrehumbert, J.B., Motter, A.E.: Beyond word frequency: bursts, lulls, and scaling in the temporal distributions of words. *PLoS One* **4**, e7678 (2009)
46. Quercia, D., Lambiotte, R., Stillwell, D., Kosinski, M., Crowcroft, J.: The personality of popular facebook users. In: *ACM CSCW 12*, pp. 955–964 (2012). <http://www.acm.org/>
47. Cover, T., Thomas, J.A.: *Elements of Information Theory*. Wiley-Interscience, New York (2006)
48. Kleinberg, J.M.: Navigation in a small world. *Nature* **406**, 845 (2000)
49. Watts, D.J., Strogatz, S.H.: Collective dynamics of ‘small-world’ networks. *Nature* **393**, 440–442 (1998)
50. Newman, M.E.J.: The structure of scientific collaboration networks. *Proc. Natl. Acad. Sci. U.S.A.* **98**, 404–409 (2001)
51. Bianconi, G.: The entropy of randomized network ensembles. *Europhys. Lett.* **81**, 28005 (2008)
52. Anand, K., Bianconi, G.: Entropy measures for networks: toward an information theory of complex topologies. *Phys. Rev. E* **80**, 045102 (2009)
53. Gómez-Gardenés, J., Latora, V.: Entropy rate of diffusion processes on complex networks. *Phys. Rev. E* **78**, 065102(R) (2008)
54. Eckmann, J.P., Moses, E., Sergi, D.: Entropy of dialogues creates coherent structures in e-mail traffic. *Proc. Natl. Acad. Sci. U.S.A.* **101**, 14333 (2004)
55. Song, C., Qu, Z., Blumm, N., Barabási, A.L.: Limits of predictability in human mobility. *Science* **327**, 1018–1021 (2010)
56. Lambiotte, R., Blondel, V.D., de Kerchovea, C., Huensa, E., Prieurc, C., Smoredac, Z., Van Dooren, P.: Geographical dispersal of mobile communication networks. *Physica A* **387**, 5317–5325 (2008)
57. Malmgren, R.D., Stouffer, D.B., Motter, A.E., Amaral, L.A.N.: A Poissonian explanation for heavy tails in e-mail communication. *Proc. Natl. Acad. Sci. U.S.A.* **47**, 18153–18158 (2008)

Temporal Motifs

Lauri Kovanen, Márton Karsai, Kimmo Kaski, János Kertész,
and Jari Saramäki

Abstract We discuss the temporal motifs approach that is aimed at detecting significant, intrinsically dynamic, mesoscopic structures and patterns in temporal networks, which cannot be seen in static or aggregated networks. Such patterns involve several nodes and their timed contacts. The approach consists of three phases: (1) identifying temporal subgraphs, (2) assigning the subgraphs to equivalence classes, and (3) assessing the relevance, surprise and significance of class-wise counts against some reference. We discuss these phases in detail, and apply the presented method to a temporal network of mobile telephone calls.

1 Introduction

The key target of the temporal network approach is to study patterns that cannot be seen if the networks in question are made static by e.g. aggregating over link activation sequences. Sometimes such patterns are of interest because they have consequences on dynamical processes at the network level (e.g. the effects of burstiness on spreading, discussed elsewhere in this book). In general, the patterns are of interest since they may help us understand how the system functions. Temporal motifs are a tool for studying the mesoscale structure of temporal networks, where *mesoscale* refers both to topology and time. In more concrete terms, we want to study sequences of node contacts that follow each other within a short time interval, detect patterns in such sequences, and group them into

L. Kovanen · M. Karsai · K. Kaski · J. Kertész · J. Saramäki (✉)
Department of Biomedical Engineering and Computational Science, Aalto University School
of Science, 00076 Aalto, Finland
e-mail: jari.saramaki@aalto.fi

J. Kertész
Center for Network Science, Central European University, Budapest, Nador u. 9., H-1051,
Hungary

equivalence classes. Finally, we want to study how often patterns in each class occur and assess their statistical significance.

The concept of *network motifs* was originally introduced for static networks by Milo et al. [1] in 2002. Before addressing the time dimension, it is useful to discuss the reasoning behind static networks motifs. Originally, network motifs were defined as classes of isomorphic induced subgraphs with significantly large cardinality, i.e., the number of isomorphic subgraphs is higher in the data than in a reference system, usually the configuration model.¹ With this definition, it turned out that similar networks had a similar set of network motifs, suggesting that motifs should have to do with the functioning of the networks and could be used to define universality classes of networks.

Since their introduction, network motifs have become a widely applied tool, especially in the study of protein interaction networks [2]. However, it has also become obvious that it is not as straightforward to consider motifs as the “building blocks” of complex networks as suggested in the title of [1], or group networks according to their motif constitution as was done in [3]. In fact, any motif analysis depends intimately on the choice of the reference, as pointed out in [4]. Even though it has become customary to take the configuration model as reference, there has been only a little discussion on why one should fix the degree distribution, but not for example the clustering, assortativity, modularity, or any other network property that is well-known to exist in real networks but not in random (Erdős-Rényi) networks. The problem of finding a reference to compare with will also haunt us with temporal motifs.

This article is based on the concepts introduced in [5]; somewhat similar ideas were also presented in [6]. The term *temporal motif* itself occurs more often in the complex networks literature because it has been used to label some different concepts. For example in [7] the term refers to sequences of events in consecutive time windows, commonly known as time-respecting paths [8]. The term *dynamic motif* is also commonly used, but the concepts it refers to vary just as much. As an example, in [9] “dynamic motif” refers to analyzing network motifs in static networks obtained by aggregating data in consecutive time windows, and [10] studies a dynamic process on a network where edges are either active or not and defines “dynamic motif” as a network motif if all of its edges are active simultaneously at least once during the process.

Carrying out an analysis with temporal motifs consists of three independent steps. The first step is to define what we are looking for: temporal subgraphs. In Sect. 2 we show how the concept of subgraph can be generalized to temporal networks, and discuss the algorithm for identifying temporal subgraphs in large data sets. After detecting temporal subgraphs, the second step is to define an equivalence relation that can be used to divide the temporal subgraphs into equivalence classes, each corresponding to a *temporal motif* (Sect. 3). This equivalence is analogous to

¹The configuration model is a random network with the same degree sequence as the empirical network.

using graph isomorphism to define static motifs. We also present an implementation for carrying out this step and discuss its limitations and possible extensions.

The two steps above allow us to count the number of motifs in a data set. The last step of the analysis is interpreting these counts, and here we face the same problem of finding a reference system that has been troublesome in the static motif analysis. Instead of providing a single reference—the temporal equivalent of the configuration model—we argue that the choice of reference depends on the goal of the study. We also present some cases where meaningful results can be obtained even without a reference.

We introduce temporal motifs in the context of communication networks where each node can communicate with at most one other node at a time. This constraint makes it somewhat easier to define temporal subgraphs, but we also discuss how this it could be relaxed and go through the issues that arise if this is done.

2 Temporal Subgraphs

Just like a network motif represents an equivalence class of subgraphs, a temporal motif represents an equivalence class of temporal subgraphs. Both “subgraph” and “equivalence class” can be easily defined for static graphs: usually one studies induced, connected subgraphs² and defines equivalence by graph isomorphism.³ In temporal networks neither of these two concepts has a natural or commonly accepted definition. In fact, there are multiple possible generalizations of the concepts of “subgraph” and “isomorphism” to temporal networks.

While some choices for these concepts are surely better than others, we believe that their definitions should ultimately depend on the goal of the analysis. Temporal subgraphs are the objects that we wish to count, and the fact that there are many possible choices for defining subgraphs in temporal networks is not necessarily a bad thing; rather, it allows us to customize the definition to the problem at hand much more freely than is possible in static networks.

There is also a computational constraint for the definition: we need to be able to count the temporal subgraphs in the data, preferably in linear time with respect to the number of events and nodes. A practical requirement for counting any objects in linear time in arbitrary data is that there are at most a linear number of the objects to count. Definitions that give an exponential number of subgraphs are computationally unfeasible. This constraint is equally relevant when we try to make sense of the results. Our goal is to make conclusions based on the number of subgraphs in the

²A graph $G = (V, L)$ is connected iff there is a path between any two nodes, or equivalently when $|L| \geq 2$, iff there is a path between any two edges. A subgraph $G' \subseteq G$ is *induced* if all nodes $v_i, v_j \in G'$ that are adjacent in G are also adjacent in G' .

³Two graphs G_1 and G_2 are isomorphic if there is a bijection $\sigma : V_1 \rightarrow V_2$ of node labels such that $\sigma(L_1) = L_2$.

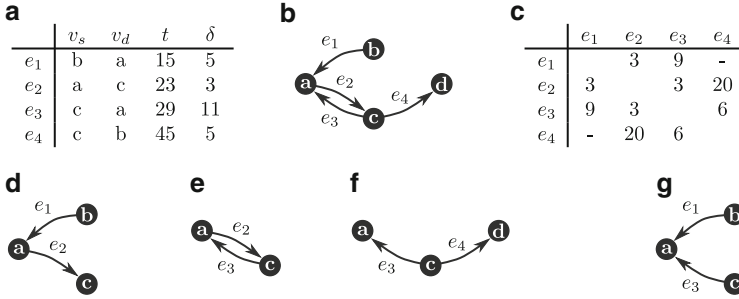


Fig. 1 (a) A directed temporal network $G_T = (V, E)$ with $V = \{a, b, c, d\}$ and $|E| = 4$. Each event consists of source node v_s , destination node v_d , starting time t and duration δ . (b) A graphical representation of G_T . (c) Time differences between adjacent event pairs. Assuming $i < j$, the value at (e_i, e_j) is $t_j - (t_i + \delta_i)$. (d–g) All two-event temporal subgraphs in the data assuming $\Delta t = 10$. The subgraph in (g) is not a valid subgraph because it skips event e_2 that for node a takes place between e_1 and e_3 . Other subgraphs are valid

data, and any definition that gives a super-linear number of subgraphs is likely to give misleading, hard-to-interpret results.

The requirement that subgraphs should be connected seems rather intuitive; in fact, the number of unconnected subgraphs becomes easily so high that counting them is out of the question. In a temporal network we should also include time when defining connectedness between events. We say that two events are Δt -adjacent if they have at least one node in common and if the time difference between the events is no more than Δt , measured from the end of the first event to the beginning of the second. This definition of adjacency immediately leads to a definition of connectivity: two events are Δt -connected if there is a sequence of Δt -adjacent events between them. A connected temporal subgraph is then a set of events where each pair of events is Δt -connected. Figure 1 illustrates these three concepts.

This definition has one small caveat. Consider a case where one node has n events that all take place with a time window Δt . Because any set of $k < n$ events is Δt -connected, this data would contain $\binom{n}{k}$ connected temporal subgraphs with k events—a super-linear number. We therefore add a requirement that for each node in the subgraph the events where that node is involved must be consecutive. Subgraphs that satisfy this condition are called *valid temporal subgraphs*. In the above example this reduces the number of k -event subgraphs to $n - k + 1$. This additional requirement is analogous to only counting *induced* subgraphs in the static case instead of all possible subgraphs. That choice also reduces the number of subgraphs and ensures they always include all relevant edges for the included nodes.

Note that valid temporal subgraphs do not necessarily contain all events that are Δt -connected to the included events. When this is the case, we call the result a *maximal* temporal subgraph. All other subgraphs involving any of the events in question are by definition completely contained inside a single maximal subgraph.

The algorithm for detecting all temporal subgraphs presented in [5] works by first finding all maximal subgraphs and then all other subgraphs by going through

Algorithm 1 FINDTEMPSUBGRAPHS returns all temporal subgraphs in data E with up to n_{\max} events that have e_0 as the earliest event. Unlike the algorithm given in [5] this one does not require constructing maximal subgraphs. $N(e)$ is the set of next and previous events of nodes in e (thus $|N(e)| \leq 4$), and t_0 denotes the starting time of e_0 . V_- is the set of excluded events; note that this set is updated, not replaced, on line 10. L_+ is a list of potential events to add. Each element is a pair (Δ_i, e_i) where $\Delta_i \geq 0$ is the shortest time difference between e_i and any other adjacent event already in the subgraph S ; if $\Delta t < \max\{\Delta_i\}$, S is no longer connected. This can be used to efficiently identify temporal subgraphs for different values of Δt . Note that the subgraphs returned by FINDTEMPSUBGRAPHS are not necessarily valid; this must be checked separately.

```

1: function FINDTEMPSUBGRAPHS( $E, n_{\max}, e_0$ )
2:    $S \leftarrow \{e_0\}$ 
3:    $V_- \leftarrow \{e_0\}$ 
4:    $L_+ \leftarrow [(\Delta_{0,i}, e_i) \mid e_i \in N(e_0), 0 \leq \Delta_{0,i} \leq \Delta t]$ 
5:   return  $\{e_0\} \cup \text{SUBFIND}(E, n_{\max}, S, V_-, L_+, t_0)$ 

6: function SUBFIND( $E, n_{\max}, S, V_-, L_+, t_0$ )
7:    $S_{\text{all}} \leftarrow \emptyset$ 
8:   for  $(\Delta_i, e_i)$  in  $L_+$  ordered by  $\Delta_i$  do
9:     if  $e_i \notin V_-$  then
10:       $V_- \leftarrow V_- \cup \{e_i\}$ 
11:       $S^* \leftarrow S \cup \{e_i\}$ 
12:       $S_{\text{all}} \leftarrow S_{\text{all}} \cup \{S^*\}$ 
13:      if  $|S^*| < n_{\max}$  then
14:         $N_+ \leftarrow \{e_j \in N(e_i) \setminus V_- \mid t_j \geq t_0, |\Delta_{i,j}| \leq \Delta t\}$ 
15:         $L_+^* \leftarrow [(\Delta_j, e_j) \in L_+ \mid \Delta_j > \Delta_i] + [(|\Delta_{i,j}|, e_j) \mid e_j \in N_+]$ 
16:         $S_{\text{all}} \leftarrow S_{\text{all}} \cup \text{SUBFIND}(E, n_{\max}, S^*, V_-, L_+^*, t_0)$ 
17:   return  $S_{\text{all}}$ 

```

the subgraphs inside the maximal subgraphs. When Δt is increased, the maximal subgraphs become larger, and eventually a giant maximal subgraph typically emerges that contains a significant fraction of all events. In this case, it may become infeasible to detect temporal subgraphs by first detecting maximal subgraphs. Then, Algorithm 1 is a good alternative, as it does not require the maximal subgraphs to be identified explicitly. In addition, Algorithm 1 gives the critical time window size for each subgraph; if Δt is smaller than this critical value, the subgraph is no longer Δt -connected. This makes it possible to efficiently study how the number of temporal motifs varies as a function of Δt .

3 From Subgraphs to Temporal Motifs

The definition of temporal subgraph is not sufficient for defining motifs—we also need to define an equivalence relation. With static motifs equivalence of subgraphs is defined by graph isomorphism: two induced, connected subgraphs correspond

to the same motif if they are identical after we disregard the identities of the nodes. When defining temporal motifs we also start by discarding node identities. An event sequence can be represented by a directed multigraph.⁴ Two temporal subgraphs can correspond to the same motif only if their underlying directed multigraphs are isomorphic. To define temporal motifs we also need to include the time dimension in the equivalence relation. We could, for example, retain all temporal information. In most cases, however, the resulting temporal motifs would be far too specific: two event sets would be equivalent only if they have the same topology and the events would occur at exactly the same time. For most types of temporal networks, such as the call network discussed later, this makes no sense. Because of this, instead of including exact times, we only retain information about the temporal order of the events. Then, two temporal subgraphs are equivalent *if they have the same topology and their events occur in the same order*.

In practice the motif corresponding to a temporal subgraph is identified by mapping all information about the topology and the temporal order of events into a directed colored graph, as shown in Fig. 2. In the simplest case, where nodes have no attributes and the only attributes associated with events are their time and direction, the mapping is done as follows: first, all nodes are given the same color (black circles in Fig. 2). Then, for each event, an additional vertex of another color (open squares) is inserted, and directed links are created from the source node to the event node, and from the event node to the target node. At this stage, the colored graph is bipartite, as there are only links between “real” nodes and event nodes. Finally, information about the temporal order of events is included by adding directed links between events in their order of occurrence, so that a directed link joins the first event node to the second event node and so on. Having done this, we have transformed the temporal subgraph into a unique colored directed graph.

In order to arrive at temporal motifs, we want to assign the colored directed graphs that represent temporal subgraphs into classes. Solving the isomorphism of such graphs is a non-trivial problem, but luckily this problem is common enough and there are several good implementations: in fact, most popular algorithms for solving graph isomorphism make use of colored nodes, that is, they solve isomorphism for colored graphs (G, π) where $\pi : V \rightarrow C$ defines the color $c \in C$ of each node. We will cover the basic ideas for solving graph isomorphism in detail in the next section.

It is worth mentioning that the existence of such algorithms is very fortunate, since we can add new layers of detail by adding new colors to the above mapping. For example, we can use different colors to represent different node types, and then distinguish motifs by the types of involved nodes. Furthermore, because of the way the mapping is constructed, we can also distinguish between events of different types. As an example, for mobile communication data, we could assign calls and text messages a different color, or study how communication patterns differ by the time of the day by coloring events according to their times (e.g. morning, day, evening, and night events).

⁴Multigraphs are graphs where multiple edges between vertices are allowed.

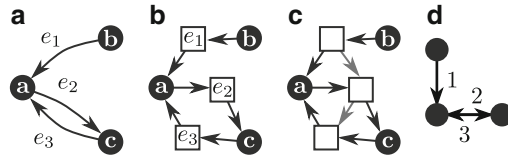


Fig. 2 Identifying the motif for a temporal subgraph. (a) A valid temporal subgraph. (b) Insert an additional vertex for each event (*squares*), making sure these vertices have a color not used by the original nodes (the “color” of a node is denoted by its shape). The direction of events is denoted by the two directed edges connecting the new vertex to the original nodes. If events are undirected we replace these by bidirectional edges. (c) Information about the temporal order of events is included by adding directed edges between the event vertices. The result is a directed, colored graph that contains all information about the topology and temporal order of events. (d) A more compact representation of the motif. The edges denote the direction of the events, and the numbers denote their temporal order. Note that the numbers are always on the side of the *arrow head*; this way reciprocated events can also be shown

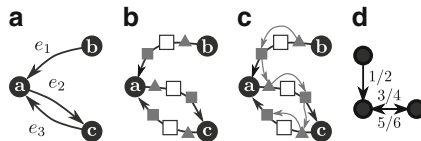


Fig. 3 Identifying the motif for a temporal subgraph when a node can have multiple simultaneous events. In this case we need to retain information on the order of both the starting and ending times of events. (a) A valid temporal subgraph. In this example we assume that e_1 ends before e_2 begins, and e_2 ends before e_3 begins. (b) Insert three new vertices for each event and connect them with a chain of directed edges denoting the direction of the event. Each of the three nodes has a different color. The color of the central vertex can be used to denote the type of the event, while the other two vertices denote the beginning and the end of the event and are assigned some other color. (c) Add directed edges to denote the temporal order of the beginning and end of events. (d) In the compact representation two numbers are now needed to represent the order of the starting and ending times of events.

Furthermore, because we use directed edges to denote the temporal order of events, we are not limited to representing the full order of events, but any partial order can be used. For example, if we wish to study spreading dynamics, it is possible to limit the temporal order of two events only if their mutual order is relevant for spreading. The order of the events is relevant to spreading when changing the order would either destroy existing time-respecting paths in the motif or create new ones. This is achieved by placing a constraint for the mutual order of two adjacent events (by adding an edge between event vertices in the graph of Fig. 2c).

Finally, what if we wish to study a system where nodes can be simultaneously involved in multiple events? Unlike the previous step of defining temporal subgraphs, the mapping step is easier to generalize to this case. As shown in Fig. 3, we now need to add three vertices for each event.

4 Isomorphism Detection and Canonical Graphs

As mentioned above, temporal motifs are identified by mapping temporal subgraphs into directed colored graphs and then using existing algorithms, such as `Bliss`⁵ [11], to solve the isomorphism. In this section we describe the basic idea of how such algorithms work.

Graph isomorphism is one of very few problems that have not been shown to be in either P or NP-complete. Instead of directly solving the isomorphism of two graphs, most algorithms solve a related problem of finding a *canonical label* $C(G)$ that satisfies the condition $C(G_1) = C(G_2) \Leftrightarrow G_1 \cong G_2$, where $G_1 \cong G_2$ means that the two graphs are isomorphic. Given a tool for finding canonical labels, it is straightforward to identify isomorphic graphs.

In this section $G = (V, L)$ is a directed graph. We also assume that the nodes are identified by integers from 1 to N , that is, $V = \{1, \dots, N\}$. Let $\text{Sym}(V)$ be the set of all permutations of V . The image of $x \in V$ in $\gamma \in \text{Sym}(V)$ is denoted by x^γ . This notion is extended to sets so that for $S \subseteq V$ we have $S^\gamma = \{x^\gamma \mid x \in S\}$, and for graphs $G^\gamma = (V, L^\gamma)$ where $L^\gamma = \{(i^\gamma, j^\gamma) \mid (i, j) \in L\}$. With this notation $G_1 \cong G_2$ if and only if there is a permutation $\gamma \in \text{Sym}(V)$ such that $G_1^\gamma = G_2$.

To illustrate these ideas, consider the following simple method for calculating canonical labels. Let $A = [a_{ij}]$ be the adjacency matrix of G and $b(G) = a_{11} \dots a_{1n} a_{21} \dots a_{nn}$ the binary number obtained by concatenating its values row by row. Now $C(G) = \min_{\gamma \in \text{Sym}(V)} \{b(G^\gamma)\}$ is a valid canonical label for graphs with N nodes, as its value does not depend on the labeling of nodes. Unfortunately, calculating $C(G)$ from this simple definition requires going through all $n!$ permutations. It is possible to calculate canonical labels more efficiently than this. The idea is that instead of going through all possible canonical labelings we only need to try a subset of them as long as we ensure that the same subset is used for isomorphic graphs.

A family of efficient algorithms are based on a backtrack search that alternates between two phases: *refinement* and *individualization*. These algorithms are based on `Nauty`⁶ [12], whose predecessor dates back to 1976. The implementation we are using, `Bliss`, was published in 2007 but is to a large extent identical to `Nauty`. `Bliss` uses more efficient data structures and includes improvements in pruning unnecessary parts of the search tree, but the description of the algorithm given here applies equally well to both `Nauty` and `Bliss`.

A central concept in the search is (ordered) *partition* $\pi = (V_1, \dots, V_m)$, an ordered sequence of subsets of V , called *cells*, whose union is V . A cell is *singular* if it has only one element, and a partition is *discrete* if all of its cells are singular. A *unit* partition has only one cell. Partition π_1 is *at least as fine* as π_2 , denoted by $\pi_1 \leq \pi_2$, if π_2 can be obtained from π_1 by replacing neighboring cells by their union

⁵<http://www.tcs.hut.fi/Software/bliss/>

⁶<http://cs.anu.edu.au/~bdm/nauty/>

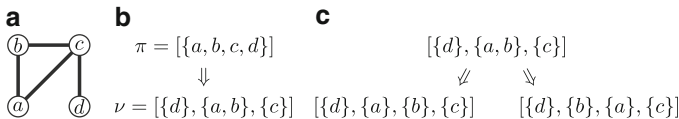


Fig. 4 Illustration of the backtrack search for calculating the canonical label for a graph. **(a)** The undirected, uncolored graph G for which we calculate canonical labels. Initially, each node has the same color, i.e. the partition is $\pi = \{\{a, b, c, d\}\}$. **(b)** Refinement. π is the original ordered partition for the uncolored graph. In the refined partition ν all nodes of one color have the same number of neighbors of each of the other colors. As an example, here the nodes $\{a, b\}$ are now of the same color (partition cells correspond to colors), and both have one neighbor of color $\{c\}$ and no neighbors of color $\{d\}$. **(c)** Individualization. We select one non-singular cell—in this case the cell $\{a, b\}$ is the only one—and create new partitions by splitting each node in turn. Here this results in two discrete partitions, the leaves in the search tree. A leaf certificate $C(G, \pi, \nu_i)$ is then calculated for each leaf ν_i , and the leaf ν_i with $C(G, \pi, \nu_i) < C(G, \pi, \nu_j) \forall j \neq i$ is selected as the canonical label

zero or more times. If $x \in V$ is included in the i^{th} cell of π , we write $\pi(x) = i$; in this way every discrete partition corresponds to a permutation $\bar{\pi} \in \text{Sym}(V)$. A *colored graph* is formally defined as pair (G, π) , where $\pi(x)$ is interpreted as the color of node x . For an uncolored graph π is a unit partition.

Every node ν in the backtrack search tree is an ordered partition. We illustrate the search for the undirected, uncolored graph shown in Fig. 4a. Since the input graph is uncolored, $\pi = \{\{a, b, c, d\}\}$.

The search starts with the refinement phase. This phase takes (G, π) as input and produces a partition $\nu = R(G, \pi) \preceq \pi$ such that in the colored graph (G, ν) every node of color i has the same number of neighbors of color j , for all i and j . For the graph in Fig. 4, the partition $\nu = \{\{d\}, \{a, b\}, \{c\}\}$ satisfies this condition: node d has no neighbors of color 1 or 2 and one neighbor of color 3, while nodes a and b have one neighbor of color 1 (each other, that is), and one neighbor of color 3.

Note that this is not the only ordered partition that fulfills the given conditions; for example $\{\{a, b\}, \{c\}, \{d\}\}$ would be equally valid. The crucial point is that however R is implemented, it must not use any information about the node labels; to be precise, $R(G^\gamma, \pi^\gamma) = R(G, \pi)^\gamma \forall \gamma \in \text{Sym}(V)$. This ensures that the same nodes are produced for isomorphic graphs. The refinement algorithm used in both `Nauty` and `Bliss` is described in [12].

The individualization phase takes (G, ν) as input, selects one non-singleton cell $V_i = S(G, \nu)$ of ν —again so that $S(G^\gamma, \nu^\gamma) = S(G, \nu)^\gamma \forall \gamma \in \text{Sym}(V)$, which can be achieved for example by selecting the first cell with the maximum size—and produces child nodes by splitting this cell. The child nodes are partitions $\nu = [V_1, \dots, \{v_j\}, V_i \setminus \{v_j\}, \dots, V_m] \forall v_j \in V_i$. In the example of Fig. 4 there is only one non-singleton cell after the initial refinement phase, and the splitting produces two new partitions as shown in Fig. 4c.

Refinement and individualization are repeated for the partitions produced until we get discrete partitions defining the leaf nodes in the tree. In Fig. 4 this happens after applying each phase only once, but in the general case multiple steps are

required. In each leaf node v we calculate a leaf certificate $C(G, \pi, v)$ defined so that it is independent of node labels in the original graph; for example $(G^{\bar{v}}, \pi^{\bar{v}})$ fulfills this condition (see [11] for proof). Because we have been careful not to use node labels during the construction of the tree, isomorphic graphs will produce isomorphic search trees, and hence the same set of leaf certificates. Now it suffices to pick one leaf certificate—say, the smallest one—to use as graph certificate.

This basic backtrack search already provides a significant improvement over the naive method of going through all permutations. For the graph in Fig. 4a we only need to compute leaf certificate for two permutations, instead of all $4! = 24$. This is however only the basic idea of the search. For example, by selecting the leaf certificate function cleverly it is possible to prune some subtrees early in the search. Even more pruning can be achieved by making use of the automorphism of the input graph.

For details of these and other improvements to the search we refer the reader to [12] and [11]. The important point is that even though isomorphisms can not be detected in polynomial time, the detection is very efficient in practice. Furthermore, because colored graphs are used internally, there is little extra cost in solving the isomorphism for colored graphs.

5 Analyzing Motif Counts

The concepts and algorithms presented so far allow counting temporal motifs in data sets with up to 10^9 events. Unfortunately, the motif counts alone do not reveal that much about the data. If there is no reference to compare with, it is in most cases impossible to say when the count value is high and when it is low. As with static motifs, a typical choice of reference is a null model, and we will therefore discuss null models below, in Sect. 5.2.

We argue that a desirable feature of any temporal motif analysis is that *the results are independent of the aggregated network*. There are two reasons for this. The first is that the static differences—those observable in the aggregate network, like the number of different static motifs, or which node types are involved, the number of nodes of each type and their average activity—easily overpower temporal differences. For example, if there is twice the number of nodes of type A than of type B , it is not too surprising if temporal motifs with type A nodes are more common. Social networks also exhibit preferred connectivity by various attributes. A typical example is homophily; similar people are more likely to be friends. If there are more edges between similar than dissimilar nodes, we would expect temporal motifs between similar nodes to be more common.

The second reason for factoring out the effect of the aggregate network is that differences in it are much easier to study, and in many cases already relatively well known. For example, aggregated networks obtained from mobile phone data sets have been studied extensively. If we devise our null model such that the results are independent of the aggregated network, we also get an independent description of

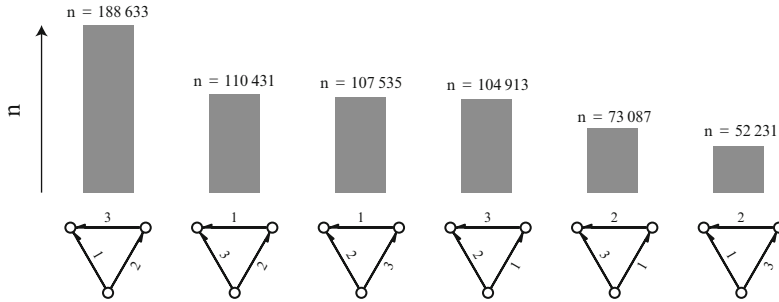


Fig. 5 Six motifs with the same underlying graph but different order of events. The *bars* show the total count for each of the motifs with $\Delta t = 10$ min. In the aggregate network it would not be possible to differentiate between the six motifs, but the large factor (3.6) between the most and least common case shows that there is a relevant difference to be made

the data, in addition to results obtained with the aggregated network. In other words, we can see patterns that are not revealed by the aggregate.

In the following sections we present example results using a mobile phone data set with $\sim 10^8$ events and $\sim 10^6$ nodes. The nodes correspond to customers of a single European mobile phone operator and the events correspond to mobile phone calls between them during a period of several months. The data set also contains meta data about the customers, such as gender and age, that can be used to distinguish different node types.

We use $\Delta t = 10$ min in all examples. This provides ample time for making a new call after ending the previous one without including too many coincidentally simultaneous calls. A full data analysis would naturally benefit from studying how sensitive the results are to changes in the time window size.

5.1 Direct Comparisons

Before considering null models it is worthwhile to note that some purely temporal results (i.e. results that are independent of the aggregate network) can be obtained even without any reference model. The first case is motifs that differ only in the temporal order of events, such as the triangles in Fig. 5 (another example is the two-chain, where the events can take place in the causal or non-causal order). Because these motifs cannot be distinguished in the aggregate network, any difference observed is purely temporal.

Motif analysis reveals that the most common triangle is 4 times as common as the rarest one. Comparison of all six motifs reveals two explanations for this difference, both well-known features of communication networks. The first is burstiness; in the four most common motifs the person making two calls makes those calls consecutively. The second explanation is causality. E.g., in the most common motif

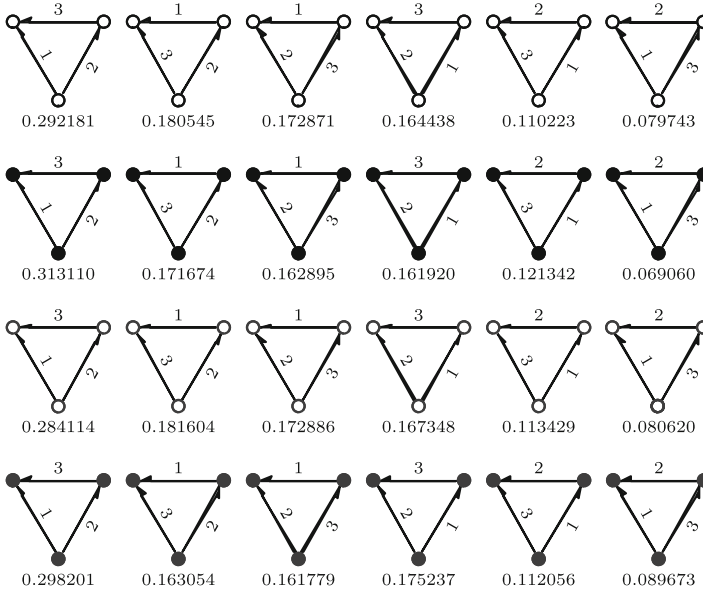


Fig. 6 Six motifs that have the same topology but differ in the order of the events, plotted separately for four different types. From *top* to *bottom*, the rows correspond to postpaid female, prepaid female, postpaid male, and prepaid male (postpaid refers to customers who are billed based on the calls made; prepaid customers pay for their calls beforehand). The numbers below the motifs show the fraction out of all motifs in each row. This value can be compared across different rows because it doesn't depend on the group size, activity or homophily. For the mobile phone data we observe only small differences between node types

(where A calls B and C, and C then calls B), the third call can be triggered by the earlier calls, as the caller C may have information on the first A–B call through the second A–C call.

When analyzing data that has different node types it is generally not possible to directly compare the counts because they mostly just reflect the differences in groups sizes, activity, and connectivity, instead of differences in temporal behavior. It is however always possible to compare the *relative* occurrence of motifs with different orders of events, when we constrain all nodes in the motif to have the same type, as illustrated in Fig. 6. The reasoning here is similar as with Fig. 5: no property of the static network can explain the relative count of the differently timed versions, and hence we are comparing purely temporal differences.

Comparing motifs that have multiple node types is unfortunately not as simple. Motif counts generally depend on the number of nodes of each type, average activity levels of different node types and their preferred connectivity. In most cases, a comparison of motifs with the same topology but different node types would just reflect these differences. Comparison of different topologies, even when keeping node type constant, is not valid either. If for example the aggregate network consists of directed triangles, then we would expect directed temporal triangles to be common as well (as compared to other kinds of triangles).

5.2 Null Models

Except for the cases listed above, we need a point of reference to compare against if we are to make statements about the prevalence of motifs. And when discussing motifs and references, it is hard not to mention null models.

Null models are often presented as a method for finding out whether the results could stem from random variations under some constraints. One of the first applications of network motifs was to test whether the number of static motifs in various networks could result from the degree distribution alone [1]. This is achieved by comparing against the motif count in the configuration model, a random network with the same degree sequence as the empirical network.

Suppose the empirical count for motif m_i is $C(m_i)$, and for the randomized networks we get the mean count $\mu(m_i)$ with standard deviation $\sigma(m_i)$. Now, if the empirical motif counts result from the degree distribution alone, we would expect the z -score

$$z_i = \frac{C(m_i) - \mu(m_i)}{\sigma(m_i)}$$

to have zero mean and unit variance. Following the standard null hypothesis framework, this equals to testing the null hypothesis

H_0 : $C(m_i)$ results from degree distribution alone.

Large deviations of z from zero suggest that the data does not support the null hypothesis.

Using null models might seem straightforward, but anyone applying null models in their analysis should be aware of possible problems involved. For example, the corresponding null hypothesis—which is almost never explicitly written out—might not be the one the researcher intended to study. And because null models are typically defined algorithmically, it might not even be obvious what the null hypothesis is. A good discussion of this and other caveats in the use of null models can be found in [4].

Complex networks are also not the first applications of null models. Very similar ideas have been used in ecology [13], and the usage have often been followed by a heated discussion on the limitations and possibilities of the method—even to the extent to earn the name *null model wars* [14].

6 Summary and Discussion

The fundamental goal of temporal network analysis is to be able to detect patterns that would be lost, were the networks in question considered static or quasi-static by aggregating over link activations over some time interval. Were this not the case, then static network analysis would suffice.

In this chapter, we have presented an approach for detecting recurrent patterns in the time-ordered sequences of events that constitute temporal networks. In essence, this approach can be boiled down to three (independent) phases: (1) defining and detecting *temporal subgraphs*, (2) assigning the detected temporal subgraphs to similarity classes (*temporal motifs*), and (3) assessing the relevance of the class-wise subgraph counts, either in relation to each other or against some carefully chosen reference system.

These phases reflect the additional complications induced by adding another degree of freedom—time. For static networks, a triangle is a triangle, and such subgraphs can readily be counted. For temporal networks, we first have to define what a triangle is; here, we have defined temporal subgraphs based on the time adjacency of events sharing nodes. For constructing similarity classes, we have designed a method of mapping temporal subgraphs to directed, colored graphs, whose isomorphism can be tackled with existing algorithms. Finally, the question of the meaning and relevance of temporal motif counts—often, the *surprise* of the counts against some assumptions about regularities in the underlying system—is clearly the most difficult of these questions. We have attempted to tackle it using comparisons between motifs that have the same numbers of nodes and events, representing structure over and above corresponding static network representations, and by carefully examining the concept of null models, with the aim of clearly laying out the meaning of null hypotheses.

Our methodology can be directly applied in studies of any temporal system of interacting agents, where interactions evolve as exclusive instantaneous events. Because the temporal motifs are based on the timings of such events, all available time-domain information is accounted for, and no simplifying assumptions are required. In general, this technique may help to highlight “hidden” correlations and functionality, and to understand how micro-level interactions induce mesoscopic-level structure that may play a role for dynamical processes that are mediated by the temporal system.

Certain possible extensions of the present framework would allow for an even broader range of applications. First, a generalization that would allow the nodes to simultaneously participate in multiple instantaneous interactions would be very useful—consider, e.g. emails sent to multiple recipients. There is a large number of systems where the node-wise interactions are non-exclusive. Potential applications include biological systems such as temporal gene regulation or protein interaction networks [15, 16], social systems of humans or animals [17] and ecological interaction networks [18]. A generalization for interval graphs, i.e. for temporal networks where events are non-instantaneous and have specified durations, would open even further possibilities, and allow for detection of temporal patterns in e.g. evolving group dynamics such as dynamics of face-to-face communication [19].

Acknowledgements The authors acknowledge financial support by the EU 7th Framework Program’s FET-Open to ICTeCollective, project no. 238597, and support by the Academy of Finland to the project “Temporal networks of human interactions”, no. 260427. Lauri Kovanen is also supported by the doctoral program Brain & Mind.

References

1. Milo, R., Shen-Orr, S., Itzkovitz, S., Kashtan, N., Chklovskii, D., Alon, U.: Network motifs: simple building blocks of complex networks. *Science* **298**(5594), 824–827 (2002)
2. Ciriello, G., Guerra, C.: A review on models and algorithms for motif discovery in protein-protein interaction networks. *Brief. Funct. Genomics Proteomics* **7**(2), 147–156 (2008)
3. Milo, R.: Superfamilies of evolved and designed networks. *Science* **303**(5663), 1538–1542 (2004)
4. Artzy-Randrup, Y., Fleishman, S.J., Ben-Tal, N., Stone, L.: Comment on “Network motifs: simple building blocks of complex networks” and “Superfamilies of evolved and designed networks”. *Science* **305**(5687), 1107 (2004)
5. Kovanen, L., Karsai, M., Kaski, K., Kertész, J., Saramäki, J.: Temporal motifs in time-dependent networks. *J. Stat. Mech. Theor. Exp.* **2011**(11), P11005+ (2011)
6. Zhao, Q., Tian, Y., He, Q., Oliver, N., Jin, R., Lee, W.-C.: Communication motifs: a tool to characterize social communications. In: *Proceedings of the 19th ACM International Conference on Information and Knowledge Management*, pp. 1645–1648. ACM, New York (2010)
7. Bajardi, P., Barrat, A., Natale, F., Savini, L., Colizza, V.: Dynamical patterns of cattle trade movements. *PLoS ONE* **6**(5), e19869+ (2011)
8. Kempe, D., Kleinberg, J., Kumar, A.: Connectivity and inference problems for temporal networks. *J. Comput. Syst. Sci.* **64**(4), 820–842 (2002)
9. Braha, D., Bar-Yam, Y.: Time-Dependent complex networks: dynamic centrality, dynamic motifs, and cycles of social interaction. In: Gross, T., Sayama, H. (eds.) *Adaptive Networks: Theory, Models and Applications*. Springer Studies on Complexity, pp. 39–50. Springer, Berlin (2009)
10. Schramm, L., Martins, V.V., Jin, Y., Sendhoff, B.: Analysis of gene regulatory network motifs in evolutionary development of multicellular organisms. In: *Proceedings of the 12th International Conference on the Synthesis and Simulation of Living Systems (ALife XII)*, pp. 133–140. MIT Press, Cambridge, MA (2010)
11. Junttila, T., Kaski, P.: Engineering an efficient canonical labeling tool for large and sparse graphs. In: Applegate, D., Brodal, G.S., Panario, D., Sedgewick, R. (eds.) *Proceedings of the Ninth Workshop on Algorithm Engineering and Experiments and the Fourth Workshop on Analytic Algorithms and Combinatorics*, pp. 135–149. SIAM, Philadelphia (2007)
12. McKay, B.D.: Practical graph isomorphism. *Congr. Numer.* **30**, 45–87 (1981)
13. Gotelli, N.J.: Research frontiers in null model analysis. *Global Ecol. Biogeogr.* **10**(4), 337–343 (2001)
14. Fox, J.: Why ecologists should refight the ‘null model wars’, *Oikos Blog*, <http://oikosjournal.wordpress.com/2011/06/01/why-ecologists-should-refight-the-null-model-wars/> (2011). Accessed 2 Sept 2012
15. Bar-Joseph, Z., Gitter, A., Simon, I.: Studying and modelling dynamic biological processes using time-series gene expression data. *Nat. Rev. Genet.* **13**, 552–564 (2012)
16. Jin, R., et al.: Identifying dynamic network modules with temporal and spatial constraints. *Pac. Symp. Biocomput.* **14**, 203–214 (2009)
17. Waters, J.S., Fewell, J.H.: Information processing in social insect networks. *PLoS ONE* **7**(7), e40337 (2012)
18. Blonder, B., Wey, T. W., Dornhaus, A., James, R., Sih, A.: Temporal dynamics and network analysis. *Methods Ecol. Evol.* **3**(6), 958–972 (2012)
19. Cattuto, C., et al.: Dynamics of person-to-person interactions from distributed RFID sensor networks. *PLoS ONE* **5**(7), e11596 (2010)

Applications of Temporal Graph Metrics to Real-World Networks

John Tang, Ilias Leontiadis, Salvatore Scellato, Vincenzo Nicosia, Cecilia Mascolo, Mirco Musolesi, and Vito Latora

Abstract Real world networks exhibit rich temporal information: friends are added and removed over time in online social networks; the seasons dictate the predator-prey relationship in food webs; and the propagation of a virus depends on the network of human contacts throughout the day. Recent studies have demonstrated that static network analysis is perhaps unsuitable in the study of real world network since static paths ignore time order, which, in turn, results in static shortest paths overestimating available links and underestimating their true corresponding lengths. Temporal extensions to centrality and efficiency metrics based on temporal shortest paths have also been proposed. Firstly, we analyse the roles of key individuals of a corporate network ranked according to temporal centrality within the context of a bankruptcy scandal; secondly, we present how such temporal metrics can be used to study the robustness of temporal networks in presence of random errors

J. Tang · I. Leontiadis · S. Scellato · C. Mascolo
Computer Laboratory, University of Cambridge 15 JJ Thomson Avenue,
Cambridge CB3 0FD, UK

V. Nicosia
Computer Laboratory, University of Cambridge 15 JJ Thomson Avenue,
Cambridge CB3 0FD, UK

Laboratorio sui Sistemi Complessi, Scuola Superiore di Catania, Via Valdisavoia 9,
95123 Catania, Italy

M. Musolesi (✉)
School of Computer Science, University of Birmingham, Edgbaston, Birmingham B15 2TT, UK
e-mail: mirco.musolesi@acm.org

V. Latora
Laboratorio sui Sistemi Complessi, Scuola Superiore di Catania, Via Valdisavoia 9,
95123 Catania, Italy

School of Mathematical Sciences, Queen Mary, University of London, E1 4NS London, UK

Dipartimento di Fisica e Astronomia and INFN, Università di Catania and INFN, Via S. Sofia 64,
95123 Catania, Italy

and intelligent attacks; thirdly, we study containment schemes for mobile phone malware which can spread via short range radio, similar to biological viruses; finally, we study how the temporal network structure of human interactions can be exploited to effectively immunise human populations. Through these applications we demonstrate that temporal metrics provide a more accurate and effective analysis of real-world networks compared to their static counterparts.

1 Introduction

Temporal graph metrics [48, 49] represent a powerful tool for the analysis of real-world dynamic networks, especially with respect to the aspects for which time plays a fundamental role, such as in the case of spreading of a piece of information or a disease. Indeed, existing metrics are not able to characterise the temporal structure of dynamic networks, for example in terms of centrality of nodes over time. For these reasons, new metrics have been introduced, such as temporal centrality, in order to capture the essential characteristics of time-varying graphs. A detailed description of the metrics used in this chapter can be found in [40].

In this chapter we will discuss a series of possible applications of temporal graph metrics to the analysis of real-world time-varying networks. This chapter is structured as follows. We will cover our work in this area and, finally, we will discuss contributions in this fields by other researchers and potential future applications, in particular in the area of the modelling of epidemic spreading.

More specifically, in Sect. 2 we analyse the roles of key individuals according to temporal centrality within the context of the Enron scandal [49]. In Sect. 3 we study how such temporal metrics can be used to study the robustness of temporal networks in presence of random errors and intelligent attacks [45]. Then, Sect. 4 we present a containment scheme for mobile phone malware which can spread via short range radio transmission [50, 51]. Finally, in Sect. 5 we discuss existing and potential applications to human epidemiology, outlining some research directions in these areas.

2 Corporate Networks

2.1 Overview

The Enron Energy Corporation started as a traditional gas and electrical utility supplier; however, in the late 1990s their main money making business came from trading energy on the global stock markets [18]. In December 2001, the Enron Energy Corporation filed for bankruptcy after it was uncovered that fraudulent accounting tricks were used to hide billions of dollars in debt [23]. This led to the eventual conviction of several current and former Enron executives [8, 55].

The investigation also brought to light the reliance of the company on traders to bring in profits using aggressive tactics culminating in intentional blackouts in California in Summer 2001. With both control over electricity plants and the ability to sell electricity over the energy markets, Enron traders artificially raised the price of electricity by shutting down power plants serving the State of California and profiting by selling electricity back at a premium [7].

During the investigation into the Enron accounting scandal, telephone calls, documents and emails were subpoenaed by the U.S. government and as such the email records of 151 user mailboxes were part of the public record consisting of approximately 250,000 emails sent and received during the period between May 1999 to June 2002 (1,137 days), leading up to the bankruptcy filing. None of the emails were anonymised and so they provide unique semantic information of the owner of each mailbox.

2.2 Temporal Graph Construction

In our analysis, we use the dataset prepared by Shetty and Adibi [47]. Since we do not have a complete picture of the interactions of users outside of the subpoenaed mailboxes we concentrate on email exchanges between the core 151 users only. Taking this email dataset, we process the complete temporal graph from 1999 to 2002 with undirected links, using windows of size $w = 24$ h and horizon $h = 1$. If an email was exchanged between two individuals in a temporal window, a link between the two nodes representing those individuals will be added to the graph representing the temporal snapshot for that time.

2.3 Semantic Value of Temporal Centrality

Figure 1 plots the static and temporal centrality rankings of employees calculated using closeness and betweenness. Examining the static centralities (left column) we note that there is little difference between the top five employees using static closeness or betweenness. Also plotting the static degree centrality of each node¹, we notice similar rankings suggesting that static analysis only favours employees who interacted with the most number of other people. Temporal closeness and temporal betweenness yield different rankings amongst the top five and the calculated Kendall-tau correlation coefficient [31] (Table 1) confirm that static-to-static metrics are strongly correlated ($\simeq 0.7$). Also note that there is low correlation (< 0.4)

¹The static degree centrality is defined as the number of edges connected to a node i , normalised by the total possible neighbour nodes $(n - 1)$ [56].

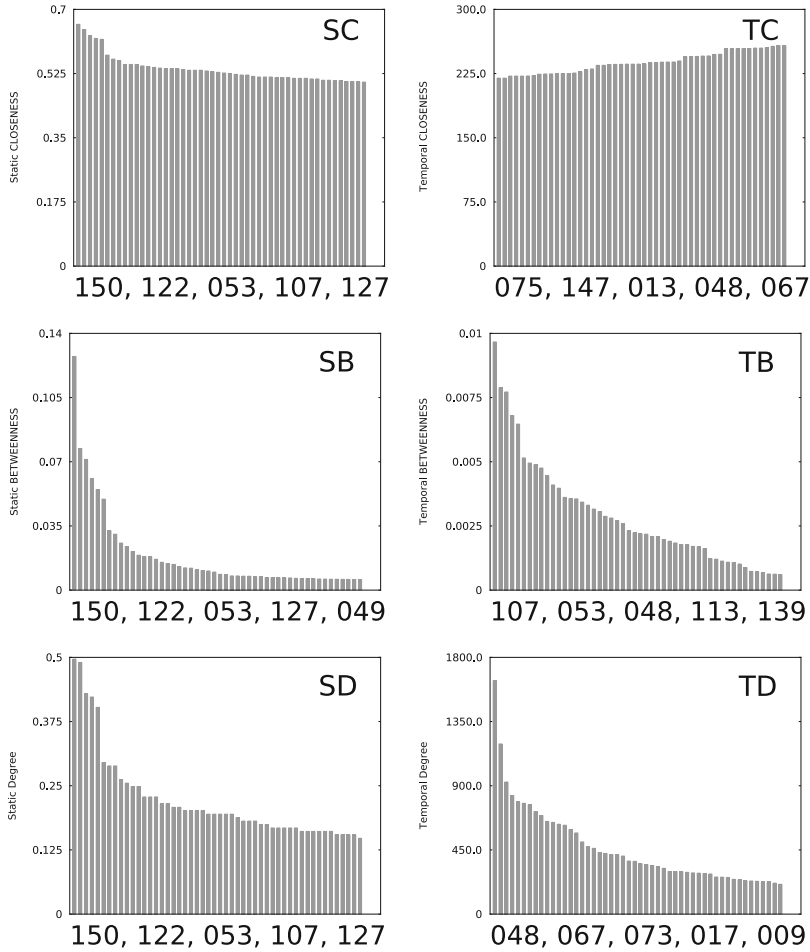


Fig. 1 Ranked distribution of top 50 statically (S) and temporally (T) central nodes. From top row: Closeness (C), Betweenness (B), and Degree (D). Top 5 node ID’s listed under each plot

between temporal metrics and static degree demonstrating that temporal analysis is not dependent on the number of people an individual interacts with.

Cross referencing the top two employee identifiers with their position within the organisation (Table 2) we identify a secretary (150) and managing director (122) as central nodes for both static closeness and betweenness; however, both temporal closeness and betweenness consistently selected employees in trading roles (053, 075, 107, 147). A secretary and a managing director are certainly important for information dissemination and central to many communication channels, as detected by static measures. However, instead the top trading executives are exclusively favoured by temporal analysis.

Table 1 Kendall-tau correlation coefficients between centralities

	SB	SC	SD	TB	TC	TD
SB	1.00	0.57	0.69	0.41	0.24	0.43
SC	–	1.00	0.70	0.36	0.22	0.31
SD	–	–	1.00	0.39	0.28	0.48
TB	–	–	–	1.00	0.43	0.34
TC	–	–	–	–	1.00	0.40
TD	–	–	–	–	–	1.00

Table 2 Roles of top centrality nodes

ID	Role	Notes
9	(Unknown)	
13	Legal	Senior Legal Specialist
17	Manager	
48	Executive	
53	Trader	
54	President	Former Head of Trading
67	Vice President	Enron Wholesale Services
73	Trader	
75	Director of Trading	
107	Trader	Head of Online Trading
122	Managing Director	
127	Chairman and CEO	
139	Director	
147	Trader	
150	Secretary	Assistant to Greg Whalley

To show that temporal analysis does not simply uncover nodes with the most interactions with other people, we also plot the temporal degree (TD) calculated as the total number of emails sent and received by each node i . Since there is a low correlation (<0.4) with temporal closeness and betweenness this shows that temporal analysis is not dependent on the number of emails sent and received by each individual.

2.4 Effectiveness of Central Nodes on Dynamic Processes

2.4.1 Trace-Driven Simulation Setup

To evaluate the role and the centrality of the employees identified by temporal and static analysis, we consider two dynamic processes. First, we simulate a simple information *dissemination process* over the temporal graph constructed from the Enron traces. The process is simulated as follows. We select the top N nodes from the ranking based on temporal closeness centrality. We place an identical message m into their (infinite) buffers. We refer to any node that has received a copy of this

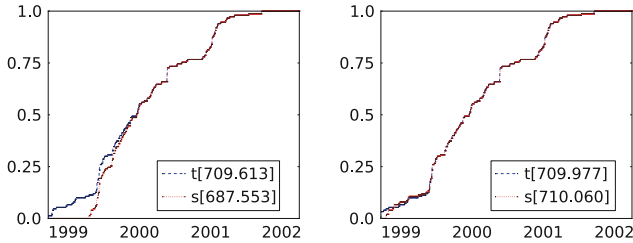


Fig. 2 Dissemination process: Dissemination ratio starting from top 2 (*left*) and top 10 (*right*) closeness source nodes. Area under curve reported in legend for temporal (t) and static (s) centrality

message as *reached*. We then replay the contact trace through time and as reached nodes make contact with an unreached node u , the message is replicated into the buffer of node u . We assume that messages are transferred instantaneously and only the first neighbour in a time window can be reached. We then repeat this for static closeness centrality and plot the dissemination ratio across time for both.

Second, to model the role of individuals as part of an information *mediation process*, we borrow concepts from the more commonly known epidemic immunisation process where the dissemination ratio of a contagion spreading throughout a static network is measured before and after certain nodes are immunised against the contagion [2]. This is analogous to measuring the spread of information (the contagion) before and after important individuals are removed from the network (such as going on holiday or being discharged) since our conjecture is that removing mediators will impact the network communication efficiency greatly.

In the trace-driven simulation, instead of a single message spreading within the organisation, we seed all employees with a different message that needs to be delivered to all other employees. This models multiple channels of communication. In order to derive a baseline performance, we start by calculating the dissemination ratio when no nodes are removed. We then remove the top N individuals identified by temporal betweenness and rerun the information spreading process. Nodes which are removed cannot receive or pass on messages. We then repeat the same process for comparison using static betweenness centrality for the ranking.

2.4.2 Evaluating Information Dissemination and Mediation

We present plots using $N = \{2, 10\}$ for information dissemination (Fig. 2) and information mediation (Fig. 3). As we can see the different pairs of traders identified by temporal analysis are better than the arbitrary nodes selected by static analysis for both disseminating information through the organisation and acting as mediators between communication channels. In the information dissemination case, although the final dissemination is the same across the long period of time, the two traders selected by temporal analysis disseminate information quicker. Only after increasing

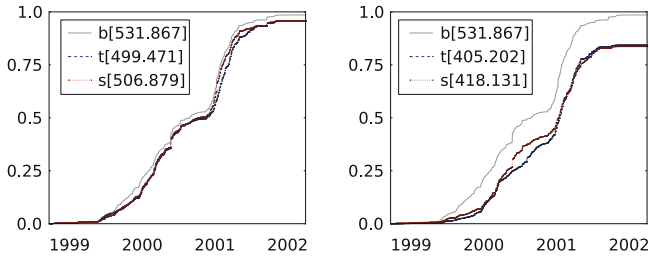


Fig. 3 Mediation process: Dissemination ratio after removing top 2 (*left*) and top 10 (*right*) betweenness nodes. Area under curve reported in legend for temporal (t), static (s) and baseline (b) where no nodes are removed

to 10 nodes the static analysis presents similar results. In the information mediation case, the final dissemination ratios for both temporal and static centrality nodes slightly decreases by removing the nodes but are comparable. However, removing the two traders gives an overall more prolonged drop in message dissemination. In the case of the removal of 10 nodes, the individuals identified by means of the temporal metrics slow the dissemination process further compared to static ones.

2.5 Summary of the Findings

This study has demonstrated the advantages of using temporal network analysis over traditional static, aggregated graphs. Although centrality rankings are quantitative measures of node importance, their physical meaning is very much qualitative. For this reason, we have shown that temporal centrality provides a more accurate identification of key people in a corporate social network where each persons role is known. Taking a second perspective, we demonstrate that temporal centrality can identify nodes which can spread and mediate information, better than static analysis. This demonstrates the importance of temporal information for applications, which are applied to real networks.

3 Network Robustness

3.1 Overview

The study of real-world communication systems by means of complex network models has provided insightful results and has vastly expanded our knowledge on how single entities create connections and how these connections are used for communication or, more generally, interaction [3]. In particular, technological networks

such as the Internet and the World Wide Web have been under scrutiny in terms of structure and dynamic behavior [22, 27]. More recently, with the widespread adoption of mobile and opportunistic networks, it has become important to develop new analytical tools to keep into account network dynamics over time [30, 32] and how this affects phenomena such as information propagation [10, 14].

At the same time, the problem of understanding whether real systems can sustain substantial damage and still maintain acceptable performance has been extensively addressed [1, 5]. Various measures of network robustness have been defined and investigated for several classes of networks, evaluating how different system can be more or less resilient against random errors or targeted attacks thanks to their underlying structural properties [15, 26].

Nonetheless, it is still unclear how to approach the study of robustness of networks by taking into account their time-varying nature: by adopting a static representation of a temporal network, important features which impact the actual performance might be missed. Thus, it becomes important to develop a robustness metric which takes into account the temporal dimension and gives insights on how a mobile network is affected by damage or change. Particularly, the fact that links are not always active means that information spreading can be delayed or even stopped and that *relative ordering in time of connection events may affect the creation of temporal paths in mobile networks*.

Our main goal is to design a novel framework for the analysis of robustness in time-varying networks. We adopt *temporal network metrics* [48] to quantify network performance and define a measure of robustness against generic network damages. At first, we study its performance on random network models to understand its properties; then we apply our method to study a real mobile network, describing how temporal robustness gives a more accurate evaluation of system resilience than static approaches.

3.2 A Framework to Evaluate Robustness of Temporal Networks

The study of robustness of complex networks has mainly focused on describing how a given performance metric of the network is affected when nodes are removed according to a certain rule. The underlying assumption is that the absence or malfunctioning of some nodes will cause the removal of their edges and, thus, some paths will become longer, increasing the distances between the remaining nodes, or completely disappear, resulting in the loss of connectivity in the whole system. In this work we will study the problem of defining and analyzing robustness in evolving networks: as a consequence, *we need to use a performance metric which includes the temporal dimension in its definition*. We choose to adopt temporal efficiency as the performance metric. We then consider random and independent failures for every node and we evaluate how the system tolerates increasing level of malfunctioning nodes.

Since a temporal graph is continuously evolving, we can evaluate how temporal efficiency changes over time by considering a value τ and evaluating $E_G(t)$ as the relative temporal efficiency of the temporal graph in the time window $[t - \tau, t]$. The effect of τ is to effectively impose an upper bound on the temporal distances, as all paths longer than τ simply do not exist. As a consequence, τ should be chosen so that any communication whose delay is longer than τ itself can be ignored.

Given a temporal graph G , we define a damage D as any structural modification on it and we define G_D as the graph resulting by the effect of the damage D on G . A damage may be the deactivation of some nodes or the removal of some edges at a particular time t_D . Because of damage D , some temporal shortest paths will be longer or will not exist any more, thus, we expect that the temporal efficiency will eventually reach a new steady value $E_{G_D} \leq E_G$. It is important to evaluate the new value of the temporal efficiency on a new temporal graph which still contains the deactivated nodes, in order to obtain a decrease in efficiency. Otherwise, we might obtain a smaller temporal graph which is more efficient than the original graph, although it has lost much of its structure. Hence, we do not consider highly dynamic systems where nodes can be constantly added or removed. Instead, we focus on evaluating the service degradation in a more controlled environment where only a number of existing nodes could fail.

We define the loss in efficiency $\Delta E(G, D)$ caused by the damage D on the temporal graph G as $\Delta E(G, D) = E_G - E_{G_D}$. Finally, we define the *temporal robustness* $R_G(D)$ of the temporal graph against the damage D as

$$R_G(D) = 1 - \frac{\Delta E(G, D)}{E_G} = \frac{E_{G_D}}{E_G} \quad (1)$$

This value is normalized between 0 and 1 and it measures the relative loss of efficiency caused by the damage: if the damage does not impact the efficiency of the graph ($E_{G_D} = E_G$) then its robustness is 1, while if the damage destroys the efficiency of the graph ($E_{G_D} = 0$) the robustness drops to 0. Temporal efficiency is a particularly suitable metric to study temporal network robustness as it denotes both longer temporal paths and the lack of paths among temporally disconnected nodes at the same time. Nonetheless, other metrics have been used to assess robustness in static systems: for instance, there could be scenarios where fast communication with small delays can be more important than global connectivity, thus other measures can be adopted. Provided that these measures can be extended to the temporal case, they can be easily integrated in our framework.

3.3 Robustness of Random Temporal Networks

In this section, we present a numerical analysis of temporal robustness for different classes of random temporal networks: an Erdős–Rényi temporal model, a Markovian temporal model and mobility-based temporal model.

3.3.1 Random Temporal Network Models

An Erdős–Rényi (ER) random graph with N nodes and parameter p is created by independently including each possible edge in the graph with probability p and it is denoted as $G(N, p)$ [19]. We generalize this model to the temporal case by creating a sequence of T ER random graphs $G(N, p)$ and we denote the resulting temporal graph as $G(N, p, T)$.

The temporal ER network model does not provide temporal correlations between consecutive graphs in the sequence. We thus consider a model where link evolution is described by a Markov process, thus enabling memory effects in network dynamics. We consider a complete graph G with N nodes. At every discrete timestep t each link may or may not be present: a temporal graph is created where the existence of each link evolves according to a two-state discrete Markov process. We denote with p the probability that a link present at time t will be removed at time $t + 1$ and with q the probability that a link which is not present at time t will be added at time $t + 1$. The steady probability of link presence then is $P_{ON} = \frac{q}{p+q}$: as a consequence, each observation of the temporal graph appears as an ER random graph with each edge present with probability P_{ON} .

We also create a random model of a temporal network by using mobility models. In this case we are introducing topological constraints: a key difference with the previous temporal models is that each node is not equally likely to connect with all the other nodes, due to the effect of spatial distance. We consider $N = 100$ nodes moving in a square area $1,000 \times 1,000$ m and we define a communication range r : at every time step, we create a graph where nodes are connected if their Euclidean distance is shorter than r . Thus, we change the probability of link presence P_{ON} by varying the communication range. Then, a temporal graph can be defined as the sequence of graphs extracted at each time step while the nodes move. We investigate two different mobility models that are implemented using the Universal Mobility Model Framework [37]: Random Waypoint Model (RWP) and Random Waypoint Group Model (RWPG). In RWP each node selects uniformly at random a location towards which it moves with speed uniformly distributed in a fixed range [5, 40] mph. As the node reaches its destination, it waits for a randomly distributed time in [0, 120] s and repeats the above steps until the end of the simulation.

In RWPG nodes are divided into two classes: there are M group leaders and $N - M$ group followers. Every group followers has its own leader so that the N nodes are divided into equally-sized groups. Each group leader selects a random target and moves towards it, according to the RWP mobility model. Group members do not select any target; instead, they follow their group leader according to the *pursuit force* [37] which is set to give a group span of 200 m.

3.3.2 Numerical Evaluation

We numerically evaluate temporal efficiency $E_G(t)$ over time, adopting a time window of $\tau = 100$, for a graph with $N = 100$ nodes: after an initial phase,

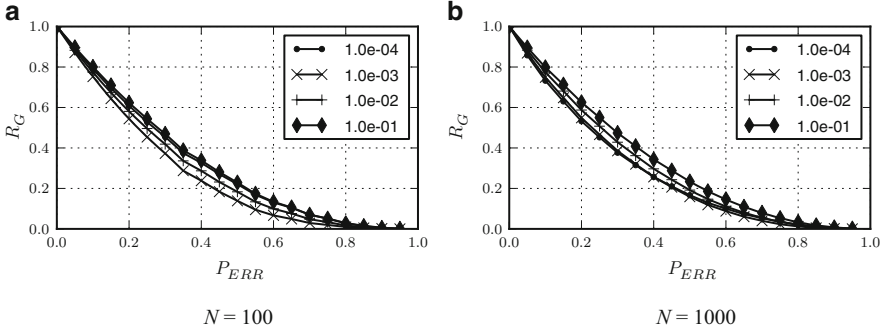


Fig. 4 Temporal robustness R_G as a function of probability of error P_{ERR} in the ER random model for different link probability p (a) 100 nodes; b) 1000 nodes). The size of the system has no impact on temporal robustness: furthermore, the system fails smoothly as the probability of error increases

the random temporal graph reaches an equilibrium state and we compute the steady value of temporal efficiency. We run each simulation for 2τ steps and we compute the average value of temporal efficiency over the last τ steps. All results have been averaged over 100 different runs. We evaluated numerically temporal robustness by deactivating each node independently with increasing probability P_{ERR} . We measure temporal efficiency before and after the failure, when the network reaches a new equilibrium state.

As reported in Fig. 4, the temporal ER model fails smoothly as we increase the fraction of removed nodes, without any sudden disruption for any value of P_{ERR} . This is a main difference with respect to what happens in the static case: for a static ER random graph there may exist a critical value of P_{ERR} which causes a breakdown of the network in several disconnected components [1]. This is not true for temporal robustness, as new paths can still appear after the damage as the network rearranges its connections. Time provides more redundancy and, hence, more resilience. Moreover, we also note that temporal robustness does not depend on system size: since it is normalized with respect to the value of temporal efficiency before the damage, it depends only on the relative drop in efficiency, not on absolute values.

As shown in Fig. 5a, temporal robustness is affected by probability of error P_{ERR} in the same way as in the temporal ER model: the system fails gradually as more nodes are removed. However, for intermediate values of P_{ON} robustness has lower values. At the same time, high and low values of P_{ON} provide the same robustness, even if the absolute value of temporal efficiency can be very different, thanks to the normalization of temporal robustness.

In the case of mobility-based temporal networks, reported in Fig. 5b, both RWP and RWPG exhibit a similar behavior: again, the network loses efficiency in a smooth way and temporal robustness is not affected by P_{ON} in this case as the spatial characteristics of the network are mainly affecting the resulting robustness.

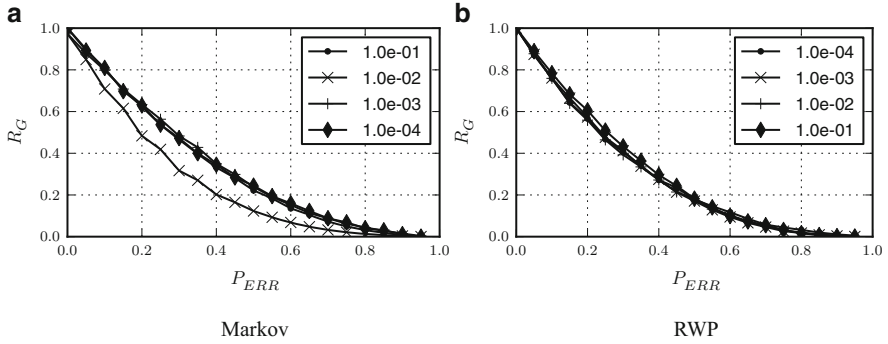


Fig. 5 Temporal robustness R_G as a function of probability of error P_{ERR} and for different values of P_{ON} for a) the Markov-based and for b) the RWP random model (RWPG does not deviate from RWP)

3.4 Case Study: Cabspotting

We have seen that temporal networks do not exhibit sudden breakdowns when nodes are being removed and that various temporal network models exhibit analogies in their resilience. We now shift our attention to real time-varying networks: our aim is to understand whether temporal robustness gives us more information than static robustness in a real case and to investigate whether random models can offer a good approximation to real networks.

3.4.1 Dataset

This case study is based on Cabspotting, a publicly available dataset of mobility traces: the Cabspotting project tracked taxi cabs in San Francisco traveling through all the Bay Area for about 2 years with the aim of gathering data about city life [41]. The vehicles were equipped with GPS sensors and every device was periodically updating its position and uploading it to a central server to be stored, along with the timestamp of the record. Thus, it is possible to reconstruct each taxi's trajectory over space. For pictorial representations of the dataset, please refer to the project website [4].

We have selected an area of about $20 \text{ km} \times 20 \text{ km}$ around the city of San Francisco and we have extracted 24 consecutive hours of mobility traces, corresponding to Wednesday, 21 May 2008. After this, we have generated an artificial contact trace by defining a communication range of 200 m for the vehicles, which roughly corresponds to WiFi connectivity range in similar scenarios [11]: whenever two cars are within this distance they can communicate to each other. Time granularity is in seconds, so we have a sequence of 86,400 graphs with 488 nodes and more than 350,000 contacts among them. The average contact duration is about 2 min while the average inter-contact time is more than 2.5 h.

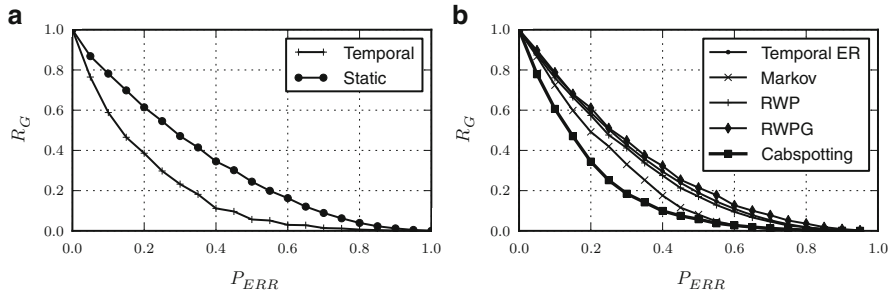


Fig. 6 Comparison between temporal robustness R_G and static robustness as a function of probability of error P_{ERR} for the Cabspotting dataset (a). The static approach overestimates system robustness. *Right:* Comparison between the temporal robustness R_G of the dataset and random null models with the same number of nodes N and P_{ON} of the Cabspotting temporal network (b)

3.4.2 Analysis

We study the reaction of the Cabspotting temporal network to random failures and compare it to our findings on random models. We adopt numerical simulation, but since the temporal dynamics of this network is not stationary, we can not compare the temporal efficiency E_G before and after a certain error, because the two temporal window will likely have already different properties. Instead, we fail nodes according to P_{ERR} at the very first time step of the temporal sequence of graphs: in this way, we can compare the average temporal efficiency over all the time for the original network and for the damaged one. We adopt a value of $\tau = 3,600$, which allows us to consider temporal paths up to 1 h, even if such longer paths can not contribute much to temporal efficiency.

The first comparison that we show in Fig. 6a is between static robustness and temporal robustness for the Cabspotting temporal network. In this case static robustness is computed on the static graph obtained by aggregating all the contacts in the trace and adopting static global efficiency as performance measure. Since the resulting static graph contains more than 100,000 edges it is clearly an overestimation of the communication properties of the real system, as not all these links are continuously available over time and some paths can not be used due to temporal ordering constraints. Indeed, static robustness appears much larger than the temporal counterparts: only temporal robustness is able to capture the realistic communication capabilities of the system and how they are affected by random failures.

Then, we attempt to understand if the various random temporal network models we have studied can be used to approximate the robustness properties of the real scenario. For each model, we compute the temporal robustness as a function of P_{ERR} for a network with the same number of nodes N and the same P_{ON} measured in the Cabspotting temporal network (about 0.005), using the same simulation parameters as in the real scenario. As reported in Fig. 6b, all temporal networks present the same

trend in network robustness, albeit random models have higher values of temporal robustness than the real network. Interestingly, the closest match is the Markov-based temporal model, while the mobility-based models are closer to the ER model than to the Cabspotting network, even if this is actually a mobility-based contact network. However, the assumptions used in mobility models require homogeneity of space and absolute freedom to move continuously and independently in a boundless area, while in reality taxis are usually constrained to move on streets and bridges and they often move together along the same direction or stop together in a particular place to wait for customers (i.e., airport or stations). The Markov model, instead, introduces the type of time correlations that appear to better mimic the real scenario. In fact, the most important aspect that needs to be captured is time ordering of events: in random mobility models connections do not follow particular time patterns, whereas real traces do (rush hour, working hours, human sleeping cycles). Only temporal robustness can take into account these unique characteristics.

3.5 Summary of the Findings

These two results provide evidence that *temporal robustness is a more accurate measure to be used on mobile networks instead of standard static approaches*. Therefore, when testing protocols and applications to be deployed in mobile networks, a temporal study is more meaningful and should not be substituted by a static approximation.

4 Mobile Malware

4.1 Overview

Smartphones are not only ubiquitous, but also an essential part of life for many people who carry such devices through their daily routine. It comes at no surprise then that recent studies have shown that the mobility of such devices mimic that of their owners' schedule [17, 54]. This fact constitutes an opportunity for devising efficient protocols and applications, but it also represents an increasing security risk: as with biological viruses that can spread from person to person, mobile phone viruses can also leverage the same social contact patterns to propagate via short-range wireless radio such as Bluetooth and WiFi. For example, when security researchers downloaded *Cabir* [53]—the first proof-of-concept piece of mobile malware—for analysis, they soon discovered the full risk potential of the mobile worm as it broke loose, replicating from the test device to external mobile phones. This event prompted the need for specially radio shielded rooms to securely test such malicious code [28].

Unlike desktop computers mobile malware can spread through both short-range radio (i.e., Bluetooth and WiFi) and long-range communication (SMS, MMS and email) [33]. Long-range malicious traffic can potentially be contained by the network operator by scanning every message against a database of known malware or spam [52], however, short-range propagation might fall under the radar of centralised service providers: effective schemes to defend against short-range mobile malware spreading are necessary. In addition, while a global patching of the devices through cellular connectivity is the natural solution and is in theory possible, in practice, due to associated costs and resource consumption, this is not ideal. For example, there are potential constraints with respect to the cellular network capacity and server bandwidth (with respect to the latter, similar issues have also investigated for software updates distribution in the Internet, see for example [25]).

4.2 Temporal Centrality Metrics for Malware

Being highly correlated with human contacts, understanding how such malware propagates requires an accurate analysis of the underlying time-varying network of contacts amongst individuals. State-of-the-art solutions on mobile malware containment have ignored two important temporal properties: firstly, the time order, frequency and duration of contacts; and secondly, the time of day a malicious message starts to spread and the delay of a patch [57, 58]. Instead, we argue that the temporal dimension is of key importance in devising effective solutions to this problem.

With this in mind, the focus of this study is to investigate the effectiveness of two containment strategies based on targetting key nodes, taking into account these temporal characteristics. We firstly investigate a traditional strategy, inspired by studies on error and attack tolerance of networks [1], exploiting static and a time-aware enhanced version of *betweenness centrality* which provide the best measure of how nodes that mediate or bridge the most communication flows. According to this strategy the nodes that act as mediators are patched to *block* the path of a malicious message. However, due to temporal clustering and alternative temporal paths, in most cases, such strategies merely *slow* the malware and does not *stop* it. In other words, a scheme based solely on immunisation of key nodes is not sufficient, instead *quick spreading* of the patch is necessary for most networks. We propose a solution based on local *spreading* of patches through Bluetooth, i.e., exploiting the same mechanism used by the malware itself. The key issue in this approach is to select the right nodes as starting points of the patching process, using *temporal closeness centrality* which ranks nodes by the speed at which they can disseminate a message to all other nodes in the network. We show that this strategy can reduce the cellular network resource consumption and associated costs, achieving at the same time a complete containment of the malware in a limited amount of time.

Table 3 Experimental datasets

	CAMBRIDGE	INFOCOM	MIT
N	18	78	100
Duration (days)	10	5	280
Contacts (avg. per day)	1,927	25,796	231
Scanning rate	30 s	2 min	5 min

4.3 Evaluation

4.3.1 Simulation Setup

To evaluate the time-aware mobile malware containment schemes, three traces of real mobile device contacts carried by humans are used: Bluetooth traces of researchers at the University of Cambridge, Computer Laboratory, as part of an emotion sensing experiment [42]; Bluetooth traces of participants at the 2006 INFOCOM conference [46]; and campus Bluetooth traces of students and staff at MIT [17]. We shall refer to these as CAMBRIDGE, INFOCOM, MIT, respectively. Table 3 describes the characteristics of each set of traces. All three datasets were constructed from mobile device co-location where participants were given Bluetooth enabled mobile devices to carry around. When two devices come into communication range of the Bluetooth radio, the device logs the colocation with the other device. For the CAMBRIDGE dataset, all 10 days are used as part of the evaluation. For the INFOCOM dataset, since devices were not handed out to participants until late afternoon during the first day, only the last 4 days are used. For the MIT dataset, we show results for the first 2 weeks of the Fall semester representing a typical fortnight of activity.

The top N_p devices are chosen according to the calculated temporal betweenness or temporal closeness centrality ranking from the temporal graph $\mathcal{G}_t^w(t_p, t_{max})$, where w is set to the finest window granularity, corresponding to the scanning rate of the devices in each dataset (for example, 30 s windows for CAMBRIDGE); and h is set to 1, since higher values of h lead to similar performance of the containment schemes. The N_m nodes that are initially infected with malicious messages are chosen uniformly randomly. The results are obtained by averaging over 100 runs for each N_p . The static centralities from the static aggregated graph over the time interval $[t_p, t_{max}]$ are also calculated for comparison.

Our evaluation is based on the following assumptions: firstly, when a node receives a patch message, it is immunised for the rest of the simulation (i.e., we assume that the malware does not mutate over time); secondly, there is always a successful file transfer between devices (errors in transmission can be taken into consideration in the assessment of the contention scheme without changing significantly the results of our work, assuming random transmission failures); thirdly, an attacker chooses nodes at random; and finally, we have no knowledge

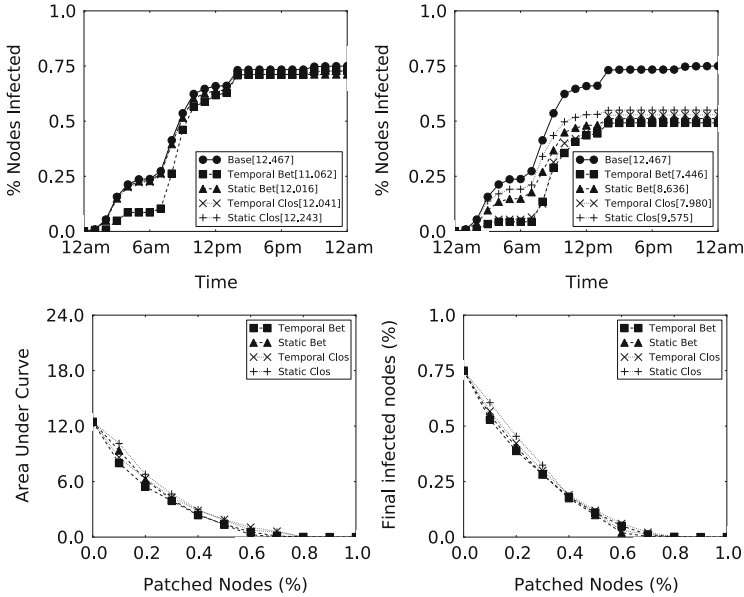


Fig. 7 INFOCOM day 4: Immunising 1 node (*top left*) and 10 source nodes (*top right*). Area under curves shown in the legend. Area (*bottom left*) and final % infected nodes (*bottom right*), as we increase the % nodes immunised (x-axis)

of which devices are compromised (otherwise the best scheme is to patch those devices immediately).

4.3.2 Non-effectiveness of Betweenness Based Patching

Starting from the results of the analysis of the effects time of day has on message spreading, we now evaluate the *best case* scenario for the containment scheme based on patching nodes (without spreading the patch) and we show that this is highly inefficient since it requires a very large number of nodes to be patched via the cellular network to be effective.

Using Day 4 of the INFOCOM trace for this example, a piece of malware is started at the beginning of the day ($t_m=12$ a.m.) and the device(s) are patched at the same time ($t_p=12$ a.m.). This is the best case scenario for two reasons: first, the temporal graph in the morning is characterised by low temporal efficiency since there are very few contacts, therefore, the malware spreads slowly; secondly, devices that are immunised immediately have the best chance of blocking malware spreading routes.

Figure 7 shows the ratio of compromised devices across time when the top 1 (top left panel) and top 10 (top right panel) devices are patched after being selected using betweenness and closeness. As we can see, temporal betweenness initially perform better than static betweenness and both temporal and static closeness (quantified

by the difference in the area under each curve, shown in the legend). However, by 7 a.m. we observe a steep rise in the number of compromised devices and by the end of the day, all curves converge to the same point. We also note that *in both cases it is not possible to totally contain the malware, suggesting that more devices need to be patched*. Taking a broader view, Fig. 7 shows the area under the curve (bottom left) and final ratio of nodes infected (bottom right) as we increase the number of patched devices. Clearly, even when the malware is started at the slowest time of day for communication, we still need to patch 80 % of the devices before we can completely stop the malware from spreading; this can be considered an impractically high number of devices to patch. Similar high percentages are also required in the MIT trace with a minimum of 45 % patched nodes.

4.3.3 Effectiveness of Closeness Based Patching (Worst Case Scenario)

Since the betweenness based containment scheme is not effective, we now evaluate the closeness based *spreading* scheme with the aim of disseminating a patch message throughout the network more quickly than a malicious message. For brevity, we do not present results on spreading based on temporal betweenness centrality since it is intuitive that this metric is not designed to quantify the speed of the patching dissemination process and, for this reason, it leads to poorer results. We start our analysis by examining a *worst case* scenario using the CAMBRIDGE dataset: a researcher receives a malicious message on their device in the early hours of Friday morning ($t_m = \text{Fri } 12 \text{ a.m.}$) and the malicious program replicates itself to any devices it meets during the day. A patch message is started a day later to try and patch all the compromised devices ($t_p = \text{Sat } 12 \text{ a.m.}$). This can be considered as the a worst case since there are more interactions and hence more opportunity for malware to spread during the day and the patch is delayed until a day later.

Figure 8 shows the spreading rate for the malicious message versus the best (left) and worst device (right) to start the patching message. These results were obtained by running simulations considering every single device as a starting point of the patching process, and then ranking them based on three *performance metrics*:

- The area under the curve (AUC), which captures the behaviour of the infection over time with respect to the number of infected devices²;
- The peak number of compromised devices (I_{max});
- The time in days necessary to achieve total malware containment (τ).

Since the AUC captures both the I_{max} and τ , the best and worst initial devices that were patched were selected using the AUC. Comparing all three measures, the case related to the selection of the worst device (right panel) is characterised by double AUC (2.62 vs. 1.07); a higher peak in compromised devices I_{max} (68 % vs. 60 %)

²The AUC is commonly used in epidemiology and medical trials [21].

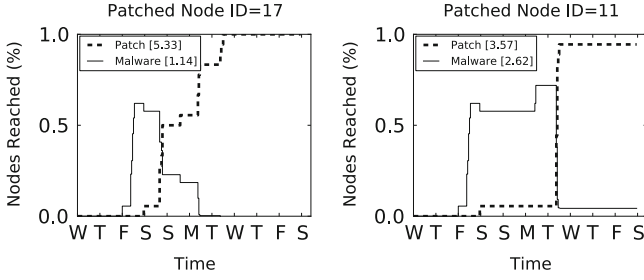


Fig. 8 CAMBRIDGE [t_m =Fri 12 a.m., t_p =Sat 12 a.m.] delivery rate (y-axis) starting a mobile worm from single node with best case patching node (*left*) and worse case patching node (*right*) shown. Area under the curve shown in the legend

and by the fact that it is not possible to fully contain the malware in a finite time τ (∞ vs. 3.3 days).

4.3.4 Sensitivity to Malware Start Time

Thus far we have only considered a single malware start time. We now take a broader view and examine the effects of a malicious message starting at different times. For each dataset the AUC, I_{max} and τ are exhaustively calculated for different malware start times at hourly intervals and increasing patch delays starting from zero (i.e., patch messages start at the same time as malicious messages) to up to 2 days. As a baseline, a naive method of randomly selecting patching nodes is also calculated, averaged over 100 runs. Figure 9 shows for each dataset the performance metrics as a function of the malware start time t_m , averaged over all patch delays. In particular, we note that the AUC and the maximum number of infected nodes I_{max} tend to follow the temporal efficiency (strictly related to human circadian rhythms); however, the total time of containment (τ) remains stable across all start times. These results demonstrate that this time-aware containment scheme is an effective method of quickly containing malware, irrespective of when the malware started. Now analysing the AUC and I_{max} , the temporal centrality curve is consistently lower than static and naive methods. Furthermore, static centrality performs worse than the naive method at some points of time; more specifically:

- For the CAMBRIDGE dataset, during the weekend a static method has a higher peak number of compromised devices (I_{max}) than the naive method, which shows that a static method is not effective at slowing down the malware from spreading.
- For the INFOCOM dataset, again I_{max} is higher than the naive method, during days 2 and 4. In addition, the AUC curve for a static method peaks with temporal efficiency during days 2, 4 and 5: this means that the malware is not contained effectively in these scenarios. Also, the total containment time (τ) is greater than that of the naive method during days 3, 4 and 5. This shows that temporal

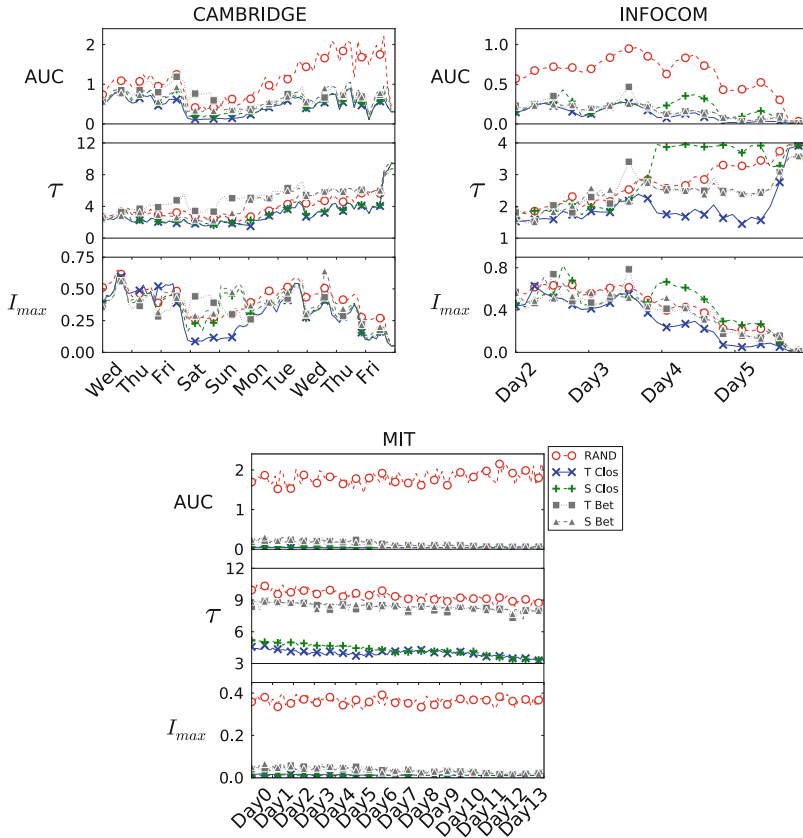


Fig. 9 Performance of temporal, static and naive node selection, across different malware start times (x-axis), averaged over all patch delays

centrality is more consistently effective for identifying the best nodes to start the patching process, compared to both static and naive methods.

- Finally, for the MIT dataset, the naive method performs extremely poorly (with high values of UAC, I_{max} and τ across all malware start times), compared to either a static or temporal method.

4.3.5 Summary of the Findings

This study demonstrates that a temporal analysis of mobile device interactions is better suited to real networks where the topology changes over time. As we have seen, a traditional strategy of patching high betweenness nodes is not effective when temporal topological information is taking into account for both the information dissemination process and also centrality calculations. Instead, we propose a

strategy that can select the best devices to spread the patch in a *competitive* fashion, using the same opportunistic encounters with other devices utilised by the malware itself.

5 Epidemics and Immunisation

A promising application area of the proposed metrics is indeed epidemics modelling in human networks [29, 36]. Currently, the vast majority of the existing models assume an underlying static network [35, 38]. By considering a static network, the *temporal order of appearance* of the links (i.e., the sequence of the contact opportunities) is somehow neglected. This fact might have significant implications on the actual realism of the mathematical model, especially in the case of small populations. Another specific aspect that might have a strong influence on the resulting model is the type of mixing patterns [39] that are present in the population.

The problem of modelling the spreading of infection in a time-varying graph and the definition of vaccination strategies given the information related to the network and epidemic dynamics (and the correlation between the two) are open and challenging research areas at the same time. Temporal centrality metrics can be used for example to prioritise the vaccination of individuals involved in an immunisation program. Moreover, temporal metrics can be used in general to study the evolution of a disease over time by providing quantitative measures of the time scale of its spreading considering the sequence of infected individuals (or geographic areas) over time.

In the recent years, some works have been focussed on the interplay between changing topology and the epidemic process taking place over the network. For example, in [44] Saramäki and Kaski present a model for studying the spreading of an infectious influenza on a dynamic small-world network, by analysing the effect of a dynamic re-wiring process on a Susceptible-Infective-Recovered-style epidemic model, deriving the equations for the epidemic threshold and spreading dynamics. In particular, the authors show how the epidemic saturation time scale varies with the size of the network and the initial conditions. In [34] the authors present the results of different vaccination strategies by simulating the dynamics of sexual disease spreading in empirical contact sequences of individuals. More specifically, the authors analyse the largest outbreak, the average outbreak sizes, and the relative advantages of the different strategies as a function of the infectivity and the duration of the infective state.

In general, social encounter networks, a typical class of time-varying networks, are attracting an increasing attention in the epidemiology community [16]. Researchers have been employing RFID and sensor techniques for extracting contact traces in order to accurately reconstruct patterns of interactions among individuals, also with respect to the duration of the contacts (see for example [6, 10, 43]). These models might also be scaled up to study disease outbreaks in cities [20].

Epidemic models have also been applied to diffusion of ideas, behaviour or lifestyle choices in social networks [9], for example in order to study the spreading of obesity [12] or smoking [13]. Another interesting and open area is the characterisation of the spreading of an epidemic and the simultaneous dissemination of information about it that might modify the behaviour of individuals (i.e., the dynamics of the underlying time-varying networks). A work in this direction is [24].

We believe that the application of the proposed metrics to these fields is indeed very promising and might contribute to increase the accuracy, and therefore, the realism of existing models and to develop new ones allowing researchers to extract valuable information and insights from them. In particular, the centrality metrics presented in this chapter and the accompanying one [40] in this book can be used to identify the key spreaders in order to define effective containment and immunisation strategies. For example, vaccination can be based on priorities assigned to the temporal centralities of the individuals in case of human diseases, whereas, as far as computer viruses are concerned, *white worms* used for patching the systems could be distributed starting from the nodes with the highest temporal closeness centrality.

6 Final Remarks

In this chapter we presented some key applications of temporal metrics to various domains such as centrality analysis in a social network, robustness and epidemiology of computer viruses and diseases. We have shown that temporal graph metrics are able to provide information about the structure of the time-varying networks and the dynamics of processes happening over them that is not possible to extract through the classic static metrics and graph representations. We hope that the case studies presented in this chapter and the discussions of open problems in the field might be considered as a starting point and a source of inspiration for future applications in these and other fields.

Acknowledgements This work was funded in part through EPSRC Project MOLTEEN (EP/I017321/1) and the EU LASAGNE Project, Contract No.318132 (STREP).

References

1. Albert, R., Jeong, H., Barabási, A.-L.: Error and attack tolerance of complex networks. *Nature* **406**(6794), 378–382 (2000)
2. Barrat, A., Barthélemy, M., Vespignani, A.: *Dynamical Processes on Complex Networks*. Cambridge University Press, Cambridge (2008)
3. Boccaletti, S., Latora, V., Moreno, Y., Chavez, M., Hwang, D.-U.: Complex networks: structure and dynamics. *Phys. Rep.* **424**(4–5), 175–308 (2006)
4. Cabspotting Project. <http://cabspotting.org/> (2009). Accessed 27 Feb 2013
5. Callaway, D.S., Newman, M.E.J., Strogatz, S.H., Watts, D.J.: Network robustness and fragility: percolation on random graphs. *Phys. Rev. Lett.* **85**(25), 5468–5471 (2000)

6. Cattuto, C., Van den Broeck, W., Barrat, A., Colizza, V., Pinton, J.-F., Vespignani, A.: Dynamics of person-to-person interactions from distributed RFID sensor networks. *PLoS ONE* **5**(7), e11596 (2010)
7. CBS News. Enron traders caught on tape. <http://www.cbsnews.com/stories/2004/06/01/eveningnews/main620626.shtml> (2004). Accessed 27 February 2013
8. CBS News. Former Enron trader pleads guilty. <http://www.cbsnews.com/stories/2004/06/16/national/main623569.shtml> (2004). Accessed 27 February 2013
9. Centola, D.: The spread of behavior in an online social network experiment. *Science* **329**(5996), 1194–1197 (2010)
10. Chaintreau, A., Hui, P., Crowcroft, J., Diot, C., Gass, R., Scott, J.: Impact of human mobility on opportunistic forwarding algorithms. *IEEE Trans. Mobile Comput.* **6**(6), 606–620 (2007)
11. Chaintreau, A., Le Boudec, J.Y., Ristanovic, N.: The age of gossip: spatial mean field regime. In: *Proceedings of SIGMETRICS '09*, pp. 109–120. ACM, New York (2009)
12. Christakis, N.A., Fowler, J.H.: The spread of obesity in a large social network over 32 years. *N. Engl. J. Med.* **357**(4), 370–379 (2007)
13. Christakis, N.A., Fowler, J.H.: The collective dynamics of smoking in a large social network. *N. Engl. J. Med.* **358**(21), 2249–2258 (2008)
14. Clauset, A., Eagle, N.: Persistence and periodicity in a dynamic proximity network. In: *Proceedings of DIMACS Workshop on Computational Methods for Dynamic Interaction Networks*, Rutgers University, Piscataway, 24–25 September 2007
15. Crucitti, P., Latora, V., Marchiori, M., Rapisarda, A.: Error and attack tolerance of complex networks. *Physica A* **340**, 388–394 (2004)
16. Danon, L., House, T.A., Read, J.M., Keeling, M.J.: Social encounter networks: collective properties and disease transmission. *J. R. Soc. Interface* **9**(76), 11 (2012)
17. Eagle, N., Pentland, A.: Reality mining: sensing complex social systems. *Pers. Ubiquit. Comput.* **10**(4), 255–268 (2006)
18. Elkind, P., McLean, B.: *The Smartest Guys in the Room: The Amazing Rise and Scandalous Fall of Enron*. New York, Penguin (2004)
19. Erdős, P., Rényi, A.: On the evolution of random graphs. *Publ. Math. Inst. Hungar. Acad. Sci.* **5**, 17–61 (1960)
20. Eubank, S., Guclu, H., Anil Kumar, V.S., Marathe, M.V., Srinivasan, A., Toroczkai, Z., Wang, N.: Modelling disease outbreaks in realistic urban social networks. *Nature* **429**(6988), 180–184 (2004)
21. Evans, C.H. Jr., Ildstad, S.T.: *Small Clinical Trials: Issues and Challenges*. National Academy of Sciences Press, Washington, DC (2001)
22. Faloutsos, M., Faloutsos, P., Faloutsos, C.: On power-law relationships of the Internet topology. In: *Proceedings of SIGCOMM '99*, pp. 251–262. ACM, New York (1999)
23. Federal Energy Regulatory Commission. Addressing the 2000–2001 Western Energy Crisis. <http://www.ferc.gov/industries/electric/indus-act/wec.asp> (2010). Accessed 27 Feb 2013
24. Funka, S., Gilada, E., Watkinsb, C., Jansena, V.A.A.: The spread of awareness and its impact on epidemic outbreaks. *Proc. Natl. Acad. Sci. U.S.A.* **106**, 6872–6877 (2009)
25. Gkantsidis, C., Karagiannis, T., Vojnovic, M.: Planet scale software updates. In: *Proceedings of SIGCOMM '06*. ACM, New York (2006)
26. Holme, P., Kim, B.J., Yoon, C.N., Han, S.K.: Attack vulnerability of complex networks. *Phys. Rev. E* **65**(5), 056109 (2002)
27. Huberman, B.A., Adamic, L.A.: Growth dynamics of the world-wide web. *Nature* **401**(6749), 131 (1999)
28. Hypponen, M.: F-secure weblog: the grand opening! <http://www.f-secure.com/weblog/archives/00000568.html> (2005). Accessed 27 Feb 2013
29. Keeling, M.J., Rohani, P.: *Modeling Infectious Diseases in Human and Animals*. Princeton University Press, Princeton (2007)
30. Kempe, D., Kleinberg, J., Kumar, A.: Connectivity and inference problems for temporal networks. *J. Comput. Syst. Sci* **64**(4), 820–842 (2002)
31. Kendall, M.G.: A new measure of rank correlation. *Biometrika* **30**(1–2), 81–93 (1938)

32. Kostakos, V.: Temporal graphs. *Physica A* **388**(6), 1007–1023 (2009)
33. Leavitt, N.: Mobile phones: the next frontier for hackers? *Computer* **38**(4), 20–23 (2005)
34. Lee, S., Rocha, L.E.C., Liljeros, F., Holme, P.: Exploiting temporal network structures of human interaction to effectively immunize populations. *PLoS ONE* **7**(5), e36439 (2012)
35. Liljeros, F., Edling, C.R., Amaral, L.A.N.: Sexual networks: implications for the transmission of sexually transmitted infections. *Microb. Infect.* **5**(2), 189–196 (2003)
36. May, R.M.: Network structure and the biology of populations. *Trends Ecol. Evol.* **21**(7), 394–399 (2006)
37. Medina, A., Gursun, G., Basu, P., Matta, I.: On the universal generation of mobility models. In: Proceedings of IEEE/ACM MASCOTS '10, Miami Beach, FL, August 2010
38. Newman, M.E.J.: *Networks: An Introduction*. Oxford University Press, Oxford (2010)
39. Newman, M.E.J.: Mixing patterns in networks. *Phys. Rev. E* **67**, 026126 (2003)
40. Nicosia, V., Tang, J., Mascolo, C., Musolesi, M., Russo, G., Latora, V.: Graph metrics for temporal networks. In: Saramäki, J., Holme, P. (eds.) *Temporal Networks*. Springer, Berlin (2013)
41. Piorkowski, M., Sarafijanovic-Djukic, N., Grossglauser, M.: CRAWDAD data set epfl/mobility (v. 2009-02-24). Downloaded from <http://crawdad.cs.dartmouth.edu/epfl/mobility> (2009). Accessed 27 Feb 2013
42. Rachuri, K.K., Musolesi, M., Mascolo, C., Rentfrow, P.J., Longworth, C., Aucinas, A.: EmotionSense: a mobile phones based adaptive platform for experimental social psychology research. In: Proceedings of UbiComp '10. ACM, New York (2010)
43. Salathé, M., Kazandjieva, M., Lee, J.W., Levis, P., Feldman, M.W., Jones, J.H.: A high-resolution human contact network for infectious disease transmission. In: Proceedings of the National Academy of Sciences of the USA, Washington, vol. 107, pp. 22020–22025, December 2010
44. Saramäki, J., Kaski, K.: Modelling development of epidemics with dynamic small-world networks. *J. Theor. Biol.* **234**(3), 413–421 (2005)
45. Scellato, S., Leontiadis, I., Mascolo, C., Basu, P., Zafer, M.: Evaluating temporal robustness of mobile networks. *IEEE Trans. Mobile Comput.* **12**(1), 105–117 (2013). <http://doi.ieeecomputersociety.org/10.1109/TMC.2011.248>
46. Scott, J., Gass, R., Crowcroft, J., Hui, P., Diot, C., Chaintreau, A.: CRAWDAD data set cambridge/haggle (v. 2009-05-29). Downloaded from <http://crawdad.cs.dartmouth.edu/cambridge/haggle> (2009). Accessed 27 Feb 2013
47. Shetty, J., Adibi, J.: Discovering important nodes through graph entropy the case of Enron email database. In: Proceedings of the 3rd International Workshop on Link Discovery, pp. 74–81. ACM, Chicago (2005)
48. Tang, J., Musolesi, M., Mascolo, C., Latora, V.: Temporal distance metrics for social network analysis. In: Proceedings of WOSN '09, Barcelona, August 2009
49. Tang, J., Musolesi, M., Mascolo, C., Latora, V., Nicosia, V.: Analysing information flows and key mediators through temporal centrality metrics. In: Proceedings of ACM SNS '10, Paris, April 2010
50. Tang, J., Mascolo, C., Musolesi, M., Latora, V.: Exploiting temporal complex network metrics in mobile malware containment. In: Proceedings of the 12th IEEE International Symposium on a World of Wireless, Mobile and Multimedia Networks (WOWMOM'11), Lucca, June 2011
51. Tang, J., Kim, H., Mascolo, C., Musolesi, M.: STOP: socio-temporal opportunistic patching of short range mobile malware. In: Proceedings of the 13th IEEE Symposium on a World of Wireless, Mobile and Multimedia Networks (WOWMOM'12), San Francisco, June 2012
52. Van Ruitenbeek, E., Courtney, T., Sanders, W.H., Stevens, F.: Quantifying the effectiveness of mobile phone virus response mechanisms. In: Proceedings of DNS '07, 2007
53. Virus description: Bluetooth-worm: symos/cabir. <http://www.f-secure.com/v-descs/cabir.shtml> (2004). Accessed 27 Feb 2013
54. Wang, P., Gonzalez, M.C., Hidalgo, C.A., Barabasi, A.-L.: Understanding the spreading patterns of mobile phone viruses. *Science* **324**(5930), 1071–1076 (2009)

55. Washington Post. Enron fraud trial ends in 5 convictions. <http://www.washingtonpost.com/wp-dyn/articles/A23034-2004Nov3.html> (2004). Accessed 27 Feb 2013
56. Wasserman, S., Faust, K.: Social Networks Analysis. Cambridge University Press, Cambridge (1994)
57. Zhu, Z., Cao, G., Zhu, S., Ranjan, S., Nucci, A.: A social network based patching scheme for worm containment in cellular networks. In: Proceedings of INFOCOM '09, IEEE, Rio de Janeiro, April 2009
58. Zyba, G., Voelker, G.M., Liljenstam, M., Mehes, A., Johansson, P.: Defending mobile phones from proximity malware. In: Proceedings of INFOCOM '09, IEEE, Rio de Janeiro, April 2009

Spreading Dynamics Following Bursty Activity Patterns

Alexei Vazquez

Abstract The dynamics of many social, technological and economic phenomena are driven by individual human actions, turning the quantitative understanding of human behavior into a central question of modern science. Recent empirical evidence indicates that the timing of individual human actions follow non-Poisson statistics, characterized by bursts of rapidly occurring events separated by long periods of inactivity. In this work we analyze how this bursty dynamics impacts the dynamics of spreading processes in computer and social systems. We demonstrate that the non-Poisson nature of the contact dynamics results in prevalence decay times significantly larger than predicted by the standard Poisson process based models. Thanks to this slow dynamics the spreading entity, namely a virus, rumor, etc., can persist in the system for long times.

1 Introduction

Human activities often mediate the spreading of infectious agents. Typical examples are the spreading of computer viruses through email communications [1, 2], the spreading of sexually transmitted diseases through sexual contacts [3–6] and the spreading of airborne infectious diseases through geographical mobility [4, 7–12]. Most of the literature on spreading processes assumes that these human activities are carried on at a constant rate and, therefore, are well represented by a Poisson process [4, 7, 8, 13–16]. However, recent evidence indicates that several human activities are rather characterized by bursty activity patterns, with short terms where the activity is executed in consecutive short intervals separated by very long intervals

A. Vazquez (✉)

Department of Radiation Oncology and Center for Systems Biology, The Cancer Institute of New Jersey, UMDNJ-RWJMS, 195 Little Albany St, New Brunswick, NJ 08903, USA
e-mail: vazqueal@umdnj.edu

[17–21]. These observations have motivated a revision of previous work on spreading processes to account for the bursty nature of human activity patterns [22–26].

The study of spreading processes following human activity patterns can be divided in two major fields: theoretical and detailed simulations. The theoretical approaches are based on models that make several simplifications, aiming to understand the major factors driving the characteristic temporal patterns of the spreading process [22, 25]. Detailed simulations aim a more precise description of the spreading process and generally incorporate human activity patterns that are as close to the reality as possible [11, 12, 27, 28].

In this chapter we introduce the reader to the generalizations that are required for the theoretical study of spreading process following bursty activity patterns. We note that, for most part, this framework has been extensively developed in the mathematical literature of point processes [29] and branching processes [30]. Our contribution is limited to the adaption of these powerful mathematical methods to the study of two instances with high impact in our society: the spread of computer viruses and sexually transmitted diseases.

2 Modeling Human Activities as Renewal Processes

We focus our attention on human activities where the duration of each activity execution is much smaller than the time interval between two consecutive executions of the activity. In this case we can represent the activity timeline by a point process in time (Fig. 1). We call the interevent time the time interval between two consecutive executions of the activity, which is also refereed as the waiting time in the renewal and queueing processes literature. We will denote by T_i the i -th interevent time. In the simplest scenario, we assume that the interevent times are positive independent identically distributed random variables. This type of point process is called a renewal process [29]. A renewal process is fully characterized by the interevent time distribution, with a probability density function $P(\tau)d\tau = \text{Prob}(\tau \leq T_i \leq \tau + d\tau)$.

When dealing with renewal processes we often calculate the distribution of the sum of two or more interevent times

$$S_n = \sum_{i=1}^n T_i \quad (1)$$

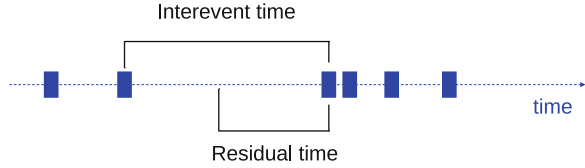
Since the T_i are independent identically distributed random variables the distribution of S_n is obtained by convolutions of the distribution of T_i

$$\text{Prob}(\tau \leq S_n \leq \tau + d\tau) = P^{*n}(\tau) \quad (2)$$

where $P^{*n}(\tau)$ denotes the n -order convolution of $P(\tau)$. $P^{*n}(\tau)$ can be calculated recursively: $P^{*1}(\tau) = P(\tau)$ and

$$P^{*n}(t) = \int_0^t d\tau P(\tau) P^{*(n-1)}(t - \tau) \quad (3)$$

Fig. 1 Point process representing the timeline of a human activity



Poisson Process

The Poisson process is a particular case of a renewal process where the activities are executed at a constant rate λ . In this case the interevent time distribution is exponential

$$P(\tau) = \lambda e^{-\lambda\tau} \tag{4}$$

and the n -order convolutions are gamma distributions

$$P^{*n}(\tau) = \frac{\lambda}{(n-1)!} (\lambda\tau)^{n-1} e^{-\lambda\tau} \tag{5}$$

The importance of the Poisson process resides on the fact that, given a renewal process with a finite mean interevent time $\langle\tau\rangle$, for time scales larger $\langle\tau\rangle$ it can be approximated by a Poisson process with rate [29]

$$\lambda = \frac{1}{\langle\tau\rangle} \tag{6}$$

where $\langle\tau\rangle = \int_0^\infty d\tau P(\tau)\tau$ is the expected interevent time. In turn, deviations from the Poisson process approximation are expected in the regime $t < \langle\tau\rangle$. The longer the mean interevent time the longer we need to wait for the Poisson process approximation to hold.

Lévy Process

When the average interevent time is not finite we cannot approximate a renewal process by a Poisson process. This is the case of interevent times distributions with a power law decay $P(\tau) \sim \tau^{-\alpha}$ for $\tau \gg \tau_0$ and $1 < \alpha < 2$, where τ_0 is a characteristic time scale. In this case we can apply a generalized central limit theorem for power law distributions concentrated in $[0, \infty)$ [29]. Specifically, in the limit $n \gg 1$ we can approximate the n -order convolution by

$$P^{*n}(\tau) \sim \frac{1}{\tau_0 n^{\frac{1}{\alpha-1}}} \mathcal{L}_{\alpha-1} \left(\frac{\tau}{\tau_0 n^{\frac{1}{\alpha-1}}} \right) \tag{7}$$

where $\mathcal{L}_\mu(x)$ represents the stable (Lévy) distribution with exponent μ and concentrated in $[0, \infty)$. The stable distributions $\mathcal{L}_\mu(x)$ are characterized by the asymptotic behavior $\mathcal{L}_\mu(x) \sim x^{-(1+\mu)}$ when $x \gg 1$. From the latter result and (7) it follows that

$$P^{*n}(\tau) \sim \tau^{-\alpha} \quad (8)$$

when $\tau \gg \tau_0 n^{\frac{1}{\alpha-1}}$. Therefore, the power law tail of the distribution is preserved upon convolution.

3 Modeling Disease Spreading as a Branching Process

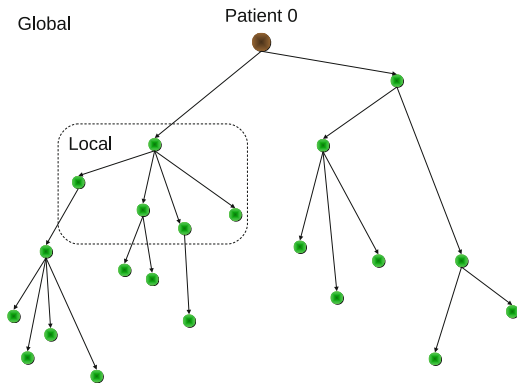
A spreading process can be represented by a causal-tree of disease transmission ([31], Fig. 2). In this tree each node represents an infected agent and each arrow represents the transmission of the disease from a primary case to a secondary case. In addition, the arrow length represents the generation time, the time elapsed from the infection of the primary case to the infection of the secondary case. We make an explicit distinction between the first infected agent (patient zero) and the remaining infected agents. The infection of patient zero comes from an exogenous source, such as an animal host in the case of human infectious diseases or a hacker in the case of computer viruses. We could think of patient zero as an agent selected at random from the agent population. However, this may not be the case for subsequently infected agents, because the spreading process introduces biases in the way agents are reached.

The theory of branching processes provides a general framework to study the causal-tree of disease transmission [30, 31]. It provides recursive rules to calculate global quantities characterizing the spreading process at the population level from the iteration of local properties characterizing the transmission from a primary case to its secondary cases (Fig. 2). Under the assumption that all cases are statistically equivalent, the local transmission is characterized by the reproductive number or average number of secondary cases generated by patient zero R_0 , the reproductive number or the number of secondary cases generated by primary cases other than patient zero R , and the probability density function of generation times $g(t)$. At the global level, the spreading process is characterized by the average number of new infections $n(t)$ between time t and $t + dt$, which is related to the local properties by the equation [30, 31]

$$n(t) = \sum_{d=1}^D R_0 R^{d-1} g^{*d}(t) \quad (9)$$

where d denotes the distance from the root and D is the maximum distance from the root. Here $R_0 R^{d-1}$ is the expected number of nodes at a distance d from the root and $g^{*d}(t)$ is the distribution of the time it takes the infection to reach a node at

Fig. 2 Causal-tree of disease transmission representing an epidemic outbreak. The *brown circle* represents patient zero



a distance d from the root, which is just the distribution of the sum of d generation times. Finally, integrating (9) over time we obtain the total number of infected agents

$$N_{\infty} = \sum_{d=1}^D R_0 R^{d-1} \tag{10}$$

4 Spreading of Computer Viruses

Computer viruses exploit different mechanisms of transmission between computers. For the sake of simplicity, we focus on the spreading of an email worm. Email worms are activated when an email user opens an infected email and, subsequently, the worm forwards itself to all email addresses in the user’s address-book. In this case the spreading process is determined by the temporal patterns of email sessions and the address-book size of email users.

Figure 3 illustrates the spreading of an email worm overlaid over email activity patterns. The dashed blue lines represent the timeline of each email user where the horizontal blue segments represent email accesses sessions. At time $t = 0$ patient-zero is infected with an email worm (e.g., deployed by a hacker). Some later time patient zero access his email account, activates the worm, which forwards itself to the email addresses in the patient-zero address book (Fig. 3, large green circle). The recipients have now the email worm hidden in an email in their inbox (Fig. 3, red circles). However, they do not transmit the virus until some later time when they access their email accounts. In the following we relate these particularities of email worm spreading to the general approach described in previous section.

In this context the reproductive number is associated with the address-book of email users. When collecting together the address-book of several users we obtain a directed email network, where each node represents an email user and there is

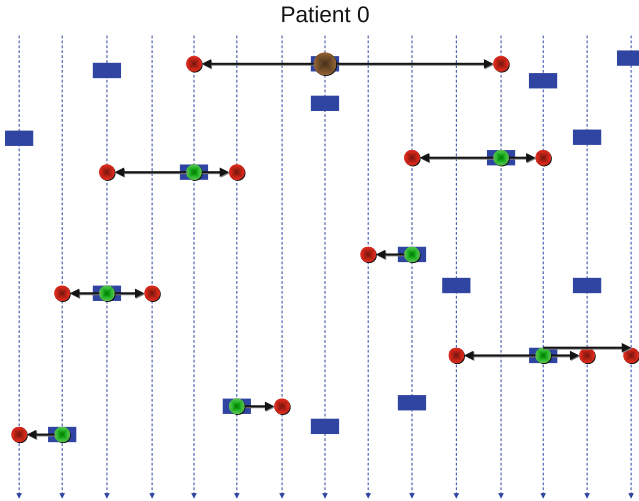


Fig. 3 Schematic representation of the spread of an email worm over the email communications of a subset of email users. The *brown circle* represents patient zero. The *blue dashed lines* represent the timeline of each user and the horizontal blue segments represent email access sessions. The *green circles* represent the activation of the email worm and subsequent transmission to other email users. The *red circles* represent the arrival of the email worm to user's inboxes

an arrow from user A to user B whenever user B is in the address book of user A. Each user is then characterized by an outdegree k_{out} , counting the number of email addresses on his address-book, and an indegree k_{in} , counting the number of other email users having his email address on their address-book. Assuming that patient zero is a user selected at random, we obtain that R_0 is given by the average outdegree

$$R_0 = \sum_{k_{out}} k_{out} p(k_{out}) \tag{11}$$

where $p(k_{out})$ is the outdegree distribution. In contrast, other infected agents are not selected at random, they are reached following the email network. Assuming that there are no correlations in the email network other than those deduced from the outdegree and indegree distributions, the probability that a user is at the other end of an arrow is proportional to its indegree. Consequently

$$R = \sum_{k_{out}} k_{out} \frac{\sum_{k_{in}} p(k_{out}|k_{in}) k_{in} p(k_{in})}{\sum_{k_{in}} k_{in} p(k_{in})} \tag{12}$$

where $p(k_{in})$ is the indegree distribution and $p(k_{out}|k_{in})$ is the outdegree distribution conditioned to users with indegree k_{in} . The difference between R_0 and R can be quite dramatic because email networks are characterized by power law distributions of indegree and outdegree [32] and the indegree and outdegree are correlated [33].

To give a quantitative estimate, let us analyze the data reported in [32], recording email communications in a university setting in a period of 112 days. We estimated the size of the address-book of a user by the number of different email addresses to who the user sent at least one email in the recorded period, obtaining $R_0 = 3.8$ and $R = 38.9$. This data indicates that R can be one order of magnitude larger than R_0 . However, these numbers may be an underestimate. For example, a direct analysis of user's address-book sizes reports $R_0 = 12.45$ [33].

Now we turn our attention to the timing of infections. The asynchronous nature of email communications results in a time lapse between the reception of an infected email and the subsequent activation and transmission (Fig. 3, across a user timeline, red to green circle). From the perspective of the user receiving the infected email, the time it receives the email from the infected sender is a time selected at random. Therefore, the generation time is the time elapsed from a randomly selected point in the receiver's timeline to the next receiver's email session. This time is known as the residual waiting time in the context of renewal processes theory [29] (Fig. 1). The distribution of residual waiting times, and thus the distribution of generating times, is related to the interevent time distribution through the equation [29]

$$g(t) = \frac{1}{\langle \tau \rangle} \int_t^\infty dt P(\tau). \quad (13)$$

Empirical Data

The empirical data indicates that the probability density function of the time between consecutive emails sent by an email user is well approximated by a power law decay followed by an exponential cutoff [22]

$$P(\tau) = A\tau^{-\alpha}e^{-\frac{\tau}{\tau_E}} \quad (14)$$

where A is a normalization factor, $\alpha \approx 1$ and τ_E depends on the dataset analyzed. For example, $\tau_E = 25 \pm 2$ days for a dataset characterizing email communications within a university setting and $\tau_E = 9 \pm 1$ months (approximately 270 days) for a dataset characterizing the email communications between users of a commercial email service provider [22]. In contrast, the Poisson approximation predicts $P_P(\tau) = \exp(-t/\langle \tau \rangle)/\langle \tau \rangle$, where the mean interevent time $\langle \tau \rangle$ takes the values 0.86 and 4.9 days for the university and commercial data, respectively. Therefore, although in both cases the interevent time distribution is characterized by an exponential decay at long times, the initial power law decay in the empirical data shifts the characteristic time of that exponential decay from days to months.

Substituting the empirical interevent time distribution (14) into (13) we obtain

$$g(t) = f(t)e^{-\frac{t}{\tau_E}} \quad (15)$$

where

$$f(t) = \frac{A}{\langle \tau \rangle} \int_t^\infty d\tau \tau^{-\alpha} e^{-\frac{t-\tau}{\tau_E}} \quad (16)$$

is a slowly-varying function of time. Substituting (15) into (9) we obtain

$$n(t) = \sum_{d=1}^D R_0 f^{*d}(t) \frac{1}{\tau_E} \frac{1}{(d-1)!} \left(\frac{Rt}{\tau_E} \right)^{d-1} e^{-\frac{t}{\tau_E}} \quad (17)$$

In the limit $t \gg \tau_1 = \tau_E D/R$ equation (17) can be approximated by

$$n(t) = N_\infty \frac{f^{*D}(t)}{\tau_E (D-1)!} \left(\frac{t}{\tau_E} \right)^{D-1} e^{-\frac{t}{\tau_E}} \quad (18)$$

To estimate the characteristic time τ_1 we use again the email network data reported in [32]. This email network has $R \approx 40$ and $D = 8$, resulting in $\tau_1 \approx 0.2\tau_E$. For the university and commercial email server setting we obtained $\tau_E \approx 25$ days and 9 months, resulting in $\tau_1 \approx 5$ days and 1.8 months, respectively. Therefore, the asymptotic expression (18) is valid beyond a few days within a university setting (thousand users) and beyond 2 months in the commercial email provider setting (million users). To better understand the implication of these time scales let us inspect (18) in more detail. First, $n(t) \sim N_\infty$, indicating that by $t \sim \tau_1$ the spreading process has reached a number of individuals proportional to the final outbreak size N_∞ , which coincides with the total number of users in the absence of any intervention. Thus, the email worm will reach epidemic dimensions within a few days in the university setting and within 2 months in the commercial provider setting. We note that the 2 months may be an overestimate because we based our calculation of R and D on data from a university setting. Second, at this point the spreading dynamics is characterized by a power law increase with an exponent D that is determined by the typical distance between users in the network. This behavior is a characteristic feature of networks with heavy-tailed degree distributions [34], independently of degree correlations [35] or the existence of multiple node types [36]. We note that this power law growth is modulated by $f^{*D}(t)$, which is itself determined by the power law behavior of the inter-email time distribution for $\tau < \tau_E$. Finally, the spreading dynamics will follow an exponential decay with a characteristic time τ_E that is of the order of 1 month for the university setting and 9 months for the commercial provider setting. This latter prediction is consistent with empirical data [22]. Prevalence data collected for six different email worms exhibits an exponential decay with a characteristic decay times between 11–14 months [22].

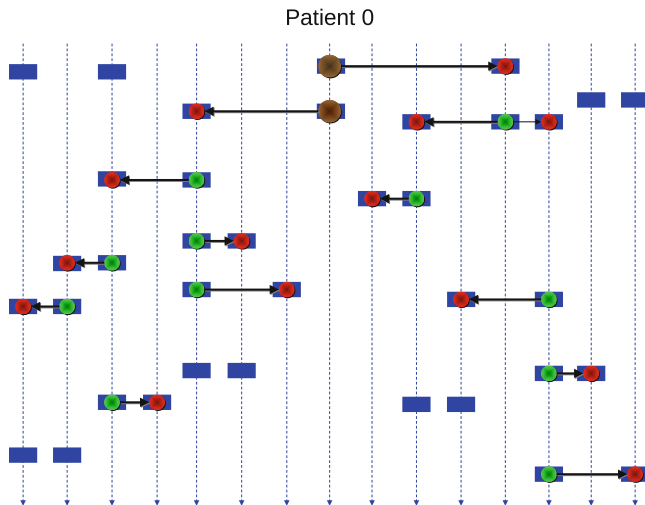


Fig. 4 Schematic representation of the spread of a sexually transmitted disease over the pattern of sexual activities of a subset of homosexual individuals. The *brown circle* represents patient zero. The *blue dashed lines* represent the timeline of each individual and the horizontal segments the time at which they engage in a sexual activity. *Green circles* represent events of disease transmission and red circles the time when individuals become infected

5 Spreading of Sexually Transmitted Diseases

The spread of sexually transmitted diseases is intimately connected with the patterns of sexual activities. For the sake of simplicity, we focus on the spread of a sexually transmitted disease in a homosexual population. Figure 4 illustrates the spread of a sexually transmitted disease overlaid over the sexual activity patterns of a set of individuals. The dashed blue lines represent the timeline of each individual where the blue segments represent the time points when individuals are involved in a sexual activity. In the simplest case, we can model the timeline of sexual activities of an individual by a renewal process [29], where the interevent times are independent equally distributed random variables with a probability density $P(\tau)$.

We note that, as a difference with the email worms (Fig. 3), the sexual activity requires the synchronous participation of at least two individuals (Fig. 4). Furthermore, an infected individual can infect other individuals at different time points (Fig. 4). The time interval to the first transmission coincides with an interevent time, the time to the second transmission coincides with the sum of two interevent times and so on. The probability density function of the sum of l interevent times is obtained from the convolution $P^{*l}(t)$.

Another important observation is that the rate λ at which sexually active individuals acquire new sexual partners is quite heterogeneous. The rate λ can be estimated as the number of sexual partners that an individual has in a given period of time. Empirical data collected for several countries reveals that the probability

density function of λ is characterized by a power tail $u(\lambda) \sim \lambda^{-\gamma}$, with an exponent $2 < \gamma < 4$ [37–40]. To take this heterogeneity into consideration we parametrize the interevent time distribution by the effective rate λ , explicitly writing $P(\tau; \lambda)$.

We assume that patient zero is an individual selected at random. Therefore, the number of secondary cases generated at time t by patient-zero is given by

$$v_0(t) = i(t)s(t)m \int_0^\infty d\lambda u(\lambda) \sum_{l=1}^\infty P^{*l}(t; \lambda) \quad (19)$$

where m is the average number of partners per sexual activity session, $i(t)$ is the probability of disease transmission upon sexual contact and $s(t)$ is the probability of stopping the disease transmission. The stopping of disease transmission generally happens when the patient becomes aware of his/her disease status, i.e. when he/she becomes symptomatic. The time between infection and the manifestation of symptoms is known as the incubation period, here denoted by τ_I . Subsequent infected individuals are biased by the rate at which they engage in sexual activities, with a probability $\lambda / \int_0^\infty d\lambda u(\lambda)\lambda$. Therefore, the number of secondary cases generated at time t by a patient other than patient-zero is given by

$$v(t) = i(t)s(t)m \frac{1}{\int_0^\infty d\lambda u(\lambda)\lambda} \int_0^\infty d\lambda u(\lambda)\lambda \sum_{l=1}^\infty P^{*l}(t; \lambda) \quad (20)$$

From (19) and (20) we can calculate the reproductive numbers and generating time distributions as follows

$$R_0 = \int_0^\infty dt v_0(t) \quad (21)$$

$$R = \int_0^\infty dt v(t) \quad (22)$$

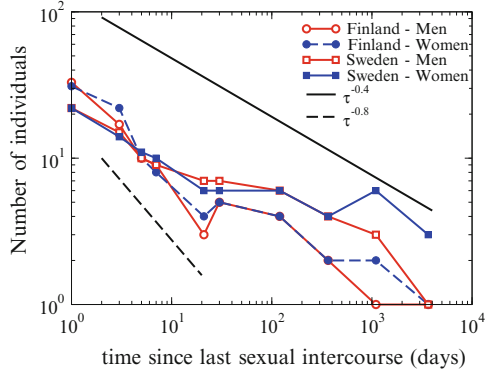
$$g_0(t) = \frac{1}{R_0} v_0(t) \quad (23)$$

$$g(t) = \frac{1}{R} v(t) \quad (24)$$

Poisson Process Approximation

When the distribution of interevent times has a finite mean, we can approximate the timeline of sexual activities by a Poisson process with rate (6). Furthermore, we assume that the probability of transmission $i(t) = i_0$ is time independent and that the patient becomes aware of its disease status at a rate $1/\tau_I$. Under these approximations we obtain $v_0 = i_0 m e^{-t/\tau_I} \langle \lambda \rangle$ and $v = i_0 m e^{-t/\tau_I} \langle \lambda^2 \rangle / \langle \lambda \rangle$, resulting in

Fig. 5 The histogram of the time since last having sexual intercourse, based on an study of Swedish and Finnish men and women



$$R_0 = i_0 m \langle \lambda \rangle \tau_I \tag{25}$$

$$R = i_0 m \frac{\langle \lambda^2 \rangle}{\langle \lambda \rangle} \tau_I \tag{26}$$

$$g_0(t) = g(t) = \frac{1}{\tau_I} e^{-\frac{t}{\tau_I}} \tag{27}$$

As mentioned above the empirical data indicates that λ follows a power law distribution $u(\lambda) \sim \lambda^{-\gamma}$ with $\gamma > 3$, but close to 3. As previously noticed [16, 41], this results in high a value of $\langle \lambda^2 \rangle / \langle \lambda \rangle$ and, consequently, a high reproductive number (26). However, the validity of the Poisson process as a model of sexual activity patterns has not been challenged so far.

Non-Poisson Nature of Sexual Activity Patterns

To test the validity of the Poisson approximation we analyzed data reporting sexual activity patterns in Sweden and Finland [42]. Specifically, we focus on reported statistics for the time since last having sexual intercourse. This time is known as the spent waiting time in the theory of renewal processes [29], i.e. the time elapsed since the last event (sexual activity in this context). The probability density function of the spent time $P_s(\tau)$ is related to that for the interevent time through the equation

$$P_s(t) = \frac{1}{\langle \tau \rangle} \int_t^\infty d\tau P(\tau) \tag{28}$$

Figure 5 reports the histogram of the time since last intercourse for Swedish and Finnish men and women. This distribution manifest a slow decay over three order of magnitudes. While the quality of the data is not sufficient to make an accurate fit, it

can be approximated by a power law decay with an exponent between -0.4 and -0.8 . From (28) it then follows that $P(\tau) \sim \tau^{-\alpha}$ and $1.4 < \alpha < 1.8$. Therefore, the interevent time of sexual activities deviates from the exponential law characterizing a Poisson process. Furthermore, since $1.4 < \alpha < 1.8$ it cannot be approximated by a Poisson process.

As discussed in Sect. 2 a feature of power law interevent time distributions with exponent $1 < \alpha < 2$ is that the power law tail is preserved under convolution. Therefore, at long times, (21) and (22) will behave as $\nu_0(t) \sim i(t)s(t)mt^{-\alpha}$ and $\nu(t) \sim i(t)s(t)mt^{-\alpha}$. Again assuming a time-independent probability of infection upon sexual contact and that patients stop transmitting the disease at a rate $1/\tau_I$, we obtain the asymptotic behavior

$$g_0(t) \sim g(t) \sim At^{-\alpha}e^{-\mu t}. \quad (29)$$

Substituting (29) in (9) we obtain the following asymptotic behavior for the spreading dynamics

$$n(t) \sim N_\infty \sum_{d=1}^D f^{*d}(t) \frac{1}{\tau_I(d-1)!} \left(\frac{Rt}{\tau_I}\right)^{d-1} e^{-\frac{t}{\tau_I}} \quad (30)$$

where $f(t) \sim At^{-\alpha}$. In the limit $t \gg \tau_1 = \tau_I D/R$, and taking into account that the convolution of $f(t)$ preserves the asymptotic power law, (29) can be approximated by

$$n(t) \sim N_\infty \frac{1}{\tau_I(D-1)!} \left(\frac{t}{\tau_I}\right)^{D-\alpha-1} e^{-\frac{t}{\tau_I}} \quad (31)$$

This predicts that the number of new infections will increase as a power law in time during the time scale $\tau_1 < \tau < \tau_I$. Empirical data collected for several countries reveals that the probability density function of λ is characterized by a power tail $u(\lambda) \sim \lambda^{-\gamma}$, with an exponent $2 < \gamma < 4$ [37–40]. As previously noticed [16, 41], this results in high a value of $\langle \lambda^2 \rangle / \langle \lambda \rangle$ and, consequently, a high reproductive number (26). No data has been reported regarding the typical distance in the network of sexual contacts, but our experience with human networks suggest that it should be small. In summary, although we do not count with an accurate estimate of D and R , the reported data suggest that the network of sexual contacts is a small-world network (small D) with a high heterogeneity in the number of sexual partners (high R), suggesting that $D/R \ll 1$. Therefore, we expect that $\tau_1 = \tau_I D/R \ll \tau_I$. In the case of HIV, the incubation time is about 10 years [5] and, therefore, we predict the manifestation of a power law growth over years. This prediction agrees with the observation of a polynomial growth in the HIV epidemics in US cities and sub-Saharan African countries [5, 43, 44]. There are some exceptions however. For Eastern European countries the HIV epidemics exhibits an exponential growth [44]. While this could be determined by narrow distribution of λ , which results in an exponential growth, we do not count with data to explain these exceptions.

6 Outlook

These analyses provide the first order approach to understand spreading processes with the underlying non-Poissonian dynamics characteristic of human activity patterns. Due to the high heterogeneity of human networks, such as the network of email communications or sexual partners, the spreading process reaches a population level in very short times. From there on the spreading process follows a power law increase in the number of new infectious, with an exponent that is determined by the characteristic distance between nodes in the network and the scaling of the interevent time distribution. This power law increase is followed by an exponential decay with a characteristic time that is very long. In the context of email worms spread, the decay time is set by the exponential tail of the inter-emails time distribution, which is of the order of 10 months. In the context of the spread of sexually transmitted diseases the decay time is set by the incubation time of the disease, which is particularly long, 10 years, for HIV.

In the context of sexually transmitted diseases, the characteristic time of the long-time exponential decay is associated with the incubation period of the disease. However, we still do not know what is the origin of the exponential decay in the emails interevent time distribution, which causes the long-time exponential decay of the spreading process in the context of computer viruses. Given the relevance of this time scale, future work should be devoted to elucidate its origin.

The generalization of these results to the case of statistically different agents can be attained with the use of the theory of multi-type branching processes [36, 45]. Extensions will be necessary, for example, to model sexually transmitted diseases in heterosexual populations, where men and women are characterized by different sexual activity patterns. Further work is required to understand the impact of correlations in the series of interevent times, precluding the use of renewal processes to model the human activity timeline. Correlations between the length of interevent times has been observed in the pattern of jobs sent to a printer by a given individual [20], mobile phone calls [46], text messages [46], email communications [46] and models of human activity [25]. How these correlations affect the spreading dynamics remains to be understood.

References

1. Harley, D., Slade, R., Gattiker, U.E.: *Viruses Revealed*. Osborne/McGraw-Hill, Berkeley (2001)
2. Chen, T.M.: *Internet Protocol J.* **6**, 4 (2003)
3. Yorke, J.A., Hethcote, H.W., Nold, A.: *Sex. Transm. Dis.* **5**, 51 (1978)
4. Anderson, R.M., May, R.M.: *Infectious Diseases of Humans*. Oxford University Press, New York (1991)
5. Brookmeyer, R., Gail, M.H.: *AIDS Epidemiology: A Quantitative Approach*. Oxford University Press, New York (1994)
6. De, P., Singh, A.E., Wong, T., Yacoub, W., Jolly, A.M.: *Sex. Transm. Infect.* **80**, 280 (2004)

7. Rvachev, L.A., Longini, I.M.: *Math. Biosci.* **75**, 3 (1985)
8. Flahault, A., Letrait, S., Blin, P., Hazout, S., Menares, J., Valleron, A.J.: *Stat. Med.* **7**, 1147 (1988)
9. Burton, D.R., Parren, P.W.H.I.: *Nature* **408**, 527 (2000)
10. Anderson, R.M., et al.: *Phil. Trans. R. Soc. Lond. B* **359**, 1091 (2004)
11. Eubank, S., et al.: *Nature* **429**, 180 (2004)
12. Colizza, V., Barrat, A., Barthelemy, M., Vespignani, A.: *Proc. Natl. Acad. Sci. USA* **103**, 2015 (2006)
13. Bailey, N.T.J.: *The Mathematical Theory of Infectious Diseases*, 2nd edn. Griffin, London (1975)
14. Daley, D.J., Gani, J.: *Epidemic Modelling: An Introduction*. Cambridge University Press, Cambridge (1999)
15. Hethcote, H.W.: *SIAM Rev.* **42**(4), 599 (2000)
16. Pastor-Satorras, R., Vespignani, A.: *Phys. Rev. Lett.* **86**, 3200 (2001)
17. Eckmann, J.P., Moses, E., Sergi, D.: *Proc. Natl. Acad. Sci. USA* **101**, 14333 (2004)
18. Barabási, A.L.: *Nature* **435**, 207 (2005)
19. Oliveira, J.G., barabási, A.L.: *Nature* **437**, 1251 (2005)
20. Harder, R., Paczuski, M.: *Physica A* **361**, 329 (2006)
21. Vazquez, A., Oliveira, J.G., Dezső, Z., Goh, K.I., Kondor, I., Barabási, A.L.: *Phys. Rev. E* **73**, 036127 (2006)
22. Vazquez, A., Balazs, R., Andras, L., Barabasi, A.L.: *Phys. Rev. Lett.* **98**, 158702 (2007)
23. Iribarren, J.L., Moro, E.: *Phys. Rev. Lett.* **103**, 038702 (2009)
24. Iribarren, J.L., Moro, E.: *Phys. Rev. E* **84**, 046116 (2011)
25. Min, B., Goh, K.I., Vazquez, A.: *Phys. Rev. E* **83**, 036102 (2011)
26. Karsai, M., Kivela, M., Pan, R.K., Kaski, K., Kertész, J., Barabási, A.L., Saramäki, J.: *Phys. Rev. E* **83**, 025102 (2011)
27. Balcan, D., Colizza, V., Gonçalves, B., Hu, H., Ramasco, J., Vespignani, A.: *Proc. Natl. Acad. Sci. USA* **106**, 21484 (2009)
28. Simini, F., González, M., Maritan, A., Barabási, A.L.: *Nature* **484**, 96 (2012)
29. Feller, W.: *An Introduction to Probability Theory and Its Applications*, vol. II. Wiley, New York (1966)
30. Harris, T.E.: *The Theory of Branching Processes*. Springer, Berlin (2002)
31. Vazquez, A.: *AMS-DIMACS Volume on Discrete Methods in Epidemiology*, pp. 163–179. AMS, Providence (2006)
32. Ebel, H., Mielsch, L.I., Bornholdt, S.: *Phys. Rev. E* **66**, R35103 (2002)
33. Newman, M.E.J., Forrest, S., Balthrop, J.: *Phys. Rev. E* **66**, R035101 (2002)
34. Vazquez, A.: *Phys. Rev. Lett.* **96**, 038702 (2006)
35. Vazquez, A.: *Phys. Rev. E* **74**, 056101 (2006)
36. Vazquez, A.: *Phys. Rev. E* **74**, 066114 (2006)
37. Liljeros, F., Edling, C.R., Amaral, L.A.N., Stanley, H.E., Berg, Y.: *Nature* **411**, 907 (2001)
38. Jones, J.H., Handcock, M.S.: *Proc. R. Soc. Lond. B Biol. Sci.* **270**, 1123 (2003)
39. Schneeberger, A., Mercer, C.H., Gregson, S.A., Fergusson, N.M., Nyamukapa, C.A., Anderson, R.M., Johnson, A.M., Garnett, G.P.: *Sex. Transm. Dis.* **31**, 380 (2004)
40. Latora, V., Nyamba, A., Simporé, J., Sylvestre, B., Diane, S., Sulvere, B., Musumeci, S.: *J. Med. Virol.* **78**, 724 (2006)
41. Callaway, D.S., Newman, M.E.J., Strogatz, S.H., Watts, D.J.: *Phys. Rev. Lett.* **85**, 5468 (2000)
42. Lewin, B., Fygl-Meyer, K., Helmius, G., Lalos, A., Mansson, S.: *Sex in Sweden*. The National Institute of Public Health Stockholm, (2000)
43. May, T.M., Anderson, R.M.: *Phil. Trans. R. Soc. Lond. B* **321**, 565 (1988)
44. Szendrői, B., Csányi, G.: *Proc. R. Soc. Lond. B Biol. Sci.* **271**, S364 (2004)
45. Mode, C.J.: *Multitype Branching Processes*. Elsevier, New York (1971)
46. Karsai, M., Kaski, K., Barabási, A.L., Kertész, J.: *Sci. Rep.* **2**, 397 (2012)

Time Allocation in Social Networks: Correlation Between Social Structure and Human Communication Dynamics

Giovanna Miritello, Rubén Lara, and Esteban Moro

Abstract Recent research has shown the deep impact of the dynamics of human interactions (or temporal social networks) on the spreading of information, opinion formation, etc. In general, the bursty nature of human interactions lowers the interaction between people to the extent that both the speed and reach of information diffusion are diminished. Using a large database of 20 million users of mobile phone calls we show evidence this effect is not homogeneous in the social network but in fact, there is a large correlation between this effect and the social topological structure around a given individual. In particular, we show that social relations of hubs in a network are relatively weaker from the dynamical point than those that are poorer connected in the information diffusion process. Our results show the importance of the temporal patterns of communication when analyzing and modeling dynamical process on social networks.

G. Miritello

Departamento de Matemáticas & GISC, Universidad Carlos III de Madrid, 28911 Leganés, Spain
Telefónica R&D, Madrid, Spain

R. Lara

Telefónica R&D, Madrid, Spain

E. Moro (✉)

Departamento de Matemáticas & GISC, Universidad Carlos III de Madrid, 28911 Leganés, Spain
Instituto de Ciencias Matemáticas CSIC-UAM-UCM-UC3M, 28049 Madrid, Spain

Instituto de Ingeniería del Conocimiento, Universidad Autónoma de Madrid,
28049 Madrid, Spain

e-mail: emoro@math.uc3m.es

1 Introduction

A quantitative understanding of human communication patterns is of paramount importance not only for a better understanding of human behavior, but also to explain the dynamics of many social, technological and economic phenomena. Examples include epidemics spreading, virus outbreaks, opinion formation, diffusion of innovation, rumors or trends [32, 41, 43]. All these processes are related to the underlying structure of the network and on the temporal activity patterns of humans, since they depend on the way humans interact and share information [3, 21, 33]. Determination of spreading paths, speed and reach in society is crucial for developing efficient strategies to propagate information (like in viral marketing [21]), to find out the influence that different people play in social networks [50] or to know how public opinion forms and spreads [17].

Most of our current understanding of spreading phenomena comes from implementing models and ideas borrowed from epidemiology on empirical or synthetic social networks [1]. Although recent works suggest that information transmission or influence is a much more involved process than disease propagation [2, 23, 48], these studies have permitted to find the deep entanglement between spreading and the complex topological patterns of the underlying network in the dynamical process [6–8, 30, 40]. Social networks are very heterogeneous: the flux of information that pass through each social tie is unevenly distributed, some individuals are more connected than others, social relationships are organized into communities, etc. These network structure heterogeneities reflect the way in which whom and how each individual is connected (and located) within the network and affect, therefore, the spreading of information. In particular, a celebrated hypothesis is that “hubs” (most connected people) [41] or those users with large centrality [30] are the key players in diffusion processes, being responsible for the largest part of the total reach of the spreading process.

Paradoxically, most of these studies of dynamical phenomena on social networks neglect the *temporal patterns* of human communications: humans act in bursts or cascades of events [3, 24, 44, 49], most social ties are not persistent [18, 31] and communications happen mostly in the form of group conversations [13, 24, 51, 52]. Since information transmission and human communication are concurrent, the temporal structure of communication must influence the properties of information spreading. Indeed, recent experiments of electronic recommendation forwarding [21] and simulations of epidemic models on email and mobile databases [26, 34, 49] found that the asymptotic speed of information spreading is controlled by the bursty nature of human communications that leads to a slowing down of the diffusion. Furthermore, in [34] it was found that not only the speed, but also the reach of information is affected by the temporal patterns of human communication. Specifically, while *burstiness of human communication* hinders the propagation of information through social ties, *group conversations* (or correlation between communication events in neighbor ties) favor the formation of local information cascades. These two competing effects shape the spreading reach and speed of

information yielding to different possible behaviors depending on the temporal properties of the information transmission.

Although identification of the key ingredients of the dynamical patterns of human communication allows to understand the evolution of the process at the network level, still there is no clear knowledge of what the roles played by the individual patterns of activity in that process are and how they correlated with the (static or aggregated) topological structure of social networks. For example, we might wonder whether static hubs, identified as those who contact a large number of people in a given time period, are also dynamical hubs, i.e., they have such communication patterns so that they retain their key role in information diffusion on temporal networks. In this contribution we analyzed this hypothesis by investigating how the different properties of temporal patterns of communication correlate with the social connectivity of an individual. More generally, this problem is related to how people allocate time among their social connections. After all, time and attention are inelastic resources and thus humans have to implement a communication strategy to maintain their social connectivity. Although static models of information diffusion assume that all ties of a given node are open at all times and information can flow at any time through any given tie, we expect attention and time constrains to shape the dynamical properties of human communication. Analyzing the communication of mobile phone calls between people, our results suggest that ties of static hubs have less transmissibility (on average) than expected and thus we find a large correlation between the static (node's degree) and dynamical properties of human communication. Taken together, these results suggest that temporal patterns of communication must be incorporated in the description and modeling of dynamical human-driven phenomena and of quantitative models of contact social networks.

This contribution is organized as follows: in Sect. 2 we describe our data and methods and review the different ways to characterize communication patterns between people. In Sect. 3 we revisit our method introduced in [34] in which we map the dynamic of human interactions onto a static representation of a social network through a quantity we call the *dynamical strength of ties*. We also study the correlation between the dynamical patterns and social connectivity of human communication in that section. Finally in the discussion we comment on our results and the possibility of using the dynamical strength of ties as a way to model temporal networks.

2 Characterizing Human Communication Patterns

To understand what features characterize human communication patterns, we study the mobile phone calls during $T_0 = 11$ months of a single mobile phone operator in a given country. The data consists of 2×10^7 phone numbers and 7×10^8 communication ties for a total of 9 billion calls between users. Call Detail Record (CDR) contains the hashed number of the caller and the receiver, the time when the call was initiated and the duration of the call. We consider only events in which the

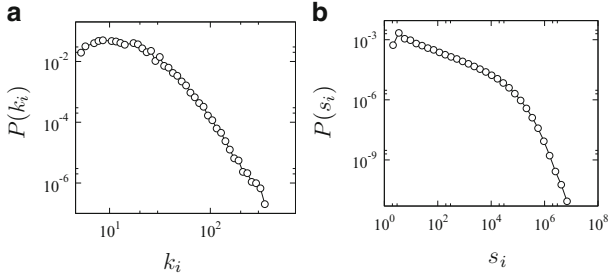


Fig. 1 Distribution of the social connectivity k_i (a) and the nodes' strength (b) in our mobile phone network

caller and the callee belong to the operator under consideration, because of partial access to the records of other operators. Finally, we only consider ties which are reciprocated, i.e., in which a call is made at least in both directions $i \leftrightarrow j$ and thus we consider that the weight of the tie w_{ij} given by the number of calls or the total amount of call time between i and j , is symmetric ($w_{ij} = w_{ji}$).¹ Our data for the connectivity of the social network, the duration of the calls, etc. are very similar to those reported in previous studies of mobile phone networks [42]. As shown in Fig. 1, we found a skewed distribution for both the nodes' social connectivity k_i in the observation time period and the strength $s_i = \sum_j w_{ij}$. In our database, we observe that the mean social connectivity is around 85, with a maximum value of around 500. For the node strength s_i instead, we found that, although the mean of this distribution is around 1.5 h in the whole period, the maximum value is about 6 h per day. This means that while the time that the larger part of the population spends on the phone per day is of the order of seconds or minutes, there is a small minority who phone more than 1 h per day. Not only the aggregated s_i , but also the ties weight w_{ij} show a long-tailed distribution, which indicates a strong heterogeneity in the way people distribute the time across their social circle. For both k_i and s_i , however, the decay is faster than a power-law, which indicates the presence of a relatively small number of hubs. This decay is probably due to the fact that we have filtered out business phone numbers, which mainly correspond to the hubs in mobile networks, a possibility also pointed out in [39].

The relationship between the social connectivity and the intensity of communication has been investigated recently by Miritello et al. in [35]: in line with previous studies for both scientific collaboration and the air-transportation networks [5], we found that the average strength $s_i(k_i)$ of nodes with degree k_i increases almost linearly with k_i , that is $s_i(k_i) \sim k_i^\beta$, with $\beta \simeq 1$. However, we observe a slightly more complex behavior for large values of k_i , where s_i starts to grow sublinearly with k_i until it saturates for very large values of k_i , which suggests the existence of

¹Similar results are found if the total amount of time is used for w_{ij} instead of the number of calls.

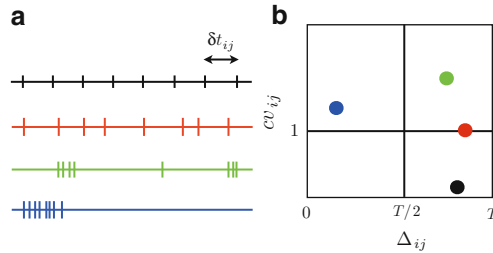


Fig. 2 (a) Schematic representation of different communication patterns within a tie for the same intensity, $w_{ij} = 8$ calls. Each vertical line correspond to a different call between i and j . (b) Bivariate representation of the coefficient of variation and stability of ties for the corresponding cases in (a)

a limit for more connected people to allocate communication time in a proportional fashion. Thus, the larger the social connectivity, the smaller the time dedicated per tie. This means that, on average, hubs have weaker communications. The observed behavior might be related to Dunbar’s theory [11] which asserts that cognitive and biological constraints limit the number of people an individual keeps social contact with. On top of those limits, in our case also temporal and monetary constraints may play their role in phone communication. In this respect, our results are similar to those found in other communication networks such as Twitter [16].

Characterizing a given communication tie by its strength (weight w_{ij}) ignores however the fact that human communication is a highly complex dynamical process. Among others, some of the implicit assumptions of considering static description of ties are that (1) communication can happen at any time, (2) human activity is Markovian and randomly distributed in time, therefore well approximated by a Poisson process, and (3) there is no correlation or causality between events.

This is exemplified in Fig. 2, where we show that many different temporal patterns of communication can correspond to the same strength of communication w_{ij} . In particular, recent research has shown that temporal patterns of human individuals are strongly inhomogeneous and deviate from the Poisson process [3, 26, 34, 49]. In the latter, the number of events during a time interval of duration T follows a Poisson distribution with mean ρT , where ρ is the rate of events and the time between consecutive events, called the *inter-event* times, follows an exponential distribution $p(\delta t) = \rho e^{-\rho t}$. As a consequence, individual actions happen at relatively regular time intervals δt and very short or very long inter-event times occur with small probability. However, human activity is bursty, which is reflected by the slowly decaying of the inter-event time probability distribution (possibly like $P(\delta t) \sim \delta t^{-1}$ for small inter-event times [3]), thus in stark contrast with the prediction of a homogeneous Poisson process. This behavior seems to be a universal feature of human activity: it has been observed in several systems driven by human activity sequences [4, 13, 15, 38, 45] and is known in literature as *bursty behavior* since long periods of inactivity are separated by intense bursts of activity. Regarding human communication, bursty behavior is found also in inter-event times between

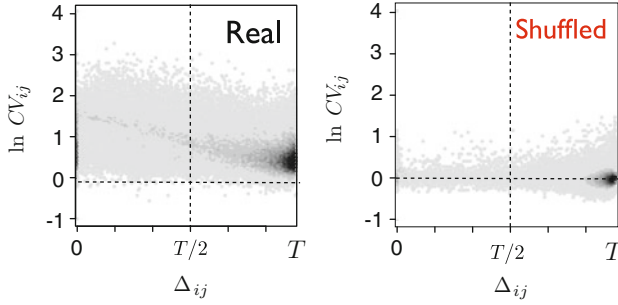


Fig. 3 Density plot of the coefficient of variation and stability of the ties in our database for the real sequence of calls (*left*) and the corresponding ones for the shuffled time stamps (*right*). To have enough statistical significance for cv_{ij} , only ties with $w_{ij} \geq 5$ are used in the plot

communications of a single person and even on events within a social tie [26, 34]. Although there are other ways to characterize (and define) burstiness [15, 27], to capture this information we use the common *coefficient of variation* cv_{ij} of the inter-event time distribution $P(\delta t_{ij})$ of a tie. It is measured as $cv_{ij} = \sigma_{ij} / \mu_{ij}$ where μ_{ij} and σ_{ij} are the mean and standard deviation of the distribution $P(\delta t_{ij})$. By definition, cv_{ij} measures the dispersion of a distribution, that is the level of heterogeneity of tie communication: the more heterogeneous the interaction is, the larger cv_{ij} . Note that for the inter-event exponential distribution in the Poisson process we have that $\sigma_{ij} = \mu_{ij}$ and thus $cv_{ij} = 1$. For the perfect deterministic process in which events happen at regular times we get $cv_{ij} = 0$, while for the bursty behavior in which $P(\delta t)$ is heavy tailed we usually have $\sigma_{ij} \gg \mu_{ij}$ and thus $cv_{ij} \gg 1$.

Although w_{ij} and cv_{ij} tell us something about the intensity and how homogeneous in time are communication events, they lack the information about how fast this happens. As shown in Fig. 2, the same amount of calls can be placed in a rather long or extremely short time window. To characterize this variability in the rhythm of communication we define the temporal stability Δ_{ij} of a tie as $\Delta_{ij} = t_{ij}^{max} - t_{ij}^{min}$, where t_{ij}^{min} and t_{ij}^{max} are, respectively, the time instants at which the first and the last communication events between i and j are observed within the observation period. A large stability ($\Delta_{ij} \simeq T_0$) indicates that the communication between i and j extends over the observation period, while a small one ($\Delta_{ij} \simeq 0$) is the signal of a short tie lifetime. In the case of a Poissonian process $\Delta_{ij} \simeq T_0$ for all ties, since time events are evenly distributed along the observation window.

As shown in Fig. 3, human communication patterns differ from equivalent Poisson process with the same number of events w_{ij} . To mimic the latter process, we shuffle the time stamps of the real events across the database, thus each call has an even probability to appear anytime within the observation window. Note that this shuffling preserves the usual circadian rhythms (nights, weekends, holidays), but destroys all possible heterogeneous patterns of communication within the ties [25]. As expected, in the shuffled Poissonian case we have that for most of the ties $cv_{ij} \simeq 1$ and $\Delta_{ij} \simeq T_0$. However, for the real case we observe that most ties show

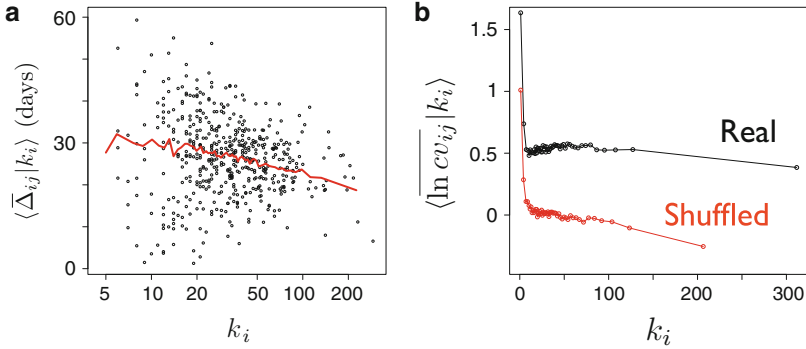


Fig. 4 (a) Scatter plot (for a small sample of individuals) and conditional mean of the average stability of the ties for a given individual $\overline{\Delta}_{ij}$ in our database as a function of her connectivity in the observation window k_i . The plot only shows the result for the real sequence of calls, since for the shuffled case $\overline{\Delta}_{ij} \simeq T$. (b) Conditional mean of the average logarithm of the coefficient of variation cv_{ij} for the real and shuffled cases as a function of k_i

bursty behavior ($cv_{ij} > 1$) and that the stability is distributed along the observation window, with the special feature that a large proportion of ties have either large stability ($\Delta_{ij} \simeq T_0$) or very small one ($\Delta_{ij} = 1$). This bimodal distribution of the lifetime of links was found also in other mobile phone databases [18] and indicates that ties are mostly long or very short, possibly signaling the very different nature of the communication involved: for example, short ties could be due to search of information within the social network, while long ties might reflect social or close relationship between individuals.

We now investigate how the dynamical properties of ties depend on the social connectivity of individuals in the observation time window k_i . As mentioned above, cognitive and monetary costs influence the aggregate amount of attention per tie for largely connected individuals [11, 16, 35]. On the other hand, we have seen that communication events are not evenly distributed across the time window. We therefore expect that the way in which people allocate time in social networks also reflects in their patterns of communication. For example, for a given w_{ij} the attention allocated in a short tie is much more localized in time than in a long tie. In addition, individuals might choose to develop more bursty communication patterns to be able to allocate more conversations within the day. In Fig. 4 we show our results for the dependence of both cv_{ij} and Δ_{ij} with k_i . Although there is no significant dependence on cv_{ij} , i.e., the burstiness of ties, for a given individual as a function of her social connectivity k_i in the time window, we observe that highly connected individuals have shorter ties. This is a clear indication that, aside from the non-trivial way in which individuals allocate time of communication among their contacts, there is also a complex way in which this attention unfolds in time. In summary, it seems that highly connected people are characterized by weaker (in terms of volume of communication) and shorter ties than moderate or low connected people.

3 Dynamical Strength of Communication Ties

It is clear that the intensity w_{ij} does not capture the whole dynamics of communication within a tie and thus it is not sufficient to describe the importance or role of that tie in the diffusion of information. To understand that role, in [34] we developed a new measure of the strength of a tie which takes into account not only the intensity of the link, but also its dynamical pattern. The idea is based on the mapping introduced by Newman in [36] in which the dynamical information diffusion process is mapped onto a static edge percolation where each tie is described by the *transmissibility* or dynamical strength, i.e., the probability that information flows through the link given the sequence of communication events between individuals. The network is then still described by a static graph, but the interaction strength between individuals now incorporates the causal and temporal patterns of their communications. As shown in [34], this procedure not only explains the qualitative behavior of the dynamics of information diffusion, but also successfully predicts, for example, the percolation threshold for the SIR (Susceptible-Infected-Recovered) model on our dataset. Obviously the dynamical strength of a tie must depend on the process under consideration. For example, its definition varies if one considers models of information diffusion like the SIR model [34], simple random walk hopping between individuals [19], or more complicated processes. In our case, since we are interested on information diffusion and/or influence, we concentrate on the simplest model of information propagation, namely the SIR epidemiological model [1]. Although recent research has highlighted that important differences exist between information diffusion and disease spreading [2,23,48], epidemiological models have been the main theoretical tools to understand how information is transmitted in social networks [10]. Moreover, they are useful methods to explore the intricate structure of social networks at large scale [26, 30, 40]. In that spirit, our aim in this section is to use the SIR model to investigate the influence of the behavior observed in the previous section on the role played by individuals in the spreading of information.

In the SIR model, individuals can be at different states of the infection dynamics and they are allowed to change their state. Individuals are initially susceptible (S) and become infected (I) with a given transmission rate λ when interact with an infected individual. At the same time, infected individuals are allowed to recover (R) at some rate μ . In our case, we consider that in each call an infected node (an individual that knows the information) can infect a susceptible node (an individual who is not aware of the information) with probability λ . Due to the synchronous nature of the phone communication, this happens regardless of who initiates the call. Nodes remain infected for a certain interval of time until they decay into the recovered state in which they do not propagate the information anymore. Although this decay into the recovered state can be very complex, for the sake of simplicity we simulate the simplest model in which nodes recover after a fixed deterministic and homogeneous time T . More general situations can be accommodated into the model such as, for example, stochastic recovery times. The information diffusion

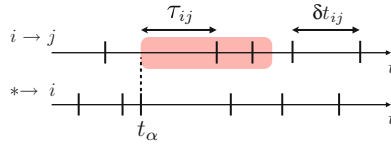


Fig. 5 Schematic view of communications events around individual i : each vertical segment indicates an event between $i \rightarrow j$ (top) and $* \rightarrow i$ (bottom). At each t_α in the $* \rightarrow i$ time series, τ_{ij} is the time elapsed to the next $i \rightarrow j$ event, which is different from the inter-event time δt_{ij} in the $i \rightarrow j$ time series. The red shaded area represents the recover time window T after t_α

is simulated starting from a unique infected seed which generates a viral cascade that grows until there are no more nodes in the infected state. As shown in [34], the simulations using the real sequence of calls between individuals show a phase transition at very small λ_c : below λ_c cascades die out very quickly, while above λ_c we find that with large probability there exists a cascade that infects a large proportion of the individuals in our social network. This percolation transition happens also around λ_c for the time-shuffled data, in which the real sequence and properties of tie interactions are destroyed mimicking Poissonian dynamics. A different behavior was however found between the real and the shuffled case below and above the percolation transition λ_c . Below λ_c , the correlations between events in neighboring ties (group conversations) favor information diffusion and thus cascades in the real case are larger than in the shuffled case. In contrast, above the percolation threshold, the burstiness of communication events hinders the propagation of information, making the reach of information smaller in the real than in the shuffled case. Thus real dynamics of interaction in social network makes information spreading more efficient at small (local) scale (below λ_c), while if information propagates easily (large λ) the reach of information in social networks is small than the one expected when a Poissonian dynamics is considered.

The observed behavior can be understand by analyzing how the communication temporal patterns affect information diffusion [34]. Spreading from user i to user j ($i \rightarrow j$) happens at the relay time intervals τ_{ij} , i.e., the time interval it takes to i to pass on to j an information he/she got from any another person $* \rightarrow i$, where $j \neq *$ (see Fig. 5). Information spreading is thus determined by the interplay between τ_{ij} and the intrinsic timescale of the infection process T . As it was shown in [34], τ_{ij} depends on the correlated and causal way in which group conversations happen, since it depends on the inter-event intervals δt_{ij} in the $i \rightarrow j$ communication but also on the possible temporal correlation with the $* \rightarrow j$ events [29, 36].

By ignoring this correlation the probability distribution function (or pdf) for τ_{ij} can be approximated by the waiting-time density for δt_{ij} given [9]:

$$P(\tau_{ij}) = \frac{1}{\delta t_{ij}} \int_{\tau_{ij}}^{\infty} P(\delta t_{ij}) d\delta t_{ij}, \tag{1}$$

where $\overline{\delta t_{ij}}$ is the average inter-event time. In this approximation, the dynamics of the transmission process only depends on the dyadic $i \rightarrow j$ sequence of communication events. In particular, the heavy-tail properties of $P(\delta t_{ij})$ found in human communication [26, 34] are directly inherited by $P(\tau_{ij})$, making the relay times much bigger than expected. Thus the more bursty the communication is, the larger the relay times are, which qualitatively explains empirical observations that heterogeneous human activity slows down information spreading [21, 22, 26, 49].

To fully understand the impact of dynamical patterns of communication on information diffusion, we follow the approach of [36] by mapping the dynamical SIR model to a static edge percolation model where each tie is described by the *transmissibility* \mathcal{T}_{ij} . The transmissibility represents the probability that the information is transmitted from i to j and it is a function of λ and T . If user i becomes infected at time t_α and the number of communication events $i \rightarrow j$ in the interval $[t_\alpha, t_\alpha + T]$ is $n_{ij}(t_\alpha)$, then the transmissibility in that interval is (see Fig. 5)

$$\mathcal{T}_{ij} = 1 - (1 - \lambda)^{n_{ij}(t_\alpha)}. \quad (2)$$

User i may become infected during any $* \rightarrow i$ communication event at t_α . Assuming these events independent and equally probable, we can average \mathcal{T}_{ij} over all the t_α events to get

$$\mathcal{T}_{ij}[\lambda, T] = \langle 1 - (1 - \lambda)^{n_{ij}(t_\alpha)} \rangle_\alpha. \quad (3)$$

If the number of $* \rightarrow i$ events is large enough, we can use a probabilistic description of (3) in terms of the probability $P(n_{ij} = n; T)$ that the number of communication events between i and j in a given time interval T is n . Thus

$$\mathcal{T}_{ij}[\lambda, T] = \sum_{n=0}^{\infty} P(n_{ij} = n; T)[1 - (1 - \lambda)^n], \quad (4)$$

which in principle can be non symmetric ($\mathcal{T}_{ij} \neq \mathcal{T}_{ji}$). This quantity represents the real probability of infection from i to j and defines what we called the *dynamical strength* of the tie. Note that \mathcal{T}_{ij} depends on the series of communication events between i and j , but also on the time series of calls received by i .

In [36] Newman studied the case in which both time series are given by independent Poisson processes in the whole observation interval $[0, T_0]$. Thus, $P(n_{ij} = n; T)$ is the Poisson distribution with rate $\rho_{ij} = w_{ij}T/T_0$, where w_{ij} is the intensity of the tie, i.e., the total number of calls from i to j in $[0, T_0]$, and so

$$\tilde{\mathcal{T}}_{ij}[\lambda, T] = 1 - e^{-\lambda\rho_{ij}} = 1 - e^{-\lambda w_{ij}T/T_0}, \quad (5)$$

which shows the one-to-one relationship between the intensity w_{ij} and the transmissibility \mathcal{T}_{ij} in the Poissonian case: the more intense the communication is, the larger

the probability of infection. However, as we have shown in [34] and in previous sections, the real $i \rightarrow j$ and $* \rightarrow i$ series are far from being independent and Poissonian. To proceed analytically, we approximate (3). For small values of λ we have $1 - (1 - \lambda)^n \simeq \lambda n$, while when $\lambda \simeq 1$ we get that $1 - (1 - \lambda)^n \simeq 1$ for $n > 0$. Thus, the transmissibility for the two regimes is given by:

$$\mathcal{T}_{ij}[\lambda, T] = \begin{cases} \lambda \langle n_{ij} \rangle_{t_\alpha} & \text{for } \lambda \ll 1 \\ 1 - P_{ij}^0 & \text{for } \lambda \simeq 1 \end{cases} \quad (6)$$

where $P_{ij}^0 = P(n_{ij} = 0; T)$ is the probability of no communication event in a time window of length T . This approximation allows us to estimate \mathcal{T}_{ij} in a much simpler way, since it depends now only on variables that can be measured from the temporal activity. In fact, (6) explains the observed behavior found in [34], since group conversations make $\langle n_{ij} \rangle_{t_\alpha}$ bigger in the real case than in the Poisson approximation, while burstiness yields to larger values of the probability of no communication in the real case than in the Poisson case and thus transmissibility is larger in the latter than in the former situation.

For $\lambda \simeq 1$, the larger the coefficient of variation cv_{ij} in a tie (i.e. the more bursty it is), the larger the probability of no event P_{ij}^0 and thus the lower the transmissibility of the tie. The same behavior is found for the lifetime of links: if communication is concentrated in a short time period, then P_{ij}^0 is large and thus the transmissibility is low. Consequently, the shorter the tie communication, the smaller the transmissibility of the ties. Since the burstiness of human communication and activity seem to be universal [3], empirical description of social networks only by their topological structure and/or the intensity w_{ij} typically overestimates the transmissibility power of ties.

Finally, we investigate whether this effect of human communication patterns is correlated with the social structure around a particular node. As shown in the previous section, intensity and lifetime of links are distributed differently among neighbors for individuals with low and large social connectivity. Since lifetime and burstiness of communication ties impact the transmissibility of links, we expect that the dependence of time allocation of communication with connectivity also translates into a dependence between k_i and the total transmissibility of an individual $\mathcal{T}_i = \sum_j \mathcal{T}_{ij}$. Note that in the Poisson case and for small values of λ , we get that $\tilde{\mathcal{T}}_{ij} \simeq \lambda w_{ij} T / T_0$ and thus $\tilde{\mathcal{T}}_i \simeq \lambda s_i T / T_0$, i.e., the transmission power of a node is proportional to the strength of the node in this approximation. However, in the real case $\mathcal{T}_i = \sum_j \mathcal{T}_{ij}[\lambda, T]$ depends both on the intensity and dynamical patterns of communication. As we see in Fig. 6a, the burstiness of ties makes individuals in general less powerful to transmit information than in the Poisson case, in the sense that their total real transmissibility is smaller than shuffled one. However, this is not an homogeneous effect in our database since, as it can be seen in Fig. 6b, the relative difference between \mathcal{T}_i in the real and shuffled cases is larger for hubs or more connected people than for poorly connected people, a manifestation in the process of information diffusion of the effect we have seen in

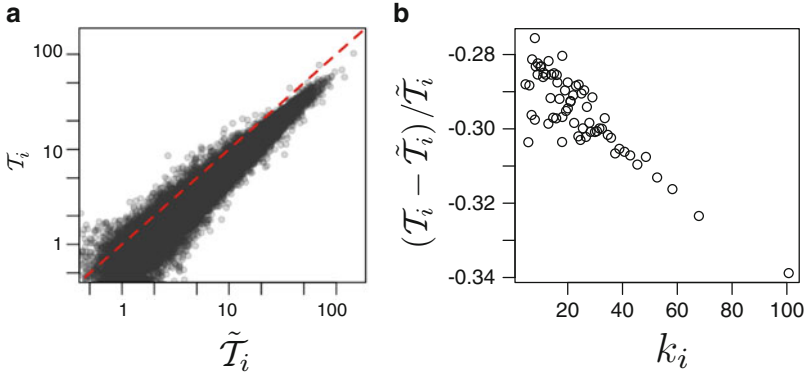


Fig. 6 (a) Comparison between the total transmissibility of individuals in the real \mathcal{T}_i and shuffled $\tilde{\mathcal{T}}_i$ call records for a random set of 10^5 users in our database. *Dashed line* is the $\mathcal{T}_i = \tilde{\mathcal{T}}_i$ line. (b) Conditional average of relative difference between the real and shuffled total transmissibility as a function of the social connectivity k_i

the previous section (i.e. hubs have shorter ties). Note that this relative difference increases with k_i meaning that \mathcal{T}_i does not grow linearly with k_i (or s_i) as $\tilde{\mathcal{T}}_i$ does. Our findings show that neither k_i or s_i are good predictors of the local spreading power or influence of a node, especially for largely connected people or hubs. In this sense, although in general static hubs (people with large k_i or s_i) have also large dynamical transmissibility, the large variability shown in Fig. 6a implies that this correspondence is not always true.

4 Discussion

In the last years there has been an increasing interest in characterizing the complex topological structure of the underlying contact network and in understanding how it affects the diffusion of information, innovation or opinions [37]. However, most of these studies neglect the temporal dimension of human communication as the fact that humans act in bursts or cascades of events [3, 24, 26, 34, 44, 49], most of ties form and decay within the observation time period [18, 31] and there are correlations between communication events [13, 24, 34, 51, 52]. These temporal heterogeneities significantly affect the current description of social networks, where ties are described by a static strength which usually only takes into account the volume of communication or intensity w_{ij} . Although w_{ij} has been shown to reflect the face-to-face interaction between two individuals [12], we have seen that the same amount of communication events can correspond to ties with completely different temporal properties, which indicates the necessity to incorporate temporal patterns of human activity in the description and modeling of human interactions. Actually,

in line with recent work on temporal networks [20, 28, 46, 47] we have shown that the current definition of social ties can be largely improved by taking into account simple temporal tie features, such as the level of burstiness of tie communication or the lifetime of the tie.

Our main contribution is that temporal properties of tie activity also reveal important information on the social topological structure around a given individual. This correlation between human communication and network topology gives important insights on the way in which people distribute their time across their network and, at the same time, it also plays a fundamental role on more global phenomena, such as influence and information spreading in social networks. Previous studies showed that the aggregated time that people dedicate to their connections is affected by cognitive and temporal constraints, which applies in particular to people with larger social circles (hubs) [11, 16, 35]. Here we have seen that time and/or attention constraints also reflect in the temporal properties of social ties. We observed in fact that, on average, social connections of highly connected individuals not only are weaker in terms of volume of communication, but they are also shorter in time. The latter result signals a time allocation strategy of individuals in their social neighborhood, which also affects the transmissibility of a given individual, i.e., her capacity to propagate a piece of information. In particular, we have found that the static picture of networks in terms of social connectivity k_i and/or intensity of communication s_i , typically overestimates the power of individuals to transmit information, an effect which is larger for more connected people.

Our mapping approach goes beyond the important application to information diffusion and it also applies to the more general and critical problem in complex networks of describing empirical temporal social networks [20]. We have shown, in fact, that a simple way to account for the temporal properties of human communication and still have a static representation of the social network, is by using the transmissibility T_{ij} as a measure of tie strength, instead of the volume of communication (number of calls or total duration) w_{ij} . While the number of communication events between a tie $i \rightarrow j$ represents the *static strength*, the transmissibility T_{ij} represents the *dynamical strength* of a tie [34]. By definition, in fact, T_{ij} incorporates not only the volume of communication w_{ij} , but also all the temporal inhomogeneities of human interaction (see (3)). The use of the dynamical strength of ties $\mathcal{T}_{ij}[\lambda, T]$ allows possible comparison of the network at different time scales and thus it can be used to obtain essential information about how and why temporal networks unfold in time. In Fig. 7 we compare a portion of the social network where the weight of each link is given by the static (a) and the dynamical (b) strength of the ties. The figure clearly shows that these two quantities may lead to quite different pictures of the topological structure of the network.

More generally, this effective static structure of temporal networks might be used in other areas of network research such as determination of influence/centrality [2], community finding algorithms [14], targeting in viral marketing [21], etc., to analyze the impact of the dynamical patterns of communication in those areas and to assess more accurately the role played by individuals or groups in dynamical process on social networks.

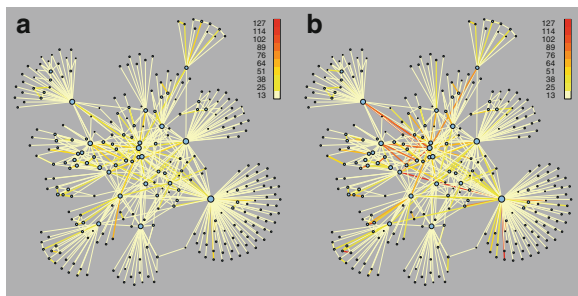


Fig. 7 (a) Temporal and (b) static structure of the mobile phone network around a randomly chosen individual where colors of the links are proportional to the strength of the ties. The strength of ties is taken as w_{ij} for the static structure, while for the sake of comparison we take the effective weight $w_{ij}(\lambda, T)^* = -T_0/(\lambda T) \ln(1 - T_{ij}(\lambda, T))$ for the temporal case. Note that in the Poisson case $w_{ij} = w_{ij}(\lambda, T)^*$. Parameters for the calculation are $\lambda = 0.5$ and $T = 15$ days. It is interesting to note that most of the strong ties present in the static structure become very weak in the temporal picture due to the burstiness and/or lifetime of links

Acknowledgements We would like to thank Telefónica for providing access to the anonymized data. E.M. and G.M. acknowledge funding from Ministerio de Educación y Ciencia (Spain) through projects i-Math, FIS2006-01485 (MOSAICO), and FIS2010-22047-C05-04.

References

1. Anderson, R.M., May, R.: Infectious Diseases in Humans. Oxford University Press, Oxford (1992)
2. Aral, S., Walker, D.: Identifying influential and susceptible members of social networks. *Science* **337**, 337–341 (2012)
3. Barabási, A.-L.: The origin of bursts and heavy tails in human dynamics. *Nat. Sci. Rep.* **435**, 207–211 (2005)
4. Barabási, A.-L.: Bursts: The Hidden Pattern Behind Everything We Do. Dutton Books, New York (2010)
5. Barrat, A., Barthélemy, M., Pastor-Satorras, R., Vespignani, A.: The architecture of complex weighted networks. *Proc. Natl. Acad. Sci. USA* **101**, 3747 (2004)
6. Barrat, A., Barthélemy, M., Vespignani, A.: Dynamical Process on Complex Networks. Cambridge University Press, Cambridge (2008)
7. Barthélemy, M., Barrat, A., Pastor-Satorras, R., Vespignani, A.: Velocity and hierarchical spread of epidemic outbreaks in scale-free networks. *Phys. Rev. Lett.* **92**, 178701 (2004)
8. Boguña, M., Pastor-Satorras, R.: Epidemic spreading in correlated complex networks. *Phys. Rev. E* **66**, 047104 (2002)
9. Breuer, L., Baum, D.: An Introduction to Queueing Theory. Springer, New York (2005)
10. Daley, D.J., Kendall, D.G.: Epidemics and rumours. *Nature* **204**, 4963, 1118 (1964)
11. Dunbar, R.: The social brain hypothesis. *Evol. Anthropol.* **6**(5), 178–190 (1998)
12. Eagle, N., Pentland, A., Lazer, D.: Inferring friendship network structure by using mobile phone data. *Proc. Natl. Acad. Sci.* **106**(36), 15274–15278 (2009)
13. Eckmann, J.-P., Moses, E., Sergi, D.: Entropy of dialogues creates coherent structures in e-mail traffic. *Proc. Natl. Acad. Sci. USA* **40**, 14333–14337 (2004)

14. Fortunato, S.: Community detection in graphs. *Phys. Rep.* **486**, 75–174 (2010)
15. Goh, K.-I., Barabási, A.-L.: Burstiness and memory in complex systems. *Europhys. Lett.* **81**, 48002 (2008)
16. Gonçalves, B., Perra, N., Vespignani, A.: Modeling users' activity on twitter networks: validation of dunbar's number. *PLoS ONE* **6**(8), e22656 (2011)
17. González-Bailón, S., Borge-Holthoefer, J., Rivero, A., Moreno, Y.: The dynamics of protest recruitment through an online network. *Sci. Rep.* **1**, 197 (2011)
18. Hidalgo, C., Rodriguez-Sickert, C.: The dynamics of a mobile phone network. *Physica A* **387**, 3017 (2008)
19. Hoffmann, T., Porter, M.A., Lambiotte, R.: Generalized master equations for non-Poisson dynamics on networks. *arXiv.org* 1112.3324v1 (2011)
20. Holme, P., Saramäki, J.: Temporal networks. *Phys. Rep.* **519**, 97–125 (2012)
21. Iribarren, J., Moro, E.: Impact of human activity patterns on the dynamics of information diffusion. *Phys. Rev. Lett.* **103**, 038702 (2009)
22. Iribarren, J., Moro, E.: Branching dynamics of viral information spreading. *Phys. Rev. E* **84**, 046116 (2011)
23. Iribarren, J.L., Moro, E.: Affinity paths and information diffusion in social networks. *Soc. Networks* **33**, 134–142 (2011)
24. Isella, L., Stehlé, J., Barrat, A., Cattuto, C., Pinton, J.-F., Van den Broeck, W.: What's in a crowd? Analysis of face-to-face behavioral networks. *J. Theor. Biol.* **166**, 166–180 (2011)
25. Jo, H.-H., Karsai, M., Kertész, J., Kaski, K.: Circadian pattern and burstiness in mobile phone communication. *New J. Phys.* **14**, 013055 (2012)
26. Karsai, M., Kivela, M., Pan, R., Kaski, K., Kertész, J., Barabási, A.-L.: Small but slow world: how network topology and burstiness slow down spreading. *Phys. Rev. E* **83**, 025102(R) (2011)
27. Karsai, M., Kaski, K., Barabási, A.-L., Kertész, J.: Universal features of correlated bursty behaviour. *Sci. Rep.* **2**, 397 (2011)
28. Karsai, M.M., Kaski, K.K., Kertész, J.J.: Correlated dynamics in egocentric communication networks. *PLoS ONE* **7**, e40612–e40612 (2011)
29. Kenan, E., Robins, J.M.: Second look at the spread of epidemics on networks. *Phys. Rev. E* **76**, 036113 (2007)
30. Kitsak, M., Gallos, L.K., Havlin, S., Liljeros, F., Stanley, H.E., Makse, H.A.: Identification of influential spreaders in complex networks. *Nat. Phys.* **6**, 888–893 (2010)
31. Kossinets, G., Watts, D.J.: Empirical analysis of an evolving social network. *Science* **311**, 5757 (2006)
32. Lazer, D., Pentland, A., Adamic, L., Aral, S., Barabási, A.-L., Brewer, N., Christakis, N.A., Contractor, N., Fowler, J., Gutmann, M., Jebara, T., King, G., Macy, M., Roy, D., Van Alstyne, M.: Computational social science. *Science* **323**, 721–723 (2009)
33. Malmgren, R.D., Stouffer, D.B., Motter, A.E., Amaral, L.A.N.: A poissonian explanation for heavy tails in e-mail communication. *Proc. Natl. Acad. Sci. USA* **105**, 18153–18158 (2008)
34. Miritello, G., Moro, E., Lara, R.: Dynamical strength of social ties in information spreading. *Phys. Rev. E* **83**, 045102(R) (2011)
35. Miritello, G., Moro, E., Lara, R., Martínez-López, R., Belchamber, J., Roberts, S.G.B., Dunbar, R.I.M.: Time as a limited resource: communication strategy in mobile phone networks. (2012). [doi:http://dx.doi.org/10.1016/j.socnet.2013.01.003](http://dx.doi.org/10.1016/j.socnet.2013.01.003)
36. Newman, M.E.J.: The spread of epidemic disease on networks. *Phys. Rev. E* **66**, 016128 (2002)
37. Newman, M.E.J.: The structure and function of complex networks. *SIAM Rev.* **45**, 167–256 (2003)
38. Oliveira, J., Barabási, A.-L.: Human dynamics: Darwin and Einstein correspondence patterns. *Nature* **437**, 1251 (2005)
39. Onnela, J.-P., Saramäki, J., Hyvönen, J., Szabó, Z., Lazer, D., Kaski, K., Kertész, J., Barabási, A.-L.: Structure and tie strengths in mobile communication networks. *Proc. Natl. Acad. Sci. USA* **104**, 7332 (2007)
40. Onnela, J.-P., Arbesman, S., González, M., Barabási, A.-L., Christakis, N.A.: Geographic constraints on social network groups. *PLoS ONE* **6**(4), e16939 (2011)

41. Pastor-Satorras, R., Vespignani, A.: Epidemic spreading in scale-free networks. *Phys. Rev. Lett.* **86**, 3200–3203 (2001)
42. Porter, M.A., Onnela, J.-P., Mucha, P.J.: Communities in networks. *Not. Am. Math. Soc.* **56**, 1082 (2009)
43. Rogers, E.: *Diffusion of Innovations*. Free Press, New York (1995)
44. Rybski, D., Buldyrev, S.V., Havlin, S., Liljeros, F., Makse, H.A.: Scaling laws of human interaction activity. *Proc. Natl. Acad. Sci. USA* **106**, 12640 (2009)
45. Rybski, D., Buldyrev, S.V., Havlin, S., Liljeros, F., and Makse, H.A.: Communication activity: temporal correlations, clustering, and growth. arXiv:1002.0216v1 (2010)
46. Tang, J., Musolesi, M., Mascolo, C., Latora, V.: Characterising temporal distance and reachability in mobile and online social networks. *ACM SIGCOMM Comp. Comm. Rev.* **40**, 1 (2010)
47. Toivonen, R., Kumpula, J., Saramäki, J., Onnela, J.-P., Kertész, J., Kaski, K.: The role of edge weights in social networks: modelling structure and dynamics. *Proc. SPIE: Noise and Stochastic in Complex Systems and Finance*, *Proc. SPIE* **6601**, 660110 (2007)
48. Ugander, J., Backstrom, L., Marlow, C., Kleinberg, J.: Structural diversity in social contagion. *Proc. Natl. Acad. Sci.* **109**(16), 5962–5966 (2012)
49. Vázquez, A., Rácz, B., Lukács, A., Barabási, A.-L.: Impact of non-poissonian activity patterns on spreading processes. *Phys. Rev. Lett.* **98**, 158702 (2007)
50. Watts, D., Dodds, P.: Influentials, networks, and public opinion formation. *J. Consum. Res.* **34**(4), 441–458 (2007)
51. Wu, T., Zhou, C., Xiaob, J., Kurthsa, J., Schellnhuber, H.: Evidence for a bimodal distribution in human communication. *Proc. Natl. Acad. Sci. USA* **107**, 18803 (2010)
52. Zhao, Q., Oliver, N.: Communication motifs: a novel approach to characterize mobile communications. In: *NetMob2010* (2010). <http://dl.acm.org/citation.cfm?id=1871694>

Temporal Networks of Face-to-Face Human Interactions

Alain Barrat and Ciro Cattuto

Abstract The ever increasing adoption of mobile technologies and ubiquitous services allows to sense human behavior at unprecedented levels of details and scale. Wearable sensors are opening up a new window on human mobility and proximity at the finest resolution of face-to-face proximity. As a consequence, empirical data describing social and behavioral networks are acquiring a longitudinal dimension that brings forth new challenges for analysis and modeling. Here we review recent work on the representation and analysis of temporal networks of face-to-face human proximity, based on large-scale datasets collected in the context of the SocioPatterns collaboration. We show that the raw behavioral data can be studied at various levels of coarse-graining, which turn out to be complementary to one another, with each level exposing different features of the underlying system. We briefly review a generative model of temporal contact networks that reproduces some statistical observables. Then, we shift our focus from surface statistical features to dynamical processes on empirical temporal networks. We discuss how simple dynamical processes can be used as probes to expose important features of the interaction patterns, such as burstiness and causal constraints. We show that simulating dynamical processes on empirical temporal networks can unveil differences between datasets that would otherwise look statistically similar. Moreover, we argue that, due to the temporal heterogeneity of human dynamics, in order to investigate the temporal properties of spreading processes it may be necessary to abandon the notion of wall-clock time in favour of an intrinsic notion of time for each individual

A. Barrat (✉)

Aix Marseille Université, CNRS UMR 7332, CPT, 13288 Marseille, France

Université du Sud Toulon-Var, CNRS UMR 7332, CPT, 83957 La Garde, France

Data Science Laboratory, ISI Foundation, Torino, Italy

e-mail: alain.barrat@cpt.univ-mrs.fr

C. Cattuto

Data Science Laboratory, ISI Foundation, Torino, Italy

e-mail: ciro.cattuto@isi.it

node, defined in terms of its activity level. We conclude highlighting several open research questions raised by the nature of the data at hand.

1 Introduction

Although social relationships and behaviors are inherently dynamically evolving, social interactions, represented by the paradigm of social networks [1] have long been studied as static entities, mostly because empirical longitudinal data have been scarce [2, 3], and often limited to relatively small groups of individuals. As new technologies pervade our daily life, digital traces of human activities are gathered at many different temporal and spatial scales and for large populations, and they promise to transform the way we measure, model and reason on social aggregates [4, 5] and socio-technical systems [6] that combine social dynamics and computer-supported interaction mechanisms (e.g., large scale on-line social networks like Twitter and Facebook). It is important to remark that, from a methodological point of view, data from technological and infrastructural proxies give access to *behavioral* networks defined in terms of the specific proxy at hand, and not to *bona fide* social networks. Digital traces have been already used as proxies to study many specific aspects of human behavior, such as geographic mobility [7–13], phone communications [14], email exchange or instant messaging [15–20], and even human mobility and proximity in indoor environments (<http://www.sociopatterns.org>) [21–24].

Due to the often high temporal resolution of emerging data sets on human interactions, the now customary representation of interactions in terms of static complex networks, which has led to countless interesting analyses and insights [1, 25–31], needs to be extended to take into account the dynamical properties of the interaction patterns, bringing forth the field of “temporal networks” [32]. This prompts fundamental and applied research on adapting and extending well-known networks observables, metrics and characterization techniques to the more complex case of a time-varying graph representations.

At the same time, the availability of high-resolution time-resolved data on human interactions does not mean that any research question should be addressed by using the full-scale and finest-resolution datasets, as they usually entail computational challenges due to the sheer size of their digital representations. Given a specific problem or research questions, understanding what is the most appropriate scale for coarse-graining the raw behavioral data, and what are the mathematical techniques and data representation that are best suited to create such synopses is a key problem in its own merit [33–35], and has been already identified as such in the specific case of epidemic simulation based on temporal social network data [36, 37].

In the context outline above, we review here recent research efforts, developed within the SocioPatterns collaboration (<http://www.sociopatterns.org>), based on large-scale datasets that describe human face-to-face interactions in various contexts, covering scientific conferences [21–23, 36, 38], hospital wards [39], schools [40], and museums [38].

2 Phenomenology

2.1 From Raw Proximity Data to Dynamical Networks

The data we describe here have been collected in deployments of the SocioPatterns (<http://www.sociopatterns.org>) social sensing infrastructure, described in [21]. This measurement infrastructure is based on wearable wireless devices that exchange low-power radio signals in a distributed fashion and use radio packet exchange rates to monitor for location and proximity of individuals. The proximity information is sent to radio receivers installed in the environment, which timestamp and log contact data. Participants are asked to wear such devices, embedded in unobtrusive wearable badges, on their chests, so that badges can exchange radio packets only when the individuals wearing them face each other at close range (about 1–1.5 m). The onboard software of the devices is tuned so that the face-to-face proximity of two individuals wearing the badges can be assessed with a probability in excess of 99% over an interval of 20 s. A “contact” between two individuals is then considered as established during a time period of 20 s if the devices worn by these individuals exchanged at least one radio packet during that interval. The contact is then considered as ongoing until a 20 s interval occurs such that no packet exchange between the devices is recorded: at that point the contact event is recorded together with its starting time and duration. Notice that in contrast to other temporal network datasets in which interactions are instantaneous events, here close-proximity and face-to-face contacts do have a finite duration.

The data gathered by the social sensing infrastructure thus give access, for each pair of participants, to the detailed list of their contacts, with starting and ending times: these data can be represented as a time-varying social network of contact within the monitored community. The temporal resolution of 20 s in assessing proximity sets the finest resolution for the temporal network representation we use, which, in the following, will be assumed to be an ordered sequence of graphs, each corresponding to a 20-s interval. Table 1 provides information and literature references on the temporal networks that will be discussed in the following.

2.2 Microscopic View

For each pair of individuals i and j , the datasets contain a list of ℓ successive time intervals $((t_{ij}^{(s,1)}, t_{ij}^{(e,1)}), (t_{ij}^{(s,2)}, t_{ij}^{(e,2)}), \dots, (t_{ij}^{(s,\ell)}, t_{ij}^{(e,\ell)}))$ during which i and j were detected to be in close-range face-to-face proximity, where $t_{ij}^{(s,a)}$ refers to the starting time (hence the superscript s) and $t_{ij}^{(e,a)}$ to the ending time of the time interval number a .

Several quantities of interest can be defined to summarize the contact patterns of each individual or pair of individuals, and to provide a statistical characterization of

Table 1 Partial list of the datasets on face-to-face proximity collected by the SocioPatterns collaboration during 2009 and 2010 and discussed in the present paper

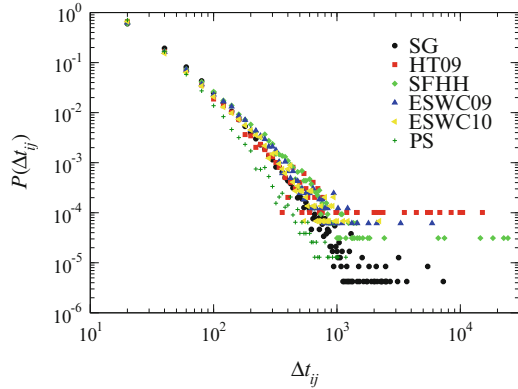
Name	Date	Venue	Event type	# persons	Duration	Reference
SG	Apr–Jul 2009	Science Gallery, Dublin, IE	Exhibition	~30,000	3 months	[38, 41, 42]
ESWC09	Jun 2009	ESWC 2009, Crete, GR	Conference	~180	4 days	[22, 23]
SFHH	Jun 2009	SFHH, Nice, FR	Conference	~400	2 days	[36]
HT09	Jul 2009	ACM Hypertext 2009, Torino, IT	Conference	~120	3 days	[43, 44]
PS	Oct 2009	Primary school, Lyon, FR	School	~250	2 days	[40, 45]
ESWC10	Jun 2010	ESWC 2010, Crete, GR	Conference	~200	4 days	[46]
(OBG)	Nov 2009	Bambino Gesù hospital, Roma, IT	Hospital	~100	10 days	[39]
(PRAMA)	Apr 2010	Practice Mapping, Gijon, ES	Exhibition	~100	10 days	[47]
(HFARM)	Jun–Jul 2010	H-Farm, Treviso, IT	Company	~200	6 weeks	–

Deployments that did not involve face-to-face detection or had less than 100 participants are not reported. Deployments with names in bold face correspond to publicly available datasets (see references). Deployments with names in parentheses are listed for reference only

contact patterns. In particular, for each pair of individuals i and j (edge $i-j$), their list of contact time intervals yields a list of contact durations $(\Delta t_{ij}^{(1)}, \dots, \Delta t_{ij}^{(\ell)})$, with $\Delta t_{ij}^{(a)} = t_{ij}^{(e,a)} - t_{ij}^{(s,a)}$ for $a = 1, \dots, \ell$. Several notions of weight w_{ij} for the edge $i-j$ can be defined on the basis of this list of contact durations, yielding weighted contact networks that describe different aspects of the empirical sequence of contacts:

- *Edge presence*: w_{ij}^p measures the contact occurrence (the superscript p stands for “presence”), with $w_{ij}^p = 1$ if at least one contact between i and j has been established, and 0 otherwise.
- *Frequency of occurrence*: The frequency $w_{ij}^n = l$ indicates how many distinct contact events have been registered between i and j , disregarding the length of each contact (the superscript n is for “number”).
- *Cumulative time in contact*: The cumulative duration of the contact $w_{ij}^t = \sum_a \Delta t_{ij}^{(a)}$ gives the sum of the durations of all contacts established between i and j (hence the superscript t).

Fig. 1 Distributions of the face-to-face contact durations measured in different environments



At the level of each individual i , the above weights w can be aggregated over all individuals j who had a contact with i , i.e., $s_i = \sum_j w_{ij}$, yielding the following notions of node strength:

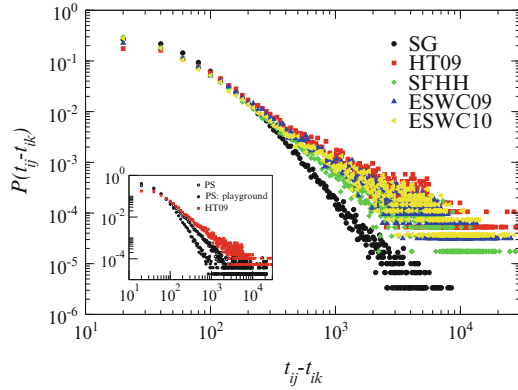
- $s_i^p = \sum_j w_{ij}^p$ gives the number of distinct individuals with whom i has established at least one contact; i.e., the degree k_i of i in the behavioral contact network.
- $s_i^n = \sum_j w_{ij}^n$ indicates the overall number of contacts in which i has been involved.
- The cumulative contact time $s_i^t = \sum_j w_{ij}^t$ corresponds to the total sum of the duration of all contacts involving individual i .¹

Of course all the quantities described above can be measured over the whole duration of the deployment, or for a restricted duration (for instance, 1 day, as is natural for conferences or the museum deployment we describe below). The choice of the aggregation time allows, for instance, to investigate the inter and intra-day variability of interaction patterns among different individuals.

A first way to uncover the complexity of the data is through a study of the statistical distributions of the duration of the contact events, and of the time intervals between contact events. As shown in Figs. 1 and 2 and discussed in [21], broad distributions spanning several orders of magnitude are observed in both cases: most contact durations and intervals between successive contacts are very short, but very long durations are also observed, and no characteristic timescale emerges. This bursty behavior is a well known feature of human dynamics and has been observed in a variety of systems driven by human actions [14, 48–50]. In the present case of close-range contacts, no simple functional form such as a power-law distribution or a log-normal distribution seems to fit the observed data over the full range of time

¹Note that s_i^t might be larger than the total time during which i has been in contact with any individual, as i could be in contact at the same time with more than one individual.

Fig. 2 Distributions of the time intervals between two successive contact events of a given individual, aggregated over the entire population



intervals. However, it is important to highlight a few important aspects of the contact duration distributions of Fig. 1.

The first observation is that the distributions approximately collapse on one another regardless of the specific context they refer to. This is remarkable as the datasets refer to very different social environments: exhibitions (SG), where visitors stream along a pre-defined path of a museum; Academic conferences (HT09, ESWC09, ESWC10), where the same tightly knit community shares a small number of social spaces for several days and meets according to a predefined schedule, large-scale conferences (SFHH) where many people do not know each other and very different social spaces coexist, such as plenary rooms and exhibition spaces. In the case of the primary school (PS), the distribution is slightly narrower, possibly due to strong schedule constraints such as the duration of breaks between lectures, or to the fact that young children tend to have less long face-to-face interactions than adults. Regardless of all these social, spatial and demographic differences, face-to-face contact behavior appears to obey the same bursty behavior across all contexts. This is an important fact for modelers, as it implies that processes relying on contact durations can be modeled by plugging into the model the empirically observed distribution, assumed to depend negligibly on the specifics of the contact situation being modeled.

A second observation deals with the origin of the contact duration heterogeneity of Fig. 1. It may be argued that the simultaneous presence of multiple timescales of human contact is responsible for the broad distribution we observe. However, as shown in [21] and related Supplementary Information, the contact durations restricted to single individuals do exhibit the same broad distribution observed for the entire social aggregate. This points to an intrinsic origin for the observed temporal heterogeneity, rooted in the way single persons arbitrate their social contacts and the use of their time. The temporal heterogeneity of contact durations, at the individual and collective level, undermines a number of simple representations for the contact network that implicitly assume some degree of statistical homogeneity. For example, when dealing with contact networks for epidemiological purpose, it is customary to summarize the contact networks between classes of individuals by

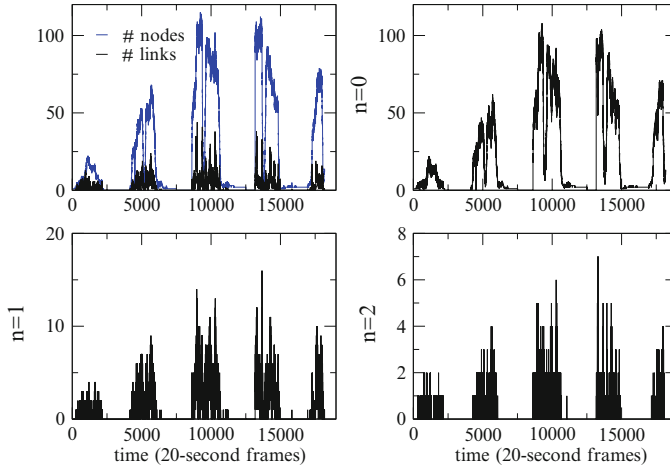


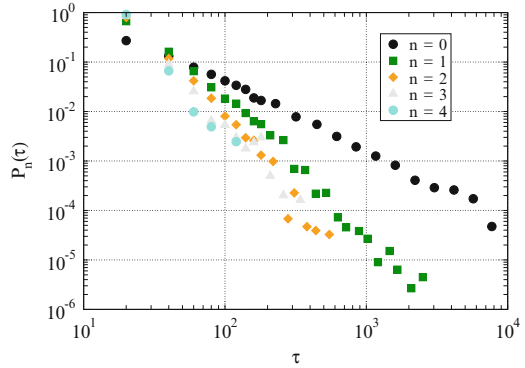
Fig. 3 Timelines of the number of: nodes and links in 20-s instantaneous networks (*top left*), isolated nodes (*top right*), groups of 2 nodes (*bottom left*), groups of 3 nodes (*bottom right*) in the ESWC09 data set

using contact matrices [51] computed from averages of contact durations. Given the highly skewed character of the actual distributions measured by using state-of-the-art techniques, these representations need to be generalized in order to suitably capture temporal and structural heterogeneities that may play a crucial role in determining the evolution of dynamical processes over contact networks.

Perhaps the most striking feature of the observed distributions are their robustness: the distributions of contact durations are extremely similar for very different contexts, populations, activity timelines, and deployment conditions. In particular, we observe the same distribution in deployments corresponding to very different sampling of the population under study (from 30% for SFHH to almost 100% for PS, HT09). This confirms the results of [21] that showed the robustness of the contact duration distribution under further resampling of the data, aimed at simulating data loss or limited population sampling. Moreover, although human activity and contact patterns are highly non-stationary, as shown by an example in Fig. 3, the contact duration distributions measured over different time windows coincide [21], unveiling a statistical stationarity in an otherwise non-stationary signal. This is consistent with similar analyses on other temporal networks, such as proximity networks [52] and networks of cattle transfers between farms [53].

On the other hand, as displayed in Fig. 2, the distribution of time intervals between successive contacts involving the same individual typically do depend on the specific context at hand. The distributions are very similar for different conferences (HT09, ESWC09, ESWC10, SFHH), but narrower for the museum and the primary school cases. Moreover, in the school case (inset in Fig. 2), spatial and behavioral sampling due to selecting only those contacts that occur in the school playground significantly affects the distributions, even though their

Fig. 4 Distributions of the lifetime (in seconds) of groups of size $n + 1$ (ESWC09)



qualitative features stay unchanged. In general, this dependence on the context of the distribution of interval durations between successive contacts means that, contrary to pair-wise interactions, more complex temporal motifs that bear relevance to the causal structure of the temporal network may depend on the specific environment.

Similar to the case of contact durations, broad distributions are also observed for the lifetimes of simple structures in the contact network, such as groups of individuals of size $n + 1$ ($n = 0$ corresponds to an isolated person, $n = 1$ to a pair of individuals, and so on), as shown in Fig. 4. These broad distributions of group lifetimes become narrower for increasing n , i.e., larger groups are less stable than smaller ones.

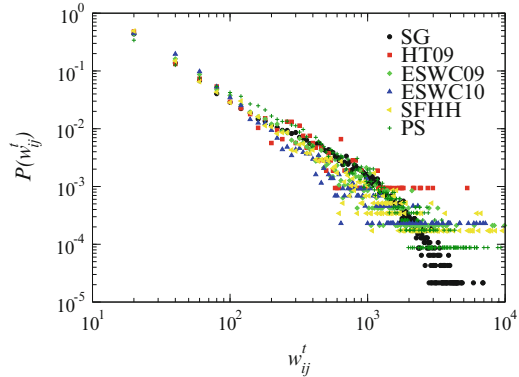
2.3 Aggregated Network View

The sequence of contact events between individuals during a given time window defines an aggregated contact network at the population level, which is a static summary of the temporal network. In this network, each node is an individual, and a link between two nodes i and j denotes the fact that the corresponding individuals have been in contact at least once during the time window under consideration. Whereas the overall topological structure of the temporal network can be encoded in a static graph, the temporal activity of individual edges $i - j$ can be summarized by suitably defined weights for the edges, such as the number of times w_{ij}^n the link was established or the cumulative duration w_{ij}^t of the contact events between i and j .

The time window considered for aggregation can range from the finest time resolution of 20 s up to the entire duration of the data set. In many contexts, it is natural to consider a specific temporal aggregation scale (i.e., daily), but different aggregation levels typically provide complementary views of the network dynamics at different scales.

Interestingly, and despite their static character, the structures of the aggregated contact networks unveil important information about the contact patterns of the

Fig. 5 Weight distributions for the daily aggregated networks. The weight w_{ij}^t gives the cumulated amount of time spent in face-to-face interaction during 1 day by individuals i and j



population. Let us first consider the statistical distributions that are typically used to describe a network. The distributions of degree (number of distinct individuals with whom a given individual has been in contact) are typically narrow, with an exponential decay at large degrees and characteristic average values that depend on the particular context [38]. On the other hand, the distributions of the cumulative contact durations are broad: most pairs of individuals have been in face-to-face proximity for a short total amount of time, but a few cumulated contact durations are very long. No characteristic interaction timescale can be naturally defined, except for obvious temporal cutoffs due to the finite duration of the measurements. As already observed in the case of the distributions of contact durations, Fig. 5 shows the similarity of the distributions obtained in very different contexts: different populations, in which individuals behave with very different goals in different spatial and social environments, display a strikingly similar statistical behavior.

Despite their statistical similarities, the aggregated networks of face-to-face proximity might have very different structures, as revealed by a visual inspection of simple force-based network layouts. For instance, Fig. 6 shows that the aggregated network of interactions during a conference day is much more “compact” than the ones describing the interactions between museum visitors. In fact, as shown in [38], a typical daily aggregated network has a much smaller diameter in a conference context than in the museum case. This difference is due to the different patterns of presence of the attendees at the monitored venue, and also to the different social contexts: in conferences participants are present during the entire conference duration and are usually engaged in interacting with known individuals and in meeting new persons. Conversely, the distribution of visit durations in the museum case is close to a log-normal, with a geometric mean around 35 min, and the visitors’ main goal is not to meet other visitors but rather to explore the space following a partially pre-defined path. As a consequence, museum visitors are unlikely to interact directly with other visitors entering the venue more than one hour after or before them, thus preventing the aggregated network from having a short diameter: there is limited interaction among visitors entering the museum at different times, and the network diameter defines a path connecting visitors that enter the venue at successive times,

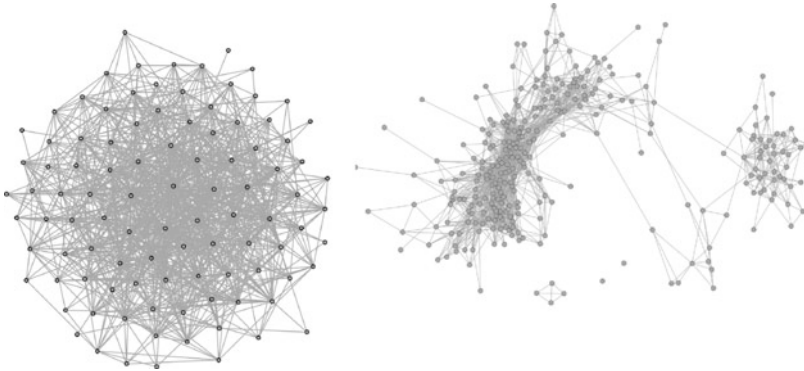


Fig. 6 Daily aggregated networks in the HT09 and SG deployments. Nodes represent individuals and edges are drawn between nodes if at least one contact event was detected during the aggregation interval. *Left*: aggregated network for 1 day of the HT09 conference. *Right*: one representative day at the SG deployment. The network layouts were generated by using the force atlas graph layout implementation available in Gephi [54]

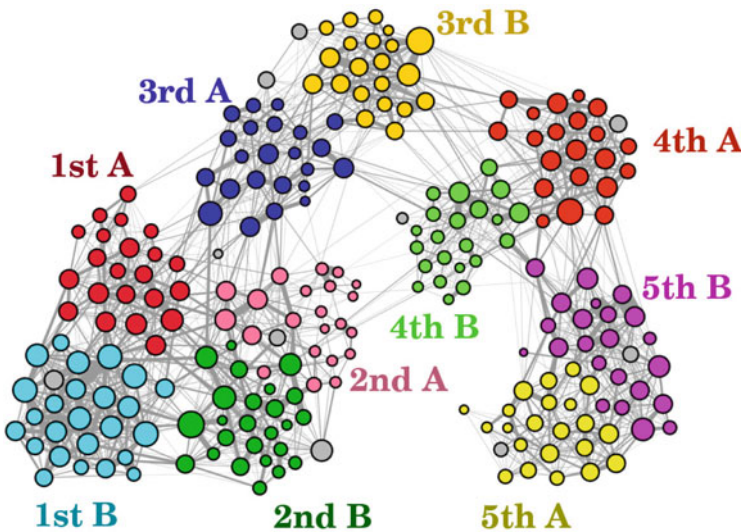


Fig. 7 School (PS) daily aggregated social network. Only links that correspond to cumulated face-to-face proximity in excess of 5 min are shown. The color of nodes indicates the grade and class of students. *Grey nodes* are teachers. The network layout was generated by using the force atlas graph layout implementation available in Gephi [54]

mirroring the longitudinal dimension of the network. These findings show that aggregated network topology and longitudinal/temporal behavioral properties are deeply interwoven.

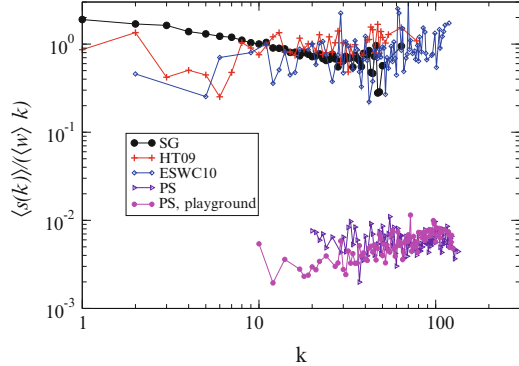
Finally, the aggregated network of contacts among school children reported in Fig. 7 represents an intermediate case: children of each class form a cohesive

structure with many links, but links between different classes, and in particular between children of different grades, are less frequent. This structure results from several combined factors that include (1) the spatial structure of the school, the grouping of students into classes, (2) the fixed association of school classes with given room for school activity, (3) the particular schedule of the school, according to which students do not go to the schoolyard or canteen at the same time and their movement as a group follows predefined spatio-temporal trajectories [40], (4) age-related homophily effects [55], which also play a role when children are free to move in the same space, such as in the playground. Overall, as shown in Fig. 7 the cumulative contact network displays a visible community structure that can be recalled using standard community-detection techniques. However, it is important to remark that the cumulated network projects out a lot of information on temporal communities, i.e., on nodes that share similar spatio-temporal trajectories and similar contact histories. For example, if a group X of nodes mixes strongly with a different group Y during a time interval $[t_1, t_1 + T]$, and the second group of nodes Y has some connections with a third group Z during $[t_2, t_2 + T]$, with $t_2 > t_1 + T$, the cumulative network representation will lose information on the group identities of X and Y and only show a single group $X \cup Y$ with connections to Z . The problem of defining and identifying temporal communities in a time-varying networks [56, 57] is a central one when trying to mine out an activity schedule (such as the school schedule) from electronic records of human interactions, and requires to suitably define null models for temporal networks that incorporate the above described heterogeneities.

These few examples show how similar statistical properties in terms of heterogeneity of contact event durations and overall face-to-face presence can in fact hide very distinct structures of aggregated networks, that are shaped by the dynamical unfolding of the contacts: the study of static aggregated networks sheds in this respect some light on the system's dynamics.

As in other cases of weighted networks [10], more insight can be gleaned by studying the *correlations* between the weights, which are here the trace of the contact dynamics, and the topology. Let us consider the strength s of each node, defined as the sum of the weights of all links inciding on it [10]. In our case, this corresponds, for each individual, to the cumulated time of interaction with other individuals. In social interaction contexts, it can be considered as at least as important as the number of distinct individuals contacted (the degree in the aggregated network), as it is a measure of the resources (time) an individual committed to social interactions. Correlations between the strength and the degree are of course expected: even for completely random durations of the contact events, a linear dependency of the average strength $\langle s(k) \rangle$ of nodes of degree k is obtained, with $\langle s(k) \rangle \sim \langle w \rangle k$, where $\langle w \rangle$ is the average link weight. A deviation of $\langle s(k) \rangle / k$ from a horizontal line thus denotes the existence of non-trivial correlations: for instance, a decreasing $\langle s(k) \rangle / k$, as observed in large-scale phone call networks [14], indicates that individuals who call more distinct individuals spend on average less time in each call than individuals who have less links.

Fig. 8 Correlation between node’s strength and degree, as measured by the average strength $\langle s(k) \rangle$ of nodes of degree k . The figure shows $\langle s(k) \rangle / (\langle w \rangle k)$, in several contexts. Distinct increasing and decreasing trends are observed, depending on the context



In the face-to-face behavioral networks we review here, two distinct behaviors have been observed, depending on the context, as shown in Fig. 8. In the museum data set (SG), $\langle s(k) \rangle / (\langle w \rangle k)$ has a clearly decreasing trend (that can be fitted by a power law with a negative exponent). On the other hand, for the aggregated networks describing the contacts in conferences (HT09 and ESWC10), $\langle s(k) \rangle / (\langle w \rangle k)$ displays consistently an increasing trend. In school settings, a rather flat $\langle s(k) \rangle / (\langle w \rangle k)$ is observed when the contacts occurring in the whole school (PS) are taken into account. This behavior has also been observed independently (Smieszek, private communication), in another dataset describing the proximity patterns of highschool students [24]. However, if only the contacts occurring in contexts where the children’s movements and contacts are not constrained (PS, playground) are considered, an increasing trend is found.

The contrasting results obtained in different contexts show that processes such as information diffusion [58, 59], frequently occurring in social contexts, will unfold in different ways. The number of distinct persons encountered does not contain enough information to estimate the spreading potential of an individual: a super-linear dependence of $\langle s(k) \rangle$ with k hints at the importance of “super-spreader nodes” with large degree [58, 59] while a sub-linear behavior indicates that the decrease in the weights of individual contacts mitigates the expected super-spreading behavior of large degree nodes.

3 Modeling Face-to-Face Dynamical Contact Networks

The phenomenology outlined in the previous sections calls for the development of new modeling frameworks for dynamically evolving networks, as most modeling efforts have been until recently devoted to the case of static networks [26–30]. Among recent models of dynamical networks [52, 60–64], we review here a model of interacting agents developed in [63, 64] in order to describe how individuals interact at short times scales.

The model considers N agents who can either be isolated or form groups (cliques). Each agent i is characterized by two variables: (i) his/her coordination number $n_i = 0, 1, 2, \dots, N - 1$ indicating the number of agents interacting with him/her, and (ii) the time t_i at which n_i was last changed. At each (discrete) time step, an agent i is chosen randomly. With a probability $p_n(t, t_i)$ that may depend on the agent's state, on the present time t and on the last time t_i at which i 's state evolved, i updates his/her state, under the following rules:

- (i) If i is isolated ($n_i = 0$), another isolated agent j is chosen with probability proportional to $p_0(t, t_j)$, and i and j form a pair. The coordination number of both agents are then updated ($n_i \rightarrow 1$ and $n_j \rightarrow 1$).
- (ii) If the agent i is already in a group, ($n_i = n > 0$), with probability λ the agent i leaves the group; in this case, the coordination numbers are updated as $n_i \rightarrow 0$, and $n_k \rightarrow n - 1$ for all the other agents k of the original group. With probability $(1 - \lambda)$ on the other hand i introduces an isolated agent j in the group, chosen with probability proportional to $p_0(t, t_j)$. The coordination numbers of all the interacting agents are then changed according to the rules $n_j \rightarrow n + 1$ and $n_k \rightarrow n + 1$ (for all k in the group).

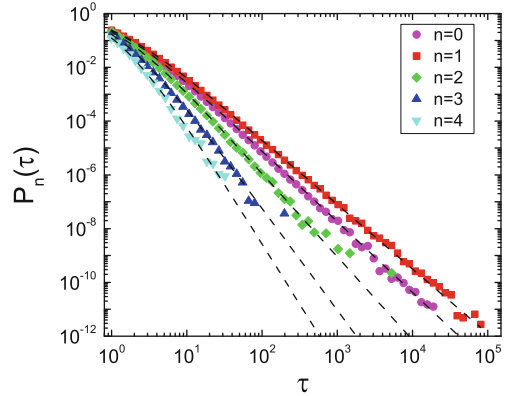
These rules define a dynamic network of contacts between the agents, whose properties depend on the probabilities p_n , which control the tendency of the agents to change their state, and on the parameter λ , which determines the tendency either to leave groups or on the contrary to make them grow.

Constant probabilities p_n correspond to Poissonian events of creation and deletion of links between individuals, and hence to narrow distributions of contact times. On the other hand, the introduction of memory effects in the definition of the p_n is able to generate dynamical contact networks with properties similar to the ones of empirical data sets [63, 64]. In particular, a reinforcement principle can be implemented by considering that the probabilities $p_n(t, t')$ that an agent with coordination number n changes his/her state decrease with the time elapsed since his/her last change of state. To this aim, we can impose $p_n(t, t') = p_n(t - t')$, with p_n decreasing functions of their arguments. This is equivalent to the assumption that the longer an agent is interacting in a group, the smaller is the probability that s/he will leave the group, and that the longer an agent is isolated, the smaller is the probability that s/he will form a new group.

The evolution equations of the number of agents in each state can be solved self-consistently at the mean-field level [63, 64] in various cases. One of the simplest is given by p_n functions scaling as $1/(t - t')$, $p_n(t, t') = \frac{b_n}{1+(t-t')/N}$, with moreover $b_n = b_1$ for every $n \geq 1$ in order to reduce the number of parameters (the model's parameters are then b_0 , b_1 , and λ). The probability distributions of the time spent in each state can then be shown to be given by power-law distributions

$$\begin{aligned}
 P_0(\tau) &\propto (1 + \tau)^{-1-b_0(3\lambda-1)/(2\lambda-1)} \\
 P_n(\tau) &\propto (1 + \tau)^{-(n+1)b_1-1} \quad \text{for } n \geq 1.
 \end{aligned}
 \tag{1}$$

Fig. 9 Distribution $P_n(\tau)$ of durations of groups of size $n + 1$, for $N = 1,000$ agents with $b_0 = b_1 = 0.7$, $\lambda = 0.8$, and a number of time steps $T_{max} = N \times 10^5$. The *dashed lines* correspond to the analytical predictions (1). From [64]



As shown in Fig. 9, these predictions are confirmed by numerical simulations.² The distributions of time intervals between successive contacts of an individual are as well power-law distributed, and the aggregated contact networks display features similar to the empirically observed ones.

The model can be easily extended to include an intrinsic heterogeneity between agents, possibly reflecting a difference in their “sociability”, or to model populations with a varying number of agents. For instance, it is possible to consider a museum-like situation in which agents enter the system, remain for a certain duration, and then leave without the possibility to re-enter it. Power-law distributions of contact durations are still observed, and the shape of the aggregated contact network closely resembles the ones observed in the museum setting. In addition, it would be possible to consider agents belonging to different groups with different mixing properties, in order to mimic as well for instance the contact dynamics in a school. Overall, this model’s versatility makes it an interesting tool for generating artificial dynamical contact networks.

4 Dynamical Processes on Dynamical Networks

Many networks are the support of dynamical processes of various nature, from random walks to synchronization or spreading phenomena [30]. Most related studies have however considered, as a first approach, dynamical phenomena unfolding on static networks. It has been shown how different topological characteristics impact the unfolding of phenomena such as epidemic spreading, with important

²The system is in a stationary state for $b_1 > 0.5$, $b_0 > (2\lambda - 1)/(3\lambda - 1)$ and $\lambda > 0.5$, while the self-consistent solution breaks down outside of this parameter region, and non-stationary behavior with the possible formation of large (system-size) groups can be observed [63, 64].

consequences such as the suppression of the epidemic threshold in very heterogeneous networks [58].

To date, few research efforts have dealt with the fact that the networks supporting these phenomena might have a dynamics of their own. Through the study of toy models of co-evolution, in which the network dynamics itself is defined as a reaction to the process unfolding on top of it, it was shown that the interplay of these two dynamics can lead to interesting and sometimes counter-intuitive effects [60]. In this context, the study of dynamical processes on dynamical (temporal) networks can have a two-fold purpose. On the one hand, it can guide the design of more realistic models, applied for instance to epidemic spreading. Dynamical processes on temporal networks can be studied to understand the relative roles of the different time scales at play, and what level of information is actually needed for the description of these processes [36]. In addition to that, the use of very simple dynamical processes, such as random walks or deterministic spreading, can be considered among the techniques developed for the study and characterization of dynamical networks, such as the ones put forward in [32,38,53,65,66]. In particular, dynamical processes can serve to probe the role of causality constraints in temporal networks, comparing the outcome of a given process (i) on the dynamical network describing the real temporal sequence of events, and (ii) on aggregated networks in which the information about the precise order of events is discarded.

In this section we focus on a simple snowball SI model of epidemic spreading or information diffusion [59]. Individuals can be either in the susceptible (S) state, indicating that they have not been reached by the “infection” (or information) yet, or they can be in the infectious (I) state, meaning that they have been infected by the disease (or that they have received the information) and can further propagate it to other individuals. In the simplest, deterministic version of such a process, every contact between a susceptible individual and an infectious one results in a transmission event, which instantaneously turns the susceptible individual into an infected one according to $S + I \rightarrow 2I$. In this simple model, infected individuals do not recover, i.e., once they transition to the infectious state they indefinitely remain in that state. The process is initiated by a single infected individual (“seed”), typically chosen at random. Despite its simplicity, such a schematic model provides interesting insight on causality constraints in dynamical networks, and on how different temporal contact patterns can lead to different outcomes. This is partially due to the fact that the SI process yields the fastest possible information propagation from the seed node to the rest of the network, thus bounding other more complex and realistic invasion processes.

4.1 SI Model as a Probe of Temporal Network Structure

Let us first consider the simplest measure of the unfolding of an SI process in a population, as given by the temporal evolution of the number of infected individuals

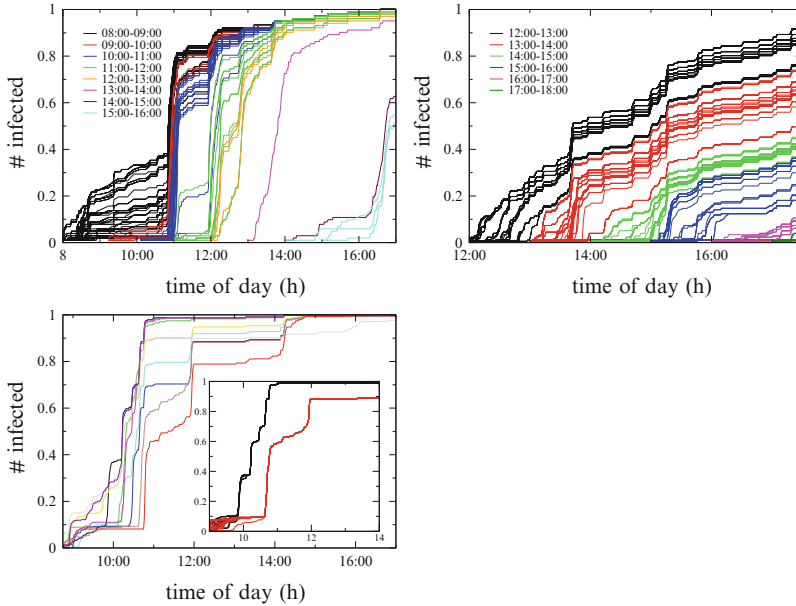


Fig. 10 Incidence curves showing the number of infected individuals as a function of time for a susceptible-infectious (SI) process simulated over 1 day of HT09 (*top-left panel*), SG (*top-right panel*) and PS (*bottom-left panel*) temporal network data. In the HT09 and SG cases (*top plots*) each curve corresponds to a different seed node and is color-coded according to the starting time of the spreading process. In the PS case (*bottom*) school, each curve is an average over the dynamics simulated for different seed nodes belonging to a given class. The inset shows individual curves for different seeds chosen in two distinct classes

(i.e., the incidence curve). Figure 10 shows that the incidence curves in different environments look qualitatively very different.

In the case of a typical day at a conference (HT09, top-left panel) few transmission events occur until the conference participants gather for the coffee break at 11am, even if the seed was present early. A strong increase in the number of infected individuals is then observed, and a second strong increase occurs during the lunch break (12 p.m.). As a result of the concentration in time of transmission events, spreading processes initiated by different seeds all achieve very similar (and high) incidence levels after a few hours, regardless of the initial seed and of its arrival time. Even epidemics started by latecomers can reach about 80 % of the community.

A very different picture is observed in the museum case (top-right panel), where the arrival time of the seed individual has a strong impact on the epidemic size: at any point in time, the number of infected individuals is strongly correlated with the arrival time of the seed. This is due to the fact that visitors stream through the venue, and those who left before the arrival time of the seed cannot be reached by the infection. Furthermore, in many cases the daily aggregated network displays multiple disconnected components, so that the spreading process stops soon after

the seed leaves and only reaches a very small portion of the total population [38]. Even on days with many visitors and a globally connected daily aggregated network, the incidence curves do not present sharp gradients as in the conference case, and later epidemics are unable to infect a large fraction of daily visitors.

In the school case (bottom-left panel) almost all students arrive at the beginning of the day, hence no effects due to heterogeneous arrival times can be observed. Similarly to the conference case, the simulated dynamics displays jumps in the number of infected individuals at specific times of the day, regardless of the seed node, and by the end of the day almost all individuals get infected. Heterogeneous invasion dynamics can be observed depending on the class of the seed node, and the differences can be related to the scheduled activities and movements of school children. Conversely, different choices for the seed node within a single class (bottom-left panel, inset) yield very similar incidence curves. This can be understood as a result of different within-class and cross-class contact patterns: contacts within individual classes are rather homogeneous compared to cross-class contacts, so that the SI process quickly reaches most nodes of the seed's class. The invasion of other classes is controlled by slower temporal structures of the contact network, which are determined by the school schedule and determine the sensitivity on the initial class.

To characterize in a more quantitative fashion the importance of the temporal structure of the network on the spreading dynamics, we can consider the number of individuals who are reachable from the seed node through paths in the (daily) cumulative contact network, and compute what fraction of them are actually reached by an SI process that takes place over the temporal contact network. The value of this ratio displays markedly different distributions in the museum and in the conference case [38]: at a conference almost all the individuals who are reachable along the cumulative contact network always get infected by the end of the day, whereas in the museum case this ratio is often much smaller than 1. Therefore, studying the dynamics of a simple SI process can uncover differences in the temporal structure of human proximity networks that cannot be detected by using simpler statistical indicators (e.g., the probability distributions of contact durations). This calls for more work aimed at using generic dynamical processes over temporal networks to define a new class of time-aware network observables that can expose important differences and similarities.

4.2 Causality-Respecting Paths

The differences in spreading patterns outlined above are due to the causality constraints inherent in the temporal character of the contact network: for instance, if node i interacts first with node j and then with node k , a message or infectious agent can travel from j to k through i , but not in the opposite direction, while in a static network both events would be equally possible.

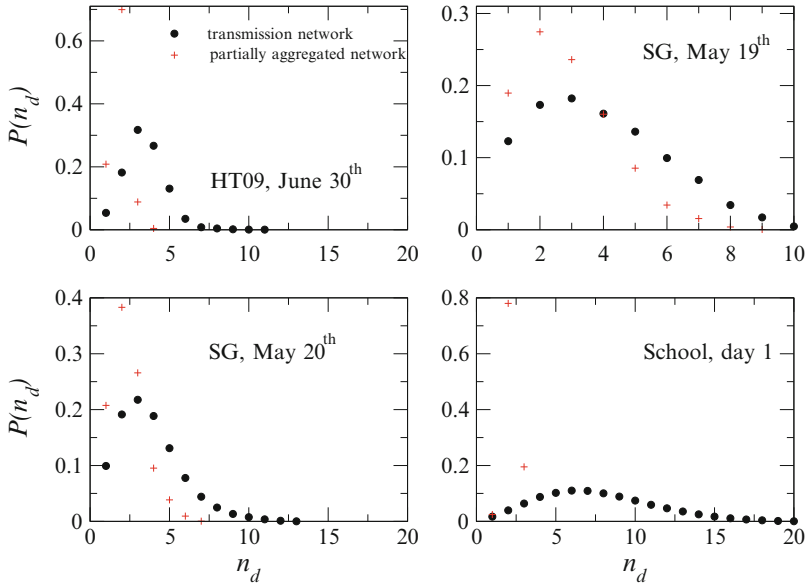


Fig. 11 Distribution of the path lengths n_d from the seed node to all the infected individuals, computed over the transmission network (*black circles*) and over the partially aggregated networks (*red pluses*). For each day the distributions are computed by varying the choice of the seed node over all individuals

It is therefore interesting to study the spreading paths of the SI process on a temporal network and on the corresponding aggregated network, as mentioned in the above Sect. 4.1. To this aim, for each seed node we define a *transmission network* along which the infection effectively spreads in the temporal network (i.e., the network whose edges are given by $S \leftrightarrow I$ contacts). Therefore, the distance along the transmission network between the seed node and another arbitrary node i gives the actual number of transmission events that occurred before the spreading process reached i , and consequently it is the length of the *fastest* path from the seed individual to the infected one which respects the causality constraints of the temporal network [53, 67, 68].

On the other hand, in an aggregated, static view of the contact network the spreading would follow the *shortest* path over the network aggregated from the time the seed first appears, as the infection can only spread along interactions occurring after the arrival of the seed node. We call this network a *partially aggregated network*.

As shown in Fig. 11, the distribution of lengths of the fastest paths turns out to be broader and shifted toward higher values than the corresponding shortest-path distributions. This holds both for the conference and for the museum case, and has also been observed in other cases [68]. The actual number of intermediaries is therefore larger on a temporal network than would be predicted by a propagation

scheme based on a static network. This difference can be understood by considering a similar example as discussed above: if node i is infected and interacts with node j , who then interacts with node k before i interacts with k , the actual (fastest) spreading path between nodes i and k has path length 2, while the shortest path has a unitary path length.

In settings in which each transmission event has a cost, or is associated with the possibility of signal loss or attenuation, such differences might play an important role and temporal effects should accordingly be taken into account carefully.

4.3 Activity Clocks

The results of the previous subsection show that, depending on the environment and on the time at which the spreading process is initiated, different spreading dynamics can be obtained. In particular, the time at which a given node is reached by the information or infection may strongly depend on collective activity patterns. In the context of message routing in networks of mobile devices [69–72], the distribution of elapsed times between the generation of the message and its arrival at given nodes is often considered as a way to evaluate the performance of a spreading protocol [73–76]. However, the non-stationary and bursty behavior of the contact and proximity networks imply that the distribution of delays between message injection and message delivery at a given node may in fact depend importantly on the time of injection of a message, or on specific details of contact and activity patterns. The left panel of Fig. 12 shows this for the case of a message that spreads over the HT09 temporal contact network according to a simple SI process initiated at two different points in time: the distribution of arrival delays computed in terms of wall-clock time is extremely sensitive to the injection time of the message and displays strong heterogeneities that cannot be captured by any simple statistical model. It is thus important to devise more robust metrics for message delivery that factor out non-stationary behaviors and temporal heterogeneities, allowing on the one hand to carry out more objective comparisons of different protocols for message spreading, and on the other hand to validate the models of human mobility (and the ensuing temporal networks) that are used to design and inform such protocols.

Some progress in the direction outlined above can be made by giving up the global notion of wall-clock time in favor of a node-specific definition of time. We imagine that each node has its own clock, and that this clock only runs when the node is involved in one or more contacts. Since the clock measures the amount of time a given node has spent in interaction, we refer to this clock as an “activity clock”. All activity clocks are set to zero at the beginning of the spreading process, when the initial message is injected into the network. Thus, the activity clock of a node measures the amount of time during which that node could have received a message propagated along the links of the temporal network, i.e., it ignores the time intervals during which the node was disconnected from the rest of the network.

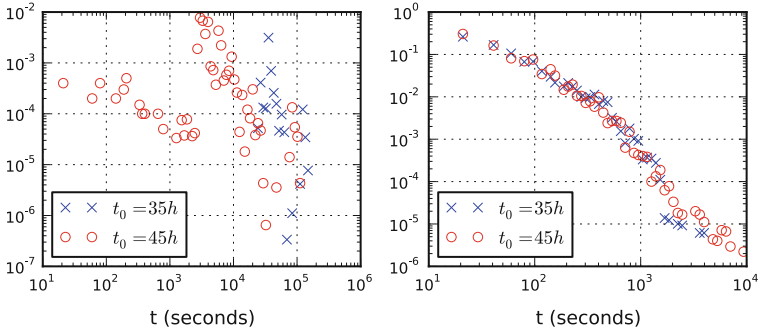


Fig. 12 Log-binned distribution of message arrival delays. The distributions are computed by simulating a simple SI process over the HT09 temporal contact network, for two different injection times of the initial message (*blue crosses* and *red circles*). *Left*: the delay interval is defined as the wall-clock time difference between the arrival of the message at a given node and the injection time of the message. *Right*: the delay interval distribution is computed by using node-specific activity clocks that only run when nodes have active links (proximity relations) to other nodes. That is, each node has a specific notion of “intrinsic” time that is defined as the cumulated time it spent in contact with other nodes

In this context, the message delivery delay for node i is defined as the value of its activity clock when the message is received, i.e., it is the elapsed time node i has spent in contact with others, from the injection time of the initial message up to the moment when the message is received by i . The right panel of Fig. 12 shows the distributions of delivery delays computed in terms of activity clocks. The distributions exhibit a smooth dependence on activity-clock time, without the strong heterogeneities observed when using wall-clock time. Most importantly, they now collapse onto one another, i.e., they are robust with respect to changes in the injection time of the message. Strikingly, they are also robust with respect to the context: as reported in [77], the same distribution is obtained for spreading processes simulated in conferences with very different schedules and contact densities.

It is important to remark that synthetic temporal networks of human contact are typically generated on the basis of a number of accepted models for the underlying human mobility in space. The quality of the models is often assessed on the basis of their ability to reproduce simple statistical observables of the temporal network, such as the probability distribution of contact durations and the distribution of times between successive contacts of a node. However, when computing the distributions of delivery delays for an SI process in terms of activity clocks, strong differences emerge between the accepted generative models and the empirical temporal networks. Specifically, as reported in [77], most of the accepted models yield delay distributions that are much narrower than those of Fig. 12, thus failing to reproduce the empirical phenomenology. This points to the need for further modeling work to design generative models of temporal networks that can correctly reproduce the empirical distributions. Notice that such differences only become visible on using activity clocks in combination with dynamical process

on the temporal network, used as a probe of properties that cannot be captured by means of customary metrics. For example, the comparison between the left and right panels of Fig. 12 shows how suitable definitions of “time” based on activity metrics of the temporal network have the power to uncover regularities that are otherwise completely shadowed by the intrinsic heterogeneities of the system. At the same time these results call for more research in several directions. In particular, it would be important to:

- Define and characterize activity clocks based on different types of node and edge metrics for temporal networks (e.g., defining time as the cumulated number of contact events, rather than as the elapsed time in contact),
- Express in terms of activity clocks the evolution of simple dynamical processes taking place on temporal networks,
- Model the form of the delay distributions observed in simulation for paradigmatic dynamical processes such as SI spreading taking place on temporal networks.

5 Conclusion

The study of empirical temporal networks is receiving increasing attention because of the availability of new data sources and because of their relevance for the detection, modeling and control of phenomena in a broad variety of socio-technical systems. To date, key questions are still open about temporal networks and dynamical processes over temporal networks.

Here we focused on high-resolution empirical temporal networks of human proximity, provided a phenomenological overview of some important properties, and reported on the impact that such properties have on paradigmatic epidemic-like processes that take place over temporal networks, with potential applications to diverse domains such as information spreading or epidemic modeling. We remark that the consolidated toolbox of statistical indicators, network metrics and generative models for static networks that has been developed over the last decade cannot be trivially generalized to the case of temporal networks. More research is thus needed in order to identify dynamical extensions of the observables designed for static network, to uncover dynamical network motifs [53, 66], and to explore entirely new characterization techniques that expose important features of the temporal-topological structure of the networks. In this respect, it will be probably fruitful to investigate simple dynamical processes over networks as a tool for uncovering relevant patterns, and as an aid to constrain and evaluate generative models for temporal networks.

We also notice that in the context of many applicative domains it is very difficult to characterize separately the dynamics of the network and that of the relevant dynamical process (e.g., the dynamics of a contact network and the dynamics of an epidemic unfolding over it): depending on the specific process, on its timescales, and on the set of properties of the process that one aims at modeling, the temporal

structure of the network can have a profoundly different relevance. For example, it has been shown that for flu-like epidemic processes, with latent and infectious timescales of the order of a few days, the temporal structure of the underlying human contact networks is negligible if one aims at modeling just the peak time of the epidemics, and is important if the goal is to model the size of the epidemics [36]. Developing a more systematic understanding of the impact that the temporal structure of a network has on a given observable is an open challenge.

The above remarks are related to another important problem, that of coarse-graining temporal network data when either explicit node/edge attributes are available or node/edge activity patterns can be clustered into classes of similar behavior. When dealing with human contact networks, this is the case of many contexts in which the population under study is structured because of roles (e.g., hospitals) and/or spatio-temporal constraints on group mobility and interactions (e.g., schools). In particular, inferring behavioral classes from temporal network data requires algorithms to mine for dynamical communities of nodes or edges that extend those available for static networks, as a temporal network may have sharply defined classes of dynamical behavior that completely disappear on considering aggregated networks obtained by projecting out time. To this end, machine learning techniques based on node/edge features or on entire activity timelines may prove effective in uncovering and characterizing behavioral regularities hidden in temporal networks. When classes are known (e.g., explicit role-based classes within a hospital population), or discovered via time-aware community detection techniques, it is often insightful to consider aggregated representations of the data based on the class attributes, such as the contact matrices commonly used in epidemiology. These customary representations, though, have been defined and investigated in order to coarse-grain static interaction networks, and they need to be generalized so that they can be used to summarize temporal networks in a way which is suitable for the relevant applicative context.

Progress in the above directions of creating synopses of temporal network data would greatly help in defining “parsimonious” models for dynamical processes, that only retain the necessary amount of information about the underlying temporal network. This also calls for work on reconciling different scales of representation of temporal network data, so that properties and dynamical processes at different levels can be related to one another. In consideration of the coming deluge of behavioral information represented in the form of temporal networks, the ability to create parsimonious but informative representations will be an increasingly valuable asset for the applications of network science.

Acknowledgements It is a pleasure to thank G. Bianconi, V. Colizza, L. Isella, A. Machens, A. Panisson, J.-F. Pinton, M. Quaggiotto, J. Stehlé, W. Van den Broeck, A. Vespignani for many interesting discussions. We also warmly thank all the collaborators who helped make the SocioPatterns deployments possible, and in particular Bitmanufaktur and the OpenBeacon project. Finally, we are grateful to all the volunteers who participated in the deployments.

References

1. Wasserman, A., Faust, K.: *Social Network Analysis: Methods and Applications*. Cambridge University Press, Cambridge (1994)
2. Padgett, J.F., Ansell, C.K.: Robust action and the rise of the Medici. *Am. J. Sociol.* **98**, 1259–1319 (1993)
3. Lubbers, M.J., Molina, J.L., Lerner, J., Brandes, U., Avila, J., McCarty, C.: Longitudinal analysis of personal networks. The case of argentinean migrants in Spain. *Soc. Networks* **32**, 91–104 (2010)
4. Lazer, D., et al.: Life in the network: the coming age of computational social science. *Science* **323**, 721 (2009)
5. Giles, J.: Computational social science: making the links. *Nature* **488**, 448 (2012)
6. Vespignani, A.: Predicting the Behavior or techno-social systems. *Science* **325**, 425 (2009)
7. Chowell, G., Hyman, J.M., Eubank, S., Castillo-Chavez, C.: Scaling laws for the movement of people between locations in a large city. *Phys. Rev. E* **68**, 066102 (2003)
8. De Montis, A., Barthélemy, M., Chessa, A., Vespignani, A.: The structure of inter-urban traffic: a weighted network analysis. *Environ. Plann. J. B* **34**, 905–924 (2007)
9. Brockmann, D., Hufnagel, L., Geisel, T.: The scaling laws of human travel. *Nature* **439**, 462–465 (2006)
10. Barrat, A., Barthélemy, M., Pastor-Satorras, R., Vespignani, A.: The architecture of complex weighted networks. *Proc. Natl. Acad. Sci. USA* **101**, 3747–3752 (2004)
11. Balcan, D., Colizza, V., Gonçalves, B., Hu, H., Ramasco, J.J., Vespignani, A.: Multiscale mobility networks and the spatial spreading of infectious diseases. *Proc. Natl. Acad. Sci. USA* **106**, 21484–21489 (2009)
12. González, M.C., Hidalgo, C.A., Barabási, A.-L.: Understanding individual human mobility patterns. *Nature* **453**, 779–782 (2008)
13. Song, C., Qu, Z., Blumm, N., Barabási, A.-L.: Limits of Predictability in Human Mobility. *Science* **327**, 1018–1021 (2010)
14. Onnela, J.-P., Saramäki, J., Hyvonen, J., Szabó, G., Argollo de Menezes, M., Kaski, K., Barabási, A.-L., Kertész, J.: Analysis of a large-scale weighted network of one-to-one human communication. *New J. Phys.* **9**, 179 (2007)
15. Eckmann, J.-P., Moses, E., Sergi, D.: Entropy of dialogues creates coherent structures in e-mail traffic. *Proc. Natl. Acad. Sci. USA* **101**, 14333–14337 (2004)
16. Kossinets, G., Watts, D.: Empirical analysis of an evolving social network. *Science* **311**, 88–90 (2006)
17. Golder, S., Wilkinson, D., Huberman, B.: Rhythms of social interaction: messaging within a massive online network. In: *Communities and Technologies 2007: Proceedings of the Third Communities and Technologies Conference*, Michigan State University, 2007
18. Leskovec, J., Horvitz, E.: Planetary-scale views on a large instant-messaging network. In: *Proceeding of the 17th International Conference on World Wide Web*, pp. 915–924. ACM, New York (2008)
19. Rybski, D., Buldyrev, S.V., Havlin, S., Liljeros, F., Makse, H.A.: Scaling laws of human interaction activity. *Proc. Natl. Acad. Sci. USA* **106**, 12640–12645 (2009)
20. Malmgren, R.D., Stouffer, D.B., Campanharo, A.S.L.O., Nunes Amaral, L.A.: On Universality in Human Correspondence Activity. *Science* **325**, 1696–1700 (2009)
21. Cattuto, C., Van den Broeck, W., Barrat, A., Colizza, V., Pinton, J.-F., Vespignani, A.: Dynamics of person-to-person interactions from distributed RFID sensor networks. *PLoS ONE* **5**(7), e11596 (2010)
22. Alani, H., Szomsor, M., Cattuto, C., Van den Broeck, W., Correndo, G., Barrat, A.: Live social semantics. In: *8th International Semantic Web Conference ISWC2009. Lecture Notes in Computer Science*, vol. 5823, pp. 698–714. Springer, Berlin (2009). http://dx.doi.org/10.1007/978-3-642-04930-9_44

23. Van den Broeck, W., Cattuto, C., Barrat, A., Szomszor, M., Correndo, G., Alani, H.: The live social semantics application: a platform for integrating face-to-face presence with on-line social networking. First International Workshop on Communication, Collaboration and Social Networking in Pervasive Computing Environments (PerCol 2010). In: Proceedings of the 8th Annual IEEE International Conference on Pervasive Computing and Communications, pp. 226–231, Mannheim, Germany (2010)
24. Salathé, M., Kazandjieva, M., Lee, J.W., Levis, P., Feldman, M.W., Jones, J.H.: A high-resolution human contact network for infectious disease transmission. *Proc. Natl. Acad. Sci. (USA)* **107**, 22020–22025 (2010)
25. Special issue of Science on Complex networks and systems. *Science* **325**, 357 (2009)
26. Dorogovtsev, S.N., Mendes, J.F.F.: Evolution of Networks: From Biological Nets to the Internet and WWW. Oxford University Press, Oxford (2003)
27. Newman, M.E.J.: The structure and function of complex networks. *SIAM Rev.* **45**, 167–256 (2003)
28. Pastor-Satorras, R., Vespignani, A.: Evolution and Structure of the Internet: A Statistical Physics Approach. Cambridge University Press, Cambridge (2004)
29. Caldarelli, G.: Scale-Free Networks. Oxford University Press, Oxford (2007)
30. Barrat, A., Barthélemy, M., Vespignani, A.: Dynamical Processes on Complex Networks. Cambridge University Press, Cambridge (2008)
31. Watts, D.: Connections: a twenty-first century science. *Nature* **445**, 489 (2007)
32. Holme, P., Saramäki, C.: Temporal networks. *Phys. Rep.* **519**, 97–125 (2012)
33. Clauset, A., Eagle, N.: Persistence and periodicity in a dynamic proximity network. In: Proceedings of the DIMACS Workshop on Computational Methods for Dynamic Interaction Networks, Piscataway (2007). Also available at <http://arxiv.org/abs/1211.7343>
34. Caceres, R.S., Berger-Wolf, T., Grossman, R.: Temporal scale of processes in dynamic networks. In: 2011 IEEE 11th International Conference on Data Mining Workshops (ICDMW), pp. 925–932 (2011)
35. Krings, G., Karsai, M., Bernharsson, S., Blondel, V.D., Saramäki, J.: Effects of time window size and placement on the structure of aggregated networks. *EPJ Data Sci.* **1**, 4 (2012)
36. Stehlé, J., Voirin, N., Barrat, A., Cattuto, C., Colizza, V., Isella, L., Régis, C., Pinton, J.-F., Khanafer, N., Van den Broeck, W., Vanhems, P.: Simulation of a SEIR infectious disease model on the dynamic contact network of conference attendees. *BMC Med.* **9**, 87 (2011)
37. Blower, S., Go, M.H.: The importance of including dynamic social networks when modeling epidemics of airborne infections: does increasing complexity increase accuracy? *BMC Med.* **9**, 88 (2011)
38. Isella, L., Stehlé, J., Barrat, A., Cattuto, C., Pinton, J.-F., Van den Broeck, W.: What's in a crowd? Analysis of face-to-face behavioral networks. *J. Theor. Biol.* **271**, 166–180 (2011)
39. Isella, L., Romano, M., Barrat, A., Cattuto, C., Colizza, V., Van den Broeck, W., Gesualdo, F., Pandolfi, E., Ravà, L., Rizzo, C., Tozzi, A.E.: Close encounters in a pediatric ward: measuring face-to-face proximity and mixing patterns with wearable sensors. *PLoS ONE* **6**(2), e17144 (2011)
40. Stehlé, J., Voirin, N., Barrat, A., Cattuto, C., Isella, L., Pinton, J.-F., Quaghiotto, M., Van den Broeck, W., Régis, C., Lina, B., Vanhems, P.: High-resolution measurements of face-to-face contact patterns in a primary school. *PLoS ONE* **6**(8), e23176 (2011)
41. <http://www.sciencegallery.com/infectious>. Downloaded on 1 August 2012
42. <http://www.sociopatterns.org/datasets/infectious-sociopatterns-dynamic-contact-networks/>. Downloaded on 1 August 2012
43. <http://www.ht2009.org/>. Downloaded on 1 August 2012
44. <http://www.sociopatterns.org/datasets/hypertext-2009-dynamic-contact-network/>. Downloaded on 1 August 2012
45. <http://www.sociopatterns.org/datasets/primary-school-cumulative-networks/>. Downloaded on 1 August 2012
46. Barrat, A., Cattuto, C., Szomszor, M., Van den Broeck, W., Alani, H.: Social dynamics in conferences: analyses of data from the Live Social Semantics application. In: 9th International Semantic Web Conference (ISWC 2010), Shanghai, China, 7–11 November 2010

47. <http://www.addith.be/projects/2010/practice-mapping/>. Downloaded on 1 August 2012
48. Barabási, A.-L.: The origin of bursts and heavy tails in human dynamics. *Nature* **435**(7039), 207 (2005)
49. Vázquez, A., Oliveira, J.G., Dezső, Z., Goh, K.-I., Kondor, I., Barabási, A.-L.: Modeling bursts and heavy tails in human dynamics. *Phys. Rev. E* **73**, 036127 (2006)
50. Barabási, A.-L.: *Bursts: The Hidden Pattern Behind Everything We Do*. Dutton Adult, New York (2010)
51. Read, J.M., Edmunds, W.J., Rile, S., Lessler, J., Cummings, D.A.T.: Close encounters of the 766 infectious kind: methods to measure social mixing behaviour. *Epidemiol. Infect.* **140**, 2117–2130 (2012)
52. Gautreau, A., Barrat, A., Barthélemy, M.: Microdynamics in stationary complex networks. *Proc. Natl. Acad. Sci. USA* **106**, 8847 (2009)
53. Bajardi, P., Barrat, A., Natale, F., Savini, L., Colizza, V.: Dynamical patterns of cattle trade movements. *PLoS ONE* **6**(5), e19869 (2011)
54. <http://www.gephi.org>. Downloaded on 1 August 2012
55. McPherson, M., Smith-Lovin, L., Cook, J.M.: Birds of a feather: homophily in social networks. *Annu. Rev. Sociol.* **27**, 415–444 (2001)
56. Tantipathananandh, C., Berger-Wolf, T., Kempe, D.: A framework for community identification in dynamic social networks. In: *KDD 07: Proceedings of 13th ACM SIGKDD on Knowledge discovery and data mining*, pp. 717–726, New York, USA (2007)
57. Seifi, M., Junier, I., Rouquier, J.-B., Iskrov, S., Guillaume, J.-L.: Stable community cores in complex networks. In: Menezes, R., Evsukoff, A., González, M.C. (eds.) *Complex Networks*. Springer, Berlin (2013)
58. Pastor-Satorras, R., Vespignani, A.: Epidemic spreading in scale-free networks. *Phys. Rev. Lett.* **86** 3200–3203 (2001)
59. Anderson, R., May, R.: *Infectious Diseases of Humans: Dynamics and Control*. Oxford University Press, Oxford (1991)
60. Gross, T., Sayama, H. (eds.): *Adaptive Networks: Theory, Models and Applications*. Springer/NECSI Studies on Complexity Series. Springer, Berlin (2008)
61. Scherrer, A., Borgnat, P., Fleury, E., Guillaume, J.-L., Robardet, C.: Description and simulation of dynamic mobility networks. *Comp. Net.* **52**, 2842 (2008)
62. Hill, S.A., Braha, D.: Dynamic model of time-dependent complex networks. *Phys. Rev. E* **82**, 046105 (2010)
63. Stehlé, J., Barrat, A., Bianconi, G.: Dynamical and bursty interactions in social networks. *Phys. Rev. E* **81**, 035101(R) (2010)
64. Zhao, K., Stehlé, J., Bianconi, G., Barrat, A.: Social network dynamics of face-to-face interactions. *Phys. Rev. E* **83**, 056109 (2011)
65. Nicosia, V., Tang, J., Musolesi, M., Russo, G., Mascolo, C., Latora, V.: Components in time-varying graphs. *Chaos* **22**, 023101 (2012)
66. Kovanen, L., Karsai, M., Kaski, K., Kertész, J., Saramäki, J.: Temporal motifs in time-dependent networks. *J. Stat. Mech.* P11005 (2011)
67. Moody, J.: The importance of relationship timing for diffusion. *Soc. Forces* **81**, 25–56 (2002)
68. Kossinets, G., Kleinberg, J., Watts, D.: The structure of information pathways in a social communication network. In: *Proceedings of the 14th ACM SIGKDD International Conference on Knowledge Discovery and Data Mining*. ACM, New York (2008)
69. Hui, P., Chaintreau, A., Scott, J., Gass, R., Crowcroft, J., Diot, C.: Pocket switched networks and human mobility in conference environments. In: *Proceedings of the 2005 ACM SIGCOMM Workshop on Delay-Tolerant Networking*, vol. 244. ACM, New York (2005)
70. Zhang, X., Neglia, G., Kurose, J., Towsley, D.: Performance modeling of epidemic routing. *Comp. Networks* **51**, 2867 (2007)
71. Boldrini, C., Conti, M., Passarella, A.: Modelling data dissemination in opportunistic networks. In: *Proceedings of the Third ACM Workshop on Challenged Networks (CHANTS2008)*, pp. 89–96. ACM, New York (2008)

72. Lee, C.-H., Eunt, D.H.: Heterogeneity in contact dynamics: helpful or harmful to forwarding algorithms in DTNs? In: Proceedings of the 7th International Conference on Modeling and Optimization in Mobile, Ad Hoc, and Wireless Networks, pp. 72–81 (2009)
73. Groenevelt, R., Nain, P., Koole, G.: The message delay in mobile ad hoc networks. *Perform. Eval.* **62**, 210 (2005)
74. Cai, H., Eun, D.Y.: Crossing over the bounded domain: from exponential to power-law inter-meeting time in MANET. In: Proceedings of the 13th Annual ACM International Conference on Mobile Computing and Networking (MOBICOM2007), pp. 159–170 IEEE Press, Piscataway (2007)
75. Miklas, A.G., Gollu, K.K., Kelvin, K.W., Saroiu, S., Gummadi, K.P., De Lara, E.: Exploiting social interactions in mobile systems. In: Proceedings of the 9th International Conference on Ubiquitous Computing (UBICOMP2007), pp. 409–428. Springer, Berlin (2007)
76. Karvo, J., Ott, J.: Time scales and delay-tolerant routing protocols. In: Proceedings of the Third ACM Workshop on Challenged Networks (CHANTS2008), pp. 33–40 ACM, New York (2008)
77. Panisson, A., Barrat, A., Cattuto, C., Ruffo, G., Schifanella, R.: On the dynamics of human proximity for data diffusion in ad-hoc networks. *Ad Hoc Networks* **10**, 1532–1543 (2012)

Social Insects: A Model System for Network Dynamics

Daniel Charbonneau, Benjamin Blonder, and Anna Dornhaus

Abstract Social insect colonies (ants, bees, wasps, and termites) show sophisticated collective problem-solving in the face of variable constraints. Individuals exchange information and materials such as food. The resulting network structure and dynamics can inform us about the mechanisms by which the insects achieve particular collective behaviors and these can be transposed to man-made and social networks. We discuss how network analysis can answer important questions about social insects, such as how effective task allocation or information flow is realized. We put forward the idea that network analysis methods are under-utilized in social insect research, and that they can provide novel ways to view the complexity of collective behavior, particularly if network dynamics are taken into account. To illustrate this, we present an example of network tasks performed by ant workers, linked by instances of workers switching from one task to another. We show how temporal network analysis can propose and test new hypotheses on mechanisms of task allocation, and how adding temporal elements to static networks can drastically change results. We discuss the benefits of using social insects as models for complex systems in general. There are multiple opportunities emergent technologies and analysis methods in facilitating research on social insect network. The potential for interdisciplinary work could significantly advance diverse fields such as behavioral ecology, computer sciences, and engineering.

D. Charbonneau (✉)

Graduate Interdisciplinary Program in Entomology & Insect Science, University of Arizona, Biological Sciences West, 1041 East Lowell, Room 235, Tucson, AZ 85721, USA
e-mail: charbonneau.daniel@gmail.com

B. Blonder · A. Dornhaus

Department of Ecology and Evolutionary Biology, University of Arizona, 1041 E Lowell St., Tucson, Arizona 85721, USA
e-mail: bblonder@email.arizona.edu; dornhaus@email.arizona.edu

1 Introduction

1.1 *Social Insect Biology*

There are currently over 1.7 million described species on earth and 1 million of these are insects. Insects can be found in nearly all habitats and the earliest insects are thought to have evolved 400 million years ago [39, 96]. Within this exceptional group there exists an even more exceptional group: the social insects. Though they only represent 2% of insect species, social insects may constitute up to 80% of insect biomass and in total outweigh vertebrates by 7 to 1 [41, 89, 104]. They are known to be one of the most ecologically successful groups in nature, dominating most terrestrial habitats. Division of labor is often cited as a primary reason for their ecological success, particularly in ants [42, 72, 90, 103].

Social insects, including particularly termites, ants, bees and wasps, live in family groups of up to millions of members, called colonies. Colonies contain only one or few “queens”, who lay eggs and ensure colony reproduction. The rest of the colony is primarily composed of workers and sometimes males. Workers ensure the maintenance and growth of the colony. When a colony matures, it produces sexuals, male drones and female queens, which leave the colony to mate and establish new colonies.

The reproductive division of labor between queens and workers is an essential component of eusociality or “true sociality”. Although workers do not reproduce themselves, they gain indirect fitness through the queen because queens and workers share a large proportion of their genes. This leads to extreme cooperation between individuals within a colony and thus group-level optimization of colony features.

1.2 *Information Exchange Networks in Social Insects*

Social insect societies are complex self-organized systems. They display sophisticated problem-solving that emerges from relatively simple individual behaviors. For example, ant and bee colonies can select the best among several nest sites that differ along multiple dimensions by a consensus-decision-making process that resembles a voting procedure. They also demonstrate division of labor, which involves individual workers adaptively allocated to different tasks (e.g. caring for eggs, larvae, and pupae or brood care; building; foraging; defense; etc.), in a way that is robust to change in demand and to individual failure or even to loss of large numbers of workers. Many of these processes are regulated by interactions between the individual agents within the colony. As such the structure and dynamics of the network of interactions will affect overall colony functioning.

Information-sharing between nestmates is thus necessary for the coordination of social insect colonies. The most commonly known means of communication among social insects are pheromone trails. However, social insects use a wide range of types

of communication including visual, acoustic, tactile, vibration, and chemical cues other than pheromone trails [37, 42]. Each of these modalities of communication has properties that could affect information flow in complex ways. For example, broadcast cues like volatile pheromones will likely have a greater range than an individual-specific cue like antennation (touching with antennae, which contain sensory organs). Broadcast cues also travel faster, though less reliably than contact signals. The type of communication will fundamentally affect network structure, as it affects how many links a single communication event creates and how connected the network will be. It also affects network dynamics by changing the speed and reliability of information flow. As such, we might expect that the structures and properties of the interaction networks for each of these methods of communication could be different and optimized for different constraints.

For example, different species of ants are optimized for different environments. When workers in mass-recruiting ants find a new food source, they lay pheromone trails on the return trip to the colony. These pheromones serve to both recruit new workers to exploit the food source as well as guide these foragers to it. Successful foragers typically add to the pheromone trails on the return trip. This creates a feedback loop where the better the food source, the more foragers will be recruited to exploit it, allowing the ants to quickly and efficiently exploit resources. In addition, this enables ants to find the shortest path to a food source through a self-organized process [7, 19]. However, studies have shown that, although pheromone laying ant species are capable of quickly exploiting food sources, they cannot quickly switch to a new, better food source because they get locked into exploiting the food source with the existing pheromone trail [8, 19, 54]. There is evidence suggesting that this phenomenon, linked to symmetry-breaking, could be explained by non-linearity of individual choice behaviors in response to signal strength [54]. This suggests that mass-recruiting species are better suited to less variable environments.

Other species have developed different means of recruitment and communication about food source locations. For example, some species engage in “tandem-running,” where a worker who finds a food source returns to the colony and recruits a second individual which then follows the leader back to the site by maintaining antennal contact. Such recruits, having learned the location of the resource, can then return and recruit more individuals in turn, thereby creating a feedback loop which increases the total number of individuals having knowledge of the food site location and who can contribute to its exploitation. Studies have shown that this means of recruitment is much better suited to exploiting sporadic and ephemeral food sources because any time an individual forager returns from a new food source, it is able to immediately recruit other workers to it [33, 83].

1.3 Why Should We Care About Social Insects?

Social insects must also balance many simultaneous constraints, such as efficient communication and movement within the colony with nest defense and limited

disease propagation. This is particularly interesting because man-made networks are also often faced with multiple constraints and social insects could serve as good model systems. For example, balancing efficient movement in termite colonies with limiting disease spread [76, 77] can easily be applied to efficient data transmission in computer networks while limiting the potential for spreading viruses or other harmful programs. Furthermore, balancing efficient movement and communication within the colony with effective nest defense could have military applications.

Colonies are sometimes spatially organized such that workers show fidelity to certain areas of the nest [44, 92]. There are often relationships between spatial location of individual workers and their task specialization [82, 92], age [91], and/or body size [44]. Although it is unclear whether spatial location is driving these relationships, it is clear that the spatial location of interacting workers will change the structure of interaction networks [10, 80]. The physical nest structure itself can also affect information flow by constraining interactions, thus limiting global and enhancing local information flow.

Many biological networks, including social insect networks, are thought to approximate scale-free networks [3, 4, 31]. Specifically, the connectivity (or degree) of biological networks often follows a power law distribution. Scale-free networks share certain properties that make them particularly interesting to study. They are typically composed of several hubs, or more central nodes, and a large number of nodes with few connections. They also belong to a class of networks known as small world networks, which have the property of rapid communication between nodes throughout the network. Lastly, scale-free networks are often robust or resilient to the removal of random nodes.

Although many biological networks have been shown to be scale-free (metabolic networks, [47]; protein–protein interactions networks, [60]; gene expression networks, [70]; gene interactions, [98]), there is still some question as to how prevalent scale-free networks are in biological systems [52]. In the case of social insect networks, there is yet to be a clear answer. Because the size of social insect colonies is often small (naturally limited to no more than a few hundred individuals), natural scales may emerge in a network and also limit the power of model-selection approaches to detecting scale-free phenomena.

In Sect. 2, we review the current literature and show that degree distribution in social insect can depend on colony size. However, when social insect networks are found to be scale-free, it is possible to transpose methods and results from these to other scale-free networks, such as computer, social or business networks, and vice versa [3].

Social insects are particularly interesting to network scientists in all fields because they are an evolved (and thus optimized) system in which the interacting parts can be individually tracked and manipulated (Fig. 1). The same cannot be said for many other model network systems, such as primate social networks [95]. This is particularly interesting because experiments can be conducted on social insect networks that might not be possible in networks in other fields. We can map many of social insect adaptive functions on to functions of interest to humans. That is, they are a simulacrum of our engineered world.

Fig. 1 Individually marked ants of the species *Temnothorax rugatulus*. Photo by Alex Wild



1.4 Role and Types of Networks in Social Insects

Most research to date has focused on interaction networks, i.e. ones where individual workers are nodes and edges are defined as interaction events between workers. The relevant interactions used as network edges can be of different types such as spatial proximity [45, 73], physical contact (usually with antennae, “antennation”) [10, 67, 80], a food exchange event [15, 68, 69, 93], or specific communication signals [38, 56]. Such studies may investigate questions relating to the propagation of disease or information through the colony, and may test specific hypotheses concerning speed of transmission, whether all individuals are equally likely to be reached by the disease/information, or whether particular individuals or subgroups of the network (e.g. foragers or the queen) will transmit information/diseases more or less quickly than the rest of the colony.

Interaction networks can be directed, i.e. interactions may have a defined directionality. This can be the case in food flow networks, where one worker gives food to another worker. Given that only a fraction of the colony is out foraging at any time, successful foragers need to be able to share food, which they can store in their crop, with other workers and brood. The process by which this food is regurgitated and shared is called trophallaxis. Food flow networks are comprised of individual ants as network nodes and edges as trophallaxis events. The duration of a trophallaxis event tends to correlate with the amount of food being transferred [21], and edges may be weighted by duration of this interaction. Food flow networks can answer questions such as: what is the mean degree of separation between foragers and nurses (individuals who care for the immature brood)? Is food channeled to particular individuals preferentially (nurses, queen)? What elements of the network structure are necessary to achieve these things? Are networks structured to increase food distribution while simultaneously decreasing disease spread?

Worker–worker contact (interaction) networks can also be used to answer important questions. However, many key questions can only be answered by looking beyond networks constructed from mere physical contacts between individuals. In ecology, plant–pollinator networks (bipartite networks between pollinator communities and plant communities) have been the focus of much research. Pollinator communities are often composed primarily of social insects [22]. These types of

networks can be used to look at the resilience of plant–pollinator communities to the disappearance of one or many pollinator species [28, 29, 43, 62, 94] and temporal variation in plant–pollinator interactions [1, 5, 78].

Beyond these networks, other extremely interesting possibilities of non-interaction networks exist. For example, it is possible to create worker–task bipartite networks where each worker is linked to the set of tasks it performs, and each task is linked to the set of workers that perform it. Research using worker–task networks would enable investigation of worker specialization and individual variation of worker specialization as well as questions of network resilience to worker loss or failure.

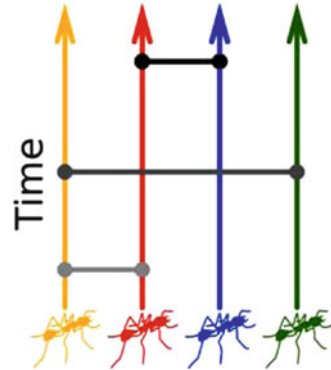
Alternatives to interaction networks include task–task networks, in which interactions are weighted and directed by the number of workers switching from one task to another [31]; worker–nest area networks, which could help investigate spatial fidelity within the nest and even nest area–nest area networks which could yield information about the movement patterns of individuals within colonies.

In this chapter, we make the case that looking beyond the worker–worker interaction networks is a necessary new direction for social insect network research. Further developing alternative network types will allow researchers to pose and answer new kinds of questions, and keep the field dynamic and exciting. Integrating networks at different organizational levels could be used to develop unified models [55]. In the following sections we review a selection of worker–worker interaction networks covering classic questions explored by these types of networks as well as two alternative network types that look at the temporal stability of bipartite plant–pollinator networks and the temporal dynamics of nest construction. We then present a worked example with original data of a task–task network in an ant colony to showcase the potential of exploring new types of networks.

2 Network Dynamics Applied to Social Insects

In recent years, networks have become increasingly popular in social insect research. Here we survey previous network research on topics that include interaction network resilience, flow (information, disease, and food), temporal stability of species interactions (plant–pollinator systems), and temporal dynamics of nest construction. Recently, researchers have focused on adding temporal elements to existing models and investigating the properties of network dynamics. Temporal networks on their own can provide insight into dynamic patterns within social insect colonies (e.g. network stability), and including a temporal dimension to static networks can yield surprising results and even invalidate conclusions drawn from static networks. The topics discussed in the following section (resource flow, group structure, task allocation, multi-species interactions) are actually dynamic processes, and as such are ideally suited to be studied from a dynamic perspective.

Fig. 2 Representation of a time-ordered network. Reproduced with permission from [10]



2.1 Worker–Worker Interaction Networks

2.1.1 Information Flow

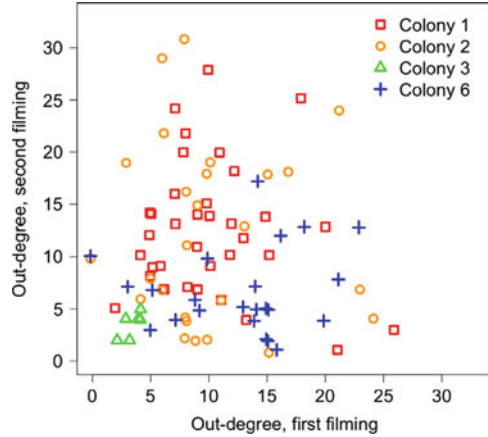
Social insect interaction networks have been described in different ways: worker interaction networks (e.g. [80]), network motifs (e.g. [100]), and temporal dynamic networks (e.g. [11]). Many complex interaction networks are adapted to inhibit or promote the transmission of disease, resources, or information between individuals. However, interactions between individuals occur over time, may be repeated, and are stochastic. These temporal dynamics are certain to affect network function, and are not captured by static network analyses. There is currently a trend in the literature to incorporate temporal dynamics into established static models and to apply methods that directly take the dynamic nature of interactions into account.

In a recent paper, Blonder and Dornhaus [10] investigated constraints on information flow in colonies of the ant *Temnothorax rugatulus*. They employed a “time-ordered network” (Fig. 2) which directly incorporates the timing of interaction events, and thus allows the tracing of possible pathways of information flow through time. The observed network of ant antennation interactions (physical touching with antennae) was compared to a diffusion model in which all individuals interact like kinetic gas particles. They compared the number of individuals reached by a message propagated from a random individual within a set time interval in the diffusion model with the observed ant interaction network. This measure can be thought of as an upper bound to information flow, as it was not determined whether each interaction actually involved transmission of information.

They found that, at large time-scales, information flow was significantly slower in ant networks than that predicted by the diffusion model, but that at small time-scales information flow was faster than predicted. This suggests that the structure of the ant network is optimized to facilitate local information flow, but also underlines the importance of using an appropriate time-scale as results may vary.

The absence of a relationship between the number of individuals a focal ant touches (out-degree) in one bout of filming compared to the next (Fig. 3) suggests

Fig. 3 Individual out-degree between the first and second observation of all colonies. Reproduced with permission from [10]



that individual ants did not consistently hold central roles within the network. This is especially interesting as many scale-free networks show consistent individual specialization.

Since this lack of individual consistency in interaction pattern was not found in other studies [45, 80], it is likely that these network properties differ between different ant species with different ecology and life history (colony size, nest types, etc.), whose individual and collective behavior is optimized for different conditions and constraints.

2.1.2 Resilience of Colony Function to Perturbation

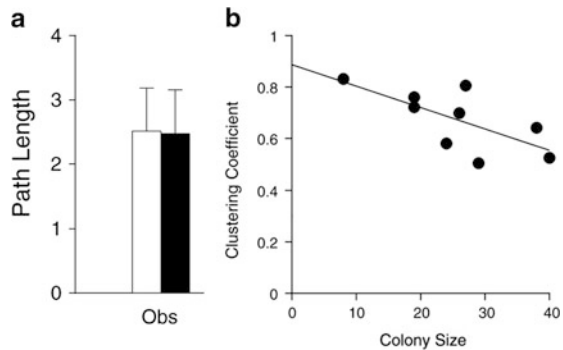
Network resilience can be broadly defined as the ability of a network to retain or restore its function after perturbation [35, 65, 106]. In the case of a computer network, this means being able to provide and maintain an acceptable level of service in the face of faults. For ecological networks such as between plants and their pollinators, this may mean having a limited extinction of plant species should several species of pollinators disappear. For social insect interaction networks, this may mean maintaining an acceptable level of function when individuals fail, either by making errors or by disappearing.

In a study looking at the resilience of a colony to the death of workers, Naug [67] assembled undirected worker–worker contact networks weighted by the frequency of interactions before and after removal of random workers from colonies of the social wasp *Ropalidia marginata* (Fig. 4). By comparing the intact and reduced networks, he showed that path lengths were maintained, thus preserving information flow throughout the colony (Fig. 5a). The wasps achieved this by an increase in connectivity amongst remaining individuals attained through an increase in the rate of interactions. As such, his results showed that interaction networks within this wasp species were resilient to the removal of random workers.

Fig. 4 The social wasp *Ropalidia marginata* (*top*) and its nest (*bottom*). *Top*: by School of Ecology and Conservation/CC-BY-2.5. *Bottom*: by Abhadra/CC-BY-2.5



Fig. 5 (a) Path length before (*white*) and after (*black*) removal of random workers. (b) Clustering coefficient decreases as colony size increases. Reproduced with permission from [67]



Naug [67] also looked at the effect of colony size, i.e. the number of individuals in the group, on network structure and properties. His results showed that smaller colonies tended to have more homogeneously connected individuals while larger colonies tended to have more heterogeneously connected individuals (Fig. 5b). Uniform connectivity in small colonies may allow all workers to have access to information about what work needs to be done. This might lead to more generalist workers in smaller colonies (if workers frequently switch tasks). On the other hand, workers in larger colonies only have access to partial information, potentially leading to behavioral specialization. This is in accord with the prevailing view in the literature that group size often correlates with task specialization ([34, 46, 50, 97], although see [26]).

However, colony sizes in this study ranged from 8 to 40 individuals which form relatively small interaction networks. Samples across more orders of magnitude would provide greater insight into the effects of colony size on network properties, but there are often natural and practical limitations to these studies. For example,

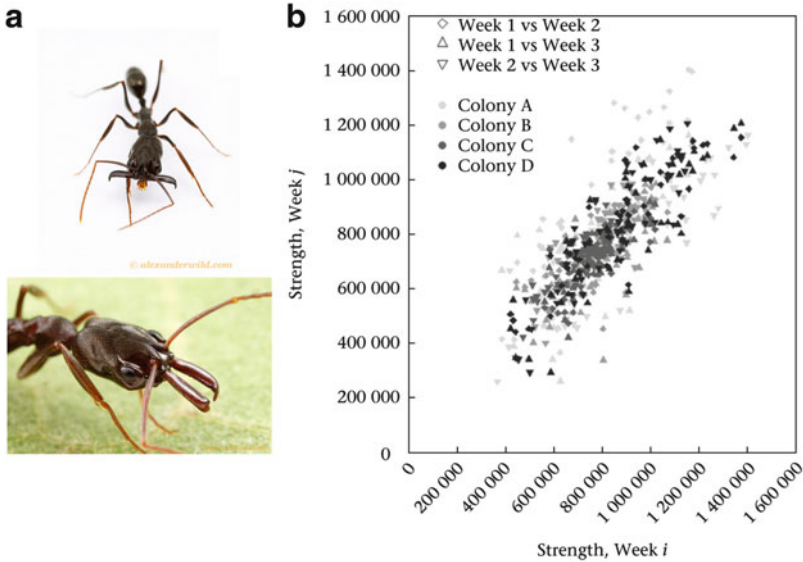


Fig. 6 (a) Ants of the genus *Odontomachus* with mandibles open at 180° and resting in closed position. These ants hold the record for fastest moving predatory appendages within the animal kingdom [75]. Photos by Alex Wild. (b) Strength of associations between workers at different times. Reproduced with permission from [45]

colonies of *Ropalidia marginata* (the wasp species used in the Naug study) typically hold no more than 200 workers and the amount of work required to collect these data increases exponentially with colony size. Thus the application of scale-free network concepts may be less relevant in these naturally small systems.

A related study looked at the stability of interaction networks and their resilience to queen removal in ants of the genus *Odontomachus*, often called “trap-jaw ants” because of their unusual mandibles (Fig. 6a). In this study, Jeanson [45] used passive microtransponders superglued to the ants to track their spatial position over a 3 week period. By assuming that ants who came in close proximity were interacting, the author created a dynamic worker–worker interaction network. His results showed that the interaction networks were stable over time and resilient to the removal of the queen, but that inter-individual differences were important in connectivity patterns (Fig. 6b). Specifically, some workers formed stronger long-lasting interactions with a smaller group of nestmates while other workers did not have privileged relationships and interacted uniformly with their nestmates.

2.1.3 Disease Transmission

Social insects, like humans, are particularly susceptible to disease because of high population density, genetic homogeneity within colonies, and high interaction rates

[105]. As such, social insects may have evolved strategies which mitigate the effects or limit the transmission of diseases.

If interaction networks are scale-free, interactions should not be uniformly distributed amongst individuals. A small number of workers should be more central and most workers should be directly connected only to a subset of the colony. One effect of this organization is that networks are particularly resilient to the random loss of some individuals [67]. It has also been shown that that highly clustered subgroups and short average path lengths, which are characteristics of scale-free networks and incidentally small world networks, should maximize efficient communication [101]. As such, we might expect that disease transmission would equally be maximized.

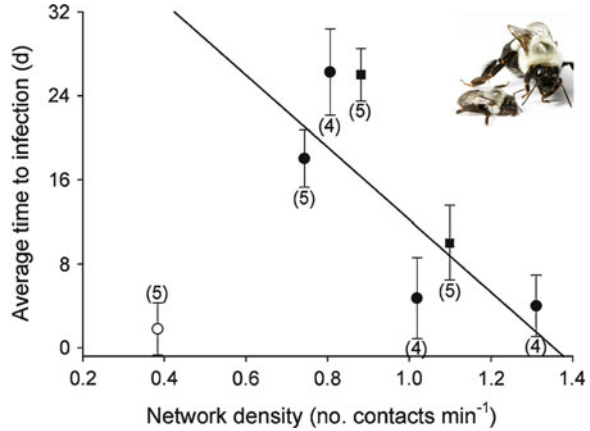
However, there could also be some evolutionary pressure to limit the spread of disease within social insect colonies. Certain features of colony organization help limit the spread of disease [67] and infection period plays an important role in the spread of disease in social insect colonies [69], as it does in human societies [51]. Indeed, one effect of clustered subgroups is that the network is partitioned which, combined with short infection periods, can result in a limited spread of disease throughout the colony because portions of the colony will die out before the disease can spread to the majority of the colony. Indeed, in an agent-based modeling study, Pie et al. [79] show that even minimal spatial segregation tends to slow the spread of disease. On the other hand, if the infection period is long, then the highly efficient communication of the network will ensure that most if not all of the colony will be infected.

A study investigating colony properties and their effects on the transmission of a contagious pathogen (*Crithidia bombi*) in bumblebee colonies (*Bombus impatiens*) used automated video tracking of uniquely identified bees to measure worker-worker contact (spatial proximity) networks within the colony and quantified the actual spread of the pathogen [73]. They showed that across colonies, rates of infection were mostly dependent on network density (average contacts per minute) where higher densities lead to higher rates of infection (Fig. 7). Furthermore, the rate of contact for individuals predicted the likelihood of infection for that individual.

Similarly, using weighted trophallaxis networks (undirected food sharing networks weighted by transfer duration) to emulate the transmission of orally transmitted pathogens rather than those transmitted simply by contact, Naug [68] shows that disease transmission in honeybee colonies is more widespread when colony interaction networks have lower clustering coefficients (degree to which nodes in a graph are clustered together). Interestingly, lower clustering coefficients and high network densities are typically associated with network resilience, which suggests a tradeoff in clustering between colony resilience to losing workers and limiting disease transmission. Both of these empirical results are supported by Pie et al. [79] who use agent-based modeling to show a nonlinear interaction between worker density and the probability of disease transmission.

A surprising fact about social insects is that a significant proportion (as much as 60 %) of colony workers is inactive at any time [27, 85]. One reason for this may be that reduced activity slows disease transmission, presumably because interaction

Fig. 7 The average time of infection from *Crithidia bombi* decreases with increasing network density (average contacts per minute) in colonies of *Bombus impatiens*. Reproduced with permission from [73]



rates in less active colonies would be lower ([79], Fig. 8). Interestingly, an empirical study found no effect of individual activity on the risk of infection [73]. Naug [68] also suggests that the location of younger individuals both within the colony and the network could have the effect of limiting their exposure to diseases.

2.1.4 Food Flow

Sendova-Franks et al. [93] looked at the network structure of trophallaxis interactions and its progression in time in the ant *Temnothorax albipennis* (Fig. 9). They also compared colonies in normal feeding situations with colonies that had been starved for 48 h. Note that this ant genus is highly starvation resistant: colonies have been shown to survive up to eight months of complete starvation [88]. Within the first 30 min, as much as 95 % of ants from starved colonies (Fig. 10, full circles) were fed, versus less than 50 % of ants in fed colonies (Fig. 10, empty circles). Increased efficiency in food distribution resulted from increased movement of internal workers away from the brood piles (eggs larvae, and pupae which are typically at the colony center) and movement of foragers carrying food further into the nest. Indeed, both the number of recipients per donor and the number of ants participating in trophallaxis increased in starved colonies. Furthermore, the distance of a vector from the centroid of internal workers to the centroid of external workers (or foragers) was shorter after starvation than in the control and the direction of this vector was parallel to that of a line going between the nest entrance and the center of the brood pile. This is particularly interesting because workers have shown spatial fidelity according to their tasks where internal workers are essentially segregated from external workers, a phenomenon which was observed in the fed colonies, but not in the starved colonies. After starved colonies had been sated, spatial segregation resumed.

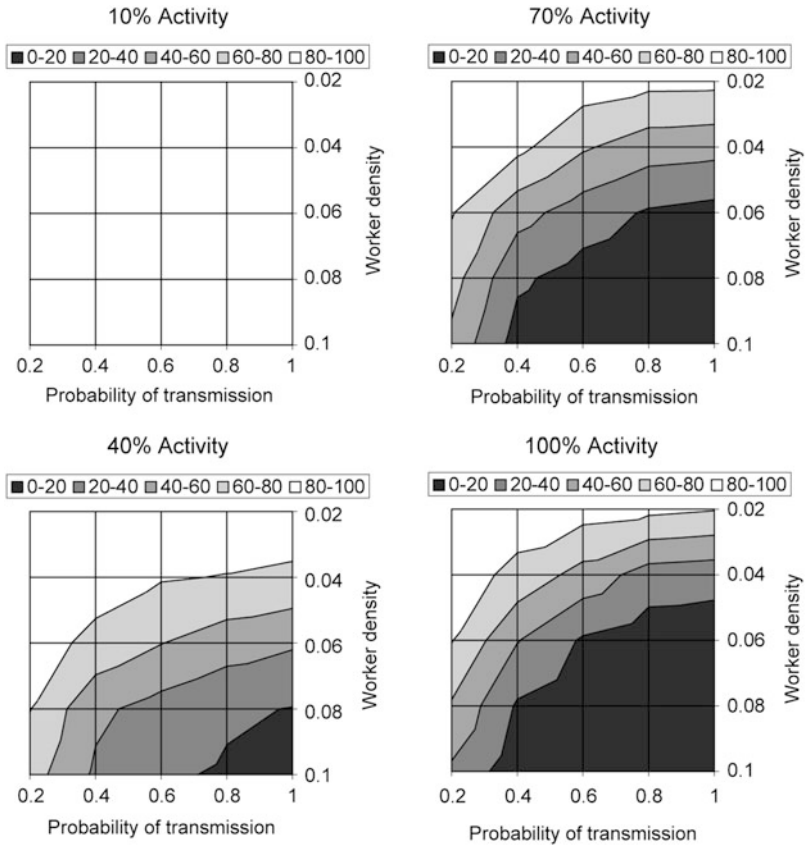


Fig. 8 Relationships between worker density, probability of transmission and colony activity obtained from an agent-based model. Reproduced with permission from [79]



Fig. 9 Nest of *Temnothorax albipennis* ants surrounded a wall of colored sand grains built by the ants. Photo by Anna Dornhaus

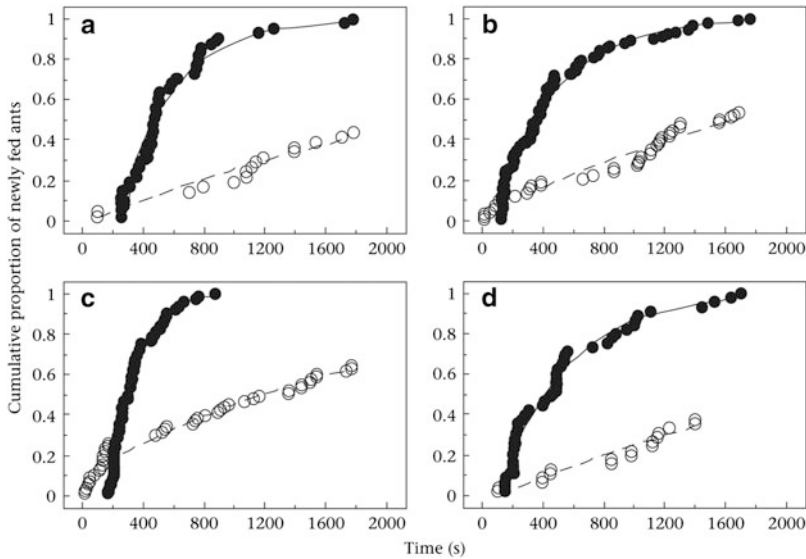


Fig. 10 The cumulative proportion of the colony fed for colonies A (a), B (b), C (c) and D (d) when that were starved for 48 h before feeding (*full circles*) and during regular feeding. Reproduced with permission from [93]

After starvation, some workers stored food rather than pass it on to other ants. They suggested that these ants are living “silos” and they may also act as food testers for the rest of the colony. Essentially, by storing large amounts of newly acquired food in these individuals the colony can test whether the food contains any toxins. If there were, only the “silo” worker would die, thus saving the rest of the colony. Otherwise, if the “silo” ant seems healthy, then the food would likely be safe. However the long-term network dynamics of food and disease flow were not directly investigated in this study.

2.2 Beyond Worker–Worker Interaction Networks

2.2.1 Temporal Stability of Species Interaction Networks

Different types of animals and plants often interact with each other in beneficial or harmful ways. For example, there is a long history of studying plant–pollinator systems, in which different species of plants are pollinated by different species of animals, usually insects [58, 86]. These interactions among different species can be thought of as plant–pollinator networks. Studies on such networks make use of theory developed in food web networks [28, 29, 43, 94]. These have allowed researchers to address questions relating to the resilience of such species networks to changes in biological community composition [62], the effects of invasive plants

on plant–pollinator networks [57], and the disruption of pollination networks due to global warming [61].

Resilience is tested by simulating a perturbation, typically by removing network nodes, and examining its effects on network topology and function. Plant–pollinator networks have been shown to be fairly resilient to removals [28, 29, 43, 94]. It is thought that resilience in pollination networks might stem from a redundancy in pollinators per plant as well as from the nested topology of the networks [62].

In the last 20 years, the question of specialists vs. generalists in plant–pollinator systems has been the subject of active debate. The idea that interactions between plants and pollinators tend toward specialization, or that plants and pollinators will coevolve towards increased fidelity, has long been widely accepted [2, 40]. However, in an extensive review, Waser et al. [99] showed evidence that perhaps generalists might be equally important and prevalent. Within the last decade, due to advances in network theory and an increasing awareness of networks, researchers have been using network approaches to address this question. Some work focused on characterizing the network properties of plant–pollinator systems such as the distribution of specialists to generalists [6, 103]. Although this work is important in understanding plant–pollinator network structure, it does leave the question of how these networks might vary in time. Indeed, research has shown that relationships between specialists and generalists are complex and that plant–pollinator networks are both asymmetric (interaction rates are not equal in each direction) and nested (species with few links have a sub-set of the links of other species), but until recently we did not know how stable these interactions were over time. A few recent studies explicitly address this issue [1, 30, 71, 78].

These studies showed that pollination network topology varied through time. Indeed, both the number and identity of interaction partners varied in time. This suggests that the relationships between plants and their pollinators may not be as strong or exclusive as expected. Indeed, within a single year of plant–pollinator interactions, a large portion of plants and pollinators seem to be specialists, but over a longer timescale interactions that were strong one year are not necessarily strong the next year (Fig. 11).

While the precise network topology of pollination networks varied through time, overall structural parameters of the network (e.g. degree centralization, connectance, nestedness, average distance, and network diameter) remained fairly constant. A large scale study spanning a wide range of latitudinal gradients shows similar results [30]. These studies are particularly interesting because they show how different patterns can appear at different timescales.

2.2.2 Temporal Dynamics of Nest Construction

Many social insects build complex nests which both constrain and facilitate collective organization. Nest often consist of multiple chambers connected by tunnels, and these have garnered much attention from researchers interested in networks. The networks created by social insect nest architecture are particularly interesting

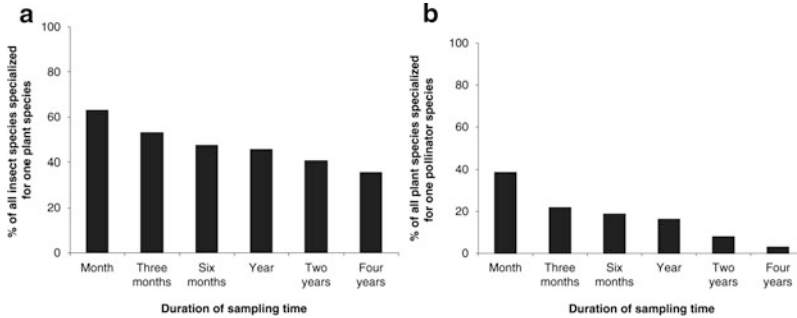


Fig. 11 Time dependence of “apparent specialization” of (a) pollinators and (b) plants. Reproduced with permission from [78]

because they show how self-organized networks can solve problems with multiple complex constraints, such as the need for efficient movement within the colony while making the nest defensible to attacks.

Over the last decade, with increasing accessibility to sophisticated computer and imaging tools and the interest in applying network approaches to biological systems, we have seen a progression of increasing complexity and detail in the studies investigating the network structure of nest architecture. Early studies focused on two-dimensional nest architecture and looked at the network properties of nest architecture such as the effects of group size on nest architecture [16], the efficiency and robustness of nest networks [18], and the relationship between topology and structural properties of nest networks [17].

More recently, researchers looked at nest networks in three-dimensional space, which better represents nest architectures of many species. Using computer tomography (CT) scanning to build three-dimensional models (Fig. 12) of nest architecture, Perna et al. [76, 77] looked at the transportation efficiency in termite nests and found that it is significantly higher than random, but below optimal transportation efficiency (Fig. 13). They proposed that this was a compromise between multiple constraints, such as efficient connectivity inside the nest, defense and resilience to attacking predators, and spatial constraints.

Recently, Minter et al. [63] investigated the temporal dynamics of nest building. Using microcomputer tomography at multiple time points over a 24 h period, they were able to track tunnel and chamber construction in time (Fig. 14).

In this study, they showed how features of the environment, specifically the presence of planes between sediment layers, would influence nest construction. When ants met with a new sediment layer, they tended to excavate more horizontally along the planes and over longer periods before continuing to tunnel downwards. They suggested that it is in fact not the planes they are responding to, but rather local heterogeneities in sediment compaction. This suggests that the importance of local information outweighs that of global information in determining individual nest construction behavior which in turn leads to the emergent phenomenon of nest structure.

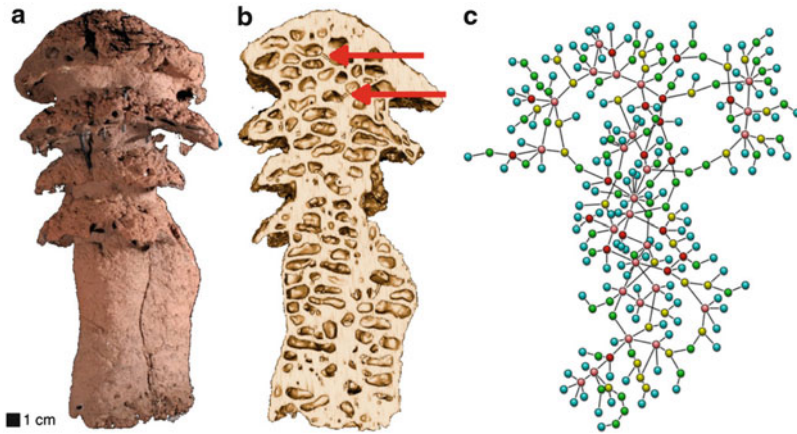


Fig. 12 (a) Above ground mushroom shaped termite nest. (b) tomographical cut of the same nest (the *arrows* indicate two of the corridors between chambers). (c) representation of chambers and galleries as a network. Nodes are chambers in the nest and edges are corridors. Reproduced with permission from [77]

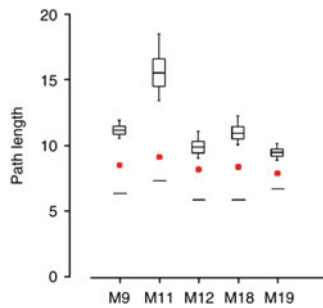


Fig. 13 Average topological path length for random spanning subgraphs (*black*), optimized spanning subgraphs (*horizontal lines*), and real gallery networks (*red circles*). Reproduced with permission from [77]

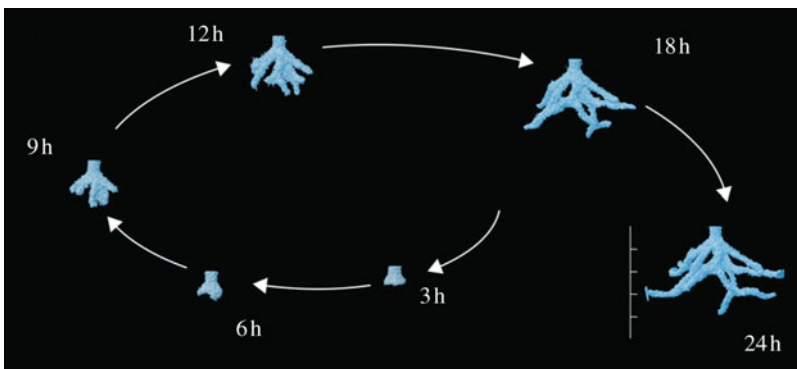


Fig. 14 Example of the progression of three-dimensional nest structure through time. Reproduced with permission from [63]

3 Even Further Beyond Worker–Worker Networks: A Task–Task Network

Networks play a role in several aspects of collective behavior in social insects. In Sect. 2 we presented a selection of the network types that have been most studied so far, including worker–worker interaction networks as well as other network types (bipartite plant–pollinator networks and nest architecture networks). We made the case for looking beyond networks of individual interactions, and employing network theory more broadly to other types of complex interacting processes. In support of this idea, we present original data worked into an example of a task–task network, i.e. defining the different tasks performed by workers in an insect colony as nodes, and each case of a worker switching between tasks as linking these nodes.

The process of allocating workers to the different jobs (“tasks”, such as foraging or nest-building) in a colony is both difficult and important to colony performance [9, 13, 36]. There is no consensus in the literature on how this is achieved in the face of changing demand for tasks and possible worker failure. To investigate this issue, we performed a temporal network analysis of the dynamics of task switching, asking if certain switching patterns were particularly common and whether the patterns of switching were stable over time. We hypothesized that workers would often rotate through certain “hub” tasks before switching to other tasks, and that flow through other tasks would be consistently low.

We collected a colony of *Temnothorax rugatulus* ants consisted of 41 workers and 2 queens in the Santa Catalina Mountains, outside of Tucson, Arizona USA in a pine forest at an altitude of approximately 8,000 ft. The collected ants were kept in the lab in artificial nests made of a piece of cardboard sandwiched between two glass slides ([27], see Fig. 15a). In the field, these ants typically nest in small rock crevices and artificial nests emulate these [32].

The ants were then painted with unique combinations of four paint spots, one on the head, one on the thorax and two on the abdomen so that they could be individually identified and tracked (Fig. 15b). Videos (5 min long) of normal colony activity were taken at four time points throughout the day: 8 am, 4 pm, 8 pm and 4 am (Fig. 15c). For each ant, the task it performed was recorded every second by an observer (see Table 1 for task list).

We first constructed a time-ordered network for each 5-min interval, creating a node for each task and an edge for each instance of a worker switching between tasks. Time-ordered networks are structures that provide a complete record of the timing of all observed interactions [11]. Here an example is shown for the first 5-min interval, qualitatively demonstrating extensive switching involving the tasks “wandering inside” (wi), “self-grooming” (sg), and “brood care” (bc), and some involving rotating through inactivity (i) (Fig. 16).

We used established techniques [11] to transform these time-ordered networks to a series of time-aggregated networks, with the aim of applying network methods in a temporal context. We chose a window size of 60 s but in this case results are robust to the choice of window size. Time aggregated networks constructed from

Fig. 15 Artificial *Temnothorax rugatulus* nest composed of a piece of cardboard sandwiched between two glass slides (a). Individually marked ants. The larger ant is a queen (b). Video recording setup of HD cameras equipped with servos filming an ant colony (c). Photos by Daniel Charbonneau

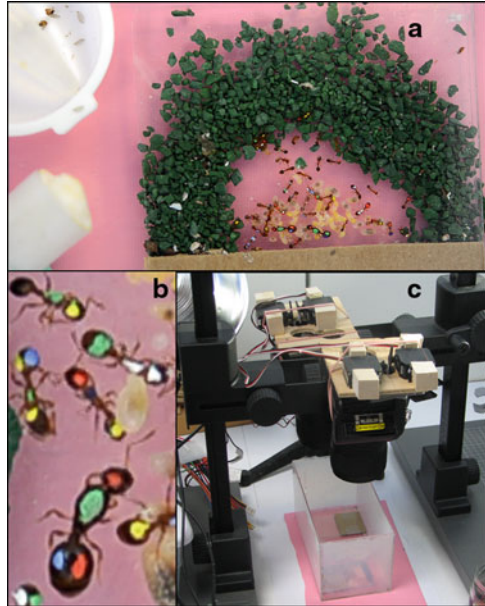


Table 1 List of possible tasks observed during video analysis and their associated codes

Code	Task
b	Nest building
f	Foraging
wo	Wandering outside nest
bc	Brood care
sg	Self-Grooming
go	Grooming other (giver)
og	Grooming other (receiver)
t	Trophallaxis
fd	Eating
wi	Wandering inside nest
i	Inactive

the first 5-min interval are shown below. These networks qualitatively demonstrate consistent patterns of flow between tasks (Fig. 17).

To quantitatively test whether workers return to a “hub” task before switching to new tasks, we measured betweenness for each task for every time-aggregated network during every interval (Fig. 18). The “wandering inside” (wi) task has the highest betweenness over nearly every time interval, demonstrating that it is a hub task. Most other tasks had consistently low betweenness. We then tested for temporal stability in the task flow by assessing trends in the betweenness of “wandering inside” (wi) over time. Within each interval, we found no significant increase or decrease (ANOVA; all $p > 0.12$). However across all intervals, there was a significant increase and then decrease in betweenness (ANOVA with linear and quadratic terms; both $p < 0.02$).

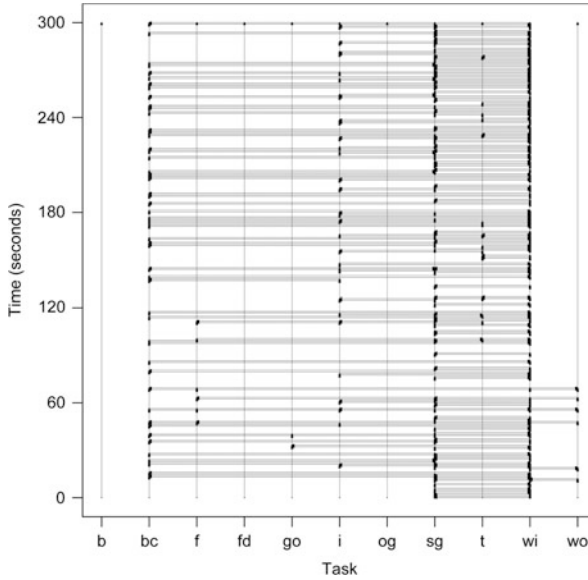


Fig. 16 Example of a time-ordered network for the first 5-min interval. Explanations of task abbreviations can be found in Table 1

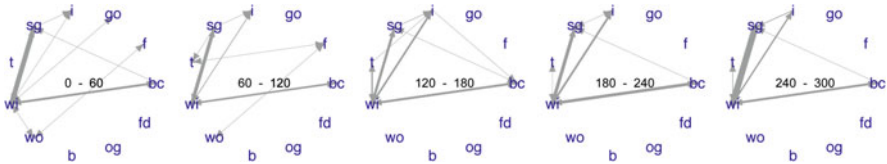


Fig. 17 Example time aggregated networks for the first 5-min interval. The numbers in the center of each network indicates the time interval in seconds. Explanations of task abbreviations can be found in Table 1

This temporal network analysis therefore indicates that there is minute-scale stability in task flow but hour-scale variation, and that most variation in task assignment is mediated through temporary assignment of workers to “wandering inside” (wi) tasks.

To interpret these results, we must first discuss the observed tasks. These fall into three separate categories. The first category, which includes all tasks with the exceptions of “wandering inside” and “inactive”, represents observable tasks that are thought to contribute to colony fitness (e.g. brood care or foraging). The second category (inactivity) is a conservative estimate of the time at which and duration during which individuals are inactive. The last category (anytime workers are wandering inside the nest but without performing an identifiable task) is less interpretable. We do not know whether they are simply being inactive, whether they are in fact performing some other yet to be identified task, whether they are simply between tasks, or whether they are looking for work to do. Some evidence in

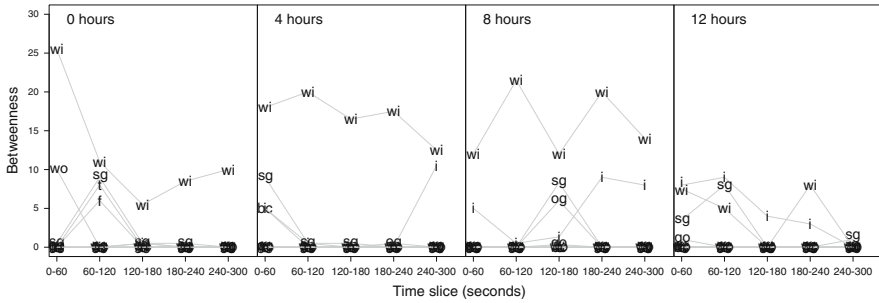


Fig. 18 Betweenness for each task for every time-aggregated network during each 60 s interval for all time points. Explanations of task abbreviations can be found in Table 1

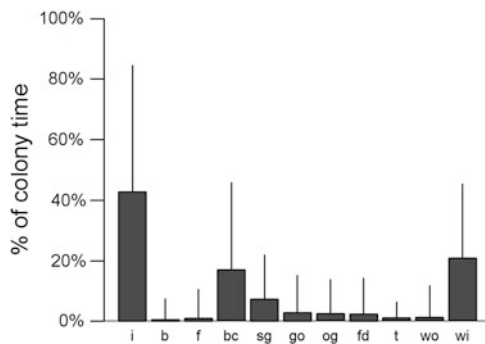


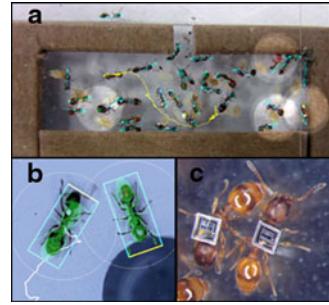
Fig. 19 Mean proportion of time spent in each task

honeybees indicates that they may be “patrolling”, i.e. collecting information about demand for work in different tasks [49].

The fact that the “wandering inside” (wi) task is a hub task (highest betweenness over nearly every time interval) suggests that the latter two possibilities are likely. Indeed, it seems as though “wandering inside” (wi) is an intermediate state between being engage in a task. We’ve shown that there is extensive switching between the tasks “wandering inside” (wi), “self-grooming” (sg), and “brood care” (bc), and some involving rotating through inactivity (i). This is likely because these are by far the tasks which workers spend most of their time doing (Fig. 19).

The temporal network approach lets us test new types of hypotheses and has identified a key behavior that deserves future study as it plays a key role in mediating between other tasks. Our task–task network quantifies the role of wandering in worker task switching in a new way as compared to other studies [48, 49]. It seems that ants must wander throughout the nest between tasks rather than awake from inactivity or directly switch from one active task to another.

Fig. 20 (a) Examples of the ant tracking tools being developed in Dr. Shin’s laboratory and (b) by Quitmeyer and Balch. (c) *Temnothorax albipennis* ants with RFID tags



4 Future Challenges and Opportunities

Many complex systems (e.g. social groups, neural networks, macro/micro-economics, etc.) can be studied with a network perspective, but these are often limited by constraints such as difficulty in acquiring high quantities of data or lack of an ethical or cost-effective way to do experiments. Social insects do not have these issues and thus provide a good model for other systems.

Because social insects are thought to employ relatively simple algorithms to achieve sophisticated group-level behaviors [19], they have been used as inspiration for the design of many artificial systems [12, 66]. Insect-inspired solutions have already been derived from foraging behavior [25], spatial sorting [59], or task allocation [13], and are used in job-shop scheduling [23], “traveling salesman” problems [24], software “agents” [74, 102], optimization of communication networks [20], and collective robotics (e.g. for planetary exploration: [14, 53]). Given the existence of a variety of methods for experimentation on social insects and that the research can be transposed to so many other fields, we expect this list to keep growing.

Although social insect colonies are tractable to observation and manipulation and offer a means of gathering real data relatively quickly, the many steps and processes required for acquiring data are still fairly time- and work-intensive. In many cases, social insect networks are created from spatial information and advances in tracking software have helped reduce the workload of acquiring this type of data. For example, Dr. Shin’s lab at the University of North Carolina Charlotte has developed a tracking tool (Fig. 20a) that can highly reliably track individual ants (96% + accurate) [81], but there are other tracking tools being developed as well (e.g. [84], Fig. 20b). The miniaturization of electronics has made it possible to use of radio-frequency identification (RFID) chips to both uniquely identify individuals and track individual movement ([64, 87], see Fig. 20c). Lastly, rapidly emerging analytical methods are being developed by social insect scientists (e.g. the R package “timeordered” that was used in the worked example. See [11] for a review).

Applying network approaches to social insect research is an emerging area and many studies are only just getting off the ground. Initial datasets were so hard to obtain that authors are reluctant to publish them completely. However, with new methods of obtaining data (e.g. video tracking) and new traditions in science (it is

becoming more common and often required by journals and NSF to publish full datasets) this is likely to change. Furthermore, there is a strong interest from social insect scientists to collaborate and share their data with network researchers and theoreticians. Indeed, social insect researchers often have the data and the biological questions which could be answered by network analyses, but lack the know-how to answer them appropriately.

The development of new network analysis tools can advance our understanding of social insect networks, but also of general organizational principles. We can transpose many social insect adaptive functions on to functions of interest to humans such as organizational structures, social and computer networks as well as physics and engineering. Social insect networks have been optimized by evolution to deal with multiple simultaneous constraints and principles derived from social insect systems can be used to find optimal network structures for multiple functions or under specific constraints.

Nonetheless, there are future challenges that need to be addressed in order for the use of the network framework to move forward. More and more the importance of including a temporal element to static networks is becoming evident. These can have drastic effects on results and even yield completely inverse results as in the case of specialist vs. generalist pollinators in pollination networks (See Sect. 2.2.1).

Furthermore, simply including a temporal element is insufficient. Finding and using an appropriate timescale is equally essential in drawing out accurate conclusions. In ant interaction networks, Blonder and Dornhaus [10] show that at small timescales, degree distribution is heterogeneous and some individuals are more central than others, but that at larger timescales degree distribution flattens out and becomes more uniform (See Sect. 2.1.4). If we only looked at the smaller timescale, we would conclude that some individuals are more central and perhaps act as communication hubs.

In this chapter, we have made the case for moving beyond worker–worker networks. This is an exciting avenue of network research that will open the possibility of answer novel questions. The framework surrounding bipartite networks will be especially important in advancing this burgeoning area of research.

Emerging technologies are facilitating the way social insect researchers gather and analyze data, but their development is also fostering a desire for interdisciplinary collaboration. Indeed, the need to develop time-saving technologies as well as the possibility of transposing research between fields is bringing together biologists, computer scientist, engineers, physicists, mathematicians, to name a few, and creating a synergism in research that we feel will be very exciting in years to come.

References

1. Alarcón, R., Waser, N.M., Ollerton, J.: Year-to-year variation in the topology of a plant–pollinator interaction network. *Oikos* **117**, 1796–1807 (2008). doi: 10.1111/j.0030-1299.2008.16987.x

2. Baker, H.G., Hurd, P.D.: Intrafloral ecology. *Annu. Rev. Entomol.* **13**, 385–414 (1968)
3. Barabási, A.L., Albert, R.: Emergence of scaling in random networks. *Science* **286**, 509–512 (1999)
4. Barabási, A., Bonabeau, E.: Scale-free networks. *Sci. Am.* **288**, 60–69 (2003)
5. Bascompte, J., Jordano, P.: Plant–animal mutualistic networks: the architecture of biodiversity. *Annu. Rev. Ecol. Evol. Syst.* **38**, 567–593 (2007)
6. Bascompte, J., Jordano, P., Melián, C.J., Olesen, J.M.: The nested assembly of plant–animal mutualistic networks. *Proc. Natl. Acad. Sci. USA* **100**, 9383 (2003)
7. Beckers, R., Deneubourg, J.L., Goss, S.: Trails and U-turns in the selection of a path by the ant *Lasius niger*. *J. Theor. Biol.* **159**, 397–397 (1992a)
8. Beckers, R., Deneubourg, J.L., Goss, S.: Trail laying behaviour during food recruitment in the ant *Lasius niger* (L.). *Insect. Soc.* **39**, 59–72 (1992b)
9. Beshers, S.N., Fewell, J.H.: Models of division of labor in social insects. *Annu. Rev. Entomol.* **46**, 413–440 (2001)
10. Blonder, B., Dornhaus, A.: Time-ordered networks reveal limitations to information flow in ant colonies. *PLoS ONE* **6**, e20298 (2011)
11. Blonder, B., Dornhaus, A., Wey, T.W., et al.: Temporal dynamics and network analysis. *Methods Ecol. Evol.* **3**, 958–972 (2012)
12. Bonabeau, E., Dorigo, M., Theraulaz, G.: *Swarm Intelligence: from Natural to Artificial Systems*. Oxford University Press, Oxford (1999)
13. Bonabeau, E., Sobkowski, A., Theraulaz, G., Deneubourg, J.L.: Adaptive task allocation inspired by a model of division of labor in social insects. *Biocomput. Emergent Comput.* 36–45 (1997)
14. Brooks, R.A., Flynn, A.M.: Fast, cheap and out of control. DTIC document (1989)
15. Buffin, A., Goldman, S., Deneubourg, J.L.: Collective regulatory stock management and spatiotemporal dynamics of the food flow in ants. *FASEB J.* **26**, 2725–2733 (2012). doi: 10.1096/fj.11–193698
16. Buhl, J., Gautrais, J., Deneubourg, J.L., Theraulaz, G.: Nest excavation in ants: group size effects on the size and structure of tunneling networks. *Naturwissenschaften* **91**, 602–606 (2004a)
17. Buhl, J., Gautrais, J., Louis Deneubourg, J., et al.: The growth and form of tunnelling networks in ants. *J. Theor. Biol.* **243**, 287–298 (2006). doi: 10.1016/j.jtbi.2006.06.018
18. Buhl, J., Gautrais, J., Solé, R.V., et al.: Efficiency and robustness in ant networks of galleries. *Euro. Phys. J. B Condens. Matter Complex Syst.* **42**, 123–129 (2004b)
19. Camazine, S., Deneubourg, J.L., Franks, N.R., et al.: *Self-Organization in Biological Systems*. Princeton University Press, Princeton (2003)
20. Di Caro, G., Dorigo, M.: AntNet: distributed stigmergetic control for communications networks. *J. Artif. Intell. Res.* **9** (1998)
21. Cassill, L.D., Tschinkel, W.R.: Regulation of diet in the fire ant, *Solenopsis invicta*. *J. Insect Behav.* **12**, 307–328 (1999)
22. Chapman, R.E., Bourke, A.F.G.: The influence of sociality on the conservation biology of social insects. *Ecol. Lett.* **4**, 650–662 (2001)
23. Cicirello, V.A., Smith, S.F.: Wasp-like agents for distributed factory coordination. *Auton. Agent. Multi-Agent Syst.* **8**, 237–266 (2004)
24. Dorigo, M., Gambardella, L.M., others: Ant colonies for the travelling salesman problem. *BioSystems* **43**, 73–82 (1997)
25. Dorigo, M., Stützle, T.: *Ant Colony Optimization*. MIT, Cambridge (2004)
26. Dornhaus, A., Holley, J.A., Franks, N.R.: Larger colonies do not have more specialized workers in the ant *Temnothorax albipennis*. *Behav. Ecol.* **20**, 922–929 (2009)
27. Dornhaus, A., Holley, J.A., Pook, V.G., et al.: Why do not all workers work? Colony size and workload during emigrations in the ant *Temnothorax albipennis*. *Behav. Ecol. Sociobiol.* **63**, 43–51 (2008)
28. Dunne, J.A.: *The Network Structure of Food Webs. Ecological Networks: Linking Structure to Dynamics in Food Webs*, pp. 27–86. Oxford University Press, Oxford (2006)

29. Dunne, J.A., Williams, R.J., Martinez, N.D.: Network structure and biodiversity loss in food webs: robustness increases with connectance. *Ecol. Lett.* **5**, 558–567 (2002)
30. Dupont, Y.L., Padrón, B., Olesen, J.M., Petanidou, T.: Spatio-temporal variation in the structure of pollination networks. *Oikos* **118**, 1261–1269 (2009). doi: 10.1111/j.1600-0706.2009.17594.x
31. Fewell, J.H.: Social insect networks. *Science* **301**, 1867–1870 (2003)
32. Franks, N.R., Mallon, E.B., Bray, H.E., et al.: Strategies for choosing between alternatives with different attributes: exemplified by house-hunting ants. *Anim. Behav.* **65**, 215–223 (2003)
33. Franks, N.R., Pratt, S.C., Mallon, E.B., et al.: Information flow, opinion polling and collective intelligence in house-hunting social insects. *Phil. Trans. R Soc. Lond. B* **357**, 1567–1583 (2002). doi: 10.1098/rstb.2002.1066
34. Gautrais, J., Theraulaz, G., Deneubourg, J.L., Anderson, C.: Emergent polyethism as a consequence of increased colony size in insect societies. *J. Theor. Biol.* **215**, 363–373 (2002)
35. Gordon, D.M.: *Interaction Patterns and Task Allocation in Ant Colonies*. Birkhäuser Verlag, Basel, Switzerland (1999)
36. Gordon, D.M.: The organization of work in social insect colonies. *Nature* **380**, 121–124 (1996)
37. Gordon, D.M.: *Ant encounters: Interaction Networks and Colony Behavior*. Princeton University Press, Princeton (2010)
38. Greene, M.J., Gordon, D.M.: Interaction rate informs harvester ant task decisions. *Behav. Ecol.* **18**, 451–455 (2007)
39. Grimaldi, D.A., Engel, M.S.: *Evolution of the Insects*. Cambridge University Press, Cambridge (2005)
40. Hodges, S.A., Arnold, M.L.: Columbinas: A geographically widespread species flock. *Proc. Natl. Acad. Sci. USA* **91**, 5129 (1994)
41. Holden, C.: Entomologists wane as insects wax. *Science* **246**, 754–756 (1989). doi:10.1126/science.2814497
42. Hölldobler, B., Wilson, E.O.: *The Ants*. Belknap Press of Harvard University Press, Cambridge (1990)
43. Ings, T.C., Montoya, J.M., Bascompte, J., et al.: Review: ecological networks – beyond food webs. *J. Anim. Ecol.* **78**, 253–269 (2009). doi: 10.1111/j.1365-2656.2008.01460.x
44. Jandt, J.M., Dornhaus, A.: Spatial organization and division of labour in the bumblebee *Bombus impatiens*. *Anim. Behav.* **77**, 641–651 (2009)
45. Jeanson, R.: Long-term dynamics in proximity networks in ants. *Anim. Behav.* **83**, 915–923 (2012). doi: 10.1016/j.anbehav.2012.01.009
46. Jeanson, R., Fewell, J.H., Gorelick, R., Bertram, S.M.: Emergence of increased division of labor as a function of group size. *Behav. Ecol. Sociobiol.* **62**, 289–298 (2007)
47. Jeong, H., Tombor, B., Albert, R., et al.: The large-scale organization of metabolic networks. *Nature* **407**, 651–654 (2000)
48. Johnson, B.R.: Global information sampling in the honey bee. *Naturwissenschaften* **95**, 523–530 (2008)
49. Johnson, B.R.: A Self-organizing model for task allocation via frequent task quitting and random walks in the honeybee. *Am. Nat.* **174**, 537–547 (2009)
50. Karsai, I., Wenzel, J.W.: Productivity, individual-level and colony-level flexibility, and organization of work as consequences of colony size. *Proc. Natl. Acad. Sci.* **95**, 8665 (1998)
51. Keeling, M.J., Rohani, P.: *Modeling Infectious Diseases in Humans and Animals*. Princeton University Press, Princeton (2008)
52. Khanin, R., Wit, E.: How scale-free are biological networks. *J. Comput. Biol.* **13**, 810–818 (2006)
53. Krieger, M.J.B., Billeter, J.B., Keller, L.: Ant-like task allocation and recruitment in cooperative robots. *Nature* **406**, 992–995 (2000)
54. Lanan, M.C., Dornhaus, A., Jones, E.I., et al.: The trail less traveled: individual decision-making and its effect on group behavior. *PLoS ONE* **7**, e47976 (2012). doi: 10.1371/journal.pone.0047976

55. Linksvayer, T.A., Fewell, J.H., Gadau, J., Laubichler, M.D.: Developmental evolution in social insects: regulatory networks from genes to societies. *J. Exp. Zool. B Mol. Dev. Evol.* **318**, 159–169 (2012). doi: 10.1002/jez.b.22001
56. Linksvayer, T.A., Fondrk, M.K., Page, R.E.: Honeybee social regulatory networks are shaped by colony-level selection. *Am. Nat.* **173**, E99–E107 (2009). doi: 10.1086/596527
57. Lopezaraiza-Mikel, M.E., Hayes, R.B., Whalley, M.R., Memmott, J.: The impact of an alien plant on a native plant–pollinator network: an experimental approach. *Ecol. Lett.* **10**, 539–550 (2007)
58. Lovell, J.H.: *The Flower and the Bee: Plant Life and Pollination*. C. Scribner's sons, New York (1918)
59. Lumer, E.D., Faieta, B.: Diversity and adaptation in populations of clustering ants. In: *From Animals to Animats. Proceedings of the 3rd International Conference on the Simulation of Adaptive Behavior*, pp. 501–508 (1994)
60. Maslov, S., Sneppen, K.: Specificity and stability in topology of protein networks. *Science* **296**, 910 (2002)
61. Memmott, J., Craze, P.G., Waser, N.M., Price, M.V.: Global warming and the disruption of plant–pollinator interactions. *Ecol. Lett.* **10**, 710–717 (2007)
62. Memmott, J., Waser, N.M., Price, M.V.: Tolerance of pollination networks to species extinctions. *Proc. R. Soc. Lond. B Biol. Sci.* **271**, 2605–2611 (2004)
63. Minter, N.J., Franks, N.R., Robson Brown, K.A.: Morphogenesis of an extended phenotype: four-dimensional ant nest architecture. *J. R. Soc. Interface* **9**, 586–595 (2011). doi: 10.1098/rsif.2011.0377
64. Moreau, M., Arrufat, P., Latil, G., Jeanson, R.: Use of radio-tagging to map spatial organization and social interactions in insects. *J. Exp. Biol.* **214**, 17–21 (2011)
65. Najjar, W., Gaudiot, J.L.: Network resilience: A measure of network fault tolerance. *IEEE Trans. Comput.* **39**, 174–181 (1990)
66. Nakano, T.: Biologically inspired network systems: a review and future prospects. *IEEE Trans. Syst. Man Cybern. C Appl. Rev.* 1–14 (2011)
67. Naug, D.: Structure and resilience of the social network in an insect colony as a function of colony size. *Behav. Ecol. Sociobiol.* **63**, 1023–1028 (2009). doi: 10.1007/s00265–009–0721-x
68. Naug, D.: Structure of the social network and its influence on transmission dynamics in a honeybee colony. *Behav. Ecol. Sociobiol.* **62**, 1719–1725 (2008)
69. Naug, D., Smith, B.: Experimentally induced change in infectious period affects transmission dynamics in a social group. *Proc. R. Soc. B Biol. Sci.* **274**, 61–65 (2007)
70. Van Noort, V., Snel, B., Huynen, M.A.: The yeast coexpression network has a small-world, scale-free architecture and can be explained by a simple model. *EMBO Rep.* **5**, 280–284 (2004)
71. Olesen, J.M., Bascompte, J., Elberling, H., Jordano, P.: Temporal dynamics in a pollination network. *Ecology* **89**, 1573–1582 (2008)
72. Oster, G.F., Wilson, E.O.: *Caste and Ecology in the Social Insects*. Princeton University Press, Princeton (1979)
73. Otterstatter, M.C., Thomson, J.D.: Contact networks and transmission of an intestinal pathogen in bumble bee (*Bombus impatiens*) colonies. *Oecologia* **154**, 411–421 (2007)
74. Parunak, H.V.D.: “Go to the ant”: Engineering principles from natural multi-agent systems. *Ann. Oper. Res.* **75**, 69–102 (1997)
75. Patek, S.N., Baio, J.E., Fisher, B.L., Suarez, A.V.: Multifunctionality and mechanical origins: ballistic jaw propulsion in trap-jaw ants. *Proc. Natl. Acad. Sci. USA* **103**, 12787–12792 (2006). doi:10.1073/pnas.0604290103
76. Perna, A., Jost, C., Couturier, E., et al.: The structure of gallery networks in the nests of termite *Cubitermes* spp. revealed by X-ray tomography. *Naturwissenschaften* **95**, 877–884 (2008a)
77. Perna, A., Valverde, S., Gautrais, J., et al.: Topological efficiency in three-dimensional gallery networks of termite nests. *Phys. A Stat. Mech. Appl.* **387**, 6235–6244 (2008b). doi: 10.1016/j.physa.2008.07.019
78. Petanidou, T., Kallimanis, A.S., Tzanopoulos, J., et al.: Long-term observation of a pollination network: fluctuation in species and interactions, relative invariance of network

- structure and implications for estimates of specialization. *Ecol. Lett.* **11**, 564–575 (2008). doi: 10.1111/j.1461-0248.2008.01170.x
79. Pie, M.R., Rosengaus, R.B., Traniello, J.F.A.: Nest architecture, activity pattern, worker density and the dynamics of disease transmission in social insects. *J. Theor. Biol.* **226**, 45–51 (2004). doi: 10.1016/j.jtbi.2003.08.002
80. Pinter-Wollman, N., Wollman, R., Guetz, A., et al.: The effect of individual variation on the structure and function of interaction networks in harvester ants. *J. R. Soc. Interface* **8**, 1562–1573 (2011). doi: 10.1098/rsif.2011.0059
81. Poff, C., Nguyen, H., Kang, T., Shin, M.C.: Efficient Tracking of Ants in Long Video with GPU and Interaction (2012)
82. Powell, S., Tschinkel, W.R.: Ritualized conflict in *Odontomachus brunneus* and the generation of interaction-based task allocation: a new organizational mechanism in ants. *Anim. Behav.* **58**, 965–972 (1999)
83. Pratt, S.C., Sumpter, D.J.T.: A tunable algorithm for collective decision-making. *PNAS* **103**, 15906–15910 (2006). doi: 10.1073/pnas.0604801103
84. Quitmeyer, A., Balch, T.: Biotrack Pack 1.5. In: Bio-Tracking. <http://www.bio-tracking.org/biotrackpack/>
85. Retana, J., Cerdá, X.: Social Organization of *Cataglyphis cursor* Ant Colonies (Hymenoptera, Formicidae): Inter-, and Intraspecific Comparisons. *Ethology* **84**, 105–122 (1990). doi: 10.1111/j.1439-0310.1990.tb00788.x
86. Robertson, C.: Flowers and Insects: Lists of Visitors to Four Hundred and Fifty-Three Flowers. C. Robertson. National Center for Ecological Analysis and Synthesis Interaction, Carlinville, IL (1929). Web Database: http://www.nceas.ucsb.edu/interactionweb/html/robertson_1929.html. Keywords: Lists plant–pollinator interactions for 456
87. Robinson, E.J.H., Smith, F.D., Sullivan, K.M.E., Franks, N.R.: Do ants make direct comparisons? *Proc. R. Soc. B* (2009). doi: 10.1098/rspb.2009.0350
88. Rueppell, O., Kirkman, R.W.: Extraordinary starvation resistance in *Temnothorax rugatulus* (Hymenoptera, Formicidae) colonies: Demography and adaptive behavior. *Insect. Soc.* **52**, 282–290 (2005). doi: 10.1007/s00040-005-0804-2
89. Samways, M.J.: Insects in biodiversity conservation: some perspectives and directives. *Biodivers. Conserv.* **2**, 258–282 (1993)
90. Schwander, T., Rosset, H., Chapuisat, M.: Division of labour and worker size polymorphism in ant colonies: the impact of social and genetic factors. *Behav. Ecol. Sociobiol.* **59**, 215–221 (2005)
91. Seeley, T.D., Kolmes, S.A.: Age polyethism for hive duties in honey bees — illusion or reality? *Ethology* **87**, 284–297 (1991). doi: 10.1111/j.1439-0310.1991.tb00253.x
92. Sendova-Franks, A.B., Franks, N.R.: Spatial relationships within nests of the ant *Leptothorax unifasciatus* (Latr.) and their implications for the division of labour. *Anim. Behav.* **50**, 121–136 (1995)
93. Sendova-Franks, A.B., Hayward, R.K., Wulf, B., et al.: Emergency networking: famine relief in ant colonies. *Anim. Behav.* **79**, 473–485 (2010)
94. Sole, R.V., Montoya, M.: Complexity and fragility in ecological networks. *Proc. R. Soc. Lond. B Biol. Sci.* **268**, 2039–2045 (2001)
95. Sueur, C., Jacobs, A., Amblard, F., et al.: How can social network analysis improve the study of primate behavior? *Am. J. Primatol.* **73**, 703–719 (2011)
96. The World Conservation Union: IUCN red list of threatened species. Summary Statistics for Globally Threatened Species (2010)
97. Thomas, M.L., Elgar, M.A.: Colony size affects division of labour in the ponerine ant *Rhytidoponera metallica*. *Naturwissenschaften* **90**, 88–92 (2003)
98. Tong, A.H.Y., Lesage, G., Bader, G.D., et al.: Global mapping of the yeast genetic interaction network. *Science STKE* **303**, 808 (2004)
99. Waser, N.M., Chittka, L., Price, M.V., et al.: Generalization in pollination systems, and why it matters. *Ecology* **77**, 1043–1060 (1996). doi: 10.2307/2265575

100. Waters, J.S., Fewell, J.H.: Information processing in social insect networks. *PLoS ONE* **7**, e40337 (2012). doi: 10.1371/journal.pone.0040337
101. Watts, D.J., Strogatz, S.H.: Collective dynamics of “small-world” networks. *Nature* **393**, 440–442 (1998)
102. Weiss, G.: *Multiagent Systems a Modern Approach to Distributed Artificial Intelligence*. MIT, Cambridge (1999)
103. Wey, T., Blumstein, D.T., Shen, W., Jordán, F.: Social network analysis of animal behaviour: a promising tool for the study of sociality. *Anim. Behav.* **75**, 333–344 (2008)
104. Wilson, E.O.: *Ants*. Bull. Am. Acad. Arts Sci. **45**, 13–23 (1991)
105. Wilson-Rich, N., Spivak, M., Fefferman, N.H., Starks, P.T.: Genetic, individual, and group facilitation of disease resistance in insect societies. *Annu. Rev. Entomol.* **54**, 405–423 (2009). doi: 10.1146/annurev.ento.53.103106.093301
106. Wuchty, S., Ravasz, E., Barabási, A.L.: The architecture of biological networks. *Complex Syst. Sci. Biomed.* 165–181 (2006)

Self-Exciting Point Process Modeling of Conversation Event Sequences

Naoki Masuda, Taro Takaguchi, Nobuo Sato, and Kazuo Yano

Abstract Self-exciting processes of Hawkes type have been used to model various phenomena including earthquakes, neural activities, and views of online videos. Studies of temporal networks have revealed that sequences of social interevent times for individuals are highly bursty. We examine some basic properties of event sequences generated by the Hawkes self-exciting process to show that it generates bursty interevent times for a wide parameter range. Then, we fit the model to the data of conversation sequences recorded in company offices in Japan. In this way, we can estimate relative magnitudes of the self excitement, its temporal decay, and the base event rate independent of the self excitation. These variables highly depend on individuals. We also point out that the Hawkes model has an important limitation that the correlation in the interevent times and the burstiness cannot be independently modulated.

1 Introduction

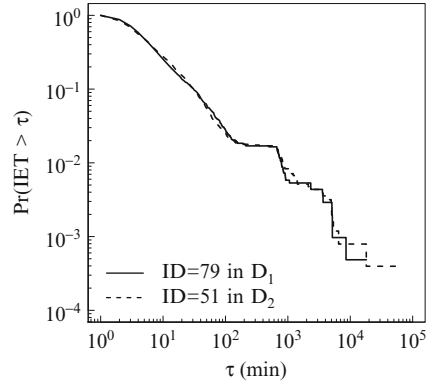
1.1 Temporal Networks

Social networks, which specify the pairs of individuals that are directly connected and those that are not, are substrates of social interactions. An important caveat in the use of social networks for understanding social behavior is that the pair of

N. Masuda (✉) · T. Takaguchi
Department of Mathematical Informatics, The University of Tokyo, 7-3-1 Hongo, Bunkyo,
Tokyo 113-8656, Japan
e-mail: masuda@mist.i.u-tokyo.ac.jp; taro.takaguchi@mist.i.u-tokyo.ac.jp

N. Sato · K. Yano
Central Research Laboratory, Hitachi, Ltd., 1-280 Higashi-Koigakubo, Kokubunji-shi,
Tokyo 185-8601, Japan
e-mail: nobuo.sato.jn@hitachi.com; kazuo.yano.bb@hitachi.com

Fig. 1 Survivor functions of the IET (i.e., probability that the IET is larger than τ) for the conversation sequences of two individuals. For each of D_1 and D_2 , the individual with the largest number of events is selected. The selected individuals in D_1 and D_2 have 2,397 and 2,886 events, respectively



directly connected individuals does not interact all the time. Social events between a pair of individuals, such as dialogues and transmission of email, are better described as a sequence of events, i.e., a collection of tagged event times, where the tag includes, for example, the identity of the two individuals, type of the event, duration, and content of dialogues. In fact, recent massive data, mostly online, and technological developments of recording devices for offline social interaction enable recording of social events with a higher temporal (and spatial) precision than before. Examples of data taken in this domain include calling activity [2], web recommendation writing [15], email traffic [1, 7, 21], online forum dealing with sexual escorts [32], human interactions in the real space [3, 16, 17, 33], to name a few. Transmission of infection or information may occur only during the period in which two individuals are involved in an event. A set of such event sequences among pairs of individuals are collectively called the temporal network [14], which is the focus of this volume. Computational models that generate realistic event sequences possessing properties such as those described in Sects. 1.2 and 1.3 would help us understand the nature of human communication behavior.

1.2 Long-tailed Interevent Time Distribution

In many empirical event sequences that we would like to model, interevent times are distributed according to a long-tailed distribution. The survivor functions (also called the complementary cumulative distributions) of IET (i.e., the probability that the IET is larger than a given value τ), are shown in Fig. 1 for two individuals in the data sets used in our previous study [33, 34] (see Sect. 4.1 for descriptions of the data).

Different mechanisms seem to explain the non-Poissonian behavior of the IET. A first mechanism that was discovered to generate power-law IET distributions is a priority queue model [1]. In this class of models, each task corresponding to an event carries a priority level and arrives at a queue. Then, the queue tends to execute

tasks with high priority; tasks with low priority are made to wait for a long time before being executed. The priority queue model has also been extended to allow for interaction of two priority queues between a pair of interacting individuals [18, 23, 28, 38]. However, some types of social interaction including conversations may not proceed like a queue. Therefore, we attempt an alternative approach in the present chapter.

1.3 IET Correlation

Another facet of actual event sequences is that they often possess positive temporal correlation. In other words, a long (short) IET is likely to be followed by a long (short) IET. This is the case even if the effect of circadian fluctuations is removed from data [19]. Although there are various methods to measure temporal correlation of the IET [8, 19], here we show it by simply measuring the conditional mean IET defined by

$$\tau^{\text{next}}(\tau) \equiv \langle \tau_{i+1} \rangle_{\tau_i \leq \tau}, \quad (1)$$

where τ_i is the i th IET in a sequence, and $\langle \cdot \rangle$ represents the average. If the IET correlation is absent, $\tau^{\text{next}}(\tau)$ is independent of τ .

The values of τ^{next} are plotted against τ in Fig. 2a–c for the conversation sequences used in Fig. 1, times of email sending and receiving in a university [6], and times of online sexual escorts by male individuals [32], respectively. We remark that long-tailed IET distributions are known for the email [1, 35] and sexual escort [32] data sets. The conditional mean IET τ^{next} increases with τ in Fig. 2a, b. Therefore, adjacent IETs are positively correlated. In Fig. 2c, τ^{next} decreases with τ for $\tau \leq 7$ and increases with τ for $\tau \geq 7$. Figure 2c suggests that those who have bought an escort tend to avoid buying a next escort within a week. This is directly shown in Fig. 2d, which shows the IET distribution. However, adjacent IETs for the sexual escort data are positively correlated on a longer time scale (Fig. 2c).

In the discrete time model proposed in [10], the probability of an event occurrence decreases if events occurred too frequently in the recent past and increases if the time since the last event becomes long. Such a mechanism may generate positive IET correlation.

1.4 Self-excitatory Stochastic Processes

An alternative mechanism that yields positive IET correlation is self-excitation. The idea is that once an individual talks with somebody, the individual is excited to talk with somebody with a higher rate. Malmgren and coworkers developed such models and applied to data [21, 22].

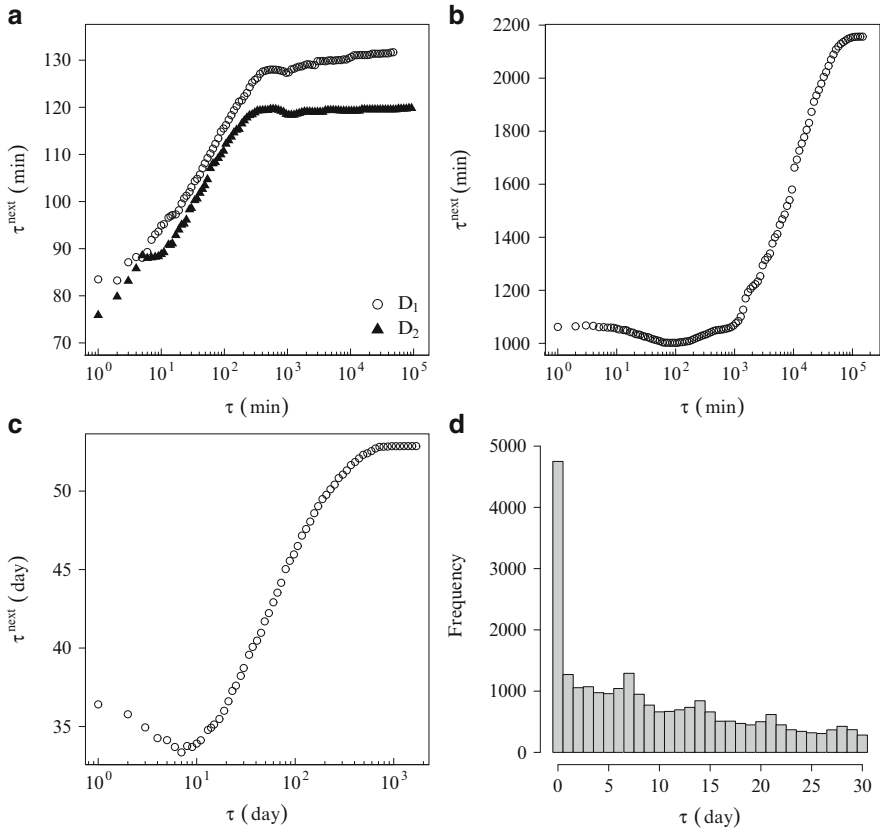


Fig. 2 Conditional mean IET defined by (1) for (a) conversation event sequences [33], (b) email logs [6], and (c) purchase of sexual escorts [32]. (d) Histogram of the IET for the data shown in (c)

In the cascading nonhomogeneous Poisson process proposed in [21], the authors assumed that the primary process is an inhomogeneous Poisson process with a periodic event rate. An event generated from the primary process is assumed to elevate the system to the active state and trigger cascades of activity. In other words, after a trigger event, a burst of events may ensue as a result of the Poisson process with a rate that is larger than the base rate of the primary process. The entire recording period is divided into alternately appearing intervals of the active state with a high event rate and the normal state with a low event rate by an adjustment of the position and number of intervals to yield a good fit to the data. As a result, the number of events contained in a burst is shown to obey an approximate exponential distribution (also see [19], which shows that the number of events in a burst obeys a power law distribution; the definition of burst is different in the two papers). With a circadian and weekly rate modulation, the cascading nonhomogeneous Poisson process is capable of producing the long-tailed IET distributions observed in the data.

Their model has many parameters to be estimated. This is common to their another model proposed in [22]. In [22], letter writing activity of each renowned individual is fitted by a cascading Poisson process model. The time unit is set to a day. The two parameters, i.e., the base event rate and tendency to write an additional letter within a time unit, are estimated on the basis of the data. Because the different parameter values are assumed for different sections of the data, the number of the parameters in the model can be large. In the case of the letter correspondence by Einstein, data are collected over 54 years, and the two parameters are estimated for each year. Therefore, there are 108 parameters.

These models [21, 22] are quite successful in capturing properties of the real event sequences. Nevertheless, it may be also fruitful to consider a much simpler self-excitatory model as a complementary approach to capture the origins of bursts (Sect. 1.2) and IET correlation (Sect. 1.3) inherent in human behavior.

A simple two state model in which normal and excited states are assumed is proposed in [19]. The model is not a hidden Markov model because the probability of staying in the excited state becomes large as the number of events that have already occurred in the current burst increases. The model reproduces properties of the original data such as the power-law IET distribution and autocorrelation function. However, statistical methods to estimate the model parameters from the data were not presented [19].

1.5 Our Approach: Hawkes Process

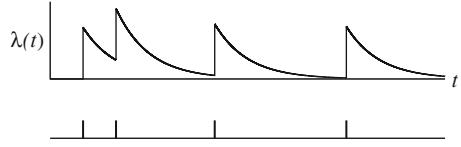
In this chapter, we fit the self-excitatory point process model called the Hawkes process [11–13, 36] to the data recorded in company offices [33, 34, 37, 39] (also see Figs. 1 and 2a). A main benefit for using the Hawkes process is that it contains a small number of parameters and is mathematically tractable; the maximum likelihood (ML) method for inferring parameter values is established for some important special cases [29].

This chapter is organized as follows. In Sect. 2, we introduce the Hawkes model and recapitulate its basic mathematical properties. In Sect. 3, we numerically investigate properties of event sequences generated by the Hawkes process. In Sect. 4, we carry out the ML estimation of the parameters of the Hawkes model and compare the data and the estimated model. In Sect. 5, we discuss the results, with an emphasis on the limitation and possible extensions of the Hawkes model for better describing human data. Mathematical details are delegated to two Appendices.

2 Hawkes Process

The Hawkes process is a self-exciting point process model that is analytically tractable. It is an inhomogeneous Poisson process in which the instantaneous event rate depends on the history of the time series of events. It is not a renewal process. The event rate at time t , denoted by $\lambda(t)$ is given by

Fig. 3 Example time course of event rate $\lambda(t)$ and the corresponding event sequence



$$\lambda(t) = \nu + \sum_{i, t_i \leq t} \phi(t - t_i), \quad (2)$$

where t_i is the time of the i th event, and $\phi(t)$ is the memory kernel, i.e., the additional rate incurred by an event. The causality implies $\phi(t) = 0$ ($t < 0$).

The Hawkes process has been used for modeling, for example, seismological data [26, 36], video viewing activities [4, 24], neural spike trains [30], and genomic data [31]. For example, in [4], time series of views of different videos on YouTube were categorized into three classes, which were characterized by different $\phi(t)$ and different time-dependent versions of ν . The Hawkes process has also been used to construct a method to estimate the structure of neural networks from given spike trains [5], analyze auto and cross correlation in data recorded from mouse retina [20], and understand the correlation between the activities of different neurons in pulse-coupled model networks of excitatory and inhibitory neurons [30]. In [31], the Hawkes process is used to model stochastic occurrences of specific genes on DNA sequences. The method to estimate a piecewise linear $\phi(t)$ based on the least square error was presented.

Depending on applications, the memory kernel $\phi(t)$ has been assumed to be a hyperbolic (i.e., power law) function [4] or a superposition of the gamma function [26]. Nevertheless, in the present work, we simply set

$$\phi(t) = \alpha e^{-\beta t} (t \geq 0) \quad (3)$$

for the following reasons. First, it allows the ML estimation of the parameters α , β , and ν [29]. Second, the Hawkes process with (3) has a small number of parameters as compared to competitive models with self excitation [21, 22, 26, 27]. It should be noted that (3) indicates that the self-exciting effect of an event decays in time. It is contrasted with a previous model in which the self-exciting effect is constant for some time and then the event rate returns to the basal rate [21]. An example time course of the event rate $\lambda(t)$ and the corresponding event sequence are shown in Fig. 3.

We define cluster of events as the set of events that are triggered by a single event occurring at the basal rate ν . In other words, all the events in a cluster are descendants of the trigger event. The expected cluster size is given by [12, 36]

$$c = \int_0^{\infty} \phi(t) dt = \frac{1}{1 - \frac{\alpha}{\beta}}, \quad (4)$$

and the stationary event rate is given by

$$\bar{\lambda} = c\nu = \frac{\nu}{1 - \frac{\alpha}{\beta}}. \quad (5)$$

The convergence of the event rate requires $\alpha < \beta$.

3 Numerical Results for Statistics of IET

In this section, we numerically examine basic properties of the Hawkes process with the exponential memory kernel. To quantify the broadness of the IET distribution, we measure the coefficient of variation (CV), defined as the standard deviation of the IET divided by the mean of the IET as follows:

$$\text{CV} = \frac{\sqrt{\sum_{i=1}^N (\tau_i - \langle \tau \rangle)^2 / N}}{\langle \tau \rangle}, \quad (6)$$

where N is the number of IETs in a given sequence and $\langle \tau \rangle \equiv \sum_{i=1}^N \tau_i / N$ is the mean IET. It should be noted that $\langle \tau \rangle$ in the limit $N \rightarrow \infty$ is equal to $1/\bar{\lambda} = (1 - \alpha/\beta)/\nu$. The Poisson process yields $\text{CV} = 1$.

We also measure the correlation coefficient for the IET [8] defined as

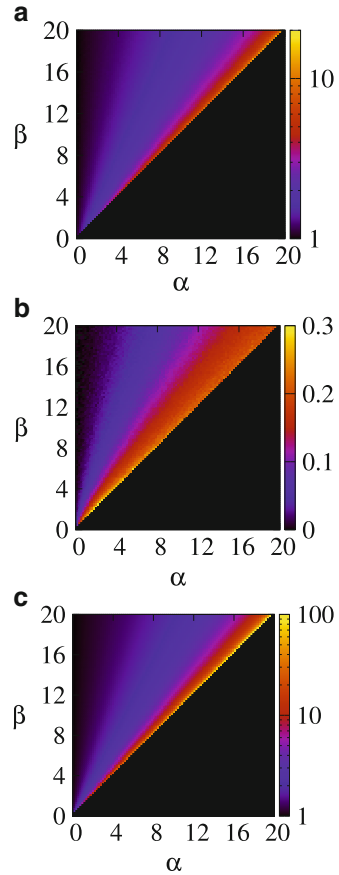
$$\frac{\sum_{i=1}^{N-1} (\tau_i - \langle \tau \rangle)(\tau_{i+1} - \langle \tau \rangle) / (N-1)}{\sum_{i=1}^N (\tau_i - \langle \tau \rangle)^2 / N}. \quad (7)$$

The Hawkes process is invariant under the following rescaling of the time and parameter values: $Ct = t'$, $\alpha = C\alpha'$, $\beta = C\beta'$, and $\nu = C\nu'$, where $C > 0$ is a constant. Therefore, we normalize the time by setting $\nu = 1$ and vary α and β . The values of CV, IET correlation, and mean cluster size c are invariant under this rescaling. For a given pair of α and β values, we generate a time series with 2×10^5 events using the method described in [25] and calculate the statistics of the IET.

The values of CV, IET correlation, and c (4) for various α and β values are shown in Fig. 4a, 4b, and 4c, respectively. Although we can more theoretically calculate CV using the expression of the IET distribution [13] (also see Appendix 1 for details), it is numerically demanding to do so. Therefore, we resorted to direct numerical simulations. The data are present only in the region $\alpha < \beta$, where the Hawkes process does not explode.

Figure 4a indicates that the Hawkes process generates a wide range of CV. A large value of $\alpha/\beta (< 1)$ yields a large CV value. This is the case for both small and

Fig. 4 Statistics of the IET obtained from the Hawkes process. **(a)** CV, **(b)** IET correlation, and **(c)** mean cluster size c for various values of α and β

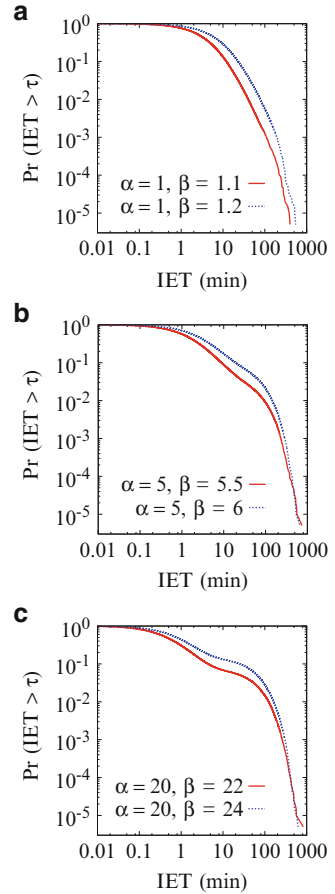


large α values. In Fig. 5, the survival function of the IET on the basis of 2×10^5 events is compared for different α and β values that satisfy $\beta = 1.1\alpha$ or 1.2α . Although the CV values are large, the IET distributions are consistently different from power law distributions. In particular, the IET distribution seems to be a superposition of multiple distributions with different time scales when α is large (Fig. 5c). It should be noted that we assumed the exponential, not long-tailed, memory kernel (3).

Figure 4b indicates that a large α/β value also yields a large IET correlation. Once the event rate increases because of recent occurrences of other events, the following IET tends to be small. Therefore, strong self-excitation in the model (i.e., large α/β) is considered to cause large IET correlation. The strength of self-excitation can be also quantified by c . Figure 4c indicates that a large α/β tends to yield a large c .

Figure 4a–c look similar, suggesting that the three quantities are correlated with each other.

Fig. 5 Survivor functions of the IET for the Hawkes process with different values of α and β



4 Fitting the Hawkes Process to the Data

4.1 Data Sets

We analyze two data sets D_1 and D_2 of face-to-face interaction logs obtained from different company offices in Japan. World Signal Center, Hitachi, Ltd., Japan collected the data using the Business Microscope system developed by Hitachi, Ltd., Japan. For technical details concerning the data collection, see [33, 37, 39]. We previously analyzed the data using different methods [33, 34]. Data sets D_1 and D_2 consist of recordings from 163 individuals for 73 days and 211 individuals for 120 days, respectively. The two individuals are defined to be involved in a conversation event, simply called the event, if their modules exchange the IDs at least once in a minute. The module has other types of data that we do not use in the present study,

such as the list of conversation partners and the duration of each event. In total, D_1 and D_2 contain 51,879 and 125,345 events, respectively.

4.2 Results of Fitting

For the entire sequence of event times obtained for each individual, we carry out the ML estimation of the parameters of the Hawkes process with the exponential memory kernel. It should be noted that we use the information about event times and not the duration of events or the partners' IDs. We slightly modify the ML method developed in [29] (see Appendix 2 for details).

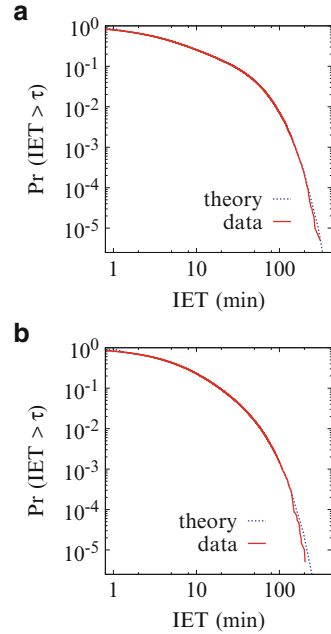
The modification is concerned with the treatment of the data during the night. Our data are nonstationary owing to the circadian and weekly rhythms. Therefore, direct application of the Hawkes process, which is a stationary point process, is invalid. In the previous literature in which different models are investigated, these rhythms are explicitly modeled [9, 21] or treated by dynamically changing the time scale according to the event rate [18]. In contrast, we omit the night part of the data from the analysis because our data are collected in company offices and therefore there is no event from late in the night through early in the morning.

In both data sets D_1 and D_2 , there is nobody in the office between four and six in the morning. Accordingly, we can partition the data into workdays without ambiguity. For each individual, we discard the workdays that contain less than 40 conversation events. We call a workday containing at least 40 events the valid day. Then, we define the first event in each valid day as trigger event and set $t = 0$. The following events on the same valid day are interpreted to be generated from the Hawkes process. The time of the last event denoted by t_{last} (denoted by $t_{N_d}^d$ in Appendix 2) is defined to be the end time of the valid day; it is necessary to specify t_{last} to apply the ML method (Appendix 2). The value of t_{last} depends on individuals even on the same day. The individual may stay in the office for a considerable amount of time after $t = t_{\text{last}}$ before leaving the office. This implies that the individual does not have conversations with others remaining in the office between $t = t_{\text{last}}$ and the time when the individual leaves the office. If this is the case, the fact that this individual does not have events for $t > t_{\text{last}}$ may affect the ML estimators. Nevertheless, we neglect this point. Finally, we obtain the likelihood of the series of events for an individual by multiplying the likelihood for all the valid days.

We apply the ML method to the individuals that possess at least 300 valid IETs (i.e., IETs derived from the valid days) during the entire period. This thresholding leaves 63 individuals in D_1 and 148 individuals in D_2 . We also exclude one individual in D_1 because the ML method does not converge for this individual.

The survivor function of the IET is compared between the data and the estimated Hawkes process in Fig. 6. The comparison is made for an individual in D_1 (Fig. 6a) and an individual in D_2 (Fig. 6b). We calculated the IET distribution for the estimated model using the theoretical method [13] (Appendix 1). The agreement between the IET distributions of the data and the estimated model is excellent.

Fig. 6 Survivor functions of the IET for two individuals. (a) Results for an individual in D_1 , who has 1,694 valid IETs during the recording period. The ML estimators are given by $\alpha = 4.91$, $\beta = 7.89$, and $\nu = 2.18$. (b) Results for an individual in D_1 , who has 1,765 valid IETs. The ML estimators are given by $\alpha = 2.45$, $\beta = 3.86$, and $\nu = 2.77$

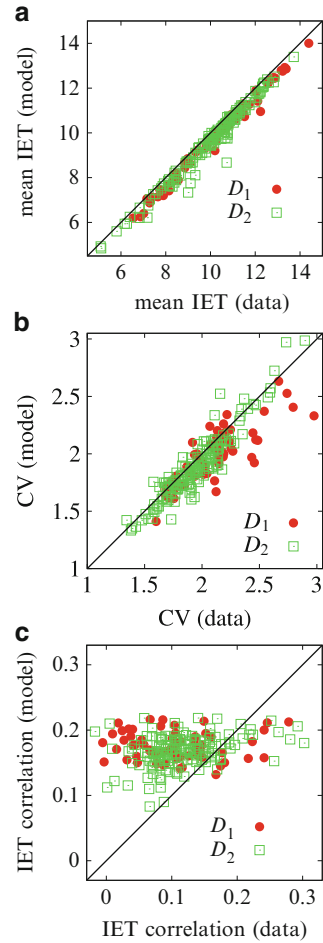


To assess the quality of the fit at a population level, we compare three statistics of the IET between the data and model for different individuals. The relationship between the mean IET obtained from the data and that obtained from the estimated model, i.e., $1/\bar{\lambda} = (1 - \alpha/\beta)/\nu$, is shown in Fig. 7a. For different individuals in both data sets, the mean IET is close between the data and the model. The Pearson correlation coefficient between the data and model are equal to 0.993 and 0.986 for D_1 and D_2 , respectively. However, the Hawkes process slightly underestimates the mean IET.

The CV values for the data and the estimated model are compared in Fig. 7b. We calculated the CV values for the estimated model on the basis of 2×10^5 events that we obtained by simulating the Hawkes process with the ML estimators α , β , and ν . Although the CV can be theoretically calculated using the ML estimators (Appendix 1), we avoided doing so because the theoretical method is computationally too costly to be applied to all the individuals. Roughly speaking, the CV values obtained from the model are close to those of the data. The Pearson correlation coefficient between the data and model are equal to 0.832 and 0.936 for D_1 and D_2 , respectively.

The IET correlation of the data and that for the estimated model are compared in Fig. 7c. We calculated the IET correlation for the estimated model by direct numerical simulations, as in the case of the CV. Figure 7c indicates that the Hawkes process does not reproduce the IET correlation for most individuals. The IET correlation for the estimated model is distributed in a much narrower range than that of the data. This is consistent with the finding that the CV and the IET correlation are positively correlated in the Hawkes process (Sect. 3). Because most individuals

Fig. 7 Comparison between the data and the estimated model. **(a)** mean IET, **(b)** CV, and **(c)** IET correlation. Each data point corresponds to one valid individual. The mean IET, CV, and IET correlation for the data are calculated on the basis of the days containing at least 40 events

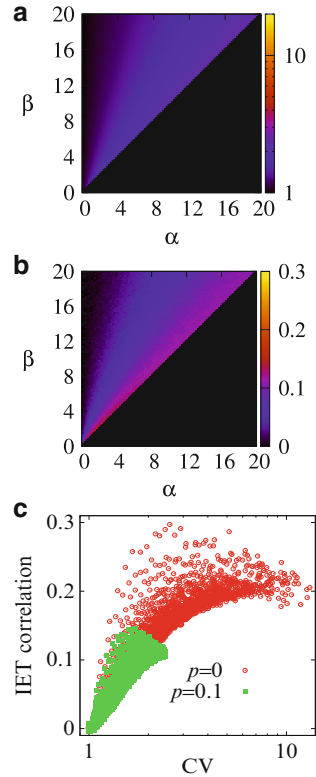


have the CV values larger than unity (Fig. 7b), the estimate of the IET correlation obtained by the model tends to be positive regardless of the estimated values of α , β , and ν . Figure 7c suggests that the Hawkes process with the exponential memory kernel is incapable of approximating the real data in terms of the IET correlation.

5 Discussion

We analyzed properties of the IET generated by the Hawkes process with an exponential memory kernel and then fitted the model to the face-to-face interaction logs obtained from company offices. The model successfully reproduced the data in

Fig. 8 Results for the modified Hawkes process with $\nu = 1$. **(a)** CV with $p = 0.1$. **(b)** IET correlation with $p = 0.1$. **(c)** Relationship between the CV and IET correlation with $p = 0$ and $p = 0.1$



terms of the IET distribution. However, the model does not explain the behavior of the IET correlation in the data.

This limitation may be because the effect of self-excitation is too strong in the Hawkes process; the event rate can be very large after a burst of events. To examine this issue, we carry out additional numerical simulations using a modified Hawkes model. We modify the model such that after each event that would increase the event rate by $\phi(0)$ in the original Hawkes process, we reset the event rate to the basal value ν with probability p . The original Hawkes process corresponds to $p = 0$. The CV and IET correlation for $p = 0.1$ and various values of α and β are shown in Fig. 8a and 8b, respectively. The values of the CV and IET correlation for $p = 0.1$ are much smaller than those for $p = 0$ (Fig. 4a, b). This is because a burst, which increases the CV and IET correlation in the Hawkes model, is forced to terminate with probability p after each event in the modified model. The CV and IET correlation values for $(\alpha, \beta) = (0.2i, 0.2j)$, where $0 \leq i < j < 100$ are plotted in Fig. 4c. For comparison, the corresponding results for $p = 0$ on the basis of the data used in Fig. 4a, b are also shown in the figure. The introduction of $p > 0$ does not decorrelate the CV and IET correlation. To explain the behavior of the IET correlation in the present data, we need different models. It seems that the

IET correlation has not been discussed in the context of social interaction data, with a notable exception [19]. We are interested in the capabilities of alternative models [10, 21, 22] in reproducing the IET correlation in the data.

In the present study, we used the exponential memory kernel because it is analytically tractable and contains only three parameters. The original Hawkes process with other memory kernels has also been applied to data [4, 26]. The ML method is available also for this case [26]. Nevertheless, we suspect that self-excitation inherent in the Hawkes process induces both high CV and positive IET correlation for a variety of memory kernels. Therefore, the use of different memory kernel may not improve the fit of the Hawkes process to our data in terms of the IET correlation.

Two-state models [19, 21, 22], in which events are produced at high and low rates in the excited and normal states, respectively, are also self-exciting. These models may be more realistic for social data than the standard Hawkes process used in this work in the sense that humans may not distinguish many different levels of self-excitation as is assumed in the Hawkes process. On the other hand, the Hawkes process with the exponential memory kernel is simpler than these models such that the ML methods are available and the parameters have simple physical meanings. Although the model by Malmgren and colleagues allows for the ML method [21], the method is quite complicated and contains many parameters. It may be desirable to develop two-state models that are simple and allow for statistical methods. Alternatively, it may be desirable to modify the Hawkes process to account for the behavior of the IET correlation in the real data.

We lack methods to compare the goodness of fit of different models, except that it is straightforward to test the validity of a model against the Poisson process (but see [21]). We need develop goodness of fit tests to compare the performance of models proposed in different papers.

Appendix 1: IET Distribution of the Hawkes Process

In this section, we explain the derivation of the IET distribution of the Hawkes process shown in [13]. Also see [36] for introduction to mathematical treatments of the Hawkes and related processes.

Consider a trigger event at $t = 0$ and the inhomogeneous Poisson process with rate function $\phi(t)$, i.e., the point process directly induced by the trigger event. The probability generating functional (PGFL) for this inhomogeneous Poisson process, denoted by H , is given by

$$\begin{aligned} H(z(\cdot)) &\equiv E \left(\prod_{i \geq 1} z(t_i) \right) \\ &= \exp \left\{ \int_0^\infty [z(t) - 1] \phi(t) dt \right\}, \end{aligned} \quad (8)$$

where $z(t)$ is a carrying function, and t_i is the time of the i th event. We define $t_0 = 0$.

The events at $t = t_i$ may induce further events. On the basis of (8), the PGFL for the inhomogeneous Poisson process including all the descendant events induced by a trigger event at $t = 0$, denoted by F , is given through the following recursive relation:

$$F(z(\cdot)) = z(0) \exp \left\{ \int_0^\infty [F(z_t(\cdot)) - 1] \phi(t) dt \right\}, \tag{9}$$

where $z_t(t') \equiv z(t' + t)$ is the time translation. On the right-hand side of (9), $z(0)$ accounts for the trigger event at $t = 0$, and $F(z_t(\cdot))$ accounts for the fact that an event triggered at time t initiates an inhomogeneous Poisson process with rate $\phi(t)$ on top of the other inhomogeneous Poisson processes going on.

We obtain the PGFL for the entire Hawkes process, denoted by G , by combining Eq. (9) and the PDFL of the homogeneous Poisson process with rate ν as follows:

$$G(z(\cdot)) = \exp \left\{ \int_{-\infty}^\infty \nu [F(z_t(\cdot)) - 1] dt \right\}. \tag{10}$$

We set $z(t) = \tilde{z}$ for $t_s \leq t \leq t_s + \Delta$ and $z(t) = 1$ otherwise. Then, $\pi(t_s, \Delta, \tilde{z}) \equiv F(z(\cdot))$ is the probability generating function (PGF) for the number of events in $[t_s, t_s + \Delta]$, with the carrying variable \tilde{z} , and

$$\pi(t_s - t, \Delta, \tilde{z}) = F(z_t(\cdot)) \tag{11}$$

is the PGF for the number of events in $[t_s - t, t_s - t + \Delta]$. Equation (9) is reduced to

$$\pi(t_s, \Delta, \tilde{z}) = \begin{cases} \exp \left\{ \int_0^{t_s+\Delta} [\pi(t_s - t, \Delta, \tilde{z}) - 1] \phi(t) dt \right\}, & t_s > 0, \\ \tilde{z} \exp \left\{ \int_0^{t_s+\Delta} [\pi(t_s - t, \Delta, \tilde{z}) - 1] \phi(t) dt \right\}, & -\Delta \leq t_s \leq 0, \\ 1, & t_s < -\Delta. \end{cases} \tag{12}$$

By setting $t_s = 0$ and combining (10) and (11), we obtain the PGF for the number of events in $[0, \Delta]$ as

$$Q_\Delta(\tilde{z}) \equiv G(z(\cdot)) = \exp \left\{ \int_{-\infty}^\Delta \nu [\pi(-t, \Delta, \tilde{z}) - 1] dt \right\}. \tag{13}$$

In particular,

$$\tilde{\pi}(t_s, \Delta) \equiv \pi(t_s, \Delta, 0) \tag{14}$$

is the probability that there is no event in $[t_s, t_s + \Delta]$ for a cluster of events originating at $t = 0$. Using (12), we obtain

$$\tilde{\pi}(t_s, \Delta) = \begin{cases} \exp \left\{ \int_0^{t_s + \Delta} [\tilde{\pi}(t_s - t, \Delta) - 1] \phi(t) dt \right\}, & t_s > 0, \\ 0, & -\Delta \leq t_s \leq 0, \\ 1, & t_s < -\Delta. \end{cases} \quad (15)$$

By setting $\tilde{z} = 0$ in (13) and using (15), we obtain the survivor function of the forward recurrence time, i.e., time to the next event from arbitrary t , as follows:

$$Q_\Delta(0) = \Pr(\text{forward recurrence time} > \Delta) = \exp \left\{ -\nu \Delta - \nu \int_0^\infty [1 - \tilde{\pi}(t, \Delta)] dt \right\}, \quad (16)$$

where \Pr denotes probability. $Q_\Delta(0)$ is the probability that the Hawkes process does not have any event in $[0, \Delta]$.

Finally, the distribution of the interevent time τ is given in the form of survivor function as

$$\Pr(\tau > t) = -\frac{dQ_\Delta(0)(t)}{dt} \Big/ \bar{\lambda}, \quad (17)$$

where the stationary event rate $\bar{\lambda}$ is given by (5).

In the numerical simulations, we adopted the Simpson's rule for calculating integrals in (15) and (16), and solved (15) by iteration.

We remark that integration of (17) by part leads to

$$\langle \tau \rangle = \frac{1}{\bar{\lambda}} \quad (18)$$

and

$$\langle \tau^2 \rangle = \frac{2}{\bar{\lambda}} \int_0^\infty Q_\Delta(0)(t) dt. \quad (19)$$

Equations (18) and (19) can serve to calculate the CV. However, we did not use them and obtained the CV by direct numerical simulations because calculating the CV via (18) and (19) is time consuming.

Appendix 2: ML Method for the Hawkes Process

In this section, we explain a slightly modified version of the ML method for the Hawkes process with the exponential memory kernel originally proposed in [29].

We let the event times be $0 \leq t_1 \leq t_2 \leq \dots \leq t_N$. Different from the usual assumption of the continuous-time point process, we allow multiple events to occur at the same time (i.e., $t_i = t_{i+1}$). Such simultaneous events actually occur in our data because of the finite time resolution of 1 min. Simultaneous events do not prevent the application of the ML method explained in the following.

For the exponential memory kernel given by (3), the event rate at time t is given by

$$\lambda(t) = \nu + \alpha \sum_{j=1}^{j_{\max}(t)} e^{-\beta(t-t_j)}, \quad (20)$$

where $j_{\max}(t)$ is the index of the last event before time t .

The likelihood of the event sequence during time period $[0, t_N]$, denoted by $L(t_1, \dots, t_N)$, is given by

$$L(t_1, \dots, t_N) = \exp\left(-\int_0^{t_N} \lambda(t) dt\right) \prod_{i=1}^N \lambda(t_i). \quad (21)$$

By substituting (20) in (21), we obtain the log likelihood for the original Hawkes process as follows [29]:

$$\log L(t_1, \dots, t_N) = -\nu t_N + \sum_{i=1}^N \frac{\alpha}{\beta} (e^{-\beta(t_N-t_i)} - 1) + \sum_{i=1}^N \log(\nu + \alpha A(i)), \quad (22)$$

where

$$A(i) = \sum_{1 \leq j < i \leq N} e^{-\beta(t_i-t_j)}. \quad (23)$$

Exactly speaking, the point process for an individual for one workday begins when the individual has arrived in the office. Because we do not know when the point process begins, we assume that the first event of each day is a trigger event. In other words, we set $t_1 = 0$ and modify (22) as

$$\log L(t_1, \dots, t_N) = -\nu t_N + \sum_{i=1}^N \frac{\alpha}{\beta} (e^{-\beta(t_N-t_i)} - 1) + \sum_{i=2}^N \log(\nu + \alpha A(i)). \quad (24)$$

For each individual, we use the days that have at least 40 events. We index such a valid day as $d = 1, 2, \dots, d_{\max}$. We denote the event times of valid day d by $0 = t_1^d \leq \dots \leq t_{N_d}^d$, where N_d is the number of events in valid day d . The log likelihood of the entire sequence is given by the summation of the log likelihood over all the valid days.

The partial derivatives of the log likelihood with respect to α , β , and ν are originally derived in [29]. In the present case, they read

$$\frac{\partial \log L}{\partial \alpha} = \sum_{d=1}^{d_{\max}} \left\{ \sum_{i=1}^{N_d} \frac{1}{\beta} (e^{-\beta(t_{N_d}^d - t_i^d)} - 1) + \sum_{i=2}^{N_d} \frac{A_d(i)}{\nu + \alpha A_d(i)} \right\}, \quad (25)$$

$$\frac{\partial \log L}{\partial \beta} = \sum_{d=1}^{d_{\max}} \left\{ -\alpha \sum_{i=1}^{N_d} \left[\frac{1}{\beta} (t_{N_d}^d - t_i^d) e^{-\beta(t_{N_d}^d - t_i^d)} + \frac{1}{\beta^2} (e^{-\beta(t_{N_d}^d - t_i^d)} - 1) \right] - \sum_{i=2}^{N_d} \frac{\alpha B_d(i)}{\nu + \alpha A_d(i)} \right\}, \quad (26)$$

$$\frac{\partial \log L}{\partial \nu} = \sum_{d=1}^{d_{\max}} \left\{ -t_{N_d}^d + \sum_{i=2}^{N_d} \frac{1}{\mu + \alpha A_d(i)} \right\}, \quad (27)$$

where

$$A_d(i) = \sum_{1 \leq j < i \leq N_d} e^{-\beta(t_i^d - t_j^d)} \quad (28)$$

and

$$B_d(i) = \sum_{1 \leq j < i \leq N_d} (t_i^d - t_j^d) e^{-\beta(t_i^d - t_j^d)}. \quad (29)$$

We obtain the ML estimates by setting the left-hand sides of (25)–(27) to 0.

We carried out the gradient descent method to estimate α , β , and ν for each individual. We repeat the substitution

$$\alpha \leftarrow \alpha + \delta \frac{\partial \log L}{\partial \alpha}, \quad (30)$$

$$\beta \leftarrow \beta + \delta \frac{\partial \log L}{\partial \beta}, \quad (31)$$

$$\nu \leftarrow \nu + \delta \frac{\partial \log L}{\partial \nu}, \quad (32)$$

where we set $\delta = 10^{-2}$. For one individual in D_2 , the ML method does not converge with $\delta = 10^{-2}$. Because it converges with $\delta = 10^{-3}$, we used this value for this particular individual.

Because the likelihood may have multiple local maxima, we started the gradient descent method with two different initial conditions, i.e., $(\alpha, \beta, \nu) = (0.6, 1.2, 0.6)$ and $(12, 24, 12)$ [hr⁻¹]. We found that the final results corresponding to the two initial conditions were identical for each individual.

For the ML method, the Hessian of the log likelihood can be explicitly given and used in combination with the Newton method [29]. However, we found that the Newton method does not converge for many individuals compared to the simple gradient descent described above. Therefore, we did not use the Newton method.

Because $\alpha, \beta, \nu \geq 0$ and $\alpha < \beta$ are needed for the Hawkes process to be well defined, we forced the parameter values to satisfy these conditions. In each update step, if the updated α becomes less than 10^{-6} , we set $\alpha = 10^{-6}$. Similarly, if $\alpha < \beta$ is violated, we set $\beta = \alpha + 10^{-6}$. If $\nu < 10^{-6}$, we set $\nu = 10^{-6}$.

The temporal resolution of our data is a minute. We set the unit time for the ML method to an hour such that our data has a resolution of $1/60$ on this timescale. The data would be too discrete for the ML method to bear accurate results if we set the unit time for the ML method to a minute. We verified that the results little changed when we made the time unit larger than one hour.

Acknowledgements N. M. acknowledges the support provided through Grants-in-Aid for Scientific Research (No. 23681033, and Innovative Areas “Systems Molecular Ethology” (No. 20115009)) from MEXT, Japan. T. T. acknowledges the support provided through Grants-in-Aid for Scientific Research (No. 10J06281) from JSPS, Japan.

References

1. Barabási, A.L.: The origin of bursts and heavy tails in human dynamics. *Nature* **435**, 207–211 (2005)
2. Candia, J., González, M.C., Wang, P., Schoenharl, T., Madey, G., Barabási, A.L.: Uncovering individual and collective human dynamics from mobile phone records. *J. Phys. A* **41**, 224015 (2008)
3. Cattuto, C., Van den Broeck, W., Barrat, A., Colizza, V., Pinton, J.F., Vespignani, A.: Dynamics of person-to-person interactions from distributed RFID sensor networks. *PLoS ONE* **5**, e11596 (2010)
4. Crane, R., Sornette, D.: Robust dynamic classes revealed by measuring the response function of a social system. *Proc. Natl. Acad. Sci. USA* **105**, 15649–15653 (2008)
5. Dahlhaus, R., Eichler, M., Sandkühler, J.: Identification of synaptic connections in neural ensembles by graphical models. *J. Neurosci. Meth.* **77**, 93–107 (1997)
6. Ebel, H., Mielsch, L.I., Bornholdt, S.: Scale-free topology of e-mail networks. *Phys. Rev. E* **66**, 035103(R) (2002)
7. Eckmann, J.P., Moses, E., Sergi, D.: Entropy of dialogues creates coherent structures in e-mail traffic. *Proc. Natl. Acad. Sci. USA* **101**, 14333–14337 (2004)
8. Goh, K.I., Barabási, A.L.: Burstiness and memory in complex systems. *Europhys. Lett.* **81**, 48002 (2008)
9. González, M.C., Hidalgo, C.A., Barabási, A.L.: Understanding individual human mobility patterns. *Nature* **453**, 779–782 (2008)
10. Han, X.P., Zhou, T., Wang, B.H.: Modeling human dynamics with adaptive interest. *New J. Phys.* **10**, 073010 (2008)
11. Hawkes, A.G.: Point spectra of some mutually exciting point processes. *J. R. Stat. Soc. B* **33**, 438–443 (1971)
12. Hawkes, A.G.: Spectra of some self-exciting and mutually exciting point processes. *Biometrika* **58**, 83–90 (1971)
13. Hawkes, A.G., Oakes, D.: A cluster process representation of a self-exciting process. *J. Appl. Prob.* **11**, 493–503 (1974)
14. Holme, P., Saramäki, J.: Temporal networks. *Phys. Rep.* **519**, 97–125 (2012)
15. Iribarren, J.L., Moro, E.: Impact of human activity patterns on the dynamics of information diffusion. *Phys. Rev. Lett.* **103**, 038702 (2009)
16. Isella, L., Romano, M., Barrat, A., Cattuto, C., Colizza, V., Van den Broeck, W., Gesualdo, F., Pandolfi, E., Ravà, L., Rizzo, C., Tozzi, A.E.: Close encounters in a pediatric ward: measuring face-to-face proximity and mixing patterns with wearable sensors. *PLoS ONE* **6**, e17144 (2011)

17. Isella, L., Stehlé, J., Barrat, A., Cattuto, C., Pinton, J.F., Van den Broeck, W.: What's in a crowd? Analysis of face-to-face behavioral networks. *J. Theor. Biol.* **271**, 166–180 (2011)
18. Jo, H.H., Karsai, M., Kertész, J., Kaski, K.: Circadian pattern and burstiness in mobile phone communication. *New J. Phys.* **14**, 013055 (2012)
19. Karsai, M., Kaski, K., Barabási, A.L., Kertész, J.: Universal features of correlated bursty behaviour. *Sci. Rep.* **2**, article No. 397 (2012)
20. Krumin, M., Reutsky, I., Shoham, S.: Correlation-based analysis and generation of multiple spike trains using Hawkes models with an exogenous input. *Front. Comput. Neurosci.* **4**, 147 (2010)
21. Malmgren, R.D., Stouffer, D.B., Motter, A.E., Amaral, L.A.N.: A Poissonian explanation for heavy tails in e-mail communication. *Proc. Natl. Acad. Sci. USA* **105**, 18153–18158 (2008)
22. Malmgren, R.D., Stouffer, D.B., Campanharo, A.S.L.O., Amaral, L.A.N.: On universality in human correspondence activity. *Science* **325**, 1696–1700 (2009)
23. Min, B., Goh, K.I., Kim, I.M.: Waiting time dynamics of priority-queue networks. *Phys. Rev. E* **79**, 056110 (2009)
24. Mitchell, L., Cates, M.E.: Hawkes process as a model of social interactions: a view on video dynamics. *J. Phys. A* **43**, 045101 (2010)
25. Ogata, Y.: On Lewis' simulation method for point processes. *IEEE Trans. Inform. Theor.* **27**, 23–31 (1981)
26. Ogata, Y.: Seismicity analysis through point-process modeling: a review. *Pure Appl. Geophys.* **155**, 471–507 (1999)
27. Ogata, Y., Akaike, H.: On linear intensity models for mixed doubly stochastic Poisson and self-exciting point-processes. *J. R. Stat. Soc. B* **44**, 102–107 (1982)
28. Oliveira, J.G., Vazquez, A.: Impact of interactions on human dynamics. *Physica A* **388**, 187–192 (2009)
29. Ozaki, T.: Maximum likelihood estimation of Hawkes' self-exciting point processes. *Ann. Inst. Stat. Math.* **31**, 145–155 (1979)
30. Pernice, V., Staude, B., Cardanobile, S., Rotter, S.: How structure determines correlations in neuronal networks. *PLoS Comput. Biol.* **7**, e1002059 (2011)
31. Reynaud-Bouret, P., Schbath, S.: Adaptive estimation for Hawkes processes; application to genome analysis. *Ann. Stat.* **38**, 2781–2822 (2010)
32. Rocha, L.E.C., Liljeros, F., Holme, P.: Information dynamics shape the sexual networks of Internet-mediated prostitution. *Proc. Natl. Acad. Sci. USA* **107**, 5706–5711 (2010)
33. Takaguchi, T., Nakamura, M., Sato, N., Yano, K., Masuda, N.: Predictability of conversation partners. *Phys. Rev. X* **1**, 011008 (2011)
34. Takaguchi, T., Sato, N., Yano, K., Masuda, N.: Importance of individual events in temporal networks. *New J. Phys.* **14**, 093003 (2012)
35. Vázquez, A., Oliveira, J.G., Dezső, Z., Goh, K.I., Kondor, I., Barabási, A.L.: Modeling bursts and heavy tails in human dynamics. *Phys. Rev. E* **73**, 036127 (2006)
36. Vere-Jones, D.: Stochastic models for earthquake occurrence. *J. R. Stat. Soc. B* **32**, 1–62 (1970)
37. Wakisaka, Y., Ohkubo, N., Ara, K., Sato, N., Hayakawa, M., Tsuji, S., Horry, Y., Yano, K., Moriwaki, N.: Beam-scan sensor node: reliable sensing of human interactions in organization. In: 2009 Sixth International Conference on Networked Sensing Systems (INSS). pp. 1–4. IEEE Press, Piscataway (2009)
38. Wu, Y., Zhou, C., Xiao, J., Kurths, J., Schellnhuber, H.J.: Evidence for a bimodal distribution in human communication. *Proc. Natl. Acad. Sci. USA* **107**, 18803–18808 (2010)
39. Yano, K., Ara, K., Moriwaki, N., Kuriyama, H.: Measurement of human behavior: creating a society for discovering opportunities. *Hitachi Rev.* **58**, 139–144 (2009)

Infering and Calibrating Triadic Closure in a Dynamic Network

Alexander V. Mantzaris and Desmond J. Higham

Abstract In the social sciences, the hypothesis of triadic closure contends that new links in a social contact network arise preferentially between those who currently share neighbours. Here, in a proof-of-principle study, we show how to calibrate a recently proposed evolving network model to time-dependent connectivity data. The probabilistic edge birth rate in the model contains a triadic closure term, so we are also able to assess statistically the evidence for this effect. The approach is shown to work on data generated synthetically from the model. We then apply this methodology to some real, large-scale data that records the build up of connections in a business-related social networking site, and find evidence for triadic closure.

1 Motivation

Many modern application areas give rise to patterns of connectivity that change over time [9]. Examples include mobile telecommunication, on-line trading, smart-metering, massive multiplayer online gaming and online social networking. Information such as ‘who called who’, ‘who tweeted who’, ‘who FaceTimed who’, and ‘people who bought his book also bought ...’ is naturally evolving over time and cannot be fully exploited through a static representation as a single time-average or snapshot. These emerging, data-rich disciplines generate large, highly-resolved network sequences that demand new models and computational tools.

This work focuses on the use of a mathematical model to describe the microscale, transient dynamics. The model, from [5], is mechanistic, incorporating the triadic closure effect that many social scientists believe to be a key driving force behind social interactions. We show how a likelihood approach can be used to calibrate the

A.V. Mantzaris · D.J. Higham (✉)

Department of Mathematics and Statistics, University of Strathclyde, Glasgow, UK

e-mail: alexander.mantzaris@strath.ac.uk; d.j.higham@strath.ac.uk

model, thereby allowing the triadic closure hypothesis to be tested statistically on real data.

The manuscript is organised as follows. In Sect. 2 we introduce the triadic closure concept and discuss some relevant work in the area. In Sect. 3 we describe the model from [5] and illustrate its use. Section 4 then explains how the likelihood—the probability of observing the microscale, edge by edge, data given a set of model parameters—can be computed and used to perform statistical inference. To illustrate the idea, we generate synthetic data from the model and reverse engineer the model parameters. In Sect. 5 we then apply these ideas to a set of online social interaction data. Section 6 gives a summary and points to future work.

2 Background

The concept of triadic closure can be traced back to the work of the sociologist Georg Simmel in the early 1900s, and was popularized by the influential article [4]. It is a key motivation for the use of *clustering coefficients* [3, 15] to summarize network properties. The basic principle can be summarized as [2, 16]

Triadic Closure, part 1: If two unconnected people in a social network have a friend in common, then there is an increased likelihood that they will become friends themselves at some point in the future.

As discussed in [2, Chap. 3], there are at least three convincing reasons why triadic closure might feature in the evolution of a social interaction network. If B and C are not currently friends, but share a common friend, A, then a new link from B to C is more likely to arise than a link between an arbitrary pair, through

Opportunity: B and C both socialize with A and hence have more chance of meeting,

Trust: A can simultaneously vouch for both B and C,

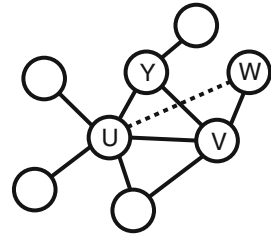
Incentive: A may view the triadic friendship as less stressful or time-consuming to maintain than the separate pair of dyads, and hence encourage the B–C link.

Based on these points, we may also argue that each extra common friend shared by B and C will increase the chance of a future B–C link. Hence, we may slightly extend the triadic closure principle above:

Triadic Closure, part 2: The likelihood that two unconnected people in a social network will become friends themselves at some point in the future increases with the number of friends they share in common.

The digital age has given rise to large scale human interaction data sets, making it feasible to test the hypothesis that changes in connectivity are driven by triadic closure. For example, Leskovec et al. [12] studied four large online social network datasets and found that “most new edges span very short distances, typically closing triangles.” Mislove et al. [14] monitored the growth of the Flickr network and found that 80% of new links “connected users that were only two hops apart, meaning that

Fig. 1 Depiction of the triangulation process, based on Fig. 6 from [12]. A new edge is produced, as shown by the *dashed line*. This dashed edge creates a triad closure between nodes U, V, and W



the destination user was a friend-of-a-friend of the source user before the new link was created”. Szell et al. [17] measured transition rates between dyadic and triadic structures for positive and negative social interactions in a massive multiplayer online game and found “overrepresentation (underrepresentation) of complete triads in networks of positive ties, and vice versa for networks of negative ties.”

Networks in neuroscience have also been observed to have an overabundance of triangles, with respect to both anatomical and functional connectivity [1, 7, 13].

In this work we aim to go beyond the realm of simply recording the incidence of network triangles by combining ideas from applied mathematics and applied statistics. Given network data, we wish to *calibrate an appropriate mechanistic model of network evolution* and simultaneously *quantify the statistical evidence in favour of triadic closure*.

The closest previous work to ours is perhaps [12], where stochastic models incorporating triadic closure were proposed and tested in a microscale/likelihood setting. To understand the class of models from [12], consider the node u in Fig. 1 (which is based on Fig. 6 from [12]). The triangulation stage adds a link to a node, w , that is two hops away from u . This is done by first choosing one of u ’s neighbours, v , according to one of the five following rules

- random: uniformly at random,
- degree: proportional to some power of the degree of node v ,
- common friends: proportional to the number of common friends shared by nodes u and v ,
- last time: proportional to some power of the time that has elapsed since v last created an edge,
- comlast: proportional to the product of (a) the number of common friends shared by nodes u and v , and (b) the time that has elapsed since v last created an edge, raised to some power.

Similarly, any of these five rules can be used to choose a neighbour, w , of v . The new link is then inserted between u and w in order to create a triad. This gives a total 25 different models, which were tested in [12] on real data in a likelihood setting. The authors concluded that the random-random model (choose v uniformly from the neighbours of u and then choose w uniformly from the neighbours of v) gives a good compromise between accuracy and simplicity.

In this work, we consider a recent stochastic triadic closure model from [5], based on the general methodology of [6]. A key difference from the versions

discussed above is that this model triangulates by directly choosing nodes w that are two hops from u , with a bias that is proportional to the number of common neighbours—directly reflecting part 2 of the triadic closure principle. Advantages of this modelling approach are that:

- A single parameter, ϵ , is used to quantify the strength of the triadic closure effect. The case $\epsilon = 0$ corresponds to no preference for triadic closure (edges appear uniformly at some basal rate). Hence, we have a nested pair of models and can test whether there is statistically significant evidence for triadic closure in the data.
- The modeling framework is sufficiently simple to allow a mean-field approximation for the evolution of the edge density. The mean-field approximation involves the same model parameters, and hence this macroscopic summary data can be used when a full likelihood computation at the microscale is not feasible. We exploit this feature in Sect. 5.

3 The Triadic Closure Model

We suppose that a fixed set of N nodes have a connectivity structure that may change at discrete, uniformly spaced, time points $t_0 < t_1 < \dots < t_K$. We let A_k denote the adjacency matrix for the network at time t_k and assume that the networks are unweighted and undirected without self-loops, so each $A_k \in \mathbb{R}^{N \times N}$ has $a_{ij} = a_{ji} = 1$ if there is an edge from node i to node j at time t_k and has $a_{ij} = a_{ji} = 0$ otherwise, with all $a_{ii} = 0$.

The triadic closure model in [5] involves two matrix-valued functions of the current state, $\omega(A_k)$, and $\alpha(A_k)$, giving the *edge death* and *edge birth* probabilities, respectively. The death probability takes the simple form

$$(\omega(A_k))_{ij} \equiv \tilde{\omega}, \quad \text{for some } \tilde{\omega} \in (0, 1). \quad (1)$$

The birth probability is defined as

$$(\alpha(A_k))_{ij} = \delta + \epsilon(A_k^2)_{ij}, \quad (2)$$

for some constants δ and ϵ . We impose $0 < \epsilon(N - 2) < 1 - \delta$ to ensure that the birth probability lies between 0 and 1.

Given the time t_k network, A_k , if there is currently no edge from i to j , then the birth probability specifies the chance that the edge will emerge at time t_{k+1} . Similarly, if i and j are connected in A_k , the death probability specifies the chance that the edge will disappear at time t_{k+1} . Conditioned on A_k , all such edge events are taken to be independent. More precisely, the model takes the form of a discrete time Markov chain over the state space of all binary, symmetric networks with N nodes, and given A_0 we may simulate a path of the chain as follows

```

for  $k = 0, 1, 2, \dots, K - 1$ 
  Compute  $\alpha(A_k)$ 
  for all disjoint pairs  $i \neq j$ 
    if  $(A_k)_{ij} = 0$  then set
       $(A_{k+1})_{ij} = 1$  with prob.  $\alpha(A_k)_{ij}$  (birth)
       $(A_{k+1})_{ij} = 0$  with prob.  $1 - \alpha(A_k)_{ij}$  (no change)
    else we have  $(A_k)_{ij} = 1$ , so set
       $(A_{k+1})_{ij} = 0$  with prob.  $\tilde{\omega}$  (death)
       $(A_{k+1})_{ij} = 1$  with prob.  $1 - \tilde{\omega}$  (no change)
    end if
  end for all pairs
end for  $k$ 

```

To understand the form of the birth probability (2), we note that the factor $(A_k^2)_{ij}$ counts the number of neighbours shared by nodes i and j at time t_k . Hence the overall birth probability is given by combining

- a basal level, δ , and
- a triadic closure term that is proportional to the number of new triangles the edge would create. Here ϵ controls the strength of the triadic closure effect.

A mean-field approximation for the evolution of a macroscopic quantity, the edge density

$$\hat{p}_k := \frac{1}{N(N-1)/2} \sum \sum_{i>j} (A_k)_{ij}, \tag{3}$$

was proposed in [5] and found to match well with real simulations. This mean-field approximation takes the form

$$p_{k+1} = (1 - \tilde{\omega})p_k + (1 - p_k) (\delta + \epsilon(N - 2)p_k^2). \tag{4}$$

An interesting feature of the iteration (4) is that there are generically three *steady states*; that is, values p^* such that $p_{k+1} = p_k = p^*$ solves (4), with only the outer two being stable. Simulations showed that both stable states could be observed in practice, and in particular for initial networks A_0 close to the intermediate, unstable steady state, the density along a path evolves to one of the two stable values in an unpredictable manner that depends on the precise micro-level detail.

To illustrate the model, and also to provide some data for the inference computations in the next section, we now show some network sequences generated by the model. In each case we used 100 nodes and 100 time points, and the initial network, A_0 , was a sample of a classical Erdős-Rényi random graph with expected edge density of p ; we denote this by $A_0 = \text{ER}(p)$.

Data Set A: $\delta = 0.0004, \tilde{\omega} = 0.01, \epsilon = 0, A_0 = \text{ER}(0.5)$.

In this case there is no triadic closure—edges appear and disappear uniformly at random. The mean-field equation (4) collapses to a linear iteration with a single, stable steady state at $p^* = 0.0385$. Figure 2 shows the adjacency matrix at selected time points, along with the edge density as a function of time. The images of the

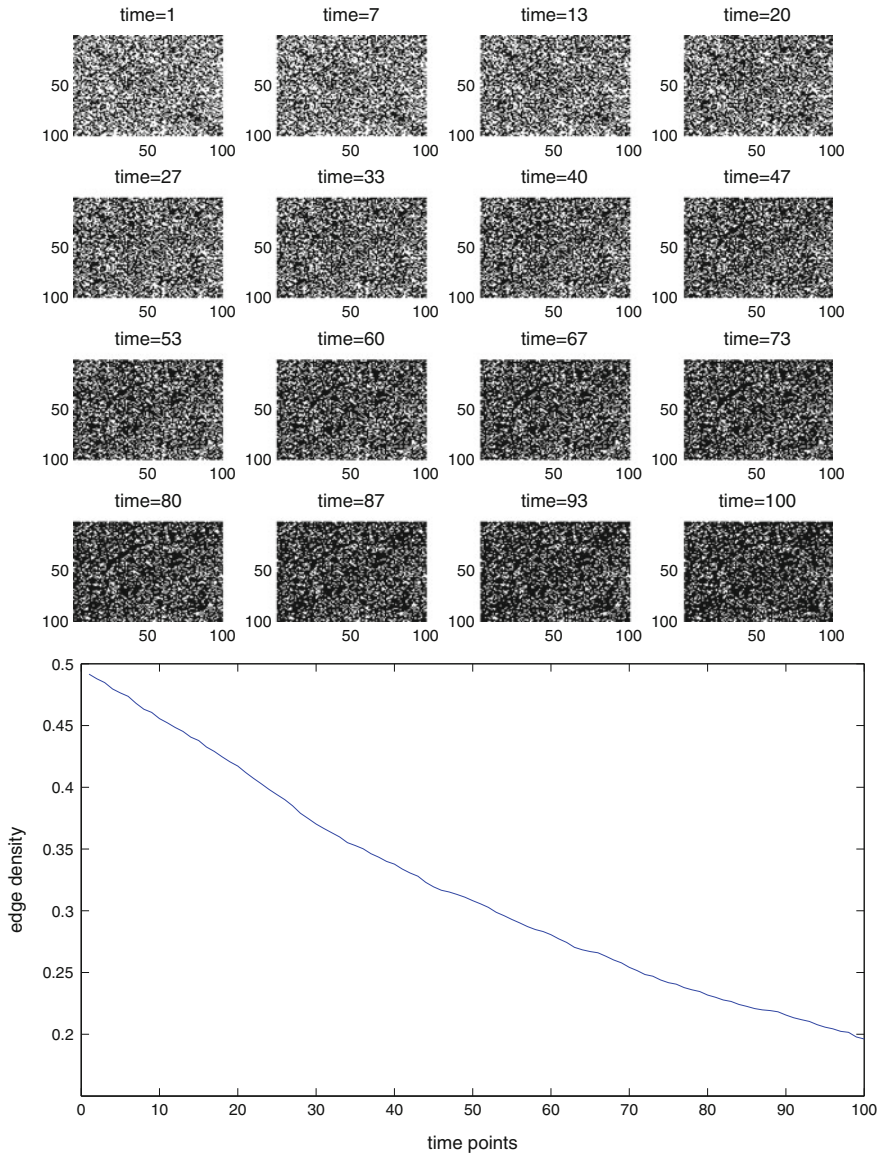


Fig. 2 Data set A. *Upper*: the adjacency matrix at selected time points. *Lower*: edge density as a function of time

adjacency matrix put a black square where the value is zero and a white square where the value is one. To show the relevance of the mean-field approximation, Fig. 3 illustrates what happens when the path is followed for a longer period; we used 1,000 time points. The mean-field approximation from (4) is superimposed over the edge density plots. Here the observed edge density at the final time point is 0.0356.

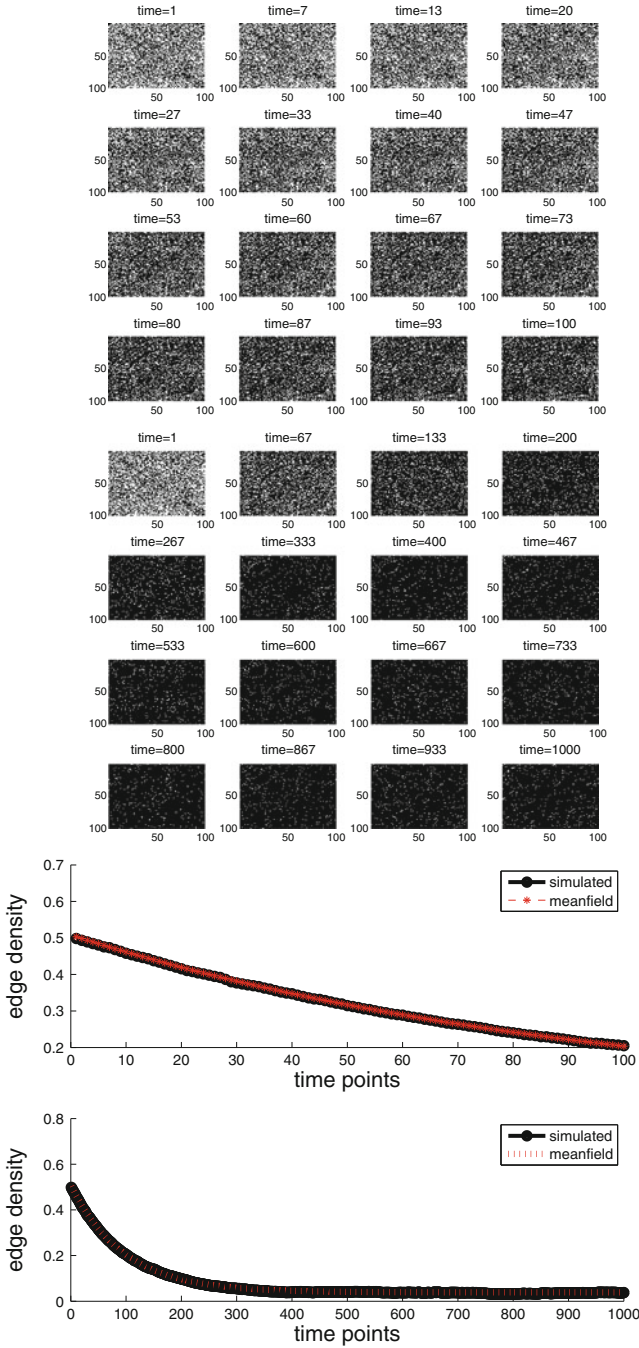


Fig. 3 Extended version of data set A. *Upper*: the adjacency matrix at selected times points up to time 1,000. *Lower*: edge density up to time 100 and time 1,000

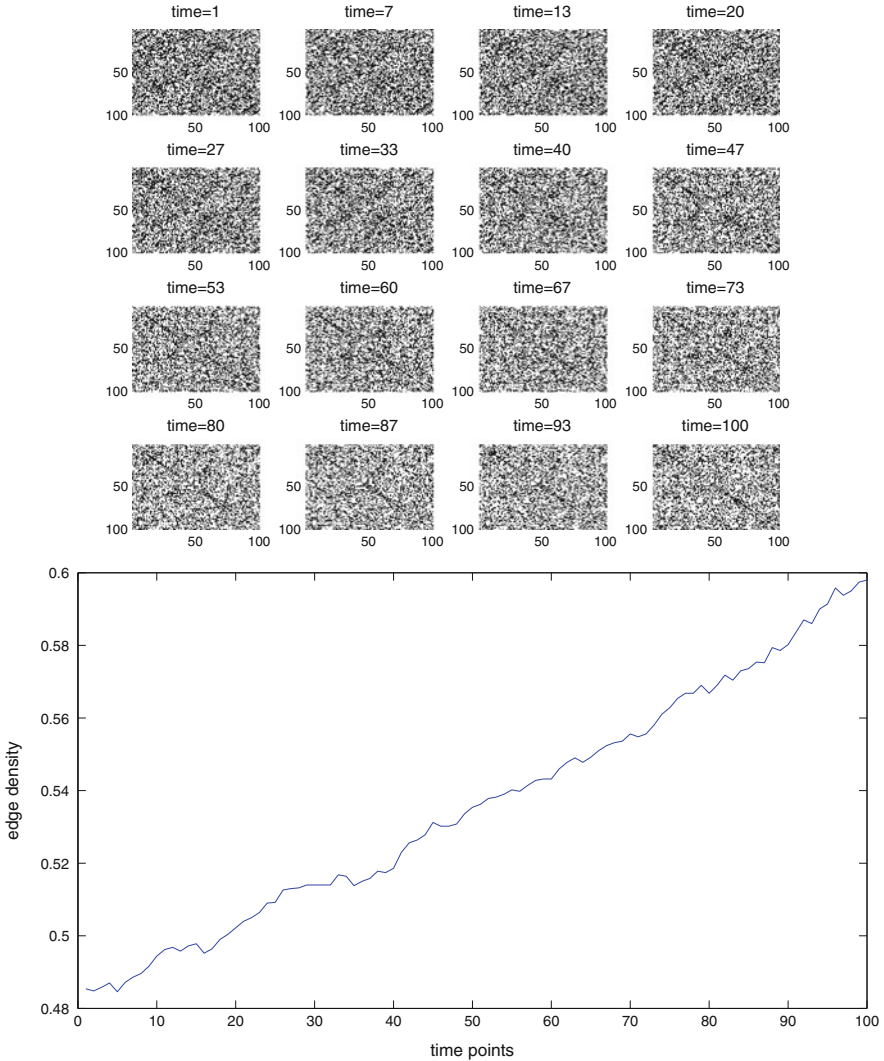


Fig. 4 Data set B. *Upper*: the adjacency matrix at selected time points. *Lower*: edge density as a function of time

Data Set B: $\delta = 0.0004$, $\tilde{\omega} = 0.01$, $\epsilon = 0.0005$, $A_0 = \text{ER}(0.5)$.

Here, the mean-field iteration has steady states 0.7215 (stable), 0.2291 (unstable) and 0.0494 (stable). Using $A_0 = \text{ER}(0.5)$ starts the paths closest to the denser of the two stable macro-states. Figure 4 shows some network snapshots along with the edge density. A longer time interval is used in Fig. 5 in order to confirm the relevance of the $p^* = 0.7215$ steady state.

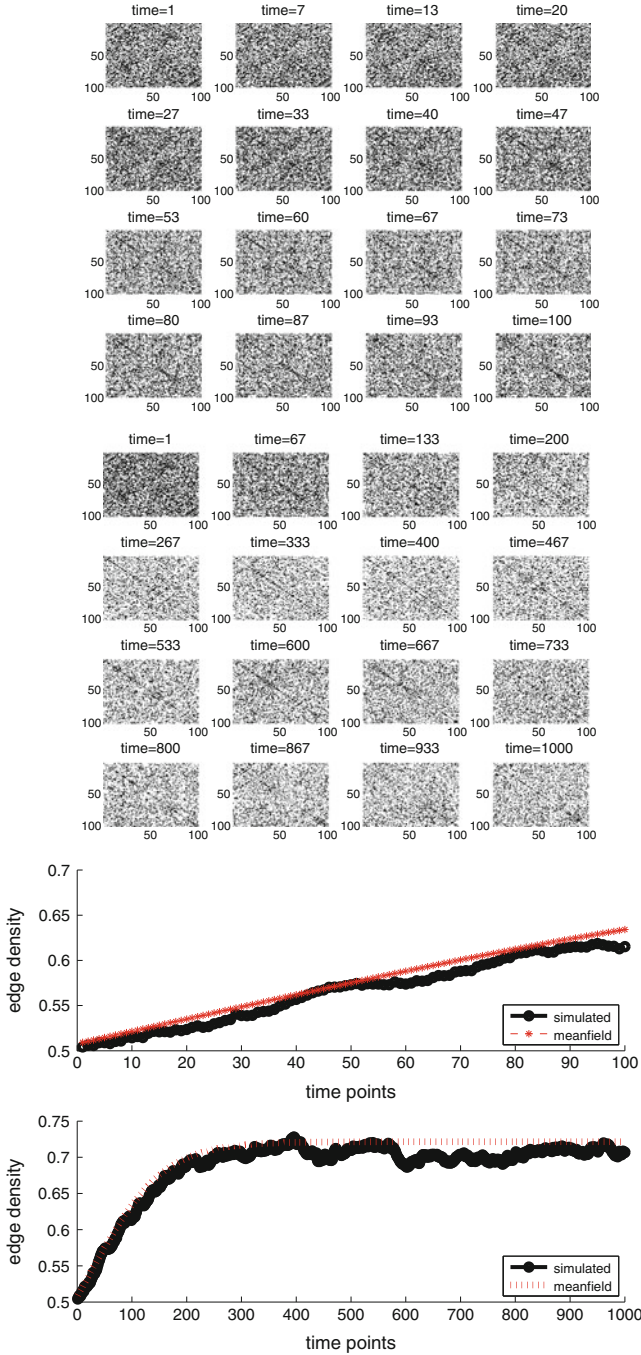


Fig. 5 Extended version of data set B. *Upper*: the adjacency matrix at selected times points up to time 1,000. *Lower*: edge density up to time 100 and time 1,000

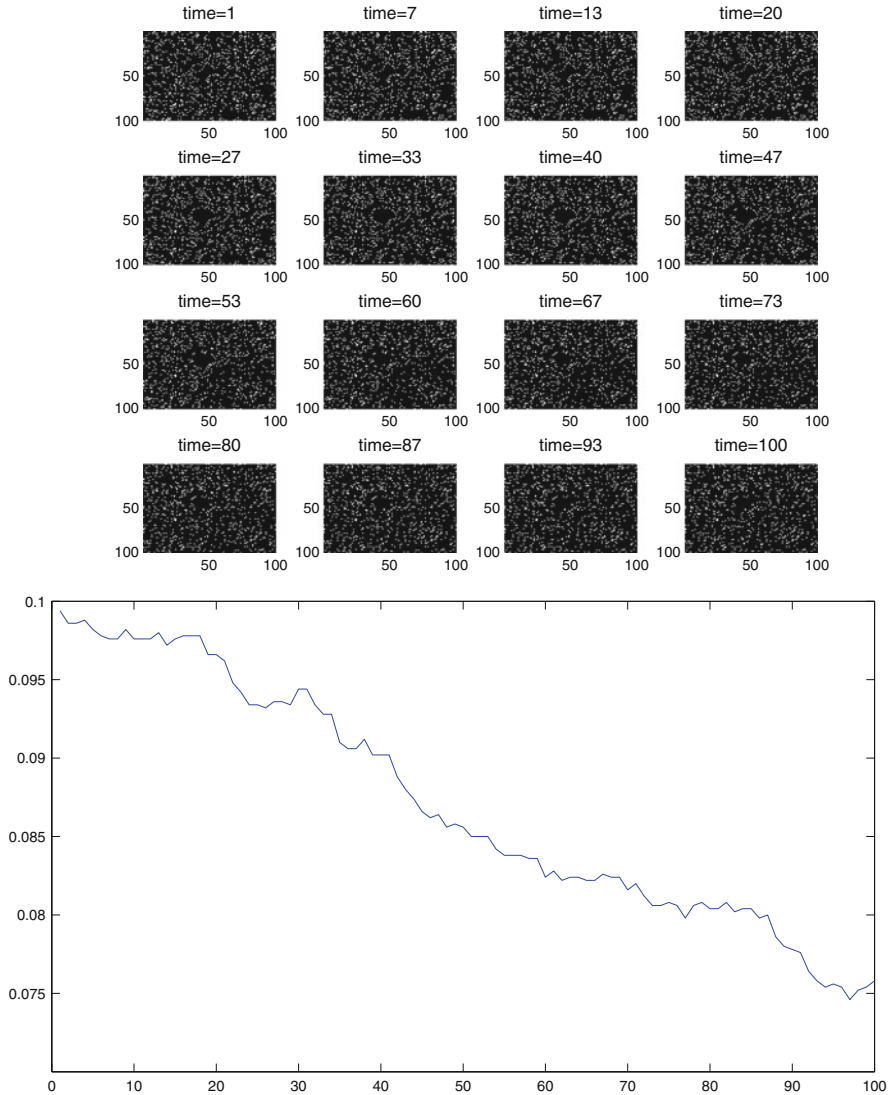


Fig. 6 Data set C. *Upper*: the adjacency matrix at selected time points. *Lower*: edge density as a function of time

Data Set C: $\delta = 0.0004$, $\tilde{\omega} = 0.01$, $\epsilon = 0.0005$, $A_0 = \text{ER}(0.1)$.

Here, we use the same model parameters as in Data Set B, but start with a less dense initial network. Figure 6 shows network snapshots and edge density, and Fig. 7 runs over a longer time period. In this case, the edge density is attracted to the other stable steady state at $p^* = 0.0494$.

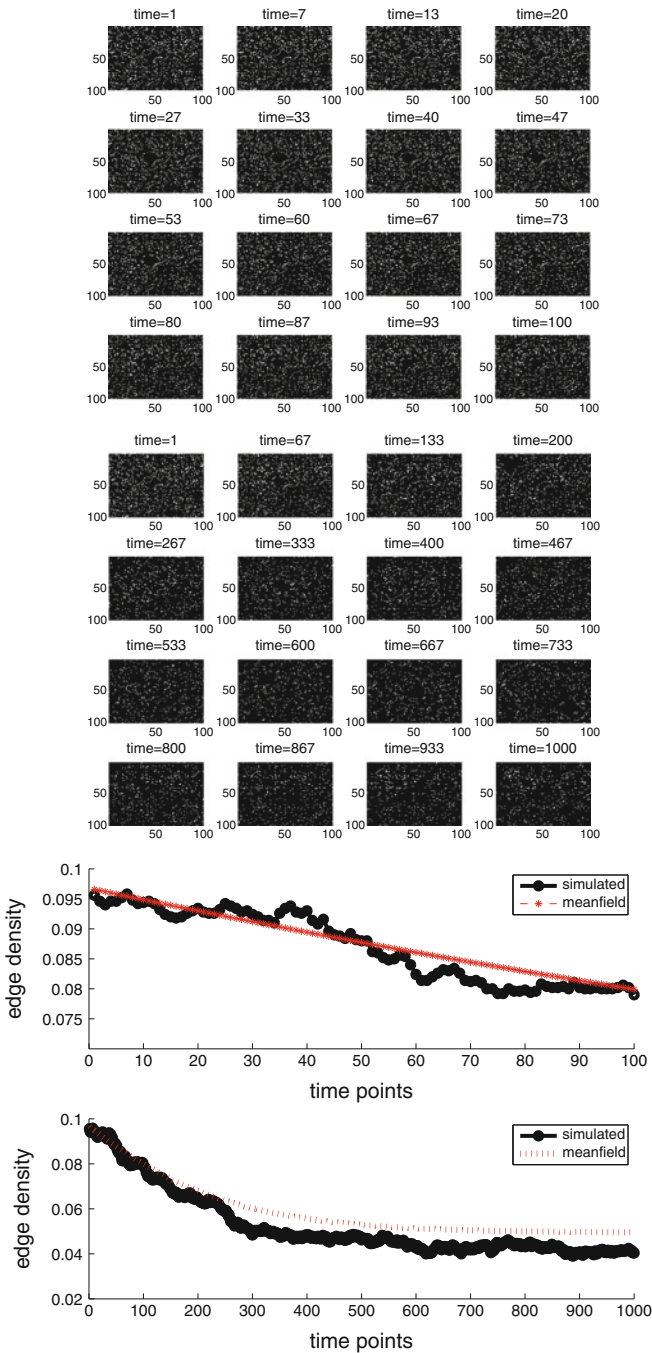


Fig. 7 Extended version of data set C. *Upper*: the adjacency matrix at selected times points up to time 1,000. *Lower*: edge density up to time 100 and time 1,000

4 Likelihood and Inference

The probabilistic nature of the model produces a natural likelihood function to feed into a calibration and inference framework. This section explains the details and tests out the idea on the data sets from Sect. 3.

Given network data A_0, A_1, \dots, A_k , that is, up to time t_k , because the model satisfies the Markov property the likelihood of observing a network A_{k+1} at time t_{k+1} depends only on A_k and is given by

$$\mathcal{L}(A_{k+1}|A_k) = \prod_{\text{Remain alive}} (1 - \tilde{\omega}) \times \prod_{\text{Become alive}} \alpha(A_k)_{ij} \times \prod_{\text{Remain dead}} (1 - \alpha)_{ij} \times \prod_{\text{Become dead}} \tilde{\omega}_{ij}.$$

Here the products are over appropriate ordered edge pairs; that is, (i, j) with $i < j$; so for example, ‘‘Remain alive’’ denotes (i, j) for which both $(A_k)_{ij} = 1$ and $(A_{k+1})_{ij} = 1$.

Now suppose that the model parameters and initial network A_0 are fixed. Any observed network sequence A_1, A_2, \dots, A_K then has likelihood

$$\mathcal{L}(A_1|A_0) \times \mathcal{L}(A_2|A_1) \times \dots \times \mathcal{L}(A_K|A_{K-1}). \quad (5)$$

The parameters which maximise the likelihood of a model may then be calculated. In this work we use straightforward grid searches over appropriate parameter ranges. We focus here on the *constrained model*, where ϵ is fixed at zero, so no triad closure effect is present, and the *unconstrained model*, where ϵ is a model parameter. The constrained model is therefore nested within the unconstrained model, which makes the application of the likelihood ratio test [18] suitable for model comparison. The likelihood ratio test value, D , is then used to compute a p-value for rejecting the null model, which is the constrained model. The value D and the difference in degrees of freedom in the unconstrained and constrained model are used as parameters for the chi-squared distribution. This allows us to compute a p-value for rejecting the null hypothesis. We take a threshold of 0.01.

The Akaike information criterion (AIC), [8], is also used here for model selection. AIC is founded in information theory. The application of AIC reinforces the results of the likelihood ratio test.

Inference for Data Set A: Here we performed a grid search of the likelihood over $\delta = 0.0001 : 0.0001 : 0.0006$ and $\tilde{\omega} = 0.0005 : 0.005 : 0.025$ for the constrained model. For the unconstrained model we also used $\epsilon = 0.0000 : 0.0001 : 0.001$.

The search for the constrained model gave $\delta_{max} = 0.0004$ and $\omega_{max} = 0.0105$ with a log likelihood of -10182.0284 . For the unconstrained model, we obtained $\delta_{max} = 0.0004$, $\omega_{max} = 0.0105$ and $\epsilon_{max} = 0$, with a log likelihood of -10182.0284 . Hence, the extra freedom offered by ϵ was clearly not relevant for this data set. The log likelihood ratio test therefore gives $D = 0$, favouring the constrained model. The marginal for ϵ is shown in Fig. 8. We can see the decay away from the true value of zero. AIC also prefers the model without triadic closure.

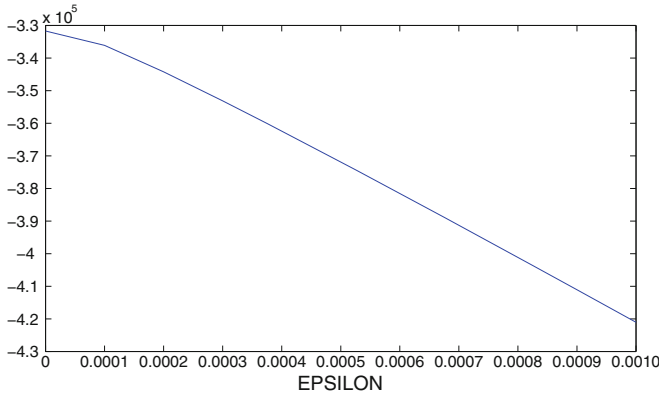


Fig. 8 Marginal for ϵ in data set A

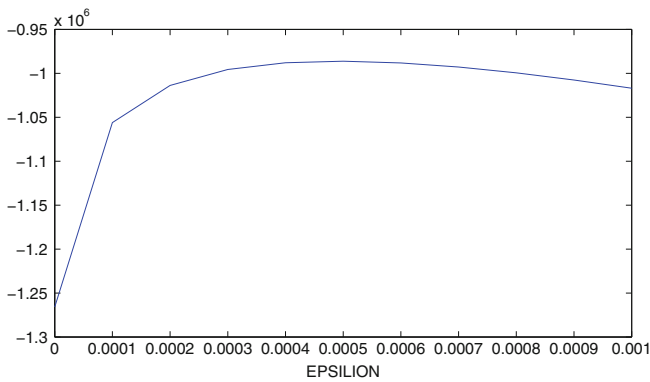


Fig. 9 Marginal for ϵ in data set B

Inference for Data Set B: Here we searched over $\delta = 0.0001 : 0.0001 : 0.0006$ and $\omega = 0.0005 : 0.005 : 0.025$ in the constrained model and also $\epsilon = 0.0000 : 0.0001 : 0.001$ in the unconstrained model. The likelihood for the constrained model is maximized at $\delta_{max} = 0.0006$ and $\omega_{max} = 0.0105$ with log likelihood of -38633.7891 . For the unconstrained model, $\delta_{max} = 0.0001$, $\omega_{max} = 0.0105$ and $\epsilon_{max} = 0.0005$ with log likelihood -31477.9615 . We note that the constrained model has a higher birth rate to compensate for the lack of triangulation. The log likelihood ratio test value is $D = 14311.6553$, so the test result is 1, favouring the triad closure model. AIC chooses the model that has triad closure as well. The marginal of ϵ , shown in Fig. 9, has a clear peak around the value of 0.0005 that was used to generate the data.

Inference for Data Set C: For the constrained model the grid search took place over $\delta = 0.0001 : 0.0001 : 0.0006$ and $\omega = 0.0005 : 0.005 : 0.025$ and for the unconstrained model we also used $\epsilon = 0.0000 : 0.0001 : 0.001$. The constrained model

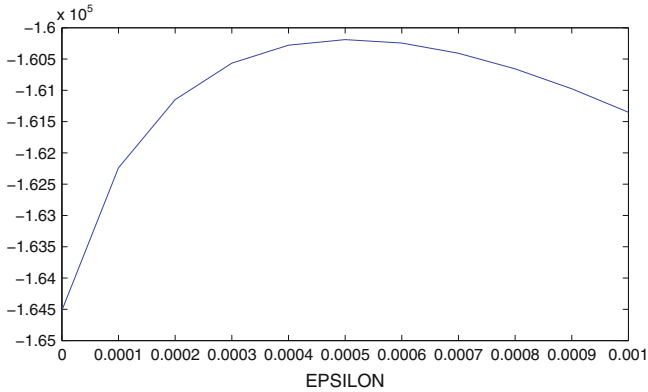


Fig. 10 Marginal for epsilon for data set C

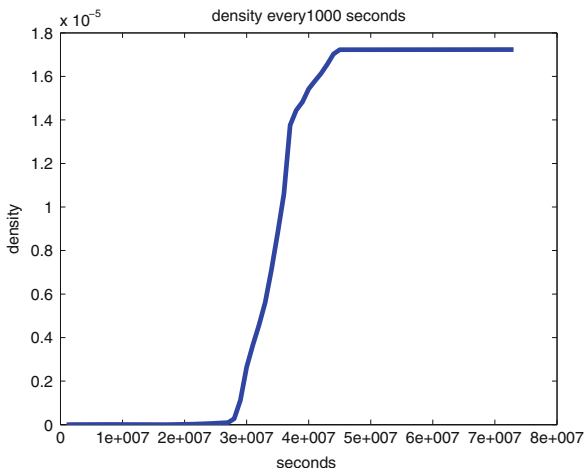
produced $\delta_{max} = 0.0006$ and $\omega_{max} = 0.0105$ with log likelihood of -5136.5503 . For the unconstrained model we have $\delta_{max} = 0.0004$, $\omega_{max} = 0.0105$ and $\epsilon_{max} = 0.0005$ with log likelihood of -5089.8203 . As for Data set B, the constrained model has a higher birth rate to balance the lack of triangulation. The log likelihood ratio test value is $D = 93.4599$, with a test result of 1, favouring the triad closure model. As well, AIC chooses the model with triad closure. The marginal of ϵ is shown in Fig. 10, and, as in Data set B, we see a peak around the value of 0.0005.

Based on these results, we conclude that the likelihood-based inference approach can produce meaningful conclusions on this type of data.

5 On-Line Social Network Data

We now apply this methodology to online social network data from [10] that relates to the Wealink (<http://www.wealink.com/>) social networking site for professionals in China. In this data set, new users (nodes) join the network over time, and a new link can be established between any pair of current users. The raw data consists of triples of the form (i, j, t) , indicating that a link has been created between nodes i and j at time stamp t . There are 26,817,840 time stamps, measured in seconds, and they range from $t = 1$ to 72,711,888 s, which is just over 841 days. The largest node id is 223,482. For the purpose of calibration and model selection, we assume that all 223,482 nodes are present (i.e. available to form links) from the initial time point, and that all links are undirected. Hence we have symmetric adjacency matrices of dimension $N = 223,482$. Edges do not disappear in this data set. Figure 11 shows how the edge density increases with time. The overall average rate of increase in Fig. 11 is 0.0038 edges per second.

Fig. 11 Density of the Wealink online social network as a function of time in seconds



By construction, there is no edge death in this data set. Hence, we fix $\tilde{\omega} = 0$. This leaves two parameters, the basal birth rate, δ , and the triadic closure strength, ϵ . Just as we did in Sect. 4 for the synthetic data, our aim is therefore to test whether there is evidence for a positive triadic closure strength.

Because of the large amount of data, we made a number of simplifications in order to reduce computational complexity to a feasible level. First, it is clear from Fig. 11 that most activity takes place over a limited time period, and hence, for our experiments, we start with the network at time 3×10^7 s and continue until time 4×10^7 s. Then, rather than treating each event separately, we divide this period into 100 equally spaced time windows and construct an adjacency matrix for each. So each adjacency matrix records an element 1 in positions (i, j) and (j, i) if nodes i and j were already linked, or formed a link in the relevant time window, and it records a zero otherwise.

Due to the excessive cost of evaluating the likelihood, we first used the mean-field approximation (4) to get a feel for an appropriate range of parameter values. Figure 12 shows the edge density increasing over the 100 discrete time points. The red circles show the corresponding mean-field solution when we fix $\epsilon = 0$ and optimize in a mean-square sense over the remaining parameter, δ ; that is, given p_0 , we consider the iteration

$$p_{k+1} = p_k + (1 - p_k)\delta$$

and minimize the mean-square deviation between $\{p_k\}_{k>0}$ and the edge density from the data. This produces a value of $\delta = 8.2059 \times 10^{-8}$ for the basal birth rate. The black crosses show the results when also allow the triadic closure strength to be nonzero; that is, we use

$$p_{k+1} = p_k + (1 - p_k) (\delta + \epsilon(N - 2)p_k^2).$$

Here, we found $\delta = 9.53 \times 10^{-8}$ and $\epsilon = 7.32 \times 10^{-16}$.

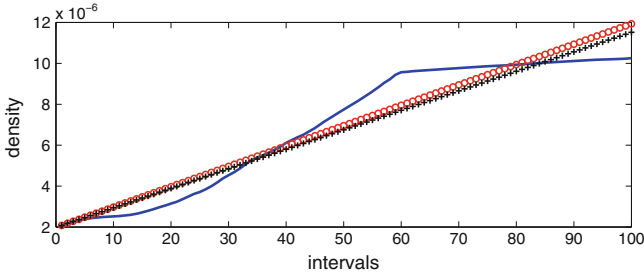


Fig. 12 *Blue solid line:* Edge density over the 100 discrete time points used for the inference. *Red circles:* edge density from best mean-field fit with ϵ fixed at zero and δ as a free parameter. *Black crosses:* edge density from best mean-field fit with both ϵ and δ as free parameters

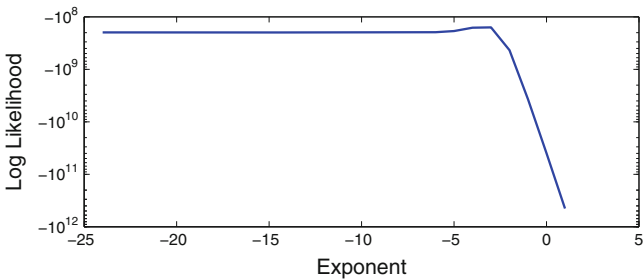


Fig. 13 Log likelihood of the triadic closure model as a function of triad closure strength, ϵ . The basal edge birth is fixed at 9.95×10^{-8} . The x -axis shows the log base 10 values used for ϵ in the search for the largest loglikelihood

Since our available computing power only permitted a full likelihood based calibration over one parameter, we then fixed $\delta = 9.95 \times 10^{-8}$ and inferred the triadic closure strength, ϵ , from the microscale data. Figure 13 shows the log likelihood as a function of ϵ . The best ϵ value gives a log likelihood of -1.58×10^8 , whereas the $\epsilon = 0$ model produces -1.97×10^8 . We find that $D = 7.81 \times 10^7$, and the triadic closure model is therefore chosen by the log likelihood ratio test. AIC also chooses the model with triadic closure.

6 Summary

Our aim in this work was to investigate calibration and inference issues for a stochastic microscale evolving network model. Edge dynamics in the model involve a term that quantifies a triadic closure effect—friends of friends tend to become friends. We showed that the presence of triadic closure can be inferred from a reasonable quantity of synthetic data, generated from the model. We then showed

that there is statistical evidence for triadic closure in real data from a business-related social networking site.

Although likelihood-based calibration and model comparison is conceptually straightforward for stochastic, Markov chain based, models of the type used here, the fundamental task is computationally challenging for large network sequences over long time periods. In this work, we were able to exploit a mean-field theory that describes the evolution of a macroscale quantity—the edge density—in terms of the model parameters.

There are many directions in which this type of work could be taken:

- other concepts from the social sciences that may determine network dynamics, such as homophily/heterophily, social distance and cultural drift [2, 11], could be quantified through mathematical models and then tested for and compared in real dynamic data sets,
- other types of interaction network, for example from telecommunication, online human behaviour and e-business, could be calibrated, compared and categorized,
- more sophisticated, customized strategies for sampling the model parameter space could be developed; for example via Markov chain Monte Carlo techniques.

Acknowledgements This work was supported by the Engineering and Physical Sciences Research Council and the Research Councils UK Digital Economy Programme, under grant EP/I016058/1. DJH was also supported by a Fellowship from the Leverhulme Trust.

References

1. Bullmore, E., Sporns, O.: Complex brain networks: graph theoretical analysis of structural and functional systems. *Nat. Rev. Neurosci.* **10**, 186–198 (2009)
2. Easley, D., Kleinberg, J.: *Networks, Crowds, and Markets: Reasoning About a Highly Connected World*. Cambridge University Press, London (2010)
3. Estrada, E.: *The Structure of Complex Networks*. Oxford University Press, Oxford (2011)
4. Granovetter, M.: The strength of weak ties. *Am. J. Sociol.* **78**(6), 1360–1380 (1973)
5. Grindrod, P., Higham, D.J.: Evolving graphs: dynamical models, inverse problems and propagation. *Proc. R. Soc. Ser. A* **466**, 753–770 (2010)
6. Grindrod, P., Higham, D.J.: Bistable evolving networks. *Internet Math.* **8**, 402–423 (2012)
7. He, Y., Chen, Z.J., Evans, A.C.: Small-world anatomical networks in the human brain revealed by cortical thickness from MRI. *Cerebr. Cortex* **17**(10), 2407–2419 (2007)
8. Hirotsugu, A.: A new look at the statistical model identification. *IEEE Trans. Automat. Contr.* **19**(6), 716–723 (1974)
9. Holme, P., Saramäki, J.: Temporal networks. *Phys. Rep.* **519**, 97–125 (2012)
10. Hu, H., Wang, X.: Evolution of a large online social network. *Phys. Lett. A* **373**(12–13), 1105–1110 (2009)
11. Jackson, M.O.: Networks and economic behavior. *Annu. Rev. Econ.* **1**, 489–513 (2009)
12. Leskovec, J., Backstrom, L., Kumar, R., Tomkins, A.: Microscopic evolution of social networks. In: Li, Y., Liu, B., Sarawagi, S. (eds.) *KDD*, pp. 462–470. ACM, New York (2008)
13. Liu, Y., Liang, M., Zhou, Y., He, Y., Hao, Y., Song, M., Yu, C., Liu, H., Liu, Z., Jiang, T.: Disrupted small-world networks in schizophrenia. *Brain* **131**(4), 945–961 (2008)

14. Mislove, A., Koppula, H.S., Gummadi, K.P., Druschel, P., Bhattacharjee, B.: Growth of the Flickr Social Network. In: Proceedings of the 1st ACM SIGCOMM Workshop on Social Networks (WOSN'08), Seattle, WA (2008)
15. Newman, M.: Networks: An Introduction. Oxford University Press, New York (2010)
16. Rapoport, A.: Spread of information through a population with socio-structural bias. *Bull. Math. Biol.* **15**(4), 523–533 (1953)
17. Szell, M., Thurner, S.: Measuring social dynamics in a massive multiplayer online game. *Soc. Network* **39**, 313–329 (2010). <http://arxiv.org/abs/0911.1084>
18. Wasserman, L.: All of Statistics: A Concise Course in Statistical Inference. Springer, New York (2004)

Dynamic Communicability Predicts Infectiousness

Alexander V. Mantzaris and Desmond J. Higham

Abstract Using real, time-dependent social interaction data, we look at correlations between some recently proposed dynamic centrality measures and summaries from large-scale epidemic simulations. The evolving network arises from email exchanges. The centrality measures, which are relatively inexpensive to compute, assign rankings to individual nodes based on their ability to broadcast information over the dynamic topology. We compare these with node rankings based on infectiousness that arise when a full stochastic SI simulation is performed over the dynamic network. More precisely, we look at the proportion of the network that a node is able to infect over a fixed time period, and the length of time that it takes for a node to infect half the network. We find that the dynamic centrality measures are an excellent, and inexpensive, proxy for the full simulation-based measures.

1 Background and Motivation

In many social interactions, the timing of the connections is vital. Suppose A meets B today and B meets C tomorrow. This makes it possible for a message, or a disease, to pass from A to B, but not from C to A. Further, the more active B happens to be tomorrow, the more potential there is for today's A–B link to have a downstream effect. Several authors have pointed out the need to account for topological dynamics when considering disease propagation. The work in [15] considers the stages that sexually transmitted diseases (STDs) pass through when infecting subpopulations of a network, and shows that the timing in the connectivity between individuals plays a crucial role. In [10] a disease is simulated with an SI model (as we use here) and an SIR alternative, over contact networks relating to high-end prostitution. Both a static and a temporal view of the

A.V. Mantzaris (✉) · D.J. Higham
Department of Mathematics and Statistics, University of Strathclyde, Glasgow, UK
e-mail: alexander.mantzaris@strath.ac.uk

interaction data is used, and the results show that temporal effects play a key role. Epidemic simulations over temporal connectivity data are also used in [7] to explore vaccination strategies. Similarly, the spread of computer malware over temporal networks is considered in [13, 14], and strategies developed for the immunisation of key nodes. The SI framework is used in [2] to characterise the global structure of a temporal network.

From a network science perspective, it is natural to seek generic *centrality* measures that rank individual nodes according to their “importance.” In the case of static network topology, there is a wealth of such measures, most of which can be traced back to the social network analysis community [4]. Devising centrality measures that apply to time-dependent networks is a more recent pursuit. The work of [12] used a shortest-path-counting approach to measure the closeness/betweenness of nodes in a time varying graph. The alternative walk-counting approach in [5] was based on a direct generalization of Katz centrality [6] to the case of time-dependent networks. A key message from [11] and [8] is that centrality measures based on a static, aggregate summary of the network will not adequately reflect the hierarchy of importance.

The question that we address in this work is

given a time-dependent network, can suitable centrality measures provide useful information about the spread of epidemics?

The question is motivated by the fact that centrality measures are typically much cheaper to compute than large-scale stochastic simulations. For this reason, we focus on the dynamic communicability approach in [5] where we can deal with all nodes simultaneously by solving a sparse linear system at each time step (that is, finding x in a matrix-vector system of the form $Ax = b$, where A has the same sparsity as the current network adjacency matrix).

In the next section we give details of the computational tasks and the data set used. Sections 3 and 4 describe the data and results, and we finish with a discussion in Sect. 5.

2 Methodology

We consider a fixed set of N nodes whose connections are recorded at an equally spaced set of time points $t_0 < t_1 < \dots < t_M$. The network at each time point is undirected and unweighted, with no self loops. So, at time t_k , we can record the state of the network in the adjacency matrix $A^{[k]} \in \mathbb{R}^{N \times N}$. Here $(A^{[k]})_{ij} = 1$ if node i has a link to node j at time t_k and $(A^{[k]})_{ij} = 0$ otherwise.

The epidemic simulations are performed in a stochastic SI framework. At each time point a node is either susceptible (S) or infectious (I). Once made infectious, a node cannot return to the susceptible state. We begin, at t_0 , by infecting a single node. Generally, to determine the status of the nodes at time t_{k+1} , we

use the following rule: for each node that was in the infectious state at time t_k , we consider all the time t_{k+1} neighbours pointed to by this node. If any such neighbour is in the susceptible state, then it is moved into the infectious state with independent probability β . More loosely, an infectious node has a fixed probability β of transmitting the infection to each of its *current* contacts.

We measure the virulence of a node in two separate ways. After starting the infection at this node, we compute

- (a) the proportion of the network infected at the final time, t_M ,
- (b) the number of time points required to infect at least half of the network.

To understand the centrality measures from [5], we need to introduce the concept of a *dynamic walk of length w from node i to node j* : this is simply any traversal from i to j along w edges that respects the arrow of time (i.e. having used an edge at time t_r , the next edge that we use must exist at time t_r or later). The ability of node i to broadcast information to node j may then be measured as the total number of dynamic walks from i to j , where a walk of length w is downweighted by the factor α^w . Here $\alpha \in (0, 1)$ is a fixed parameter that reduces the influence of longer walks. In the case of a single time point, this measure reduces to the classical Katz centrality [6], which may be computed through the matrix resolvent, $(I - \alpha A)^{-1}$. Generalizing to multiple time points in this way, we arrive at the expression

$$\mathcal{Q} = (I - \alpha A^{[0]})^{-1} (I - \alpha A^{[1]})^{-1} \dots (I - \alpha A^{[M]})^{-1}, \tag{1}$$

where \mathcal{Q}_{ij} measures how well node i can broadcast information to node j . To obtain a single coefficient for node i we sum over all nodes in the network to obtain the *broadcast centrality*. In practice, since we plan to use this measure to rank the nodes, it is reasonable to normalize, which avoids numerical underflow/overflow, leading to the iteration

$$\hat{\mathcal{Q}}^{[k]} = \frac{\hat{\mathcal{Q}}^{[k-1]} (I - \alpha A^{[k]})^{-1}}{\left\| \hat{\mathcal{Q}}^{[k-1]} (I - \alpha A^{[k]})^{-1} \right\|}, \tag{2}$$

for $k = 0, \dots, M$, with $\hat{\mathcal{Q}}^{[-1]} = I$ and $\|\cdot\|$ representing the Euclidean matrix norm. The broadcast centrality for node i is then given by $\sum_{j=1}^N \left(\hat{\mathcal{Q}}^{[k]} \right)_{ij}$.

Just as in the original Katz version, this centrality measure involves a parameter, α . In order for the matrix inverses to exist, we require α to be less than

$$\alpha^* := \min_{0 \leq k \leq M} (\rho(A^{[k]})^{-1}),$$

where $\rho(\cdot)$ denotes the spectral radius. Tests in [5] indicated that the results are not sensitive to the choice of α , and in all tests here we use $\alpha = 0.9\alpha^*$.

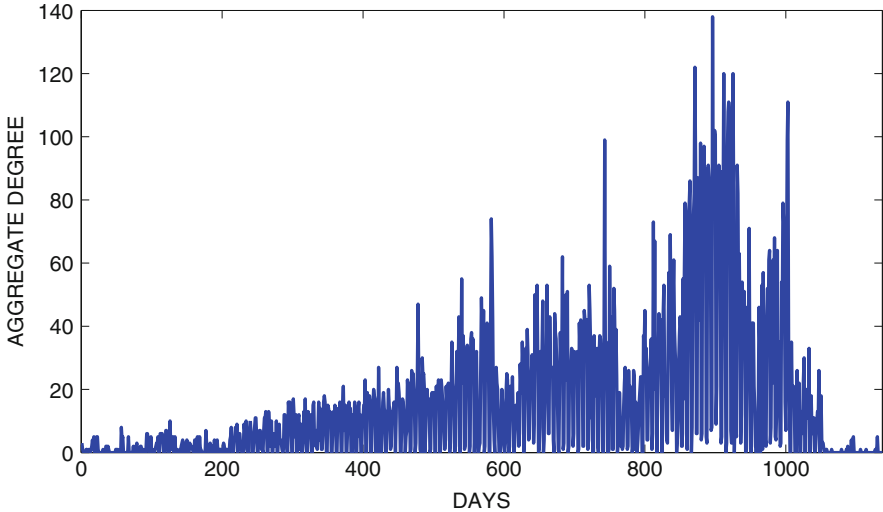


Fig. 1 The static aggregate degree each day for all of the nodes (Enron employees)

3 Data

We perform the tests on real social interaction data that records email exchanges between former Enron employees [3, 9]. There are $N = 151$ individuals, and we summarize activity into daily time slices: an undirected edge between i and j indicates that at least one email (including *cc* and *bcc*) passed between the two individuals. Figure 1 shows a plot of the static aggregate degree each day for all the nodes. Because the start date is arbitrary, we smooth out its influence by repeating computations over a sliding window that covers half the overall period; that is, 568 of the 1,036 consecutive days. So the first window runs from day 1 to day 568, the second window runs from day 2 to day 569, and so on. In this manner, we create 568 distinct evolving networks, each involving $M + 1 = 568$ consecutive days. Results are averaged over all windows.

For each of the 568 windows, we compute the broadcast centralities and, with each node in turn as a starting point for infection, perform one SI simulation. In practice we found that computing the broadcast centralities was typically an order of magnitude faster than computing $N = 151$ paths of the SI model, one from each starting state.

For a small number of windows/starting node combinations, the infection level remained below 50% at the final time point. For simplicity, these runs were omitted from the averaging process when we measured the average time to infect 50% of the population. For this reason, we regard the proportion of the network infected at the final time as the more robust of the two SI-based measures.

Table 1 Symbols for company position

President	Hexagram
CEO	Pentagram
Executive	Pentagram
Legal	Diamond
Vice President	Hexagram
Director of Trading	Square
Managing Director	Upward triangle
Manager	Right facing triangle
Director	Left facing triangle
In House Lawyer	Diamond
Trader	Square
Employee	Plus
Secretary	Circle
All others	Small dot

Table 2 Correlation coefficients relating to Figs. 3, 7 and 11 for broadcast versus proportion of the network infected

β	Pearson	Kendall Tau	Spearman
0.2	0.85	0.70	0.88
0.5	0.88	0.82	0.94
1.0	0.94	0.81	0.94

The Enron data set also provides the positions of most employees within the company. For completeness, we display this information in our figures. Table 1 indicates the symbols that we use. However, in the results that follow there does not appear to be any clear pattern based on these semantic labels.

4 Results

The SI simulations were repeated for three different choices of the infection probability, β . In each case, we provide two dimensional scatter plots (one point for each node) that compare, in a pair-wise fashion, (a) the proportion of the network infected at the final time point, (b) the time taken to infect 50% of the network, and (c) the natural logarithm of the broadcast centrality. The corresponding Pearson, Kendall Tau and Spearman correlation coefficients for (a)–(c) are reported in Table 2.

We also scatter plot the aggregate degree—that is, the total number of edges involving the node over all time points—against the proportion of the network infected.

We emphasize that the broadcast centrality and aggregate degree are independent of the parameter β in the SI model.

Fig. 2 Infected proportion versus time for 50 % of the network to be infected for $\beta = 0.2$

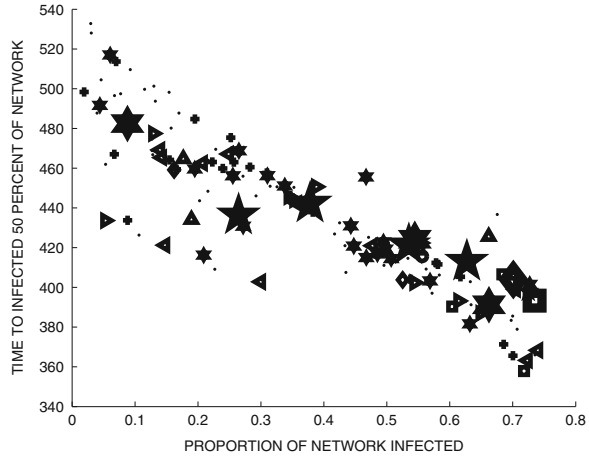
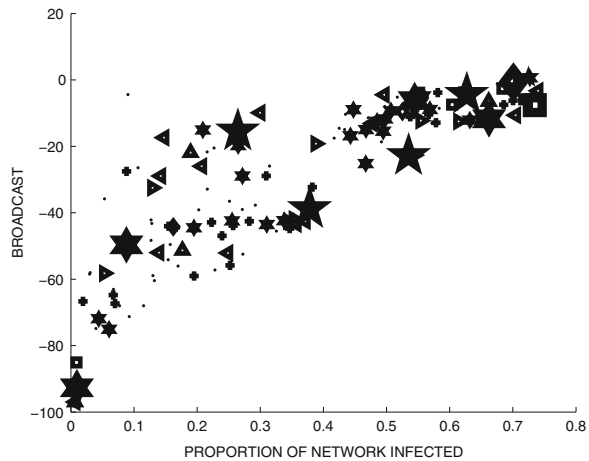


Fig. 3 Broadcast centrality versus infected proportion for $\beta = 0.2$



4.1 Infection Rate $\beta = 0.2$ Results

For $\beta = 0.2$, Fig. 2 focuses on the SI model and compares the infected proportion against the time to infect 50%. These are seen to have a strong negative correlation, and hence, in terms of ranking the nodes by infectiousness, they are broadly comparable.

The broadcast centrality is compared with the infected proportion in Fig. 3 and with the time to infect 50% in Fig. 4. In both cases, we see strong correlations.

In Fig. 5 we show the aggregate degree against the infection level. Although most of the very high degree nodes are typically strong infectors, the relationship is far from linear and breaks down at the lower levels. We also emphasize that the

Fig. 4 Broadcast centrality versus time to reach 50% network infection for $\beta = 0.2$

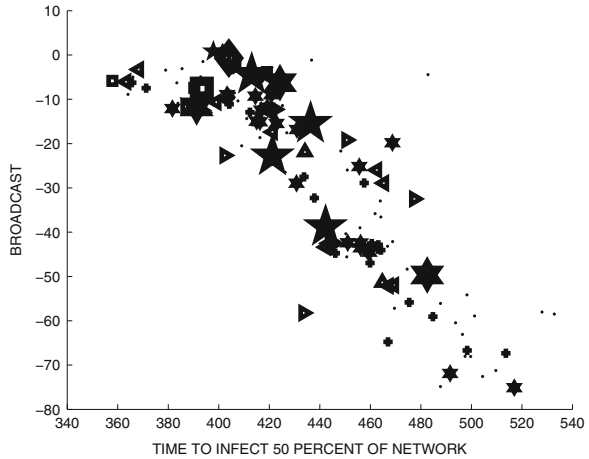
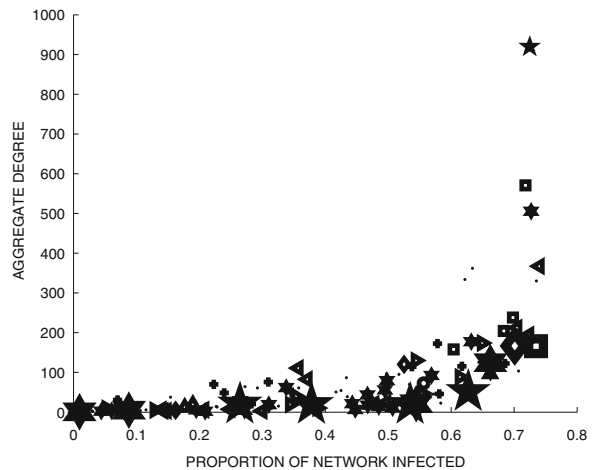


Fig. 5 Aggregate degree versus infected percentage for $\beta = 0.2$



integer-valued nature of nodal degree makes it liable to produce more ties when used to rank nodes.

4.2 Infection Rate $\beta = 0.5$ Results

We now repeat the experiments from Sect. 4.1 with a stronger infection rate of $\beta = 0.5$.

Figure 6 shows the infected proportion against the time to infect. We see that the two measures are inversely correlated more tightly than in the $\beta = 0.2$ case, shown in Fig. 2.

Fig. 6 The infected proportion against the time for 50% of the network to be infected for $\beta = 0.5$

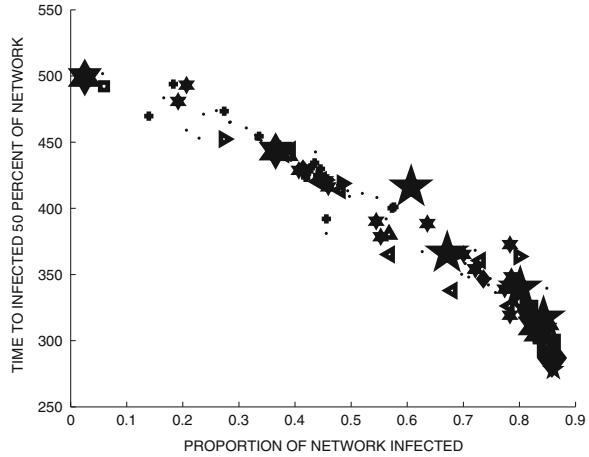
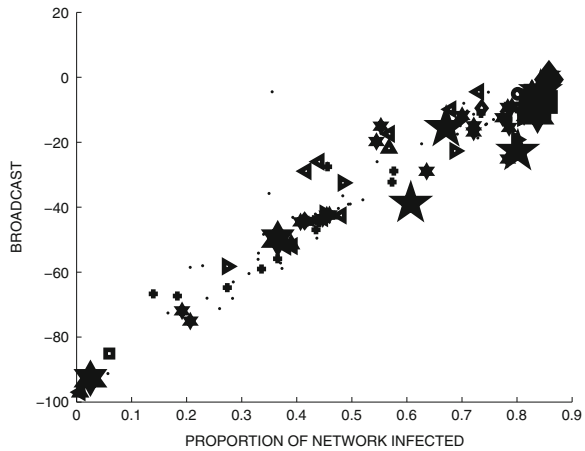


Fig. 7 Broadcast centrality versus infected proportion for $\beta = 0.5$



Figures 7 and 8 compare the broadcast centrality with infected proportion and time to infect 50%, respectively. The performance of the broadcast measure as a proxy seems to improve slightly over the $\beta = 0.2$ case. This is confirmed in Table 2 in terms of the three correlation coefficients.

Figure 9 shows the aggregate degree against infected proportion and the effect observed for $\beta = 0.2$ is now further exaggerated.

4.3 Infection Rate $\beta = 1.0$ Results

The final set of tests uses $\beta = 1.0$ in the SI model. In this case the disease transmission is no longer stochastic.

Fig. 8 Broadcast centrality versus time to reach 50% network infection for $\beta = 0.5$

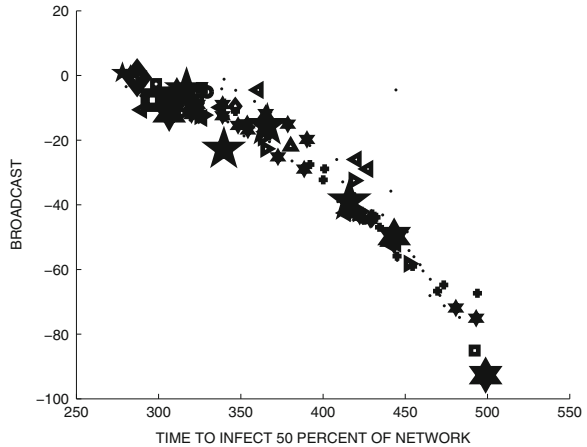
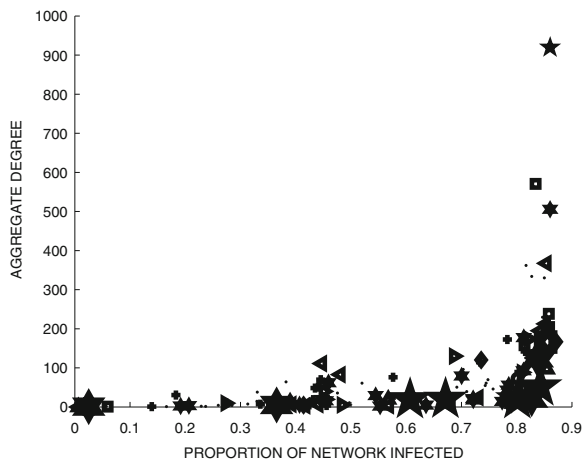


Fig. 9 Aggregate degree versus infected proportion for $\beta = 0.5$



Following the format of the previous subsections, Fig. 10 shows the infected proportion against the time for 50% infection, and Figs. 11 and 12 compare broadcast centrality with infected proportion and time to reach 50% network infection, respectively. In this case, looking at the SI model in isolation, we see a build up of virulent nodes in Fig. 10 that have a similar ability to infect around 85–90% of the network, but vary quite considerably in their time taken to infect the first 50%. The picture is ‘spoilt’ by the faster infectors being unable to ‘finish off’ the final 10% of nodes. To some extent this behaviour is also reflected in Fig. 11, where some of the very high broadcasters are underperforming in terms of their relative ability to infect a very high proportion of the network. The results in Fig. 12, where broadcast is compared with time to infect 50% of the network, show a smoother relationship. We conclude that in this high-infection-rate, sparse-connectivity regime, the time

Fig. 10 Infected percentage versus time for 50 % of the network to be infected for $\beta = 1.0$

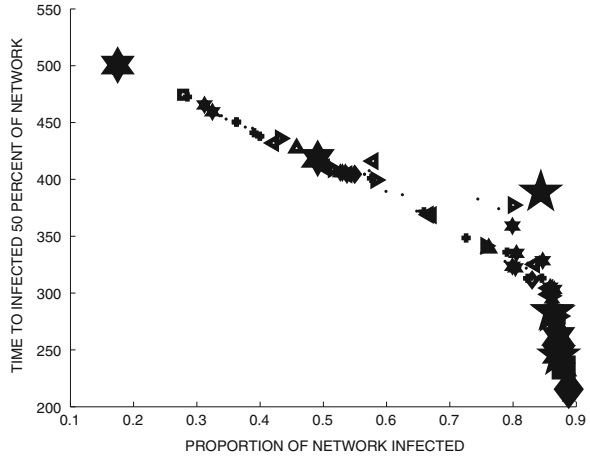
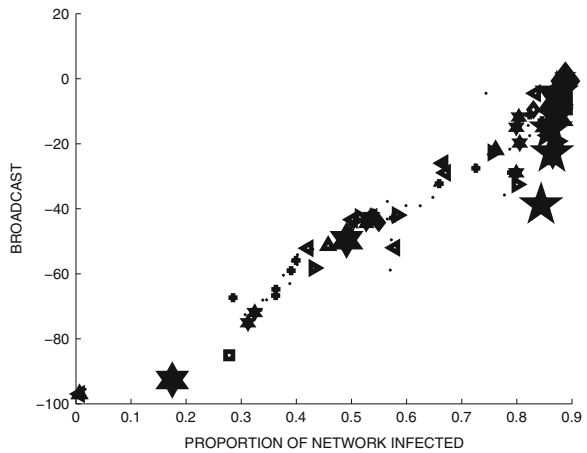


Fig. 11 Broadcast centrality versus infected proportion for $\beta = 1.0$



to infect 50 % is a more realistic measure of a node’s virulence than the infected proportion after a fixed, long time horizon.

Finally, Fig. 13 shows again that the aggregate degree is a poor predictor of the infected network proportion.

5 Discussion

We are concerned here with quantifying properties of a time-dependent interaction network in terms of epidemic spread. Our results indicate that ranking nodes according to their broadcast centrality from [5] can operate as an accurate, and relatively inexpensive, proxy for more detailed rankings of their ability to spread

Fig. 12 Broadcast centrality versus time to reach 50% network infection for $\beta = 1.0$

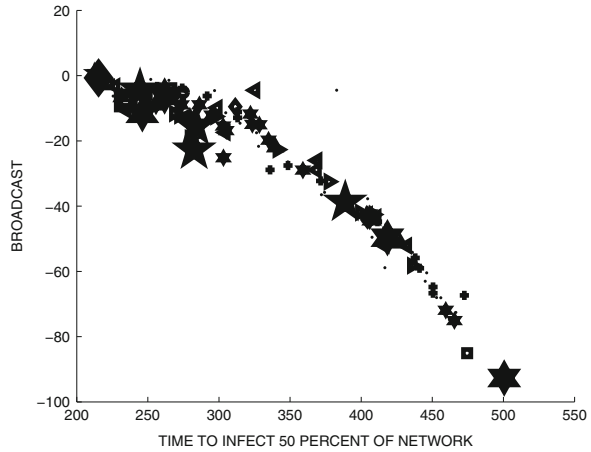
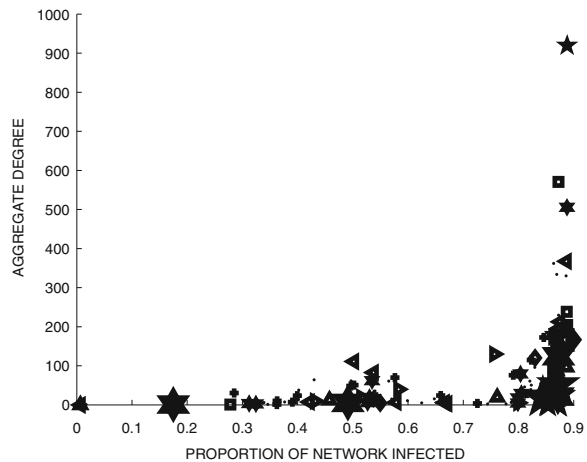


Fig. 13 Aggregate degree versus infected proportion for $\beta = 1.0$



infection based on averaging over microscale simulations. In particular, the results were insensitive to infection probability in the microscale model. By contrast, simply judging a node by its overall bandwidth does not provide a useful picture.

There are many avenues for extending this type of study. For example:

- Further investigation is needed to test whether improvements will arise from fine tuning the Katz-style downweighting parameter α used in the broadcast centrality measure, as a function of the infection probability, β .
- Other types of interaction data could be used to generate the underlying dynamic topology.
- The accompanying *receive centrality* measure from [5] can be tested as a proxy for the vulnerability of a node to infection.
- More complex compartmental epidemic models could be investigated, including SIS and SIR. In this case, our intuition is that the straightforward dynamic walk

counting approach of [5] will be less successful, and hence new classes of time-respecting network centrality measures will be required.

- In addition to local node-based information, global summaries, such as an appropriate, dynamic, version of the basic reproduction number, R_0 , could be compared with network features. A study of this type has recently been performed for the case of a static network in [1].

Acknowledgements This work was supported by the Engineering and Physical Sciences Research Council and the Research Councils UK Digital Economy Programme, under grant EP/I016058/1. DJH was also supported by a Fellowship from the Leverhulme Trust.

References

1. Ames, G., George, D., Hampson, C., Kanarek, A., McBee, C., Lockwood, D., Achter, J., Webb, C.: Using network properties to predict disease dynamics on human contact networks. *Proc. Biol. Sci.* **278**(1724), 3544–3550 (2011)
2. Barrat, A., Cattuto, C.: Temporal networks of face-to-face human interactions. In: Holme, P., Saramäki, J. (eds.) *Temporal Networks*. Springer, Berlin (2013)
3. Carvalho, V.R., Cohen, W.: Recommending recipients in the Enron email corpus. Tech. Rep. CMU-LTI-07-005, Carnegie Mellon University (2007)
4. Estrada, E.: *The Structure Of Complex Networks*. Oxford University Press, London (2011)
5. Grindrod, P., Higham, D.J., Parsons, M.C., Estrada, E.: Communicability across evolving networks. *Phys. Rev. E* **83**, 046120 (2011)
6. Katz, L.: A new index derived from sociometric data analysis. *Psychometrika* **18**, 39–43 (1953)
7. Lee, S., Rocha, L.E.C., Liljeros, F., Holme, P.: Exploiting temporal network structures of human interaction to effectively immunize populations. *PLoS ONE* **7**, e36439 (2012)
8. Mantzaris, A.V., Higham, D.J.: A model for dynamic communicators. *Eur. J. Appl. Math.* **23**, 659–668 (2012)
9. Nicosia, V., Tang, J., Mascolo, C., Musolesi, M., Russo, G., Latora, V.: Graph metrics for temporal networks. In: Holme, P., Saramäki, J. (eds.) *Temporal Networks*. Springer, Berlin (2013)
10. Rocha, L.E.C., Liljeros, F., Holme, P.: Simulated epidemics in an empirical spatiotemporal network of 50,185 sexual contacts. *PLoS Comput. Biol.* **7**, e1001109 (2011)
11. Tang, J., Musolesi, M., Mascolo, C., Latora, V., Nicosia, V.: Analysing information flows and key mediators through temporal centrality metrics. In: *SNS '10: Proceedings of the 3rd Workshop on Social Network Systems*, pp. 1–6. ACM, New York (2010). doi:<http://doi.acm.org/10.1145/1852658.1852661>
12. Tang, J., Scellato, S., Musolesi, M., Mascolo, C., Latora, V.: Small-world behavior in timevarying graphs. *Phys. Rev. E* **81**, 055101 (2010)
13. Tang, J., Mascolo, C., Musolesi, M., Latora, V.: Exploiting temporal complex network metrics in mobile malware containment. In: *Proceedings of IEEE 12th International Symposium on a World of Wireless Mobile and Multimedia Networks (WOWMOM)*, Published by IEEE (2011)
14. Tang, J., Leontiadis, I., Scellato, S., Nicosia, V., Mascolo, C., Musolesi, M., Latora, V.: Applications of temporal graph metrics to real-world networks. In: Holme, P., Saramäki, J. (eds.) *Temporal Networks*. Springer, Berlin (2013)
15. Wasserheit, J.N., Aral, S.O.: The dynamic topology of sexually transmitted disease epidemics: implications for prevention strategies. *J. Infect. Dis.* **174** (1996)

Random Walks on Stochastic Temporal Networks

Till Hoffmann, Mason A. Porter, and Renaud Lambiotte

Abstract In the study of dynamical processes on networks, there has been intense focus on network structure—i.e., the arrangement of edges and their associated weights—but the effects of the temporal patterns of edges remains poorly understood. In this chapter, we develop a mathematical framework for random walks on temporal networks using an approach that provides a compromise between abstract but unrealistic models and data-driven but non-mathematical approaches. To do this, we introduce a stochastic model for temporal networks in which we summarize the temporal and structural organization of a system using a matrix of waiting-time distributions. We show that random walks on stochastic temporal networks can be described exactly by an integro-differential master equation and derive an analytical expression for its asymptotic steady state. We also discuss how our work might be useful to help build centrality measures for temporal networks.

1 Introduction

A wide variety of systems are composed of interacting elements (e.g., nodes connected by edges) and can be represented as networks. Important examples include the Internet, highways and other transportation systems, and many social

T. Hoffmann

Department of Physics, University of Oxford, Oxford, OX1 3RH, UK

e-mail: tillahoffmann@gmail.com

M.A. Porter

Oxford Centre for Industrial and Applied Mathematics, Mathematical Institute and CABDyN

Complexity Centre, University of Oxford, Oxford, OX1 3LB, UK

e-mail: porterm@maths.ox.ac.uk

R. Lambiotte (✉)

Department of Mathematics, University of Namur, Namur, Belgium

e-mail: renaud.lambiotte@fundp.ac.be

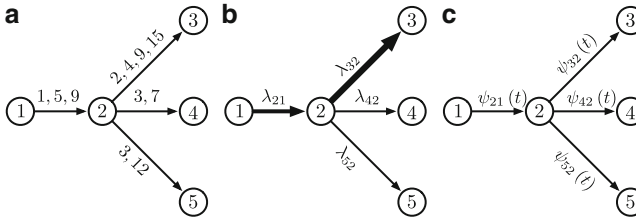


Fig. 1 Different levels of abstraction to model dynamics on temporal networks. In this illustration, a walker steps from node 1 to node 2 and then jumps to one of the latter's three neighbors. When studying dynamics on temporal networks, researchers tend to either (a) perform numerical simulations on empirical networks using the observed times at which edges are active between nodes or (b) develop mathematically-tractable Markovian models that neglect temporal patterns (typically by considering only aggregations of the interactions between nodes). In this chapter, we aim at finding (c) an intermediate level of modelling, in which we replace the sequence of activation times by a stochastic model that preserves a system's inter-event distribution. We thereby balance the amount of data included in the description with the description's simplicity

and biological systems. Because of the ubiquity of network representations, the study of networks has emerged as one of the fundamental building blocks in the study of complex systems [6, 13, 43].

Unfortunately, most empirical studies of networks thus far have been based on observations of snapshots of systems. Similarly, most theoretical efforts have focused on static network properties (such as degree distribution or modularity) and their effects on dynamical processes such as diffusion or epidemic spreading. In its current state, network theory thus fails to properly model a wide range of complex systems, in which interactions need not be active permanently but rather might switch on only temporarily. Observations in financial markets [49]; email [3, 12, 33, 39], letter [44], and online [34, 36] communication networks; face-to-face contacts [24]; movie rentals [4]; and many other situations have illustrated that the time intervals between edge activations can be distributed nontrivially, and the ensuing dynamics thus tend to deviate significantly from Poisson processes. It has also been shown that such burstiness yields radically different dynamics on networks. This makes it crucial to go beyond modelling dynamical systems on static networks by also considering the dynamics of the networks themselves [8, 14, 15, 22, 27, 29, 31, 40, 47, 51, 53, 55, 56].

A natural framework to study many time-dependent complex systems is to use temporal networks [21], in which one accounts for the timings of interactions instead of assuming static connectivity (e.g., by employing data aggregation) or that interactions take place at a uniform rate. Two approaches (see Fig. 1) have been used to add a temporal dimension to networks to account for constraints imposed by temporality on spreading processes. First, one can perform simulations on temporal graphs for which a time series of the presence versus absence of edges is deduced directly from empirical observations [27, 47]. However, such a computational approach has a significant drawback, as it relies entirely on numerical simulations

and is unable to provide a general picture of such problems. Second, one can use an abstract approach by developing spreading models that nevertheless attempt to incorporate realistic temporal statistics. Such models can then be studied either mathematically or using numerical simulations [53, 56]. In this second approach, an underlying network is studied as a fluctuating entity that is typically driven by a stationary stochastic process. This approach is nice because it is amenable to mathematical analysis [18, 22, 23, 26, 40], and it also provides a more accurate picture of time-dependent complex systems than do static networks.

In this chapter, which is a modified version of [20], we take the second approach and develop a mathematical framework to explore the effect of non-Poisson inter-event statistics on random walks. To do this, we apply the concept of a generalized master equation [41], which is traditionally defined on regular lattices, to the study of continuous-time random walks on arbitrary networks. Generalized master equations are a standard tool in non-equilibrium statistical physics; they lie at the heart of the theory for anomalous diffusion, and their applications range from ecology [32] to transport in materials [30]. Our choice regarding what dynamics to consider is motivated by the importance of random walks as a way to (i) understand how network structure affects dynamics and (ii) uncover prominent structural features of networks.

The rest of this chapter is organized as follows. We first introduce basic concepts of random walks on static networks and then introduce a model for stochastic temporal networks. We then derive a generalized master equation to describe random walks on stochastic temporal networks. We examine the stationary solution of this equation and show that it is determined by an effective transition matrix whose dominant eigenvector can be calculated rapidly even for very large networks if they are sparse. After checking that the generalized master equation reduces to standard rate equations when the underlying process satisfies Poisson statistics, we validate theoretical predictions using numerical simulations. Finally, we discuss the implications of our work for constructing centrality measures of nodes in temporal networks.

2 Random Walks on Static Networks

In this section, we review basic properties of random walks on static networks. The structure of a network is described by an $N \times N$ adjacency matrix A , where N is the number of nodes in the system. By definition, the adjacency matrix component A_{ij} gives the weight of an edge going from j to i . The adjacency matrix reflects the underlying network structure, on which various dynamical processes (e.g., diffusion) can occur. The simplest process that can be defined on a network is a discrete-time, unbiased random walk. At a given step of such a process, a walker located at a node j follows a particular edge leaving j with a probability proportional to the edge's weight.

The probability mass function (PMF) $n_{i;t}$ for a walker to occupy node i at time t evolves according to the equation

$$n_{i;t+1} = \sum_j T_{ij} n_{j;t}, \quad (1)$$

where T_{ij} , a component of the transition matrix T , represents the probability to jump from j to i and is defined as

$$T_{ij} = A_{ij}/s_j^{\text{out}}, \quad (2)$$

where the out-strength

$$s_j^{\text{out}} = \sum_i A_{ij}$$

of node j is the total weight of the edges leaving node j . Note that the PMF is equivalent to the expected density of an infinite ensemble of random walkers. Because the total number of walkers is conserved, the columns of T_{ij} are normalized:

$$\sum_i T_{ij} = \frac{1}{s_j^{\text{out}}} \sum_i A_{ij} = 1.$$

The condition $\sum_i n_{i;t} = 1$ is thus verified for all times t . The dynamical process (1) with transition matrix components (2) has been studied in detail, and a wide variety of its properties are known for many different types of networks [10]. For instance, consider a network that is undirected, which implies that $A_{ij} = A_{ji}$ and that the strength of node j is $s_i = s_i^{\text{out}}$, and also suppose that it is connected and non-bipartite. The above discrete-time random walk then converges to a unique equilibrium solution p with components

$$p_i = s_i/W, \quad (3)$$

where $W = \sum_i s_i$.

By construction, p is the dominant eigenvector (i.e., the eigenvector corresponding to the maximum positive eigenvalue) of the transition matrix. Its corresponding eigenvalue is 1, so it satisfies

$$\sum_j T_{ij} p_j = p_i.$$

When modelling diffusion, it is often desirable (and more realistic) to allow walkers to jump in an asynchronous fashion. A natural way to implement such a situation is to switch from a discrete-time to a continuous-time perspective [37]. One then needs to use a so-called *waiting-time distribution* (WTD), which determines the time that is spent by a walker on a node before traversing one of the available edges. The most common assumption is to use an exponential WTD:

$$\psi(i;t) = \lambda_i e^{-\lambda_i t},$$

for which the process is Markovian. The rates λ_i at which a walker jumps can in general be non-identical and depend on the node i on which the walker is located. Such continuous-time random walks are governed by the differential equation

$$\frac{dn_i}{dt} = \sum_j \left(\frac{A_{ij}}{s_j} \lambda_j - \lambda_i \delta_{ij} \right) n_j \equiv - \sum_j L_{ij} n_j, \quad (4)$$

where L_{ij} is the component of the Laplacian matrix describing the dynamics and $n_i(t)$ is the PMF to find a walker on node i at time t . For undirected networks, the stationary solution has components

$$p_i = \frac{s_i}{Z \lambda_i}, \quad (5)$$

where $Z = \sum_i s_i / \lambda_i$ is a normalization constant. One can interpret the quantity p_i as the frequency at which a node i is visited multiplied by the characteristic time $\langle t_i \rangle \approx 1/\lambda_i$ spent on it. This frequency is proportional to s_i , which is the same as for discrete-time random walks (3). Standard choices for the jumping rates include the uniform rate $\lambda_i = 1$, for which

$$L_{ij} = \delta_{ij} - A_{ij}/s_j, \quad (6)$$

and a rate $\lambda_i = s_i$ proportional to node strength, for which

$$L_{ij} = s_i \delta_{ij} - A_{ij}. \quad (7)$$

These are the two standard types of graph Laplacians. With the choice (7), the steady-state solution of a Poisson random walk is uniform (i.e., $p_i = 1/N$, which is independent of A) regardless of the topology and edge weights of a network.

3 Stochastic Temporal Networks

The models that we described in Sect. 2 overlook temporal patterns of the activation of edges by assigning a single scalar A_{ij} to represent an aggregation of the activity between nodes i and j . Such an aggregate measure of the importance of the connection between i and j is often understood as the rate at which edges are selected by a walker, and one can certainly use this perspective in (4). The probability for an edge to be selected in a time interval dt is thus independent of the time that has elapsed since the process started [19]. This Markovian assumption facilitates theoretical analysis, but it is accurate only for systems in which the rate at which events take place is not history-dependent.

To go beyond a Markovian picture, we propose to study random walks on networks that evolve in time in a stochastic manner. We assign to each edge an inter-event time distribution that determines when an edge is accessible for transport.

The dynamics of a network are thus characterized by an $N \times N$ matrix $\psi(t)$ of waiting-time distributions $\psi_{ij}(t)$ that determine the appearance of an edge emanating from node j and arriving at node i . We also assume that the edges remain present for infinitesimally small times. That is, no network edge is present except at random instantaneous times determined by $\psi(t)$, when a single edge is present. From now on, we employ the following terminology. We use \mathcal{G} to denote an underlying graph that determines which edges are allowed and which are not, and $\psi_{ij}(t)$ determines a dynamic graph in which edges appear randomly according to the assigned waiting times. We use such a random process to model the transitions of a random walker moving on \mathcal{G} . By construction, a walker located at a node j remains on it until an edge leaving j toward some node i appears. When such an event occurs, the walker jumps to i without delay and then waits until an edge leaving i appears.

There are several ways that one can set up the WTDs $\psi_{ij}(t)$. One option is to consider the processes leading to steps being associated with an *active* walker. In this case, the walker's clock is reinitialized when it makes a step to a node. For example, gossip traversing a social network might be modeled using an active walker because the process of broadcasting gossip restarts when the gossip is received by a new contact. Another option is to consider the processes leading to steps being associated with a *passive* walker. In this case, the edges' clocks are reinitialized when they are activated. A virus spreading across a social network might be modeled using a passive walker because interactions among people are not (primarily) initiated by a virus. In the present work, we consider the case of an active walker in which a WTD corresponds to the probability for an edge to occur between times t and $t + dt$ after the random walker arrives on node j at time $t = 0$ (recall that the clock is reset when the walker arrives at a node).

It follows from the definition of the WTDs as probability distribution functions that

$$\int_0^{\infty} \psi_{ij}(t) dt = 1.$$

The probability that an edge appears between j and i before time t is

$$\int_0^t \psi_{ij}(t') dt',$$

and the probability that it does not appear before time t is therefore

$$\chi_{ij}(t) \equiv 1 - \int_0^t \psi_{ij}(t') dt'. \quad (8)$$

If a transition from j to i is not allowed, then the corresponding element $\psi_{ij}(t)$ is equal to 0 for all times.

It is important to distinguish between the WTD $\psi_{ij}(t)$ of the process that might lead to a step along a network and the probability distribution $T_{ij}(t)$ for actually making a step from j to i . This distinction is necessary because all of the processes

on a node are assumed to be independent of one another, but the probability to make a step depends on all of the processes. As an illustration, consider a walker on a node j with only one outgoing edge to i . The probability distribution function (PDF) to make a step to i at time t after having arrived on j is then

$$T_{ij}(t) = \psi_{ij}(t) .$$

However, if there exists another edge leaving j (e.g., an edge to node k), then the PDF to make a transition to i is modified, as a step to i only occurs if the edge to i appears before the one going to k . In this situation,

$$T_{ij}(t) = \psi_{ij}(t) \chi_{kj}(t) .$$

In general, the PDF to make a step from j to i accounting for all other processes on j is

$$\begin{aligned} T_{ij}(t) &= \psi_{ij}(t) \times \prod_{k \neq i} \chi_{kj}(t) \\ &= \psi_{ij}(t) \times \prod_{k \neq i} \left(1 - \int_0^t \psi_{kj}(t') dt' \right) . \end{aligned} \tag{9}$$

Equation (9) emphasizes the importance of the temporal ordering of the edges in the random walk. In particular, it gives greater importance to edges that tend to appear before others and are thus more likely to be traversed by a random walker.

4 Generalized Montroll-Weiss Equation

We now focus on the trajectories of a random walker exploring the stochastic temporal network that we described in Sect. 3. We closely follow the standard derivation of the Montroll-Weiss (MW) equation [41], which is traditionally defined on regular lattices, and we generalize it to an arbitrary N -node network of transitions. We are interested in finding the PMF $n_i(t)$ for a walker to occupy node i at time t . The PMF is given by the integral over all probabilities $q_i(t')$ of having arrived on node i at time $t' \leq t$, weighted by the probability $\phi_i(t - t')$ of not having left the node since then:

$$n_i(t) = \int_0^t \phi_i(t - t') q_i(t') dt' . \tag{10}$$

Taking the Laplace transform

$$\hat{n}_i(s) \equiv \mathcal{L}\{n_i(t)\} = \int_0^\infty n_i(t) e^{-st} dt$$

allows us to exploit the fact that the convolution in (10) reduces to a product in Laplace space:

$$\hat{n}_i(s) = \hat{\phi}_i(s) \hat{q}_i(s) . \quad (11)$$

We obtain the quantity $\hat{\phi}_i(s)$ in (11) as follows. The probability distribution to make a step from node i to any other node is

$$T_i(t) = \sum_{j=1}^N T_{ji}(t) . \quad (12)$$

The PDF to remain immobile on node i for a time t is thus given by

$$\phi_i = 1 - \int_0^t T_i(t') dt' ,$$

whose Laplace transform is

$$\hat{\phi}_i(s) = \frac{1}{s} \left(1 - \hat{T}_i(s) \right) . \quad (13)$$

The quantity $\hat{q}_i(s)$ is the Laplace transform of the PDF $q_i(t)$, which describes the probability of arriving on node i exactly at time t . One calculates it by accounting for all k -step processes that can lead to such an event [50]:

$$q_i(t) \equiv \sum_{k=0}^{\infty} q_i^{(k)}(t) ,$$

where $q_i^{(k)}(t)$ represents the probability to arrive on node i at time t in exactly k steps. Note that the PDF at node i is related to that at node j by the recursion relation

$$q_i^{(k+1)}(t) = \int_0^t d\tau \sum_j T_{ij}(t-\tau) q_j^{(k)}(\tau) . \quad (14)$$

In other words, the probability to arrive on node i in $k+1$ steps is the probability to arrive at any other node j in k steps weighted by the probability of making a step $j \rightarrow i$ at the required time. Upon taking a Laplace transform, (14) becomes

$$\hat{q}_i^{(k+1)}(s) = \sum_j \hat{T}_{ij}(s) \hat{q}_j^{(k)}(s) .$$

Summing over all k and adding $\hat{q}_i^{(0)}(s)$ yields

$$\hat{q}_i^{(0)}(s) + \sum_{k=0}^{\infty} \hat{q}_i^{(k+1)}(s) = \sum_j \hat{T}_{ij}(s) \sum_{k=0}^{\infty} \hat{q}_j^{(k)}(s) + \hat{q}_i^{(0)}(s) ,$$

which can also be written in terms of matrices and vectors as

$$\hat{q}(s) = \hat{T}(s) \hat{q}(s) + \hat{q}^{(0)}(s) .$$

Noting that $q^{(0)}(t) = n(0) \delta(t)$, we see that the last term is simply $n(0)$, which leads to the following solution in Laplace space:

$$\hat{q}(s) = \left(I - \hat{T}(s) \right)^{-1} n(0) . \quad (15)$$

We insert the expression (13) for $\hat{\phi}_i(s)$ and the expression (15) for $\hat{q}_i(s)$ into the equation for the PMF (11) to obtain a generalization of the MW equation [41] that applies to arbitrary network structures:

$$\begin{aligned} \hat{n}_i(s) &= \frac{1}{s} \left(1 - \hat{T}_i(s) \right) \sum_k \left(I - \hat{T}(s) \right)_{ik}^{-1} n_k(0) \\ &= \sum_{jk} \frac{1}{s} \left(I_{ij} - \hat{T}_i(s) \delta_{ij} \right) \left(I - \hat{T}(s) \right)_{jk}^{-1} n_k(0) . \end{aligned}$$

In terms of vectors and matrices, we write this as

$$\hat{n}(s) = \frac{1}{s} \left(I - \hat{D}_T(s) \right) \left(I - \hat{T}(s) \right)^{-1} n(0) , \quad (16)$$

where the diagonal matrix \hat{D}_T has components given by

$$\left(\hat{D}_T \right)_{ij}(s) \equiv \hat{T}_i(s) \delta_{ij} .$$

Equation (16) is a formal solution in Laplace space for the PMF of a random walk whose dynamics are governed by the WTDs $\psi_{ij}(t)$. However, taking the inverse Laplace transform to obtain the PMF as a function of time does not in general yield closed-form solutions.

The non-Markovian nature of equation (16) becomes clear after taking an inverse Laplace transform and returning to a description in the original time variable. This leads to the integro-differential equation

$$\frac{dn}{dt} = \left(T(t) * \mathcal{L}^{-1} \left\{ \hat{D}_T^{-1}(s) \right\} - \delta(t) \right) * K(t) * n(t) , \quad (17)$$

where \mathcal{L}^{-1} denotes the inverse Laplace transform and

$$f * g = \int_0^t d\tau f(t - \tau) g(\tau)$$

denotes convolution with respect to time. The *memory kernel* K characterizes the amount of memory in the dynamics [2] and is defined in Laplace space by

$$\hat{K}(s) \equiv \frac{s\hat{D}_T(s)}{I - \hat{D}_T(s)}.$$

Because of the convolutions, the temporal evolution of the PMF at time t depends on the states of the system at all times since the initial condition.

Although the integro-differential equation (17) is instructive, it is difficult to manipulate in practice, and it is often significantly easier to analyze the associated Laplace-space equation (16). For example, the total number of walkers is conserved if and only if

$$\frac{d}{dt} \sum_i n_i(t) = 0,$$

which is difficult to verify in the time domain. We refer the reader to our paper [20] for a detailed derivation of (17) and a proof in Laplace space that the total number of walkers is indeed conserved.

5 Asymptotic State

5.1 Preliminaries

Based on our analysis of random walks on static networks, we expect the walker distribution to reach a unique steady-state solution as $t \rightarrow \infty$ as long as any node can be reached from any other node. The asymptotic steady-state PMF p satisfies

$$p = \lim_{t \rightarrow \infty} n(t) = \lim_{s \rightarrow 0} s\hat{n}(s),$$

so

$$p = Mn(0), \tag{18}$$

where the matrix

$$M \equiv \lim_{s \rightarrow 0} \left(I - \hat{D}(s) \right) \left(I - \hat{T}(s) \right)^{-1}$$

maps the initial state $n(0)$ to the final state p . In the limit $s \rightarrow 0$, one can expand the exponential in the definition of the Laplace transform to first order:

$$\begin{aligned} \left[\hat{D}_T(s) \right]_{ij} &= \int_0^\infty (1-st) T_j(t) \delta_{ij} dt + O(s^2) \\ &= (1-s\langle t_j \rangle) \delta_{ij} + O(s^2) \\ &= (I - sD_{(t)})_{ij} + O(s^2), \end{aligned}$$

where the resting time

$$\langle t_j \rangle = \int_0^\infty t T_j(t) dt \tag{19}$$

is the mean time spent on node j and the diagonal matrix $D_{\langle t \rangle}$ has components given by

$$[D_{\langle t \rangle}]_{ij} \equiv \langle t_j \rangle \delta_{ij}.$$

Similarly, one can use the approximation

$$\begin{aligned} \hat{T}_{ij} &= \int_0^\infty [1 - st + O(s^2)] T_{ij}(t) dt \\ &= \mathbb{T}_{ij} \left(1 - s \int_0^\infty t \frac{T_{ij}(t)}{\mathbb{T}_{ij}} dt + O(s^2) \right) \\ &= \mathbb{T}_{ij} [1 - s \langle t_{ij} \rangle + O(s^2)], \end{aligned} \tag{20}$$

where $\langle t_{ij} \rangle$ is the mean time before making a step $j \rightarrow i$ and the components of the *effective transition matrix* \mathbb{T} are

$$\mathbb{T}_{ij} \equiv \int_0^\infty T_{ij}(t) dt. \tag{21}$$

We write (20) in matrix form as

$$\hat{T} = \mathbb{T} - s \mathbb{T} \circ \langle t \rangle + O(s^2),$$

where \circ denotes the Hadamard component-wise product. This yields our final expression:

$$M = \lim_{s \rightarrow 0} \left[s D_{\langle t \rangle} (I - \mathbb{T} - s \mathbb{T} \circ \langle t \rangle)^{-1} + O(s^2) \right]. \tag{22}$$

5.2 Effective Transition Matrix

Before focusing on the stationary state p in (18), we discuss the properties of \mathbb{T} . The matrix element \mathbb{T}_{ij} is the probability of making a step $j \rightarrow i$ for any time $t \in [0, \infty)$. Thus, $\mathbb{T}_{ij} \geq 0$ for all i and j . Additionally,

$$\sum_i \mathbb{T}_{ij} = 1, \tag{23}$$

so \mathbb{T} is a stochastic matrix (which we call the “effective transition matrix” of the stochastic process). Because we have assumed that \mathcal{G} is strongly connected, the stochastic matrix is irreducible and its dominant eigenvector x satisfies

$$\mathbb{T}x = x, \tag{24}$$

which has an eigenvalue of 1 and is unique [52]. As we will see below, the matrix \mathbb{T} plays an important role in determining the asymptotic state of the system as $t \rightarrow \infty$.

By definition, (23) is equivalent to the condition

$$\int_0^\infty T_j(t) dt = 1,$$

which is expected to be true if node j is connected to at least one other node.¹ Therefore, a transition from j to some other node is guaranteed to occur eventually if one allows infinite time. To show this, we use (9) and (12) to obtain

$$\begin{aligned} T_j(t) &= \sum_{i=1}^N T_{ij}(t) = - \sum_{i=1}^N \left(\frac{d\chi_{ij}(t)}{dt} \times \prod_{k \neq i} \chi_{kj}(t) \right) \\ &= - \frac{d}{dt} \left(\prod_{i=1}^N \chi_{ij}(t) \right). \end{aligned}$$

Integrating over the entire time domain yields

$$\begin{aligned} \int_0^\infty T_j(t) dt &= - \int_0^\infty dt \times \frac{d}{dt} \left(\prod_{i=1}^N \chi_{ij}(t) \right) \\ &= - \left(\prod_{i=1}^N \chi_{ij}(t) \right) \Big|_{t=0}^\infty = 1, \end{aligned}$$

because $\chi_{ij}(0) = 1$ and $\chi_{ij}(\infty) = 0$ when the edge $j \rightarrow i$ exists in the underlying graph \mathcal{G} .

5.3 Steady-State Solutions

The matrix M in (22) maps any initial condition onto a unique vector as long as the underlying graph \mathcal{G} consists of a single strongly connected component [20]. The

¹This condition holds in our setting, as we have assumed that the underlying graph \mathcal{G} of potential edges is strongly connected.

steady-state solution p is then given by the dominant eigenvector of the matrix M . In practice, it is easier to obtain the least dominant eigenvector of its inverse

$$\begin{aligned} M^{-1} &= \lim_{s \rightarrow 0} \frac{1}{s} [I - \mathbb{T} - s\mathbb{T} \circ \langle t \rangle] D_{\langle t \rangle}^{-1} \\ &= \lim_{s \rightarrow 0} \left[\frac{1}{s} (I - \mathbb{T}) D_{\langle t \rangle}^{-1} - (\mathbb{T} \circ \langle t \rangle) D_{\langle t \rangle}^{-1} \right]. \end{aligned} \quad (25)$$

In the limit $s \rightarrow 0$, the eigenvectors of M^{-1} tend to the eigenvectors of the matrix

$$C \equiv (I - \mathbb{T}) D_{\langle t \rangle}^{-1},$$

because the second term in the second line of (25) becomes negligible in comparison to the first term. Thus, in the limit $s \rightarrow 0$, finding the dominant eigenvector of M reduces to finding the least dominant eigenvector of C . It follows that

$$\begin{aligned} Cp &= (I - \mathbb{T}) D_{\langle t \rangle}^{-1} D_{\langle t \rangle} x \\ &= Ix - \mathbb{T}x = 0, \end{aligned}$$

where we recall that x is the dominant eigenvector of \mathbb{T} . Therefore, the steady-state solution is

$$p = \beta D_{\langle t \rangle} x, \quad (26)$$

where β is a normalization constant.

The equilibrium solution in (26) takes a particularly simple form that is similar to the stationary solution (5) for Markovian continuous-time random walks on static networks. The time spent on node i is given by the frequency to arrive on i multiplied by the waiting time $\langle t_i \rangle$ spent on i . One can compute this solution easily even for very large graphs, because deriving \mathbb{T} from ψ is straightforward and one can compute the dominant eigenvector of a large matrix using standard, efficient techniques (such as the power method [38]).

5.4 Example: Edges Governed by Poisson Processes

We now focus on the particular case in which the underlying network \mathcal{G} is undirected and the edge dynamics are governed by Poisson processes. The WTDs are then given by exponential distributions [52]

$$\psi_{ij}(t) = \lambda_{ij} e^{-\lambda_{ij} t}, \quad (27)$$

where λ_{ij} is the characteristic rate for the transition $j \rightarrow i$. In this situation, (9) becomes

$$T_{ij}(t) = \lambda_{ij} e^{-\lambda_{ij}t} \prod_{l \neq i} \left(1 - \int_0^t \lambda_{lj} e^{-\lambda_{lj}t'} dt' \right) = \lambda_{ij} e^{-\Lambda_j t}, \quad (28)$$

and (12) becomes

$$T_j(t) = \sum_{i=1}^N \lambda_{ij} e^{-\Lambda_j t} = \Lambda_j e^{-\Lambda_j t},$$

where the aggregate transition rate from node j is defined as $\Lambda_j \equiv \sum_{i=1}^N \lambda_{ij}$. It follows from (28) that the effective transition matrix \mathbb{T} satisfies

$$\mathbb{T}_{ij} = \frac{\lambda_{ij}}{\sum_{i=1}^N \lambda_{ij}} = \frac{\lambda_{ij}}{\Lambda_j}. \quad (29)$$

The probability to follow an edge is thus proportional to its weight, and we recover the usual rate equation (4). In particular, we obtain

$$\frac{dn_i}{dt} = \sum_j \lambda_{ij} n_j(t) - \Lambda_i n_i(t), \quad (30)$$

so the dynamics are governed by the combinatorial Laplacian $L_{ij} = \lambda_{ij} - \Lambda_i \delta_{ij}$ of a weighted network defined by the adjacency matrix λ with components λ_{ij} . As we discussed in Sect. 2, the steady-state solution p is thus uniform (independent of the details of the rate matrix λ).

Equation (30) shows that a random walk on a stochastic temporal network driven by (27) is equivalent to a Poisson continuous-time random walk on a static network that is constructed by aggregating a temporal network by counting the number of times edges appear between each pair of nodes.

5.5 Numerical Experiments

In this section, we consider a toy example of a completely connected graph with $N = 3$ nodes to illustrate how the nature of the WTDs can affect dynamics.

We suppose that the WTDs for the processes occurring on the edges have different functional forms and different characteristic times (see Fig. 2), and we compare this non-Poisson situation to a situation with edges governed by Poisson processes with the same mean rates. In our example, the characteristic-rate matrix

$$\lambda = \begin{pmatrix} 0 & 1 & 2 \\ 1 & 0 & 3 \\ 2 & 3 & 0 \end{pmatrix}$$

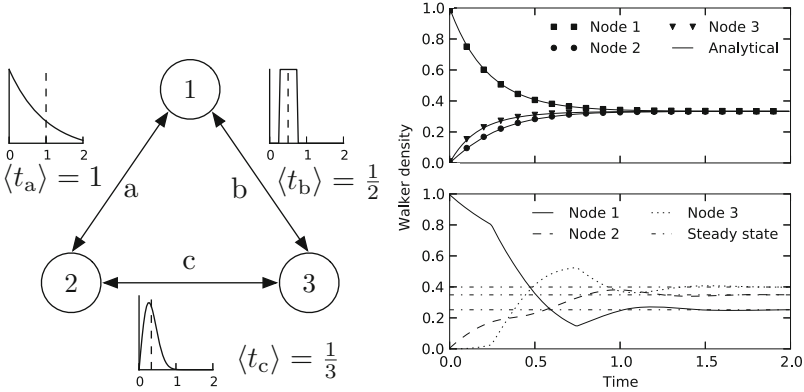


Fig. 2 (Left) Illustration of random-walk dynamics on an undirected network with $N = 3$ nodes and no self-loops. The waiting-time distributions for the edges a , b , and c are exponential, uniform, and Rayleigh, respectively. Their corresponding means are $\langle t_a \rangle$, $\langle t_b \rangle$, and $\langle t_c \rangle$. (Right) Mean temporal evolution of the PMFs obtained from 10^6 numerical simulations for (upper panel) Poisson and (lower panel) non-Poisson processes. In the former case, we also plot the corresponding analytical solutions of the rate equation. The error bars are smaller than the width of the curves that we used for plotting. For the non-Poisson example, we obtain the steady-state PMFs from (26)

Table 1 Comparison of the effective transition matrix, dominant eigenvector, mean resting times, and stationary solution for a Poisson random walk and a non-Poisson random walk on a toy network with $N = 3$ nodes

Symbol	Eq.	Poisson	Non-Poisson
Effective transition matrix (\mathbb{T})	(21)	$\begin{pmatrix} 0.000 & 0.250 & 0.400 \\ 0.333 & 0.000 & 0.600 \\ 0.667 & 0.750 & 0.000 \end{pmatrix}$	$\begin{pmatrix} 0.000 & 0.387 & 0.772 \\ 0.273 & 0.000 & 0.228 \\ 0.727 & 0.613 & 0.000 \end{pmatrix}$
Dominant eigenvector (x)	(24)	$(0.250, 0.333, 0.417)^T$	$(0.392, 0.200, 0.408)^T$
Mean resting time ($\langle t_i \rangle$)	(19)	$(0.333, 0.250, 0.200)^T$	$(0.273, 0.387, 0.301)^T$
Stationary solution (p)	(26)	$(0.333, 0.333, 0.333)^T$	$(0.349, 0.252, 0.399)^T$

Incorrect normalizations of PMFs are due to rounding errors.

is identical in both situations. However, the resulting effective transition matrices, mean resting times, and stationary solutions differ (see Table 1). We plot the temporal evolution of the PMFs in Fig. 2 to illustrate the differences between the two situations. We obtain PMFs from numerical simulations of random walks with all walkers located at node 1 initially. The system relaxes towards a stationary solution in both cases, but this stationary solution clearly depends on the nature of the WTDs, as walkers tend to be underrepresented on node 1 for the non-Poisson dynamics. See our paper [20] for additional numerical experiments and other details.

6 Discussion

In this chapter, we developed a mathematical framework that allows one to incorporate nontrivial temporal statistics into the study of networks. We proposed a simple stochastic model for temporal networks and considered how stochastic processes on edges can affect diffusion processes. In particular, we conducted an analytical study of a random walk on stochastic temporal networks in which we demonstrated that its dynamics are driven by an integro-differential master equation. Despite the complexity of this non-Markovian process, we found an analytical expression for its asymptotic steady-state solution and verified its validity using numerical experiments.

We believe that our approach offers an interesting compromise between abstract but unrealistic models and data-driven but non-mathematical approaches for studying temporal networks. However, our work does suffer from limitations that might hinder its applicability in practical contexts, and attempting to remove these limitations offers several interesting research directions. First, we summarized the temporal statistics using only inter-event time distributions and thereby neglected other correlations, such as those involving three or more events [28]. Second, we examined stationary-state dynamics of temporal networks, and many systems that can be modeled using temporal networks do not attain stationary states (due, for example, to daily or weekly patterns). Finally, we implicitly assumed when solving the generalized Montroll-Weiss equation (16) that the first moments of $\psi_{ij}(t)$ and $T_{ij}(t)$ are finite. In Sect. 5.1, we performed a small- s expansion and used the quantities $\langle t_j \rangle$ and $\langle t_{ij} \rangle$ in our calculations. These operations are not valid when it is not possible to define a characteristic waiting time between two steps. (This occurs, for example, when the Laplace transform of the WTDs behaves near $s = 0$ like $1 - as^\alpha$, where $\alpha < 1$ [2].) Because empirical observations of WTDs in real-world systems often have heavy tails [3], it would be interesting to extend our results to this situation.

We expect our approach to pave the way for the development of new tools that consider both network structure and network dynamics [37]. For example, there is an urgent need for the development of approaches to analyze networks that properly take into account the temporal dynamics of edges [17, 42, 45, 54]. A direct application of our work is to define a modified version of PageRank centrality (which is sometimes called simply PageRank) [7], as well as modified versions of related measures [43], to measure the importance of nodes with respect to the dynamics of a random walker on a temporal network. PageRank is a conservative [16], non-local measure of node *centrality* (i.e., of a node's importance [43]) that has been applied to a huge variety of networks across a broad range of scholarly disciplines both in its original form [5, 38, 43, 46] and in slight variations of it [1, 9, 35]. The PageRank vector is usually defined for discrete-time random walks, and the components of this vector are given by the frequency at which the corresponding nodes are visited in the $t \rightarrow \infty$ limit. The PageRank vector is equal to the dominant eigenvector of the transition matrix T , whose components are given by (2). Constructing an analog of PageRank is somewhat

more complicated for a continuous-time process, as the steady-state PMF p and frequency of visits x are now different in general. As we have discussed in this chapter, these two quantities are related by the relation $p = \beta D_{(t)} x$ at stationarity, where $D_{(t)}$ is the mean time spent on a node before leaving it. To ensure that the standard PageRank vector is recovered in the Poisson limit, we choose to use x for the PageRank centrality of a continuous-time process. Accordingly, we define PageRank on stochastic temporal networks as the dominant eigenvector of the effective transition matrix \mathbb{T} , as this gives more importance to edges that are visited more by walkers due to the temporal order of their appearance. It would be interesting to explore the properties of this centrality measure and to compare it to PageRank and other existing (conservative) notions of centrality. It would also be interesting to develop non-conservative centrality notions for temporal networks, and one has to consider processes other than random walks to do that [16]. Other possible applications of our work include the construction of random-walk-based measures of network modularity [11, 42, 48] or node similarity [25] for stochastic temporal networks.

Acknowledgements This chapter is based on [20], which contains additional calculations and numerical simulations. RL would like to acknowledge support from FNRS (MIS-2012-F.4527.12) and Belspo (PAI Dysco). MAP acknowledges a research award (#220020177) from the James S. McDonnell Foundation and a grant from the EPSRC (EP/J001759/1). We thank T. Carletti, J.-C. Delvenne, P. J. Mucha, M. Rosvall, and J. Saramäki for fruitful discussions, and we thank P. Holme for helpful comments in his review of this manuscript.

References

1. Allesina, S., Pascual, M.: Googling food webs: can an eigenvector measure species' importance for coextinctions? *PLoS Comput. Biol.* **5**, e1000494 (2009)
2. Balescu, R.: *Statistical Dynamics*. Imperial College Press, London (1997)
3. Barabási, A.-L.: The origin of bursts and heavy tails in human dynamics. *Nature* **435**, 207 (2005)
4. Beguerisse Díaz, M., Porter, M.A., Onnela, J.-P.: Competition for popularity in catalog networks. *Chaos* **20**, 043101 (2010)
5. Bergstrom, C., West, J., Wiseman, M.: The eigenfactor metrics. *J. Neurosci.* **28**, 11433 (2008)
6. Boccaletti, S., Latora, V., Moreno, Y., Chavez, M., Hwang, D.-U.: Complex networks: Structure and dynamics. *Phys. Rep.* **424**, 175–308 (2006)
7. Brin, S., Page, L.: The anatomy of a large-scale hypertextual Web search engine. In: *Proceedings of the 7th International Conference on World Wide Web (WWW)*, pp. 107–117, Elsevier, Amsterdam, The Netherlands (1998)
8. Caley, P., Becker, N.G., Philp, D.J.: The waiting time for inter-country spread of pandemic influenza. *PLoS ONE* **2**, e143 (2007)
9. Callaghan, T., Mucha, P.J., Porter, M.A.: Random walker ranking for NCAA Division IA football. *Am. Math. Mon.* **114**, 761–777 (2007)
10. Chung, F.: *Spectral Graph Theory*. CBMS Regional Conference Series in Mathematics, No. 92. American Mathematical Society, Providence (1996)
11. Delvenne, J.-C., Yaliraki, S., Barahona, M.: Stability of graph communities across time scales. *Proc. Natl. Acad. Sci. USA* **107**, 12755 (2010)

12. Eckmann, J.-P., Moses, E., Sergi, D.: Entropy of dialogues creates coherent structures in e-mail traffic. *Proc. Natl. Acad. Sci. USA* **101**, 14333 (2004)
13. Evans, T.S.: Complex networks. *Contemp. Phys.* **45**, 455 (2004)
14. Fernández-Gracia, J., Eguíluz, V., San Miguel, M.: Update rules and interevent time distributions: slow ordering versus no ordering in the voter model. *Phys. Rev. E* **84**, 015103 (2011)
15. Ferreira, A.: On models and algorithms for dynamic communication networks: the case for evolving graphs. In: *Proceedings of 4e Rencontres Francophones sur les Aspects Algorithmiques des Télécommunications (ALGOTEL2002)*, pp. 155–161, INRIA Press, Mèze, France (2002)
16. Ghosh, R., Lerman, K., Surachawala, T., Voevodski, K., Teng, S.-T.: Non-conservative diffusion and its application to social network analysis. *arXiv:1102.4639* (2011)
17. Grindrod, P., Parsons, M.C., Higham, D.J., Estrada, E.: Communicability across evolving networks. *Phys. Rev. E* **83**, 046120 (2011)
18. Hethcote, H.W., Tudor, D.W.: Integral equation models for endemic infectious diseases. *J. Math. Biol.* **9**, 37 (1980)
19. Hoel, P., Port, S., Stone, C.: *Introduction to Probability Theory*. Houghton Mifflin, Boston, MA (1971)
20. Hoffmann, T., Porter, M.A., Lambiotte, R.: Generalized master equations for non-Poisson dynamics on networks. *Phys. Rev. E* **86**, 046102 (2012)
21. Holme, P., Saramäki, J.: Temporal networks. *Phys. Rep.* **519**, 97 (2012)
22. Iribarren, J.L., Moro, E.: Impact of human activity patterns on the dynamics of information diffusion. *Phys. Rev. Lett.* **103**, 038702 (2009)
23. Iribarren, J.L., Moro, E.: Branching dynamics of viral information spreading. *Phys. Rev. E* **84**, 046116 (2011)
24. Isella, L., Stehlé, J., Barrat, A., Cattuto, C., Pinton, J.-F., Van den Broeck, W.: What's in a crowd? Analysis of face-to-face behavioral networks. *J. Theor. Biol.* **271**, 166 (2011)
25. Jeh, G., Widom, J.: SimRank: a measure of structural-context similarity. In: *KDD'02: Proceedings of the eighth ACM SIGKDD international conference on Knowledge discovery and data mining*, pp. 538–543, ACM, New York, NY (2002)
26. Karrer, B., Newman, M.E.J.: A message passing approach for general epidemic models. *Phys. Rev. E* **82**, 016101 (2010)
27. Karsai, M., Kivela, M., Pan, R.K., Kaski, K., Kertész, J., Barabási, A.-L., Saramäki, J.: Small but slow world: how network topology and burstiness slow down spreading. *Phys. Rev. E* **83**, 025102(R) (2011)
28. Karsai, M., Kaski, K., Barabási, A.-L., Kertész, J.: Universal features of correlated bursty behaviour. *Sci. Rep.* **2**, 397 (2012)
29. Kempe, D., Kleinberg, J., Kumar, A.: Connectivity and inference problems for temporal networks. *J. Comp. Sys. Sci.* **64**, 820 (2002)
30. Kenkre, V.M., Andersen, J.D., Dunlap, D.H., Duke, C.B.: Unified theory of the mobilities of photo-injected electrons in naphthalene. *Phys. Rev. Lett.* **62**, 1165 (1989)
31. Kivela, M., Pan, R.K., Kaski, K., Kertész, J., Saramäki, J., Karsai, M.: Multiscale analysis of spreading in a large communication network. *J. Stat. Mech.* P03005 (2012)
32. Klafter, J., Sokolov, I.M.: Anomalous diffusion spreads its wings. *Phys. World* **18**, 29 (2005)
33. Kleinberg, J.: Bursty and hierarchical structure in streams. *Data Min. Knowl. Disc.* **7**, 373 (2003)
34. Kumar, R., Novak, J., Raghavan, P., Tomkins, A.: On the bursty evolution of blogspace. In: *Proceedings of the 12th International Conference on World Wide Web (WWW)*, pp. 568–576, ACM, New York, NY (2003)
35. Lambiotte, R., Rosvall, M.: Ranking and clustering of nodes in networks with smart teleportation. *Phys. Rev. E* **85**, 056107 (2012)
36. Lambiotte, R., Ausloos, M., Thelwall, M.: Word statistics in blogs and RSS feeds: Towards empirical universal evidence. *J. Informetrics* **1**, 277 (2007)
37. Lambiotte, R., Sinatra, R., Delvenne, J.-C., Evans, T.S., Barahona, M., Latora, V.: Flow graphs: Interweaving dynamics and structure. *Phys. Rev. E* **84**, 017102 (2011)

38. Langville, A., Meyer, C.: *Google's PageRank and Beyond: The Science of Search Engine Rankings*. Princeton University Press, Princeton (2006)
39. Malmgren, R.D., Stouffer, D.B., Motter, A.E., Amaral, L.A.N.: A Poissonian explanation for heavy tails in e-mail communication. *Proc. Natl. Acad. Sci. USA* **105**, 18153 (2008)
40. Miritello, G., Moro, E., Lara, R.: Dynamical strength of social ties in information spreading. *Phys. Rev. E* **83**, 045102(R) (2011)
41. Montroll, E.W., Weiss, G.H.: Random walks on lattices. *J. Math. Phys.* **6**, 167 (1965)
42. Mucha, P.J., Richardson, T., Macon, K., Porter, M.A., Onnela, J.-P.: Community structure in time-dependent, multiscale, and multiplex networks. *Science* **328**, 876 (2010)
43. Newman, M.E.J.: *Networks: An Introduction*. Oxford University Press, London (2010)
44. Oliveira, J.G., Barabási, A.-L.: Darwin and Einstein correspondence patterns. *Nature* **437**, 1251 (2005)
45. Pan, R.K., Saramäki, J.: Path lengths, correlations, and centrality in temporal networks. *Phys. Rev. E* **84**, 016105 (2011)
46. Radicchi, F.: Who is the best player ever? A complex network analysis of the history of professional tennis. *PLoS ONE* **6**, e17249 (2011)
47. Rocha, L.E.C., Liljeros, F., Holme, P.: Information dynamics shape the sexual networks of Internet-mediated prostitution. *Proc. Natl. Acad. Sci. USA* **107**, 5706 (2010)
48. Rosvall, M., Bergstrom, C.: Maps of information flow reveal community structure in complex networks. *Proc. Natl. Acad. Sci. USA* **105**, 1118 (2008)
49. Sabatelli, L., Keating, S., Dudley, J., Richmond, P.: Waiting time distributions in financial markets. *Eur. Phys. J. B* **27**, 273 (2002)
50. Scher, H., Lax, M.: Stochastic transport in a disordered solid. I. *Theor. Phys. Rev. B* **7**, 4491 (1973)
51. Starnini, M., Baronchelli, A., Barrat, A., Pastor-Satorras, R.: Random walks on temporal networks. *Phys. Rev. E* **85**, 056115 (2012)
52. Stewart, W.J.: *Probability, Markov Chains, Queues, and Simulation: The Mathematical Basis of Performance Modeling*. Princeton University Press, Princeton (2009)
53. Takaguchi, T., Masuda, N.: Voter model with non-Poissonian interevent intervals. *Phys. Rev. E* **84**, 036115 (2011)
54. Tang, J., Musolesi, M., Mascolo, C., Latora, V.: Characterising Temporal Distance and Reachability in Mobile and Online Social Networks. In: *Proceedings of the 2nd ACM SIGCOMM Workshop on Online Social Networks (WOSN'09)*, pp. 118–124, ACM, New York, NY (2009)
55. Tang, J., Scellato, S., Musolesi, M., Mascolo, C., Latora, V.: Small-world behavior in time-varying graphs. *Phys. Rev. E* **81**, 055101(R) (2010)
56. Vazquez, A., Balazs, R., Andras, L., Barabási, A.-L.: Impact of non-Poisson activity patterns on spreading processes. *Phys. Rev. Lett.* **98**, 158702 (2007)

A Temporal Network Version of Watts's Cascade Model

Fariba Karimi and Petter Holme

Abstract Threshold models of cascades in the social and economical sciences explain the spread of opinion and innovation as an effect of social influence. In threshold cascade models, fads or innovation spread between agents as determined by their interactions to other agents and their personal threshold of resistance. Typically, these models do not account for structure in the timing of interaction between the units. In this work, we extend a model of social cascades by Duncan Watts to temporal interaction networks. In our model, we assume agents are influenced by their friends and acquaintances at certain time into the past. That is, the influence of the past ages and becomes unimportant. Thus, our modified cascade model has an effective time window of influence. We explore two types of thresholds—thresholds to fractions of the neighbors, or absolute numbers. We try our model on six empirical datasets and compare them with null models.

1 Introduction

Threshold models of cascades have been studied extensively in social and economical literature. The examples of the phenomena they seek to explain include diffusion of innovation, rumors and diseases, strikes, voting behavior and migration. Diffusion models such as Bass model [3] are canonical models. These assume that

F. Karimi
IceLab, Department of Physics, Umeå University, 90187 Umeå, Sweden
e-mail: fariba.karimi@physics.umu.se

P. Holme (✉)
IceLab, Department of Physics, Umeå University, 90187 Umeå, Sweden
e-mail: petter.holme@physics.umu.se

Department of Energy Science, Sungkyunkwan University, Suwon 440–746, Korea
e-mail: holme@skku.edu

Department of Sociology, Stockholm University, 10691 Stockholm, Sweden

the individual choice of action is independent from the total number of interactions of the individuals. However, sociologist Mark Granovetter [9] proposed thresholds to influence as a rational action. This insight comes from that in many situations there must be a point where the net benefits of performing an action exceeds the net costs. This also reflects the fact that many decisions need the group size to be considered. For example, the costs of joining a riot would probably decrease as the group size increases. Granovetter further proposes two main factors that influence spreading in threshold scenarios—social structure and timing of social action. In this chapter, we focus on the latter factor.

Social psychologist Bibb Latané [16] proposed social impact theory to explain social influence as a multiplicative function of strength, immediacy (an inverse function of physical distance) and the number of sources of influence. In the threshold model of cascades, we only investigate effects of the third factor (that the influence is proportional to the number of people involved). The threshold itself corresponds to the individual's persistence to change his or her state. Threshold models have been studied for uniform or heterogeneous threshold values [9, 22]. Dodds and Watts [4] showed that minor manipulation of individuality threshold can have a major impact on spreading phenomena. Here, for simplicity (like in [24]), we assume an identical threshold value for all individuals.

This chapter is inspired by Watts' threshold model of cascades in networks [24]. This work explains for example how new innovation can make a cascade of adaptation solely by network interactions. Even though this approach does not represent the reality of innovation adaptation, it gives an estimation of the importance of networks in the spreading process. In the threshold model, the agents' decision of action is binary choice, for examples the decision of choosing a brand for a same product. In this model, the individuals' choice of action depends only on other neighborhood choice. In Schelling's words, we have model of binary choice with externalists.

We extend the work of [14] where we present a generalization of a threshold model to temporal networks [10, 15]. Temporal networks, the theme of this book, are networks that encodes information about when things happen not only about which nodes that are in contact. We contrast our generalised model to the behavior of the original, static-network version. In our model (as in Watts's model), all the agents initially have the same state, and the thresholds are homogeneously distributed over the population. During the simulation, the agents change their states according to their interaction with their neighborhood and time of these interactions. We study two types of thresholds—fractional and absolute—corresponding to whether the individual respond to the fraction of neighbors with a deviating opinion, or to the absolute number of such neighbors. We note that while fractional thresholds are most common in the social and economic literature, absolute threshold models are used in bootstrap percolations and self-organized criticality which focus on local dependency [1, 7].

2 Methods

We consider a system of *vertices* (agents) and *edges* (vertices that at some point are in contact with each other). The system can be represented as a network G with a set of vertices V and a set of edges E . Every edge is associated with a set of times of interaction events. These interactions are bidirectional.

Each vertex or agent in the network has a *state*. State can be either 0 or 1. We call vertices with state 0 *non-adopters*. Vertices with state 1 correspond to *adopters*. Initially all the vertices in the network have state 0 (non-adopters). We start by randomly choosing a vertex and assign the state to 1. This initial vertex with state 1 can, according to the diffusion-of-innovation literature [22], be interpreted as an innovator advertising a new product. Here, for simplicity, we only divide the population into adopters and non-adopters. We thus study cascades of adoption from adopters to non-adopters. Choosing random vertex and repeating the simulation for large number of realizations ensures that the results come from large-scale network properties rather than the initial agent's position in the network.

We run the dynamic of interactions in the chronological orders. Influential interactions are those that occur within a *time window* θ in the past. This means that agents change their initial state 0 to 1, depending on the contacts within a the mentioned time window. If, within the time window, the fraction (or number) of adopters among the agent's neighbors exceeds the threshold value, then the agent changes state to 1. In ours (and Watts') setup, an adopter remains adopter for the rest of the simulation. The motivation of the latter is just to simplify the model.

Let us denote the total population by N and the number of adopters (as a function of time) $N_{\text{adopters}}(t)$. The cascade size is calculated as follows (and averaged over at least 200 runs of simulations)

$$\Omega(t) = \frac{\langle N_{\text{adopters}}(t) \rangle}{N} \quad (1)$$

Let ϕ be the threshold value in which agent change their state accordingly. Let a_i denote the number of adopters vertex i meets in a time window θ . Here c_i denotes total number of contacting neighbors that vertex i has within the time window θ . In the case of fractional threshold values, we count the fraction of adopters in the neighborhood of a vertex i within a time window as follows

$$f_i = \frac{a_i}{c_i} \quad (2)$$

The state of adoption occurs according to the following conditions

$$Pr[\text{adopting from vertex } i] = \begin{cases} 1 & \text{if } f_i \geq \phi \\ 0 & \text{if } f_i < \phi \end{cases} \quad (3)$$

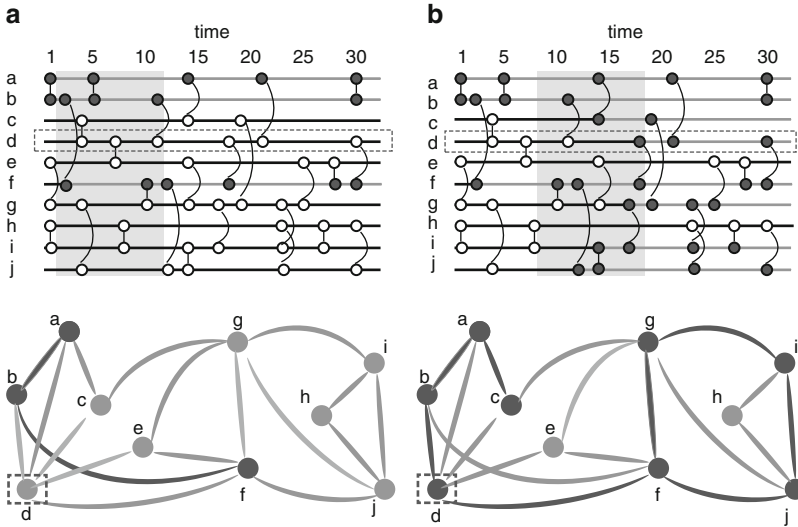


Fig. 1 An illustration of our temporal-network cascade model. In the panel (a), vertex d does not change its state according to the time window and value of threshold. In panel (b), vertex d reaches the criteria to change its state

For the case of absolute threshold model, let Φ be the absolute number of adopters that vertex i needs to meet within the time window θ to be able to change its state to 1. The condition for the change of state is the following

$$Pr[\text{adopting for vertex } i] = \begin{cases} 1 & \text{if } f_i c_i \geq \Phi \\ 0 & \text{if } f_i c_i < \Phi \end{cases} \quad (4)$$

Figure 1 illustrates the model. Contacts are illustrated in a time line. Shaded circles indicate adopters, white or gray circles indicate non-adopters. The threshold here is assumed to be $\phi = 0.5$ and the time window $\theta = 10$. As time progresses, the time window slides through each contact and the vertices are updated according to their contacts within the time window. In panel (a), vertex d does not change its state even though it is in contact with an adopter. At another time, panel (b), vertex d changes its color because inside the current time window, the fraction of adopters exceeds the threshold.

3 Empirical Datasets

We test our model on six empirical datasets stemming from different types of human interactions. The datasets were obtained with all individuals anonymized to protect their privacy. All datasets have been used in previous studies. The first

Table 1 Summary of properties of the datasets

Data	No. vertices	No. contacts	Time duration	Resolution
Email	3,188	309,125	82 days	Second
Online dating	29,341	536,276	512 days	Second
Internet community messages	329	434	500 days	Second
Internet community forum	2,384	291,151	500 days	Second
Prostitution	16,730	50,632	2,232 days	Day
Conference	113	20,818	3 days	20 s

dataset consists of self-reported sexual contacts from a Brazilian online forum where sex-buyers rate and discuss female sex-sellers [19]. The second dataset comes from email exchange at a university [6]. It was used in [2] to argue that human behavior often comes in bursts. The third datasets was collected at a 3-day conference from face-to-face interactions between conference attendees [13]. The fourth dataset comes from a Swedish Internet dating site where the interaction ranges from partner seeking to friendship oriented [11]. The fifth and sixth datasets come from a Swedish forum for rating and discussing films [20]. One of these datasets represents comments in a forum that is organized so that one can see who comments on whom. The other datasets comes from email-like messages. Table 1 summarizes details of datasets such as number of vertices, number of contacts, sampling time and time resolution. Some of the datasets like movie forum, email and conference contacts can be underlying structure for the spreading of social influence, like fads or ideas, or computer viruses. The sexual-contact dataset and perhaps also the online dating datasets, one can argue represent the structure over which sexually transmitted infections can spread.

4 Fractional-Threshold Model

4.1 *Effect of Threshold Values and Time Windows on Cascade Size*

In this section, we investigate the effect of varying time windows θ and threshold values ϕ on the size of cascade. The cascade size Ω is defined as the fraction of adopters over the whole population. The size of cascade can vary from 0 to 1. Results in all sections are the outcome of at least 200 simulation runs with different random seed. Therefore, the size of cascade we report is the average over that many simulation runs.

The threshold is fixed and identical for all individuals. As the threshold increases, the agents are more resistance to change their initial states. In Watts's model, the cascade cannot occur if the threshold value is too low [24]. Introducing a time window enables cascades to happen for higher threshold values. For short time windows only

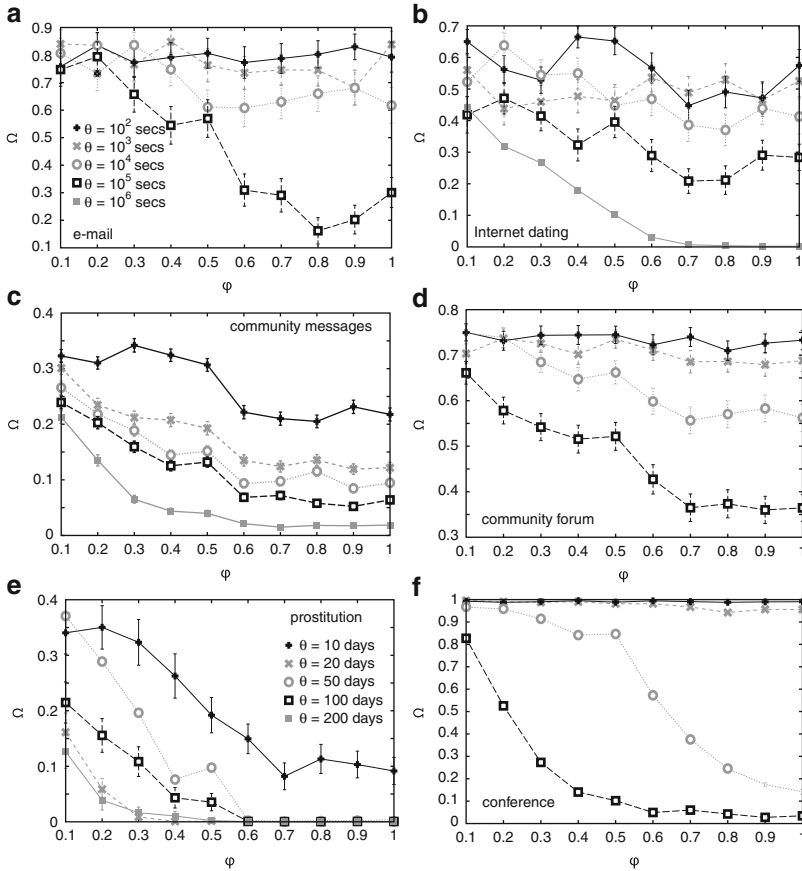


Fig. 2 Cascade size Ω versus threshold values ϕ from 0.1 to 1.0 for various time window sizes θ . The error bars indicate the standard error over 200 runs of cascade simulations

the most recent contacts counts. As larger time window integrate more influence, it can require more time to reach the threshold . It has been shown that in the static case, there is an upper limit for the threshold value beyond which no cascade can occur [24]. Since the static case is equivalent to the temporal case when θ is equal to the duration of the data, the limiting threshold value will be at least as large in the temporal case. In Fig. 2, we show the effect of increasing θ and ϕ on cascade size Ω for six empirical datasets. In short time windows, individuals meet fewer people and meeting one adopter is enough to change the state. This behavior is similar to (hypothetical) disease spreading models with 100% per-contact transmission probability.

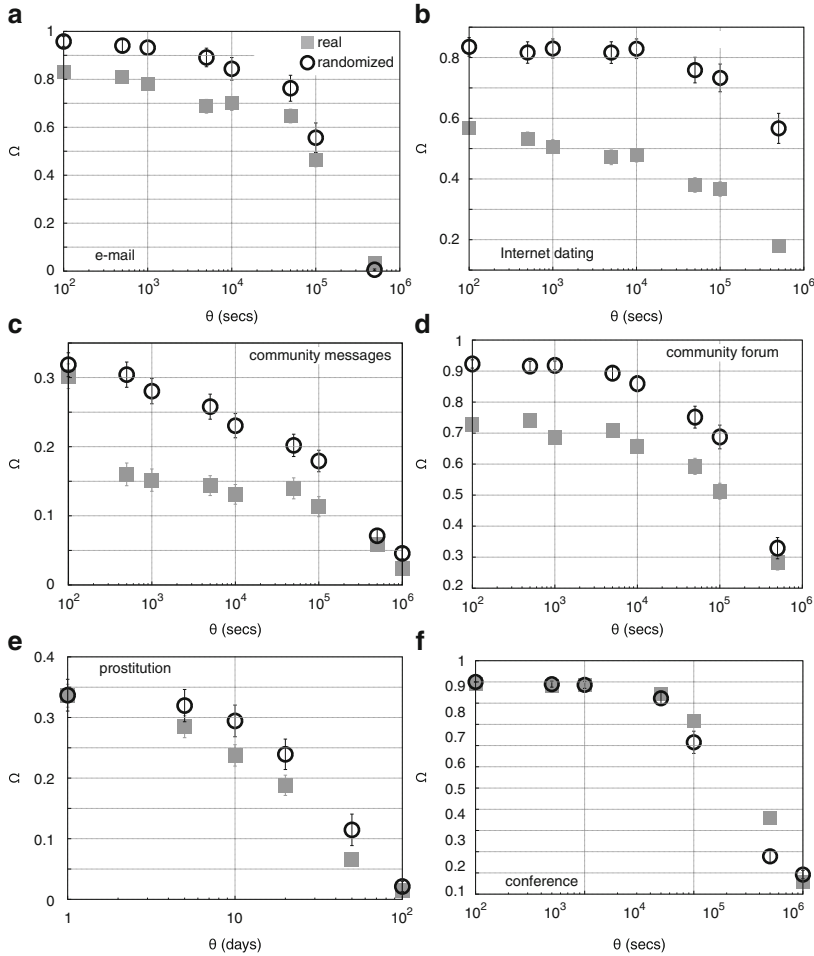


Fig. 3 Cascade size versus time-window size for fixed value of the threshold ($\phi = 1/2$). To verify the effect of temporal correlations, we compare the data to a null model by reshuffling time stamps. The figures show that, except the conference data, temporal correlations slow down the cascade size compare to the randomized networks without temporal structure. The *error bars* indicate the standard error over 150 runs of cascade simulations. The legend in panel (a) applies to all panels except (e)

4.2 Effect of Temporal Structure on Cascade Size

Now we will focus more on the effect of temporal structure of contacts on the cascade size. Bursty behavior of contacts meaning that high intensity of contact activity in short interevent time and followed by no activity in long time intervals [2, 8]. Studies have shown the burstiness can influence spreading over the contacts [23]. Here we examine the burstiness effect by applying our cascade

Table 2 Properties of the aggregated (and hence static) networks

The data	Connectance	Burstiness	Clustering coefficient	Assortativity
Prostitution	0.0002	0.44	0.00 [0.00]	-0.10[-0.02]
Email	0.006	0.68	0.06 [0.07]	-0.25[-0.22]
Conference	0.34	0.74	0.50 [0.48]	-0.12[-0.17]
Online dating	0.0002	0.65	0.00 [0.00]	-0.04[-0.04]
Internet community forum	0.012	0.80	0.43 [0.40]	-0.24[-0.30]
Internet community messages	0.007	0.65	0.05 [0.08]	-0.54[-0.51]

Connectance is the fraction of all possible links that are realized in a network [5]. Burstiness is high activity in short inter-event time followed by long range of no activity [8]. The clustering coefficient measures the fraction of triangles relative to the number of connected triples [18]. Assortativity measures the correlation of the degrees at either side of an edge [18]. Clustering coefficient and assortativity for null models are written in brackets

model on the six empirical datasets and compare the cascade size on the real and reshuffled time stamps. This reshuffled time stamps model (null model) follow [15]. It preserves network structures such as degree distribution and number of contacts. The null model is implemented by randomly reshuffling time stamps of contacts between pairs of nodes. Therefore burstiness and autocorrelations on single edges and pairwise correlations of edge pairs is destroyed. The null model, however, retains the global temporal statistics (number of events at given time, etc. [15]).

Figure 3 represents results of changing the size of the time window on cascade size for six empirical datasets. We choose the fractional threshold value to be $\phi = 0.5$. Studies have been shown that in a laboratory experiments individuals' choice is well described by the threshold 0.5 [17].

The cascade size Ω decreases as a function of time window θ . This is not surprising since larger time window associate with more interaction per individuals and decrease the fraction of adopters one meets. For the very large time window the cascade behavior is similar to the static threshold model—that cascade does not happen for larger threshold values [24]. When θ is large enough, the temporal order of events no longer matters, exactly as we see in Fig. 3 for large time windows.

For almost all datasets the null model has larger cascade size compare to the real datasets. In fact, other studies also suggest that the time correlation of events slows down the spreading [15]. For the case of conference data, the real and null model are overlapping for the small or large time windows. For intermediate-sized time windows the real datasets has larger cascade sizes compare to the null model. We will try to explain this in terms of the network statistics. In the case of conference data, the network is densely connected (see Table 2). This high connectance guarantees that, for the small and medium time windows, sufficient fraction of adopters are exposed to individuals. For the intermediate time windows, the temporal correlation plays an important role. This is especially strong in the conference data since it is organized around specific activities such as talks, poster sessions,

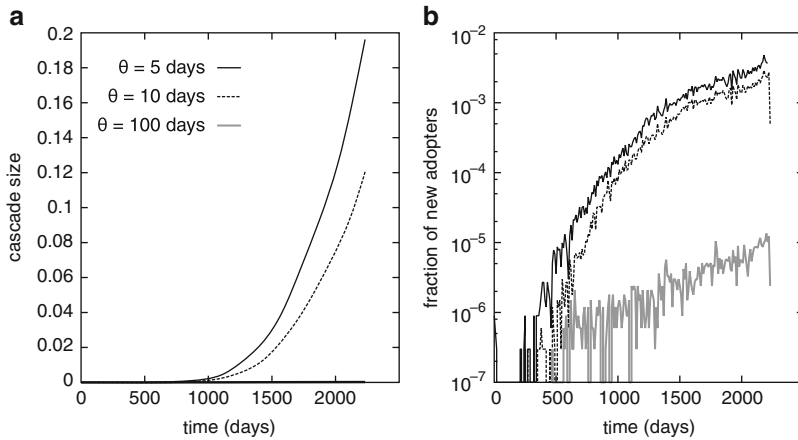


Fig. 4 Evolution of cascade sizes versus sampling time for the prostitution dataset. The threshold is $\phi = 0.70$

coffee and lunch breaks. Typically, networks of high assortativity have a densely connected subgraph—for the conference data, the entire network is such a densely connected graph.

5 The Time Evolution of Adoption in the Fractional Threshold Model

Spreading dynamics have been studied in SI models of contagion and compared with null models [15]. It has also been shown that heterogeneity in human activity affects the spreading [12]. In this section, we study the spreading dynamics on the population on empirical datasets. In addition, we also study how the number of new adopters evolves over time in different time window sizes. We investigate the time evolution of the cascades by two types of plots. The first is the aggregated cascade size over time which has been defined in (1). The other plot is based on the number of new adopters for each time step in the evolving network. Figures 4–9 show these two plots separately for each dataset.

The general pattern we observe here is that increasing the time window implies a decrease in the speed of the cascades. The larger time windows take more time for the vertex to change state. This effect is furthermore highly non-linear—sometimes the change is dramatic, sometimes hardly visible. The heterogeneity in the daily pattern is responsible for jagged increase of cascades. This effect is specifically clear in the curves of new adopters as a function of time. We also note that the growth is convex in some cases, concave in others (i.e. the cascade accelerates,

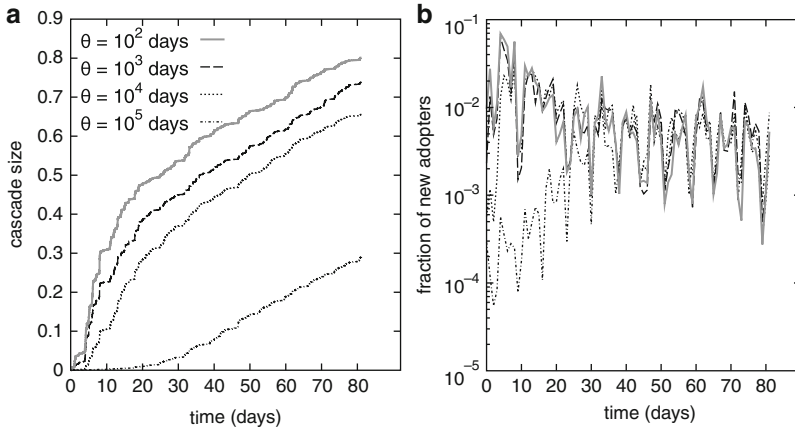


Fig. 5 Evolution of cascade size versus sampling time for the email dataset. The threshold is $\phi = 0.70$

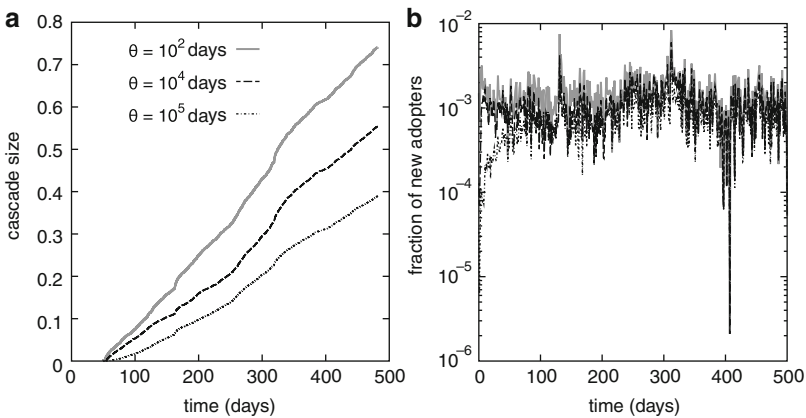


Fig. 6 Evolution of cascade size versus sampling time for the community forum dataset. The threshold is $\phi = 0.70$

like Fig. 4, after a quiet start. This is presumably related to the sparseness of this dataset and the fact that the overall activity in it grows with time. For Figs. 6 and 9 the outbreak progresses close to linearly. This is interesting in context of the Fig. 7 which represents the same set of users as Fig. 6 but a different type of activity (forum posts rather than e-mail like messages). This could suggest that opinion cascades spreads faster in open discussions than in person-to-person communication.

The datasets of Internet community messages and conference encounters are two examples of rather small networks with the distinctive difference that the community

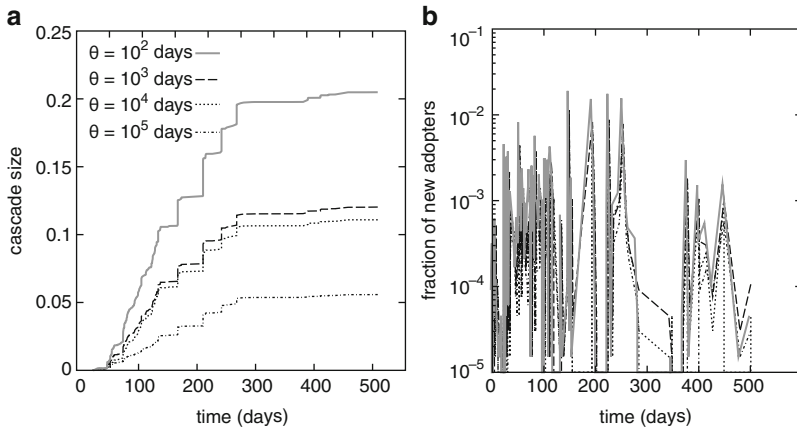


Fig. 7 Evolution of cascade size versus sampling time for the community messages dataset. The threshold is $\phi = 0.70$

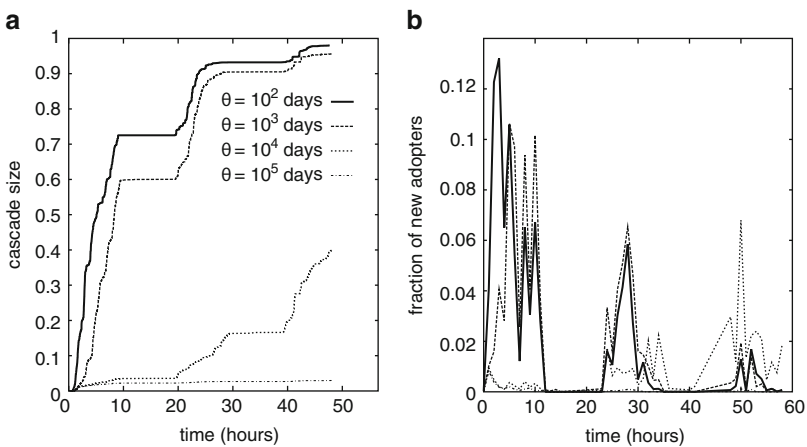


Fig. 8 Evolution of cascade size versus sampling time for the conference dataset. The threshold is $\phi = 0.70$

message data is sparse and conference network is dense. In the adoption dynamics, we see a similar pattern in both datasets—that as new adopters emerge over time, the activities speed up. The size of the cascades in the conference data seem to be much higher than the community message data due to it being more densely connected.

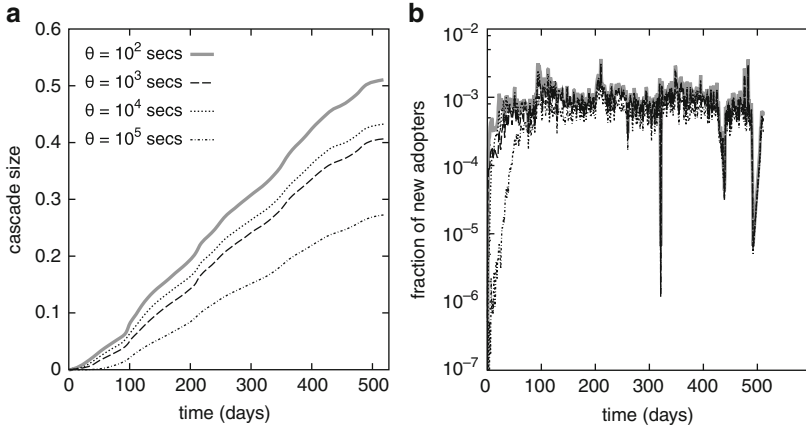


Fig. 9 Evolution of cascade size versus sampling time for the dating dataset. The threshold is $\phi = 0.70$

6 Absolute Threshold Model

The fractional threshold models explain only parts of socio-economical spreading processes. In reality individuals may have different threshold in different interactions. Even a single discussion with a relative or close friend can be sufficient for changing an opinion. In this chapter, we denote absolute threshold models, Φ , the sufficient number of adopters the individual has to meet to change state, (4). One can assume that in many situations, the reality is somewhere in between pure fractional or pure absolute threshold.

In Fig. 10, we show the cascade size as a function of various time windows. We fixed the absolute threshold value for all cases $\Phi = 3$. As the figure shows, the cascade size increase by increasing the time window θ . In larger time window, the chance of meeting three adopters increase. Interestingly, for the time-reshuffled models, this is not the case. In fact, the time order in the empirical datasets boost the cascade compare to randomized time order. In conference data, Fig. 10f, the sampling time is short therefore the time order does not play a major role. The increase in the cascade size by increasing the time window is the opposite from the fractional threshold models. Exposing to more contacts in fractional model, decrease the fraction of adopters in the time window. Moreover opposite to the fractional threshold model, the null model in absolute threshold model has lower cascade size compare to empirical data. Thus as temporal correlation in fractional threshold model slows down the cascades. In the absolute threshold models the opposite effect occurs. In the case of community messages—Fig. 10c—since number of contacts is low there are large error bars that do not rule out an increasing θ -dependence.

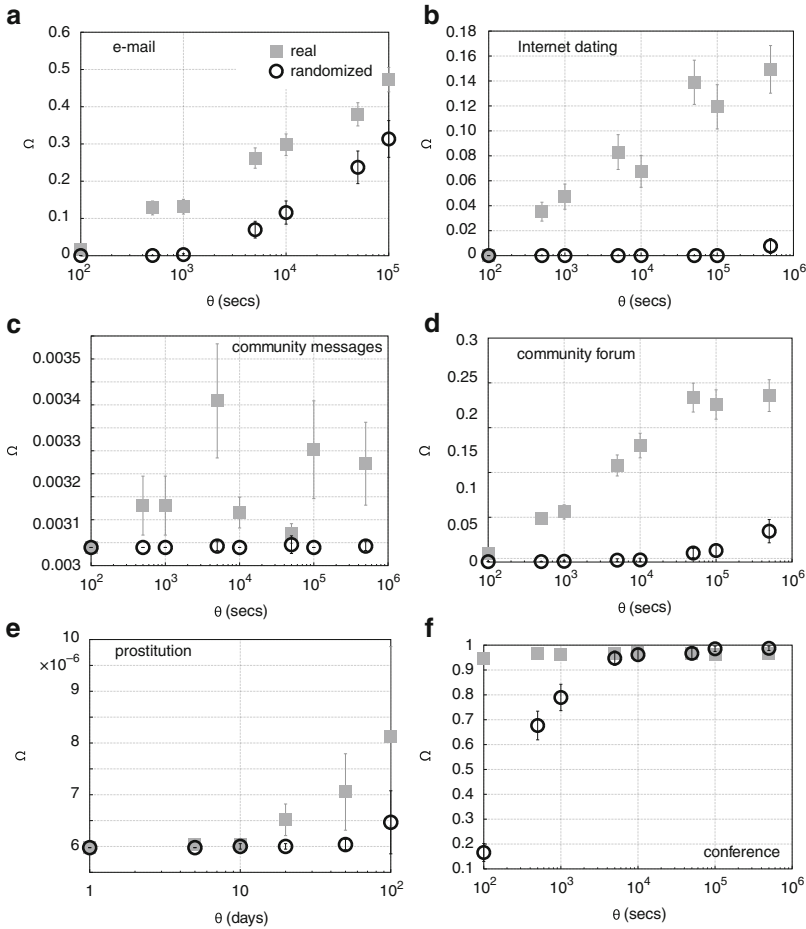


Fig. 10 Cascade size versus time windows for the absolute-threshold model. The threshold is $\Phi = 3$. To investigate the effect of temporal correlations, we compare the data to a null model where the times of the contacts are randomly shuffled. In most cases, the temporal structure makes the cascades larger as the time windows increase. The *error bars* indicate the standard error over 200 runs of cascade simulations

7 Discussion

We proposed an extension of Watts's cascade model [24] to temporal networks where the influence is integrated over a sliding window of the contacts. This model builds on the key assumption that people are influenced by contacts dating some time back into the past but not influenced by very old contacts. We studied two variants of the model, one where people respond to a threshold of the fraction of adopters among their neighbors and another where they respond to the absolute

number of such contacts. We find that the dynamics of cascades are heavily affected by the timing of contacts in the temporal networks.

There is a qualitative difference between the fractional- and absolute-threshold models. In the former case, the cascade sizes decrease with time-window size; in the latter case, it is the other way around. Moreover, the response to randomization is different—for the fractional-threshold case the temporal-network structure makes the cascades larger, whereas in the absolute-threshold case, randomization decreases the size of cascades. This is interesting in the light of [15] where the authors argue that burstiness slows down spreading phenomena. In this case, the authors have models of contagion in mind, but their conclusion seems not to generalize to threshold models (as was also observed in [21] and [14]).

We also note that the time evolution of the cascades differs from dataset to dataset where the more sparsely connected systems show accelerating outbreaks. This cannot only be explained by that it takes longer time for a cascade to take off as there are some datasets where cascades fail to reach a large proportion of the population for a large part of parameter space. It is indeed hard to single out one temporal network structure that controls the cascade dynamics. But the average number of contacts per edge and the connectance (or average degree in the aggregated network) seem to be two important quantities.

We believe there are interesting open questions regarding threshold models in temporal networks; the main one being what structures—temporal or topological—that control spreading phenomena in temporal networks.

Acknowledgements The authors acknowledge financial support by the Swedish Research Council and the WCU program through NRF Korea funded by MEST R31–2008–10029. The authors thank Taro Takaguchi for comments.

References

1. Balogh, J., Pittel, B.G.: Bootstrap percolation on the random regular graph. *Random Struct. Alg.* **30**, 257–286 (2007)
2. Barabási, A.L.: The origin of bursts and heavy tails in human dynamics. *Nature* **435**(7039), 207–211 (2005)
3. Bass, F.: A new product growth model for consumer durables. *Manag. Sci.* **50**, 1833–1840 (1969)
4. Dodds, P.S., Watts, D.J.: Universal behavior in a generalized model of contagion. *Phys. Rev. Lett.* **92**, 218701 (2004)
5. Dunne, J.A., Williams, R.J., Martinez, N.D.: Food-web structure and network theory: The role of connectance and size. *Proc. Natl. Acad. Sci. USA* **99**, 12917–12922 (2002)
6. Eckmann, J.P., Moses, E., Sergi, D.: Entropy of dialogues creates coherent structures in e-mail traffic. *Proc. Natl. Acad. Sci. USA* **101**, 14333–14337 (2004)
7. Fontes, L.R.G., Schonmann, R.H.: Bootstrap percolation on homogeneous trees has 2 phase transitions. *J. Stat. Phys.* **132**, 839–861 (2008)
8. Goh, K.I., Barabási, A.L.: Burstiness and memory in complex systems. *EPL* **81**, 48002 (2008)

9. Granovetter, M.: Threshold models of collective behavior. *Am. J. Sociol.* **83**(6), 1420–1443 (1978)
10. Holme, P., Saramäki, J.: Temporal networks. *Phys. Rep.* **519**, 97–125 (2012)
11. Holme, P., Edling, C.E., Liljeros, F.: Structure and time-evolution of an internet dating community. *Soc. Network* **26**, 155–174 (2004)
12. Iribarren, J.L., Moro, E.: Impact of human activity patterns on the dynamics of information diffusion. *Phys. Rev. Lett.* **103**, 038702 (2009)
13. Isella, L., Stehlé, J., Barrat, A., Cattuto, C., Pinton, J.F., Van den Broeck, W.: What's in a crowd? Analysis of face-to-face behavioral networks. *J. Theor. Biol.* **271**, 166–180 (2011)
14. Karimi, F., Holme, P.: Threshold model of cascades in temporal networks (2012). E-print 1207.1206
15. Karsai, M., Kiveliä, M., Pan, R.K., Kaski, K., Kertész, J., Barabási, A.L., Saramäki, J.: Small but slow world: how network topology and burstiness slow down spreading. *Phys. Rev. E* **83**, 025102 (2011)
16. Latané, B.: Dynamic social impact: the creation of culture by communication. *J. Comm.* **46**, 13–25 (1996)
17. Latané, B., L'Herrou, T.: Spatial clustering in the conformity game: dynamic social impact in electronic groups. *J. Pers. Soc. Psychol.* **70**, 1218–1230 (1996)
18. Newman, M.E.J.: *Networks: An introduction*. Oxford University Press, Oxford (2010)
19. Rocha, L.E.C., Liljeros, F., Holme, P.: Information dynamic shape the sexual networks of internet-mediated prostitution. *Proc. Natl. Acad. Sci. USA* **107**, 5706–5711 (2010)
20. Said, A., De Luca, E.W., Albayrak, S.: How social relationships affect user similarities. In: *Proceedings of the ACM IUI'10 Workshop on Social Recommender Systems* (2010)
21. Takaguchi, T., Masuda, N., Holme, P.: Bursty communication patterns facilitate spreading in a threshold-based epidemic dynamics (2012). E-print 1206.2097
22. Valente, T.W.: *Network Models of the Diffusion of Innovations*. Hampton Press, Gresskill (1995)
23. Vazquez, A., Raćz, B., Lukaćs, A., Barabási, A.L.: Impact of non-poissonian activity patterns on spreading processes. *Phys. Rev. Lett.* **98**, 158702 (2007)
24. Watts, D.J.: A simple model of global cascades on random networks. *Proc. Natl. Acad. Sci. USA* **99**, 5766–5771 (2002)

Timing Interactions in Social Simulations: The Voter Model

Juan Fernández-Gracia, Víctor M. Eguíluz, and Maxi San Miguel

Abstract The recent availability of huge high resolution datasets on human activities has revealed the heavy-tailed nature of the interevent time distributions. In social simulations of interacting agents the standard approach has been to use Poisson processes to update the state of the agents, which gives rise to very homogeneous activity patterns with a well defined characteristic interevent time. As a paradigmatic opinion model we investigate the voter model and review the standard update rules and propose two new update rules which are able to account for heterogeneous activity patterns. For the new update rules each node gets updated with a probability that depends on the time since the last event of the node, where an event can be an update attempt (exogenous update) or a change of state (endogenous update). We find that both update rules can give rise to power law interevent time distributions, although the endogenous one more robustly. Apart from that for the exogenous update rule and the standard update rules the voter model does not reach consensus in the infinite size limit, while for the endogenous update there exist a coarsening process that drives the system toward consensus configurations.

1 Introduction

Individual based models of collective social behavior include traditionally two basic ingredients: the mechanism of interaction and the network of interactions [1]. The idea of choosing a mechanism of interaction, such as random imitation [2–4] or threshold behavior under social pressure [5–7], is to isolate this mechanism and to determine its consequences at the collective level of emergent properties. The network of interactions determines who interacts with whom. The topology

J. Fernández-Gracia · V.M. Eguíluz (✉) · M.S. Miguel
IFISC, Instituto de Física Interdisciplinar y Sistemas Complejos (CSIC-UIB), Campus Universitat
Illes Balears, 07122 Palma de Mallorca, Spain
e-mail: victor@ifisc.uib-csic.es

of the network incorporates among other things the heterogeneity of ties among individuals. In addition ties can be non persistent, so that the network structure changes with time. In particular, the network and the state of the individuals can evolve in similar time scales (co-evolution). Such entangled process of *dynamics of the network* and the *dynamics on the network* can describe how to go from *interacting with neighbors* to *choosing neighbors* [8–12]. A third ingredient of individual based models, which was not considered in detail in the past, is the timing of interactions: When do individuals interact? The usual assumption in simulation models was that of a constant rate of interaction. In this paper we revise this assumption addressing the consequences of the heterogeneity in the timing of interactions.

Addressing this question is timely due to the availability of massive and high resolution data on human activity patterns. Information and knowledge extracted from this data needs to be included in a realistic modeling of collective social behavior. Indeed, many interevent time distributions measured recently in empirical studies about human activities such as e-mail communication, surface mail, timing of financial trades, visits to public places, long-range travels, online games, response time of cybernauts, printing processes and phone calls, among others [13–22], show heavy tails for large times. Motivated by these findings there are two current lines of research:

- Origin of these heavy-tailed distributions
 - These heavy tails have been explained based on circadian cycle and seasonality, via a non-homogeneous Poisson process with a cascading mechanism [13,20].
 - Root these heavy tails in the way individuals organize and prioritize their tasks, which can be modeled through a priority queuing model [14,17,21,22]. See chapter “Burstiness: Measures, Models, and Dynamic Consequences”.
- Effects of this interaction timing heterogeneity on certain dynamics: independently of the origin of this feature it has been noticed that a non-homogeneous interaction in time can give rise to non-trivial behavior. An example considered so far in some detail is spreading and infection dynamics: SI-type spreading dynamics have been investigated, showing that this peculiar timing gives rise to a slowing down of the dynamics that cannot be explained just by a change of time scale but it changes the functional form of the prevalence of a disease [16–19]. See chapter “Spreading Dynamics Following Bursty Activity Patterns”.

Our work [23] goes along the second of these research lines. It considers the implementation of human activity patterns in simulation models of interacting individuals, and the consequences of the timing of interactions. As an illustrative model we explore this general question in the context of the voter model [2,3]. The voter model is a very stylized model that serves as a null model for the competition of two equivalent states under a dynamics of random imitation. A difference with previous work in spreading and infection dynamics is that in the voter model each individual can be in two equivalent states. Then the question is when the

system reaches consensus in either of these two states or when there is asymptotic dynamical coexistence of the two states. We will see that the answer to this question depends crucially on the timing of interactions. Related work on the voter model, discussed later, include the papers by Stark et al. [24], Baxter [25], and Takaguchi and Masuda [26].

In Sect. 2 we revise the definition of the voter model and the different quantities used to monitor its macroscopic dynamics. Section 3 considers the voter model dynamics with different standard update rules, *i.e.*, update rules that incorporate a constant rate of interaction. In Sect. 4 we introduce new update rules to account for heterogeneous activity patterns. We consider two update rules: *endogenous update*, coupled to the dynamics of the states of the agents; and *exogenous update* which is independent of the states of the agents. Section 5 includes a discussion of our results and related work.

2 The Voter Model

2.1 Definition of the Voter Model

The voter model is a microscopic model first considered in Ref. [2] in 1973 as a model for the competition of species for their habitats, and named *voter model* in Ref. [3] in 1975 as the natural interpretation of its rules in terms of opinion dynamics [1, 4]. However it has been investigated not just in the context of social dynamics but also in fields such as probability theory [3] and population dynamics [2].

The voter model consists of a set of N agents placed on the nodes of an interacting network. The links of the network are the connections among agents. Two nodes are first neighbors if they are directly connected by a link in the network. The agents have a binary variable (opinion, state. . .) which can take the values $+1$ or -1 . The behavior of the agents is characterized by an imitation process, because, whenever they interact, they just copy the state of a randomly chosen first neighbor.

The model has two absorbing configurations, *i.e.*, configurations in which the dynamics stop, which consist either of all agents in state $+1$ or in state -1 . These absorbing configurations are also typically called *consensus*, as the whole population has agreed in the same state.

This model has been studied by computer simulations using what we later define as *random asynchronous update* for node dynamics. In this case the basic steps in the dynamics are:

1. Randomly choose an agent i with opinion x_i .
2. Randomly choose one of i 's neighbors, j , with opinion x_j . Agent i adopts j 's opinion; $x_i(t + 1/N) = x_j(t)$.
3. Resume at 1.

The alternative link dynamics is considered in Ref. [27].

Usually the time is measured in units of N basic steps, *i.e.*, a Monte Carlo step, following the idea that every agent gets updated on average once per unit time.

2.1.1 Macroscopic Description

A basic question is under which conditions consensus will be reached and how. In order to answer this question we have to define some macroscopic quantities which will describe the state of the system and its dynamical behavior.

Magnetization $m(t)$: It is the average state of the population and is defined as

$$m(t) = \frac{1}{N} \sum_{i=1}^N x_i.$$

Density of interfaces $\rho(t)$: It is the fraction of links connecting agents with different states. It is defined as

$$\rho(t) = \frac{\# \text{ of links between } -1 \text{ and } +1}{\# \text{ of links in the network}} = \frac{1}{\sum_{i=1}^N k_i} \left(\sum_{\langle ij \rangle} \frac{1 - x_i x_j}{2} \right),$$

where $\langle ij \rangle$ stands for summing over neighboring nodes.

In numerical simulations finite size effects come into play. In finite size systems consensus will be reached, but we have to differentiate if consensus is reached due to the inherent dynamics or to a finite size fluctuation. We use averages over many realizations to extract the mean behavior. This is what is called an ensemble average and will be denoted by $\langle \cdot \rangle$. When doing the ensemble averages some conservation laws can be found. For the case of regular networks, where every node has the same number of neighbors (same degree), the ensemble average of the magnetization $\langle m(t) \rangle$ is conserved under node dynamics [27,28]. For this reason the magnetization is not a good order parameter and we have to define the density of interfaces ρ , which in general is not conserved. This is a proper order parameter as it measures the degree of order in the system. It is nonzero while the system is not in one of the absorbing states and is zero otherwise. A decrease of $\rho(t)$ describes the coarsening process with growth of domains with agents in the same state. If the network is heterogeneous, i.e., the degrees of the nodes are not all the same, the conservation law for $\langle m(t) \rangle$ breaks down unless we use link dynamics.

In order to gain more insight into the dynamics for finite size systems we also introduce two other quantities to characterize the dynamics. These quantities are:

Survival probability $S(t)$: It is the probability that a realization of the system has not reached one of the absorbing states at time t . The mean time $\langle T \rangle$ to reach consensus is then given by¹

¹ $S(t)$ is the probability of being in an active configuration at simulation time t . Then the probability of reaching an absorbing state at time t is $\frac{d}{dt}(1 - S(t)) = -\frac{d}{dt}S(t)$. The average time to reach consensus is then $\langle T \rangle = -\int_0^\infty (t \frac{d}{dt}S(t))dt$ and, integrating by parts one finds that $\langle T \rangle = \int_0^\infty S(t)dt$.

$$\langle T \rangle = \int_0^\infty S(t) dt.$$

Density of interfaces averaged over surviving runs $\langle \rho^*(t) \rangle$: This quantity is basically the same as the density of interfaces, but disregarding the realizations that have already reached an absorbing state when doing the ensemble average. It tells us the degree of order in the system for the realizations that are still in an active state. This quantity is related to the density of interfaces averaged over all realizations by

$$\langle \rho(t) \rangle = S(t) \langle \rho^*(t) \rangle.$$

A novel quantity in the study of the voter model has to be introduced in order to characterize the temporal activity patterns. This quantity is:

Interevent time (IET) distribution $M(\tau)$: It is the probability that, given two consecutive changes of state of a node, the time interval between them equals τ . We will also use the complementary cumulative distribution² of this, $C(\tau) = 1 - \int_0^\tau M(t) dt$.

3 Standard Update Rules

In this section we review standard update rules used in simulations of agent based models (ABM's). We also investigate the behavior of the voter model for these different rules. In ABM's agents are placed on the nodes of a network. The state of the agents is characterized by a variable that can take one of various values. The specific dynamics tells how the states of the nodes are updated. But in addition to the dynamical rules, simulation incorporate rules that determine when an agent is given the opportunity to update her state. Standard update rules implement a homogeneous pattern of updates in time.

The simulations all over this chapter were done with random initial conditions, *i.e.*, every agent has the same probability in the beginning to have one state or the other, and setting their initial time since the last change of state equal to zero.

3.1 Definitions of Standard Update Rules

Typically the update rules implemented are

- *Asynchronous update*: At each simulation step only one of the agents is updated. The unit of time is typically defined as N simulation steps (a Monte Carlo step), where N is the number of agents in the system.

²In the remainder we will refer to the complementary cumulative distribution just as cumulative distribution.

- *Random asynchronous update (RAU)*: The agents are updated in a random order.
- *Sequential asynchronous update (SAU)*: The agents are always updated in the same order.
- *Synchronous update (SU)*: All the agents are updated at the same time. The time is measured in units of simulation steps.

The most commonly used update for the voter model has been the RAU. Most of the results have been derived for that update. As we can see from the definitions of these standard update rules, there exists a well defined characteristic time between two consecutive updates of the same node. In the case of SAU and SU every agent is updated exactly once per unit time, while for RAU this only happens on average.

3.2 Voter Model with Standard Update Rules

In Fig. 1 we can see the outcome of the simulations on a complete graph, a random graph of average degree $\langle k \rangle = 6$ and on a scale-free graph of average degree $\langle k \rangle = 6$. The figure includes plots of the averaged density of active links $\langle \rho(t) \rangle$, the evolution of ρ in a single realization and the survival probability $S(t)$. The cumulative IET distribution $C(\tau)$ is plotted for the three updates and the three different networks in Fig. 2. The question of interest is whether $C(\tau)$ is Poisson-like or a more heterogeneous distribution.

Results for RAU, SAU and SU are plotted together for comparison purposes. We observe that the averaged density of active links $\langle \rho(t) \rangle$, the survival probability $S(t)$ and the tail of the cumulative IET distribution $C(\tau)$ display an exponential decay $\exp(-t/\tau(N))$, with a characteristic time that depends on the system size. These characteristic times have been extracted by fitting the data for many system sizes and computing the scaling behavior of $\tau(N)$. The results of this analysis are summarized in Table 1 for the different update rules and networks. Both the average density of interfaces $\langle \rho(t) \rangle$ and the survival probability $S(t)$ display the same characteristic time. This feature gives rise to the appearance of a plateau in the density of interfaces averages over surviving runs, as $\langle \rho^*(t) \rangle = \langle \rho(t) \rangle / S(t)$, which is a signature of the system not being ordered by the dynamics.

Our results indicate that the voter model has the same qualitative dynamical behavior under RAU, SAU and SU node update rules. These results can be summarized as follows:

Density of active links:

$\langle \rho(t) \rangle$: For the ensemble average over all realizations we find an exponential decay in

$$\langle \rho(t) \rangle \propto e^{-t/\tau(N)}$$

with a characteristic time that scales as $\tau(N) \propto N$ for a complete graph and random graphs. For the case of Barabási-Albert scale-free graphs the scaling is compatible with the analytical result $\tau(N) \propto N / \log(N)$ [27, 29, 30]. We can see

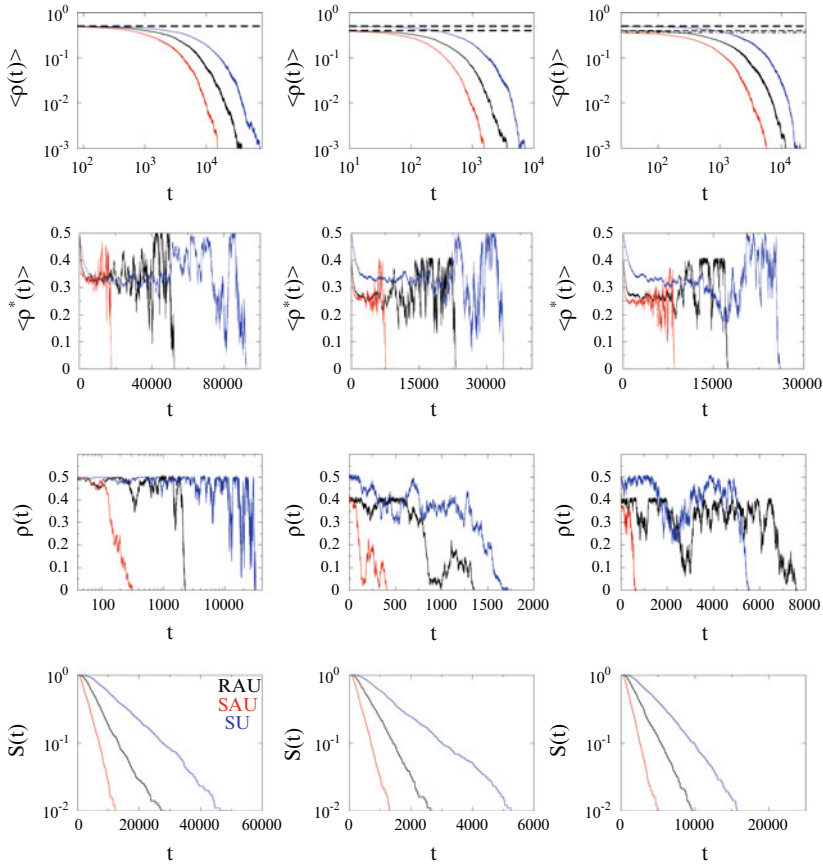


Fig. 1 The voter model under the usual update rules (RAU in black, SAU in red and SU in blue) on different networks. All the averages were done over 1,000 realizations. The *left column* is for a complete graph, *middle column* for a random graph with average degree $\langle k \rangle = 6$ and *right column* a scale-free graph with average degree $\langle k \rangle = 6$. *Top row* contains plots for the average density of interfaces $\langle \rho \rangle$ with *dashed lines* at the value of the plateau that will only exist in the thermodynamic limit, *second row* shows the density of interfaces averaged only over surviving runs $\langle \rho^* \rangle$, *third row* shows the density of interfaces for single realizations and the *bottom row* contains the survival probability. System size is $N = 1,000$

that the characteristic time diverges with the system size, so that $\langle \rho(t) \rangle$ remains constant in the infinite size limit for any of these networks. This is telling us already that the system is not reaching an ordered state in the thermodynamic limit.

$\langle \rho^*(t) \rangle$: Decays exponentially until it reaches a plateau. The plateau height is independent of the system size, meaning that, on average, the realizations that have not yet reached an absorbing state stay at a disordered state with a finite and large fraction of active links.

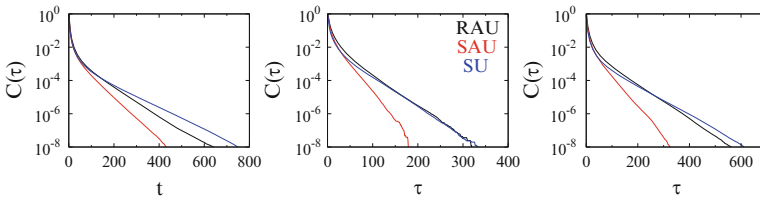


Fig. 2 Cumulative IET distributions for the voter model under the usual update rules (RAU in black, SAU in red and SU in blue) on different networks. All the averages were done over 1,000 realizations. *Left plot* is for a complete graph, *middle plot* for a random graph with average degree $\langle k \rangle = 6$ and *right plot* for a scale-free graph with average degree $\langle k \rangle = 6$. System size is $N = 1,000$

Table 1 System size dependence of the characteristic times in the density of active links, $\langle \rho(t) \rangle$ and in the cumulative distribution of interevent times, $C(t)$, for different network topologies and node update rules

		RAU $\tau(N)$	SAU $\tau(N)$	SU $\tau(N)$
CG	$\langle \rho \rangle S(t)$	$N/2$	$0.23(4)N^{1.01(2)}$	$0.9(1)N^{1.01(2)}$
	C	$0.63(7)N^{0.47(2)}$	$0.33(4)N^{0.50(1)}$	$0.6(1)N^{0.51(2)}$
RG $\langle k \rangle = 6$	$\langle \rho \rangle S(t)$	$0.57(7)N^{0.99(2)}$	$0.34(6)N^{0.97(2)}$	$1.0(1)N^{1.01(2)}$
	C	$1.0(2)N^{0.47(2)}$	$0.38(6)N^{0.51(2)}$	$0.74(9)N^{0.51(2)}$
SFG $\langle k \rangle = 6$	$\langle \rho \rangle S(t)$	$0.25(5)N^{0.88(2)}$	$0.19(3)N^{0.92(5)}$	$1.6(4)N^{0.84(3)}$
	C	$0.35(7)N^{0.52(2)}$	$0.18(7)N^{0.53(4)}$	$1.0(3)N^{0.43(3)}$

CG stands for complete graph, RG for random graph and SFG for scale-free graph

Survival probability:

$S(t)$: The survival probability decays exponentially,

$$S(t) \propto e^{-t/\tau(N)},$$

with the same characteristic time as $\langle \rho(t) \rangle$. Thus when combining $\langle \rho(t) \rangle / S(t) = \langle \rho^*(t) \rangle$ we find a constant value for $\langle \rho^*(t) \rangle$. The mean times to reach consensus for finite systems are well defined. In the infinite size limit, as $\tau(N)$ diverges with the system size, we can conclude again that the system does not reach an ordered state and the survival probability is just equal to one for all times in the thermodynamic limit.

Cumulative IET distribution:

$C(\tau)$: This distribution shows an exponential tail,

$$C(t) \propto e^{-t/\tau'(N)},$$

indicating that there is a well defined average IET. The characteristic time in the exponential tail scales approximately as

$$\tau'(N) \propto \sqrt{N}.$$

These are the features shared by all standard node update rules. There are also differences, since the precise characteristic times and the plateau heights of $\langle \rho(t) \rangle$ and $\langle \rho^*(t) \rangle$ depend on the update rule. See top row in Fig. 1 where the plateaus for the different update rules are plotted with a dashed black line. It is clear that the difference between RAU and SAU update rule lies in correlations that will be present in SAU and not in RAU. For the case of SU, the differences come from the fact that for this update rule the dynamics is purely discrete. Still the main result is that the qualitative behavior is the same: for these three update rules the system remains, in the thermodynamic limit, in an active disordered configuration for the voter model dynamics in a complete graph and in complex networks of infinite effective dimensionality such as Erdős-Rényi and Barabási-Albert networks. Also the activity patterns are very homogeneous, with a well defined IET.

4 Update Rules for Heterogeneous Activity Patterns

A set of N agents are placed on the nodes of a network of interaction, as was explained generally for agent based models in Sect. 3. Each agent i is characterized by its state x_i and an internal variable that we will call *persistence time* τ_i . For any given interaction model (Ising, voter, contact process, ...), the dynamics is as follows: at each time step,

1. With probability $p(\tau_i)$ each agent i becomes active, otherwise it stays inactive;
2. Active agents update their state according to the dynamical rules of the particular interaction model;
3. All agents increase their persistence time τ_i in one unit

The persistence time measures the time since the last event for each agent. Typically an event is an interaction (*exogenous update*: active agents reset $\tau = 0$ after step (ii)) or a change of state (*endogenous update*: only active agents that change their state in step (ii) reset $\tau = 0$) (Fig. 3).

There are two interesting limiting cases of this update when $p(\tau)$ is independent of τ : when $p(\tau) = 1$, all agents are updated synchronously; when $p(\tau) = 1/N$, every agent will be updated on average once per N unit time steps. The latter corresponds to the usual random asynchronous update (RAU). We are interested in non-Poissonian activation processes, with probabilities $p(\tau)$ that decay with τ , that is, the longer an agent stays inactive, the harder is to activate. To be precise, we will later consider that

$$p(\tau) = \frac{b}{\tau}, \quad (1)$$

where b is a parameter that controls the decay with τ . This mechanism is similar to the reinforcement dynamics explained in chapter “Models, Entropy and Information of Temporal Social Networks”. An alternative mechanism, also based on a process

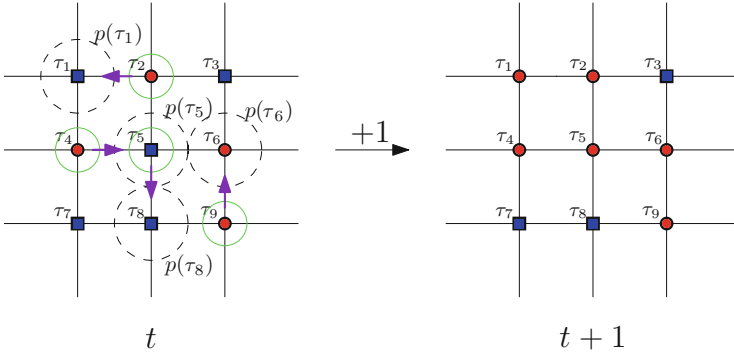


Fig. 3 Example of the new update rule. Every agent gets updated with her own probability $p(\tau_i)$, being τ_i her persistence time. The two possible states of the nodes are represented by *blue squares* and *red circles*. The node or nodes inside a *black dashed circle* are the ones that are updated. The nodes inside a *green circle* are the randomly chosen neighbors for the interaction and the purple arrow tells in which direction the state will be copied

with memory is the Hawkes process discussed in chapter “Self-exciting Point Process Modeling of Conversation Event Sequences”.

We expect the IET distribution $M(t)$ to be related to the activation probability $p(\tau)$. Neglecting the actual dynamics and assuming that at each update event, the agent changes state we can find an approximate relation between $M(t)$ and $p(\tau)$. Recall that $M(t)$ is the probability that an agent changes state (updating and changing state coincide in this approximation) t time steps after her last change of state. Therefore the probability that an agent has not changed state in $t - 1$ time steps is $1 - \sum_{j=1}^{t-1} M(j)$ and the probability of changing state having persistence time t is $p(t)$. Therefore we can write for t larger than one:

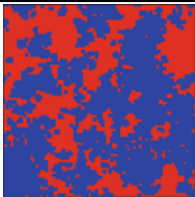
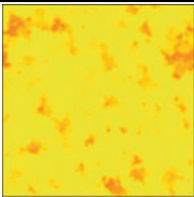
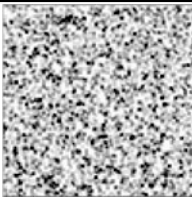
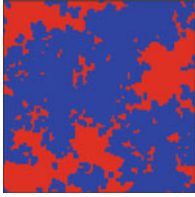
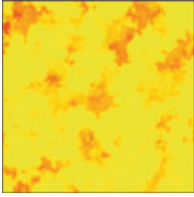
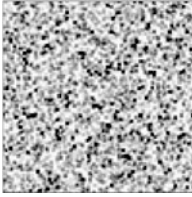

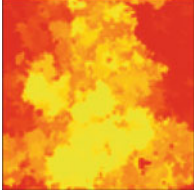
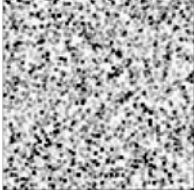
$$\left(1 - \sum_{j=1}^{t-1} M(j) \right) p(t) = M(t), \tag{2}$$

with $p(1) = M(1)$. Taking the continuous limit and expressing this equation in terms of the cumulative IET distribution we obtain

$$d \ln(C(t)) = -p(t)dt. \tag{3}$$

Setting $p(\tau) = b/\tau$ the cumulative IET distribution decays as a power law $C(t) \sim t^{-\beta}$ with $\beta = b$. Numerical simulations show that this approximation holds for the voter model on a fully connected network for endogenous updates and for a small range of b -values in the exogenous update for any topology of the ones considered in this study. The modification of the model is investigated more exhaustively for the case in which the cumulative IET distribution is a power law $C(\tau) \propto \tau^{-\beta}$, but

Table 2 Evolution of the voter model on a square lattice of 100×100 nodes with random asynchronous update (RAU)

Time	Configuration	Time since state change	Time since update
$t = 1$			
$t = 10$			
$t = 100$			

The first column of images shows the states of the nodes in blue and red, the second one shows the time since the last change of state of each node, with red being a long time and yellow a small time. The third column shows the time since the last update, being dark gray for a long time and light gray for a small time. The updates of the nodes follow a Poisson process with a characteristic time of one Monte Carlo step. The third column shows three equivalent snapshots (spatial white-noise), because of the lack of memory of the system. The growth of domains proceeds via interfacial noise dynamics (first column). Nodes change state quite frequently, except when the system is approaching consensus (see middle column)

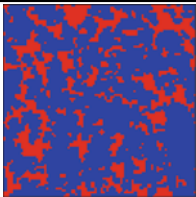
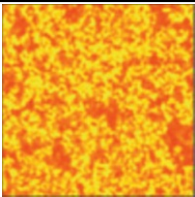
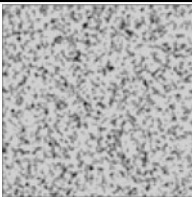
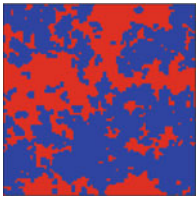
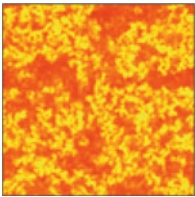
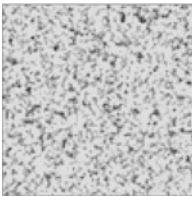
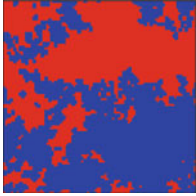
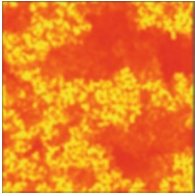
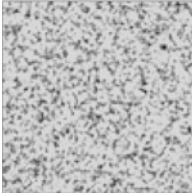
any distribution $C(\tau)$ can be plugged into the definition of $p(\tau)$ (3). In fact the case $\beta = 1$ will be studied in more detail.

When applied to the voter model the new update rule changes the transition rates for node-dependent rates that are function of the persistence time of each node.

4.1 Application to the Voter Model

First of all, and to have a better idea of the kind of dynamics that arise from the new update rules, we exemplify them in Tables 2–4. In those tables we show snapshots of the evolution of the voter model under the different update rules on a square lattice. In particular we show the configuration of nodes states, times since the last change

Table 3 Evolution of the voter model on a square lattice of 100×100 nodes with *exogenous update*

Time	Configuration	Time since state change	Time since update
$t = 1$			
$t = 10$			
$t = 100$			

Color codes as in Table 2. We observe the same coarsening process (growth of domains) as with RAU (first column). Nodes also change state quite frequently (second column), with nodes that have kept their state for a longer time only inside of domains of the same state. Nevertheless, times since the last update (third column) do not show any specific pattern: some form of $1/f$ spatial noise with nodes updated in the same way

of state and time since last update at different points in time: for RAU (Table 2), for exogenous update (Table 3) and for endogenous update (Table 4).

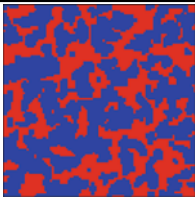
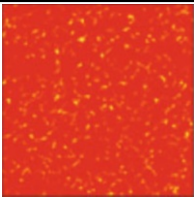
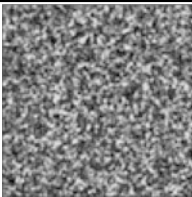
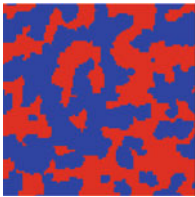
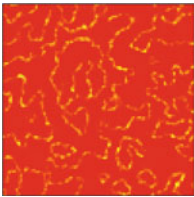
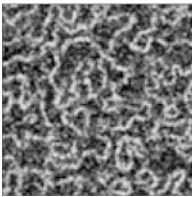

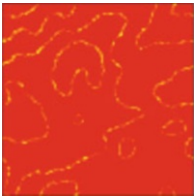

4.1.1 Voter Model with Exogenous Update on Complex Networks

If instead of the standard update rules discussed in Sect. 3.2 we now use the exogenous version of the new update, the agents will not be characterized only by its state x_i , but also by their internal time τ_i , *i.e.*, the time since their last update event.

The simulation steps for this modified voter model are as follows:

1. With probability $p(\tau_i)$ every agent i is given the opportunity of updating her state by interacting with a neighbor.
2. If the agent interacts, one of its neighbors j is chosen at random and agent i copies j 's state. $x_i(t + 1) = x_j(t)$. Agent i resets $\tau_i = 0$.

Table 4 Evolution of the voter model on a square lattice of 100×100 nodes with *endogenous update*

Time	Configuration	Time since state change	Time since update
$t = 1$			
$t = 10$			
$t = 100$			

Color codes as in Table 2. The effect of this update on the dynamics is striking and the same patterns are observed in the three columns. First, endogenous update introduces surfaces tension in the dynamics, so that the coarsening process (growth of domains) is now driven by curvature reduction (first column). In the second column we observe that the time since the last change of state is only small in the boundaries separating nodes with different states. Given that this time is now coupled to the update process, the same patterns are observed in the third column: the nodes at the interface (the ones which have changed less time ago) are updated much more frequently than the nodes in the bulk of a cluster of each state

3. The time is increased by a unit and we return to 1 to keep on with the dynamics.

For an activation probability $p(\tau) = 1/\tau$, *i.e.*, $\beta = 1$ we ran simulations on a complete graph, on random graphs of different average degrees, and on a Barabási-Albert scale-free graph of average degree $\langle k \rangle = 6$ and for different system sizes (see Fig. 4).

Our results can be summarized as follows:

Density of active links $\langle \rho(t) \rangle$ and $\langle \rho^(t) \rangle$* : When averaged over all runs, $\langle \rho(t) \rangle$ decays with different rates depending on the interaction networks and system sizes. For bigger system sizes the decay slows down, reaching a plateau in the large N limit (top row of Fig. 4). When averaged over active runs $\langle \rho^*(t) \rangle$ reaches a plateau (second row of Fig. 4), which is independent of the system

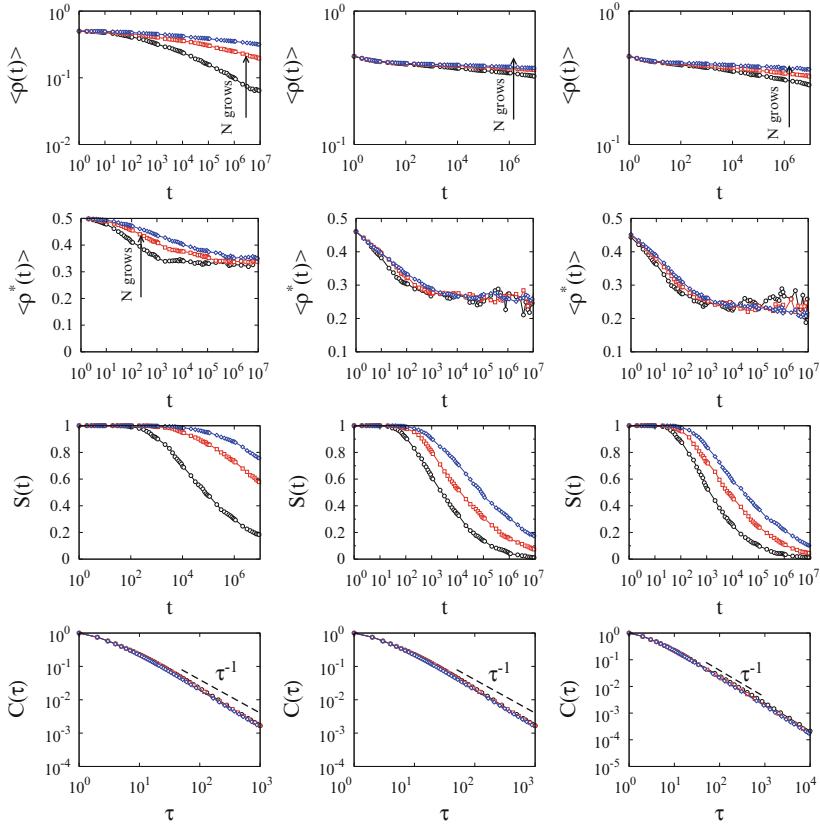


Fig. 4 Characteristics of the voter model with *exogenous update* for several networks. Left column is for complete graphs of sizes 300 in black, 1,000 in red and 4,000 in blue. Middle column is for random graphs with average degree $\langle k \rangle = 6$ and sizes 1,000 in black, 2,000 in red and 4,000 in blue. Right column is for scale-free graphs with average degree $\langle k \rangle = 6$ and sizes 1,000 in black, 2,000 in red and 4,000 in blue. Top row shows plots of the average density of interfaces $\langle \rho \rangle$, second row shows the density of interfaces averaged over surviving runs $\langle \rho^* \rangle$, middle column shows the survival probability $S(t)$ and right column shows the cumulative IET distribution $C(\tau)$. The averages were done over 1,000 realizations

size, showing that living runs stay, on average, on a dynamical disordered state, as happens with standard update rules.

Survival probability $S(t)$: No realizations order in some time, until the survival probability decays in a nontrivial way. It is not a purely exponential decay, but decays faster than any power law. Therefore no normalization problems are expected. See third row of Fig. 4.

Cumulative IET distribution $C(\tau)$: Develops a power law tail consistent with the exponent $\beta = b$, which in this case is set to 1, as we could expect if the approximation of (3) holds. See bottom row of Fig. 4.

The dynamics does not order the system with the exogenous update.

4.1.2 Voter Model with Endogenous Update on Complex Networks

We now use the endogenous update for the voter model. This is just the same as the exogenous update rule, but in this case the internal time of each agent i , τ_i , is the time since her last change of state. In this way the update rule is coupled to the states of the agents.

The simulation steps for the modified voter model that we study are as follows:

1. With probability $p(\tau_i)$ every agent i is given the opportunity of updating her state by interacting with a neighbor.
2. If the agent interacts, one of its neighbors j is chosen at random and agent i copies j 's state. $x_i(t + 1) = x_j(t)$.
3. If the update produces a change of state of node i , then τ_i is set to zero.
4. The time is updated to a unit more and we return to 1 to keep on with the dynamics.

The question now is if this modification will lead to qualitative changes in the outcome of the dynamics of the voter model.

For an activation probability $p(\tau) = 1/\tau$, i.e., $\beta = 1$ we ran simulations on a complete graph, on random graphs of different average degree, and on a Barabási-Albert scale-free graph of average degree $\langle k \rangle = 6$ and for different system sizes (see Fig. 5).

The exponents in the power laws of the quantities plotted in Fig. 5 are summarized in Table 5 for the cases of complete, random and scale-free graph with mean degree $\langle k \rangle = 6$. We can see from the table that, increasing the average degree of the random networks we get results that get closer to the ones on a complete graph.

Our results can be summarized as follows:

Density of active links $\langle \rho(t) \rangle$ and $\langle \rho^(t) \rangle$:* When averaged over all runs, $\langle \rho(t) \rangle$ decays as a power law with different exponents depending on the interaction network (see top row in Fig. 5). When averaged over active runs $\langle \rho^*(t) \rangle$ we see that it decays as a power law until it reaches a plateau whose height depends on the system size and is smaller for bigger system sizes (see second row in Fig. 5), which tells that *the system is heading towards consensus*, contrary to what happens with the standard update rules. This is one of the main results of the present work.

Survival probability $S(t)$: It is one until it decays, also like a power law (see third row in Fig. 5). The exponents are in all cases smaller or around 1, so that *the average time to reach consensus diverges for all system sizes*. Remember that the mean time to reach consensus is $\langle T \rangle = \int_0^\infty S(t)dt$. So, a proper average consensus time is not defined.

Cumulative IET distribution $C(\tau)$: Develops a power law tail (see bottom row in Fig. 5). For a complete graph and a random network with high degree we recover an exponent β in the tail of the interevent times cumulative distribution $C(\tau)$ that matches the one we wanted it to follow given our calculations and our choice

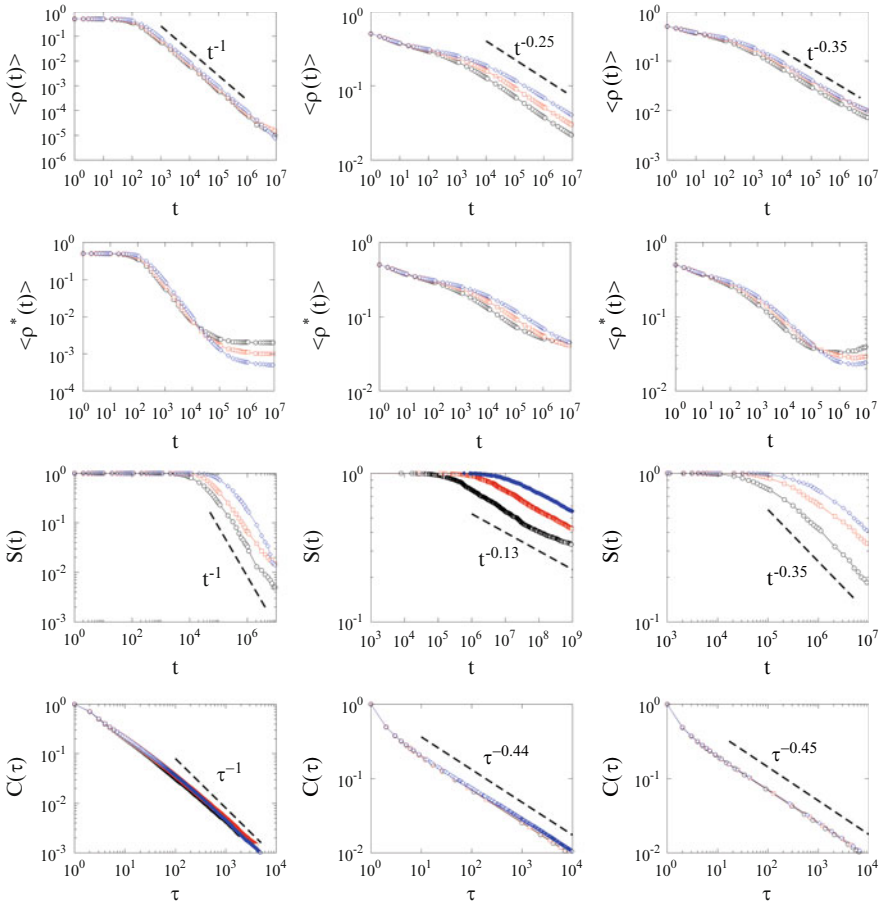


Fig. 5 Characteristics of the voter model with *endogenous update* for several networks. *Left column* is for complete graphs of sizes 300 in black, 1,000 in red and 4,000 in blue. *Middle column* is for random graphs with average $\langle k \rangle = 6$ and sizes 1,000 in black, 2,000 in red and 4,000 in blue. *Right column* is for scale-free graphs with average degree $\langle k \rangle = 6$ and sizes 1,000 in black, 2,000 in red and 4,000 in blue. *Top row* shows plots of the average density of interfaces $\langle \rho \rangle$, *second row* shows the density of interfaces averaged over surviving runs $\langle \rho^* \rangle$, *third row* shows the survival probability $S(t)$ and *bottom row* shows the cumulative IET distribution $C(\tau)$. The averages were done over 1,000 realizations

Table 5 Exponents for the power law decaying quantities $\rho(t)$, $S(t)$ and $C(\tau)$ for the voter model with the endogenous update rule

	$\langle \rho(t) \rangle \propto t^{-\gamma}$	$S(t) \propto t^{-\delta}$	$C(\tau) \propto t^{-\beta}$
Complete graph	$\gamma = 0.985(5)$	$\delta = 0.95(2)$	$\beta = 0.99(3)$
Random graph $\langle k \rangle = 20$	$\gamma = 0.99(1)$	$\delta = 0.82(1)$	$\beta = 0.94(4)$
Random graph $\langle k \rangle = 6$	$\gamma = 0.249(4)$	$\delta = 0.13(1)$	$\beta = 0.45(1)$
Scale-free graph $\langle k \rangle = 6$	$\gamma = 0.324(7)$	$\delta = 0.32(1)$	$\beta = 0.46(1)$

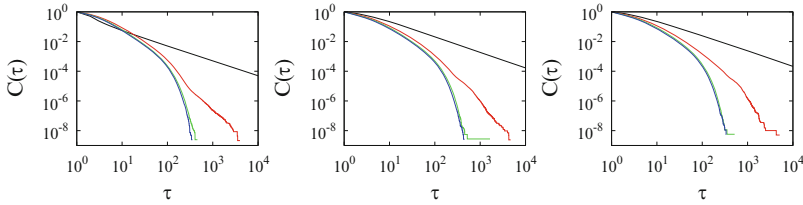


Fig. 6 *Exogenous update*: cumulative IET distribution $C(\tau)$ for different values of the parameter b (black $b = 1$, red $b = 2$, green $b = 3$, blue $b = 4$) appearing in the activation probability $p(\tau)$ for complete graph (left), random graph with $\langle k \rangle = 6$ (middles) and Barabási-Albert scale-free network with $\langle k \rangle = 6$ (right) and for system size $N = 1,000$

$p(\tau) = 1/\tau$. For the other two networks, random and scale-free with $\langle k \rangle = 6$ we recover that the tail behaves approximately as $1/\sqrt{\tau}$.

The dynamics orders the system with the endogenous update through a coarsening process that leads to the divergence of the mean time to reach consensus for all system sizes. As a summary, the complete graph case gives us already the qualitative behavior: for the voter model with exogenous update the timescales are much larger than in the voter model with RAU, but it has the same qualitative behavior: the system doesn't order in the thermodynamic limit, but stays in a disordered dynamical configuration with asymptotic coexistence of both states. This contrasts with what happens with the endogenous update, where the timescales are also perturbed, but with the difference that a coarsening process occurs, slowly ordering the system. We have checked that the ensemble average of the magnetization $\langle m(t) \rangle = \frac{1}{N} \sum_{i=1}^N \langle s_i(t) \rangle$ is conserved for the exogenous update, whereas for the endogenous update this conservation law breaks down, as previously discussed in Ref. [24]. The non-conservation of the magnetization leads to an ordering process. The conservation law is broken due to the different average values of the persistence time in both populations of agents (+1 and -1) leading to different average activation probabilities.

4.1.3 Varying the Exponents of the Cumulative IET Distribution $C(\tau)$

As was shown in Sect. 4 the exponent in the cumulative IET distribution $C(\tau) \propto \tau^{-\beta}$ should be related to the parameter b appearing in the activation probability $p(\tau) = b/\tau$. If every time we let an agent be updated, this one changes state, this relation is such that $\beta = b$. When introducing the dynamics, this relation is not so clear and depends also on the kind of network where the dynamics are taking place. In Fig. 6 we can see the interevent times cumulative distributions for different values of b for the exogenous update.

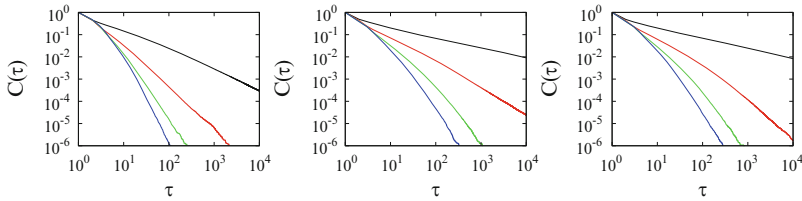


Fig. 7 *Endogenous update*: cumulative IET distribution $C(\tau)$ for different values of the parameter b (black $b = 1$, red $b = 2$, green $b = 3$, blue $b = 4$) appearing in the activation probability $p(\tau)$ for complete graph (left), random graph with $\langle k \rangle = 6$ (middle) and Barabási-Albert scale-free network with $\langle k \rangle = 6$ (right) and for system size $N = 1,000$

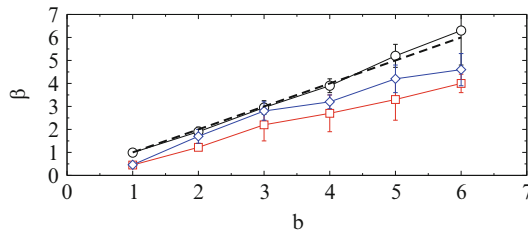


Fig. 8 *Endogenous update*. Relation of β , the exponent of the cumulative IET distribution $C(t) \sim t^{-\beta}$, and b , the parameter in the function $p(\tau) = b/\tau$ for three different topologies; fully connected (circles), random with $\langle k \rangle = 6$ (squares) and scale free with $\langle k \rangle = 6$ (diamonds) networks. As a guide to the eye we plot the curve $\beta = b$ with a dashed line. The bars stand for the associated standard errors of the measures

We can see that for $b = 1$ the power law tail is recovered with an exponent that matches $\beta = b$. For higher values of b the form of the tail is rapidly lost and we have cumulative IET distribution $C(\tau)$ are similar to those with standard update rules, i.e., do not display heavy tails.

In Fig. 7 we can see the interevent times cumulative distributions for different values of b for the endogenous update.

The endogenous update rule has a wider range of b -values for which the heavy tail is recovered. We measured the exponents of the tails for different values b in the different topologies. The results can be seen in Fig. 8.

Surprisingly, for the case of the complete graph, we recover the relation predicted, i.e., a linear relation between β in the cumulative distribution function and b , the parameter in the probability $p(\tau)$.

In the case of other topologies we find that the relation $b - \beta$ is not the one predicted in the case of no interactions, but it displays a reminiscent behavior of the one observed for a complete graph: the exponent β found in the cumulative interevent time distribution increases monotonically with the parameter b in the activation probability.

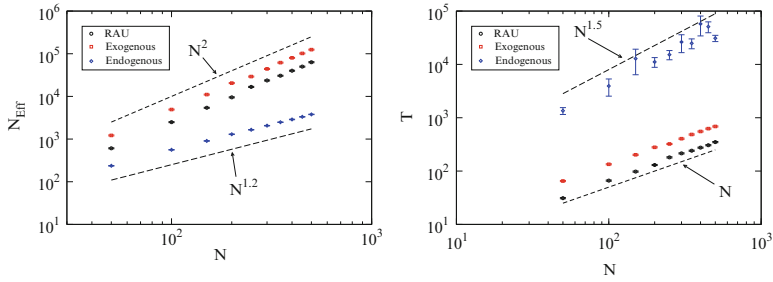


Fig. 9 On the *left* we can see the scaling of the number of effective events with system size for a complete graph and three different update rules, RAU, exogenous and endogenous. On the *right* we can see the scaling of the consensus time with system size for a complete graph and three different update rules, RAU, exogenous and endogenous

4.1.4 Effective Events

An interesting feature is the number of effective events, *i.e.*, updates that result in a change of state, are needed to get to consensus. It happens that for the usual update rules and the exogenous update, the scaling with system size is the same, while the endogenous update follows a different scaling (cf. left plot in Fig. 9 for the case of complete graph), signaling the difference due to the coarsening process that appears for the endogenous update. Furthermore the number of effective events needed with the endogenous update to order the system is much less than with the other update rules. This efficiency in ordering is due to the coarsening process that occurs with the endogenous update. Even though, in terms of time steps, the exogenous update is much slower, such that the time to reach consensus diverges. In the right plot of Fig. 9 we see a time for reaching consensus for the endogenous update, but this time will diverge if the sample of realizations taken for the average is big enough.

5 Discussion

The take home message of this work is to beware of social simulations of interacting individuals based on a constant activity rate: Human activity patterns need to be implemented as an essential part of social simulation. We have shown that heterogeneous interevent time distributions can produce a qualitative change in the voter model of social consensus, leading from dynamical coexistence of equivalent states to ordering dynamics. More specifically, we have shown that for standard update rules (SAU, RAU, SU) of the voter model dynamics in networks of high dimensionality (Fully connected, random, scale free) the system remains in long lived disordered dynamical states of coexistence of the two states, and activity patterns are homogeneous with a well defined characteristic interevent time. A power law tail for the cumulative interevent time distribution is obtained

with two forms of the update rule accounting for heterogeneous activity patterns. For an exogenous update rule the dynamics is still qualitatively the same than for standard update rules: the system does not order, remaining trapped in long lived dynamical states. However, when the update rule is coupled to the states of the agents (endogenous update) it becomes part of the dynamical model, modifying in an essential way the dynamical process: there is coarsening of domains of nodes in the same state, so that the system orders approaching a consensus state. Also the times to reach consensus in the endogenous version of the update rule are such that a mean time to reach consensus is not well defined. In fact the scaling of effective events needed for consensus is able to give a signature of which of the updates is ordering the system. In summary, when drawing conclusions from microscopic models of human activity, it is necessary to take into account that the macroscopic outcome depends on the timing and sequences of the interactions. Even if recovering heterogeneous interevent time distributions the type of update (exogenous vs. endogenous rule) can modify the ordering dynamics.

Recent research on human dynamics has revealed the “small but slow” paradigm [17, 18], that is, the spreading of an infection can be slow despite the underlying small-world property of the underlying network of interaction. Here, with the help of a general updating algorithm accounting for realistic interevent time distributions, we have shown that the competition of two states can lead to slow ordering not only in small-world networks but also in the mean field case. Our results provide a theoretical framework that bridges the empirical efforts devoted to uncover the properties of human dynamics with modeling efforts in opinion dynamics.

Works closely related to our research are those in Refs. [24–26]. Stark et al. [24] introduced an update rule similar to our *endogenous update* and focused on consensus times. However they did not explore heavy tail distribution for the interevent intervals. They found that by slowing the dynamics, introducing a probability to interact that decays with the time since the last change of state, consensus formation could be actually accelerated. Baxter [25] introduced a time dependence in the flip rates of the voter model. He explored the case when the flip rates vary periodically obtaining that consensus times depended non-trivially on the period of the flip-rate oscillations, having larger consensus times for larger periods, until it saturates. Finally, Takaguchi and Masuda [26] investigated some variations of the voter model, where the intervals between interactions of the agents were given by different distributions. The models they used are similar to our *exogenous update*. They found that the times to consensus in the case of a power law distributed interevent interval distribution were enlarged, in agreement with our results.

Possible future avenues of research following the ideas of this work are to study other dynamics and topologies. An example is the possibility that fat-tailed IET distributions appear as a consequence of topological traps in the network of interaction under majority rule dynamics. These traps can lead to anomalous scaling of consensus times for a majority rule dynamics [31, 32]. A consensus time is a global property of the system, but it remains unclear if this is also reflected in the microscopic dynamics, giving rise to broad IET distributions.

Acknowledgements We acknowledge financial support from the MINECO (Spain) and FEDER (EU) through projects FISICOS (FIS2007-60327) and MODASS (FIS2011-24785). JFG acknowledges support from the Government of the Balearic Islands through the Conselleria d'Educaci, Cultura i Universitats and the ESF.

References

1. Castellano, C., Fortunato, S., Loreto, V.: Statistical Physics of social dynamics. *Rev. Mod. Phys.* **81**, 591 (2009)
2. Clifford, P., Sudbury, A.: A model for spatial conflict. *Biometrika* **60(3)**, 581 (1973)
3. Holley, R., Liggett, T.M.: Ergodic theorems for weakly interacting infinite systems and the voter model. *Ann. Prob.* **3(4)**, 643 (1975)
4. San Miguel, M., Eguíluz, V.M., Toral, R., Klemm, K.: Binary and multivariate stochastic models of consensus formation. *Comp. Sci. Eng.* **7**, 67 (2005)
5. Granovetter, M.: Thresholds models of collective behavior. *Am. J. Soc.* **83**, 1420 (1978)
6. Watts, D.: A simple model of global cascades on random networks. *Proc. Natl. Acad. Sci. USA* **99**, 5766 (2002)
7. Centola, D., Eguíluz, V.M., Macy, M.W.: Cascade dynamics of complex propagation. *Phys. A* **374**, 449 (2007)
8. Zimmerman, M., Eguíluz, V.M., San Miguel, M.: Economics with heterogeneous interacting agents. *Lect. Notes Econ. Math. Syst.* **503**, 73 (2001)
9. Zimmerman, M., Eguíluz, V.M., San Miguel, M.: Coevolution of dynamical states and interactions in dynamic networks. *Phys. Rev. E* **69**, 065102 (2004)
10. Vazquez, F., Eguíluz, V.M., San Miguel, M.: Generic absorbing transition in coevolution dynamics. *Phys. Rev. Lett.* **100**, 108702 (2008)
11. Gross, T., Blasius, B.: Cascade dynamics of complex propagation. *J. R. Soc. Interface* **5**, 259 (2008)
12. Vazquez, F., González-Avella, J.C., Eguíluz, V.M., San Miguel, M.: Time-scale competition leading to fragmentation and recombination transitions in the coevolution of network and states. *Phys. Rev. E* **76**, 046120 (2007)
13. Malmgren, R.D., Stouffer, D.B., Campanharo, A.S.L.O., Amaral, L.A.N.: On universality in human correspondence activity. *Sci.* **325**, 1696 (2009)
14. Gama Oliveira, J., Barabási, A.-L.: Darwin and Einstein correspondence patterns. *Nature* **437**, 1251 (2005)
15. Eckmann, J.-P., Moses, E., Sergi, D.: Entropy dialogues creates coherent structures in e-mail traffic. *Science* **325**, 1696 (2009)
16. Iribarren, J.L., Moro, E.: Impact of human activity patterns on the dynamics of information diffusion. *Phys. Rev. Lett.* **103**, 038702 (2009)
17. Vázquez, A., Rácz, B., Lukács, A., Barabási, A.-L.: Impact of non-poissonian activity patterns on spreading processes. *Phys. Rev. Lett.* **98**, 158702 (2007)
18. Karsai, M., Kivela, M., Pan, R.K., Kaski, K., Kertész, J., Barabási, A.L., Saramäki, J.: Small but slow world: how network topology and burstiness slow down spreading. *Phys. Rev. E* **83**, 025102 (2011)
19. Min, B., Goh, K.I., Vazquez, A.: Spreading dynamics following bursty human activity patterns. *Phys. Rev. E* **83**, 036102 (2011)
20. Malmgren, R.D., Stouffer, D.B., Motter, A.E., Amaral, L.A.N.: A poissonian explanation for heavy tails in e-mail communication. *Proc. Natl. Acad. Sci. USA* **105**, 18153 (2008)
21. Barabási, A.-L.: The origin of bursts and heavy tails in human dynamics. *Nature* **435**, 207 (2005)
22. Vázquez, A., Gama Oliveira, J., Dezsö, Z., Goh, K.-I., Kondor, I., Barabási, A.-L.: Modeling bursts and heavy tails in human dynamics. *Phys. Rev. E* **73**, 036127 (2006)

23. Fernández-Gracia, J., Eguíluz, V.M., San Miguel, M.: Update rules and interevent time distributions: slow ordering versus no ordering in the voter model. *Phys. Rev. E* **84**, 015103 (2011)
24. Stark, H.-U., Tessone, C.J., Schweitzer, F.: Decelerating microdynamics can accelerate macrodynamics in the voter model. *Phys. Rev. Lett.* **101**, 018701 (2008)
25. Baxter, G.J.: *J. Stat. Mech.*: A voter model with time dependent flip rates. *Theor. Exp.* **2011**, P09005 (2011)
26. Takaguchi, T., Masuda, N.: Voter model with non-Poissonian interevent intervals. *Phys. Rev. E* **84**, 036115 (2011)
27. Suchecki, K., Eguíluz, V.M., San Miguel, M.: Conservation laws for the voter model in complex networks. *Europhys. Lett. J. B* **69**, 228 (2005)
28. Klemm, K., Serrano, M.A., Eguíluz, V.M., San Miguel, M.: A measure of individual role in collective dynamics. *Sci. Rep.* **2**, 292 (2012)
29. Vázquez, F., Eguíluz, V.M.: Analytical solution of the voter model on uncorrelated networks. *New J. Phys.* **10**, 063011 (2008)
30. Sood, V., Redner, S.: Voter model on heterogeneous graphs. *Phys. Rev. Lett.* **94**, 178701 (2005)
31. Castelló, X., Toivonen, R., Eguíluz, V.M., Saramäki, J., Kaski, K., San Miguel, M.: Anomalous lifetime distributions and topological traps in ordering dynamics. *Europhys. Lett.* **79**, 66006 (2007)
32. Toivonen, R., Castelló, X., Eguíluz, V.M., Saramäki, J., Kaski, K., San Miguel, M.: Broad lifetime distributions for ordering dynamics in complex networks. *Phys. Rev. E* **79**, 016109 (2009)